Imperial College London

Faculty of Medicine

Department of Medicine

Division of Brain Sciences

Centre for Neuroinflammation and Neurodegeneration

INVESTIGATING THE NEUROPROTECTIVE EFFECTS OF HISTONE DEACETYLASE INHIBITORS IN PARKINSON'S DISEASE

Ian Francis Harrison

A thesis submitted in fulfilment of the requirements for the degree of Doctor of Philosophy in the Faculty of Medicine of Imperial College London, and for the Diploma of Imperial College London

October 2014

For Grandma,
and Grandad Cakey.

Declaration of Originality

I declare that this thesis is my own work and has not been submitted in any form for another degree or diploma at any university or other institution of tertiary education. Information derived from the published or unpublished work of others has been acknowledged in the text and a list of references is given.

Ian Francis Harrison

17th October 2014

Copyright Declaration

The copyright of this thesis rests with the author and is made available under a Creative Commons Attribution Non-Commercial No Derivatives licence. Researchers are free to copy, distribute or transmit the thesis on the condition that they attribute it, that they do not use it for commercial purposes and that they do not alter, transform or build upon it. For any reuse or redistribution, researchers must make clear to others the licence terms of this work.

Acknowledgements

First and foremost I am indebted to my supervisor Prof David Dexter. It has been a privilege to work with David throughout these past 4 years during which time he has served as an inspiration for me as an early career researcher. I am truly thankful for him giving me the opportunity to work on this exciting project within his group. He has provided constant support over the course of my PhD and has displayed endless patience with me on both good days and bad. I hope one day to be able to pass on the legacy of true mentorship to others the way he has to me.

Much of the work presented in this thesis could not have been achieved without the help of both internal and external collaborators for which I am hugely thankful. I am extremely grateful to both Drs Anthony Vernon and Bill Crum at Kings College London for their work on the tensor based morphometry analysis. Likewise to Dr Matt Fuchter and his group at Imperial College for synthesising and characterising the novel sirtuin2 inhibitor. Both of these collaborations have provided an extra dimension to the research presented here and I am indebted to them for their efforts.

The MRI work presented here would not have been possible without the staff at the former Biological Imaging Centre at Imperial College. Drs Marzena Wylezinska-Arridge, Jordi Tremoleda Lopez and Willy Gsell, showed unending patience with me while learning this complicated technique and for that I am hugely grateful.

I am also thankful to the Parkinson's UK tissue bank for providing the human tissue samples for the work presented here, also to the staff at the tissue bank for their help with this. Particular thanks to Louisa, who's technical support of the human work in this thesis has been second to none. I would also like to express my thanks to the brain donors and their families, who have made this work possible.

My fellow 'Dexter-ites' have provided such a supportive lab environment for me over the past years. I thank each and every one of them for their tireless support: Mike, Tamara, Daniel, Emma and Ilse. Also to former Dexter BSc and MRes student of mine: Andy, Hiba and Ntida, thanks so much for your help. And to former Dexter lab member Dr Liz Ash for her patience in teaching me stereotaxic surgery and behavioural testing. Lastly to my 'work-wife' Claire, who's provided everything from friendship, support, a shoulder to cry on, and a person to moan to! Thanks so much for everything you've done over the past three years, my time at Imperial just wouldn't have been the same without you across the office.

The Wolfson Neuroscience Laboratories within the Centre for Neuroinflammation and Neurodegeneration have become a second home to me over the last few years, I mean this quite literally during the writing of this thesis! This would not be the case without my colleagues and friends within the department. Special thanks to you all for keeping me sane throughout this time, and giving me a much needed excuse to leave my desk and eat cake every Monday afternoon! Extra special thanks to Eleanor and Reneé, their support and friendship over the past four years has been incredible. Also it's safe to say those late nights and weekends spent running PCRs and Westerns just wouldn't have been the same without them!

Also to all of my friends outside the lab, their support has been hugely appreciated. I don't know what I'd do without having such an amazing bunch of friends like them. Particular thanks to my former flat mate Lewis, for providing a much needed ear to bend at the end of a long day of failed experiments. He's seen me at both my high and low points, and if it wasn't for him tentatively knocking on my door and bringing me more coffee before he went to bed, early and late stage assessment just wouldn't have got done! Also to my best friend Kate, who's provided truly unending friendship and support over the past years. No matter how busy she is, she'll always take ten minutes out of her day to listen to me moan, and later insists on dragging me out to the nearest pub to listen some more. She is a true friend and I can't thank her enough for her support.

Also to my family, my sister Kim has been a great support and provider of statistical know-how throughout these past years, and what to say about Mum and Dad? One could not ask for more supportive parents and their love, generosity and financial help throughout the entirety of my time in higher education has been astounding. I hope in return I've made them proud of me, it's the very least I can do.

Last but certainly not least, my wonderful girlfriend Laura. Words cannot describe how supportive she's been to me over the past 3 years. Even when coming home late from work every single day for weeks on end, she's still there waiting for me with a glass of wine poured and a smile on her face. Her unending love, patience and encouragement have picked me up and spurred me on when I've needed it most, and for that reason I owe the success of this thesis most of all to her.

Abstract

Parkinson's disease (PD) is the most common movement disorder and the second most common neurodegenerative disease affecting around 4 million people worldwide. Movement symptoms in PD are primarily due to degeneration of dopaminergic nigrostriatal neurons. These symptoms can be partially controlled by dopamine replacement therapies, however long term use of these drugs lead to debilitating side-effects and more importantly do not protect degenerating dopaminergic neurons from death. Hence novel neuroprotective strategies are sought. Recent evidence implicates αSynuclein accumulation, the hallmark of degenerating neurons in PD, with perturbed epigenetic acetylation of histone proteins around which DNA is coiled. A misbalance between the activities of the two enzyme classes responsible for control of histone acetylation, histone acetyltransferases and histone deacetylases (HDACs), have been linked to cell death in animal models of neurodegeneration. It is therefore hypothesised that if this pathogenic imbalance can be rectified with the use of HDAC inhibitors (HDACIs) then neurodegeneration observed in PD can be avoided. Here, the first evidence of altered histone acetylation and perturbed HDAC isoform expression in degenerating regions of the human Parkinsonian brain are demonstrated. Cell culture studies using dopaminergic neuronal and microglial cell lines demonstrate that dependent on the HDAC class(s) or isoform(s) inhibited, HDACIs are capable of inducing neuroprotection and reduction of microglial activation *in vitro*. Study of two broad-spectrum HDACIs *in vivo*, in the lactacystin rat model of PD demonstrate that, also dependent on isoform inhibition, HDACIs cause dose-dependent histone acetylation and upregulated expression of neurotrophic and neuroprotective factors, resulting in dopaminergic nigrostriatal neuroprotection and reduction of morphological changes and motor behavioural deficits detected through magnetic resonance imaging and behavioural testing respectively. Taken together the data herein provide compelling evidence to support the concept that dependent on isoform specificity, HDACIs represent a novel class of neuroprotective therapeutics for the treatment of PD.

Table of Contents

List of Figures

Page Number

Chapter One

Chapter Two

Chapter Three

Chapter Four

Chapter Five

Chapter Six

Chapter Seven

Chapter Eight

List of Tables

Page Number

Chapter One

Chapter Two

Chapter Three

Chapter Four

Chapter Five

Chapter Six

Chapter Seven

Abbreviations

6-OHDA	6-Hydroxydopamine
ABC	Avidin Biotin Complex
ABTS	2,2'-azino-bis(3-ethylbenzothiazoline-6-sulphonic acid
AD	Alzheimer's Disease
ALS	Amylotrophic Lateral Sclerosis
ANOVA	Analysis of Variance
AOI	Area of Interest
BBB	Blood Brain Barrier
Bcl	B-Cell Lymphoma
BDNF	Brain Derived Neurotrophic Factor
BSA	Bovine Serum Albumin
CBP	CREB Binding Proteins
cDNA	Complimentary Deoxyribonucleic Acid
COMT	Catecholiamine-o-methyl Transferase
C_T	Threshold Cycle
CV	Coefficient of Variance
DAT	Dopamine Transporter
dH_2O	Distilled Water
DJ-1	Daisuke Junko-1
DMSO	Dimethyl Sulphoxide
DNA	Deoxyribonucleic Acid
DNMT	DNA Methyltranferases
DPBS	Dulbecco's Phosphate Buffered Saline
DTT	Dithiothreitol
ELISA	Enzyme-Linked Immunosorbant Assays
fPD	Familial Parkinson's Disease
GABA	γ-amino butyric acid
GDNF	Glial Derived Neurotrophic Factor
GNAT	Gcn5-related acetyltransferases
GSN	Gelsolin
HAT	Histone Acetyltransferase
HD	Huntington's Disease
HDAC	Histone Deacetylase
HDACI	Histone Deacetylase Inhibitor
HDM	Histone Demethylases
HMT	Histone Methyltransferases
HRP	Horseradish Peroxidase
HSP	Heat Shock Protein
ICC	Intra-Class Correlation Coefficient
IL	Interleukin
iNOS	Inducible Nitric Oxide Sythase
L-DOPA	L-3,4-dihydroxyphenylalanine
LPS	Lipopolysaccharide
LRRK2	Leucine-rich Repeat Kinase 2
LSD	Lysine-specific Histone Demethylase 1
MAO	Monoamine Oxidase
MAO-A	Monoamine Oxidase Type-A
MAO-B	Monoamine Oxidase Type-A
MeCP2	Methyl-CpG Binding Protein 2
MEMS	Multi-slice Spin-echo Pulse Sequence
MFB	Medial Forebrain Bundle
MPP+	1-methyl-4-phenylpyridinium
MPTP	1-methyl-4-phenyl-1,2,3,6-tetrahydropyridine
MR	Magnetic Resonance
MRI	Magnetic Resonance Imaging
mRNA	Messenger Ribonucleic Acid
MYST	MOZ, Ybf2/Sas3, Sas2 and Tip60
NAD+	Nicotinamide Adenine Dinucleotide
NADPH	Nicotinamide Adenine Dinucleotide Phosphate
NED	N-1-napthylethylenediamine
NO	Nitric Oxide
NR	Neutral Red
NSAID	Non-Steroidal Anti-Inflammatory Drug
PBS	Phosphate Buffered Saline
PBST	Phosphate Buffered Saline with Tween20
PBSTX	Phosphate Buffered Saline with TritonX
PD	Parkinson's Disease
PET	Positron Emission Tomography
PINK1	PTEN-induced Kinase 1
PSI	Sythetic Proteasome Inhibitor
PTFE	Polytetrafluroethylane
PUKTB	Parkinson's UK Tissue Bank
PVDF	Polyvinylidene Fluoride
qRT-PCR	Quantitatve Real Time Polymerase Chain Reaction
RIPA	Radio-Immunoprecipitation Assay
RNA	Ribonucleic Acid
RNase	Ribonuclease
ROS	Reactive Oxygen Species
RT	Room Temperature
SAH	S-adenosyl-homocysteine
SAM	S-adenosyl-methionine
SCFA	Short Chain Fatty Acid
SIR2	Silent Information Regulator 2
SNpc	Substantia Nigra pars compacta
SOD-1	Superoxide Dismutase 1
SPECT	Single Photon Emission Computed Tomography
TH	Tyrosine Hydroxylase
TNFα	Tumour Necrosis Factor α
UCHL-1	Ubiquitin Carboxy-terminal Hydrolase L1
UPS	Ubiquitin Proteasome System
αSyn	αSynuclein

Publications/Conference Presentations Arising From Thesis

Publications

DI FRUSCIA, P., ZACHARIOUDAKIS, E., LIU, C., MONIOT, S., LAOHASINNARONG, S., KHONGKOW, M., **HARRISON, I. F**., KOLTSIDA, K., REYNOLDS, C. R., SCHMIDTKUNZ, K., JUNG, M., CHAPMAN, K. L., STEEGBORN, C., DEXTER, D. T., STERNBERG, M. J., LAM, E. W.-F. & FUCHTER, M. J. (2014) The Discovery of a Highly Isoform Selective 5,6,7,8-Tetrahydrobenzo[4,5]thieno[2,3-d]pyrimidin-4(3H)-one SIRT2 Inhibitor that is Neuroprotective in an in vitro Parkinson's Disease Model. *ChemMedChem,* 13.

HARRISON, I. F. & DEXTER, D. T. (2013) Epigenetic targeting of histone deacetylase: Therapeutic potential in Parkinson's disease? *Pharmacology & Therapeutics,* 140**,** 34-52.*

PIENAAR, I. S., **HARRISON, I. F.**, ELSON, J. L., BURY, A., WOLL, P., SIMON, A. K. & DEXTER, D. T. (2013) An animal model mimicking pedunculopontine nucleus cholinergic degeneration in Parkinson's disease. *Brain Structure and Function***,** 1-22.

Oral Presentations

HARRISON, I.F., CRUM, W.R., VERNON, A.C. & DEXTER, D.T. (2014) Neuroprotective effects of valproate, an epigenetic histone deacetylase inhibitor, in Parkinson's disease: A preclinical MRI study. Oral presentation at *Neuroprotection: Basic mechanisms and translational potential, 9th Brain Research Conference,* Washington DC, USA, November 2014.

Poster Presentations

HARRISON, I.F. & DEXTER, D.T. (2013) Investigating The Neuroprotective Effects Of Valproate, An Epigenetic Histone Deacetylase Inhibitor, In Parkinson's Disease Using Preclinical Magnetic Resonance Imaging. Poster at *The Movement Disorder Society's 17th International Congress of Parkinson's Disease and Movement Disorders, Sydney, Australia,* Volume 28, June 2013 Abstract Supplement

HARRISON, I.F., BURY, A., DEXTER, D.T., PIENAAR, I.S. (2013) Cholinergic Cell Loss And Altered Morphology Accompanied By Structural Changes Affecting The Pedunculopontine Nucleus In The Lactacystin Rat Model Of Parkinson's Disease. Poster at *The Movement Disorder Society's 17th International Congress of Parkinson's Disease and Movement Disorders, Sydney, Australia,* Volume 28, June 2013 Abstract Supplement

HARRISON, I.F. & DEXTER, D.T. (2013) Investigating the Effects of Histone Deacetylase Inhibitors in Parkinson's Disease Using Preclinical Magnetic Resonance Imaging, Poster at *BNA 2013: Festival Of Neuroscience*

HARRISON, I.F. & DEXTER, D.T. (2012) Investigating the Effects of Histone Deacetylase Inhibitors in Parkinson's Disease Using Preclinical Magnetic Resonance Imaging, Poster at *Parkinson's UK Research Conference 2012*

HARRISON, I.F. & DEXTER, D.T. (2011) Magnetic Resonance Imaging as a tool for longitudinal monitoring in the lactacystin model of Parkinson's disease and studying the neuroprotective effects of valproate, Poster at *New York Academy of Sciences 2011 - Animal Models and Their Value in Predicting Drug Efficacy and Toxicity Conference*

* Parts of 'Chapter One – Introduction' are reprinted from *Pharmacology & Therapeutics*, **140**, HARRISON, I.F. & DEXTER, D.T., "Epigenetic targeting of histone deacetylase: Therapeutic potential in Parkinson's disease?" Pages 32-52, Copyright 2013, with permission from Elsevier. See appendix 1.

Chapter One

Introduction

1 – Introduction

1.1 – Overview of Chapter

Parkinson's disease (PD) is the most common movement disorder and the second most common neurodegenerative, affecting around 4 million people worldwide. Despite its abundance in today's society, current pharmacotherapy for PD is lacking, only able to partially tackle symptoms of the disorder yet unable to stop the progressive degeneration of neurons. Epigenetics, the process by which gene activity is altered without altering genetic information, has long attracted interest in neurodegenerative disease, due to the multifactorial origins of pathology. Epigenetic factors are thought to contribute to neuronal cell death in PD, and it is suggested that alteration in epigenetic regulation could hold therapeutic promise against neurodegeneration. One way by which this can be achieved is through histone remodelling; via acetylation and deacetylation of the histone proteins around which deoxyribonucleic acid (DNA) is coiled. This chapter will firstly summarise and review the current understanding of the clinical presentation, neuropathology, treatment and modelling of PD before reviewing the primary literature on the pharmacological targeting of histone acetylation for the treatment of PD.

1.2 – Parkinson's Disease

1.2.1 – History

Historically numerous sources describe symptoms which resemble PD, including biblical texts, an ancient Egyptian papyrus (12th Century B.C.), an Ayurvedic medical treatise (10th Century B.C.) and the writings of Galen, a Roman physician and surgeon (2nd Century A.D.) (Lees, 2007, Garcia-Ruiz, 2004). However despite having roots in prehistoric medicine, PD was first described in western medicine in 1817 by London physician James Parkinson (Goetz, 2011). In his iconic essay entitled "An Essay on the Shaking Palsy", he provides symptomatic description for the first time of six patients displaying what we now describe as Parkinsonian symptoms (Parkinson, 2002, Goetz, 2011). However it was not for another 60 years after the publication of Parkinson's original essay, that the term 'Parkinson's disease' was used in place of its former title, *paralysis agitans* (shaking palsy), by French neurologist and professor of anatomical pathology, Jean-Martin Charcot (Lees, 2007).

1.2.2 – Epidemiology

1.2.2.1 – Prevalence and Incidence

The prevalence of PD in industrialised countries is estimated to be around 0.3% of the general population. Being a disease of the elderly its prevalence increases greatly with age to around 1% of those aged over 60 years (Nussbaum and Ellis, 2003). It is known to be more prevalent in industrialised countries and also in Caucasian compared with Afro-American and Asian populations (de Lau and Breteler, 2006, Mayeux et al., 1995). Similarly some studies have found a greater incidence of PD in men than women (de Lau and Breteler, 2006), thought to be attributable to the neuroprotective effects of oestrogens however this remains debated (Saunders-Pullman, 2003, Gillies et al., 2004). In terms of incidence, the prevalence of PD translates to between 8-19 per 100,000 people diagnosed per year dependent upon the population studied (de Lau and Breteler, 2006). Early onset PD being diagnosed before age 50 accounts for just 10% of cases and hence incidence in people aged 60 years and above is greater than in young populations (de Lau and Breteler, 2006). The prevalence of PD translates to significant economic burden: the total cost per year in the UK estimated to be between £449 million and £3.3 billion (Findley, 2007).

1.2.2.2 – Genetic Risk Factors and Familial PD

Familial forms of PD (fPD) are thought to account for approximately 10% of PD cases. Study of fPD has identified at least 17 autosomal dominant and autosomal recessive mutations associated with varients of the disease, providing essential clues about the molecular mechanisms of disease pathogenesis (Houlden and Singleton, 2012). Of the autosomal dominant genes associated with PD, leucine-rich repeat kinase 2 (*LRRK2*) is far the most common, mutations in which accounting for 10%

of fPD (Spatola and Wider, 2014), associated with disruption of *LRRK2*'s cellular pathways involved with regulating neuronal dendrite formation and growth (Cookson, 2010b). Similarly, *LRRK2* mutation has also been linked to the aggregation of αSynuclein (αSyn) a dominant pathological hallmark of PD (Lin et al., 2009, Tong and Shen, 2009). Likewise alterations in *SNCA*, the gene responsible for encoding αSyn have also been noted: duplications, triplication and point mutations in families leading to PD and atypical forms of PD (Spatola and Wider, 2014). Autosomal recessive mutations have also been noted to be associated with fPD. For example mutations in *PINK1* (PTEN-induced kinase 1) and *DJ-1* (Daisuke Junko-1) have been shown to both result in mild Parkinsonism, thought to be attributable to the convergence of *PINK1* and *DJ-1* in the induction of oxidative stress (Cookson, 2010a). Dopaminergic neurons, the population of neurons known to degenerate most prolifically in PD, have a uniquely weak tolerance to oxidative stress and mitochondrial dysfunction, hence the Parkinsonian phenotype upon mutation in either of these genes, attributed to its kinase function in the mitochondria (*PINK1*) and coordinating cellular response to oxidative stress (*DJ-1*) (Cookson, 2010a). Autosomal recessive mutations in *PARK2* are thought to account for 50% of early onset fPD (Padmaja et al., 2012). Parkin, the product of this gene, is a ligase protein crucially involved in the ubiquitin mediated proteosomal degradation of proteins. This system is known also to be involved in sporadic PD, thought to be linked to the failure of protein degradation in degenerating neurons in the brains of sufferers (McNaught and Jenner, 2001, Tofaris et al., 2001, McNaught et al., 2002a). Genetic studies have also identified a number of susceptibility genes, polymorphisms in which are thought to contribute significantly to a person's genetic risk of developing PD. For example, *UCH-L1* (Ubiquitin Carboxy-terminal Hydrolase L1) is also involved in ubiquitin mediated proteosomal degradation, resulting in cytosolic accumulation of abnormal protein in neurons leading to their demise (Maraganore et al., 2004).

1.2.2.3 – Environmental Risk Factors

The first evidence that environmental factors may be involved in the development of PD came from the coincidental discovery of the neurotoxin 1-methyl-4-phenyl-1,2,3,6-tetrahydropyridine (MPTP) (Langston et al., 1983). Discovered as being a by-product of the crude sythesisis of an illicit meperidine derivative by a group of drug addicts, when administered intravenously this MPTP contaminant produced striking Parkinsonian symptoms in the four users (Langston et al., 1983). This by-product, MPTP, was later shown to be readily converted in the brain in astrocytes to 1-methyl-4-phenylpyridinium (MPP+), the pyridinium ion, catalysed by monoamine oxidase type-B (MAO-B). MPP+ is then taken up by the dopamaine transporter (DAT) into dopaminergic neurons causing inhibition of mitochondrial complex I leading quickly to neuronal cell death (Przedborski et al., 2000). MPTP is now routinely used to model PD *in vivo* in mice and primates, causing progressive

nigrostriatal neurodegeneration when injected peripherally, depending on the extent and duration of treatment. Similarly the active metabolite MPP+ is used to model dopaminergic degeneration *in vitro*.

The discovery of MPTP led to a surge of epidemiological studies into environmental factors which could be associated with increased incidence of PD. Farming and living in rural areas were quickly identified as surrogate markers associated with increased incidence of PD, moreover an increased incidence of PD was observed in those with agricultural occupations (Gorrell et al., 1996, de Lau and Breteler, 2006). Farming and rural residency are often associated with increased exposure to herbicides and pesticides hence it was demonstrated that the herbicide paraquat and the pesticide rotenone are also potent mitochondrial complex I inhibitors like MPTP (Betarbet et al., 2000). Both of these toxins are now used alongside MPTP for the modelling of PD in animals.

Exposure to metals such as iron, manganese, copper, lead, zinc, mercury and aluminium have also been suggested as possible risk factors for the development of PD, due to the accumulation of metals within affected brain regions in PD (Dexter et al., 1989b, Gorell et al., 1999). For example, exposure to magnesium ore is known to be toxic towards the basal ganglia, resulting in development of Parkinsonian symptoms (Huang, 2007). Furthermore, inhalation of magnesium fumes from welding has led to a suggested explanation of the increase incidence of PD in welders (Jankovic, 2005).

Numerous lifestyle choices have also more recently been implicated in risk of developing PD. For example, multiple epidemiological studies suggest that cigarette smoking reduces the risk of developing PD (Kiyohara and Kusuhara, 2011). Although the mechanism behind this finding is still not conclusive, it is suggested that the increase of dopamine release in the dopaminergic reward pathways by nicotine in cigarette smoke may be responsible for the decreased risk. Additional to this, nicotine is also thought to act as an antioxidant and alters activity of MAO-B adding further weight to its beneficial effects against PD (Quik et al., 2012). Studies of the neuroprotective effects of nicotine in animals models of PD are conflicting however, positive finding only being reported in some animal models (Maggio et al., 1998), but not in others (Pauly et al., 2004). Interestingly it has also been shown that nicotine-free tobacco smoke is capable of inducing neuroprotection in a drosophila model of PD (Trinh et al., 2010), highlighting the possibility that the active neuroprotectant in cigarette smoke may well not be nicotine at all. Coffee consumption has also been linked to PD, however it is far more clear in this instance that caffeine is the active agent: caffeine consumption being inversely related to the risk of developing PD (Costa et al., 2010). Caffeine has therefore been shown to be neuroprotective in animal models of PD (Chen et al., 2001). Interestingly however this correlation is only noted in men, it being later confirmed that this is due

to the effect of oestrogen at inhibiting the neuroprotective effects of caffeine (Xu et al., 2006). Also of note, caffeine acts directly as an adenosine A_{2A} receptor antagonist, which has also been proposed as a potential non-dopaminergic treatment for PD itself (Armentero et al., 2011).

Lastly, inflammation is thought to play a significant role in PD pathogenesis, in particular the activation of the brain's innate immune cells, the microglia, inducing parenchymal release of numerous pro-inflammatory cytokines and cytotoxic factors contributing to neurodegeneration. Likewise it has been discovered that non-steroidal anti-inflammatory drugs (NSAIDs), principally ibuprofen, when taken two times per week, reduce the risk of development of PD by 45% (Chen et al., 2005a, Chen et al., 2003).

1.2.3 – Clinical Presentation

1.2.3.1 – Diagnosis

Following the Queens Square Brain Bank clinical criteria for the probable diagnosis of PD (figure 1.1) (Gibb and Lees, 1988), a patient suspected of having PD is primarily diagnosed with 'Parkinsonian syndrome', which is defined as displaying bradykinesia (slowness of initiation of voluntary movement with progressive reduction in speed and amplitude of repetitive action) co-presented with at least one of either muscle rigidity, 4-6 Hz rest tremor, or postural instability not caused by primary visual, vestibular, cerebellar, or proprioceptive dysfunction (Jankovic, 2008). Any disorder which results in striatal dopamine depletion or direct damage of the striatuim can result in Parkinsonism hence the second stage of PD diagnosis is to exclude other diseases associated with Parkinsonism, e.g. supernuclear palsy, multiple system atrophy and corticobasal degeneration. However, PD is the most common cause of Parkinsonism, constituting ~80% of cases (Hughes et al., 1992). Three or more of a list of 'supportive prospective positive criteria for PD' are then used to confirm the diagnosis of 'probably PD'. For example, unilateral onset, rest tremor present and the progressive nature of the disorder (figure 1.1) (Gibb and Lees, 1988). It is important to note here however that even after fulfilment of the diagnostic criteria, the patient is only diagnosed 'probable PD', confirmed diagnosis only able to be made post-mortem (Tolosa et al., 2006). In more recent years however, the advances in clinical imaging have enabled this diagnosis pathway to be supplemented with sensitive imaging protocols e.g. single photon emission computed tomography (SPECT) using the dopamine transporter ligand Ioflupane (^{123}I) (de la Fuente-Fernández, 2012), capable of differentiating PD from Parkinsonism syndrome adding confidence to the eventual clinical diagnosis.

Figure 1.1 – Queens Square Brain Bank clinical diagnostic criteria
Clinical criteria used in the UK for the diagnosis of probable PD (Gibb and Lees, 1988).

Step 1 ***Diagnosis of Parkinsonian syndrome***

- Bradykinesia (slowness of initiation of voluntary movement with progressive reduction in speed and amplitude of repetitive actions)
- And at least one of the following:
    - muscular rigidity
    - 4-6 Hz rest tremor
    - postural instability not caused by primary visual, vestibular, cerebellar, or proprioceptive dysfunction.

Step 2 ***Exclusion criteria for Parkinson's disease***

- History of repeated strokes with stepwise progression of parkinsonian features
- History of repeated head injury
- History of definite encephalitis
- Oculogyric crises
- Neuroleptic treatment at onset of symptoms
- More than one affected relative
- Sustained remission
- Strictly unilateral features after 3 years
- Supranuclear gaze palsy
- Cerebellar signs
- Early severe autonomic involvement
- Early severe dementia with disturbances of memory, language, and praxis
- Babinski sign
- Presence of cerebral tumour or communicating hydrocephalus on CT scan
- Negative response to large doses of levodopa (if malabsorption excluded)
- MPTP exposure

Step 3 ***Supportive prospective positive criteria for Parkinson's disease***
(Three or more required for diagnosis of probable Parkinson's disease)

- Unilateral onset
- Rest tremor present
- Progressive disorder
- Persistent asymmetry affecting side of onset most
- Excellent response (70-100%) to levodopa
- Severe levodopa-induced chorea
- Levodopa response for 5 years or more

1.2.3.2 – Motor Symptoms

PD presents clinically as a quartet of cardinal symptoms which can be identified with the acronym TRAP: *T*remor at rest, *R*igidity, *A*kinesia (or bradykinesia) and *P*ostural instability (Jankovic, 2008). Perhaps the most important of these, due to its relevance in diagnosis is akinesia (or bradykinesia). Literally meaning 'absence of movement', akinesia is slowness or lack of movement characteristic of PD. Bradykinesia is probably the more realistic description however given the presentation in PD, referring to the slowness of movement more commonly experienced by patients (Berardelli et al., 2001). Bradykinesia affects all voluntary and involuntary movement, encompassing difficulties with planning, initiating and executing movement (Berardelli et al., 2001). This initially manifests as slowness in performing everyday tasks and reduced reaction times however commonly secondarily manifests as loss of facial expression, impaired swallowing, decreased blinking and reduced arm swing whilst walking (Jankovic, 2008). Resting tremor is by far the symptom most synonymous with PD, presenting most predominantly in the extremities between frequencies of 4 to 6Hz (Jankovic, 2008). Parkinsonian tremor is often associated with a characteristic 'pill-rolling' motion in the thumb and fingertips which is suppressed during voluntary movement and during sleep (Jankovic, 2008). This symptom itself is not necessarily debilitating or disabling but can often cause psychological suffering due to the stigmatism associated with PD and the conspicuous nature of a resting tremor. Rigiditiy in the muscles is often one of the most frequent early manifestations of PD but it is often misdiagnosed as arthritis (Jankovic, 2008). In PD this often is accompanied by the 'cogwheel' phenomenon, in which circular jerking rigiditiy in flexion, extension and rotation about a joint are observed with a background of tremor, which continues throughout an entire movement (Jankovic, 2008). This increased resistance with movement can lead to pain whilst moving and hence can be become difficult to manage for patients. Postural instability is one of the later manifestations of PD, observed after the onset of most other clinical symptoms (Jankovic, 2008). It is detected clinical using the 'pull test', in which a patient is pulled quickly backwards or forwards by the shoulders: used to assess the degree of retropulsion or propulsion respectively. Taking more than two steps or the absence of any postural response is indicative of abnormal postural stability. In the elderly PD populations this is the most common cause of falls and risk of hip fractures (Williams et al., 2006).

1.2.3.3 – Non-Motor Symptoms

Non-motor symptoms of PD are generally associated with the advanced stages of the disease, however some of the non-motor symptoms, e.g. olfactory disturbances, constipation and depression can often occur earlier in the disease (Chaudhuri et al., 2006). The non-motor symptoms associated with PD are wide-ranging, and the occurrence and combination of non-motor symptoms experienced by individual PD sufferers vary greatly. The symptoms which are currently well know

can be categorised into five main groups: neuropsychiatric, sleep disorders, autonomic, sensory, and other (table 1.1) (Chaudhuri et al., 2006). The neuroanatomical and neurochemical substrates for most of these symptoms are starting to become better understood, however the pathophysiology associated with many of these symptoms still remains elusive.

1.2.4 – Neuropathology

The cardinal clinical symptoms of PD (tremor, rigidity, akinesia and postural instability) are generally accepted to be the result of neurodegeneration of dopaminergic nigrostriatal pathways within the central nervous system of sufferers (Dexter and Jenner, 2013). Degeneration is most notable within neuromelanine positive neurons in the Substantia Nigra pars compacta (SNpc), the mescencephalic brain nucleus responsible for the synthesis of the neurotransmitter, dopamine, hence production of the classic gross neuropathological finding of SNpc depigmentation (figure 1.2). Dopaminergic pathways project from the SNpc to the striatum, the subcortical brain nucleus composed of the caudate and putamen, responsible for the planning and modulation of movement. Therefore degeneration of these pathways in PD leads to loss of striatal dopamine and the clinical presentation of disrupted movement and motor based symptoms. At the onset of neurodegeneration, movement symptoms do not typically appear due to the existence of compensatory mechanisms of dopaminergic neurons, i.e. increased dopamine release, upregulation of dopaminergic receptors and reduced reuptake of dopamine by adjacent neurons. Therefore by the onset of movement based symptoms, it is known that 60-70% of neurons in the SNpc have already degenerated, and ~80% of striatal dopamine has been depleted (Riederer and Wuketich, 1976).

The neuropathological hallmark of degenerating neurons in the PD are concentric hyaline intracytoplasmic inclusions composed predominatly of a synaptic protein called αSyn (Spillantini et al., 1997). These ubiquitinated aggregates form intraneuronal structures known as Lewy bodies and dystrophic neurites known at Lewy neurites, which cause numerous detrimental consequences for their inhabiting cells (section 1.2.5). Lewy body like inclusions have also been shown to be present in glial cells in the midbrain of PD patients (Mochizuki et al., 2002), indicative of microglial phagocytosis of affected neurons (Fellner and Stefanova, 2013). In PD however these microglial inclusions are distinctly different from those found in other neurodegenerative disorders, such as in multiple system atrophy which is characterised by cytoplasmic microglial inclusions (Fellner and Stefanova, 2013). The cellular consequences of αSyn accumulation in Lewy formations are yet to be fully elucidated, however associated events in neurons such as oxidative stress, mitochondrial dysfunction, altered proteolysis, inflammation and excitotoxicity are thought to lead rapidly to neuronal death (Lee and Trojanowski, 2006a).

Table 1.1 – Non-Motor Symptoms of Parkinson's Disease
Range of non-motor symptoms associated with the development and progression of PD. Symptoms known to be (partly) treatable with existing dopaminergic therapies used for the treatment of motor symptoms shown in italics (Chaudhuri and Schapira, 2009).

Neuropsychiatric	**Sleep disorders**	**Autonomic**	**Sensory**	**Other**
Depression, apathy, anxiety	*Restless legs and periodic limb movements*	*Bladder disturbances*	*Pain*	*Non-motor fluctuations*
Anhedonia	*REM behaviour disorder*	Sweating	Paraesthesia	*Fatigue*
Cognitive dysfunction	REM loss of atonia	*Erectile impotence*	Olfactory disturbances	Weight loss/gain
Attention deficits	Non-REM sleep-related movement disorders	Gastrointestinal symptoms	Visual dysfunction	
Dementia	Excessive daytime somnolence	*Dribbling of saliva*		
Confusion	Vivid dreaming	Reflux, vomiting		
Panic Attacks	Insomnia	Nausea		
Attention deficit	*Sleep-disordered breathing*	*Constipation*		

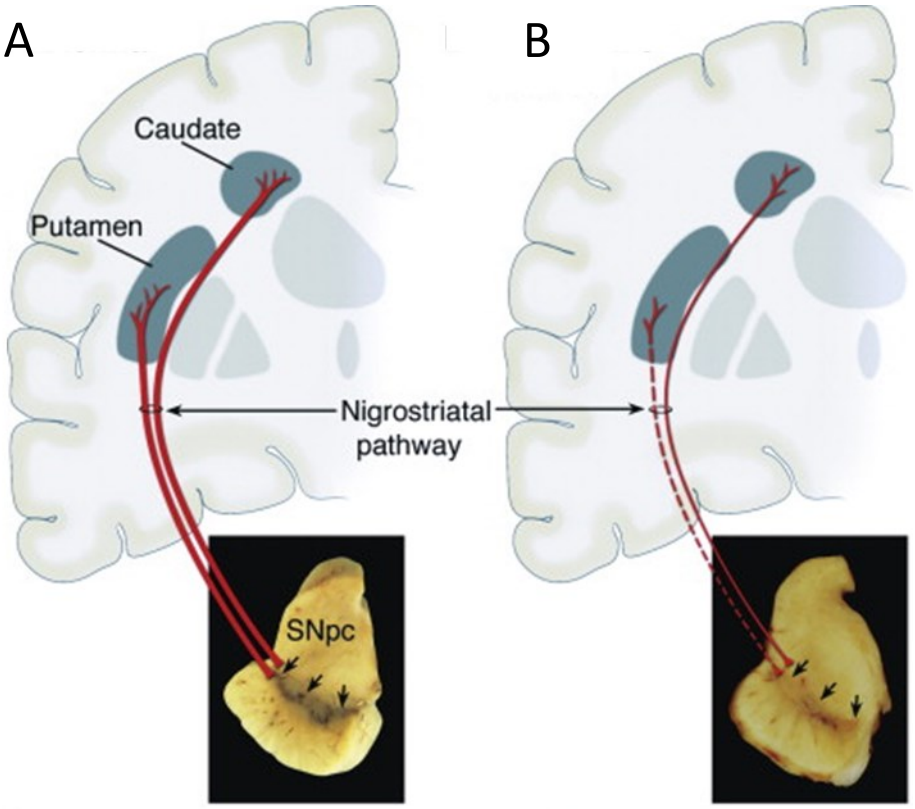

Figure 1.2 – Degeneration of Nigrostriatal Pathways in PD
Cartoon and cross section of dopaminergic projections from the SNpc to the striatum (composed of the caudate and putamen) of (A) normal subjects and (B) PD patients (adapted from Dauer and Przedborski, 2003).

Although neurodegeneration in PD is often thought to be confined to the SNpc and related dopaminergic nuclei, it is now well known that Lewy body pathology and αSyn deposition extends well beyond the dopaminergic centres: into noradrenergic, serotinergic, γ-amino butyric acid (GABA)-ergic and cholinergic neurotransmitter systems (Lim et al., 2009) located in the locus coeruleus, reticular formation of the brain stem, raphe nucleus, dorsal motor nucleus of the vagus, basal nucleus of Meynert, amygdala, and hippocampus etc., suggesting a common pathogenic process with the SNpc (Dexter and Jenner, 2013). In 2003, Braak and colleagues proposed that αSyn deposition begins in the dorsal motor nucleus of vagus (stage 1), from where they suggested it spreads upwards via the pons (stage 2) to the midbrain (stage 3), to the basal prosencephalon and mesocortex (stage 4) and onto the neocortex (figure 1.3) (Braak et al., 2003). The initial Braak stages (1-2) are therefore pre-motor symptom development: these symptoms only becoming evident from stage 3-4 onwards due to excessive dopaminergic degeneration in the midbrain. Although it has been noted that not all cases of PD strictly follow this staging system (Kalaitzakis et al., 2008), this progressive nature of αSyn pathology may well provide explanation for the progressing symptomology associated with PD development. For example, early αSyn pathology in the olfactory bulb leading to the olfactory disturbances experienced by patients prior to the motor based symptoms as a result of pathology within the midbrain and SNpc. Pathology then spreading in a rostral direction causing the development of dementia and neuropsychiatric symptoms synonymous with late stage PD.

1.2.5 – Pharmacotherapy and Current Approaches to Treatment

PD is characterised by degeneration of the dopaminergic nigrostriatal pathways, hence the primary route of pharmacotherapy lies in dopaminergic replacement strategies. Due to the inability of dopamine to cross the blood brain barrier (BBB), its synthetic precursor, L-3,4-dihydroxyphenylalanine (L-DOPA) is given orally which crosses the BBB with ease and is converted in the brain to dopamine via the enzyme DOPA decarboxylase (Whitfield et al., 2014, Poewe et al., 2010). L-DOPA administration therefore increases the concentration of this important neurotransmitter for nigrostriatal signalling and hence transiently alleviates the motor based symptoms of PD. L-DOPA however is also converted to dopamine in the peripheral as well as the central nervous system. This can result in peripheral hyperdopaminergia and hence it is now standard clinical practice to administer L-DOPA with a peripheral DOPA decarboxylase inhibitor (i.e. carbidopa) enabling L-DOPA to cross the BBB intact (Whitfield et al., 2014). For 40 years L-DOPA has very much become the ‘gold standard’ for the treatment of PD however in the majority of cases long

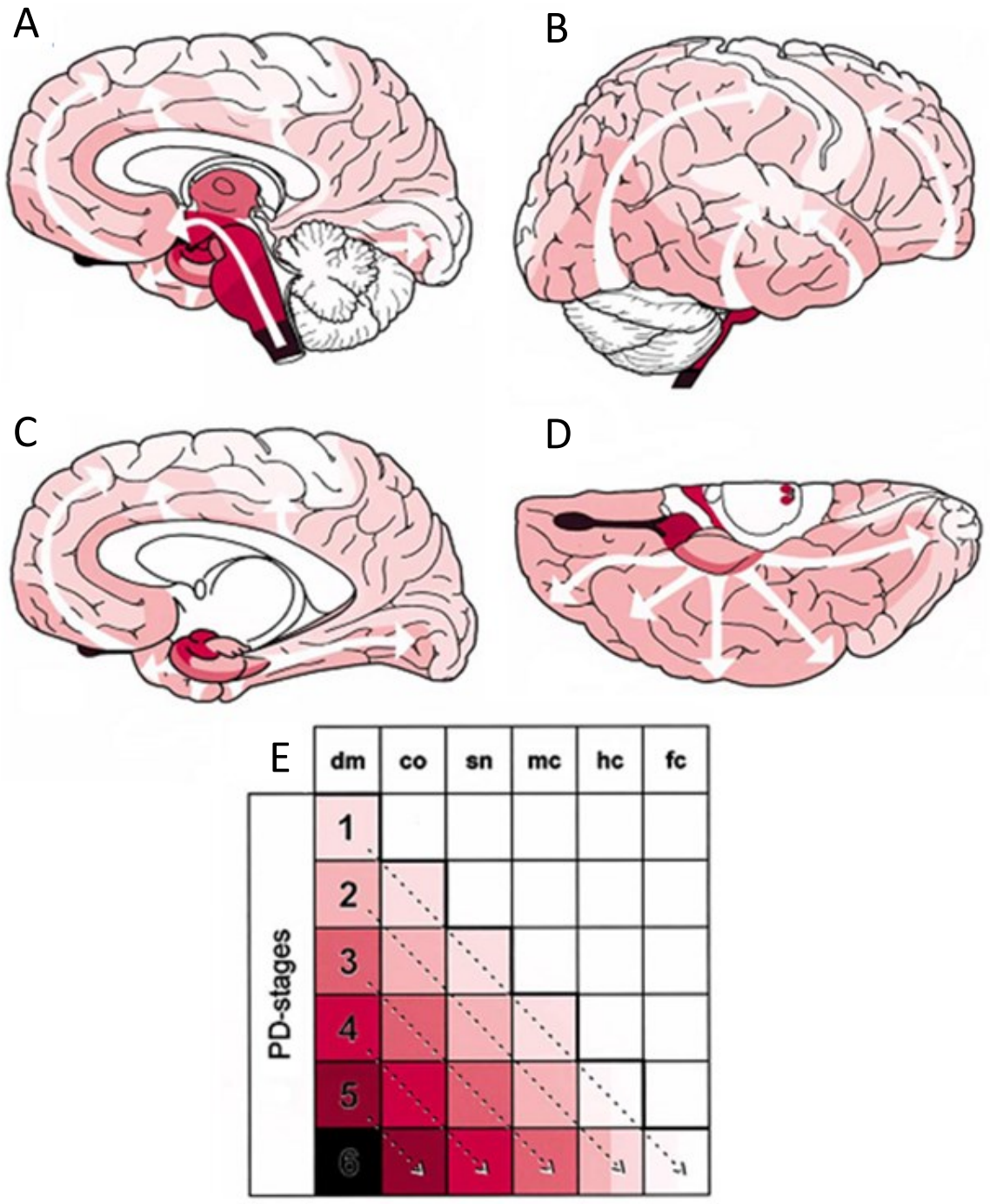

Figure 1.3 – Braak's Staging of αSyn Pathology in Sporadic PD
Ascending course of αSyn pathology within the brain during PD progression. The darker the shade of pink, the more pronounced the αSyn pathology is in the area. (A-D) Various views of the brain. (E) Topographic expansion of αSyn progression from left to right, and growing severity from top to bottom. Abbreviations: co, coeruleus–subcoeruleus complex; dm, dorsal motor nucleus of the glossopharyngeal and vagal nerves; fc, first order sensory association areas, premotor areas, as well as primary sensory and motor fields; hc, high order sensory association areas and prefrontal fields; mc, temporal mesocortex; sn, substantia nigra (adapted from Braak et al., 2003).

term use leads to the development of well characterised 'L-DOPA induced dyskinesia'. L-DOPA is therefore often combined with other drugs acting on the dopaminergic system, lowering the effective dose and limiting the development of drug induced dyskinesia (Buck and Ferger, 2010, Poewe et al., 2010). For example, synaptic dopamine can be increased with the use of drugs such as amantadine, which increases pre-synaptic release of dopamine. Similarly, synaptic dopamine can also be increased with the use of inhibitors of dopamine degradation enzymes, e.g. catecholamine-o-methyl transferase (COMT) inhibitors such as tolcapone and entacapone, and monoamine oxidase (MAO) inhibitors such as selegline and rasagiline. Direct dopaminergic receptor agonism is often also used, through administration of drugs such as apomorphine, pergolide, pramipexole and ropinirole (figure 1.4) (Poewe et al., 2010, Buck and Ferger, 2010). These drugs only correct the deficit in dopamine however and such do not return patients to full normal function.

Recent advances in deep brain stimulation have led to even greater use of surgical treatment of PD patients, in direct electrical stimulation of areas such as the Subthalamic nucleus and the Globus Pallidus interna (Foltynie and Hariz, 2010). Stimulation of such brain nuclei have been proven to benefit resting and postural tremor, truncal and limb rigidity, and limb or axial bradykinesia, as well as improvements in the severity and frequency of fluctuations and dyskinesias (Krack et al., 1997). This plethora of therapeutic options available for the treatment of PD has therefore revolutionised its management, allowing for therapeutic control of many motor symptoms. However, none of these drugs provide long term protection against continual dopaminergic neuronal cell death. Additionally, these drugs have very little effect on non-motor symptoms (table 1.1) which are the main determinants for deteriorating quality of life and patient care costs, hence more novel neuroprotectant agents are sought.

1.2.6 – Mechanisms of Neurodegeneration

The deposition of insoluble misfolded protein, be it nuclear, cytoplasmic or extracellular is a feature of numerous neurodegenerative diseases (Soto, 2003). This common feature suggests that protein deposition is in some way neurotoxic. There are numerous mechanisms by which this neurotoxicity could occur, many of which are known to contribute to the neurotoxic effects of αSyn aggregates in PD. However, these pathogenic factors are by no means mutually exclusive, quite the contrary. In fact many of the factors thought to contribute to neurodegeneration in PD interact with one another, adding multiple layers of complexity to the pathogenesis of the disease (figure 1.5).

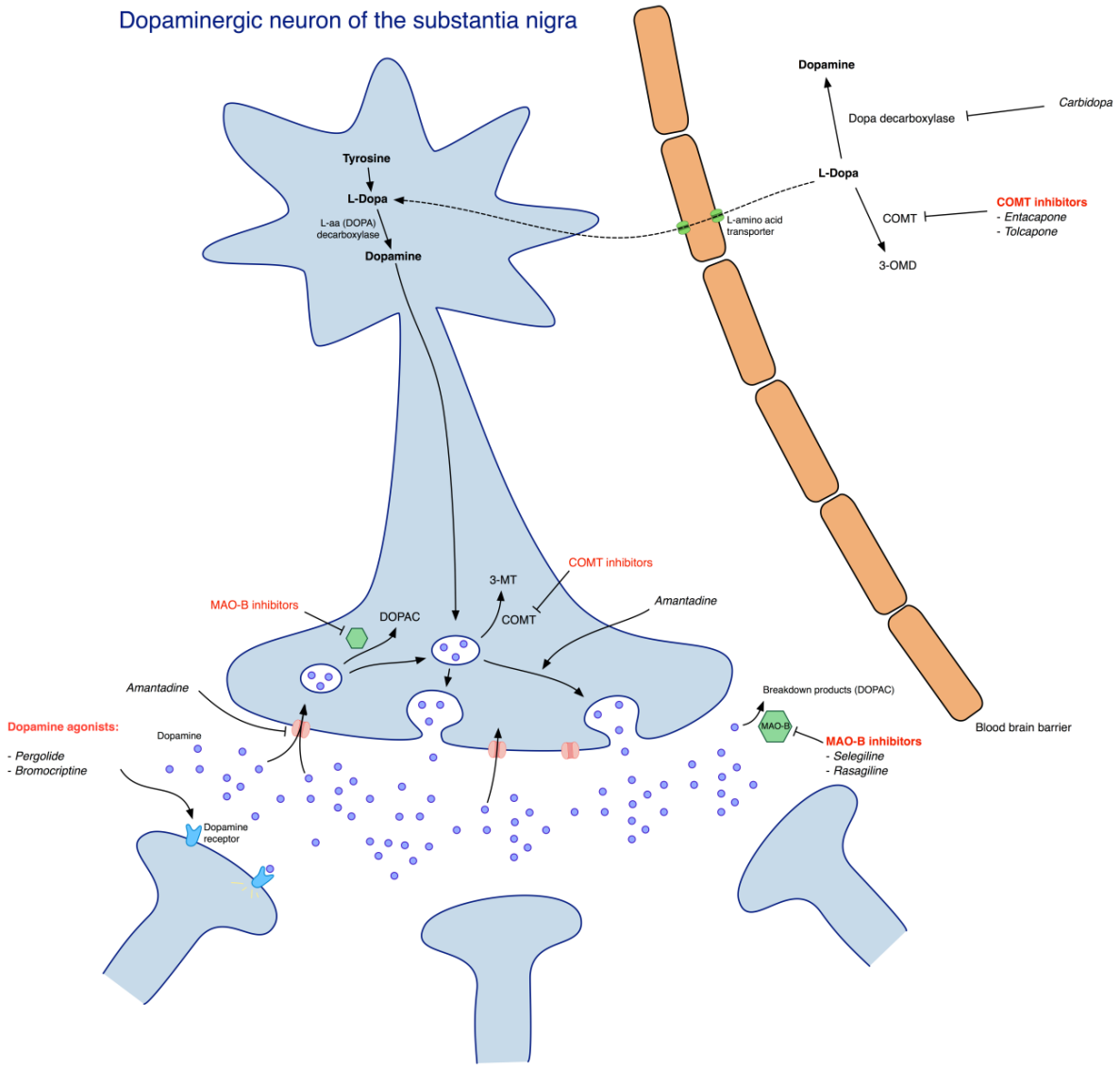

Figure 1.4 – Dopaminergic Therapeutic Strategies for Parkinson's Disease
Various therapeutic points of intervention shown in red, leading to increased dopamine content for signalling in the degenerating SNpc (adapted from Rang et al., 2007).

1.2.6.1 – Mitochondrial Dysfunction and Oxidative Stress

Evidence for the involvement of mitochondrial dysfunction and oxidative stress in the pathogenesis of PD came from the discovery of MPTP (section 1.2.2.3). MPTP causes selective dopaminergic neurodegeneration following its inhibition of mitochondrial complex 1 and blockade of the electron transport chain, resulting in energy starvation and the production of cytotoxic reactive oxygen species (ROS) and oxidative stress (Przedborski et al., 2000). Furthermore two genes associated with fPD are mitochondrial in nature: PINK1 and DJ-1, adding weight to the involvement of mitochondria in Parkinsonian neurodegeneration (Cookson, 2010a). Dopaminergic neurons themselves are particularly susceptible to oxidative stress, given the presence of ROS generating enzymes such as monoamine oxidase in this cell type, and the ability of dopamine to autooxidise. ROS themselves are very difficult to detect, however markers of oxidative stress have been extensively shown in the SNpc in PD, e.g. lipid peroxidation, and protein and DNA oxidation (Yoritaka et al., 1996, Dexter et al., 1989a, Zhang et al., 1999, Alam et al., 1997). In PD it is therefore thought that αSyn aggregates impact on mitochondrial function, for example it has been observed that transgenic mice overexpressing αSyn treated with MPTP exhibit significantly more mitochondrial abnormalities than saline or wild type mice treated with MPTP (Song et al., 2004). Moreover mutant αSyn has been previously shown to localise at the mitochondrial membrane leading to dysfunction and oxidative stress (Parihar et al., 2008). Likewise, oxidative stress leads to oxidation of iron species within degenerating dopaminergic neurons, leading to exacerbation of αSyn accumulation (Levin et al., 2011).

1.2.6.2 – Altered Proteolysis

The extensive accumulation of misfolded protein in PD, predominantly αSyn, coupled with its minimal clearing, led to investigation of the function of the ubiquitin proteasome system (UPS) in the disease. Additionally, two mutations associated with fPD take place in the genes of UPS elements: *PARK2* (parkin) and *UCH-L1*. Investigation of the function of the UPS in PD led to the discovery that there are specific alterations in catalytic activity of UPS elements in the SNpc in PD (McNaught and Jenner, 2001, Tofaris et al., 2001, McNaught et al., 2002a). Furthermore, administration of UPS inhibitors such as proteasome inhibitor 1 (PSI) to cell culture systems and directly into animal brains, led to degeneration of dopaminergic neurons (McNaught et al., 2002b, McNaught et al., 2002c). Additionally, it was observed that UPS inhibition in cell culture led to a cascade of events including both mitochondrial dysfunction as well as oxidative stress (Hyun et al., 2003). UPS inhibition therefore presents a pivotal mechanism of cell death in PD, capable of exacerbating other known factors in neuronal demise in the disease.

1.2.6.3 – Inflammation

The suggestion that inflammation may also contribute to neuronal cell death in PD came from the discovery that activated microglia are present in the SNpc of PD patients (McGeer et al., 1988). Upon activation, microglia upregulate their expression and secretion of inflammatory cytokines such as interleukin 1-β (IL-1β), IL-6 and tumour necrosis factor-α (TNFα) as well as activation inducible nitric oxide synthase (iNOS) resulting in production of nitric oxide (NO) and nitrative stress by microglial cells. Correspondingly each of these changes were shown to be present in PD brains (Hirsch et al., 2003). Pro-inflammatory cytokines such as these initiate and amplify the immune response of microglia and in concert with iNOS exert neurotoxicity (Stoll et al., 2000). Likewise, lipopolysaccharide (LPS), a potent inducer of microglia has been shown to initiate selective dopaminergic neurodegeneration when acutely injected into the SNpc in rats (Herrera et al., 2000).

1.2.6.4 – Excitotoxicity

Because of the circular nature of signalling within the basal ganglia, neurodegeneration within the SNpc leads to increased glutamatergic firing in the Subthalamic Nucleus (Rodriguez et al., 1998). It is thought that this over activation leads to excitotoxic damage of target structures, such as the Globus Palidus interna, Substantia Nigra pars reticulata, Pedunculopontine Nucleus, and most importantly the SNpc. Activation of glutamatergic receptors on nigral dopaminergic neurons leads to release of intracellular calcium, which in turn is thought to mediate excitotoxic cell death through a number of pathways (Marambaud et al., 2009). For example, intracellular calcium activates calcium dependent proteases and lipases which damage critical structural proteins and lipid membranes. Similarly, increased cytoplasmic calcium can lead to activation of iNOS and mitochondrial damage leading to production of ROS and oxidative stress leading to neurodegeneration (section 1.2.6.1).

1.2.7 – Modelling Parkinson's Disease in Animals

As has been described above, a number of the mechanistic studies seeking to understand the neurodegeneration associated with PD have utilised toxins known to induce Parkinsonian pathology in humans, e.g. MPTP. Additionally, others have used genetic aspects of the disease: genes known to be associated with fPD to model differing aspects of Parkinsonian neurodegeneration, i.e. αSyn accumulation. From these studies it is becoming increasingly clear that neurodegeneration in PD is a hugely complex affair with multifactorial origins. Taken together, it is apparent that clues from human post-mortem tissue, epidemiological studies and cell culture systems can go some way to investigating the roots and causes of the disease, however animal models are vital in aiding more complex investigations of disease pathogenesis. Likewise, animal models are pivotal in testing the efficacy of disease modifying agents against the progressing pathology associated with PD.

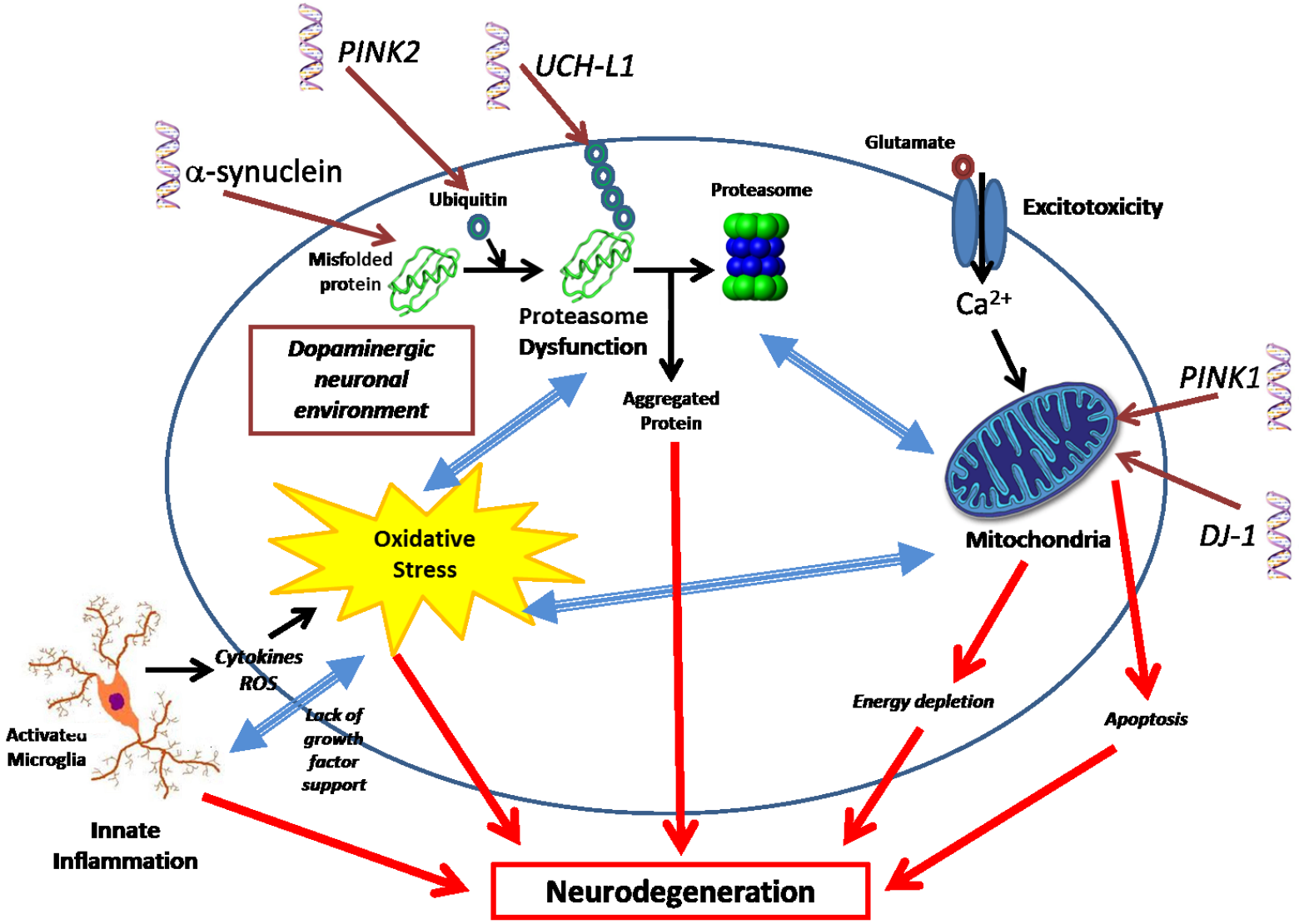

Figure 1.5 – Mechanisms of Neurodegeneration in Parkinson's Disease

Key molecular mechanisms which contribute to neurodegeneration of dopaminergic neurons in the SNpc in PD. Blue arrows interactions between the molecular mechanism associated with neurodegeneration. Double helix structures indicate common gene mutations found in fPD. Abbreviations: ROS, reactive oxygen species (adapted from Dexter and Jenner, 2013).

The ‘holy grail’ in PD research would be an animal model which recapitulates the sporadic and progressive nature of the disease, mirroring the complex anatomical spread of an even more complex mechanism of neurodegeneration throughout the brain, all the while modelling motor and non-motor symptoms of the disease. To date, no such model exists. That being said, numerous animal models are now used in PD research which model a wide range of the spontaneous, progressive, mechanistic and symptomatic aspects of the disease using both genetic and toxin based approaches.

1.2.7.1 - Gene Based Models

It may seem counter intuitive to study rare genetic forms of a common sporadic disease, however it is expected that there is a phenotypic similarity between the genetic and sporadic forms of the disease, them sharing pathogenic mechanisms. Overexpression of either wild-type or mutant αSyn in drosophila leads to αSyn positive inclusions and loss of dopaminergic neurons as well as motor behavioural changes (Feany and Bender, 2000). Most importantly these behavioural changes are alleviated upon treatment with dopaminergic therapeutics (section 1.2.5) known to address motor symptoms in human PD (Pendleton et al., 2002). The A53T mutation of the *SNCA* gene in mice has been shown to produce αSyn positive Lewy body like inclusions in addition to neuropathological changes such as neuronal atrophy, dystrophic neurites and astrocytosis with a severe motor phenotype (Giasson et al., 2002, Matsuoka et al., 2001, Lee et al., 2002). These animals however are void of nigral pathology questioning their relevance as a model of PD itself. Similarly there are mixed results using viral vector approaches to overexpress human αSyn in the SNpc of rats: αSyn accumulation being consistently demonstrated however whether this results in cell loss in the SNpc continues to be debated (Lo Bianco et al., 2002, Kirik et al., 2002). More recent studies using different viral vector strategies and injection of αSyn fibrils to induce αSyn pathology have shown encouraging results however, demonstrating nigrostriatal neurodegeneration, dopamine depletion and a motor behavioural phenotype in experimental animals (Luk et al., 2012, Oliveras-Salva et al., 2013). These studies were published post-initiation of the studies presented here; however they represent an exciting development in the field of PD animal modelling. Mixed results have also been seen in animals using overexpression of parkin, DJ-1, PINK1 and LRRK2: changes in striatal function, altered morphology of dopaminergic neurons, changes in other monoaminergic systems, inflammatory change all being observed yet animals lacking dopaminergic neurodegeneration (Goldberg et al., 2003, Chen et al., 2005b, Kitada et al., 2007, Li et al., 2009). Despite the lack of dopaminergic neurodegeneration in these models there is still value in them, allowing for investigation of the effects of mutations associated with fPD.

1.2.7.2 - Toxin Based Models

Toxin based models on the other hand are designed such that toxins are used which specifically result in dopaminergic neuronal degeneration, providing a more relevant platform on which to test the efficacy of novel neuroprotective therapies. Additionally, because of specific dopaminergic neurodegeneration, animals exhibit motor specific symptoms quantifiable through a number of behavioural test paradigms. The difficulty with using such toxins however is that many of them require direct intracerebral administration into either the SNpc, striatum or medial forebrain bundle (MFB) to cause localised Parkinsonian degeneration. High concentrations of toxins are required to cause dopaminergic degeneration and behavioural consequences making control of neuronal exposure and time course of pathology difficult to control. Similarly, a limitation of such models lies in the fact that toxin administration is often acute, animals by no means model the progressive nature of the disorder unlike gene based approaches. That being said, a number of toxins allow chronic treatment and neuropathological development, i.e. administered peripherally via osmotic mini-pump, or administration into areas such as the striatum which cause a more gradual profile of degeneration.

Based mainly on epidemiological findings of environmental factors known to induce dopaminergic neurodegeneration (section 1.2.2.3), and the pathways associated with neurodegeneration in PD (section 1.2.5) numerous toxins are used to induce Parkinsonian neurodegeneration *in vivo* (table 1.2). For example toxins which induce oxidative stress (6-hydroxydopmine (6-OHDA) and paraquat), nitrative stress and neuroinflammation (LPS), mitochondrial dysfunction (rotenone, MPTP and MPP+), excitotoxicity (glutamate, quinolinic and ibotinic acid), proteasomal dysfunction (PSI, epoximycin, lactacystin) are used to induce dopaminergic neurodegeneration *in vivo* and produce animal models of PD (Dexter and Jenner, 2013). Based on their mechanism of action, differing sites of administration are required. For example environmental toxins such as MPTP and rotenone can be given peripherally because of their ability to cross the BBB and cause SNpc dopaminergic neurodegeneration. However, due to their poor BBB penetrance, toxins such as 6-OHDA need to be administered at their site of action to cause oxidative stress responsible for initiating cell death within the area. Similarly, the speed of neurodegeneration associated with administration of an intracerebral toxin depends greatly on its site of injection (Jonsson, 1983). Injections in the MFB for example induce a fast lesion: pathological effects of the toxin spreading both rostrally to the striatum and caudally to the SNpc simultaneously. A slower development of pathology would be induced as a result of toxin administration to the SNpc, whereby it takes some time for dopaminergic terminals within the striatum to become dysfunctional. Similarly, an even more gradual development of degeneration would occur when

toxins are administered to the striatum due to the retrograde degeneration of dopaminergic neurons. It is of note however that the several of these toxin based models fail to mirror one of the principle pathological features of PD, that being altered protein accumulation, apart from the proteasome inhibitors.

Table 1.2 – Toxins Used to Model Parkinson's Disease
Toxins used to model PD in vivo based on modelling elements of pathology associated with the disease, and the sites/routes of administration. *remains debated Abbreviations: LPS, lipopolysaccharide; 6-OHDA, 6-hydroxydopamine; MFB, medial forebrain bundle; SNpc, Substantia Nigra pars compacta; MPTP, 1-methyl-4-phenyl-1,2,3,6-tetrahydropyridine; MPP+, 1-methyl-4-phenylpyridinium, PSI, proteasome inhibitor 1 (adapted from Dexter and Jenner, 2013).

Pathology Modelled	Toxin(s)	Site(s) of Administration
Oxidative Stress	6-OHDA	SNpc, MFB, striatum
	Paraquat	Peripherally
Nitrative Stress	LPS	SNpc, striatum, peripherally
Mitochondrial Dysfunction	Rotenone	Peripherally
	MPTP and MPP+	Peripherally
Excitotoxicity	Quinolinic acid	SNpc and striatum
	Ibotinic acid	SNpc and striatum
	Glutamate	SNpc and striatum
Proteasomal Dysfunction	PSI	SNpc and peripherally*
	Epoximycin	SNpc and peripherally*
	Lactacystin	SNpc and peripherally*
Glial Cell Activation	LPS	SNpc, striatum, peripherally

1.3 – Epigenetic Regulation of Gene Expression

All cells inherit the same genetic material and code. However, the regulation of these genes which enables cells to retain their unique physical and biological phenotype in line with the specific tissue or organ to which they reside varies from cell to cell. This collection of regulatory mechanisms is hence named the epigenome (literally meaning 'above the genome'): the combination of DNA and histone post-translational modifications and related interacting proteins that together package the genome and help define the transcriptional programme of a given cell (Arrowsmith et al., 2012, Bernstein et al., 2007). Dynamic changes in epigenetic regulation therefore underlie the physiological basis of cell function and crucially enable its malleability in response to environment (Meaney, 2010). Likewise by extension, perturbations of these epigenetic mechanisms are now known to play a pivotal role in a number of disease states, from cancer to metabolic disease and from neuropsychiatric to neurodegenerative disorders (Portela and Esteller, 2010).

To enable the highly compact packaging of the eukaryotic genome, DNA is tightly coiled around histone proteins forming nucleosome structures which make up chromatin (figure 1.6). Electrostatic interactions between the negatively charged DNA and positively charged octamers of four highly basic histone proteins (H3, H4, H2A and H2B) as well as a linker histone (H1) enable this wrapping. Each 147 base pairs of DNA are tightly coiled around each histone octamer. However, in order for promoter and transcriptional factors to have access to the DNA, its packaging needs to be highly dynamic and changeable. Hence, molecular masking and unveiling of promoter sequences along with local interactions between histone molecules with one another and with their surrounding DNA enables the changeability in chromatin structure vital for transcriptional activation and repression. A large number of molecular mechanisms contribute to this epigenetic regulation of genes. In order for us to understand how any of these mechanisms can be advantageously manipulated for the treatment of PD, we must first understand the relevance of their dysregulation in PD and the physiological impact their manipulation has upon disease state. Below, the two most abundant and important mechanisms will be introduced and a brief explanation of how they are thought to be relevant in PD.

1.3.1 – DNA Methylation

The brain as an organ displays the highest level of DNA methylation in the body, however this equates to just ~1% of nucleic acid bases being methylated (Ehrlich et al., 1982). DNA methylation, unlike histone post-translational modification, is less transiently dynamic, playing a vital role in longer term repression of gene expression (Miranda and Jones, 2007, Moore et al., 2012, Rottach et al., 2009). The covalent methylation of the 5' position of cytosine residues in CpG dinucleotides in

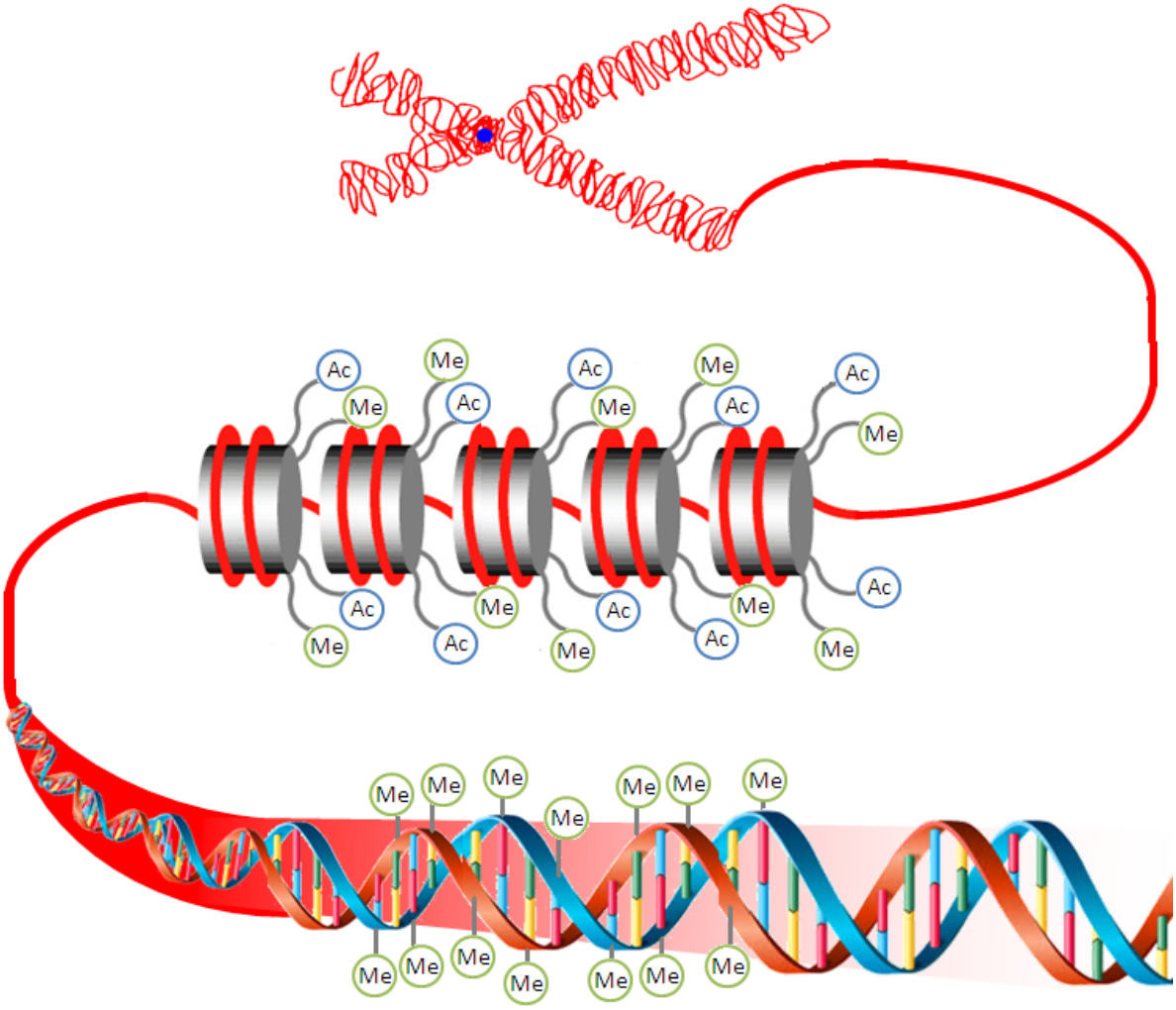

Figure 1.6 – Packaging of DNA into Chromatin and the Epigenome
DNA is tightly coiled around cores of eight histone proteins to form nucleosomes. Post-translational modification sof these histone proteins (acetylation and methylation, amongst others) as well as direct modification of DNA (methylation) help control the compression of this structure and enable transcriptional factor access to DNA. Abbreviations: Ac, acetyl; Me, methyl (reproduced with permission from Harrison and Dexter, 2013).

the DNA sequence is catalysed by DNA methyltranferases (DNMTs) (Miranda and Jones, 2007, Rottach et al., 2009). There are three DNMTs known to be active in mammals: DNMT1, the maintenance DNMT which maintains the methylation pattern of CpG sites which have been previously established by DNMT3a and DNMT3b, the *de novo* DNMTs, which are active mainly during development (Miranda and Jones, 2007, Rottach et al., 2009). The main methyl (CH_3) donor for DNMT mediated methylation is S-adenosyl-methionine (SAM), a compound which results from one-carbon metabolism of numerous B vitamins, such as folic acid, B6 and B12 (Miranda and Jones, 2007, Rottach et al., 2009). Therefore, the potential of CpG methylation is partially dependent on the ratio between SAM and its unmethylated counterpart: S-adenosyl-homocysteine (SAH). The large majority of CpG dinucelotides in the mammalian genome are richly methylated resulting in gene repression through both physical blocking of DNA to transcription factors (Miranda and Jones, 2007, Rottach et al., 2009) and via recruitment of methyl binding proteins such as methyl-CpG binding protein 2 (MeCP2), which further exacerbate this blockade and are thus associated with gene silencing (Fuks, 2005, Fuks et al., 2003).

In sporadic PD patients, it has been noted that there is impaired one-carbon metabolism in areas such as the SNpc, putamen and cortex: reducing DNA methylation of intron 1 of the αSyn gene, *SNCA*, linking DNA demethylation to αSyn expression (Jowaed et al., 2010). Furthermore, demethylation of a CpG rich island in *SNCA* was identified in PD patients (Matsumoto et al., 2010). It was shown using cell culture that demethylation of this region of the SNCA gene resulted in increased expression of αSyn (Matsumoto et al., 2010). Similarly, a recent collaborative project identified methylation and expression changes in a further three PD risk gene variants (*PARK16/1q32, GPNMB and STX1B*) in PD patients, indicating that *SNCA* is not the only hypomethylated gene subjected to altered epigenetic regulation in PD (IPDGC and WTCCC, 2011). Lastly, for obvious reasons, the maintenance DNMT, DNMT1, is most abundantly located in the nuclear compartment. However, it was discovered recently that there is a reduction in nuclear DNMT1, combined with a translation to the cytoplasm, in post-mortem PD brains as well as in the brains of αSyn transgenic mice (Desplats et al., 2011). This sequestration of DNMT1 to the cytoplasm was shown to result in global DNA hypomethylation in both human and transgenic αSyn mice brains, including CpG islands in the *SNCA* gene (Desplats et al., 2011). These effects were partially reversed in cell culture and transgenic animal experiments by overexpressing DNMT1, indicating that αSyn might mediate aberrant subcellular localisation of DNMT1 in PD (Desplats et al., 2011).

1.3.2 - Post-Translational Histone Modifications

As well as direct methylation of promoter sequences, gene expression profiles are also modulated by the extent of chromatin packaging, which determines how accessible the genome is to transcriptional factors. Appropriately, chromatin can be condensed, hence becoming transcriptionally inactive (heterochromatin) or relaxed, becoming transcriptionally active (euchromatin). This process of condensing and relaxing the genome is controlled principally through histone post-translational modification (Maze et al., 2012). Histones are subjected to a number of covalent modifications including but not limited to phosphorylation, ubiquitination, sumoylation, acetylation and methylation (Maze et al., 2012). In fact, proteins recruited to the sites of CpG methylation induce gene silencing not only through blockade of DNA but also through recruitment of histone modifying enzymes such as histone methyl transferases and histone deacetylases (Fuks, 2005, Fuks et al., 2003). This crosstalk between the epigenetic mechanisms is only just beginning to be understood (Fuks, 2005).

1.3.2.1 - Histone Methylation/Demethylation

First described in 1964 (Allfrey et al.), histone methylation is a dynamic process which involves the methylation of either arginine or lysine residues on the N-terminal tails of either H3 or H4 histone proteins to bring about a transcriptional change (Kouzarides, 2007). This methylation itself is facilitated, on arginine residues, by arginine specific histone methyltransferases (HMTs) and accordingly on lysine residues by lysine specific HMTs (Habibi et al., 2011). As is the case with DMNTs and DNA methylation, both arginine and lysine specific HMTs use SAM as a cofactor and methyl donor (Arrowsmith et al., 2012). Correspondingly, this methyl group is then returned to SAH after cleavage from either the histone lysine or arginine residue by histone demethylases (HDMs): either the Jumonji C family of 2-oxoglutarate-dependent demethylases (Tsukada et al., 2006), or the flavin-dependent enzymes lysine-specific histone demethylase 1 (LSD1) and LSD2 (Shi et al., 2004).

To add further complexity, multiple methylation valences of lysine and arginine residues on histone proteins H3 and H4 are also possible: lysine residues can be either monomethylated, dimethylated or trimethylated and similarly arginine residues can be either monomethylated or dimethylated (Habibi et al., 2011). In addition, arginine residues can be methylated either symmetrically or asymmetrically, an intricacy which has been shown to be associated with differing functional consequences (Habibi et al., 2011). Accordingly, methylation does not affect the structure of chromatin directly as the addition of a methyl group does not change the charge of the lysine or arginine residue. Instead, the methylated sites act as recognition sites for other proteins that either aid condensation of chromatin or recruit other transcriptionally regulating proteins (Arrowsmith et al., 2012). The functional effect of histone methylation on transcriptional activation is therefore

dependent on the site of the residue within the histone tail and the degree to which it is methylated (Kouzarides, 2007). For example, both positive transcriptional methylation marks (histone protein H3 lysine 4 (H3-Lys4), H3-Lys36, H3-Lys79; H3-Arg2, H3-Arg17, H3-Arg26 and H4-Arg3) and negative transcriptional methylation marks (H3-Lys9, H3-Lys7, H3-Lys36, and H4-Lys20; H4-Arg8 and H4-Arg3) exist (Habibi et al., 2011, Maze et al., 2012).

In 2008, Nicholas and colleagues measured the level of the positive histone methylation mark H3-Lys4-me3 in striatal neurons (Nicholas et al., 2008). It was shown in both the murine and primate MPTP models of PD that a reduction of this methylation mark was associated with a depletion of dopamine in these neurons (Nicholas et al., 2008). Moreover, the active site structure of MAO-A and B has significant sequence homology to LSD1 (Shi et al., 2004). Therefore, it has been shown that the classical MAO inhibitor tranylcypromine inhibits demethylation by LSD1 (Lee and Trojanowski, 2006b, Mimasu et al., 2008, Schmidt and McCafferty, 2007). This was accompanied by a global increase in H3-Lys4-me2 in the P19 embryonic carcinoma cell line (Lee et al., 2006, Schmidt and McCafferty, 2007). This has great implications in PD in that the treatment of patients with MAO inhibitors such as Selegiline and Rasagaline could contribute to the rectification of the reduced H3-Lys4 methylation levels previously described in PD models by Nicholas and colleagues (2008). Nevertheless, far greater understanding of the role of LSD1 in PD is required to understand how this could contribute to disease aetiology and pathophysiology.

1.3.2.2 - Histone Acetylation/Deacetylation

Histone acetylation, like histone methylation, was first described in 1964 (Allfrey et al.), and is a highly dynamic process regulated by two classes of enzyme: histone acetyltransferases (HATs) and histone deacetylases (HDACs). HATs are categorised into three families: the Gcn5-related acetyltransferases (GNATs); the MOZ, Ybf2/Sas3, Sas2 and Tip60 (MYST)-related HATs; and p300/CREB binding proteins (CBP) HATs. All of these use acetyl-coenzyme A as an acetyl group donor to transfer an acetyl group to the ε-amino of lysine residues on the N-terminal tails of the four core histones, H2A, H2B, H3 and H4 (Roth et al., 2001). Addition of an acetyl group to lysine neutralises the positive charge of the residue (figure 1.7), hence reducing the electrostatic interaction between the lysine in the histone tail and the negatively charged phosphate group on DNA which disrupts the inter- and intra-nucleosomal interactions between the histone and DNA (Grayson et al., 2010). This causes a relaxation in the structure of chromatin, otherwise referred to as euchromatin, and allows transcriptional factor access to the DNA. Deacetylation of lysine residues is facilitated by HDACs, which remove the acetyl groups from the ε-amino of lysine restoring the positive charge and causing a condensation of chromatin, known as heterochromatin, thus repressing transcription. In addition to enabling transcription through remodelling of chromatin, acetyl-lysine residues serve as

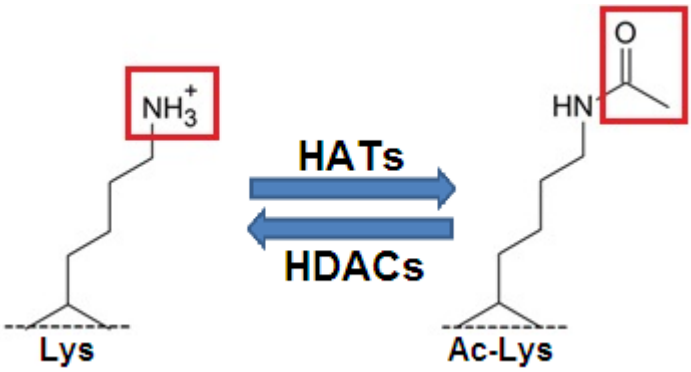

Figure 1.7 – Acetylation of Histone Lysine Residues
Addition of an acetyl group to a histone lysine residue neutralises its positive charge, reducing the electrostatic interaction between histone tail lysine residues and negatively charged phosphate groups on DNA. Abbreviations: Ac-Lys, acetyl-lysine; Lys, lysine; HATs, histone acetyl transferases; HDACs, histone deacetylase (reproduced with permission from Harrison and Dexter, 2013).

recognition sites for transcriptional activators that contain protein motifs known as bromodomains, thus indirectly facilitating transcriptional initiation (Grayson et al., 2010). Crosstalk between acetylation and methylation at specific residues further influences transcriptional activation, for example, simultaneous methylation and deacetylation of H3-Lys9 has been shown to cause stringent silencing of surrounding genes (Fuks, 2005). To this end, of the numerous histone lysine acetylation sites, some appear to be more crucial in the switching from heterochromatin to euchromatin, for example this methylated and acetylated residue H3-Lys9 and also another residue in histone protein H4: H4-Lys16 (Shahbazian and Grunstein, 2007).

In health, a tightly controlled equilibrium exists between HAT and HDAC activity enabling the dynamic control of transcription (figure 1.8) (Dietz and Casaccia, 2010, Saha and Pahan, 2006). In neurons, such a harmonized balance is therefore conducive to appropriate regulation of gene expression and subsequently facilitates appropriate neuronal homeostasis (Saha and Pahan, 2006). Therefore, it is thought that if an imbalance of HAT/HDAC was to occur then neuronal cell death would likely follow, implicating the possibility of HAT/HDAC misbalance in disease (Dietz and Casaccia, 2010, Saha and Pahan, 2006). Rouaux and colleagues in 2003 were the first researchers to identify alterations of histone acetylation levels in neurodegeneration, by demonstrating that histone acetylation levels were decreased globally in neurons accompanied by a decrease in HAT CBP/p300. Authors observed increased levels of histone deacetylation in both an *in vitro* model of cortical neuronal cell death induced by activation of amyloid precursor protein signalling, a hallmark of Alzheimer's disease (AD), and in an *in vivo* model of Amylotrophic Lateral Sclerosis (ALS): the G86R mutant Superoxide Dismutase 1 (SOD-1) mouse displaying motor neuron degeneration (Rouaux et al., 2003). Since then, histone hypoacetylation has become heavily implicated in numerous neurodegenerative diseases, especially PD. For example, in PD it has also been shown that αSyn accumulation promotes histone H3 hypoacetylation as ascertained from overexpression studies in SH-SY5Y cells as well as in an *in vivo* αSyn transgenic drosophila model (Kontopoulos et al., 2006). No direct binding was observed between αSyn and H3 therefore the effect of reduced acetylation of H3 is said to likely be through histone 'masking': the mechanism through which transcription is inhibited by ataxin-3, a polyglutamine containing protein involved in Huntington's disease (HD) (Li et al., 2002). Therefore it is theorised that the accumulation of misfolded αSyn promotes neurotoxicity in PD by 'masking' histone proteins: preventing histone acetylation, condensing chromatin, repressing gene expression and ultimately leading to cell death. Accumulations of misfolded proteins such as αSyn are a commonality in a number of neurodegenerative diseases and it is therefore thought this histone hypoacetylation could be at least partly responsible for the induction of cell death in these disorders. The use of HDAC inhibitors (HDACIs) to restore the imbalance between HAT/HDACs is

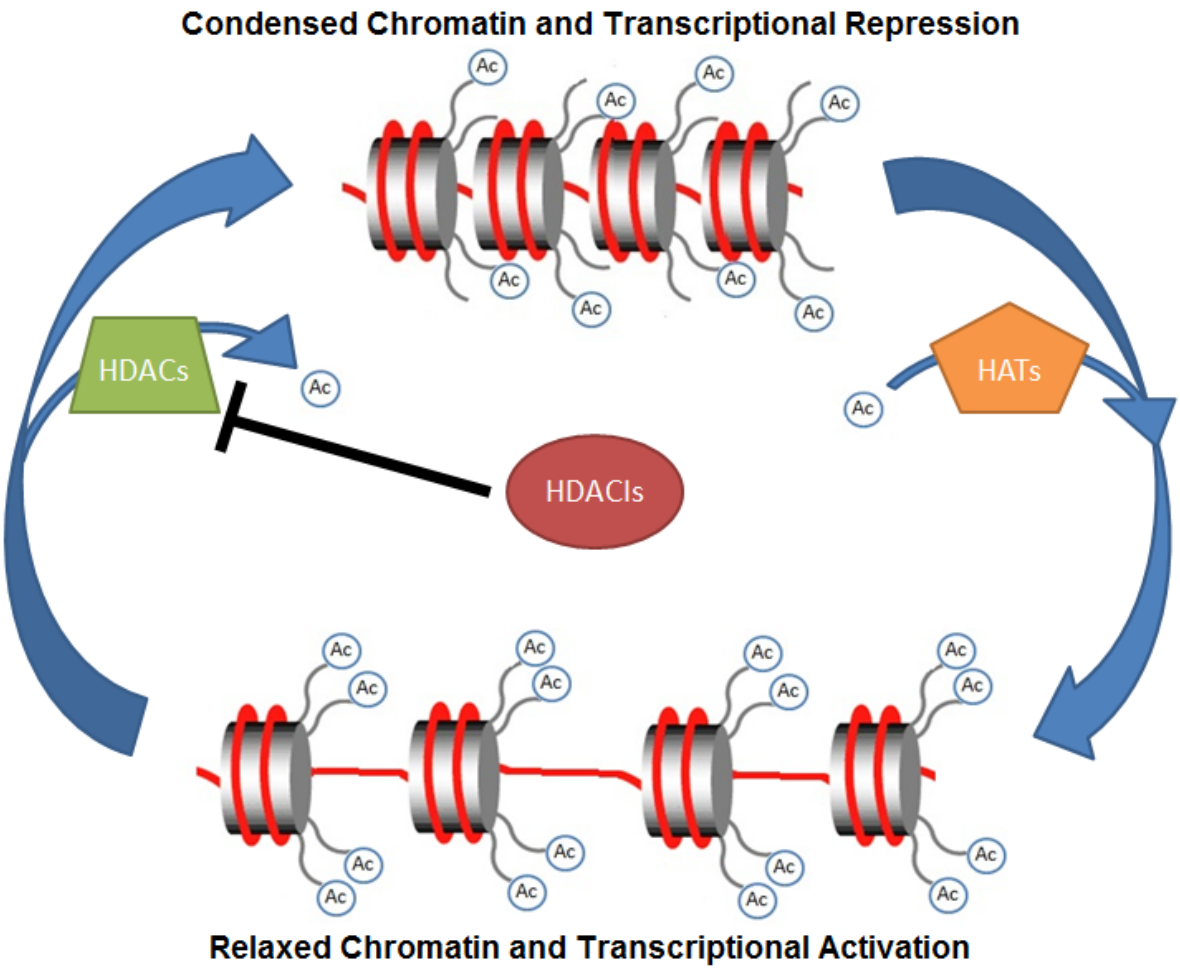

Figure 1.8 – Histone Acetylation Dependent Relaxation and Condensation of Chromatin
Relaxation and condensation of chromatin is facilitated by acetylation and deacetylation of histone proteins respectively. The level of histone acetylation depends on the interplay between HATs and HDACs. Inhibition of HDACs results in a net increase of histone acetylation, relaxation of chromatin and transcriptional activation. Abbreviations: Ac, acetyl; HATs, histone acetyl transferases; HDACs, histone deacetylases; HDACIs, histone deacetylase inhibitors (reproduced with permission from Harrison and Dexter, 2013).

therefore becoming a popular area of neurodegenerative research (Chuang et al., 2009, Dietz and Casaccia, 2010, Hahnen et al., 2008, Kazantsev and Thompson, 2008, Saha and Pahan, 2006): in AD (Xu et al., 2011), in motor neuron diseases such as ALS (Echaniz-Laguna et al., 2008, Schmalbach and Petri, 2010), HD (Butler and Bates, 2006, Sadri-Vakili and Cha, 2006), Multiple Sclerosis (Faraco et al., 2011), and most relevant to this thesis, PD. However to understand the relevance of inhibiting HDACs, we must first understand the functionality of HDACs and more importantly their expression patterns both within the cell and the brain.

1.4 – Histone Deacetylase

HDACs are conserved between yeast and man. To date 18 human HDAC isoforms have been characterised, and based on their sequence homologies and co-factor dependencies they have been phylogenetically categorised into 4 main classes: class I, II (a and b), III and IV (table 1.3) (Xu et al., 2007). Classes I, II and IV are all zinc dependent enzymes containing zinc-dependent catalytic domains. Class III on the other hand work independently of zinc, however require nicotinamide adenine dinucleotide (NAD+) for their enzymatic activity (Saunders and Verdin, 2007, Blander and Guarente, 2004). Class I HDACs include HDACs 1, 2, 3, and 8, and share high sequence homology in their catalytic sites with yeast RPD3 deacetylase (Xu et al., 2007). Class II HDACs are closely related to yeast Hda1 and include HDACs 4, 5, 6, 7, 9, 10. This class is further subcategorised into class IIa, consisting of HDACs 4, 5, 7 and 9, which contain only one catalytic site, and class IIb consisting of HDACs 6 and 10, which contain two catalytic sites (Xu et al., 2007). Class III, the NAD+ dependent class, are structurally and enzymatically distinct from other HDAC classes and share homology with yeast silent information regulator 2 (SIR2) (Blander and Guarente, 2004, Saunders and Verdin, 2007). This class comprises of sirtuin 1, 2, 3, 4, 5, 6, and 7 (Blander and Guarente, 2004, Outeiro et al., 2008, Saunders and Verdin, 2007, Haigis and Sinclair, 2010). Lastly, class IV consists of HDAC 11 alone, due to conserved residues within its catalytic core region shared by both class I and II (Xu et al., 2007).

Despite their principle role in the cell being to deacetylate histone proteins in the nucleus, the different classes and isoforms of HDACs vary in their sub-cellular localisation (table 1.3) (Haigis and Sinclair, 2010, Konsoula and Barile, 2012, Outeiro et al., 2008, Salminen et al., 1998). Similarly in the brain, expression of the different classes of HDACs varies between cell types: expression is restricted mainly to neurons however numerous classes are known to be present in glia (Broide et al., 2007). Likewise in the brain, the expression level of HDAC isoforms varies from nucleus to nucleus. There has been no distribution study of the expression of class III HDACs (the sirtuins) in the brain, however the expression levels of the 11 'classical' HDAC isoforms, i.e. classes I, II and IV, were studied and the relative expression patterns mapped in the rat brain in 2007 using high-resolution *in situ* hybridization study of 56 brain regions in the rat brain (Broide et al.). Related to PD it is of interest that the majority of HDAC expression in the SNpc is limited mainly to HDAC 2, 3, 4, 5, and 11, however lower levels of HDAC 1, 6, 7, 8 and 9 also exist here (table 1.4) (Broide et al., 2007). Moreover in this study, HDAC 10 was not detected in the SNpc at all (Broide et al., 2007).

The role of HDACs in epigenetic regulation is to reverse the effects of HATs, by catalysing the deacetylation of N-terminal tails of histone proteins. This facilitates a condensation of chromatin structure which prevents transcription factor access to DNA, thus leading to transcriptional repression. HDACs are therefore effective deacetylating enzymes; however their activity is not

restricted to histone proteins. A recent phylogenetic study of bacterial HDACs revealed that all four classes of HDACs preceded the evolution of histone proteins, suggesting that the primary function of HDACs may have been towards non-histone proteins (Gregoretti et al., 2004). For example, at least 50 acetylated non-histone proteins of known biological function are known to act as substrates for HDACs (Glozak et al., 2005, Spange et al., 2009). Notably, non-histone targets include transcription factors and co-regulators, signalling mediators, nuclear hormone receptors and cytoskeletal elements (Glozak et al., 2005, Spange et al., 2009).

It is evident that HDACs represent a vast and diverse class of deacetylating enzyme and given their distinct expression patterns in the brain and in the cell they represent an ideal target for therapeutic inhibition. To that end, recent years have witnessed increasing interest in, and vast acceleration of the development of both broad isoform non-selective inhibitors as well as isoform selective inhibitors of HDACs (Burridge, 2013, Carey and La Thangue, 2006). Hence, the functional roles of HDACs have largely been inferred from their inhibition using either broad-spectrum class inhibitors or more recently designed isoform selective inhibitors.

Table 1.3 – Sub-Cellular Localisation of Histone Deacetylases
Abbreviations: HDAC, histone deacetylase; NAD+, nicotinamide adenine dinucleotide (adapted from Harrison and Dexter, 2013).

Histone Deacetylase Class	Protein(s)	Sub-Cellular Location
Class I *(Zn^{2+} Dependent)*	HDAC1	Nucleus
	HDAC2	Nucleus
	HDAC8	Nucleus
	HDAC3	Shuttles between nucleus and cytoplasm
Class IIa *(Zn^{2+} Dependent)*	HDAC4	Shuttles between nucleus and cytoplasm
	HDAC5	Shuttles between nucleus and cytoplasm
	HDAC7	Shuttles between nucleus and cytoplasm
	HDAC9	Nucleus-cytoplasm
Class IIb *(Zn^{2+} Dependent)*	HDAC6	Cytoplasm
	HDAC10	Cytoplasm
Class III *(NAD+ Dependent)*	Sirtuin1	Nucleus
	Sirtuin2	Cytosol
	Sirtuin3	Mitochondria
	Sirtuin4	Mitochondria
	Sirtuin5	Mitochondria
	Sirtuin6	Nucleus
	Sirtuin7	Nucleolus
Class IV *(Zn^{2+} Dependent)*	HDAC11	Nucleus

Table 1.4 – Brain Regional Expression of Histone Deacetylases

Summary of the regional expression of histone deacetylase in the rat brain, as ascertained through high resolution *in situ* hybridisation analysis performed by Broide et al. (2007). Expression is listed and scored from low to high (0-5) (adapted from Harrison and Dexter, 2013).

	HDAC 1	HDAC 2	HDAC 3	HDAC 4	HDAC 5	HDAC 6	HDAC 7	HDAC 8	HDAC 9	HDAC 10	HDAC 11
Olfactory bulb	2.5	3.5	4	4	4	1.5	1	1	0.5	0.5	4.5
Cortex	2	3	3.5	3.5	3.5	1	0.5	0.5	0.5	0.5	4
Caudate putamen	0.5	2	3	1	3	0.5	0.5	0	0	0	4
Nucleus accumbens	0.5	2	3	1	3	0.5	0.5	0	0	0	4
Globus palidus	0	0	1	0.5	1	0	0	0	0	0	2
Amygdala	2.5	3	3.5	3	3	1	1	1	0.5	0.5	4.5
Hippocampus	2.5	4.5	5	4.5	5	2	1	2	1	1	4
Choroid plexus	2	0	3	0	2	0	0	0	0	0	0
Substantia nigra - compacta	1	1.5	3.5	2.5	3.5	1	1	1	1	0	4
Substantia nigra - reticulata	0.5	1	1	1	1.5	0	0	0	0	0	3
Hypothalamus	1	1.5	3.5	2.5	3.5	1	0.5	0.5	0	0	4.5
Pons	1.5	2	2.5	2.5	3	1	0.5	0.5	0.5	0	4.5
Cerebellum	4	4	5	5	5	1.5	1.5	2	0.5	0	4
Medulla	0.5	1.5	3	2	2.5	0.5	0.5	0.5	0	0	3
Spinal cord	1	2	2.5	2	2.5	0.5	0.5	0.5	0	0	3.5
	22	**31.5**	**47**	**35**	**46**	**12**	**9**	**9.5**	**4.5**	**2.5**	**53.5**

1.5 – Histone Deacetylase Inhibitors

HDACIs have shown to be efficacious in numerous disorders: for example sickle-cell anaemia, diabetes and immune disorders (Lawless et al., 2009). However, they are most commonly therapeutically used and studied as anti-cancer agents. HDAC inhibition emerged as a potential therapeutic strategy to reverse aberrant epigenetic changes associated with cancer a number of years ago (Bolden et al., 2006, Marks et al., 2001a) and hence HDACIs have since been shown to cause growth arrest, differentiation and/or apoptosis of many tumours cells by altering the transcription of a small number of genes (Marks et al., 2001b). Subsequently, clinical trials are on-going of the use of HDACIs in various cancers: non-small cell cancers and hepatocellular carcinomas, leukaemia and t-cell lymphoma (Minucci and Pelicci, 2006, Wagner et al., 2010).

It seems counter intuitive that a drug class studied for therapy in cancer, where cells refuse to die, could be efficacious for a neurodegenerative disease such as PD, where cells prematurely die in the midbrain. However, a number of cell systems have emerged in recent years which represent a substantial pathological convergence between cancer and PD (Devine et al., 2011). For example, alterations in protein folding and degeneration, cell cycle and DNA repair, mitochondria and oxidative stress, and chronic inflammation are all implicated in both cancer and PD (Devine et al., 2011). It is therefore not unreasonable to suggest that a drug class with such a varied scope of action such as HDACIs would represent a viable therapeutic option for both cancer as well as PD.

Small molecule HDACIs which inhibit the zinc dependent classes of HDACs, fall into 4 main classes according to their chemical structure: hydroxamates, cyclic peptides, short chain fatty acids and benzamides (figures 1.9 and 1.10). It is important to note that these small-molecule HDACIs do not affect class III HDACs, the sirtuins, due to the structural and functional dissimilarity between this class of HDACs and classes I, II and IV. However, a number of sirtuin inhibitors have now been developed both isoform selective and isoform non-selective (figures 1.9 and 1.10). Below the currently available chemical classes of HDACIs will be introduced in terms of their chemical structure and pharmacological mechanisms of action, and the isoforms they are known to display most potency for.

1.5.1 - Hydroxamates

Hydroxamate based inhibitors are composed of three main elements: the hydroxamic acid (-CO-NH-OH), a hydrophobic linker, and a polar tail (figure 1.9). Each of the elements of the inhibitor is thought to interact with a different part of the catalytic site of the HDAC (Marks et al., 2004, Villar-Garea and Esteller, 2004). The hydroxamate moiety is thought to bind to the zinc ion in the catalytic domain of HDACs thus inactivating the enzyme (Marks et al., 2004, Villar-Garea and Esteller, 2004). It

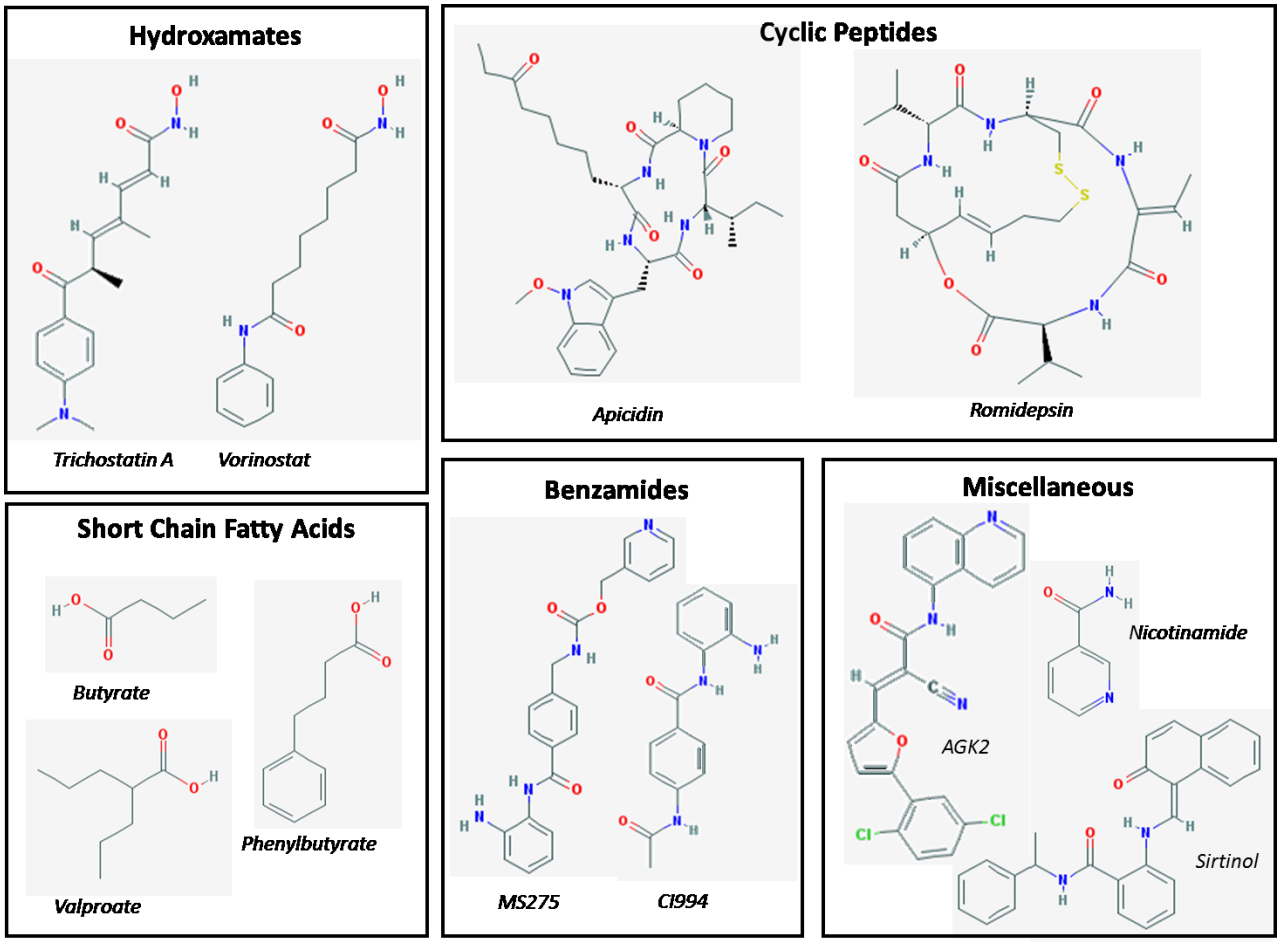

Figure 1.9 – Chemical Classes of Histone Deacetylase Inhibitors
Inhibitors of the zinc dependent HDACs can be divided into 4 main classes dependent on their chemical structure: hydroxamates, short chain fatty acids, cyclic peptides and benzamides. Inhibitors of the NAD+ dependent HDACs however vary greatly in their structure, see miscellaneous (adapted from Harrison and Dexter, 2013).

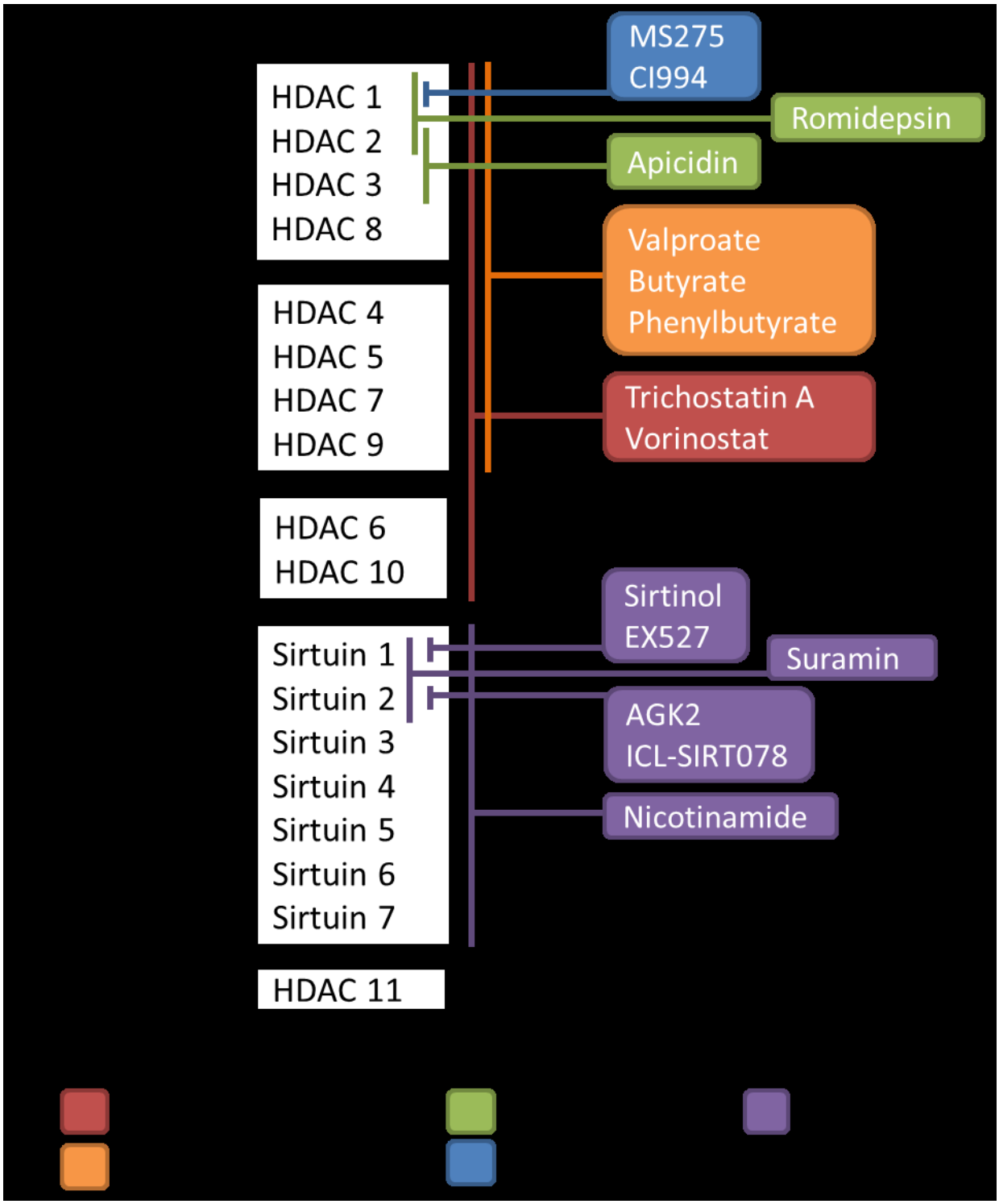

Figure 1.10 – Target Selectivity of Isoform Specific and Isoform Non-Specific Histone Deacetylase Inhibitors
Abbreviations: HDAC, histone deacetylase; NAD+, nicotinamide adenine dinucleotide; Zn^{2+}, zinc (adapted from Harrison and Dexter, 2013).

is for this reason that hydroxamates are known to only inhibit classes of HDACs which share the same zinc dependent catalytic site: classes I and II HDACs only (figure 1.10). The large majority of hydroxamate HDACIs act as pan-HDACIs meaning that they possess no profound isoform selectivity within the zinc dependent classes (Hahnen et al., 2008). In general, drugs within this class of HDACIs are known to have relatively short half-lives, however possess long lasting effects (Plumb et al., 2003).

A large number of hydroxamate containing HDACIs have now been engineered, for example Scriptaid, Oxamflatin, Belinostat, Dacinostat, Panobinostat, Givinostat and Abexinostat (Grayson et al., 2010, Wagner et al., 2010, Xu et al., 2007). A number of these compounds are now in various stages of clinical development for cancers (Wagner et al., 2010). However, the two most clinically advanced and most prominent hydroxamate HDACIs are trichostatin A and vorinostat, both of which cross the BBB (Chuang et al., 2009), hence highlighting them as targets from neurological conditions such as PD.

1.5.2 – Cyclic Peptides

A number of cyclic peptides act as HDACIs as they too are thought to interact with the catalytic zinc ion site of HDACs to cause inhibition (Furumai et al., 2002). However, due to the large variation in chemical structure among peptides (figure 1.9), peptide HDACIs exert inhibition of various different specific HDAC isoforms. Nevertheless, the development and research into the use of cyclic peptide drugs has been somewhat lacking, there being only two notable examples of drugs of this class to date: apicidin and romidepsin. Apicidin displays selectivity for HDAC2 and HDAC3 (and HDAC8) while romidepsin shows potent efficacy for inhibition of HDAC1 and HDAC2 (and HDAC4) (figure 1.10) (Khan et al., 2008). Due to their structurally dependent selectivity for HDAC isoforms, cyclic peptide HDACIs remain an encouraging template for development of HDACIs with selectivity for differing combinations of HDAC isoforms, limiting the likely side effects with their treatment.

1.5.3 – Short Chain Fatty Acids

Short chain fatty acids (SCFAs), compared with other HDACIs, are relatively small, simple structured compounds, the molecular weights of which do not much exceed 150g/mol (figure 1.9). The three most notable drugs within this class are valproate, butyrate and phenylbutyrate. Most SCFAs share HDAC isoform inhibition profiles: inhibiting the action of classes I and IIb with most efficacy (figure 1.10) (Grayson et al., 2010). Compared with the other HDACIs described thus far, SCFAs are relatively less potent, working in the range of millimoles rather than nanomoles (Grayson et al., 2010, Hahnen et al., 2008). It is thought that this weak potency is attributable to their inability to

access the zinc cation in the HDAC active-site pocket, which appears to be pivotal to the deacetylation catalysis (Lu et al., 2003). It therefore appears likely that SCFAs use mechanisms other than direct interface with the catalytic site of HDACs to bring about inhibition. SCFAs do however have hugely diverse properties, and due to their small molecular weights are able to cross the BBB with ease (Xu et al., 2007). SCFAs hence remain an encouraging class of HDACIs for neuroscience research.

1.5.4 - Benzamides

As opposed to SCFAs, cyclic peptides and hydroxamates, benzamides represent a new relatively selective class of HDACI which exhibit a relatively long half-life as compared with other potent HDACIs (Glozak et al., 2005). Two notable drugs within this class are currently in clinical trial for cancers: MS275 and CI994 (figure 1.9) (Grayson et al., 2010). Both MS275 and CI994 selectively inhibit HDAC1 (and HDAC3 to a lesser extent) over other HDAC isoforms within class I (figure 1.10). They therefore represent an exciting new population of HDAC inhibiting agents being designed selectively against individual HDAC isoforms. The vast majority of pan-HDACIs described above exhibit some toxic effects due to their wide selectivity for numerous HDACs and other off target effects. Design of more isoform specific HDACIs will lead to an even greater potential of the use of HDACIs in diseases other than cancers where HAT/HDAC activity is known to be perturbed, such as PD.

1.5.5 - Miscellaneous

Thus far all of the classes of HDACIs mentioned exhibit selectivity for the classical zinc dependent HDAC classes. However, as has already been alluded to, the NAD+-dependent class of HDACs represents a large functional sub-group of HDACs. Class III HDACs are structurally and enzymatically distinct from classes I, II and IV, therefore HDACIs which interact with this class do not fit into any of the previous mentioned chemical structural groups of classical HDACIs. Class III HDACs are NAD+-dependent and therefore they require the binding of an NAD+ molecule in their active site to enable deacetylation (Spange et al., 2009). Nicotinamide is a competitive inhibitor of all 7 sirtuin HDACs due to its ability to competitively bind to the NAD+ binding site of Sirtuins, preventing NAD+ from binding and thus inhibiting deacetylation of acetylated substrates such as histone proteins. Nicotinamide represents an encouraging HDACI in neuroscience due to its ability to cross the BBB when given orally, a feature that few HDACIs possess (Spector, 1987). Another more specific inhibitor of this class of HDACs is suramin, a symmetric polyanionic nephthylurea, which itself and its structural homologs has been shown to inhibit both sirtuin1 and sirtuin2 isoforms within the class

(Gregoretti et al., 2004). Moreover, more specific inhibitors of sirtuin1 alone have also been identified: sirtinol (Trapp et al., 2007) and EX527 (Gertz et al., 2013). Likewise specific inhibitors of sirtuin2 have also now been developed: AGK2 (Outeiro et al., 2007) and in collaboration with Dr Matthew Fuchter and colleagues (Department of Medicinal Chemistry, Imperial College London), ICL-SIRT078 (Di Fruscia et al., 2014).

1.6 – Histone Deacetylase Inhibitors in Parkinson's Disease

HDACIs have been theorised to be efficacious in neurodegenerative disease. Yet the mechanism of action in how histone acetylation is transferred to neuroprotection still remains elusive. Neuroprotection and neurotrophicity are thought to be maintained through the combined transcriptional and non-transcriptional effects of HDACIs. Inhibition of HDACs reduces the deacetylation of histones which is therefore thought to lead to chromatin relaxation and activation of multiple gene products conducive to neurotrophicity, anti-inflammation and subsequently neuroprotection. For example, brain derived neurotrophic factor (BDNF), glial derived neurotrophic factor (GDNF), heat shock protein 70 (Hsp70), αSyn, B-cell lymphoma (Bcl)-2, Bcl-XL, p21 and gelsolin (GSN) have all been shown to be induced upon HDACI treatment (Chuang et al., 2009, de Ruijter et al., 2003). Similarly, non-transcriptional effects of HDACs i.e. the non-histone targets of HDAC catalysed deacetylation, are also thought to be involved in aiding neuroprotection (Glozak et al., 2005). For example, inhibition of HDACs increases the acetylation of α-tubulin, a non-histone target, which increases microtubule stabilisation and axonal transportation aiding the release of BDNF and neuroprotection (Zhang et al., 2003). Additionally, gathering evidence highlights the multicellular involvement of HDAC inhibitors with other brain cells: immuno-modulatory effects in microglia, and reducing astrocyte and T-cell mediated inflammation (Dietz and Casaccia, 2010). It is apparent that the mechanism of neuroprotection of HDACIs is likely to be multi-targeted. Given the multi-faceted origins of PD pathogenesis, HDACIs seem like an optimistic candidate for therapy.

The distinct patterns of expression of HDACs in the brain crossed with the large number of compounds now available designed to selectively target specific isoforms and combinations of isoforms of HDACs, position HDACIs as an excellent therapeutic target in neuroscience. However current research of the use of HDACIs in neurodegeneration is limited to those that have been previously shown to cross the BBB (Kazantsev and Thompson, 2008, Morrison et al., 2007). Regardless, inhibition of HDAC classes has been observed to normalize the deficiency of histone acetylation in numerous *in vitro* and *in vivo* models of PD leading to stringent neuroprotection. Similarly non-transcriptional consequences of HDAC inhibition have also been observed in models relevant to PD, such as improvement of microtubule stability due to acetylation, aiding neuroprotection. In addition, as detailed above, multiple neuroprotective and neurotrophic factors have been identified to be upregulated as a result of HDACI mediated histone hyperacetylation, not only in neurons but also in microglia and astrocytes. Table 1.5 summarises evidence of the use of the most abundantly researched HDACIs with reference to PD: from the effects of drug treatment in cell culture models of PD cytotoxicity and immune cell activation, to the effects of HDACIs in the well-established animal models of the disease. HDACI mediated neuroprotection is therefore likely

achieved through an amalgamation of these effects: microtubule stabilisation in conjunction with numerous neurotrophic and neuroprotective agents being upregulated simultaneously to evoke a neuroprotective parenchymal environment inauspicious to neuronal cell death.

It is of note however that the *in vivo* models of PD used thus far for assessing the neuroprotective effects of HDACIs have not involved altered protein accumulation. αSyn accumulation is the principle pathological feature of PD and hence to truly rationalise the use of HDACIs for the treatment of PD in the clinic, their neuroprotection must be demonstrated in animal models which recapitulate aggregation of altered proteins in dopaminergic nigral neurons to cause neurodegeneration. Additionally, many of the studies assessing the neuroprotective effects of HDACIs use pre-treatment regimes in which the HDACI is delivered prior to toxin administration as a prophylactic treatment. These studies fail to model the clinical scenario in which HDACIs would be used; hence further investigation of this neuroprotective drug class should focus on their neuroprotective effects when administered after toxin lesioning.

Given the small molecular nature of the vast majority of HDACIs, they embody an exciting target for therapy for neuroscience due to their ability to traverse the BBB with ease. The multi-targeted and multi-cellular neuroprotective and neurotrophic affects induced upon HDACI treatment make HDACIs one of the most disease relevant drug class being investigated in PD today. Further study to facilitate our understanding of the consequences of HDAC isoform inhibition and their effects in producing neuroprotection are now required to further refine the prospective use of HDACIs in this complex disorder and translate their use to the clinic.

Table 1.5 – Evidence of Neuroprotection/Anti-Inflammation in Models of Parkinson's Disease
Abbreviations: HDAC, histone deacetylase; LPS, lipopolysaccharide; MPP+, 1-methyl-4-phenylpyridinium; MPTP, 1-methyl-4-phenyl-1,2,3,6-tetrahydropyridine; 6-OHDA, 6-hydroxydopamine; αSyn, α-Synuclein.

Chemical Class	Drug	Inhibitor Type	HDACs Inhibited	BBB Permeable	Neuroprotection/Anti-Inflammation Demonstrated *In Vitro* (Model (Reference))	Neuroprotection/Anti-Inflammation Demonstrated *In Vivo* (Model (Reference))
Hydroxamates	Trichostatin A	Pan-Inhibitor	Classes I, IIa and IIb	Yes	**LPS** (Suh et al., 2010, Chen et al., 2007) **MPP+** (Wu et al., 2008a, Wu et al., 2008b) **Glutamate** (Leng and Chuang, 2006)	None reported
	Vorinostat	Pan-Inhibitor	Classes I, IIa and IIb	Yes	**MPP+** (Kidd and Schneider, 2010, Chen et al., 2012) **LPS** (Chen et al., 2012)	None reported
Cyclic Peptides	Apicidin	Isoform-Specific	HDAC2 and 3	Yes	**Glutamate** (Marinova et al., 2009)	None reported
Short Chain Fatty Acids	Valproate	Pan-Inhibitor	Classes I and IIa	Yes	**LPS** (Peng et al., 2005, Chen et al., 2007, Chen et al., 2006, Wu et al., 2008b) **Glutamate** (Leng and Chuang, 2006) **6-OHDA** (Monti et al., 2007) **Rotenone** (Pan et al., 2005) **MPP+** (Kidd and Schneider, 2010)	**Rotenone** (Monti et al., 2010) **6-OHDA** (Monti et al., 2012) **MPTP** (Kidd and Schneider, 2011, Castro et al., 2012)
	Butyrate	Pan-Inhibitor	Classes I and IIa	Yes	**MPP+** (Kidd and Schneider, 2010, Wu et al., 2008b) **LPS** (Chen et al., 2007)	**6-OHDA** (Rane et al., 2012)
	Phenylbutyrate	Pan-Inhibitor	Classes I and IIa	Yes	**Glutamate** (Leng and Chuang, 2006) **LPS** (Roy et al., 2012) **6-OHDA** (Zhou et al., 2011)	**MPTP** (Gardian et al., 2004, Roy et al., 2012, Zhou et al., 2011) ***SNCA* (A30P+A53T)** (Ono et al., 2009) **Rotenone** (Inden et al., 2007)
Miscellaneous	Nicotinamide	Pan-Inhibitor	Class III	Yes	**MPP+** (Jia et al., 2008)	**MPTP** (Anderson et al., 2006, Anderson et al., 2008, Xu et al., 2012) **αSyn overexpression** (Jia et al., 2008)
	AGK2	Isoform-Specific	Sirtuin2	?	**αSyn overexpression** (Outeiro et al., 2007)	**αSyn overexpression** (Outeiro et al., 2007)

1.7 – Aims

It is hypothesised that histone hypoacetylation and transcriptional dysfunction contribute to the pathological process of neurodegeneration in PD, hence HDAC inhibition is neuroprotective. This thesis therefore has the following aims to assess this hypothesis. Firstly, although accumulating evidence implicates histone hypoacetylation and transcriptional dysfunction in the pathogenesis of neurodegenerative diseases such as PD, the findings of pathogenic histone hypoacetylation and transcriptional dysfunction have yet to be confirmed in the brains of PD patients: all work previously being described in animal and cellular models of neurodegeneration. Similarly, it is thought that pathogenic histone hypoacetylation is in part due to the 'masking' effects of αSyn accumulates towards histone proteins (Rouaux et al., 2003). Its remains to be questioned however as to the expression levels of the HDACs themselves in degenerating regions of the Parkinsonian brain: perhaps in concert with αSyn 'masking' of histone protein, PD pathology is directly driving a misbalance in expression between HATs and HDACs in degenerating nuclei. The first aim of this thesis is therefore to:

1. Quantify the level of histone acetylation in degenerating regions on the Parkinsonian brain in relation to healthy age matched controls, and conduct expression profiling of HDAC isoforms in these same brain regions, with the aim of identifying targetable HDAC isoforms for treatment in PD.

From the previous studies discussed above, it remains unknown as to whether isoform-specific or pan-HDAC inhibitors present most efficacy for neuroprotection in models of Parkinsonian neurodegeneration. Similarly, it is unknown which of the numerous HDAC subclasses presents greatest neuroprotective efficacy. This is thought mainly due to previous unavailability of specific subtype inhibitors. However, in recent years the development of HDACIs have advanced hugely: a large variety of both isoform-specific and non-specific inhibitors now being available. Nevertheless, at present, the PD field is not keeping up with the recent flourish in HDACI development: notable examples of isoform-specific drugs such as MS275 and EX527 have yet to be tested in models of PD. The second aim of this thesis is therefore to:

2. Test the potential of a range of isoform specific and pan-HDACIs at reducing dopaminergic neurodegeneration and microglial activation *in vitro*, with the aim of identifying suitable lead compounds for further investigation *in vivo.*

Historically, successful treatment of the classical animal models of PD has translated little to success in clinical trials. Therefore, in order to bridge this gap between bench and bedside the neuroprotective effects of HDACIs must be validated appropriately in more clinically translatable animal experiments. For example, as has already been discussed, at time of symptom onset and presentation to the clinic, a large majority of cell loss is already apparent within the SNpc of PD patients. Therefore, for greater clinical relevance and translatability, preclinical studies seeking to determine the neuroprotective effects of HDACIs in PD need to be designed such that the drug treatment is administered after neurodegeneration is induced in the animal model, i.e. after toxin administration. The third aim of this thesis is therefore to:

3. Determine the neuroprotective and behavioural effects of delayed start HDACI treatment in the progressive lactacystin lesion animal model of PD, and attempt to elucidate the mechanism by which HDACI mediated neuroprotection is achieved.

In order to achieve these aims, human brain tissue donated at post mortem will firstly be utilised from the Parkinson's UK Tissue Bank (PUKTB), at Imperial College London, to profile the level of histone acetylation and HDAC isoform expression in degenerating regions of the Parkinsonian brain with relation to controls. Cell culture studies will then be performed the test the efficacy of a number of HDACIs at reducing toxin induced neurodegeneration in a mesencephalic dopaminergic cell line, and activation in a microglial cell line, with the aim of identifying lead compounds for study *in vivo*. The lactacystin rat model of PD will then be established and the neuropathology induced as a result of toxin administration will be profiled using behavioural test paradigms and magnetic resonance imaging. Following the profiling of this model it will be challenged with two effective broad spectrum HDACIs identified from cell culture studies to determine if they are capable of inducing neuroprotection *in vivo*. A number of molecular and cellular analyses will then be conducted on animal tissue samples in attempt to elucidate the mechanism by which HDACI mediated neuroprotection is achieved.

Chapter Two

Materials and Methods

2 - Materials and Methods

2.1 - Outline of Chapter

In this chapter the materials and methods used for investigation of the use of HDACIs as disease modifying agents in PD are outlined. Firstly the materials and methods used for isolation and extraction of messenger ribonucleic acid (mRNA) and protein samples from human PD and control brain tissue for the profiling of histone acetylation and HDAC expression are detailed. Secondly the materials and methods used for *in vitro* cell culture experiments for the initial screening of the neuroprotection and anti-inflammatory effects of HDACI compounds are detailed with particular focus on the assays used for quantification of cell viability and microglial activation in cell lines. Thirdly the materials and methods used for *in vivo* experiments using the lactacystin rat model of PD are detailed including the behavioural tests and magnetic resonance imaging conducted throughout the duration of the animal studies. Finally, the reagents and protocols used for all cellular and molecular analyses of samples obtained from these previously described human, cell culture, and animal experiments are detailed.

2.2 – Human Tissue Experiments

2.2.1 – Introduction

In order to rationalise the use of HDACIs as possible disease modifying therapeutic agents for PD, the level of histone acetylation and HDAC expression was first profiled in the human condition to confirm that a pathological misbalance exists. For this, brain tissue from PD patients and age matched controls was utilised from the PUKTB at Imperial College London. Protein and mRNA was extracted from samples of whole brain tissue from a number of regions of interest, for quantification of histone acetylation and HDAC expression respectively.

2.2.2 – Human Brain Tissue Samples

Human brain tissue samples (PD and controls) were obtained from the PUKTB at Imperial College London, and all experiments using the tissue samples were previously approved by the PUKTB's Ethical Review Panel. Post-mortem (<24hrs) human brain tissue was removed from the body of the donor, and prepared and dissected using a standardised dissection protocol (Vonsattel et al., 1995). Dissected brain blocks were then snap frozen in isopentane pre-chilled on dry ice and stored at -80°C until further use.

2.2.3 - mRNA and Protein Extraction From Whole Brain Tissue

For extraction of mRNA and protein from whole brain tissue samples, 30mg of tissue from the brain block containing the region of interest was collected into ribonuclease (RNase)-free microcentrifuge tubes. Tissue was then homogenised for sequential extraction of mRNA and protein using the RNeasy® Plus Universal Mini Kit (Qiagen, Crawley, UK).

2.2.3.1 – Tissue Homogenisation and Phase Separation

Tissue was homogenised in 900µl of QIAzol® Lysis Reagent (Qiagen) using a tissue homogeniser (Tissue Tearor, Model 985370-395, BioSpec Products Inc, USA). After incubation of the homogenate at room temperature (RT) for 5mins, genomic DNA was eliminated by addition of 100µl of Qiagen gDNA Elimination Solution and mixed by inversion for 15s. 180µl of chloroform was then added and samples mixed again before being left at RT for 5mins. Samples were centrifuged at 12,000 x g for 15mins at 4°C to separate into phases: an upper aqueous phase containing RNA, a solid interphase containing DNA, and a lower phenol phase containing protein.

2.2.3.2 – mRNA Extraction and Quantification

The upper, aqueous phase was removed to a new RNase-free microcentrifuge tube and 600µl of 70% ethanol was added to precipitate RNA. This RNA containing solution was then passed through a Qiagen RNeasy Mini spin column to bind and collect RNA onto the column membrane. This was then

washed twice with Qiagen Buffer RWT and once with Qiagen Buffer RPE before drying the membrane via high speed centrifugation. RNA was then eluted from the column with RNase free water and quantified. Due to the ability of nucleic acids to absorb ultraviolet light, it is possible to quantify their concentration in a solution using a spectrophotometer which measures sample absorption at 260 and 280nm. For this a NanoDrop ND-1000 spectrophotometer (Thermo Fischer Scientific, Waltham, MA) was used. The RNA concentration for each sample was then calculated using the Beer-Lambert law:

$$\boldsymbol{A = log_{10}\frac{I_0}{I} = \varepsilon lc}$$

Where:

$\boldsymbol{A} = absorbance$
$\boldsymbol{I_0} = intensity\ of\ light\ passing\ through\ the\ reference\ cell$
$\boldsymbol{I} = intensity\ of\ light\ passing\ through\ the\ sample\ cell$
$\boldsymbol{\varepsilon} = extinction\ coefficient\ of\ RNA\ (0.025(ng/\mu l^{-1})cm^{-1})$
$\boldsymbol{l} = length\ of\ solution\ the\ light\ passes\ through\ (cm)$
$\boldsymbol{c} = concentration\ of\ the\ sample\ (ng/\mu l)$

In order to assess the purity of RNA samples, absorbance at 260 and 280nm was utilised. 'Pure' RNA is generally accepted to have an $A_{260/280}$ ratio of ~2. RNA purity of samples was therefore verified by an average $A_{260/280}$ ratio of 1.99 (range 1.97-2.01). See figure 2.1 for a representative example of the absorbance vs. wavelength plot produced by an RNA sample used to calculate its concentration and assessment of its purity. RNA samples were then stored at -80°C until further quantitative real time polymerase chain reaction (qRT-PCR) analysis (see section 2.5.3).

2.2.3.3 – Protein Extraction and Quantification

For extraction of protein, 300µl of 100% ethanol was added to the solid interphase and lower phenol phase, of the centrifuged tissue homogenate and mixed by inversion. Samples were then left at RT for 3mins before being centrifuged at 2,000 x g at 4°C for 2mins to sediment DNA. The phenol/ethanol supernatant containing the protein fraction was transferred to new microcentrifuge tubes and 1.5ml of isopropenol was added to precipitate protein. Samples were left at RT for 10mins before being centrifuged at 12,000 x g for 10mins at 4°C. The supernatant was removed and 2ml guanidine-ethanol solution (0.3M guanidine hydrochloride in 95% ethanol) was added to the protein pellet and samples centrifuged at 7,500 x g for 5mins at RT. This step was repeated twice before the supernatant was removed and 2ml 100% ethanol added to the pellet. The tubes were centrifuged again at 7,500 x g for 5mins at RT and the supernatant then removed to allow the protein pellet to air dry. The pellet was then resuspended in 500µl of urea-dithiothreitol (DTT) solution (10M Urea,

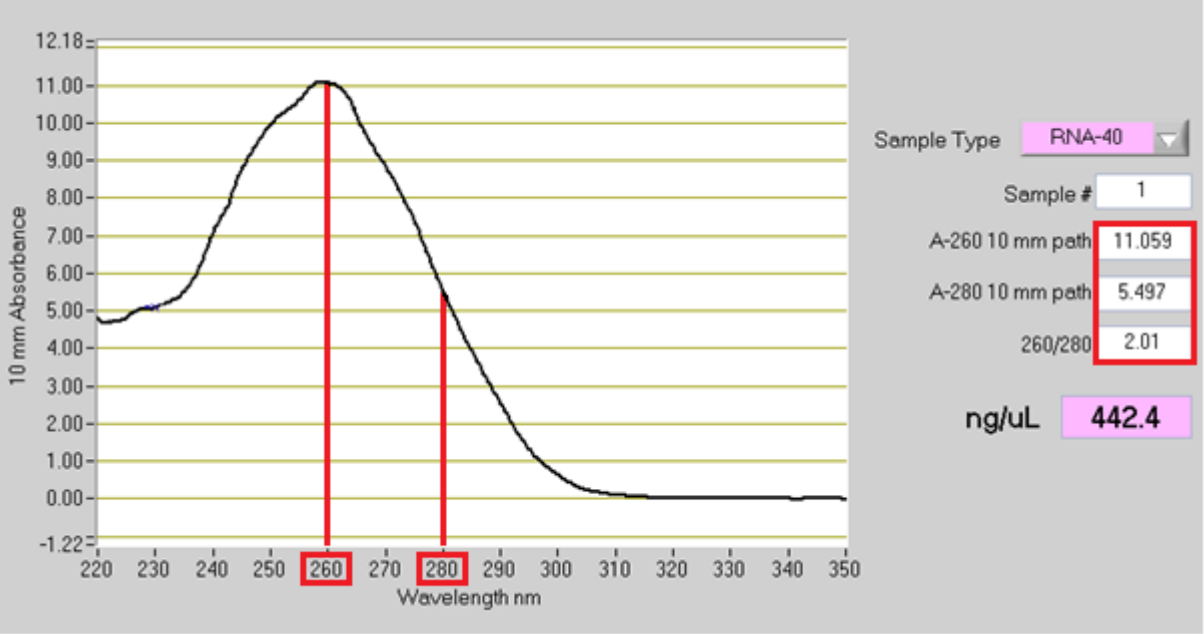

Figure 2.1 – Quantification and Assessment of RNA Purity Using Spectrophotometry

Absorbance vs. wavelength plot produced by an RNA sample used to calculate its concentration and assessment of its purity. The Beer-Lambert law is used to convert the absorbance of the sample at 260nm to RNA concentration using its known extinction coefficient, $0.025(ng/\mu l)^{-1}cm^{-1}$. The ratio of the samples absorbance at 260 and 280nm is used for assessment of sample's RNA purity.

50mM DTT in water) and sonicated 10 times in short bursts. Samples were then centrifuged at 10,000 x g for 10mins at RT and the supernatant removed to new microcentrifuge tubes and quantified. For this the 96 well plate variant of the Bradford assay was used. The Bradford assay, originally developed by Marian M. Bradford (1976), relies on Coomassie Brilliant Blue G-250 in the Bradford reagent binding to protein causing an absorbance shift from 465nm to 595nm wavelength. Briefly, in triplicate, 5µl of each protein sample was loaded into a 96 well plate. In addition, a set of protein standards was loaded in parallel with each plate by loading 5µl of a solution of known protein concentration (0 - 1.4mg/ml bovine serum albumin (BSA) in distilled water (dH_20)) to wells in triplicate. 250µl of Bradford reagent (Sigma, Poole, UK) was then added to each well containing protein samples or standards, and the plate shaken rapidly on a microtitre plate shaker for 20mins at RT. The light absorbance at 595nm was then read using a 96 well plate reader (VersaMax Microplate Reader, Molecular Devices, CA, USA). A standard curve of the spectrophotometric reading of A_{595} for each standard, minus the reading for the standard void of protein was plotted against its protein concentration (see figure 2.2 for representative example). The slope of the line of best fit of this data set was then used for calculation of the protein concentration for protein samples. Protein samples were stored at -20°C until further Western blot analysis (see section 2.5.4).

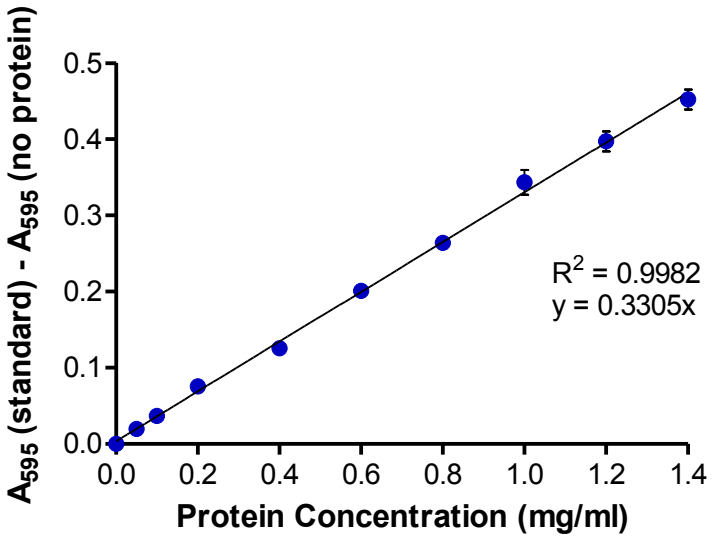

Figure 2.2 – Bradford Assay Standard Curve

For each Bradford assay plate a standard curve was constructed using solutions of known protein concentration (0 – 1.4mg/ml BSA in dH_2O) run in triplicate. The slope of the resulting line of best fit was used in order to translate the A_{595} for each sample into protein concentration. Protein standards were prepared by dissolving BSA into dH_2O and were stored at -20°C between uses. Standards were used for a maximum of five freeze/thaw cycles before fresh solutions were made. Data presented as mean ± SEM, n=3.

2.3 - *In Vitro* Experiments

2.3.1 – Introduction

To investigate the potential neuroprotective and anti-inflammatory effects of HDACIs against Parkinsonian cellular pathology, *in vitro* cell culture models of neuronal cell death and microglial activation were utilised. Cell lines were treated with toxins designed to model the pathophysiological scenario of microglial activation and neuroinflammation, and dopaminergic cell death associated with PD. At optimised time points cells were then treated with HDACIs and numerous assays subsequently performed to determine if they were able to alleviate the effects of these agents and therefore act with a neuroprotective and/or anti-inflammatory phenotype, *in vitro*.

The rat dopaminergic $1RB3A_{N27}$ (N27) cell line is a line of undifferentiated neurons originally derived from an immortalised clone of rat dopaminergic neurons by transfecting foetal mescencephalon cells with the plasmid vector $pSV3_{neo}$, which carries the LTa gene from the SV40 virus (Prasad et al., 1994). This cell line possesses both biochemical and physiological properties of dopaminergic neurons (Adams et al., 1996), making it an ideal candidate cell line for the modelling of the Parkinsonian dopaminergic neuronal cell death *in vitro*. In this thesis neuronal cell death was induced in this cell line with the use of the irreversible UPS inhibitor, lactacystin. Since the discovery that the UPS becomes dysfunctional in PD, UPS inhibitors such as PSI, epoxomycin, MG-132 and lactacystin have been used in attempt to generate animal models of PD. Lactacystin was first shown to induce neuronal cell death, *in vitro*, in PC12 cells, a catacholaminergic cell line, in 2001 (Rideout et al.). Subsequently, it has been shown extensively to recapitulate Parkinsonian dopaminergic neuronal cell death, *in vivo*, in rats (McNaught et al., 2002b, Niu et al., 2009, Vernon et al., 2010, Lorenc-Koci et al., 2011, Pienaar et al., 2013). Lactacystin covalently binds to catalytic subunits of the 20/26S proteosome, preventing accessibility of ubiquitinated proteins to the catalytic sites of UPS elements and therefore causes the cytoplasmic accumulation of unwanted proteins (McNaught et al., 2002b, McNaught et al., 2002c). This results in formation of ubiquitin/αSyn immunopositive inclusions in lactacystin treated dopaminergic neurons and subsequent neurodegeneration, both *in vitro* (McNaught et al., 2002c) and *in vivo* (McNaught et al., 2002b, Niu et al., 2009, Vernon et al., 2010, Lorenc-Koci et al., 2011, Pienaar et al., 2013). In this study, lactacystin is therefore used to model Parkinsonian neuronal cell death in the N27 cell line. Cell cultures were then treated with HDACIs to determine if the histone acetylation induced as a result of drug treatment was able to reduce/prevent the neuronal cell death observed by lactacystin.

The mouse microglial (N9) cell line was originally derived through oncogenic retroviral transformation of embryonic day 13 mouse microglial cells (Righi et al., 1989). N9 cells have been shown to be devoid of astrocytic and neuronal cell surface markers but stably retain microglial

phenotypic cell surface markers, and most importantly are stringently activated upon treatment with LPS (Righi et al., 1989) making them an ideal cell line for the study of microglial activation *in vitro*. LPS is found in the outer membrane of Gram-negative bacteria and acts as endotoxin capable of potent stimulation of microglia (Nakamura et al., 1999). When cultured and treated with LPS, primary microglia display a multi-faceted profile of activation: adopting an activated amoeboid morphology, upregulating pro-infammatory cytokines such as TNF-α, IL-6 and IL-1β, and activation of iNOS resulting in production of NO (Nakamura et al., 1999). LPS has therefore been used extensively for modelling the inflammatory profile of microglial activation in PD and has been used *in vivo* to induce microglial activation and subsequent nigral dopaminergic neuronal cell death to model inflammatory aspects of the disease in rats (Liu and Bing, 2011, Hoban et al., 2013). In this study, LPS is therefore used to model microglial activation in the N9 cell line. Cell cultures were then treated with HDACIs to determine if the histone acetylation induced as a result of drug treatment was able to reduce/prevent the microglial activation observed by LPS.

2.3.2 – Cell Culture Experiments

All *in vitro* experiments were carried out in ventilated sterile hoods (u.v. light irradiated and cleaned with 70% ethanol) with autoclaved or ethanol-sterilized equipment and latex gloves. Care was taken to ensure sterile conditions were maintained throughout the experimentation period by maintaining appropriate hood screen height and ventilation level. Incubators were cleaned monthly with 70% ethanol and water reservoirs replaced weekly with autoclaved water containing SigmaClean® Water Bath Treatment (Sigma). For experiments in 96 well plates, experimental conditions were conducted in triplicate, and repeated independently at least three times. For experiments in 6 well plates, experimental conditions were not replicated in each plate however experiments were repeated independently at least three times.

2.3.3 – N27 Neuronal Cell Line

N27 cells were maintained in 75cm^2 cell culture flasks (Corning, NY, USA) in RPMI 1640 medium (Sigma) supplemented with 10% foetal calf serum, 2mM L-glutamine, 50U/ml Penicillin and 50µg/ml Streptomycin (henceforth referred to as complete N27 medium) in a humidified incubator temperature controlled at 37°C and with 5% CO_2 ventilation. For experimentation, neurons were seeded into 6 or 96 well plates at densities of 500 and 10 x 10^3 cells/well respectively and left for 24hrs to allow neurons to readopt their natural morphology. On the day of experiments cell medium was removed and replaced with fresh complete N27 medium (2ml or 100µl per well for 6 well and 96 well plates respectively).

2.3.4 – N9 Microglial Cell Line

N9 cells were maintained in 75cm^2 cell culture flasks (Corning) in Dulbecco's Modified Eagle's Medium (Sigma) supplemented with 5% foetal calf serum, 4mM L-glutamine, 50U/ml Penicillin and 50µg/ml Streptomycin (henceforth referred to as complete N9 medium) in a humidified incubator temperature controlled at 37°C and with 5% CO_2 ventilation. For experimentation, microglia were seeded into 6 or 96 well plates at densities of 500 and 10 x 10^3 cells/well respectively and left for 24hrs to allow microglia to readopt their natural resting state morphology. On the day of experiments cell medium was removed and replaced with fresh complete N9 medium (2ml or 100µl per well for 6 well and 96 well plates respectively).

2.3.5 - Passaging/Seeding Cells

Once confluency was reached (around every 3-4 days) cells were passaged by trypsinisation (N27 cells) or scraping (N9 cells) for either seeding for experimentation or replatting for maintenance. Cell cultures were maintained up to a passage number 45 before being discarded.

2.3.5.1 - Trypsinisation of N27 Cells

Spent medium was removed from the flask and cells were washed with 5ml sterile Dulbecco's Phosphate Buffered Saline (DPBS) (Sigma) to remove any trypsin inhibitors found in the foetel calf serum in the culture medium. 5ml trypsin (Sigma) was then added to the flask and cells left to incubate for 2-3mins. After this time the flask was tapped strongly against the palm multiple times to detach all adherent cells. This cell suspension was collected and centrifuged at 1,200 x g for 5mins to pellet the cells. The supernatant was then removed and the cell pellet resuspended in warmed complete N27 medium. The number of viable cells in this suspension was then calculated by mixing 10µl of the suspension with 10µl of Trypan blue stain (Sigma) and manually counting the number of unstained (viable) cells within a 0.1µl volume of this mixture utilising a haemocytometer. Appropriate dilutions were made of the cell suspension in complete N27 medium to seed cells at the desired densities for experimentation (in either 6 or 96 well plates (Corning) at densities of 500 and 10 x 10^3 cells/well respectively). Seeded plates were returned to the incubator for 1hr to allow the cells to adhere to the well surface. Wells were then washed in warmed complete N27 medium to remove any dead/unadherant cells and appropriate volumes of medium replaced (2ml or 100µl per well for 6 well and 96 well plates respectively). Remaining cells not used for seeding plates were used to repopulate a new 75cm^3 flask and maintained as previously mentioned.

2.3.5.2 – Scraping of N9 Cells

Spent medium was removed from the flask and cells were washed twice with warmed complete N9 medium. 10ml of complete N9 medium was then added to the flask and cells scraped manually from the surface using a sterile cell scraper (VWR). The resulting cell suspension was then collected and centrifuged at 1,200 g for 5mins to pellet the cells. The supernatant was then removed and the cell pellet resuspended in warmed complete N9 medium. The number of viable cells in this suspension was then calculated by mixing 10µl of the suspension with 10µl of Trypan blue stain (Sigma) and manually counting the number of unstained (viable) cells within a 0.1µl volume of this mixture utilising a haemocytometer. Appropriate dilutions were made of the cell suspension in complete N9 medium to seed cells at the desired densities for experimentation (in either 6 or 96 well plates at densities of 500 and 10 x 10^3 cells/well respectively). Seeded plates were returned to the incubator for 1hr to allow the cells to adhere to the well surface. Wells were then washed in warmed complete N9 medium to remove any dead/unadherant cells and appropriate volumes of medium replaced (2ml or 100µl per well for 6 well and 96 well plates respectively). Remaining cells not used for seeding plates were used to repopulate a new 75cm^3 flask and maintained as previously mentioned.

2.3.6 - Freezing/Thawing Cells

In order to have a stock of cells with low passage number, cells were aliquoted and frozen. Once confluency had been reached in a 75cm^3 flask, cells were dislodged from the surface (by either trypsinisation (N27) or scraping (N9)) and collected as previously described. The cell pellet was resuspended in warmed complete medium and viable cells quantified using Trypan blue as also previously described. This cell suspension was then diluted with complete medium in the absence of antibiotics and with 10% dimethyl sulphoxide (DMSO) added, to give a final concentration of 200 x 10^3 cells/ml. 500µl of this cell suspension was aliquoted into freezing vials and placed into a cryopreservation freezing chamber at -20°C for 1hr before being placed at -80°C overnight and then moved to a liquid nitrogen store for long term storage.

Frozen cells were thawed by adding 200µl of warmed complete medium to the frozen aliquot and placing at 37°C for ~10mins. The vial was then vortexed and the cell suspension diluted in 10ml of warmed complete medium. This suspension was then centrifuged at 1,200 x g for 5mins and the DMSO containing medium removed. The cell pellet was then resuspended in 10ml warmed complete medium and incubated in a 25cm^2 flask until cells had recovered from the thawing procedure. Cells were then passaged as previously described and transferred to a 75cm^3 flask.

2.3.7 - MTS Assay

The MTS assay was used as an endpoint determination of the relative number of viable cells remaining in culture after incubation with toxins and/or HDACIs for varying time points. The MTS reagent (3-(4,5-dimethylthiazol-2-yl)-5-(3-carboxymethoxyphenyl)-2-(4-sulfophenyl)-2H-tetrazolium, inner salt) is a tetrazolium compound which is reduced by nicotinamide adenine dinucleotide phosphate (NADPH) or NAD+ produced by dehydrogenase enzymes in metabolically active cells (Berridge and Tan, 1993) to produce coloured formazan product (see figure 2.3). Therefore the spectrophotometric absorbance at 490nm is directly proportional to the number of metabolically active, viable cells remaining after the appropriate incubation period with the MTS reagent.

For performing the MTS assay the CellTiter 96® AQ_{ueous} One Solution Cell Proliferation Assay Kit (Promega, WI, USA) was used as per the manufacturer's instructions. Briefly, after incubation of cells with the test compound(s) for the appropriate time period in a 96 well plate in triplicate, 20µl of the CellTiter 96® AQ_{ueous} One Solution reagent was added directly to each well containing 100µl of cell culture medium. Plates were then incubated at 37°C in a humidified incubator temperature with 5% CO_2 ventilation for 3hrs. Absorbance was read using a 96-well plate reader (VersaMax Microplate Reader, Molecular Devices) at 490nm. The absorbance at 490nm (A_{490}) was then converted to % of control group and data expressed as mean ± standard error or mean (SEM).

2.3.8 - Neutral Red Assay

The neutral red (NR) assay was also used as an endpoint determination of the relative number of viable cells remaining in culture after incubation with toxins and/or HDACIs for varying time points. This assay, first described in 1983 (Parish and Mullbacher), is based on the ability of viable cells to incorporate and bind a supervital dye, NR (Repetto et al., 2008). At physiological pH, the dye is weakly cationic enabling it to passively penetrate the membrane of the cell and accumulate in the lysosome. Once inside, due to the proton gradient of the lysosome maintaining a pH lower than that of the cytoplasm, the dye becomes charged and is retained within the lysosome (see figure 2.4) (Repetto et al., 2008). The dye can then be extracted from viable cells using an acidified ethanol solution and the absorbance of the solubilised dye quantified spectrophotometrically at 540nm. The assay therefore depends on viable cells being able to maintain a pH gradient, consequently if the cell dies the pH gradient is reduced and the dye cannot be retained: the absorbance of the solubilised dye is therefore directly proportional to the number of viable cells

For performing the NR assay a previously published protocol was followed (Repetto et al., 2008). Briefly, NR stock solution (4mg/ml NR dye (Sigma) in DPBS) was dissolved into complete cell culture medium (either N9 or N27 depending on the cell line tested) to give a final concentration of

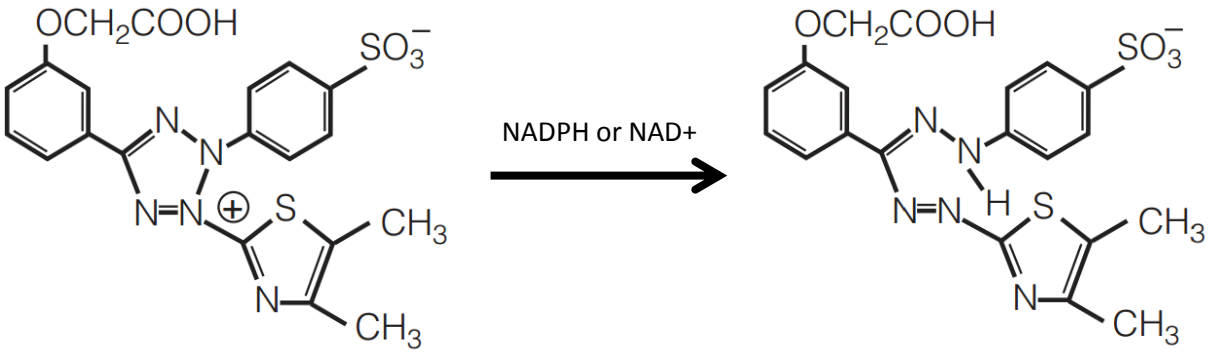

MTS ***Formazan***

Figure 2.3 – MTS Assay Chemistry
The MTS reagent is added directly to wells containing cells in which the viability is to be determined. NADPH or NAD+ produced by dehydrogenase enzymes in metabolically active cells reduces the MTS reagent to a coloured product, formazan, the concentration of which is then measured spectrophotometrically at 490nm.

40µg/ml NR (henceforth referred to as NR medium) and incubated at 37°C for 24hrs. To perform the assay, after incubation of cells with the test compound(s) for the appropriate time period in a 96 well plate in triplicate, the test medium was removed by aspiration and replaced with 100µl neural red medium. Plates were then incubated at 37°C in a humidified incubator temperature controlled at 37°C and with 5% CO_2 ventilation for 3hrs. After this time cells were inspected using an inverted microscope to confirm intracellular precipitation of NR. The NR medium was removed by aspiration from wells and cells washed by adding 150µl DPBS and removing by aspiration. 150µl of NR destain solution (50% ethanol, 49% water, 1% glacial acetic acid) was then added to wells before plates were shaken rapidly on a microtitre plate shaker for 10mins to solubilise the dye. Absorbance was read using a 96-well plate reader (VersaMax Microplate Reader, Molecular Devices) at 540nm. The absorbance at 540nm (A_{540}) was then converted to % of control group and data expressed as mean ± SEM.

2.3.9 - Bradford Assay

The NR assay was followed sequentially by determination of total protein content in the same well as an additional endpoint measure of relative cell viability using a variation of the Bradford assay (Arranz and Festing, 1990). The Bradford assay, originally developed by Marian M. Bradford (1976), relies on Coomassie Brilliant Blue G-250 in the Bradford reagent binding to protein causing an absorbance shift from 465nm to 595nm wavelength. In the context described here following the NR assay, cell containing wells are washed multiple times to remove dead cells before the remaining viable cells are lysed and their protein content solubilised. Bradford reagent is then added directly to this cell lysate in parallel to its addition to a set of standards of known protein concentration in order to translate the spectrophotometric absorbance at 595nm to protein concentration and therefore to the starting number of viable cells.

Briefly, after spectrophotometric reading of the wells for the NR assay, the neural red destain solution was removed from wells by aspiration before cells were washed three times with 150µl DPBS. Cells were then lysed and proteins solubilised by addition of 50µl sodium hydroxide (0.1M) solution. A set of protein standards was run in parallel with each plate by addition of 50µl sodium hydroxide (0.1M) solution to 5µl of a known concentration of protein (0 - 1.4mg/ml BSA in dH_20) run in triplicate. 200µl of Bradford reagent (Sigma) was then added to each well and plates were shaken rapidly on a microtitre plate shaker for 20mins. Absorbance was read using a 96-well plate reader (VersaMax Microplate Reader, Molecular Devices) at 595nm. A standard curve of the spectrophotometric reading at A_{595} for each standard, minus the reading for the standard void of protein was plotted against its protein concentration (see figure 2.2 for representative example).

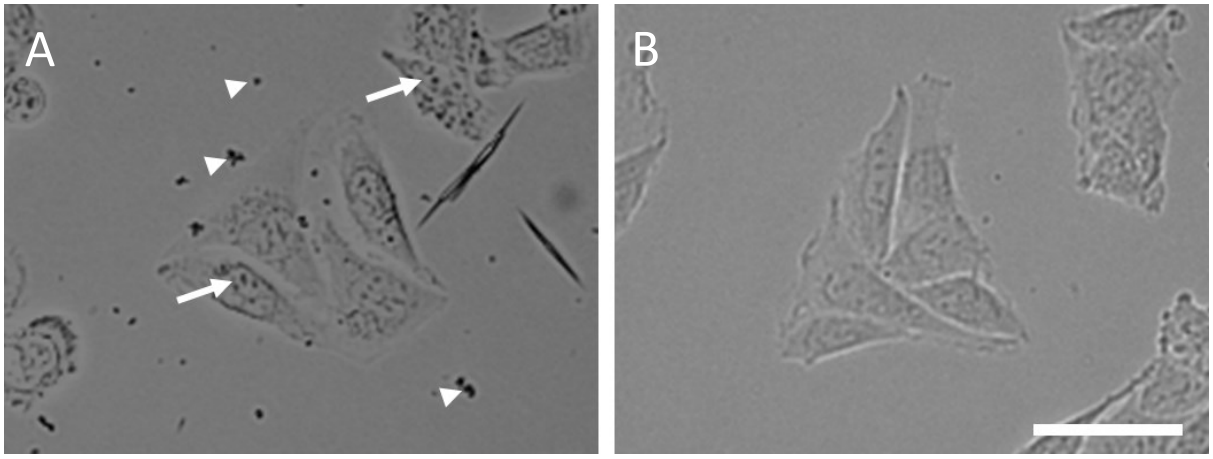

Figure 2.4 – Incorporation of Neutral Red into the Lysosomes of N27 Cells
Cultured N27 cells incubated with (A)/without (B) NR in the growth medium for 3hrs. Arrows designate incorporation of NR into the lysosome of cells indicating cell viability. Arrowheads designate NR crystals in the medium. Scale bar equal to 50µm.

The slope of the line of best fit of this data set was then used for calculation of the protein concentration for cell lysates. Data was then converted to % of control group and data expressed as mean ± SEM.

2.3.10 – Griess Assay

NO is a simple molecule with vast biological function. It acts not only as potent mediator of vasodilation but also as a neurotransmitter in the brain, and a key mediator in pathological defence (for review see Bredt and Snyder, 1994). As part of their function as resident immune modulators in the brain, upon their activation, microglia upregulate iNOS resulting in production of NO (Possel et al., 2000). NO is then available to react with ROS produced by the mitochondrial respiratory chain in the formation of neurotoxic peroxynitrites (Possel et al., 2000). NO has a short half-life in biological systems due to its auto-oxidation into two primary, stable and non-volatile metabolites: nitrite (NO_2^-) and nitrate (NO_3^-). The Griess assay, first developed by Peter Griess over 100 years ago (Griess, 1879) is a method of detection of one of these metabolites: nitrite. In this thesis this assay was therefore used as an end point determination of nitrite concentration in microglial cell cultures as indicator of NO production by upregulation of iNOS by microglia, and by extension, an indicator of microglial activation. The assay itself works on the principle that NO_2^- reacts with sulfanilamide in the Griess reagent to form a diazonium salt intermediate that subsequently reacts with N-1-napthylethylenediamine (NED) to form a coloured azo dye (see figure 2.5). The absorbance of this coloured compound can then be quantified spectrophotmetrically at 540nm.

For performing the Griess assay, after incubation of microglial cells with the test compound(s) for the appropriate time period in a 6 well plate, the medium was removed and centrifuged at 1,200 x g for 5mins to removed cell debris. 100µl of medium samples were pipetted into a 96 well plate in triplicate. In parallel, a set of standards of known nitrite concentration (0 - 50µM sodium nitrite in complete N9 medium) were run in triplicate in order to translate the spectrophotometric reading to nitrite concentration. 100µl of Greiss Reagent (Sigma) was then added directly to each well and plates were shaken rapidly on a microtitre plate shaker for 10mins. Absorbance was read using a 96-well plate reader (VersaMax Microplate Reader, Molecular Devices) at 540nm. A standard curve of the spectrophotometric reading at A_{540} for each standard, minus the reading for the standard void of nitrite was plotted against its nitrite concentration (see figure 2.6 for representative example). The slope of the line of best fit of this data set was then used for calculation of the nitrite concentration for medium samples and data expressed as mean ± SEM.

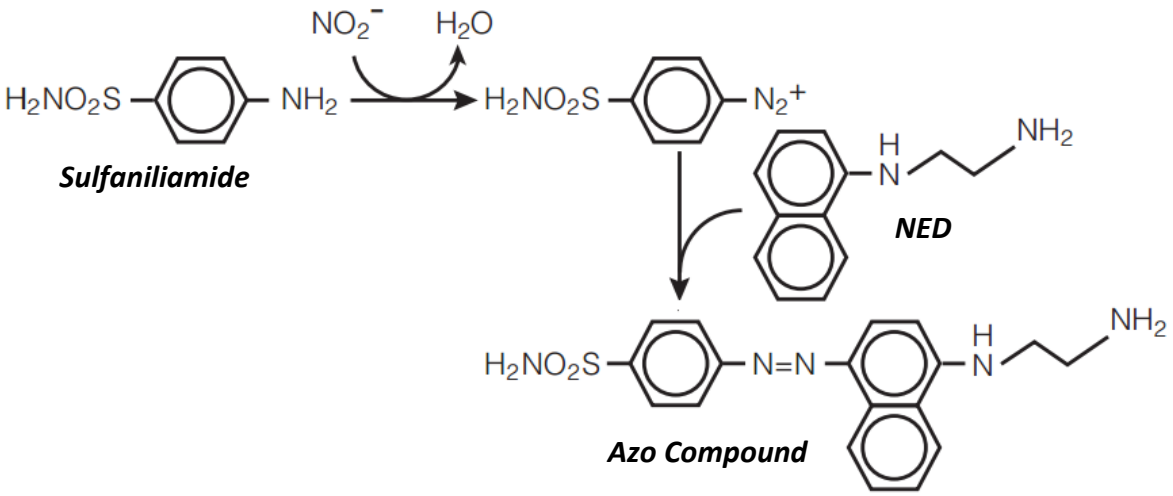

Figure 2.5 – Griess Assay Chemistry
One of the metabolites of NO, NO_2^- is quantified in the Griess assay by its primary reaction with sulfaniliamide in the Greiss reagent to for an intermediate. This then subsequently reacts with N-1-napthylethylenediamine dihydrochloride (NED) to form a coloured azo compound which is then measured spectrophotometrically at 540nm.

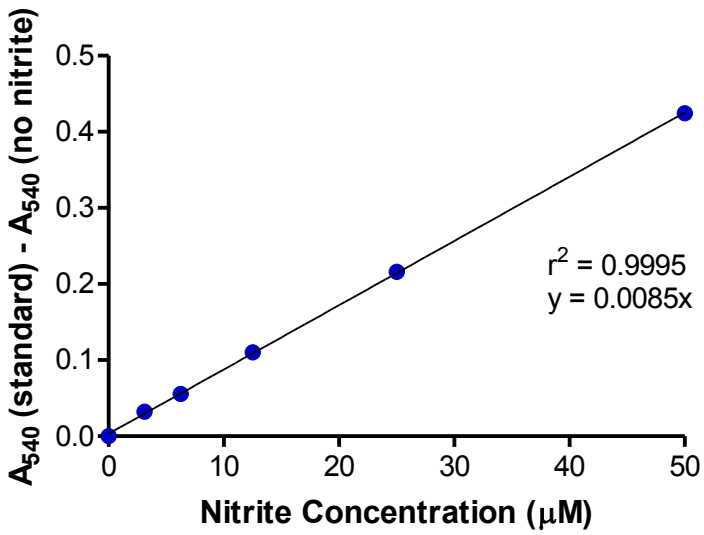

Figure 2.6 – Griess Assay Standard Curve
For each Griess assay plate a standard curve was constructed using solutions of known protein concentration (0 – 1.4mg/ml BSA in dH_2O) run in triplicate. The slope of the resulting line of best fit was used in order to translate the A_{540} for each sample into nitrite concentration. Nitrite standards were prepared by dissolving sodium nitrite into complete N9 medium. Standards were freshly prepared for each plate. Data presented as mean ± SEM, n=3.

2.3.11 – TNFα Enzyme-Linked Immunosorbent Assays

Enzyme-Linked Immunosorbant Assays (ELISAs) exploit the specificity of antibodies for a protein of interest to capture and detect the target protein. Amplification reaction steps in the sandwich format ELISA allow for efficient detection of minute amounts (pg/ml) of protein of interest (figure 2.7). In this thesis, in conjunction with Griess assays, ELISAs were used for the detection and quantification of TNFα, a pro-inflammatory cytokine secreted from microglial cell cultures as an indicator of microglial activation. Briefly, 96 well plates are firstly coated with a capture antibody which captures the protein of interest, here TNFα, from the cell culture medium sample. A biotinylated detection antibody is then added which then also binds to the protein of interest. The biotin signal from this antibody is then amplified by addition of an avidin-peroxidase conjugate, creating a complex with multiple peroxidase molecules. The conversion of the colourless 2,2'-azino-bis(3-ethylbenzothiazoline-6-sulphonic acid) (ABTS) substrate is catalysed by the peroxidase enzyme, resulting in a soluble green product which can be quantified spectrophotometrically.

For performing TNFα ELISAs, murine TNFα ELISA development kits (Peprotech Ltd., London, UK) were used as per the manufacturer's instructions. Briefly, the surface of a high binding EIR/RIA 96 well plate (Corning) was coated with the anti-TNFα capture antibody (1µg/ml in phosphate buffered saline (PBS)) overnight at RT. After this time, wells were washed four times in PBST (PBS with 0.05% Tween-20). Non specific binding was then blocked by incubating wells with PBS with 1% BSA for 1hr at RT. Wells were then washed again four times with PBST and incubated with either sample or standard (0 – 2ng/ml TNFα in PBS with 0.05% Tween-20 and 0.1% BSA) run in triplicate and incubated for 2hrs at RT. Wells were then washed again four times in PBST and incubated with anti-TNFα detection antibody (0.25µg/ml) for a further 2hrs at RT. Wells were washed again four times in PBST and incubated in avidin complex (1:2000 TNFα in PBS with 0.05% Tween-20 and 0.1% BSA) for 30mins at RT. Wells were then washed a final four times in PBST and 100µl of ABTS added to each well. Absorbance was read using a 96-well plate reader (VersaMax Microplate Reader, Molecular Devices) at 405nm and 650nm. Colour development was monitored for ~45mins and the reading in which the A_{405nm} was ≤0.2 for the 0ng/ml TNFα standard and ≤1.4 for the 2ng/ml TNFα as per the manufacturer's instruction. A standard curve of the spectrophotometric reading at A_{405} minus the reading at A_{650} was then plotted against TNFα concentration (see figure 2.8 for representative example). The equation of this line of best fit was then used for calculation of the TNFα concentration for medium samples and data expressed as mean ± SEM.

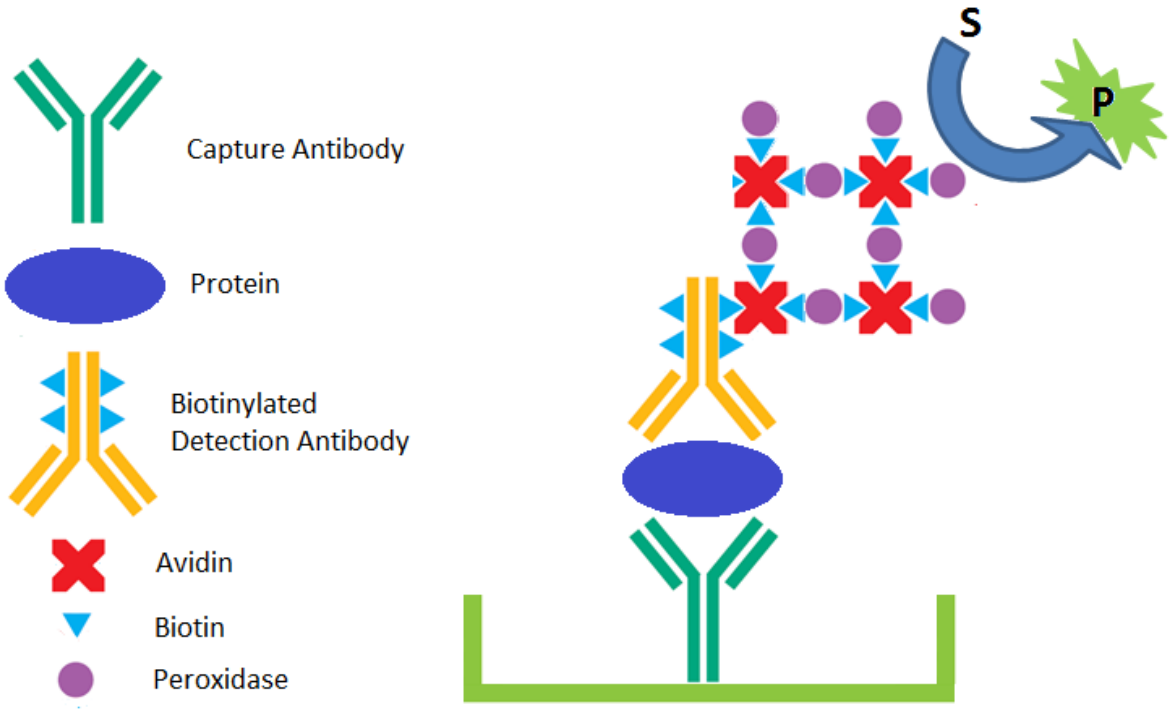

Figure 2.7 – Sandwich Format Enzyme-Linked Immunosorbant Assay
The well is firstly coated with a capture antibody specific to the protein of interest. The sample/standard is then added and the protein of interest binds directly to this capture antibody. A biotinylated detection antibody is then added which also binds to the protein of interest. The biotin signal on the capture antibody is then amplified by addition of the avidin-peroxidase conjugate, creating a complex with multiple peroxidase molecules. The conversion of the colourless 2,2'-azino-bis(3-ethylbenzothiazoline-6-sulphonic acid) (ABTS) substrate is catalysed by the peroxidase enzyme, resulting in a soluble green product which can be quantified spectrophotometrically at 405nm. Abbreviations: S, ABTS substrate; P, ABTS product.

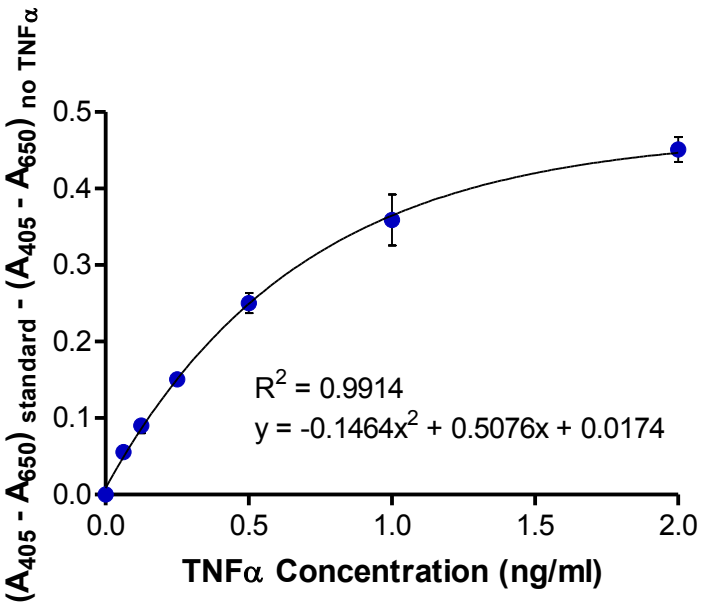

Figure 2.8 – TNFα ELISA Standard Curve
For each TNFα ELISA plate a standard curve was constructed using solutions of known TNFα concentration (0 – 2ng/ml in PBS with 0.05% Tween-20 and 0.1% BSA run in triplicate. The equation of the resulting line of best fit was used in order to translate the A405-A650 for each sample into TNFα concentration. Standards were freshly prepared for each plate. Data presented as mean ± SEM, n=3.

2.3.12 – Protein Extraction and Quantification

To determine the effects of cell culture treatments on the expression level of proteins of interest, cells were lysed and containing proteins solubilised for subsequent Western blot analysis (see section 2.5.4). For this Radio-Immunoprecipitation Assay (RIPA) buffer (Sigma) was used as per the manufacturer's instructions. Briefly, after incubation of cells with the test compound(s) for the appropriate time period in a 6 well plate, the growth medium was removed and cells were washed twice with ice cold DPBS to remove any residual medium. After this cells were incubated with RIPA buffer with 1% protease inhibitor cocktail (Sigma) (200µl/well) on ice for 5mins. Cells were then scraped manually from the surface using a sterile cell scraper (VWR) to remove and lyse residual cells. Cell lysate was collected and clarified to remove denatured nucleic acid by centrifugation at 8,000 x g for 10mins at 4°C. The protein containing supernatant was then transferred to new tubes and quantified using the Bradford assay (see figure 2.2.3.3). Proteins were then stored at -20°C until further Western blot analysis (see section 2.5.4).

2.4 - *In Vivo* Experiments

2.4.1 – Introduction

To assess the potential neuroprotective effects of HDACIs *in vivo*, an animal model of PD was utilised which recapitulates the formation of neurotoxic protein inclusions within the SNpc to cause progressive dopaminergic cell death via a mechanism similar to that observed in PD. This animal model was then systemically treated on a daily basis with differing doses of HDACIs to determine if the drugs used were able to delineate the course of the animal model of the disease, *in vivo*. Magnetic resonance imaging of the rat brain *in situ* and motor behavioural testing of the animals throughout each study were utilised to elucidate the temporal effects of HDACI treatment on brain structure and motor symptomology of the model.

In this thesis the lactacystin rat model was chosen to model PD for *in vivo* study. As has been previous described since the discovery of lactacystin's ability induce neuronal cell death, *in vitro*, in PC12 cells in 2001 (Rideout et al., 2001), it has been extensively used to recapitulate Parkinsonian dopaminergic neuronal cell death, *in vivo*, in rats (McNaught et al., 2002b, Niu et al., 2009, Vernon et al., 2010, Lorenc-Koci et al., 2011, Pienaar et al., 2013). By irreversibly inhibiting elements of the UPS, lactacystin causes the cytoplasmic accumulation of unwanted proteins including ubiquitin/αSyn immunopositive aggregates in nigral dopaminergic neurons when stereotaxically injected into the SNpc of rats (McNaught et al., 2002b, McNaught et al., 2002c). This intracellular accumulation results in progressive nigral neurodegeneration and subsequent progressive development of motor behavioural deficits. For example neurological scoring of lactacystin lesioned animals has previously been shown to gradually worsen post-lesioning: rats displaying progressive deficits in spontaneous motility and horizontal bar, grasping reflex and placing reaction tests (Vernon et al., 2010). Similarly lactacystin lesioned rats have also previously been shown to display deficits in forelimb grip strength, reduced performance on an accelerating rotarod and ostensible circling behaviour after apomorphine challenge (Vernon et al., 2010, Vernon et al., 2011). In this study, the lactacystin rat model was therefore used to model PD *in vivo* and subsequently treated with HDACIs to determine the effects of the drugs on the progression of the disease model.

2.4.2 - Experimental Animals

All animal procedures were carried out in accordance with the Home Office Animals (Scientific Procedures) Act, 1986 (PPL No.: 70/7398 held by Prof David Dexter; PIL No.: 30/8231 held by Mr Ian Harrison) and were previously approved by Imperial College London's Ethics Review Panel. Male Sprague-Dawley rats (250±10g, Charles River, UK) were housed in groups of two or three at 21±1°C

on a 12-hour light-dark cycle with relative humidity maintained at 55±10%. Standard rat chow and drinking water were available *ad libitum* throughout the duration of the study.

2.4.3 - Stereotaxic Lesioning of the Substantia Nigra in Rats

Prior to performing lactacystin lesioning of experimental animals, to test experimenter lesioning accuracy, the left SNpc of a group of male Sprague-Dawley rats (n=5) was stereotaxically lesioned with 6-OHDA using the same procedure detailed below. Lesioning accuracy was deemed acceptable given the development of amphetamine induced rotations in all animals (data not shown).

The left SNpc in male Sprague-Dawley rats was stereotaxically lesioned using the irreversible proteasome inhibitor, lactacystin. Animals were anaesthetised by inhalation of 5% isoflurane (IsoFlo®, Abbot Laboratories, Maidenhead, UK) vaporised into O_2 at a flow rate of 2l/min in an anaesthetic induction chamber. Once the animal was sufficiently anaesthetised as determined by the lack of a pedal pinch reflex response, it was moved to stereotaxic frame (Kopf Instruments, Tujunga, USA) and maintained under anaesthesia using a nose cone delivering 1-2% isoflurane vaporised into O_2 at a flow rate of 1.5l/min. The animal was positioned into the horizontal skull position (see figure 2.9A) by fitting non-traumatic ear bars into the ear canals of the animal and tightening the nose clamp with the incisor bar positioned at 3.3mm below the interaural line. Analgesia was administered in the form of buprenorphine (Vetergesic, Alstoe Animal Health, York, UK) injected intramuscularly in the femoral muscle (0.1ml/kg of 0.3mg/ml solution) and local anaesthesia was applied to the top of the head in the form of bupivacaine (Bupivicaine, Taro, Tipperary, Ireland) injected subcutaneously at four sites along the midline (0.02ml of 0.25% solution per site). Fluid replacement (glucosaline, 5ml of 0.18% NaCl, 4% Glucose, administered i.p.) was given prior to surgery as well as eye lubrication (Lacri-lube, Allergan, Buckinghamshire, UK) applied to the surface of the eyes to prevent their dehydration. A midline incision was made on the top of the head and the subcutaneous tissue was scraped away to reveal the surface of the skull. Bregma was identified (see figure 2.9B) and the location of the SNpc was identified with reference to it (coordinates in relation to bregma: anterio-posterior, -5.2mm, medio-lateral, +2.5mm, see figure 2.9C (Paxinos and Watson, 2009)). A small burr hole was made in the skull above the location of the SNpc using a microdrill. A Hamilton syringe was filled with 10µg of lactacystin (2.5µg/µl in sterile (0.9%) saline, total volume 4µl) and mounted onto the stereotaxic frame. The tip of the needle was placed on the surface of the brain and the needle was advanced ventrally to the location of the SNpc (coordinates in relation to bregma: ventral-dorsal, -7.6mm, see figure 2.9C (Paxinos and Watson, 2009)). The lactacystin was injected at a rate of 1µl/min and the needle left *in situ* for a further 3mins before being retracted slowly. The wound was sutured closed with 4 or 5 surgeons' knots

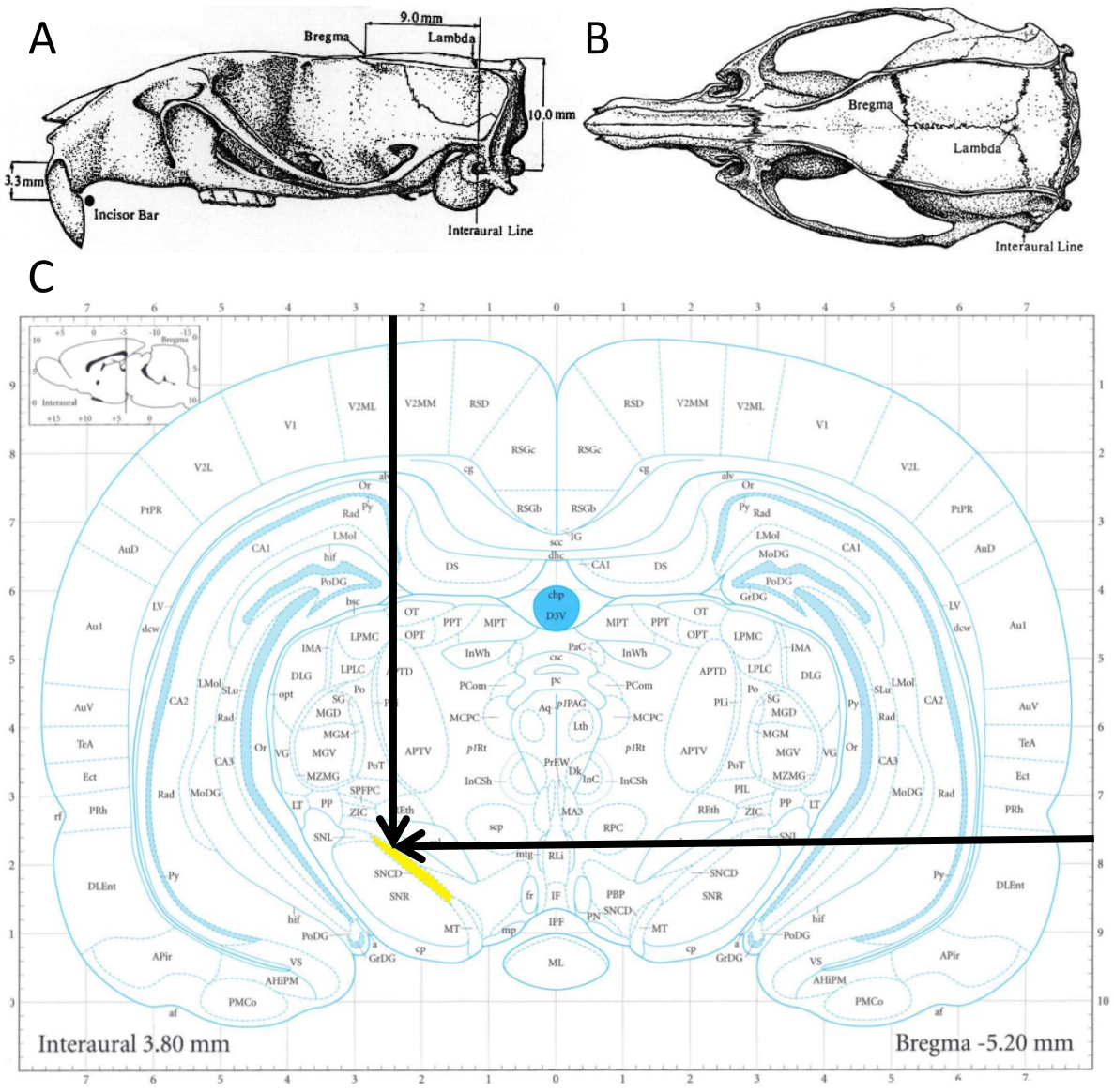

Figure 2.9 – Coordinates Used for Stereotaxic Lesioning of the Substantia Nigra pars compacta
(A) Horizontal positioning of the rat brain in the sterotaxic frame, defined by the incisor bar being positioned 3.3mm below the interaural line. (B) Top down view of the rat skull, indicating the location of bregma. (C) Stereotaxic coordinates used for injection into the left SNpc (yellow) (anterio-posterior, -5.2mm, medio-lateral, +2.5mm, ventral-dorsal, -7.6mm) (adapted from Paxinos and Watson, 2009).

using 4-0 polyamide suture material (Ethicon, New Jersey, USA). Animals were then removed from the stereotaxic frame and place in a heated recovery chamber until conscious. Fusiderm was then applied along the site of the sutures daily for 3 days following surgery to prevent infection and itching of the wound when healing. Sutures were removed once the wound had healed completely (~10days post-surgery). Standard rat chow was supplemented with wet diet for 5 days following surgery, and animal weight and general health was checked daily to ensure recovery. Animals were culled if post-surgical weight reached 80% of pre-surgical. Throughout the duration of all animal studies conducted here, two animals were culled on this basis.

2.4.4 - Behavioural Testing

Due to the unilateral lesioning of the SNpc of animals, two behavioural tests were employed to assess asymmetry in motor function. Animals were routinely handled in order to calm and enhance reliability when testing.

2.4.4.1 - Vertical Cylinder Test

To assess asymmetry in forelimb motor function the vertical cylinder test was employed (Schallert et al., 2000). Briefly, animals were placed into a Perspex cylinder (200mm diameter by 300mm height, see figure 2.10A) and rearing behaviour was recorded with a video camera for either ten complete rears or 3mins. Forelimb movements were examined using frame by frame analysis of video recordings. Forelimb use during each complete rear was analysed in terms of which forelimb the animal used to 'push-off', 'explore' and 'land'. 'Push-off' was defined as the independent use of either forelimb or simultaneous use of both forelimbs to push away from the base of the cylinder when rearing. 'Explore' was defined as the initial placement of either forelimb or simultaneous placement of both forelimbs on the walls of the cylinder. 'Land' was defined as the initial placement of either forelimb or simultaneous placement of both forelimbs on the base of the cylinder. The percentage of contralateral forelimb use was calculated as:

$$\boldsymbol{N} = \frac{(no.uses\ of\ contralateral\ forelimb + \tfrac{1}{2}\, no.uses\ of\ both\ forelimbs\ simultaneously) \times 100}{(no.uses\ of\ ipsilateral\ forelimb + contralateral\ forelimb + both\ forelimbs\ simultaneously)}$$

2.4.4.2 - Amphetamine Induced Rotation Test

Rotational asymmetry was assessed using the amphetamine induced rotation test (Ungerstedt and Arbuthnott, 1970). Briefly, animals were administered amphetamine (D-amphetamine sulphate (5mg/kg i.p.), Sigma) to induce rotational behaviour. Amphetamine competitively inhibits dopaminergic reuptake via the DAT (Fleckenstein et al., 2007), mediating reverse transport of dopamine into the synaptic cleft and also facilitates the movement of dopamine out of vesicles into

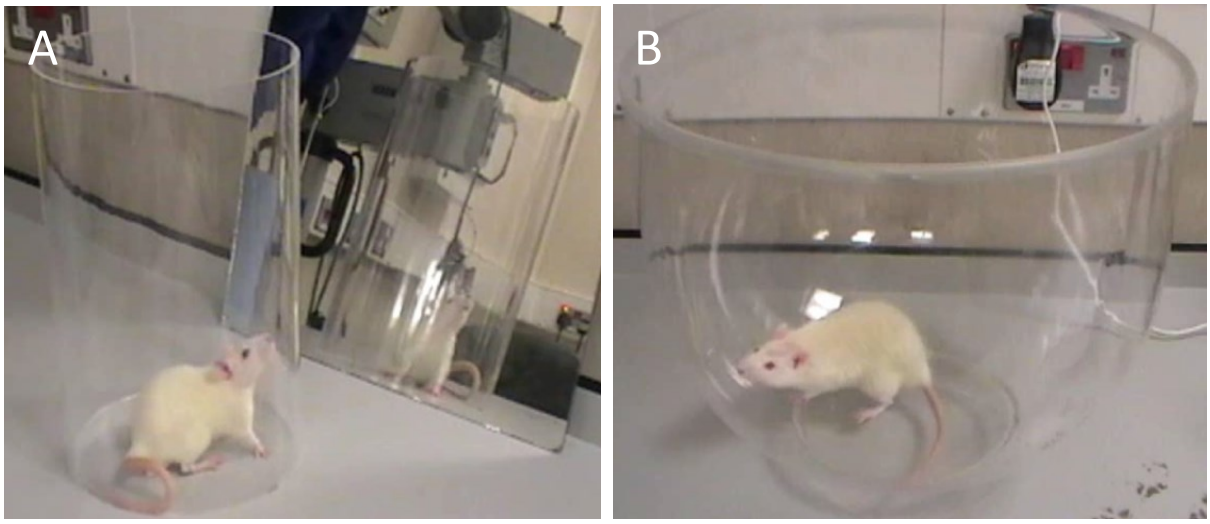

Figure 2.10 – Apparatus Used for Behavioural Testing
(A) For the vertical cylinder test animals were placed in a Perspex cylinder (200mm diameter by 300mm height) with a mirror positioned in order to observe forelimb movement when the animal was facing away from the camera. (B) For amphetamine induced rotations animals were injected with amphetamine (5mg/kg i.p.) to induce rotational behaviour and placed in a clear test arena (400mm diameter by 360mm height, Circling Bowl, Harvard Apparatus, USA) and recorded for 30mins.

the cytoplasm. This results in synaptic release of dopamine and therefore causes dopaminergic transduction to synapsed neurons. Due to the imbalance of dopaminergic neurons between hemispheres after lesioning, this causes rotational behaviour. Animals were therefore placed in a clear test arena (400mm diameter by 360mm height, Circling Bowl, Harvard Apparatus, USA, see figure 2.10B) for 30mins to acclimatise, after which time rotational behaviour was recorded for 30mins and the numbers of contraversive and ipsiversive rotations were counted in bins of 5 minutes. The net number of ipsiversive rotations per 5 minute bin was calculated as:

$$\boldsymbol{N} = (no.of\ ipsiversive\ rotations) - (no.of\ contraversive\ rotations)$$

The area under the curve produced by plotting N against time for the 30mins was then calculated as a measure of amphetamine induced rotational asymmetry.

2.4.5 - Magnetic Resonance Imaging of the Rat Brain

2.4.5.1 - Image Acquisition

T_2 weighted (T_2W) magnetic resonance images of the rat brain *in situ* were acquired using a 4.7 Tesla DirectDrive horizontal small bore magnetic resonance imaging (MRI) scanner (Varian, Palo Alto, CA, USA) and a separate 72mm quadrature birdcage head radiofrequency coil (M2M Imaging, OH, USA) linked to a Linux-based control console running Vnmrj acquisition software (v2.3, Varian, Palo Alto, CA, USA). Animals were anaesthetised by inhalation of 5% isoflurane (IsoFlo®, Abbot Laboratories, Maidenhead, UK) vaporised into O2 at a flow rate of 2l/min in an anaesthetic induction chamber. Once the animal was sufficiently anaesthetised as determined by the lack of a pedal pinch reflex response, it was moved to an MRI compatible polytetrafluroethylane (PTFE) bed (M2M Imaging, OH, USA) and maintained under anaesthesia using a nose cone delivering 1-2% isoflurane vaporised into O2 at a flow rate of 1.5l/min. Depth of anaesthesia was monitored using a respiratory balloon (SA Instruments, Stoney Brook, NY, USA) placed under the animal's chest and body temperature of the animal was monitored and maintained at 37°C using a rectal probe and heated fan (SA Instruments, Stoney Brook, NY, USA), respectively (see figure 2.11). The head of the animal was immobilised using a PTFE stereotaxic head holder after topical administration of Xylocaine Spray (Lidocaine, 10mg per ear) and EMLA cream within the ear canal for topical pain relief and displacement of air. Eye lubrication (Lacri-lube, Allergan, Buckinghamshire, UK) was applied to the surface of the eyes to prevent their dehydration. Scout images were firstly acquired to ensure correct positioning of the animal within the centre of the magnetic bore. T_2W images were then acquired using a multi-echo, multi-slice spin-echo pulse sequence (MEMS) previously designed for rat structural rat brain imaging by Dr. Marzena Wylezinska-Arridge (Biological Imaging Centre, Imperial College London), with the

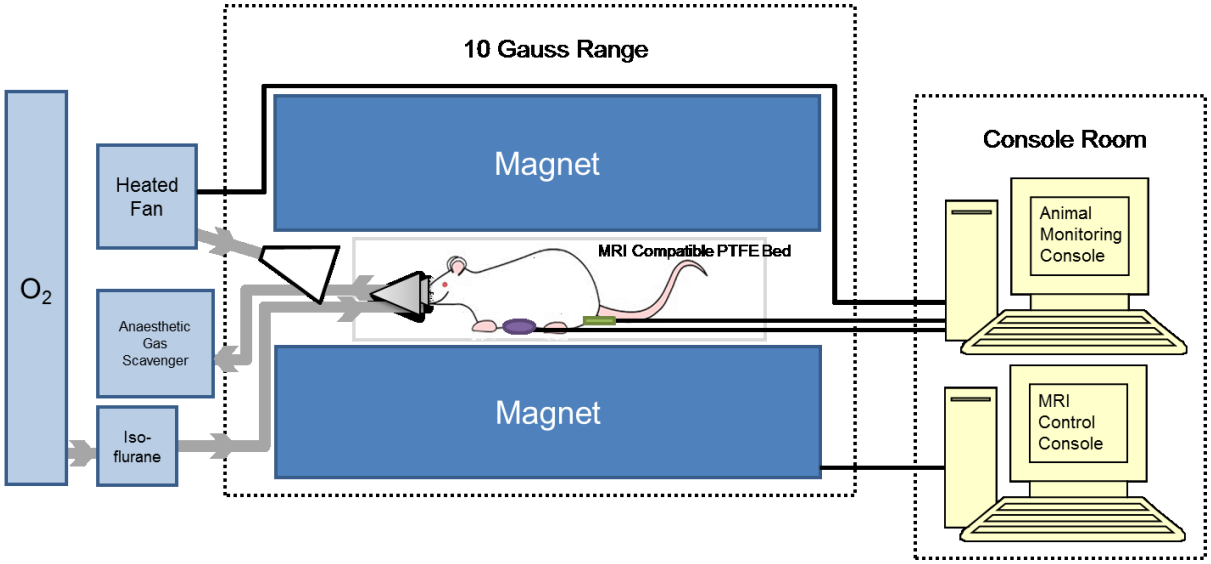

Figure 2.11 – MRI Scanner and Physiological Monitoring Equipment Setup
Animal was maintained under anaesthesia by positioning into an MRI compatible PTFE stereotaxic head holder and bed fitted with a nose cone delivering isoflurane vaporised into O_2. Depth of anaesthesia was monitored by placing a respiratory balloon (purple) under the animal's chest which was connected to the animal monitoring console in the console room. Delivery of isoflurane was adjusted (generally 1.5-2%) to maintain the respiratory rate at 60-70 breaths/min. Body temperature was monitored using rectal thermometer (green) connected to the animal monitoring console in the console room. Warm air was delivered to the magnetic bore (generally 35.5-37.5°C) to maintain the body temperature at 36.5-37.5°C. Physiological parameters were monitored throughout the scanning session and scanning was abandoned and the animal recovered if it showed any sign of physiological distress.

following scan parameters: FOV = 35 mm × 35 mm; matrix = 192 × 192; TR = 5155.2 ms; TE = 10, 20, 30, 40, 50, 60, 70, 80, 90, 100 ms; 4 averages, scan duration 1hr 5mins 59s. Fifty contiguous 0.5mm thick coronal slices with an in plane resolution of 256 × 256μm were acquired such that the entire brain of each animal was covered. Once scanning was completed, animals were removed from the magnetic bore to a heated recovery chamber. Following full recovery from anaesthesia, animals were returned to their home cages. Each animal received a maximum of four MRI scans spaced no less than 7days apart. Throughout the duration of all animal studies conducted here, two animals were culled due to physiological complications in the scanner.

2.4.5.2 - Image Post-Processing

Post-acquisition, magnetic resonance (MR) images were transferred from the console to a workstation and visually inspected for motion or intensity artefacts. No scans were excluded on this basis. Images corresponding to the ten TE times used (TE = 10, 20, 30, 40, 50, 60, 70, 80, 90, 100 ms) were summed using the "Z Project" function in ImageJ (v1.4, Rasband, U. S. National Institutes of Health, USA) before the fifty resulting images were stacked. Parametric T_2 relaxation maps from the fifty images were obtained using the "T_2 Calculation" function in the 'MRIAnalysisPak' plugin for ImageJ and the resulting fifty images were also stacked.

2.4.5.3 – Confirmation of Correct Needle Placement

To confirm that all of the lesioned animals received lactacystin to the left SNpc, MRI scans acquired at week 1 post-lesion were examined to confirm the location of stereotaxic injection of the toxin. The SNpc containing plate of the rat brain atlas (-5.2mm from bregma) was overlaid on the acquired T_2W MR image of the rat brain most resembling the size and shape of the brain in the atlas plate (figure 2.12). Accurate lactacystin lesioning was accepted if the needle tract was visible on the MR image (confirming anterio-posterior positioning) and the end of the needle tract was located above the left SNpc (confirming medio-lateral, and ventral-dorsal positioning).

2.4.5.4 – Manual Segmentation Analysis

For regional volumetric analysis, ImageJ software (v1.4) was used to manually delineate and measure the area of brain structures on T_2W MR images. Six brain regions (whole brain, lateral ventricles, corpus striatum, hippocampus, midbrain and cerebellum) were delineated based on anatomical landmarks previously described (Vernon and Modo, 2011) and with reference to the rat brain stereotaxic map (Paxinos and Watson, 2009) (see table 2.1 and figure 2.13). Volumes were then calculated by multiplying the sum of the areas for a given structure on all MR slices in which it appears, by the MR image slice thickness (0.5mm). Brain volumes were then expressed as a percentage change from each animal's baseline scan.

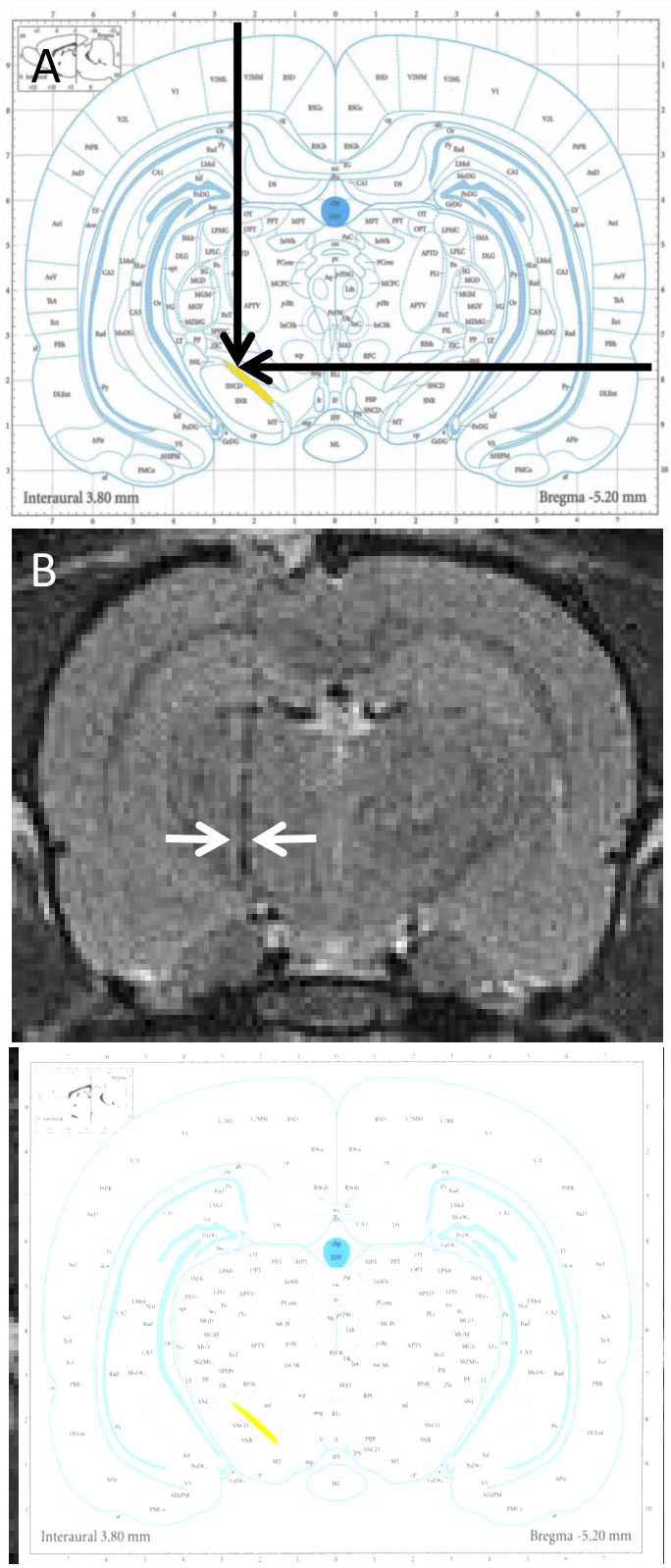

Figure 2.12 - Confirming Lesion Site Accuracy in Lactacystin Injected Animals
The SNpc containing plate of the rat brain atlas (A), was overlaid on the acquired T_2W MR image of the rat brain most resembling the size and shape of the brain in the atlas plate (B) in order to confirm lesion site accuracy in the left SNpc. (C) Accurate lactacystin lesioning was accepted if the needle tract was visible on the MR image (confirming anterio-posterior positioning) and the end of the needle tract was located above the left SNpc (confirming medio-lateral, and ventral-dorsal positioning).

Table 2.1 – Anatomical Criteria for Delineation of Brain Structures from MR Images
Description of anatomical landmarks and criteria used for the delineation of brain structure for manual segmentation analysis of MR images (anatomical reference taken from Vernon et al., 2010, Vernon et al., 2011, Paxinos and Watson, 2009). See figure 2.13 for further details.

Brain Region	Anatomical Criteria Used For Measurement
Whole Brain	Base of olfactory bulb to the last slice containing cortex
Lateral Ventricles	Defined from brain tissue by intense contrast of CSF
Corpus Striatum	Defined with reference to the corpus callosum, external capsule, anterior comissure and lateral ventricles
Midbrain	Defined with reference to dorsal hippocampal formation
Hippocampus	Defined with reference to corpus callosum and external capsule
Cerebellum	Defined with reference to fourth ventricles and brainstem as a guide

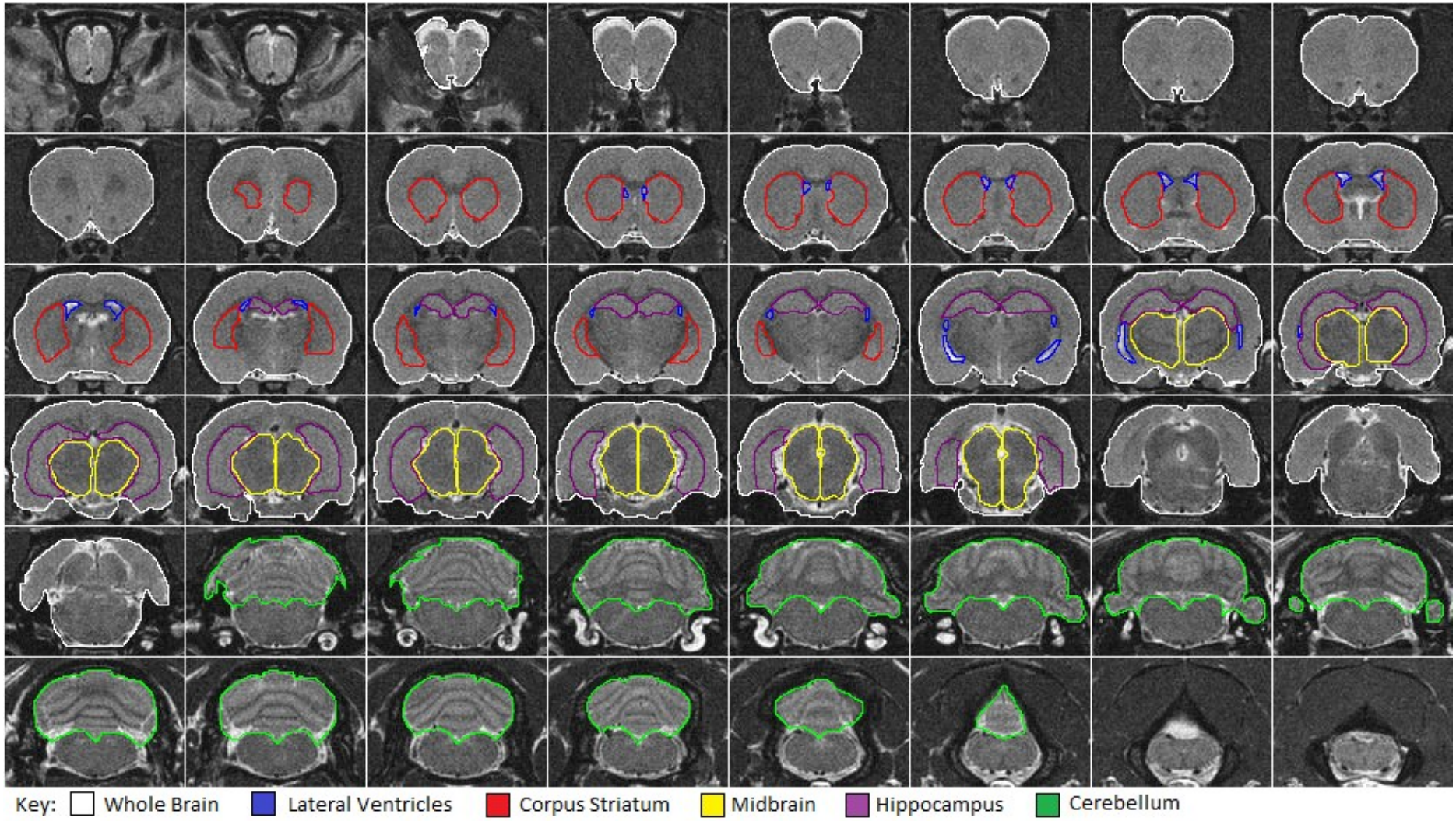

Figure 2.13 – Volumetric Manuel Segmentation Analysis of the Rat Brain from Magnetic Resonance Images.
Representative MR images of the brain of a suigically naïve rat used for volumetric manual segmentation analysis, indicating the delineation of six brain structures: whole brain, lateral ventricles, corpus striatum, hippocampus and cerebellum. See table 2.1 for anatomical criteria used (anatomical reference taken from Vernon et al., 2010, Vernon et al., 2011, Paxinos and Watson, 2009).

2.4.5.5 – Tensor Based Morphometry

The number of regions that can be studied using manual segmentation analysis is limited by the ability of the operator to reliably define anatomical boundaries using the inherent tissue contrast in the image. In addition, whilst manual segmentation can be robust and informative it is subject to operator bias, relatively insensitive to subtle anatomical changes and lacks sub-regional specificity. In contrast Tensor Based Morphometry (TBM) is an automated image analysis tool which allows unbiased detection of changes in individual voxels across the whole brain (Crum et al., 2013a, Kielar et al., 2012, Hua et al., 2008). Therefore in collaboration with Drs Anthony Vernon and William Crum at King's College London, T_2W images were also analysed using an automated TBM pipeline (Crum et al., 2013a). Briefly, a single, well-positioned good-quality control animal scan was chosen as an initial reference for rigid (6 degrees of freedom) and rigid + scaling (9 degrees of freedom) registration using a robust population approach (Crum et al., 2013b). Then, a template image was constructed as the mean of the registered control group scans and used as the reference in subsequent processing. High-dimensional non-rigid registration was applied to each scan to warp it onto the control template, and thereby obtain maps of apparent local volume difference for each scan, encoded as the Jacobian determinant at each voxel (Crum et al., 2013a). Non-parametric t-tests at each voxel were used to detect differences in the Jacobian determinants between each study group and the control group and thereby infer differences in volume across groups (Bullmore et al., 1999). Significance values were corrected for multiple comparisons using the False Discovery Rate with q=0.05 (Genovese et al., 2002).

2.4.5.6 – Measurement of T_2 Relaxivity

For T_2 relaxivity measurements the stack of fifty T_2W MR images was synchronised with the corresponding stack of fifty T_2 relaxivity maps such that signal intensity values for T_2 from T_2 relaxivity maps could be measured using T_2W images as anatomical reference. T_2 relaxivity values were determined in the corpus striatum and midbrain in both the ipsilateral and contralateral hemispheres using the same anatomical landmarks and with reference to the stereotaxic brain map as mentioned above (see table 2.1 and figure 2.13). Due to the poor resolution of MR images the SNpc could not be delineated manually. Therefore T_2 relaxivity was measured in the SNpc by placing a square region of interest of area 1.35mm^2 over the area approximate to the SNpc for each SNpc containing slice using the corresponding T_2W image and the rat stereotaxic brain map as reference (see figure 2.14). All T_2 relaxivity measurements were expressed as the ratio between the ipsilateral and contralateral hemisphere: the T_2 signal intensity ratio.

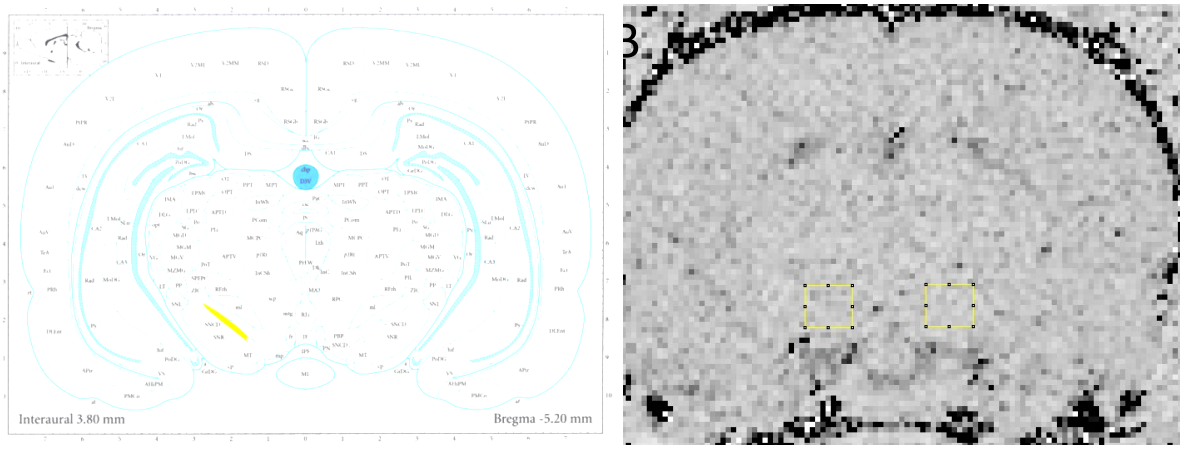

Figure 2.14 – Measurement of T_2 Relaxivity in the Substantia Nigra

Due to the poor resolution of the MR images, instead of manual delineation, a square region of interest (1.35mm^2) was placed over the area approximate to the SNpc using the corresponding T_2W image and the rat stereotaxic brain map as reference. (A) Representative T_2W image of the rat brain at the level of the SNpc (~-5.2mm from bregma) with regions of interest placed over the area approximate to the SN. (B) Synchronised corresponding T_2 relaxivity map from which measurements were taken (anatomical reference taken from Paxinos and Watson, 2009).

2.4.5.7 – Image Analysis Reliability Validation

To ensure that manual scan analysis was performed with consistent accuracy, a single scan was chosen at random and manually analysed (manual segmentation analysis and measurement of T_2 relaxivity) five times by a single rater for assessment of intra-rater reliability. Each result was plotted in terms of its percentage deviation from the mean of all five analyses, to provide a graphical illustration of intra-rater reliability (see figure 2.15). The standard deviation of these values, otherwise known as the Coefficient of Variation (CV), were all below the threshold of 5% indicative of robustly reliable manual segmentation and measurement of T_2 relaxivity by the single rater (see table 2.2). To confirm these findings statistically, an intra-class correlation coefficient (ICC) was also calculated for each set of five results. An ICC of ≥0.99 was observed in all datasets.

2.4.6 – Tissue Collection and Preparation

At the end of the each study period, animals were sacrificed according to Home Office Schedule 1 procedures using inhalation of CO_2. Animals were decapitated and the brain quickly dissected out of the skull onto ice. Using a rodent brain matrix, each brain was cut coronally at ~-4.16mm from bregma (Paxinos and Watson, 2009) at the level of the infundibular stem to produce forebrain and hindbrain blocks containing the frontal cortex and SNpc respectively. Frontal brain tissue was snap frozen on dry ice and stored at -80°C prior to mRNA and protein extraction (see section 2.4.7) and subsequent qRT-PCR (see section 2.5.3) and Western blot (see section 2.5.4) analysis respectively. The hindbrain block was firstly fixed by incubation in 4% paraformaldehyde in PBS (pH7.4) for 72hrs at 4°C before being cryoprotected by incubation in 30% sucrose in PBS until the tissue was observed to have sunk. Blocks were then snap frozen in isopentane pre-chilled on dry ice and stored at -80°C for subsequent immunohistochemical analysis (see section 2.5.2).

2.4.7 - mRNA and Protein Extraction and Quantification

RNA and protein from 30mg samples of rat frontal brain tissue were sequentially extracted using the RNeasy® Plus Universal Mini Kit (Qiagen, Crawley, UK) as previously described in section 2.2.3. After quantification, mRNA and protein samples were stored at -80 and -20°C respectively for subsequent qRT-PCR (see section 2.5.3) and Western blot (see section 2.5.4) analysis.

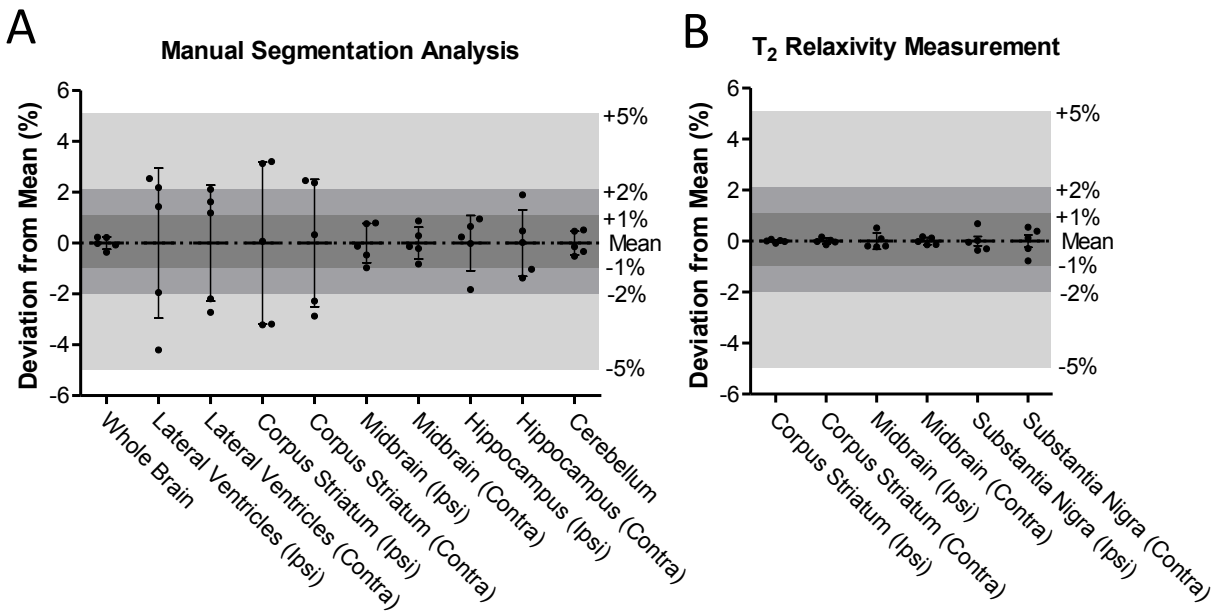

Figure 2.15 – Magnetic Resonance Image Analysis Reliability Validation
(A) Intra-rater reliability validation of manual segmentation analysis of rat brain MR images. (B) Intra-rater reliability validation of T_2 relaxivity analysis of brain MR images. The CV value for each brain structure is below the threshold of 5% indicative of robustly reliable segmentation and measurement of T_2 relaxivity by the single rater.

Table 2.2 – Magnetic Resonance Image Analysis Reliability Validation

Intra-rater reliability validation of manual segmentation and T_2 relaxivity measurement analysis of rat brain MR images. (The CV value for each brain structure is below the threshold of 5% indicative of robustly reliable segmentation and measurement of T_2 relaxivity by the single rater. Abbreviations: Ipsi, ipsilateral; Contra, contralateral; μ, mean; σ, standard deviation; CV, coefficient of variation; ICC, intra-class correlation coefficient.

	μ	σ	%CV (σ/μ)		ICC
Manual Segmentation Analysis					
Whole Brain	1569.957	3.820845	0.243373	**	≥0.99
Lateral Ventricles (Ipsi)	2.487815	0.073312	2.946838	*	≥0.99
Lateral Ventricles (Contra)	2.115199	0.04817	2.277328	*	≥0.99
Corpus Striatum (Ipsi)	70.76143	2.253864	3.185159	*	≥0.99
Corpus Striatum (Contra)	64.14539	1.610684	2.510989	*	≥0.99
Midbrain (Ipsi)	57.10785	0.441424	0.772966	**	≥0.99
Midbrain (Contra)	57.57048	0.362582	0.629806	**	≥0.99
Hippocampus (Ipsi)	56.04614	0.610481	1.089247	*	≥0.99
Hippocampus (Contra)	52.13673	0.67881	1.30198	*	≥0.99
Cerebellum	273.8156	1.29047	0.471292	**	≥0.99
T_2 Relaxivity Measurement					
Corpus Striatum (Ipsi)	0.902329	0.000529	0.058587	***	≥0.99
Corpus Striatum (Contra)	0.896312	0.001018	0.113525	**	≥0.99
Midbrain (Ipsi)	0.47492	0.001501	0.316155	**	≥0.99
Midbrain (Contra)	0.470919	0.000669	0.141992	**	≥0.99
Substantia Nigra (Ipsi)	0.481655	0.001993	0.413882	**	≥0.99
Substantia Nigra (Contra)	0.482868	0.002585	0.53534	**	≥0.99

2.5 – Cellular and Molecular Analyses

2.5.1 - Introduction

To investigate the histone acetylation profile and expression levels of HDACs in human PD, as well as assess the neuroprotective effects of HDACIs on a molecular and cellular level within the animal models of PD used here, numerous molecular and cellular biological techniques were used. Firstly, in order to quantify the amount of dopaminergic cell loss and neuroprotection associated with lactacystin lesioning and HDACI treatment in animal studies, the dopaminergic neurons within the SNpc were directly quantified in rat brains. For this the brains of animals which were removed at the end of each study were cryosectioned, immunohistochemically stained and the number of dopaminergic neurons within the SNpc stereologically counted. In addition to this, as previously described, mRNA and protein were extracted from human brain tissue samples, rat brain tissue samples and cell culture systems, for quantification of the expression of genes and proteins of interest. For gene expression analysis, RNA was first converted to complementary DNA (cDNA), and quantitative real-time polymerase chain reactions used to assess the relative expression of numerous neuroprotective proteins thought to change upon treatment with HDACIs as well as the level of HDACs themselves. Correspondingly, Western blot analysis was used to quantify the level of histone acetylation directly in extracted protein samples.

2.5.2 – Immunohistochemical Staining of the Rat SNpc

Cells were immunohistochemically labelled for either tyrosine hydroxylase (TH) or MHC Class II RT1B (clone OX6) (OX6). TH is the rate limiting enzyme in monoamine synthesis and it is therefore used here to stain dopaminergic neurons in the SNpc since this is the only population of monoaminergic neurons within this nucleus. In SNpc containing sections however the ventral tegmental area (VTA) is also present which is dopaminergic. Therefore for quantification of dopaminergic TH positive neurons specifically in the SNpc defined boundaries were employed to delineate it from the adjacent VTA (Carman et al., 1991) (see section 2.5.2.3). The OX6 clone of MHC Class II however is a marker specific to activated microglia in the brain (Ogura et al., 1994). It is therefore used here to stain activated microglia present in the SNpc of rats. In addition to immunohistochemical staining, tissue sections were counterstained with cresyl violet to stain the Nissl body present in all neurons. This stain was performed and quantified in conjunction with quantification of TH immunopositive cells to confirm neuronal cell loss as opposed to potential loss of TH expression.

2.5.2.1 – Crysectioning

Following removal of the hindbrain from rats, the tissue was fixed, cyroprotected, snap frozen and stored at -80°C for subsequent immunohistochemical analysis. Prior to cryosectioning, hindbrain

tissue was embedded in Optimal Cutting Temperature compound and equilibrated to -22°C in a cryostat (Bright Instruments, UK) for 1hr. 30µm-thick coronal sections of the hindbrain block were then cryosectioned and collected throughout the extent of the SNpc (-4.8 to -6.3mm from bregma) (Paxinos and Watson, 2009), and thaw mounted onto SuperFrost® Plus slides (VWR). Slides were then stored at -80°C until immunohistochemically stained.

2.5.2.2 – Immunohistochemistry

For immunohistochemistry, the Avidin-Biotin Complex (ABC)/peroxidase method of immunohistochemistry was used (see figure 2.16) (Key, 2009). Firstly, tissue sections were brought to RT and left to thaw, dry and anneal onto the slides for approximately 2hrs. Due to post-fixation of brain tissue, sections had a very high level of endogeneous peroxidase activity. To block this, sections were incubation in 0.3% H_2O_2 stabilised in either methanol (TH) or PBS (OX6) for 45mins. Sections were then rehydrated in a descending series of alcohol washes (100%, 100%, 90%, 70% and 50% ethanol in dH_2O) followed by dH_2O and then PBSTX (PBS with 0.1% Triton-X), each for 5mins. Non-specific antibody binding was then blocked by incubation with either 20% normal goat serum (TH) or 20% normal horse serum in PBSTX for 1hr at RT before incubating the sections with the primary antibody, either Rabbit Polyclonal Anti-TH (1:1000, Millipore, MA, USA) or Mouse Monoclonal Anti- MHC Class II RT1B**,** clone OX6 (1:1000, Serotec, Oxford, UK) in PBSTX for 24hrs at RT. Sections were then washed in PBSTX (3 x 5min washes) and incubated in the secondary antibody, either Biotinylated Goat Anti-Rabbit Secondary Antibody (TH) or Biotinylated Horse Anti-Mouse Secondary Antibody, (VectorLabs, Perteborough, UK) at 1:200 in PBSTX for 1hr at RT. Sections were then washed again (PBSTX, 3 x 5min washes) and incubated in ABC (Vectastain Elite ABC Kit, VectorLabs) for a further 1hr at RT. Sections were then washed thoroughly in Tris-Buffered Saline (TBS) (pH8.4) (3 x 5min washes). Primary antibody binding was then visualised by incubating tissue sections with 3,3'-Diaminobenzidine (DAB) (DAB peroxidase substrate kit, VectorLabs). When the DAB colour development was deemed sufficient (visualised microscopically, ~5min incubation), the reaction was stopped by washing sections in dH_2O before sections were counterstained using cresyl violiet. For this slides were incubated in cresyl violet solution (0.1% in dH_2O) for 3mins. Sections were then washed thoroughly in dH_2O before being differentiated and dehydrated in an ascending series of alcohol washes (70%, 90%, 100% and 100% ethanol in dH_2O) followed by two washes of xylene. Sections were then mounted under cover slips using DPX. See figure 2.17 for example of TH immunohistochemical staining.

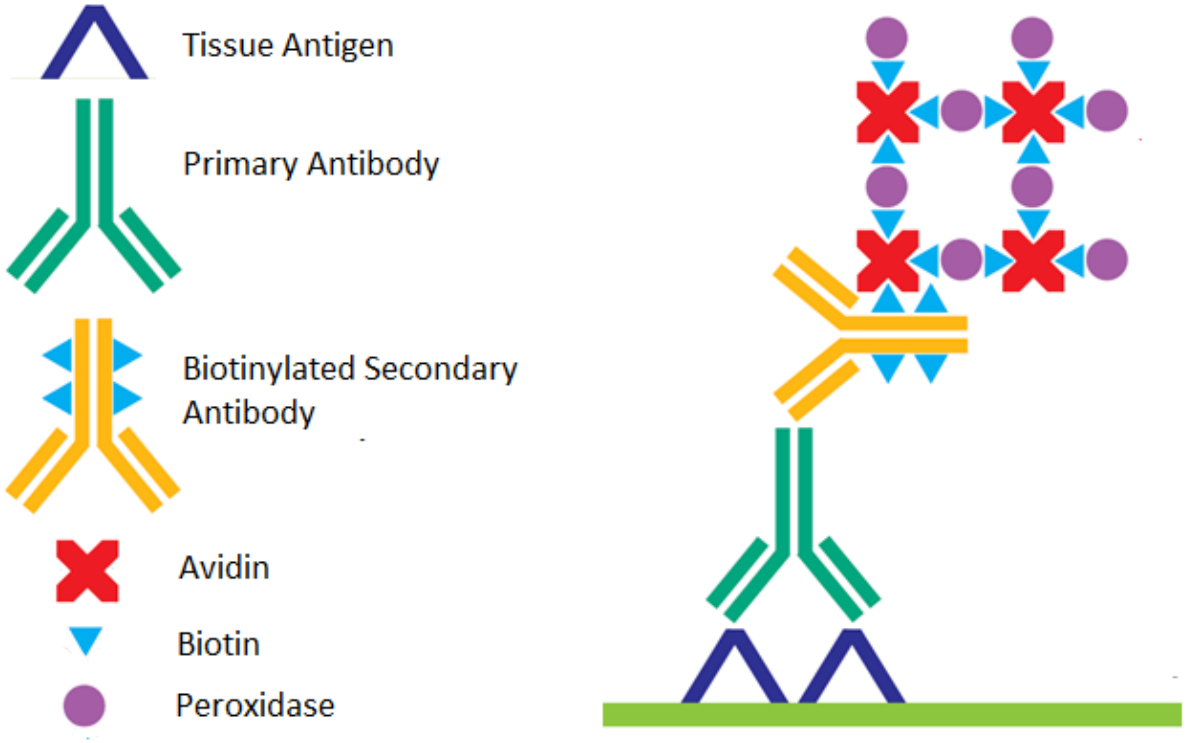

Figure 2.16 - Avidin-Biotin Complex/Peroxidase Immunohistochemistry
The presence of the tissue antigen is firstly detected by the primary antibody which becomes tightly bound to its target epitope. The secondary antibody is then added which binds to the Fc region of the primary antibody forming a complex. The biotin signal on the secondary antibody is them amplified by addition of the avidin-biotin complex (ABC), creating a complex with multiple peroxidase molecules. The peroxidase activity of the ABC is then used to catalyse the conversion of 3,3'-Diaminobenzidine (DAB) to a brown insoluble DAB precipitate, hence labelling the tissue antigen (adapted from Key, 2009).

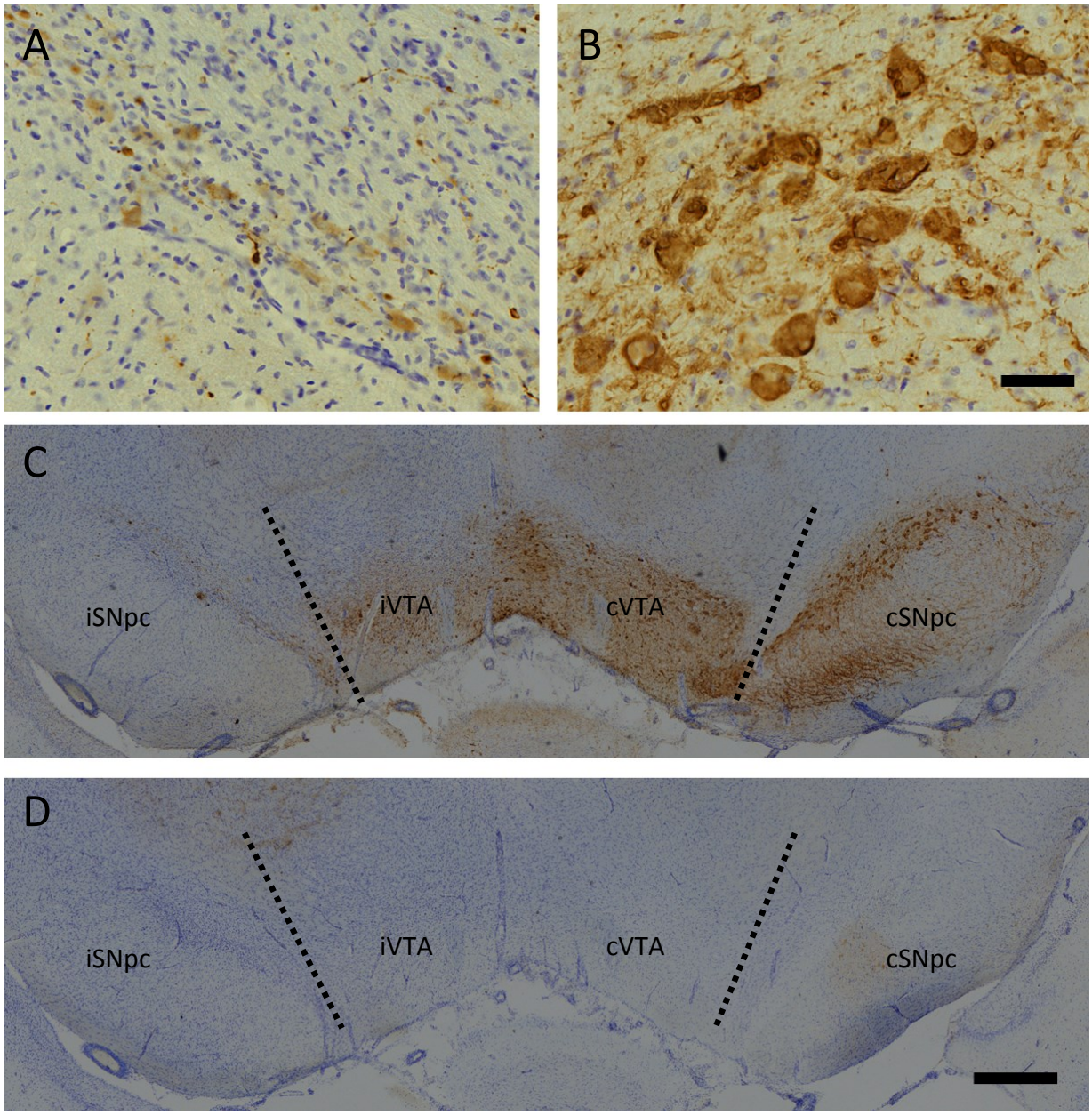

Figure 2.17 – Tyrosine Hydroxylase Immunohistochemistry in the Rat SNpc
Representative images of TH immunoreactivity in the rat SNpc. (C) Image of the ipsilateral and contralateral SNpc (iSNpc and cSNpc respectively) with the ipsilateral and contralateral VTA (iVTA and cVTA respectively) included. (A and B) High magnification images show close up examples of TH immunopositive cells in the SNpc of both hemispheres. (D) Negative control section consecutive to that shown in (C) which was stained with the same protocol but not incubated with TH primary antibody. Low magnification images taken at x4 magnification, scale bar equal to 50µm. High magnification images taken at x20 magnification, scale bar equal to 500µm.

2.5.2.3 - Stereological Cell Quantification of Dopaminergic Neurons in the SNpc

To quantify the number of TH positive (TH+) and Nissl positive (Nissl+) cells in the SNpc of rat brains, the unbiased optical fractionator method of stereological cell quantification was used as previously described (West et al., 1991). For this, a computer based stereology software system (ImagePro, MediaCybernetics, PA, USA) attached to a Nikon Eclipse E8—microscope (Nikon Instruments, Surrey, UK) and JVC 3CCD camera (JVC, London, UK) was used. Nissl+ neurons were identified by their pyramidal shape and blue intracellular Nissl body staining with a visible nucleus. TH+ neurons were identified by their brown immunopositive cell body and pyramidal shape with a visible nucleus Stereological estimates of cell numbers were made in all five previously published stereotaxic regions of the rat SNpc, defined as A-E (-4.8, -5.3, -5.6, -5.8 and -6.3mm from bregma respectively) (Carman et al., 1991). Briefly, of every sixth section, a tiled image was taken at x4 magnification, and the ipsilateral and contralateral SNpc were delineated manually with reference to previously published boundaries, to create areas of interest (AOI) (see figure 2.18A). Using the uniform systematic random sampling method with a sampling fraction of 2, the computer system then placed counting frames (140 x 160µm) across the entirety of the AOI. The numbers of TH+ and Nissl+ cells in each of the placed counting frames were then counted at x10 magnification. To avoid edge effects, "acceptance" and "forbidden" lines were used: cells crossing either the north or east borders were included in the count, whereas cells crossing either the south or west borders were excluded from the count (see figure 2.18B). The height of the optical dissector was also then calculated for each section, by measuring the average height of the counted optical plane relative to the section thickness using a Heidenhain microcator (Heidenhain, Traunreut, Germany). For each section the number of TH+ and Nissl+ was then calculated using the following equation:

$$\boldsymbol{N} = \boldsymbol{n}\left(\frac{\mathbf{1}}{\boldsymbol{ssf}}\right)\left(\frac{\mathbf{1}}{\boldsymbol{asf}}\right)\left(\frac{\mathbf{1}}{\boldsymbol{hsf}}\right)$$

Where:

$\boldsymbol{N} = total\ estimated\ number\ of\ cells\ for\ series\ of\ 6\ sections$

$\boldsymbol{n} = total\ number\ of\ counted\ cells$

$\boldsymbol{ssf}\ (\boldsymbol{section\ sampling\ fraction}) = {}^{1}/_{6}$

$$\boldsymbol{asf}\ (\boldsymbol{area\ sampling\ fraction}) = \frac{area\ of\ counting\ frame\ (22400\mu m^2) \times no.of\ frames\ counted}{area\ of\ AOI\ (\mu m^2)}$$

$$\boldsymbol{hsf}\ (\boldsymbol{height\ sampling\ fraction}) = \frac{height\ of\ counted\ optical\ plane\ (\mu m)}{total\ height\ of\ tissue\ section\ (\mu m)}$$

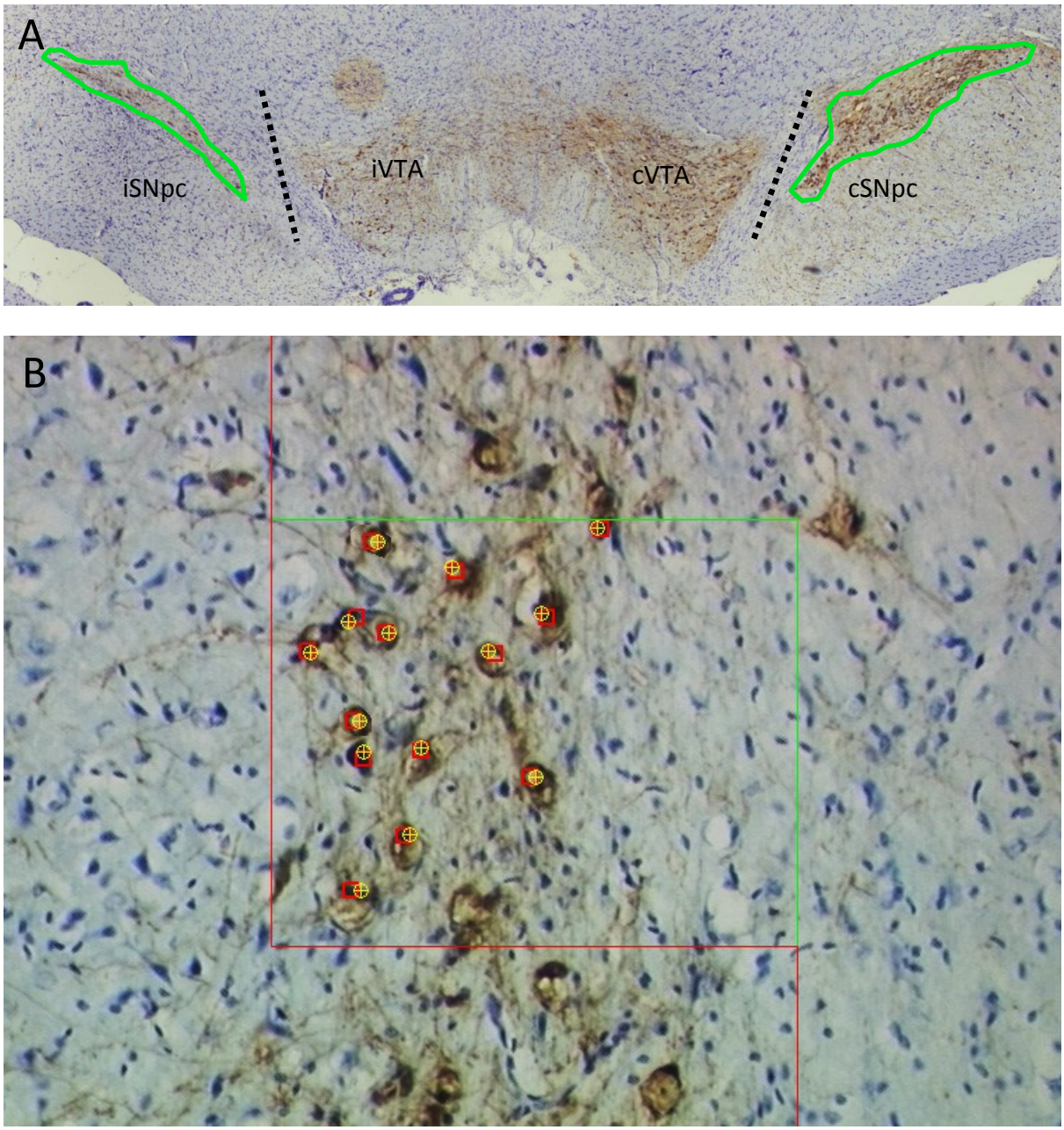

Figure 2.18 – Stereological Cell Quantification
(A) Representative example tiled image of a TH immunohistochemically stained tissue section of a lactacystin lesioned rat brain used for manual delineation of the AOI of the ipsilatreral (iSNpc) and contralateral (cSNpc) SNpc (delineated in green) with reference to previously defined boundaries (Carman et al., 1991) for stereological counting. (B) Representative counting frame used for quantification of TH+ (red marker) and Nissl+ (yellow marker) within the SNpc at x10 magnification. To avoid edge effects, "acceptance" (green) and "forbidden" (red) lines were used.

2.5.3 – Gene Expression Analysis

2.5.3.1 – cDNA Synthesis

500ng of extracted RNA from each sample, quantified spectrophotometrically (section 2.2.3), was reverse transcribed using the QuantiTect® reverse transcription kit according to the manufacturer's instructions with integrated removal of genomic DNA contamination (Qiagen). Briefly, genomic DNA was eliminated by incubation of 500ng of extracted RNA with 2µl of Qiagen gDNA Wipeout Buffer at 42°C for 2mins. A master mix was then made of 1µl Quantitect Reverse Transcriptase, 4µl Quantitect Reverse Transciption Buffer and 1µl Reverse Transciption Primer Mix, which was added to the RNA containing sample and incubated at 42°C for 15mins. After this time the reverse transcription enzyme was inactivated by incubating the sample at 95°C for 3mins. The resulting cDNA samples were stored at -20°C until qRT-PCR analysis.

2.5.3.2 – qRT-PCR

qRT-PCR experiments were performed using the Brilliant® II QPCR master mix with low ROX (Agilent Technologies UK Ltd, Edinburgh, UK) and an Mx3000P™ real-time PCR system with MxPro software (v4.10, Stratagene, La Jolla, CA, USA). For quantification of the level of expression of each gene in each sample, in a 96 Well Optical Reaction Plate (Applied Biosystems®, Life Technologies, Paisley, UK), 20µl reactions were set up in triplicate, and run in duplex with the reference gene (novel reference gene XPNPEP1 (X-prolyl aminopeptidase (aminopeptidase P) 1)). This novel reference gene was included specifically as it has been previously shown to remain constant in post-mortem tissue between numerous diseases of the CNS (Durrenberger et al., 2012). Each reaction contained 10µl of Brilliant® II QPCR master mix, 7µl of RNase-free water, 1µl template cDNA sample (see section 2.5.3.1) and 2µl (1µl gene of interest + 1µl reference gene) of PrimeTime™ qPCR assays (table 2.3 and 2.4, Integrated DNA technology, Coralville, IA, USA). After loading reaction mixtures into wells the plate was sealed using MicroAmp Optical 8-Cap Strips (Life Technologies), and spun to collect reagents at the bottom of each tube. The plate was then loaded into the Mx3000P™ real-time PCR system and reactions were carried out using the following optimised cycling protocol: 95°C for 10 min, then 60 cycles with a 3-step program (95°C for 30s, 55°C for 30s and 72°C for 30s) as these denaturing, annealing and extension temperatures were observed to work most efficiently with the PrimeTime™ qPCR assays in combination with the Brilliant® II QPCR master mix (data not shown). Fluorescence data collection was performed during the annealing (55°C) step. A negative control for each PrimeTime™ qPCR assay containing no cDNA template was run in each plate. Similarly an inter-plate calibrator for each PrimeTime™ qPCR assay, created by pooling control cDNA samples, was also run in each plate.

Table 2.3 – Probe and Primer Sequences of Human PrimeTime™ qPCR Assays

All PrimeTime™ qPCR assays were obtained from Integrated DNA Technology (Coralville, Iowa, USA) and contained 2.5nM of probe, 5nM of primer 1 and 5nM of primer 2. Abbreviation: A, adenine; C, cytosine; G, guanine; T, thymine; HEX™, Hexachlorofluorescein; IABkFQ, Iowa Black® FQ; Fwd, forward; Rev, reverse.

Gene Name	Protein Product		Sequence
XPNPEP1	XPNPEP1	Probe	**5'-/5HEX/CTTTGGGAA/ZEN/CCTCTTTCTCCAGCCA/3IABkFQ/-3'**
		Fwd Primer	*5'-CGAAACTCCTCAGCTTTGTCA-3'*
		Rev Primer	*5'-CTGTTGCTCTCTGTGAACTCT-3'*
TH	TH	Probe	**5'-/56-FAM/ACGTCTCAA/ZEN/ACACCTTCACAGCTCG/3IABkFQ/-3'**
		Fwd Primer	*5'-GGTCTCTAGATGGTGGATTTTGG -3'*
		Rev Primer	*5'-TGCTAAACCTGCTTCTTCTCC -3'*
HLADPA1	HLA-DPα1	Probe	**5'-/56-FAM/CCTAAGTCC/ZEN/TCTTCTGTTCAGATATTTTGTCACC/3IABkFQ/-3'**
		Fwd Primer	*5'-GTTTGTAGGGCAGCTGGAG-3'*
		Rev Primer	*5'-CACCGTCCTCATCATAAAGTCTC -3'*
HDAC1	HDAC1	Probe	**5'-/56-FAM/AACGTTGAA/ZEN/TCTCTGCATCTGCTTGC/3IABkFQ/-3'**
		Fwd Primer	*5'-ACAGAACCACCAGTAGACAAC -3'*
		Rev Primer	*5'-CCATCCGTCCAGATAACATGTC -3'*
HDAC2	HDAC2	Probe	**5'-/56-FAM/CCAATATCC/ZEN/CTCAAGTCTCCTGTGCC/3IABkFQ/-3'**
		Fwd Primer	*5'-GACAGCATAGTATTTGCCTTTTCC -3'*
		Rev Primer	*5'-CAACAGATCGTGTAATGACGGT -3'*
HDAC3	HDAC3	Probe	**5'-/56-FAM/CGATGACTG/ZEN/CCCAGTGTTTCCCG/3IABkFQ/-3'**
		Fwd Primer	*5'-CTGTGTAACGCGAGCAGAA -3'*
		Rev Primer	*5'-CACCAATATGCAAGGCTTCAC -3'*
HDAC4	HDAC4	Probe	**5'-/56-FAM/TCCTCAATA/ZEN/AAAAGAAGGCGCTGGC/3IABkFQ/-3'**
		Fwd Primer	*5'-TGGAAATGCAGTGGTTCAGAT -3'*
		Rev Primer	*5'-AGCTCAAGAACAAGGAGAAGG -3'*
HDAC5	HDAC5	Probe	**5'-/56-FAM/CCAACGCCA/ZEN/GCTTCCTGCAG/3IABkFQ/-3'**
		Fwd Primer	*5'-GTTCCCGACCTGACATCC -3'*
		Rev Primer	*5'-TTGACATCACCGCAGCTC -3'*
HDAC6	HDAC6	Probe	**5'-/56-FAM/TCCTTTCAG/ZEN/GCCCGGTTTGCT/3IABkFQ/-3'**
		Fwd Primer	*5'-ACCAACATCAGCTCTTCCTT -3'*
		Rev Primer	*5'-CATTGCCTCTGGGATGACA -3'*
HDAC7	HDAC7	Probe	**5'-/56-FAM/CGGCATTCC/ZEN/CTACAGAACCCTGG/3IABkFQ/-3'**
		Fwd Primer	*5'-GGCAAAAAGCTGCTGAGC -3'*
		Rev Primer	*5'-AAGAACAGTCCATCCCAACAG -3'*
HDAC8	HDAC8	Probe	**5'-/56-FAM/CAAAGAATG/ZEN/CACCATACTGGCCCG/3IABkFQ/-3'**
		Fwd Primer	*5'-TGAGATAACAAAAACCAGATGCTTC -3'*
		Rev Primer	*5'-GTCCCGAGTATGTCAGTATGTG -3'*
HDAC9	HDAC9	Probe	**5'-/56-FAM/AAATCATTC/ZEN/CGTGAGCCGCCATC/3IABkFQ/-3'**
		Fwd Primer	*5'-GAGCTTTGATCCAATGATGTGTG -3'*
		Rev Primer	*5'-TCAGCAACGAAAGACACTCC -3'*
HDAC10	HDAC10	Probe	**5'-/56-FAM/CTTCACTGT/ZEN/CAACCTGCCCTGGA/3IABkFQ/-3'**
		Fwd Primer	*5'-GTAGTCAGCGTTTCCCATCC -3'*
		Rev Primer	*5'-CTTTCCTGCGAGAGTCAGATG -3'*

SIRT1	Sirtuin1	Probe	**5'-/56-FAM/CTCGATGTC/ZEN/CTAGGTGCCCAGC/3IABkFQ/-3'**
		Fwd Primer	*5'-GTTTCATGATAGCAAGCGGTTC -3'*
		Rev Primer	*5'-GTCATGGTTCCTTTGCAACAG -3'*
SIRT2	Sirtuin2	Probe	**5'-/56-FAM/TGACCTTGG/ZEN/AAGGGGTGGCC/3IABkFQ/-3'**
		Fwd Primer	*5'-CTCCCACCAAACAGATGACTC -3'*
		Rev Primer	*5'-TCTCCCAGACGCTCA -3'*

Table 2.4 – Probe and Primer Sequences of Rat PrimeTime™ qPCR Assays

All PrimeTime™ qPCR assays were obtained from Integrated DNA Technology (Coralville, Iowa, USA) and contained 2.5nM of probe, 5nM of primer 1 and 5nM of primer 2. Abbreviation: A, adenine; C, cytosine; G, guanine; T, thymine; HEX™, Hexachlorofluorescein; IABkFQ, Iowa Black® FQ; Fwd, forward; Rev, reverse.

Gene Name	Protein Product		Sequence
XPNPEP1	XPNPEP1	Probe	**5'-/5HEX/CCATCATTC/ZEN/ACTACGCGCCGATCC/3IABkFQ/-3'**
		Fwd Primer	*5'-GTTCCATCCTTGTACTGAGCA-3'*
		Rev Primer	*5'-TTCCCAACGATTTCCAGCA-3'*
SNCA	α-Synuclein	Probe	**5'/56-FAM/CTTCTCAGC/ZEN/CACTGTTGTCACTCCA/3IABkFQ/-3'**
		Fwd Primer	*5'-CCCTCCAACATTTGTCACTTG-3'*
		Rev Primer	*5'-GCGTCCTCTATAGGTTCCA-3'*
BDNF	BDNF	Probe	**5'-/56-FAM/CAGCAAAGC/ZEN/CACAATGTTCCACCA/3IABkFQ/-3'**
		Fwd Primer	*5'-GCAACCGAAGTCTGAAATAACCA-3'*
		Rev Primer	*5'-GACACATTACCTTCCAGCATCT-3'*
GDNF	GDNF	Probe	**5'-/56-FAM/CGCTGACCA/ZEN/GTGACTCCAATATGCC/3IABkFQ/-3'**
		Fwd Primer	*5'-CAGTCTTTTGATGGTGGCTTG-3'*
		Rev Primer	*5'-GCCGAAGACCACTCCCT-3'*
HSPA1A	Hsp70	Probe	**5'-/56-FAM/CCGTGTTGT/ZEN/GGACAGTTGGTTGTG/3IABkFQ/-3'**
		Fwd Primer	*5'-TGAGTGGAATGGACAGGAAAG-3'*
		Rev Primer	*5'-CATAATCAGAACTGTGCGAGTCT-3'*
GSN	Gelsolin	Probe	**5'-/56-FAM/CGCCAGGAA/ZEN/CCTCTTCGATCACAA/3IABkFQ/-3'**
		Fwd Primer	*5'-CATCAGTAGCCAGGTCTTCC-3'*
		Rev Primer	*5'-GGCTTAAGGACAAGAAGATGGA-3'*
BCL2	Bcl-2	Probe	**5'-/56-FAM/CAGGATAAC/ZEN/GGAGGCTGGGATGC/3IABkFQ/-3'**
		Fwd Primer	*5'-CCAGGAGAAATCAAACAGAGGT-3'*
		Rev Primer	*5'-GATGACTGAGTACCTGAACCG-3'*
BAD	BAD	Probe	**5'-/56-FAM/CCATAGTCC/ZEN/CAGCCCTCCATG/3IABkFQ/-3'**
		Fwd Primer	*5'-CATCCCTTCATCTTCCTCAGTC-3'*
		Rev Primer	*5'-GACAGGCAGCCAATAACAGT-3'*

2.5.3.3 – Data Analysis

Relative gene expression was determined using the comparative C_T ($\Delta\Delta C_T$) method (Livak and Schmittgen, 2001) normalising to the expression of the reference gene and the appropriate control group. Briefly, fluorescence was plotted against cycle number and a florescence threshold line (the value of which was determined empirically for each gene) was placed in the exponential phase of the resulting line. A threshold cycle (C_T) value (cycle number at which the fluorescence generated within the reaction crosses the threshold line) for each reaction was calculated and the resulting values averaged for replicates. For each sample the ΔC_T was then calculated as given by the following equation:

$$\Delta \boldsymbol{C_T} = \boldsymbol{C_T}(\boldsymbol{gene\ of\ interest}) - \boldsymbol{C_T}(\boldsymbol{reference\ gene})$$

This ΔC_T value was then normalised to the appropriate control group by subtracting the mean ΔC_T for that group, as given by the following equation:

$$\Delta\Delta \boldsymbol{C_T} = \Delta C_T(sample) - mean\Delta C_T(appropriate\ control\ group)$$

The amount of the target gene of interest, normalized to an endogenous reference gene and relative to the appropriate control group was then calculated, as given by the following equation:

$$\boldsymbol{2^{-\Delta\Delta C_T}}$$

The resulting expression values were converted to fold changes from the appropriate control group and data expressed as mean ± SEM.

2.5.3.4 – Validation of the Comparative C_T Analysis Method

For the $\Delta\Delta C_T$ method of analysis to be valid, it is assumed that the efficiency of the target gene amplification and the efficiency of the reference gene amplification are approximately equal (Livak and Schmittgen, 2001). To test whether this was the case for the PrimeTime™ qPCR assays used, a standard curve for each amplicon was run utilising a single sample known to express all genes (calibrator cDNA described previously) diluted serially. A semi-logarithmic plot of C_T values generated vs. log of the amount of input nucleic acid was then plotted (see figure 2.19A and B). The probe efficiencies (E) were then calculated using the slope of the resulting lines (see figure 2.19A and B) and the following equation:

$$\boldsymbol{E}\ (\%) = \left(\boldsymbol{10^{-1/slope} - 1}\right) \times \boldsymbol{100}$$

The ΔC_T for each standard was then calculated (see above) and plotted against log of the amount of input nucleic acid: the slope of which must be <0.1 to pass validation (see figure 2.19C and D). All genes displayed slopes of <0.1 (range 0.019-0.089).

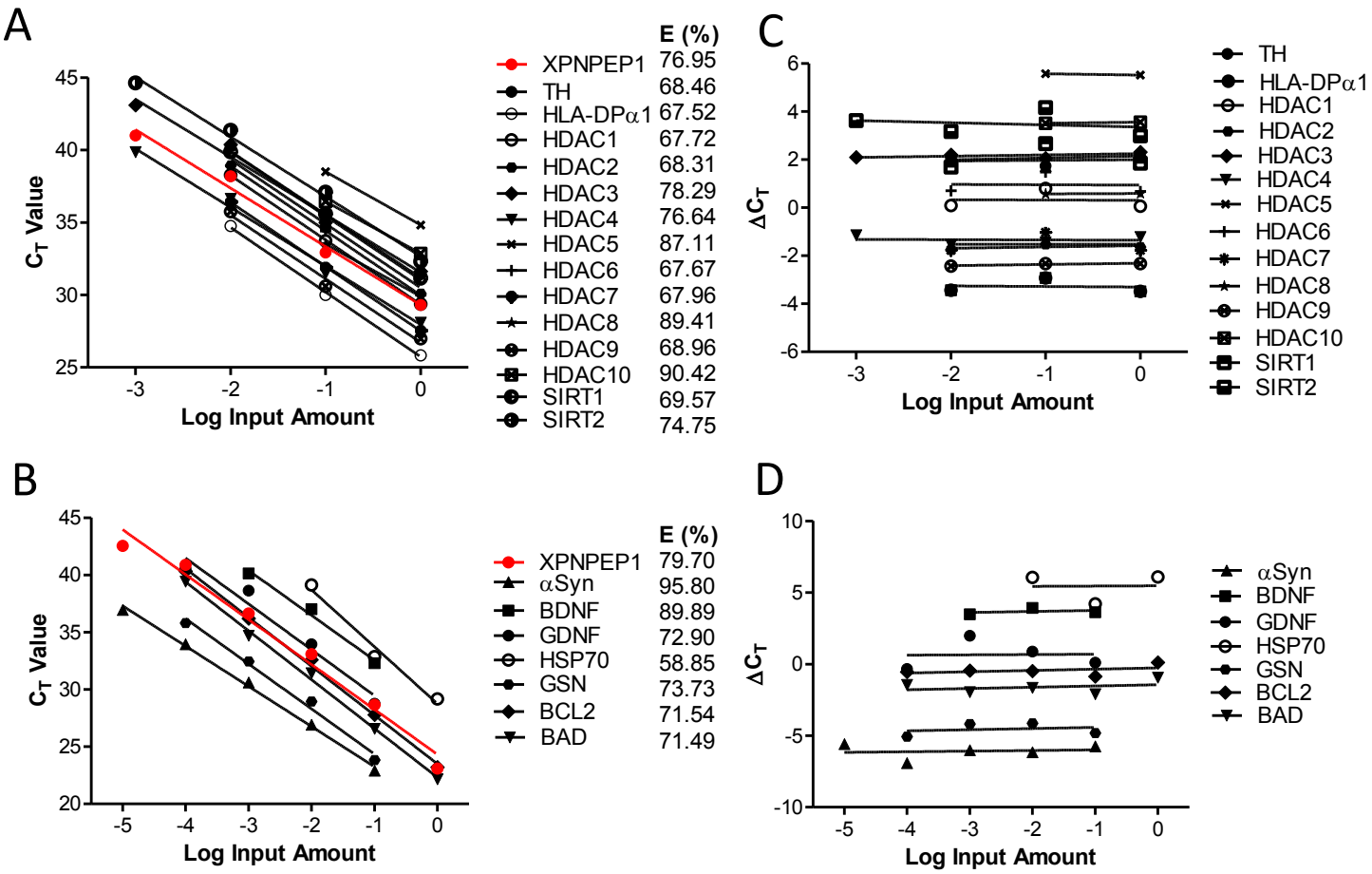

Figure 2.19 – Validation Experiments For Comparative C_T Analysis Method
Semi-logarithmic plots of C_T values generated for each (A) human and (B) rat PrimeTime™ qPCR assay vs. log of input amount of nucleic acid, used for calculated of probe efficiencies. Semi-logarithmic plots of ΔC_T vs. log of input amount of nucleic acid for (C) human and (D) rat PrimeTime™ qPCR assays, used for testing the validity of the comparative C_T method. All genes displayed slopes of <0.1 (range 0.019-0.089).

2.5.4 – Protein Expression Analysis

To assess the expression levels of proteins of interest, chemiluminescent Western blot analysis was employed (see figure 2.20). For this, the appropriate volume of Laemmli sample buffer (Sigma) was added to 10µg of extracted protein sample and incubated at 95°C for 15mins to denature the protein and disrupt any secondary/tertiary/quaternary structures precluding antibody binding. Samples were then loaded onto 1mm thick 15-well hand-cast 15% Tris-Glysine gels and proteins separated by electrophoresis in Tris-Glycine running buffer (0.25M Tris-Base, 2M Glycine, and 1% Sodium Dodecyl Sulphate) for ~40mins at a constant current of 60mA. Proteins were transferred to polyvinylidene fluoride (PVDF) membrane (pore size, 0.45µm) using semi-dry transfer (20V for 45mins) in transfer buffer (0.25M Tris-Base, 2M Glycine, 20% methanol). Membrane was then equilibrated in TBST (TBS with 0.2% Tween-20) before non-specific binding was blocked (see table 2.5 for details). Membranes were then washed in TBST before being incubated in primary antibody (see table 2.5 for details). Membranes were washed again in TBST and incubated in horseradish peroxidase (HRP)-conjugated secondary antibody (see table 2.5 for details). Membranes were washed again in TBST and incubated in chemiluminescent developing substrate (Clarity Western ECL Substrate, Bio-Rad, Hemel Hempstead UK) for 1min. Membranes was then wrapped in cling film and positioned into a Hypercassette™ (GE Healthcare Life Sciences, Buckinghamshire, UK). In the dark, high performance chemiluminescent film (GE Healthcare Life Sciences) was then exposed to membranes and films developed using a film developer (Konica, SRX-101A, Konica Minolta, NJ, USA). Protein bands were then quantified using densitometry analysis software (ImageJ, v1.4).

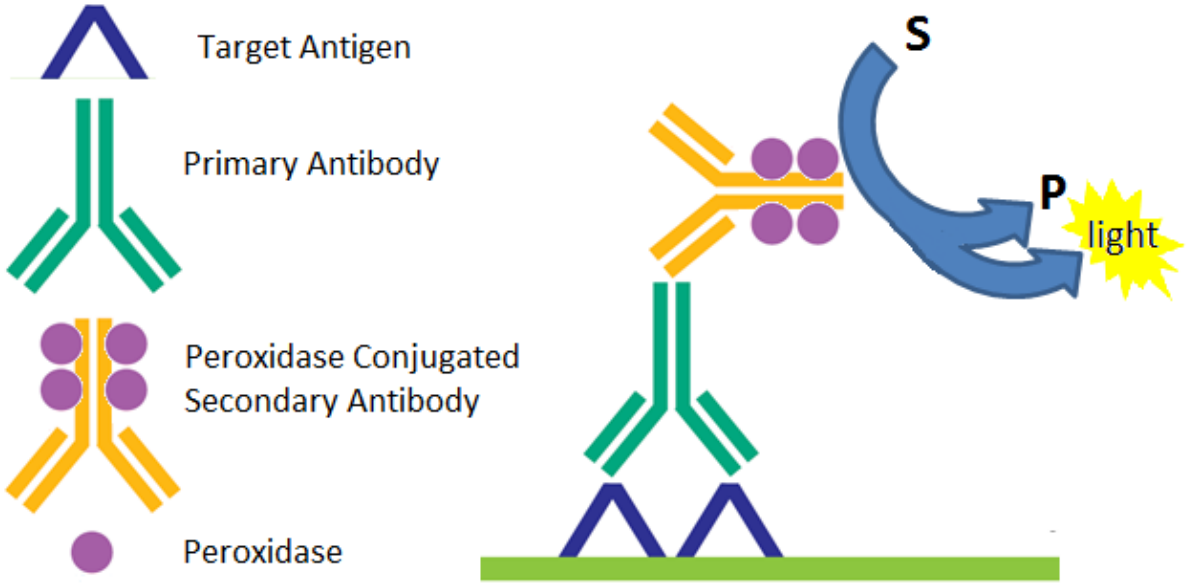

Figure 2.20 – Chemiluminescent Western Blot Analysis
The presence of the target antigen is firstly detected by the primary antibody which becomes tightly bound to its target epitope. The secondary antibody, conjugated to horseradish peroxidase, is then added which binds to the Fc region of the primary antibody forming a complex. The conversion of the chemiluminescent substrate is catalysed by the peroxidase enzyme on the secondary antibody, resulting in the conversion product and light being emitted. This is then detected through exposure to chemiluminescent film. Abbreviations: S, chemiluminescnet substrate; P, chemiluminescent product.

Table 2.5 – Antibodies Used for Western Blotting

Incubations and blocking conditions used for Western blotting. Abbreviation: BSA, bovine serum albumin; FCS, foetal calf serum; TBS-T, tris-buffered saline containing 0.2% tween-20; HRP, horseradish peroxidase; RT, room temperature.

Antigen	Molecular Weight	Blocking Conditions	Primary Antibody	Primary Antibody Incubation Conditions	Secondary Antibody	Secondary Antibody Incubation Conditions
***Histone H3 acetylated on lysine 9* (AcH3-K9)**	~ 17kDa	5% non-fat milk in TBST for 1hr at RT	Rabbit polyclonal anti-AcH3-K9 (Sigma)	1:10,000 in TBST for 1hr at RT	HRP-conjugated goat anti-rabbit (Vector Labs)	1:10,000 in TBST for 1hr at RT
β-Actin	~ 42kDa	Either 5% BSA or non-fat milk in TBST for 1hr at RT	Mouse monoclonal anti-β-actin (Abcam, Cambridge, UK)	1:20,000 in TBST for 1hr at RT	HRP-conjugated horse anti-mouse (Vector Labs)	1:10,000 in TBST for 1hr at RT
Tyrosine Hydroxylase	~ 62kDa	5% BSA in TBST for 1hr at RT	Rabbit polyclonal anti-TH (Millipore)	1:1,000 in 1% BSA in TBST with 0.01% NaN_3 for 20hrs at RT	HRP-conjugated goat anti-rabbit (Vector Labs)	1:10,000 in TBST for 1hr at RT
NeuN	~ 46/48kDa	5% BSA in TBST for 1hr at RT	Mouse monoclonal anti-NeuN (Millipore)	1:1,000 in 1% BSA in TBST with 0.01% NaN_3 for 20hrs at RT	HRP-conjugated horse anti-mouse (Vector Labs)	1:10,000 in TBST for 1hr at RT
Iba-1	~ 17kDa	3% foetal calf serum in TBST for 1hr at RT	Rabbit polyclonal anti-Iba-1 (Wako, Osaka, Japan)	1.67ug/ml in 3% FCS in TBST for 20hrs at 4°C	HRP-conjugated goat anti-rabbit (Vector Labs)	1:2,000 in 3% FCS in TBST for 1hr at RT

2.6 - Materials and Sources

Lactacystin and LPS were both obtained from Enzo Life Sciences Ltd. (Exeter, UK). Valproate, Nicotinamide, Sodium Butyrate and EX527 were all obtained from Sigma-Aldrich Chemical Co. Ltd (Pool, UK). Trichostatin A, AGK2 and Suramine were all obtained from Tocris Bioscience Ltd. (Bristol, UK). Apicidin was obtained from Enzo Life Sciences Ltd. (Exeter, UK). MS275 was obtained from Stratech Scientific Ltd. (Suffolk, UK). RNA extraction and reverse transcription kits were obtained from Qiagen Ltd. (Crawley, UK). qRT-PCR mastermix was obtained from Agilent Technologies UK Ltd. (Edinburgh, UK). PrimeTime™ qPCR Assays were all obtained from Integrated DNA Technology (Coralville, Iowa, USA). ELISA kits were obtained from Peprotech Ltd. (London, UK). Primary antibodies were obtained from either Sigma-Aldrich Chemical Co. Ltd. (Poole, UK), Millipore Ltd. (MA, USA), Abcam Ltd. (Cambridge, UK) or Wako Chemicals Ltd. (Osaka, Japan). Secondary antibodies, serums, ABC kits, and DAB peroxidase substrate kits were obtained from VectorLabs (Peterborough, UK). Unless otherwise stated all other reagents were obtained from either Sigma-Aldrich Chemical Co. Ltd. (Poole, UK) or VWR (Lutterworth, UK).

2.7 - Statistical Analysis

Unless otherwise stated all data is presented as mean ± SEM based on *n* independent observations. For individual comparisons, either two-tailed paired or unpaired Student t-tests were used. For multiple comparisons either one way or two way (repeated measures) analyses of variance (ANOVA) were used with Bonferroni post-hoc tests for multiple comparisons. For multiple comparisons to a single control group a one way ANOVA was used with Dunnet's post-hoc tests for multiple comparisons. Individual tests conducted on each dataset are detailed in the 'Experimental Design' section of each chapter. Unless otherwise stated statistical significance is indicated in figure legends using the following system: $p<0.05$ (*, $^{\#}$), $p<0.01$ (**, $^{\#\#}$), $p<0.001$ (***, $^{\#\#\#}$), $p<0.0001$ (****, $^{\#\#\#\#}$). All statistical tests were performed using GraphPad Prism (v5.0 for Windows, GraphPad Software, San Diego, CA, USA).

Chapter Three

Histone Acetylation and HDAC Expression in Parkinson's Disease

3 – Histone Acetylation and HDAC Expression in Parkinson's Disease

3.1 – Introduction

In healthy cells there is a tightly controlled equilibrium between the effects of HATs and HDACs enabling histone (de)acetylation and the dynamic control of transcription (Dietz and Casaccia, 2010, Saha and Pahan, 2006). In healthy neurons this therefore results in appropriate regulation of gene expression and subsequently facilitates appropriate neuronal homeostasis (Saha and Pahan, 2006). In neurodegenerative disease, however there is known to be an imbalance between the activity of HATs and HDACs in favour of histone deacetylation, thought to be pathogenic in disease progression (Dietz and Casaccia, 2010, Saha and Pahan, 2006, Rouaux et al., 2003). This misbalance in neurodegeneration was first noted in both an *in vitro* model of cortical neuronal cell death induced by activation of amyloid precursor protein signalling, a hallmark of AD, and in an *in vivo* model of ALS: the G86R mutant SOD-1 mice displaying motor neuron degeneration (Rouaux et al., 2003). More specific to PD, it was later demonstrated that αSyn accumulation itself promotes histone H3 hypoacetylation as ascertained from overexpression studies in SH-SY5Y cells as well as in an *in vivo* αSyn transgenic drosophila model, thought to be achieved through αSyn 'masking' acetylation sites on histone proteins (Kontopoulos et al., 2006). From these findings then it is hypothesised that the misbalance in HAT/HDAC activity could be rectified with the use of HDACIs to reduce the extent of cell death exhibited in the SNpc in PD.

Thus far pathogenic histone hypoacetylation and transcriptional dysfunction have yet to be confirmed as being present in the brains of PD patients: all work previously being described in animal and cellular models of neurodegeneration. The acetylation level of histone proteins within degenerating regions of the Parkinsonian brain must therefore be quantified and compared with age matched control subjects to confirm this hypothesis in the human disease. This represents a vital stage in the drug development process as without confirming the dysregulation of histone acetylation and trascitpional dysfunction in primary diseased tissue, the use of HDACIs for the treatment of PD cannot truly be rationalised. The first part of this chapter will therefore focus on quantifying histone acetylation levels in the midbrain, putamen and fontal cortex of control human brain tissue and brain tissue from both early (ePD, Braak stage 3/4) and late (lPD, Braak stage 6) stage PD cases from the PUKTB at Imperial College London with the aim of determining if histone acetylation is indeed a function PD development and/or if histone acetylation maps with the spreading of pathology in the Parkinsonian brain. Although it is thought that pathogenic histone hypoacetylation is in part due to the 'masking' effects of αSyn accumulates towards histone proteins, it remains unanswered whether the expression levels of the HDACs themselves in degenerating regions of the PD brain are affected in PD: studies thus far focussing on directly

measuring histone acetylation rather than expression levels of the enzymes responsible for (de)acetylating histone proteins. Due to the well-defined link between HDACs and cancer, expression studies have been conducted in a number of tumour types demonstrating their alteration in diseased tissue (Poyet et al., 2014, Pacheco and Nielsen, 2012, Yeung et al., 2004, Zhang et al., 2004, Wilson et al., 2006). To the authors knowledge however such a study is yet to be conducted in the neurodegenerative diseased brain, the only study of diseased brain tissue being conducted upon astrocytoma brain tumours (Lucio-Eterovic et al., 2008). The second part of this chapter therefore focuses on profiling the expression level of the various HDAC isoforms in levels in the midbrain, putamen and fontal cortex of control human brain tissue and brain tissue from both early (Braak stage 3/4) and late (Braak stage 6) stage PD cases with the aim of determining if HDAC isoform expression is indeed a function PD development and/or if perturbation of HDAC expression maps with the spreading of pathology in the Parkinsonian brain.

3.2 – Aims of Chapter

The aims of this chapter are therefore to:

1. Determine whether histone acetylation is affected in the Parkinsonian brain
    a. Using tissue from early (ePD, Braak stage 3/4) and late (lPD, Braak stage 6) stage PD cases and age matched controls, quantify the level of histone acetylation in the midbrain, putamen, and frontal cortex.
    b. Determine whether histone acetylation is affected in these brain regions in the Parkinsonian brain, and to what extent.
2. Determine whether the level of HDAC isoform expression is affected in the Parkinsonian brain
    a. Quantify the difference in expression levels of various HDAC isoforms between the midbrain, putamen and frontal cortex in control brain tissue.
    b. Using tissue from early (ePD, Braak stage 3/4) and late (lPD, Braak stage 6) stage PD cases and age matched controls, quantify the expression levels of various HDAC isoforms in the midbrain, putamen, and frontal cortex.
    c. Determine whether changes of expression in any of the HDAC isoforms are present in these brain regions of the Parkinsonian brain, and to what extent.

3.3 – Experimental Design

3.3.1 – Quantification of Histone Acetylation and Gene Expressions in the Parkinsonian Brain

Human brain tissue from cases of early (Braak stage 3/4, ePD, n=8) and late (Braak stage 6, lPD, n=12) stage pathologically confirmed PD, as well as age matched controls (n=10) was obtained from the Parkinson's UK Tissue Brain Bank. Table 3.1 for full description of control and PD cases used. For each case, 30mg of tissue from the brain block containing the midbrain, the putamen or frontal cortex was collected. Protein and mRNA were simultaneously extracted from tissue samples (section 2.2.3) for further analysis. The level of histone acetylation was quantified in protein samples by performing Western blot analysis for a commonly acetylated histone lysine residue, AcH3-Lys9 (section 2.5.4). Extracted mRNA from each region was converted to cDNA and the expression levels of cellular markers (TH for dopaminergic neurons and HLA-DPα1 for activated microglia) were firstly quantified using qRT-PCR (section 2.5.3). The expression levels of HDAC1 to 10, and sirtuin1 and 2 was then similarly quantified using qRT-PCR (section 2.5.3).

3.3.2 – Statistical Analysis

All data is presented as mean ± SEM. Western blot and qRT-PCR were analysed using two-way ANOVA with Bonferroni post-tests to compare individual groups. All statistical tests were performed using GraphPad Prism (v5.0 for Windows, GraphPad Software, San Diego, CA, USA).

Table 3.1 – Control and Parkinson's Disease Cases Utilised

Abbreviations: PMI, post-mortem interval; AAD, age at death; AAO, age at onset; DD, disease duration; PD, Parkinson's disease; ePD, early Parkinson's disease; lPD, late Parkinson's disease. Total row at bottom of each table: mean shown in bold, SEM shown in italic.

Control Case	Sex	PMI (hrs)	AAD (yrs)	Cause of Death
PDC08	F	17	71	Myocardial infarction
PDC23	F	23	78	Unknown
PDC26	F	23	80	Breast carcinoma with spinal metastasis; carcinosarcoma uterus
PDC28	F	11	84	Pancreatic cancer
PDC30	M	17	77	Conductive cardiac failure. Chronic kidney disease. Osteoporosis. Malignant neoplasm of prostate
PDC34	M	12	90	Respiratory failure secondary to bronchial cancer
PDC50	F	28	80	End stage primary pulmonary hypertension
PDC53	F	22	89	Not reported
C032	M	22	88	Prostate cancer, bone metastases
C037	M	5	84	Bladder cancer, pneumonia
n=10	**4M:6F**	**18**	**82.1**	
		2.2	*1.9*	

ePD Case	Sex	PMI (hrs)	AAD (yrs)	AAO (yrs)	DD (yrs)	Braak (stage)	Cause of Death	PD Medication
PD07	M	22	78	70	10	3	Pneumonia	Sinemet, Orphenadrine, Amantadine
PD14	M	21	79	67	12	3	Not reported	Ropinirole, Madopar, Artane, Amitriptyline, Hyoscine, Risperidone
PD22	F	14	76	65	14	4	Not reported	Selegiline, Madopar, Cabergoline
PD36	M	10	76	66	10	3	Unknown	Madopar
PD63	F	10	80	67	13	4	Not reported	Sinemet, Entacapone, Sinemet, Selegiline
PD86	F	22	87	77	9	4	Gastrointestinal bleeding	Madopar, Amantadine, Selegiline
PD109	M	9	72	66	6	4	Cardio-respiratory arrest; aspiration pneumonia	Pergolide, Selegiline, Sinemet , Sinemet, Cabergoline
PD204	F	5	86	68	18	3	Not reported	Selegiline, Madopar, Cabergoline, Roprinirole
n=8	**4M:4F**	**14.1**	**79.3**	**68.3**	**11.5**	**3.5**		
		2.4	*1.8*	*1.4*	*1.3*	*0.2*		

lPD Case	Sex	PMI (hrs)	AAD (yrs)	AAO (yrs)	DD (yrs)	Braak (stage)	Cause of Death	PD Medication
PD01	F		87	76	12	6	Not reported	Madopar, Sinemet, Selegiline
PD16	F	14	85	67	18	6	Bronchopneumonia and breast cancer with metastasis	Madopar, Sinemet, Bromocriptine, Pergolide, Lysuride, Selegiline
PD23	M	28	82	75	7	6	Not reported	Sinemet, Pramipexole
PD28	M	14	82	65	18	6	Not reported	Sinemet preparations, Cabergoline, Bromocriptine, Pergolide, Selegiline
PD41	M	6	77	67	10	6	Not reported	Selegiline; Benzhexol; Sinemet; Pergolide; Pramipexole; Quetiapine; Paroxetine.
PD45	M	16	80	60	19	6	Not reported	Sinemet, Ropinirole, Selegiline, Entacapone, Tolcapone, Cabergoline
PD67	M	10	83	74	9	6	Not reported	Madopar Sinemet, Selegiline, Pergolide, Ropinirole, Tolcapone, Entacapone
PD79	F	22	78	59	19	6	Chest infection	Fludrocortisone, Sulpiride, Sinemet, Dothiepin, Selegiline, Madopar, Dispersible, Amitriptyline, Madopar, Sertraline, Artane, Propranolol
PD93	F	22	81	67	14	6	Not reported	Madopar, Madopar, Cabergoline, Sulpiride, Selegiline, Olanzapine, Amantadine
PD99	M	10	82	72	11	6	Pneumonia, fractured neck of femur, pulmonary embolisms, COPD	Pramipexole, Benzhexol, Sinemet, Madopar
PD104	M	15	75	50	25	6	Pancreatic cancer	Sinemet, Madopar Dispersible, Madopar, Madopar, Pergolide, Entacapone, Disipal, Galantamine, Benzhexol, Bromocriptine, Selegiline
PD180	F	15	85	70	15	6	Not reported	Sinemet, Selegiline, Risperidone, Pergolide, Haloperidol, Rivastigmine
n=12	**7M:5F**	**15.6** *1.9*	**81.4** *1.0*	**66.8** *2.2*	**14.8** *1.5*	**6** *0*		

3.4 – Results

3.4.1 – Expression of TH and HLA-DPα1 in Brain Tissue Samples

Firstly the expression levels of TH, the rate limiting enzyme in monoamine synthesis, were quantified in midbrain and putamen tissue samples as an indicator of dopaminergic cell content in these brain regions. Additionally, the expression levels of HLA-DPα1, a MHC protein known to be present on activated microglia, were quantified in midbrain, putamen and frontal cortex tissue samples as an indicator of activated microglial cell content in these brain regions. Quantification of both of these cellular markers revealed significant differences in expression across brain regions and with disease progression (figure 3.1). In line with degeneration of dopaminergic neurons in the SNpc in PD, there was a disease dependent reduction of TH expression in midbrain tissue samples (early and late PD cases, 0.549 ± 0.345 and 0.219 ± 0.089 fold change from control cases respectively, $p>0.05$ and $p<0.05$). No overt changes in TH expression were observed in putamen samples with disease progression. With HLA-DPα1 expression however, increases were observed in the midbrain in both early and late stage PD cases, however these differences did not reach significance. In the putamen however significant increases in HLA-DPα1 expression were observed in both early and late stage PD cases compared to controls (early and late stage PD cases, 2.127 ± 0.369 and 2.094 ± 0.476 fold change from control, $p<0.05$ in both comparisons). In the frontal cortex however, reductions in HLA-DPα1 expression were observed in both early and late PD cases, however these changes did not reach significance. Summary of changes shown in table 3.2.

3.4.2 – Histone Acetylation in the Parkinsonian Brain

Quantification of a commonly acetylated histone residue (AcH3-Lys9) in whole brain tissue protein extracts from the midbrain, putamen and frontal cortex revealed significant differences in histone acetylation across brain regions and with PD progression (figure 3.2). An increase in histone acetylation was observed in the midbrain with disease progression: a subtle increase in AcH3-Lys9 being observed in early PD cases and significantly more AcH3-Lys9 in late stage PD cases (early and late PD cases, 116.86 ± 32.93% and 174.58 ± 19.22% of control respectively, $p>0.05$ and $p<0.05$). No significant changes in histone acetylation were observed in the putamen. In contrast, a significant increase of histone acetylation was observed in the frontal cortex of early PD cases (early PD cases, 180.44 ± 30.50% of control, $p<0.05$ and 0.001 compared to control and late stage PD cases respectively). In the frontal cortex of late PD cases however a non-significant reduction of histone acetylation was observed. Summary of changes shown in table 3.2.

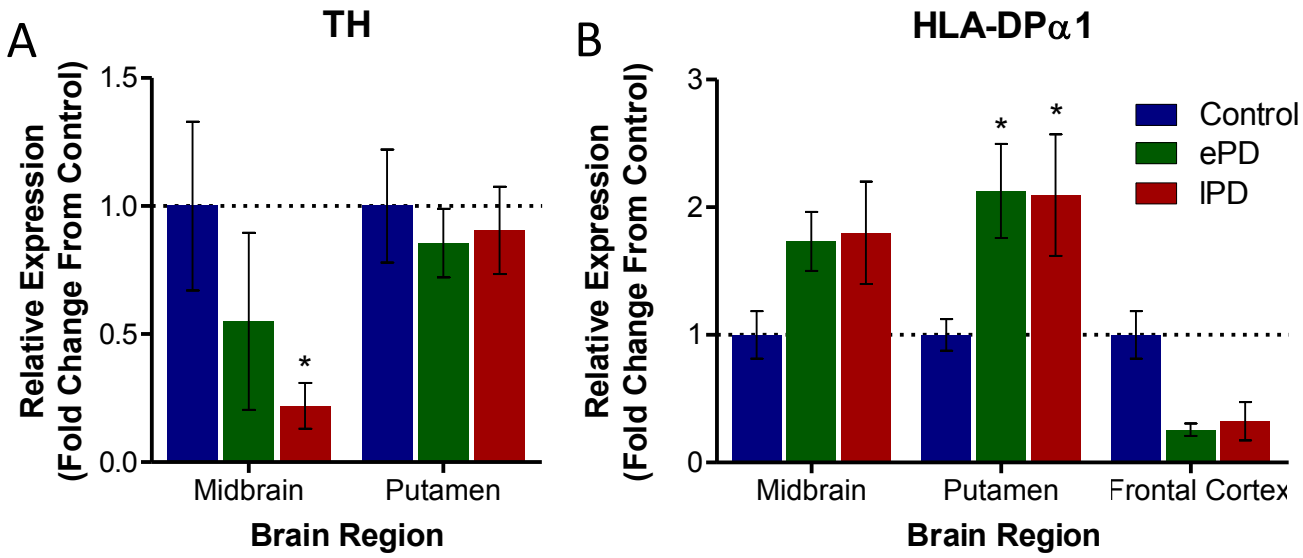

Figure 3.1 – Dopaminergic Neurons and Activated Microglial in the Parkinsonian Brain
Expression of (A) TH and (B) HLA-DPα1 in the midbrain, putamen and frontal cortex of control and early and late stage PD brains. Statistical significance from control group indicated with asterisks: *p<0.05. n=8-12 per group. Abbreviations: ePD, early stage PD; lPD, late stage PD.

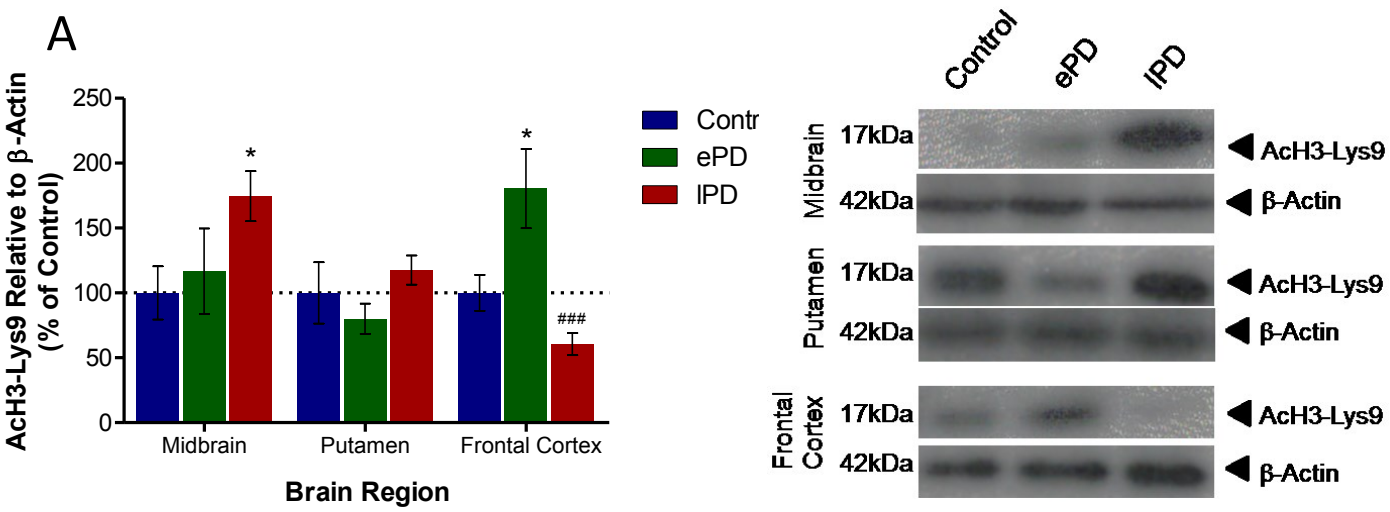

Figure 3.2 – Histone Acetylation in the Parkinsonian Brain

Histone protein H3 acetylated on lysine 9 was quantified in protein extracts of from tissue sample of the midbrain, putamen and frontal cortex of control, early and late stage PD brains. (A) Densitometry analysis of the AcH3-Lys9 band relative to the β-actin band used as a loading control. (B) Representative blot of data presented in (A). (C) Correlation analyses between Braak staging of αSyn pathology in each case and amount of AcH3-Lys9 in the (i) midbrain, (ii) putamen and (iii) the frontal cortex. Statistical significance from control group indicated with asterisks: *p<0.05. Statistical significance from early PD group indicated with hashes: ###p<0.001. n=8-12 per group. Abbreviations: ePD, early stage PD; lPD, late stage PD.

3.4.3 – HDAC Distribution in the Human Brain

To ascertain the differences in expression level of HDAC isoforms in the healthy brain between the three brain regions examined, HDAC isoform expression in the putamen and frontal cortex were firstly compared with that in the midbrain of control cases. A number of differences were observed in HDAC class I isoform expression (figure 3.3A). Compared with its expression in the midbrain, there was a reduced and increased level of HDAC1 expression in the putamen and the frontal cortex respectively, however these differences did not reach significance. No difference in expression of HDAC2 was observed between the midbrain, putamen and frontal cortex. HDAC3 expression was reduced in both the putamen and frontal cortex compared with the midbrain, however similarly these differences did not reach statistical significance. HDAC8 expression however was significantly less in the putamen compared with the midbrain (0.071 ± 0.026 fold change from midbrain expression, $p<0.05$). Conversely, HDAC8 expression was observed to be significantly more in the frontal cortex compared to both the midbrain and the putamen (2.856 ± 0.700 fold change from control, $p<0.001$ compared to both midbrain and putamen expression). Differences in expression were also observed in HDAC Class IIa isoform expression (figure 3.3B). HDAC4 showed non-significant reduced expression in the putamen and increased expression relative to the midbrain in the frontal cortex. HDAC5 expression was observed to be greater in the putamen however and less in the frontal cortex compared with the expression in the midbrain. HDAC7 on the other hand was markedly reduced compared with the midbrain in the putamen, yet significantly greater HDAC7 expression was observed in the frontal cortex (1.844 ± 0.588 relative to midbrain expression, $p<0.001$ compared to putamen expression). No change in expression of HDAC9 was observed between the midbrain and the putamen, however a large increase in HDAC9 expression was observed in the frontal cortex. This difference however was non-significant. Differences in expression of HDAC Class IIb isoforms between brain regions was also observed (figure 3.3C). A reduction and increase in HDAC6 expression was observed in the putamen and frontal cortex compared to the midbrain respectively. However HDAC10 expression was unchanged between the midbrain and putamen, yet significantly increased in the frontal cortex (1.945 ± 0.541 relative to midbrain expression, $p<0.05$ compared to both midbrain and putamen expression). Greatest differences between regional expressions of HDACs were observed in the sirtuin class of HDACs (figure 3.3D). No significant alterations in sirtuin1 or 2 expressions were observed between putamen and midbrain expression. However significantly greater expression levels of both sirtuin1 and 2 compared to the midbrain were observed in the frontal cortex (sirtuin1 and 2 expression, 2.670 ± 0.632 and 4.748 ± 0.867 fold change from midbrain expression respectively, $p<0.05$ and $p<0.001$).

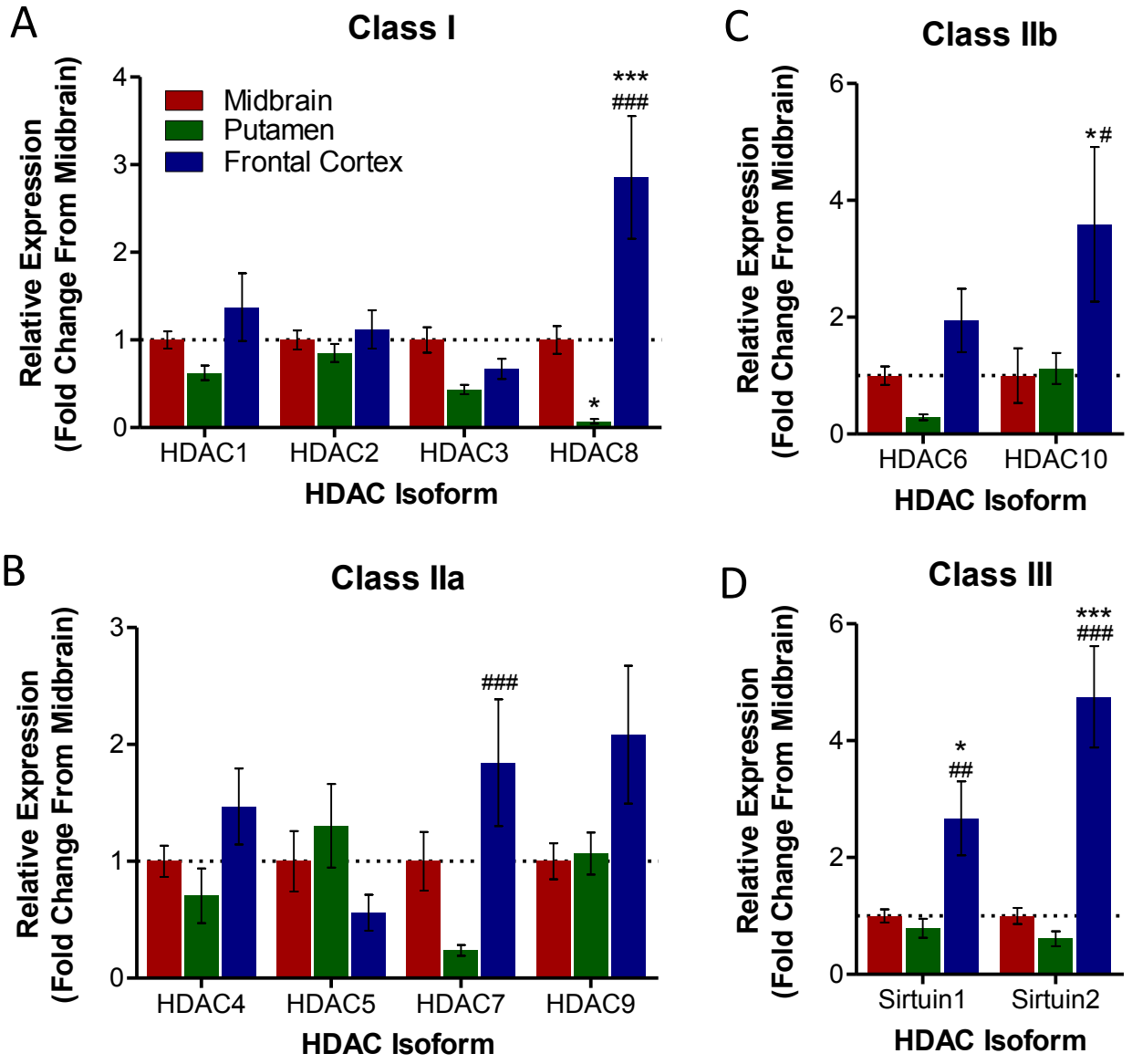

Figure 3.3 – HDAC Distribution in the Human Brain

Expression of (A) Class I, (B) Class IIa, (C) Class IIb and (D) Class III HDACs in the putamen and frontal cortex of the control human brain relative to their expression in the midbrain. Statistical significance from midbrain expression indicated with asterisks: *p<0.05, ***p<0.001. Statistical significance from putamen expression indicated with hashes: ##p<0.01, ##p<0.001. n=8-12 per group.

3.4.4 – HDAC Isoform Expression in the Parkinsonian Brain

qRT-PCR analysis of the expression level of HDAC class I isoforms revealed significant differences in expression across brain regions and with PD progression (figure 3.4). With HDAC1 expression, no changes were observed in the midbrain or putamen however a significant reduction of expression was observed in the frontal cortex of PD brains, both early and late stage PD, compared to controls (early and late stage PD, 0.194 ± 0.057 and 0.413 ± 0.104 fold change from control respectively, $p<0.01$ and $p<0.05$). With HDAC2 expression, little or no change was observed in the midbrain however in the putamen a subtle disease dependent increase in HDAC2 expression was observed. This however was not significant. Similar with the case of HDAC1, HDAC2 expression was reduced in the fontal cortex in PD brains, this however also did not reach statistical significance. HDAC3 however, was shown to significantly reduce in PD in both the midbrain and the frontal cortex (HDAC3 expression in early and late stage PD midbrain, 0.429 ± 0.048 and 0.501 ± 0.067 fold change from control respectively, $p<0.01$ in both comparisons, HDAC3 expression in early and late stage PD frontal cortex, 0.412 ± 0.067 and 0.377 ± 0.071 fold change from control respectively, $p<0.01$ and $p<0.001$ respectively). There was no change of HDAC3 expression however in the putamen. With HDAC8 expression, no change was observed in the midbrain however HDAC8 was disease dependently upregulated in the putamen, reaching statistical significance from controls in late stage PD (early and late stage PD, 0.152 ± 0.347 and 2.317 ± 0.439 fold change from control respectively, $p>0.05$ and $p<0.05$). A reduction was also observed in HDAC8 expression in the frontal cortex in PD brains, however this change was not significant. Summary of changes shown in table 3.2.

Significant changes were also observed in the expression of class IIa HDACs (figure 3.5). No change was observed in the HDAC4 expression in the midbrain yet an increase of HDAC4 expression in the putamen was observed with disease progression, reaching statistical significance in late stage PD cases (1.627 ± 0.155 and 1.847 ± 0.303 fold change from control in early and late stage cases, $p>0.05$ and $p<0.05$). A reduction in HDAC4 expression was also observed in PD cases compared with controls. Reductions in midbrain and frontal cortex HDAC5 expression were observed, however they did not reach significance. No change in HDAC5 expression was observed in the putamen. A disease dependent reduction in HDAC7 was observed in the midbrain, reaching statistical significance from control in late stage PD cases (early and late stage PD cases, 0.681 ± 0.119 and 0.429 ± 0.070 fold change from control respectively, $p>0.05$ and $p<0.05$). No change in HDAC7 expression was observed in the putamen however a statistically significant reduction in HDAC7 was observed in both early and late stage PD cases in the frontal cortex. With HDAC9 expression, no changes were observed in the midbrain or putamen expression however reductions in expression were observed in both early and late stage PD cases. Summary of changes shown in table 3.2.

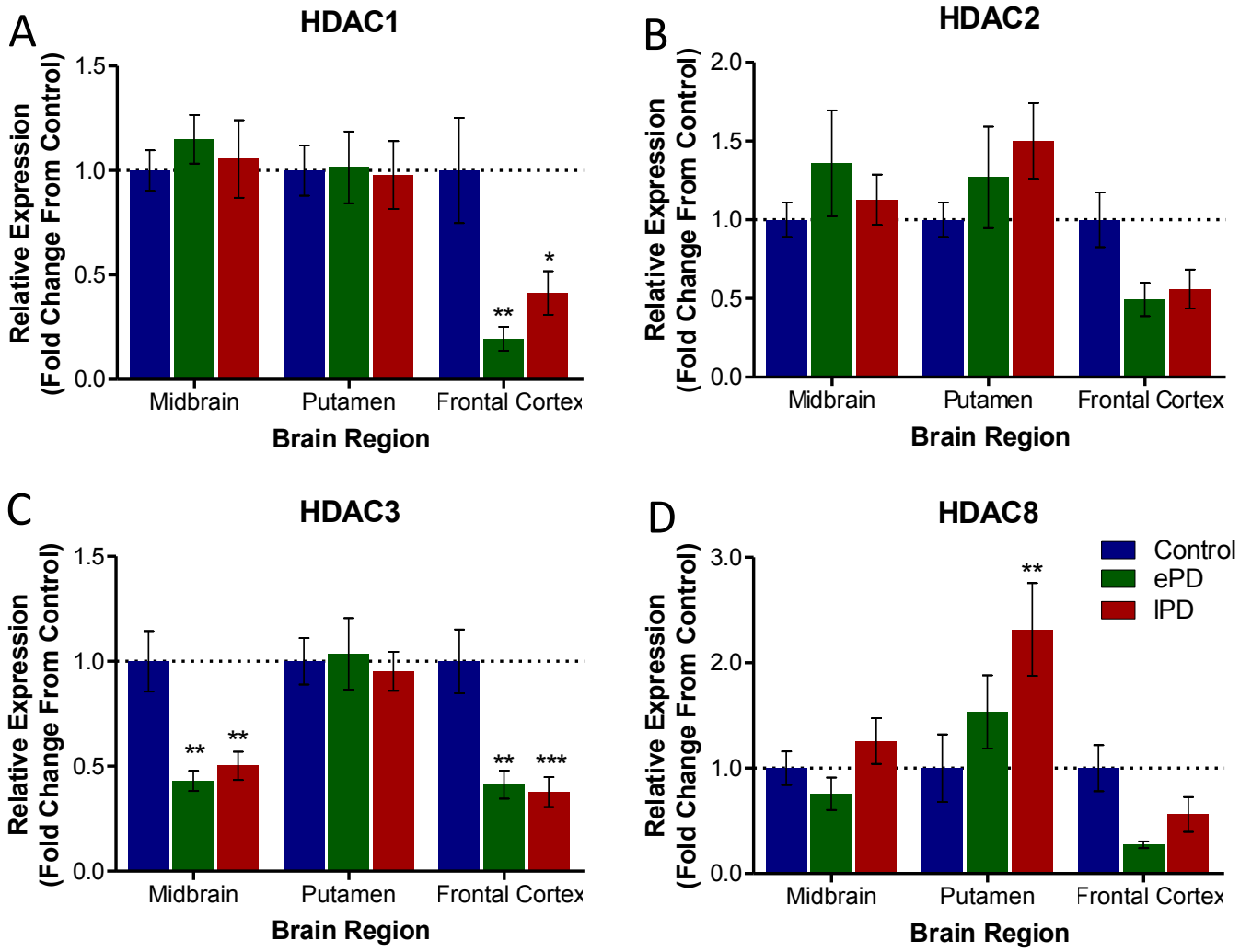

Figure 3.4 – HDAC Class I Expression in the Parkinsonian Brain
Expression of (A) HDAC1, (B) HDAC2, (C) HDAC3 and (D) HDAC8 in the midbrain, putamen and frontal cortex of control and early and late stage PD brains. Statistical significance from control group indicated with asterisks: *p<0.05; **p<0.01, ***p<0.001. n=8-12 per group. Abbreviations: ePD, early stage PD; lPD, late stage PD.

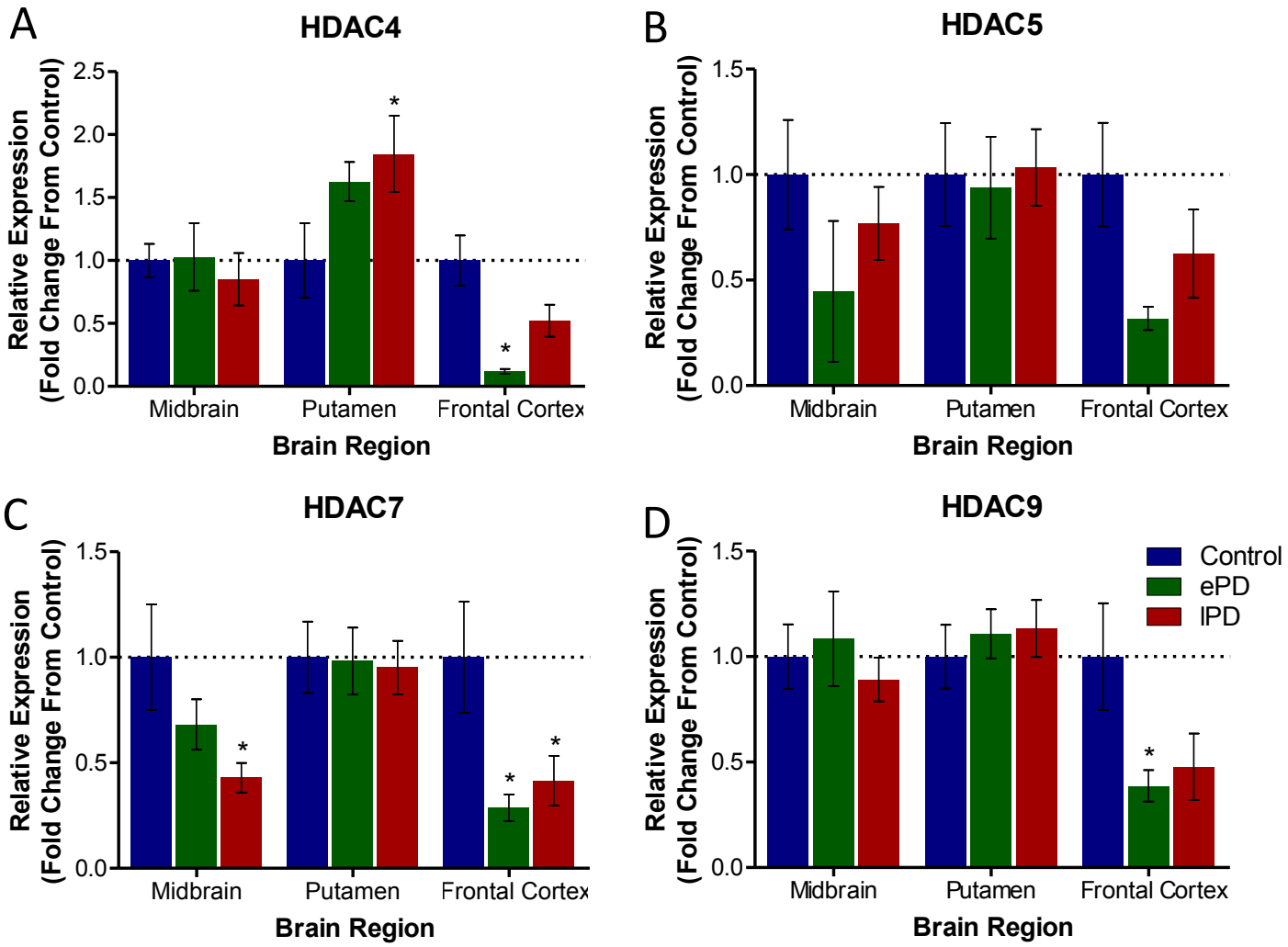

Figure 3.5 – HDAC Class IIa Expression in the Parkinsonian Brain
Expression of (A) HDAC4, (B) HDAC5, (C) HDAC7 and (D) HDAC9 in the midbrain, putamen and frontal cortex of control and early and late stage PD brains. Statistical significance from control group indicated with asterisks: *p<0.05. n=8-12 per group. Abbreviations: ePD, early stage PD; lPD, late stage PD.

Changes were also observed in HDAC class IIb expression in PD brains (figure 3.6). An increase and a decrease were observed in midbrain HDAC6 expression in early and late stage PD cases respectively (early stage PD cases, 1.330 ± 0.285, and late stage PD cases, 0.703 ± 0.109 fold change from control, $p<0.05$). Slight non-significant increases in HDAC6 expression were also observed in the putamen. However significant reductions in HDAC6 expression were observed in both early and late stage PD cases compared with controls (early and late stage PD cases, 0.125 ± 0.021 and 0.379 ± 0.093 fold change from control respectively, $p<0.01$ and $p<0.05$). A decrease in HDAC10 expression was observed in the midbrain of late stage PD brains, however no changes were observed in the expression of this HDAC in the putamen. Similar to those changes above, reductions were also observed in HDAC10 expression in the frontal cortex of both early and late stage PD cases, however these did not reach significance. Summary of changes shown in table 3.2.

With expression of class III HDACs, the sirtuins, a number of changes were similarly observed (figure 3.7). Despite not displaying any changes in sirtuin expression in disease cases in the midbrain, a significant increase in sirtuin1 expression was shown in the putamen, more so in early stage PD cases as opposed to late (sirtuin1 expression in early and late stage PD cases, 2.240 ± 0.295 and 1.600 ± 0.157 relative to control respectively, $p<0.001$ and $p<0.05$). Significant reductions on the other hand were observed in sirtuin1 expression in the frontal cortex of both early and late stage PD cases ($p<0.01$ in both comparisons). A similar pattern of changes was also observed with sirtuin2 expression. No significant changes were observed in the midbrain however a greater level of sirtuin2 expression was observed in the putamen compared with controls, this reached significance in late stage PD cases (late stage PD cases, 1.597 ± 0.295 fold change from control, $p<0.05$). Additionally, reductions in sirtuin2 expression were observed in the frontal cortex of both early and late stage PD cases. Summary of changes shown in table 3.2.

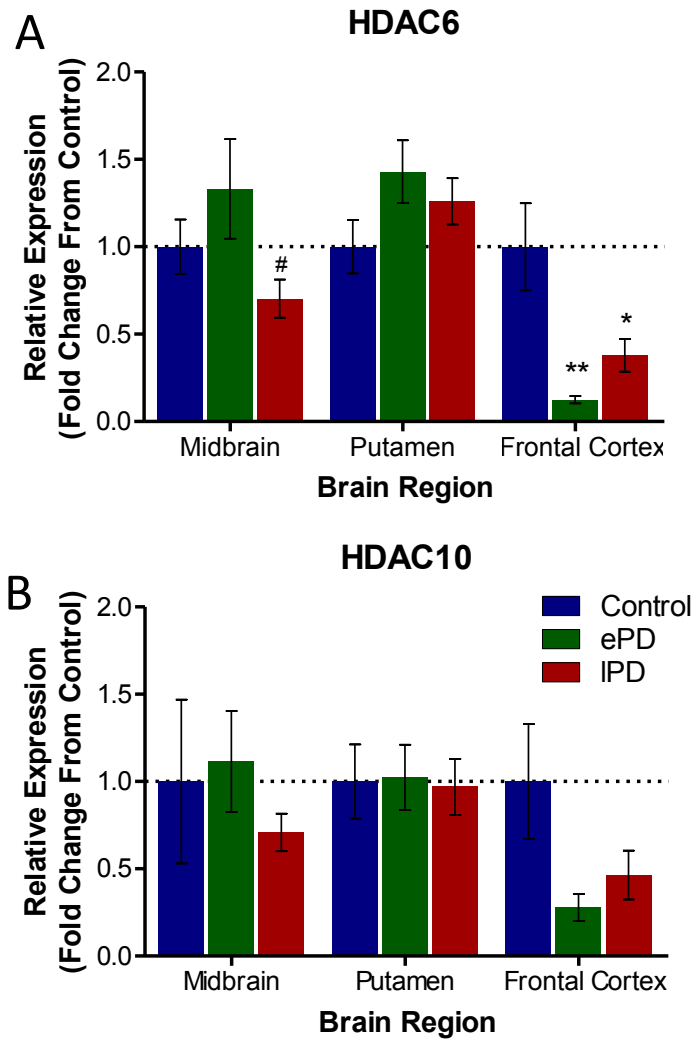

Figure 3.6 – HDAC Class IIb Expression in the Parkinsonian Brain

Expression of (A) HDAC6 and (B) HDAC10 in the midbrain, putamen and frontal cortex of control and early and late stage PD brains. Statistical significance from control group indicated with asterisks: *p<0.05. Statistical significance from early PD group indicated with hashes: #p<0.05. n=8-12 per group. Abbreviations: ePD, early stage PD; lPD, late stage PD.

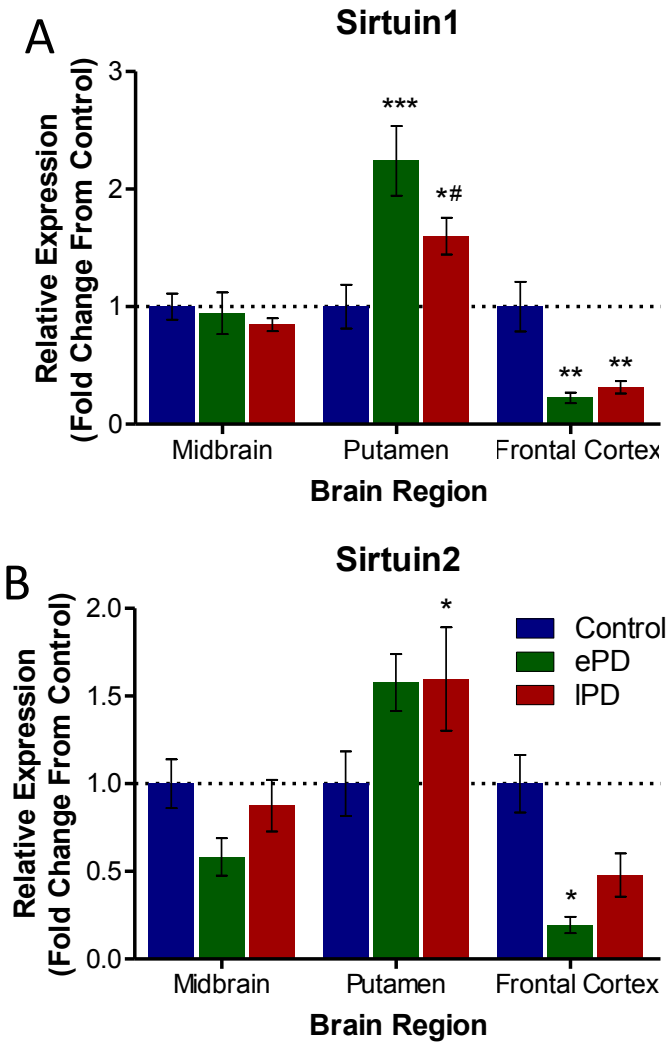

Figure 3.7 – HDAC Class III Expression in the Parkinsonian Brain

Expression of (A) sirtuin1 and (B) sirtuin2 in the midbrain, putamen and frontal cortex of control and early and late stage PD brains. Statistical significance from control group indicated with asterisks: *p<0.05; **p<0.01, ***p<0.001. Statistical significance from early PD group indicated with hashes: #p<0.05. n=8-12 per group. Abbreviations: ePD, early stage PD; lPD, late stage PD.

Table 3.2 – Summary of Changes with Parkinson's Disease

Summary of the changes observed in TH and HLA-DPα1 expresson, histone acetylation, and HDAC isoform expression in the midbrain, putamen and frontal cortex with PD development. Arrows designate changes: ↑increase, ↓decrease, ↔no overt change. First arrow designates change in early PD, second arrow designates change in late PD from control.

	Midbrain	***Putamen***	***Frontal Cortex***
TH	↓↓	↔↔	
HLA-DPα1	↑↑	↑↑	↓↓
AcH3-Lys9	↑↑	↔↔	↑↓
HDAC1	↔↔	↔↔	↓↓
HDAC2	↔↔	↑↑	↓↓
HDAC3	↓↓	↔↔	↓↓
HDAC8	↔↔	↑↑	↓↓
HDAC4	↔↔	↑↑	↓↓
HDAC5	↓↓	↔↔	↓↓
HDAC7	↓↓	↔↔	↓↓
HDAC9	↔↔	↔↔	↓↓
HDAC6	↔↓	↔↔	↓↓
HDAC10	↔↓	↔↔	↓↓
Sirtuin1	↔↔	↑↑	↓↓
Sirtuin2	↓↔	↑↑	↓↓

3.5 – Discussion

It has been observed here that a number of changes exist in levels of both histone acetylation and HDAC expression in regions of the Parkinsonian brain (table 3.2). Accompanying these changes, as would be expected, a reduction in TH expression was observed in the midbrain of PD disease cases which worsens with disease progression. Added to this were increases in HLA-DPα1, a marker of microglial activation, in both the midbrain and putamen. Dependent on the isoform, expression of many of the HDACs were observed to either be unchanged or reduced with disease progression in the midbrain. In contrast, increases of a number of the HDAC isoforms were observed in the putamen. The frontal cortex however was shown to present marked reductions in the expression levels in the majority of the HDAC isoforms tested here. Careful interpretation of these data will add insight into the possible pathogenic effects of alterations of HDAC expression in PD.

This is the first instance in which HDAC isoform expression in the Parkinsonian brain has been quantified. Due to the well-defined link between HDACs and cancer, expression studies have been conducted in a number of tumour types demonstrating their alteration in diseased tissue (Poyet et al., 2014, Pacheco and Nielsen, 2012, Yeung et al., 2004, Zhang et al., 2004, Wilson et al., 2006). Yet to the authors knowledge such a study is yet to be conducted in the neurodegenerative diseased brain, the only study of diseased brain tissue being conducted upon astrocytoma brain tumours (Lucio-Eterovic et al., 2008).

Based on the findings by Broide et al (2007), in the rat SNpc, HDAC expression is confined mainly to HDAC3, 4, 5 and 11. Lower levels of expression of HDAC1, 2, 6, 7, 8 and 9 are also known to be present in the SNpc however, yet HDAC10 is thought to be absent. In the putamen, HDAC2, 3, 5 and 11 are known to be most abundant, with lower levels of expression of HDAC1, 4, 6 and 7, and absence of HDAC8, 9 and 10. In the frontal cortex however, all of the 'classical' HDACs are known to be present: HDAC1, 2, 3, 4, 5 and 11 are expressed most abundantly with lower levels of expression of HDAC6, 7, 8, 9 and 10. It is important to note however that these *in situ* findings were based on HDAC expression in the rat brain and hence while still of relevance to the current study, do not translate directly to HDACs in the human brain. For example here however, mRNA for HDACs 1-10 and sirtuin1 and 2 were all detected in the midbrain, putamen and frontal cortex, yet due to the comparative method of qRT-PCR analysis used it is impossible to tell from the current data as to the absolute amounts of HDAC mRNA expression in each of these brain regions. However a number of differences were detected in the relative expression of HDAC isoforms from their expression in the midbrain of control tissue. In the putamen for example, reduced expression of HDAC1, 3, 6, 7, and 8, and sirtuin1 and 2 were observed relative to the midbrain. Whereas in the frontal cortex, greater expression levels of HDAC4, 6, 7, 8, 9, and 10, and sirtuin1 and 2 were observed compared to the

midbrain. It is difficult to directly comment on the agreement of these findings in humans compared to those previously published in rats due to the 'relative' rather than 'absolute' quantifications of HDAC isoform expressions presented here and by Broide et al (2007). However given the findings of altered HDAC isoform expression in PD presented here and the implication of HDACIs for neuroprotection in PD, a full mapping of HDAC isoform expression in the human brain is warranted. To the best of the authors' knowledge, a full study of HDAC isoform expression using *in situ* hybridisation in the human brain is yet to be conducted. Likewise the brain distribution of the sirtuins is yet to be mapped in either rat or human. Advances have recently been made in the development of radiolabelled HDACIs and HDAC substrates for Positron Emission Tomography (PET) imaging however, allowing direct imaging of HDACs within the brains of conscious patients. Due to the unavailability of many isoform specific HDACIs, it may be some time before HDAC isoforms themselves can be directly images in humans. This represents an exciting prospect however, given the implication shown here of HDAC expression in PD pathogenesis.

A reduction in histone acetylation in degenerating neurons was first observed by Caroline Rouaux and colleagues (2003) which was soon confirmed in cells overexpressing αSyn: Kontopoulos and colleagues (2006) suggesting that this is due to αSyn 'masking' histone proteins directly resulting in a reduction in histone acetylation and subsequent cell death. In the midbrain, in human PD however, it has been observed here that an increase in histone acetylation exists rather than a decrease. However a reduction in TH expression was also observed in the region suggestive of dopaminergic neuronal degeneration. Perhaps then because of the reduced population of dopaminergic neurons in the midbrain in PD, which according to the literature exhibit a reduction in histone acetylation, any decrease in acetylation observed in the remaining cells is diluted in this brain region by the histone acetylation level of glial and other neuronal cell populations present. Likewise, in these same samples an increase in HLA-DPα1 expression was also observed, suggestive of an increased population of activated microglia. Upon activation, microglia upregulate their expression of numerous cytokines and immunomodulatory factors, therefore it is thought that chromatin would be in a relaxed, acetylated state, allowing for transcription factor access to DNA. In accordance with increased expression of HLA-DPα1 in the midbrain, an overall increase in histone acetylation was observed. In conjunction with these changes, reduced expression of HDAC3, 5 and 7 were observed with PD development and a reduction of HDAC6 and 10 in late stage PD cases was also observed. Additionally the expression levels of other HDACs remain unchanged from control. These changes are observed on a background of severe neuronal degeneration within the midbrain, i.e. 45.1 and 78.0% loss of TH expression in early and late stage cases respectively. The static nature or subtle reductions in HDAC isoform expression observed in the midbrain with PD development,

combined with the significant neurodegeneration in this region perhaps suggest then that HDAC expression is actually increased in surviving neurons. Further study of isolated degenerating neurons is therefore warranted to help elucidate the role of increased HDAC expression in these cells, and help understand the implications of such an increase in PD pathogenesis.

In the putamen however, there was only a subtle reduction in TH expression, yet significant increases of HLA-DPα1 expression in both early and late stage PD. In line with previously findings however (Kontopoulos et al., 2006, Rouaux et al., 2003), it would be assumed that degenerating dopaminergic projections from the SNpc to this area, despite being only projections and therefore not expressing the same magnitude of TH which would be expressed in the cell body in the SNpc, would exhibit histone deacetylation. Yet because of the coincidental increase in activated microglia in this area it is thought that these two changes counteract each other, resulting in the lack of either histone acetylation or deacetylation observed. What is interesting however, are the increases of HDAC isoform expression in this area. Though because of the lack of change in acetylation, it would be reasonable to assume that corresponding increases in the expression of HATs were also evident in the putamen in PD. HDAC isoforms, as has been previously discussed however, have numerous non-histone effects, many of which could be linked to pathogenesis in PD. The disease dependent increases of expression of HDAC2, 4 and 8 as well as sirtuin1 and 2 therefore warrant further investigation as to their effects when overexpressed.

According to Braak staging, the frontal cortex does not typically become affected in PD until Braak stage 6, i.e. late PD (Braak et al., 2003). However in both the early (Braak stge 3/4) and late (Braak stage 6) stage PD cases examined here, a reduction in HLA-DPα1, a marker of activated microglia, was observed in this brain region. In line with this reduction in activated microglia in the area, reduced expression of all of the HDAC isoforms was similarly observed. What is most interesting about the results presented here however are the changes in histone acetylation in the frontal cortex. Despite the apparent lack of Parkinsonian pathology in the frontal cortex of early PD cases, in line with the reduction of HDAC expression, a significant increase in histone acetylation is observed. However, in late stage PD cases, where αSyn pathology is known to have reached the frontal cortex, in conjunction with a similar reduction in microglia marker expression to early PD cases, histone acetylation in the frontal cortex of these late stage cases is reduced. Likewise, HDAC expression in these late stage cases, with many of the isoforms is slightly greater than that of the early stage cases. These findings therefore corroborate those previously described in which αSyn pathology was shown to cause histone deacetylation: histone acetylation observed in early stage PD cases where αSyn pathology is known not to be present in the frontal cortex, whereas histone

deacetylation is observed once αSyn pathology becomes evident in this brain region, with both regions displaying similar levels of microglial marker expression.

Although the current dataset, for the first time, identifies perturbations in histone acetylation and HDAC isoform expression in the Parkinsonian brain, it is important to note that in the current study protein and mRNA were extracted from whole brain tissue sections from the post-mortem brain block containing a region of interest, rather than from either dopaminergic neurons or microglia specifically. In the midbrain samples for example, a mixed population of both degenerating dopaminergic neurons and activated microglial would therefore exhibit a profile of acetylation and HDAC expression unrepresentative of either cell type, but the histone acetylation and HDAC expression in the brain region alone. This therefore, makes interpretation of the data difficult when trying to ascertain acetylation and HDAC expression in an individual population of cells within it. Similarly, the astrocytes and oligodendrocytes have yet to be considered, their histone acetylation status and HDAC expression patterns will too affect that observed in whole brain tissue samples, adding further complexity to the dataset. Although it has been surmised above as to the contribution of both neurons and microglia to the changes observed, this remains conjecture. To truly understand the state of histone acetylation and HDAC expression in degenerating dopaminergic neurons and/or activated microglia in PD, techniques such as laser capture microdissection need be utilised to isolate specific cell types from a region of interest and conduct protein and mRNA analysis on the resulting extracts. Until then the result presented here can only give an indication of the acetylation and HDAC expression within degenerating regions of the brain.

Reductions in the expression of all of the HDAC isoforms was seen here in the frontal cortex, however what is most interesting is the alterations in the expression levels of HDAC isoforms in the other two brain regions examined, which play a greater role in PD pathogenesis: the midbrain and the putamen. With the exception of only a few HDAC isoforms, it is interesting to note that expression of a given HDAC isoform is affected in either the midbrain or putamen, rarely both. For example, in the midbrain, expression of HDAC3, 5, 7, 6 and 10, and sirtuin2 are reduced, whereas in the putamen, expression of HDAC2, 4, 6 and 8, and sirtuin1 and 2 are increased. This makes identification of specific HDAC isoforms for targeting with HDAC very difficult, as it would appear many of them are affected in PD. Similarly, the fact that expression of a HDAC isoform is affected in either the midbrain or putamen, but rarely in both indicates that perhaps specific HDAC isoforms are differentially affected by regional pathogeneses. Of note however, unlike the other HDACs investigated here, the expression levels of HDAC6 and sirtuin2 were affected in both the midbrain and putamen, highlighting their priority for further investigation in neuroprotective and anti-inflammatory strategies. Likewise, it may be possible that HDAC isoforms are differentially affected

in different cell types, further investigation should therefore focus on identifying the effects of specific HDAC inhibition on PD pathogeneses.

3.6 – Conclusions

To conclude it has been observed here that a number of changes exist in the levels of both histone acetylation and HDAC expression in regions of the Parkinsonian brain. In the midbrain, disease dependent histone acetylation is accompanied by downregulation of a number of HDAC isoforms. In the putamen however, histone acetylation remains unchanged from controls, however marked increases in HDAC isoforms unaffected in the midbrain are seen. In the frontal cortex however, reductions in the expression levels of all the HDAC isoforms quantified here were observed, yet this was accompanied by increased histone acetylation in early stage PD cases, and reduced histone acetylation in late stage PD cases. The observed changes in HDAC isoform expression highlight HDAC6 and sirtuin2 for further investigation for neuroprotective and anti-inflammatory therapeutic strategies, due to the altered expression levels in both the midbrain and putamen in PD cases. Data presented here demonstrate the first quantification of histone acetylation and HDAC expression in the PD brain.

Chapter Four

Neuroprotective and Anti-Inflammatory Effects of Histone Deacetylase Inhibitors *In Vitro*

4 – Neuroprotective and Anti-Inflammatory Effects of Histone Deacetylase Inhibitors *In Vitro*

4.1 – Introduction

HDACIs have been theorised to be efficacious in PD. Yet the mechanism of action in how histone acetylation is transferred to neuroprotection still remains elusive. Neuroprotection and neurotrophicity are thought to be maintained though the combined transcriptional and non-transciptional effects of HDACIs. Inhibition of HDACs reduces the deacetylation of histones which is therefore thought to lead to chromatin relaxation and activation of multiple gene products conducive to neurotrophicity, anti-inflammation and subsequently neuroprotection. For example, BDNF, GDNF, Hsp70, αSyn, Blc-2, Bcl-XL, p21 and GSN have all been shown to be upregulated upon HDACI treatment (de Ruijter et al., 2003, Chuang et al., 2009). Similarly, non-transcriptional effects of HDACs i.e. the non-histone targets of HDAC catalysed deacetylation, are also thought to be involved in aiding neuroprotection (Glozak et al., 2005). For example inhibition of HDACs increases the acetylation of α-tubulin, a non-histone target, which increases microtubule stabilisation and axonal transportation aiding the release of BDNF leading to neuroprotection (Zhang et al., 2003). Additionally, gathering evidence highlights the multicellular involvement of HDACIs on other brain cells, such as: immuno-modulatory effects in microglia, and reduction of astrocytic and T-cell mediated inflammation (Dietz and Casaccia, 2010). It is apparent then that the mechanism of neuroprotection of HDACIs is likely to involve several targets, achieved through an amalgamation of these effects: microtubule stabilisation in conjunction with the upregulation of numerous neurotrophic and neuroprotective agents in neurons, immunomodulation of microglia and reduction of astrocytic inflammation simultaneously to evoke a neuroprotective parenchymal environment inauspicious to neuronal cell death.

Regardless of the neuroprotective mechanism of action, inhibition of HDAC classes using small HDAC inhibiting compounds have been observed to normalise the deficiency of histone acetylation in numerous *in vitro* and *in vivo* models of PD leading to stringent neuroprotection. Inhibition of HDACs present an excellent therapeutic target in neuroscience given the distinct patterns of expression of HDACs in the brain crossed with the large number of compounds now available designed to selectively target specific isoforms and combinations of HDAC isoforms. However, thus far it remains unknown which of the numerous HDAC subclasses present greatest neuroprotective efficacy in the mescencephalic dopaminergic neurons which are susceptible to degeneration in PD. Additionally, it remains unclear which of the HDAC subclasses present most efficacy in modulating the innate immune response in the brain, which is thought to contribute to the neuroprotective effects of this drug class. This chapter therefore aims to better understand the

effects of inhibiting specific HDAC isoforms, classes and groups of classes *in vitro*, in systems modelling both Parkinsonian neuronal degeneration and neuroimmune cell activation, in lieu of identifying lead HDACI compounds to proceed to preclinical study in subsequent chapters.

Based on their HDAC inhibiting specificity, ten HDACI compounds were chosen for study including both isoform specific and pan-HDAC inhibitors (table 4.1). Firstly, two pan-inhibitors of HDAC classes I and IIa were chosen: valproate and butyrate. These short chain fatty acids are relatively small, simple structured compounds with molecular weights not much exceeding 150g/mol. Despite strong selectivity over other HDAC classes, these compounds have relatively low potencies for HDAC classes I and IIa working in the range of millimoles rather than nanomoles (Grayson et al., 2010). Trichostatin A is also a pan-inhibitor or HDAC classes I and IIa but which also inhibits class IIb. It is a hydroxymate and therefore inhibits the zinc dependent HDAC classes with relatively equal potency (Khan et al., 2008). Nicotinamide was also chosen which acts as a pan-inhibitor of class III HDACs due to its ability to competitively bind to the NAD+ binding site of the sirtuin HDACs (Avalos et al., 2005). It is therefore thought to inhibit the activity of all seven sirtuin HDACs with relatively equal potency. MS275 was also chosen which selectively inhibits HDAC1, and to a lesser extent HDAC3 (Grayson et al., 2010). This benzamide is part of a relatively new selective class of HDACIs. Apicidin was also studied which is a cyclic peptide which specifically inhibits HDAC2, HDAC3 and to a lesser degree, HDAC8 (Khan et al., 2008). The relatively large compound suramin was also included in the study. This symmetric polyanionic nephthylurea compound inhibits both sirtuin1 and sirtuin2 isoforms of HDACs (Gregoretti et al., 2004, Trapp et al., 2007). In addition to this pan-inhibitor of both sirtuin1 and 2, isoform selective inhibitors of both sirtuin1 and sirtuin2 were also included for study. EX527 was included due to its ability to selectively inhibit sirtuin1 (Gertz et al., 2013), whilst AGK2 selectively inhibits sirtuin2 (Outeiro et al., 2007). Furthermore, in collaboration with Dr Matthew Fuchter and colleagues (Department of Medicinal Chemistry, Imperial College London), a novel sirtuin2 inhibitor synthesised in-house was also included for study, shown to exhibit far greater potency and specificity for sirtuin2 than other commercially available inhibitors (Di Fruscia et al., 2014).

The neuroprotective effects of these HDACIs will firstly be assessed *in vitro* in the N27 rat mescencephalic dopaminergic neuronal cell line. Neurodegeneration in this cell line will be induced using the irreversible UPS inhibitor, lactacystin. By convalently binding to elements of the UPS, lactacystin causes formation of ubiquitin/αSyn immunopositive inclusions leading to subsequent cell death (McNaught et al., 2002b, McNaught et al., 2002c). Cell cultures will then be treated with HDACIs to determine if the histone acetylation induced as a result of drug treatment is able to reduce/prevent the neuronal cell death induced by lactacystin. The potential of the ten HDACIs at

Table 4.1 – HDACIs Studied
HDACIs used in the current study, the chemical class of HDACI to which they belong, their molecular weight and the HDAC class(es)/isoform(s) which they inhibit.

Drug	Chemical Class	Molecular Weight (g/mol)	HDAC Class(es)/Isoform(s) Inhibited
Valproate	Short Chain Fatty Acid	166.20	Classes I and IIa
Butyrate	Short Chain Fatty Acid	87.10	Classes I and IIa
Trichostatin A	Hydroxamate	302.37	Classes I, IIa and IIb
Nicotinamide	Miscellaneous	122.12	Class III
MS275	Benzamide	376.41	HDAC1 (and 3)
Apicidin	Cyclic Peptide	623.78	HDAC2 and 3 (and 8)
Suramin	Miscellaneous	1297.29	Sirtuin 1 and 2
EX527	Miscellaneous	248.71	Sirtuin 1
AGK2	Miscellaneous	434.27	Sirtuin 2
ICL-SIRT078	Miscellaneous	482.00	Sirtuin 2

reducing microglial activation will then also assessed *in vitro,* in a mouse N9 microglial cell line. When cultured and treated with LPS, this microglial cell line displays a multi-faceted profile of activation: adopting an activated amoeboid morphology, upregulating pro-infammatory cytokines such as TNF-α, IL-6 and IL-1β, and activation of iNOS resulting in production of NO. Cell cultures will then be treated with HDACIs to determine if the histone acetylation induced as a result of drug treatment is able to reduce/prevent the microglial activation induced by LPS.

4.2 – Aims of Chapter

The aims of this chapter are therefore to:

1. Test the potential of a range of isoform specific and isoform non-specific HDACIs at reducing lactacystin induced cell death in the rat mescencephalic dopaminergic N27 neuronal cell line.
    a. Confirm the suitability of the N27 cell line at modelling Parkinsonian dopaminergic neuronal cell death *in vitro* by confirming their expression of markers of dopaminergic neurons
    b. Optimise an appropriate concentration and incubation period of lactacystin to be used to model neurodegeneration in N27 cells for subsequent neuroprotection studies, and quantify changes in histone acetylation induced as a result of incubation of N27 cells with lactacystin for the optimised time period and concentration
    c. Optimise an appropriate time period in which to pre-treat N27 cells with candidate neuroprotective HDACIs in subsequent neuroprotection studies
    d. Test the potential of a range of isoform specific and isoform non-specific HDACIs against lactacystin induced neurodegeneration in the N27 cell line
2. Test the potential of a range of isoform specific and isoform non-specific histone deacetylase inhibitors at reducing LPS induced activation in the mouse N9 microglial cell line.
    a. Confirm the suitability of the N9 cell line at modelling microglial activation *in vitro* by confirming their expression of markers of microglial cells
    b. Optimise an appropriate concentration and incubation period of LPS to be used to model microglial activation in N9 cells for subsequent activation reduction studies and quantify changes in histone acetylation as a result of incubation of N9 cells with LPS for the optimised time period and concentration
    c. Optimise an appropriate time period in which to pre-treat N9 cells with candidate neuroprotective HDACIs in subsequent activation reduction studies
    d. Test the anti-inflammatory effects of a range of isoform specific and isoform non-specific HDACIs against LPS induced microglial activation in the N9 cell line

4.3 – Experimental Design

4.3.1 - Testing the Neuroprotective Potential of HDACIs at Reducing Lactacystin Induced Cell Death in the Rat Mescencephalic Dopaminergic N27 Neuronal Cell Line

In order to accurately and reliability test the potential of a range of isoform specific and non-specific HDACIs at reducing lactacystin induced cell death in the rat mescencephalic dopaminergic N27 neuronal cell line, a number of parameters needed to be confirmed and optimised. Firstly the suitability of the cell line at modelling Parkinsonian dopaminergic neuronal cell death *in vitro*, the concentration and time period in which to incubate N27 cells with lactacystin in subsequent neuroprotection studies, and an appropriate pre-treatment incubation period with HDACIs. For these experiments a number of different *in vitro* study designs were used dependent on the parameter being tested/optimised. These study formats are described below (graphical illustration in figure 4.1)

The suitability of the N27 cell line at modelling Parkinsonian dopaminergic neuronal cell death *in vitro* was firstly confirmed by verifying N27 cell expression of markers of dopaminergic (TH) neurons (NeuN). For this, N27 cells were seeded at increasing densities in a 6 well plate 24hrs prior to them being lysed and the TH and NeuN content of lysates analysed using Western blot analysis (figure 4.1A). In addition, a lysate of N9 cells was run simultaneously as a negative control which should not express either TH or NeuN.

In order to test the potential of HDACIs against the neurotoxic effects of lactacystin in the N27 cell line, a concentration of lactacystin capable of inducing an appropriate sub-maximal level of cell death firstly needed to be optimised. For this N27 cells were seeded at 10 x 10^3 cells/well into 96 well plates 24hrs prior to being treated with either lactacystin (0.2 to 10µM) or vehicle (PBS) and left to incubate for 24hrs. After this time the MTS, NR, and Bradford assays were conducted on cell containing wells to quantify the level of cytotoxicity induced as a result of lactacystin incubation (figure 4.1B). To elucidate the timecourse of lactacystin toxicity in N27 cells and for optimisation of the most appropriate incubation period of N27 cells in lactacystin, N27 cells were firstly seeded at 10 x 10^3 cells/well into a 96 well plate 24hrs prior to being treated with the concentration of lactacystin previously identified as being capable of causing an appropriate sub-maximal level of neurodegeneration in N27 cultures after 24hrs. Cell cultures were left to incubate in this concentration of lactacystin for a range of timepoints (0 to 72hrs) before MTS, NR, and Bradford assays were conducted on cell containing wells to quantify the level of cytotoxicity caused by lactacystin exposure for these timepoints (figure 4.1C). The change in histone acetylation as a result of incubation of N27 cells with the optimised concentration of lactacystin for the optimised time period was then quantified by firstly seeding N27 cells at 500 x 10^3 cells/well into a 6 well plate 24hrs

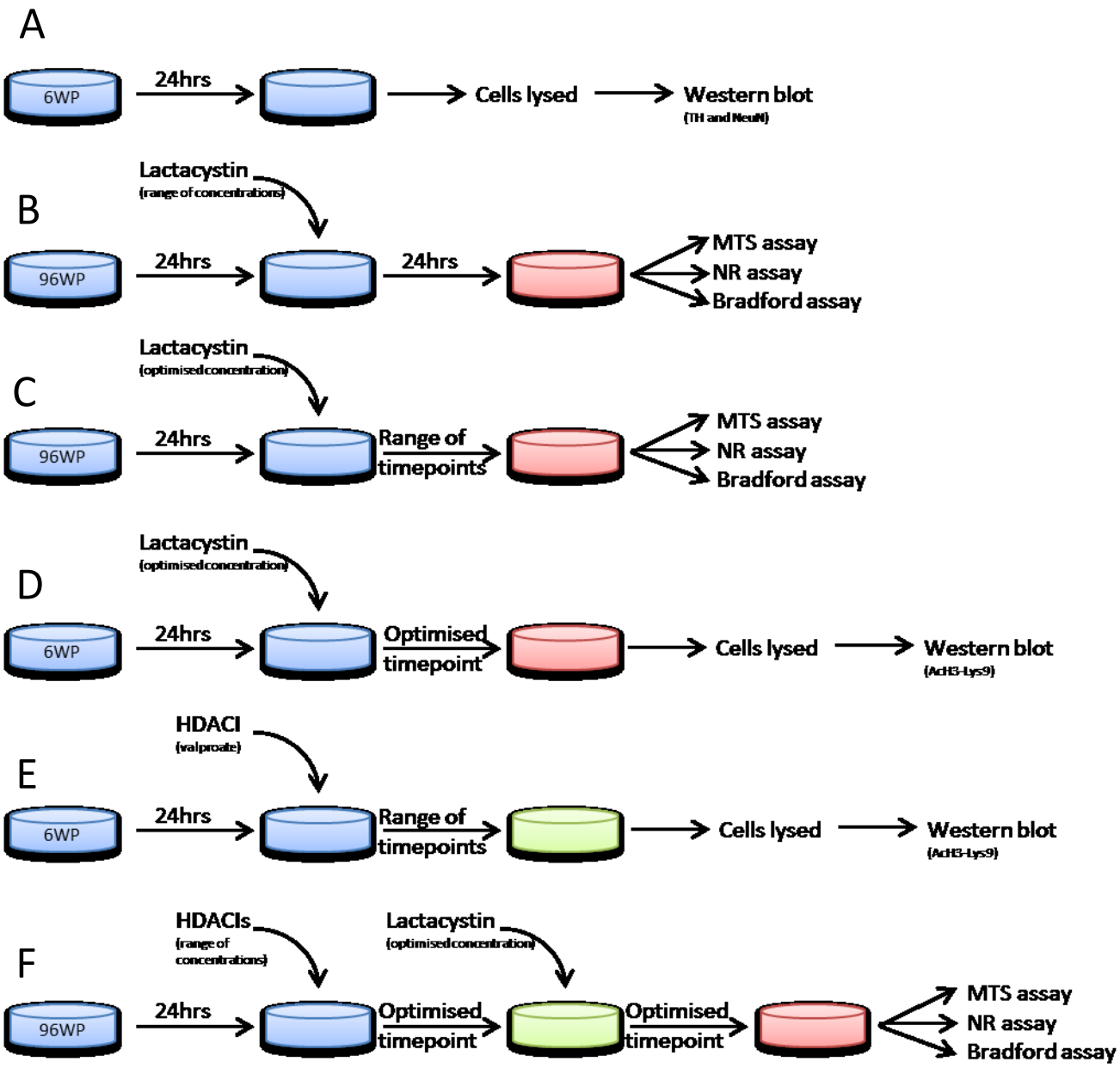

Figure 4.1 – N27 Cell Culture Study Design Schematics

Schematic of study designs used for (A) verification of N27 expression of TH and NeuN, (B) optimisation of lactacystin concentration used to induce a sub-maximal level of neurodegeneration in subsequent studies, (C) optimisation of lactacystin incubation period used to induce sub-maximal level of neurodegeneration in subsequent studies, (D) quantifying the extent of histone acetylation after incubation of N27 cells will previously optimised concentration and incubation period with lactacystin, (E) optimisation of pre-treatment incubation period with HDACIs required to induce histone hyperacetylation in N27 cells and (F) testing the neuroprotective potential of a range of isoform specific and isoform non-specific HDACIs against lactacystin induced neurodegeneration in the N27 cell line. Abbreviations: 6WP, 6 well plate; 96WP, 96 well plate.

prior to them being incubated with either the previously established optimal concentration of lactacystin or vehicle (PBS) for the previous established time period. Cells were then lysed and the level of histone acetylation quantified using Western blot analysis for AcH3-Lys9 (figure 4.1D).

Due to the transcription dependent mechanism of HDACIs, cell cultures were pre-treated with HDACIs in order to allow for appropriate transcription and translation to occur prior to toxin administration. To establish the optimal timepoint at which to pre-treat cells with HDACIs, histone acetylation was measured after treatment with a reference HDACI, valproate, due to it being extensively shown to cause histone hyperacetylation *in vitro* and *in vivo* (Gottlicher et al., 2001, Kidd and Schneider, 2010, Kidd and Schneider, 2011, Leng and Chuang, 2006, Marinova et al., 2009, Pan et al., 2005, Phiel et al., 2001). N27 cells were seeded at 500 x 10^3 cells/well into a 6 well plate 24hrs prior to them being treated with valproate (1µM) and incubated for a range of timepoints (0 to 72hrs). After this time cells were then lysed and the level of histone acetylation as a result HDACI treatment was then quantified using Western blot analysis for AcH3-Lys9 (figure 4.1E).

Finally to test the neuroprotective potential of a range of isoform specific and isoform non-specific HDACIs against lactacystin induced neurodegeneration in the N27 cell line, N27 cells were seeded at 10 x 10^3 cells/well into a 96 well plate 24hrs prior to them being pre-treated with either vehicle (PBS) or HDACIs at a range of concentrations (nine 10-fold serial dilutions of a saturated stock solution in PBS) and left to incubate for the previously established optimal timepoint for HDACI pre-treatment. After this time, lactacystin or vehicle (PBS) was then added to cell cultures containing HDACIs/vehicle at the optimised concentration required for submaximal neurodegeneration and left to incubate for the optimised time period. After this time MTS, NR and Bradford assays were conducted on HDACI/lactacystin treated cells to quantify the level of HDACI induced neuroprotection against lactacystin (figure 4.1F).

4.3.2 - Testing the Potential of HDACIs at Reducing LPS Induced Activation of the Mouse N9 Microglial Cell Line

In order to accurately and reliably test the potential of a range of isoform specific and non-specific HDACIs at reducing LPS induced activation in the mouse N9 microglial cell line, a number of parameters needed to be confirmed and optimised. Firstly the suitability of the cell line at modelling microglial activation *in vitro*, the concentration and time period in which to incubate N9 cells with LPS in subsequent activation reduction studies, and an appropriate pre-treatment incubation period with HDACIs. For these experiments, like above, a number of different *in vitro* study designs were used dependent on the parameter being tested/optimised. These study formats are described below (graphical illustration in figure 4.2).

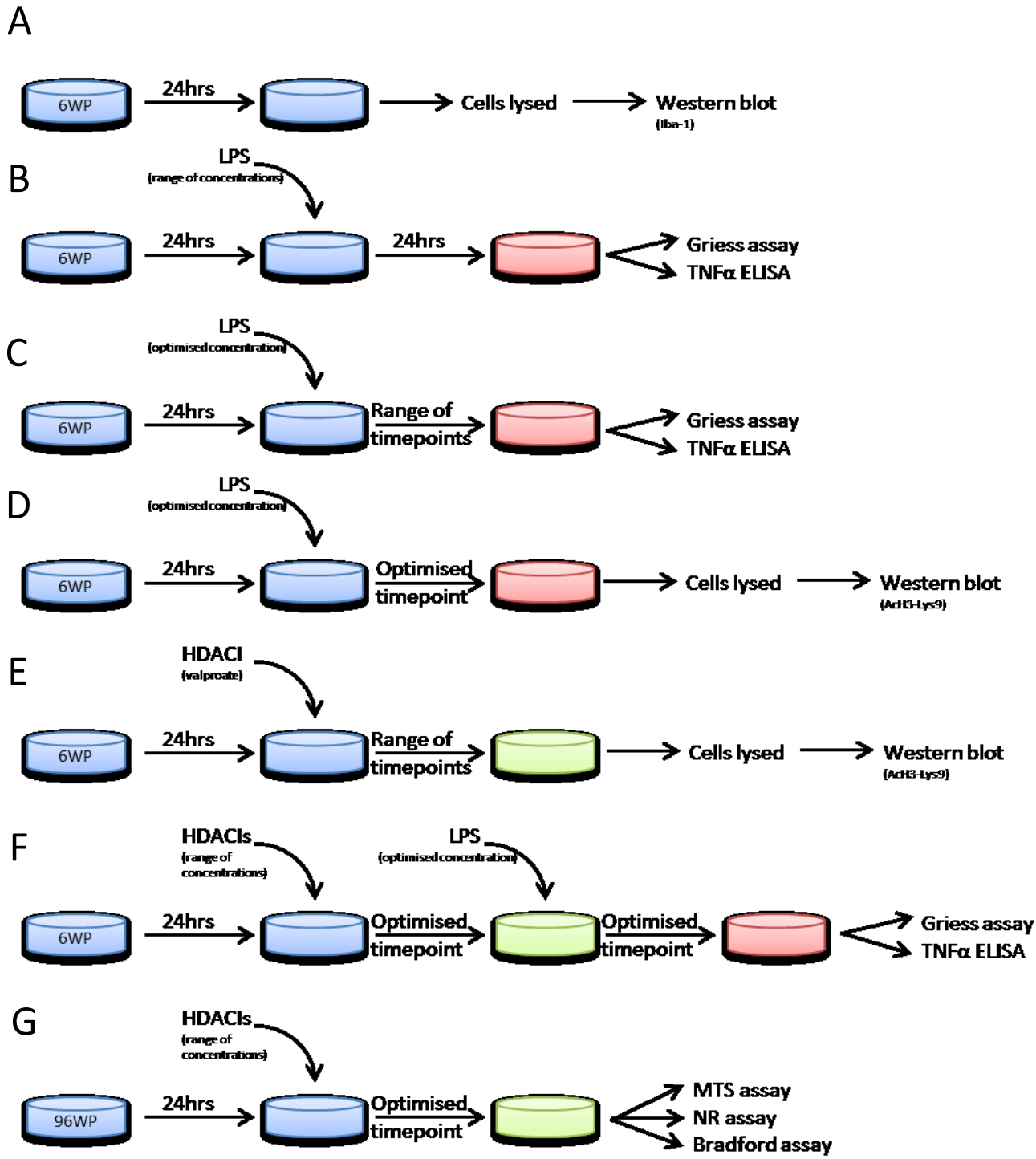

Figure 4.2 – N9 Cell Culture Study Design Schematics

Schematic of study designs used for (A) verification of N9 expression of Iba-1, (B) optimisation of LPS concentration used to induce a sub-maximal level of activation in subsequent studies, (C) optimisation of LPS incubation period used to induce sub-maximal level of activation in subsequent studies, (D) quantifying the extent of histone acetylation after incubation of N9 cells will previously optimised concentration and incubation period with LPS, (E) optimisation of pre-treatment incubation period with HDACIs required to induce histone hyperacetylation in N9 cells, (F) testing the potential of a range of isoform specific and isoform non-specific HDACIs at reducing LPS induced activation of N9 microglial cells and (G) confirming N9 cell viability after HDACI treatment. Abbreviations: 6WP, 6 well plate; 96WP, 96 well plate.

The suitability of the N9 cell line at modelling microglial activation *in vitro* was firstly confirmed by verifying N9 cell expression of a marker of microglia, Iba-1. For this, N9 cells were seeded at increasing densities in a 6 well plate 24hrs prior to them being lysed and the Iba-1 content of lysates analysed using Western blot analysis (figure 4.2A). In addition, a lysate of N27 cells was run simultaneously as a negative control which should not express Iba-1.

In order to test the potential of HDACIs at reducing LPS induced activation of the N9 cell line, a concentration of LPS capable of inducing an appropriate sub-maximal level of microglial activation firstly needed to be optimised. For this, N9 cells were seeded at 500 x 10^3 cells/well into 6 well plates 24hrs prior to them being treated with either LPS (3.90 to 1000ng/ml) or vehicle (PBS) and left to incubate for 24hrs. After this time the medium was removed from cells and Griess assays for NO quantification and ELISAs for TNFα were conducted to quantify the level of activation induced as a result of LPS incubation (figure 4.2B). To elucidate the timecourse of LPS activation of N9 cells and for optimisation of the most appropriate incubation period of N9 cells in LPS, N9 cells were firstly seeded at 500 x 10^3 cells/well into a 6 well plates 24hrs prior to them being treated with the concentration of LPS previously identified as being capable of causing an appropriate sub-maximal level of microglial activation in N9 cultures after 24hrs. Cell cultures were left to incubate in this concentration of LPS for a range of timepoints (0 to 48hrs) before the medium was removed from cells and Griess assays for NO quantification and ELISAs for TNFα were conducted to quantify the level of activation induced as a result of LPS exposure for these timepoints (figure 4.2C). The change in histone acetylation as a result of incubation of N9 cells with the optimised concentration of LPS for the optimised time period was then quantified by firstly seeding N9 cells were seeded at 500 x 10^3 cell/well into a 6 well plate 24hrs prior to them being incubated with either the previously established optimal concentration of LPS or vehicle (PBS) for the previously established time period. Cells were then lysed and the level of histone acetylation quantified using Western blot analysis for AcH3-Lys9 (figure 4.2D).

Due to the transcription dependent mechanism of HDACIs, cell cultures were pre-treated with HDACIs in order to allow for appropriate transcription and translation to occur prior to toxin administration. To establish the optimal timepoint at which to pre-treat cells with HDACIs, histone acetylation was measured after treatment with a reference HDACI, valproate, due to it being extensively shown to cause histone hyperacetylation *in vitro* and *in vivo* (Gottlicher et al., 2001, Kidd and Schneider, 2010, Kidd and Schneider, 2011, Leng and Chuang, 2006, Marinova et al., 2009, Pan et al., 2005, Phiel et al., 2001). N9 cells were seeded at 500 x 10^3 cells/well into a 6 well plate 24hrs prior to them being treated with valproate (1μM) and incubated for a range of timepoints (0 to

72hrs). After this time cells were then lysed and the level of histone acetylation as a result HDACI treatment was then quantified using Western blot analysis for AcH3-Lys9 (figure 4.2E).

Finally to test the potential of a range of isoform specific and isoform non-specific HDACIs against LPS induced activation in the N9 cell line, cells were firstly seeded in 6 well plates 24hrs prior to them being pre-treated with either vehicle (PBS) or HDACIs at a range of concentrations (nine 10-fold serial dilutions of a saturated stock solution in PBS) and left to incubate for the previously established optimal timepoint for HDACI pre-treatment. After this time, LPS or vehicle (PBS) was then added to cell cultures containing HDACIs/vehicle at the optimised concentration required for submaximal activation and left to incubate for the optimised time period. After this time the medium was removed from cells and Griess assays for NO quantification and ELISAs for TNFα were conducted to quantify the level of HDACI induced reduction of LPS induced activation (figure 4.2F). In addition, to confirm that any reduction in NO and TNFα observed were not simply the result of cytotoxicity caused by the HDACI compound, cell viability assays were conducted on cells treated with the HDACIs for the time period and concentration used in previous microglial activation studies. Briefly N9 cells were seeded in 96 well plates and left for 24hrs to readopt their natural morphology. After this time cells were incubated with the concentrations of HDACIs previously used in microglial activation reduction studies for the same time period. MTS, NR and Bradford assays were then conducted on HDACI treated cell culture wells to quantify the extent of cytotoxicity, if any, exerted by the HDACI compounds (figure 4.2G).

4.3.3 - Statistical Analysis

For experiments conducted in 96 well plates, well conditions were replicated in triplicate in each plate, the mean of which was calculated for each experiment. All experiments were repeated independently at least three times. All data is expressed as mean ± SEM between independent replicates. For correlation analysis between cellular markers (TH, NeuN and Iba-1) and seeded cell number, linear regression analyses were performed. For lactacystin and LPS dose and time response studies in N27 and N9 cells respectively, a one way ANOVA with post-hoc Dunnet's multiple comparison test, comparing all groups to the control column for each dataset. Semi-log plot data were fitted onto variable slope sigmoidal dose-response curves, and the estimated IC_{50} and R^2 values quoted. Western blot AcH3-Lys9 data for the effects of lactacystin and LPS in N27 and N9 cells respectively were analysed using individual unpaired student t-tests. Western blot AcH3-Lys9 data for the effects of HDACI treatment of N9 and N27 cells was analysed using a one way ANOVA with post-hoc Dunnet's multiple comparison test, comparing all groups to the control column for each dataset. All neuroprotection and microglial activation reduction study data in N27 and N9 cells

respectively was analysed using a one way ANOVA with post-hoc Dunnet's multiple comparison test, comparing all groups to the vehicle treated column for each dataset. All statistical tests were performed using GraphPad Prism (v5.0 for Windows, GraphPad Software, San Diego, CA, USA).

4.4 – Results

4.4.1 – Confirming the Expression of TH and NeuN in N27 Cells

N27 cells were seeded at increasing densities in 6 well plates 24hrs prior to being lysed. In addition, a well void of cells and a well containing N9 cells (seeded at 20 x 10^5 cells/well) were also included as negative controls which should not contain either TH or NeuN. The TH and NeuN protein content of well lysates was then analysed using Western blot analysis. As expected the wells containing no cells and the well containing N9 cells did not show expression of TH or either splice variant of NeuN (figure 4.3A). N27 cells seeded at increasing densities however demonstrated linearly increasing expression of TH and both spice forms of NeuN with cell number, indicative of N27 cellular expression of both markers (figure 4.3B, R^2>0.98 in all linear regression analyses).

4.4.2 – Concentration and Incubation Period of Lactacystin with N27 Cells To be Used in Subsequent Neuroprotection Studies

4.4.2.1 - Optimising Concentration of Lactacystin

N27 cells were seeded in 96 well plates 24hrs prior to the addition of lactacystin (at a range of concentrations) or vehicle (PBS). Cells were then left to incubate for 24hrs before MTS, NR, and Bradford assays were conducted on cell containing wells to quantify the level of cytotoxicity induced as a result of lactacystin incubation. In each of the three cell viability assays used here, concentrations ≥0.5µM of lactacystin demonstrated significantly reduced survival of N27 cells in culture (figure 4.4Ai, Bi and Ci). When semi-log plots of these data were constructed, each of the three assays shown here illustrated that lactacystin induced cytotoxicity through a sigmoidal profile with lactacystin concentration (figure 4.4Aii, Bii and Cii). From this data, 0.75µM lactacystin was chosen for subsequent studies due to its ability to produce a suitably robust sub-maximal level of cytotoxicity in all assays (61.81 ± 1.51%, 49.38 ± 5.99% and 51.37 ± 5.79% of control in MTS, NR and Bradford assays respectively, p<0.01 in all comparisons).

4.4.2.2 - Optimising Incubation Period of Lactacystin

N27 cells were seeded in 96 well plates 24hrs prior to the addition of lactacystin (75µM). Cells were then left to incubate for a range of timepoints before MTS, NR, and Bradford assays were conducted on cell containing wells to quantify the level of cytotoxicity induced as a result of lactacystin incubation for the time periods examined. In each of the three cell viability assays used here, timepoints ≥9hrs demonstrated significantly reduced survival of N27 cells in culture (figure 4.5A1, Bi and Ci). When semi-log plots of these data were constructed, each of the three assays shown here illustrated that lactacystin induced cytotoxicity through a sigmoidal profile with time (figure 4.5Aii, Bii and Cii). From these semi-log plots it was also evident that the majority of lactacystin induced cell

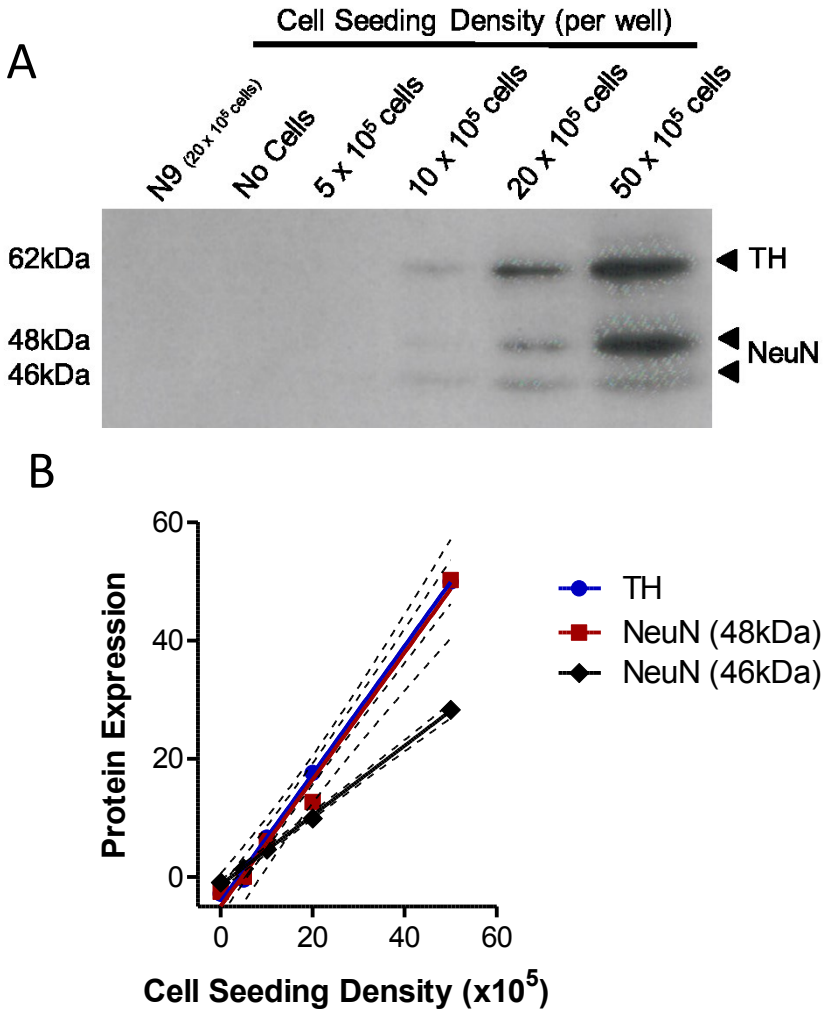

Figure 4.3 – Confirmation of N27 Expression of Dopaminergic Neuronal Markers
TH and NeuN protein content of lysates from N27 cells seeded at increasing densities were quantified using Western blot analysis for confirmation of N27 expression of markers of dopaminergic neurons. In addition a well void of cells and a well containing N9 cells (seeded at 20 x 105 cells/well) were also included as negative controls which should not contain either TH or NeuN. Equal volumes of cell lysates for each well were run on a Western blot to confirm expression of dopaminergic (TH) and neuronal (NeuN) markers. (B) Densitometry analysis of TH and NeuN bands confirming linear expression of both cellular markers with cell density. Lines indicate linear regression lines of best fit with respective 95% confidence intervals (dotted lines). (A) Representative blot of data presented in (B).

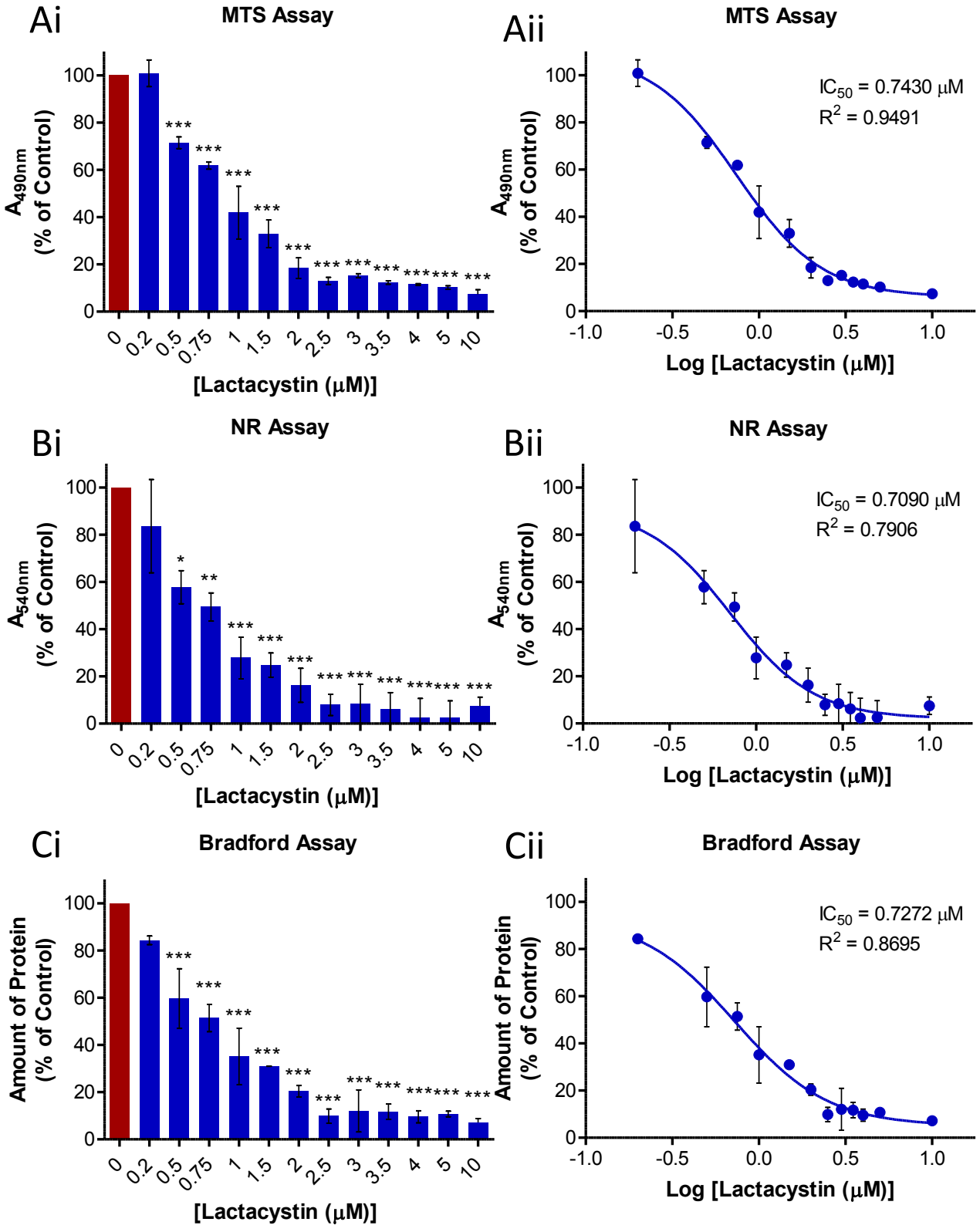

Figure 4.4 – Optimising Lactacystin Dose for Subsequent Neuroprotection Studies in N27 Cells
N27 cells were incubated in a range of concentrations of lactacystin for 24hrs in order to quantify the extent cytotoxicity as a result of lactacystin. After lactacystin treatment, MTS, NR and Bradford assays for cell viability were conducted. (Ai, Bi and Ci) Dose response data from the MTS, NR and Bradford assays respectively indicating significance from vehicle treated cells and (Aii, Bii and Cii) dose response data plotted as semi-logarithmic plot indicating IC_{50} and respective R^2 values for MTS, NR and Bradford assays respectively. Statistical significance from control cells indicated using asterisks: *p<0.05, **p<0.01, ***p<0.001. n=3.

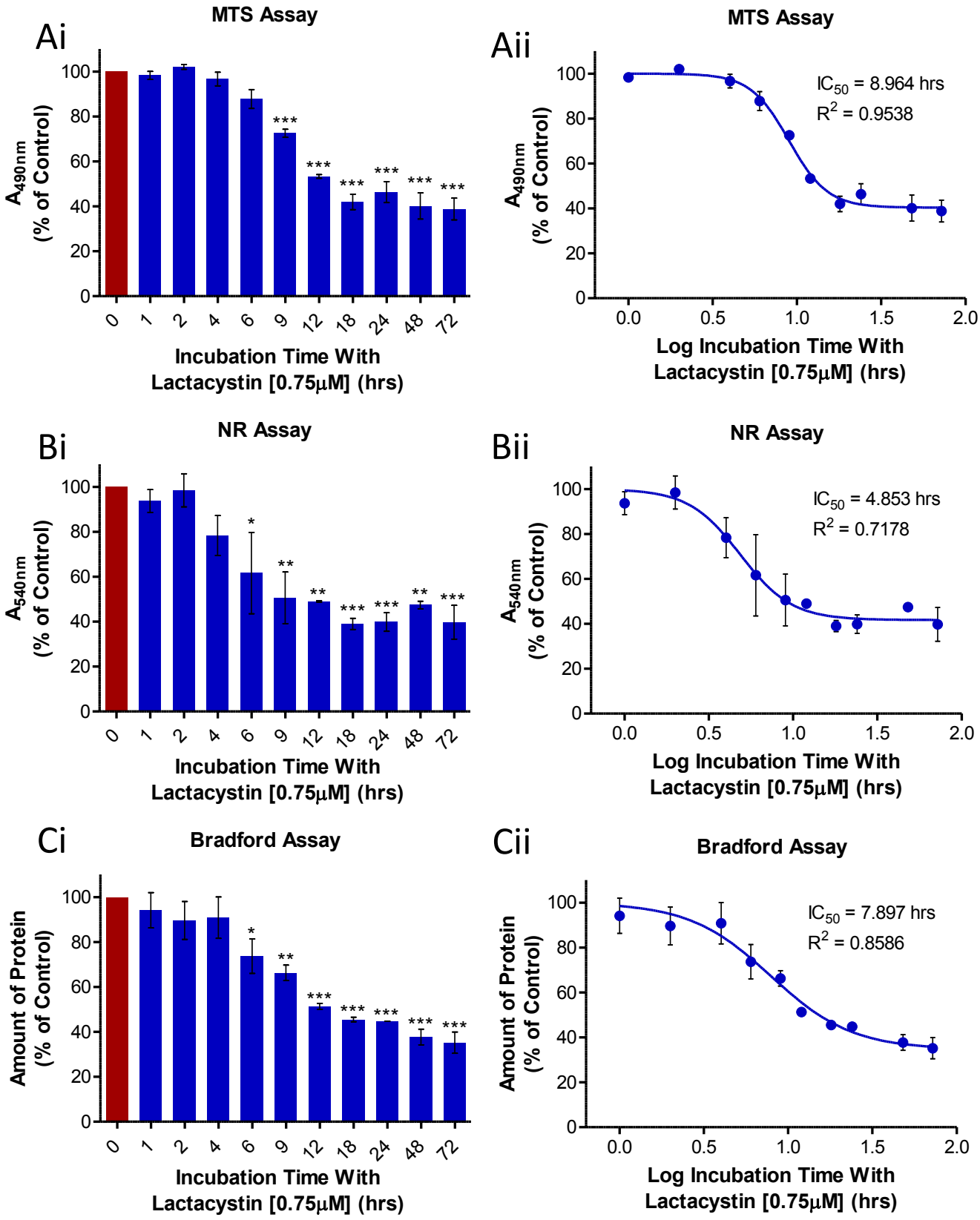

Figure 4.5 – Optimising Lactacystin Incubation Period for Subsequent Neuroprotection Studies in N27 Cells
N27 cells were incubated with lactacystin (0.75μM) for a range time periods in order to quantify the extent cytotoxicity as a result of lactacystin. After lactacystin treatment, MTS, NR and Bradford assays for cell viability were conducted. (Ai, Bi and Ci) Timecourse data from the MTS, NR and Bradford assays respectively indicating significance from untreated cells and (Aii, Bii and Cii) timecourse data plotted as semi-logarithmic plot indicating IC_{50} and respective R^2 values for MTS, NR and Bradford assays respectively. Statistical significance from control cells indicated using asterisks: *p<0.05, **p<0.01, ***p<0.001. n=3.

death occured between ~6 and 18hrs of incubation, after which time neurodegeneration plateaued and the number of surviving population remained unchanged. From this data, 24hrs lactacystin incubation was chosen for subsequent studies due to the fact that lactacystin induced neurodegeneration has come to an end by this timepoint allowing for robust detection of sub-maximal cytotoxicity in all assays.

4.4.2.3 – Histone Acetylation in Lactacystin Treated N27 Cells

For quantification of histone acetylation in N27 cells treated with the chosen concentration of lactacystin for the chosen incubation period, N27 cells were seeded in 6 well plates 24hrs prior to incubation with either lactacystin (0.75µM) or vehicle (PBS) for 24hrs. After this time cells were lysed and the AcH3-Lys9 content of lysates quantified using Western blot analysis (figure 4.6). There was significantly less AcH3-Lys9 in cell lysates from cells treated with lactacystin than vehicle treated cells indicative of histone deacetylation with lactacystin treatment (lactacystin treated, 0.187 ± 0.040 vs. vehicle treated cells, 0.348 ± 0.049, $p<0.05$).

4.4.3 – Incubation Period of HDACIs with N27 Cells To be Used in Subsequent Neuroprotection Studies

For optimisation of the appropriate pre-treatment incubation period of HDACIs to be used in subsequent neuroprotection studies, cells were seeded in 6 well plates 24hrs prior to incubation with the reference HDACI, valproate (1µM) for a range of time periods. After this time cells were lysed and the AcH3-Lys9 content of lysates quantified using Western blot analysis. There was a significant time dependent increase in AcH3-Lys9 in HDACI treated cells indicative of time-dependent histone acetylation with HDACI (valproate) treatment (figure 4.7). This increase in histone acetylation however did not become significantly different from control cell lysates until 48hrs (cells treated with valproate for 48 and 72hrs, 0.315 ± 0.038 and 0.361 ± 0.057 respectively compared to control cells, 0.091 ± 0.031, $p<0.05$ and $p<0.01$ respectively).

4.4.4 – Neuroprotective Potential of Isoform Specific and Isoform Non-Specific HDACIs against Lactacystin Induced Neurodegeneration in N27 Cells

After optimisation of the concentration and incubation period of lactacystin most suitable for inducing neurodegeneration in N27 cells, and the appropriate pre-incubation period this cell line with a HDACI the neuroprotective potential of a number of HDACIs, both isoform specific and non-specific, were tested *in vitro* in the N27 mescencephalic dopaminergic cell line. Cells were seeded in 96 well plates 24hrs prior to incubation with varying concentrations of the HDACI for 48hrs. After this time lactacystin (0.75µM) was added to cell cultures containing HDACIs/vehicle and incubated

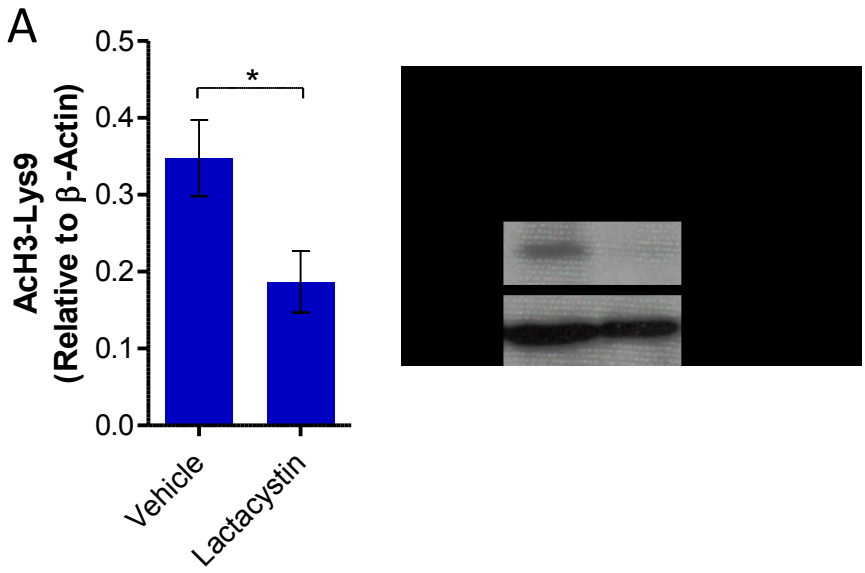

Figure 4.6 – Histone Acetylation in Lactacystin Treated N27 Cells
AcH3-Lys9 content of lysates from N27 cells treated with either lactacystin (0.75μM) of vehicle (PBS) for 24hrs were quantified by Western blot analysis. (A) Densitometry analysis of AcH3-Lys9 bands relative to β-actin used as a loading control demonstrate that there is significantly less histone acetylation in lactacystin compared to vehicle treated cells. (B) Representative blot of data presented in (A). Statistical significance indicated using asterisks: *p<0.05, **p<0.01, ***p<0.001. n=3.

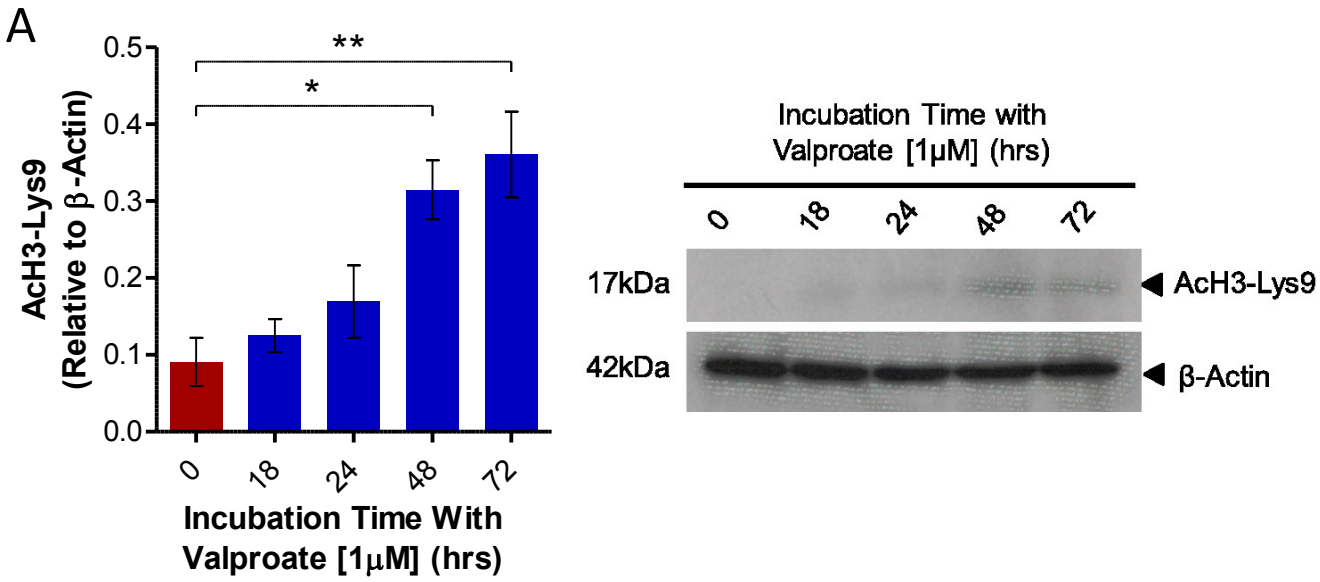

Figure 4.7 – Histone Acetylation in HDACI Treated N27 Cells

AcH3-Lys9 content of lysates from cells treated with valproate (1μM) for a range of incubation periods were quantified by Western blot analysis. (A) Densitometry analysis of AcH3-Lys9 bands relative to β-actin used as a loading control demonstrate that histone acetylation increases with incubation time with valproate. (B) Representative blot of data presented in (A). Statistical significance indicated using asterisks: *$p<0.05$, **$p<0.01$. n=3.

for a further 24hrs. After this time MTS, NR and Bradford assays were conducted on HDACI/lactacystin treated cells to quantify the level of HDACI induced neuroprotection against lactacystin.

4.4.4.1 – Neuroprotective Effects of Isoform Non-Specific HDACIs

In all three cell viability assays used here, toxicity of N27 cells was observed in concentrations of valproate ≥10μM, reaching significance from vehicle treated cells at the highest concentrations (figure 4.8A). In cells treated with lower concentrations of valproate however a very subtle neuroprotective effect was observed in two of the three cell viability assays used (NR and Bradford assays). This effect was most pronounced in cells treated with 1μM valproate, however neither of these differences reached statistical significance. A similar profile of toxicity and neuroprotection were observed in cells treated with butyrate (figure 4.8B): in all three cell viability assays used, toxicity of N27 cells was observed in concentrations of butyrate ≥100μM, reaching significance from vehicle treated cells at the highest concentrations. Likewise neuroprotection was observed in two of the three cell viability assays used. A subtle level of neuroprotection was observed in Bradford assays of butyrate treated cells most notable at 1 and 10μM however these effects did not reach significance. In NR assays of butyrate treated cells however a notable neuroprotective effect was observed at 100nM, 1μM and 10μM butyrate, reaching statistical significance from vehicle treated cells (100nM, 1μM and 10μM butyrate treated cells, 77.03 ± 7.99, 81.21 ± 9.42 and 85.62 ± 11.16% cell viability respectively compared to vehicle treated cells, 50.80 ± 2.61% cell viability, $p<0.05$, $p<0.01$ and $p<0.001$ respectively).

Toxicity of N27 cells was observed in concentrations of trichostatin A ≥10nM in all three cell viability assays, reaching significance from vehicle treated cells at higher concentrations (figure 4.9A). No overt neuroprotective effects are observed with lower trichiostatin A concentrations however.

Like with other pan-inhibitors discussed thus far, nicotinamide was toxic to N27 cells at higher concentrations, however this toxicity did not become apparent with nicotinamide until incubation with very high concentrations, several degrees of magnitude higher than others: toxicity becoming apparent at concentration ≥10mM (figure 4.9B). Similarly, no overt neuroprotection was observed against lactacystin toxicity with nicotinamide treatment. The NR assay shows some evidence of neuroprotection though given the large error the concentrations in question (10nM and 1μM) and the lack of an effect observed in other cell viability assays, this appears to be artefact.

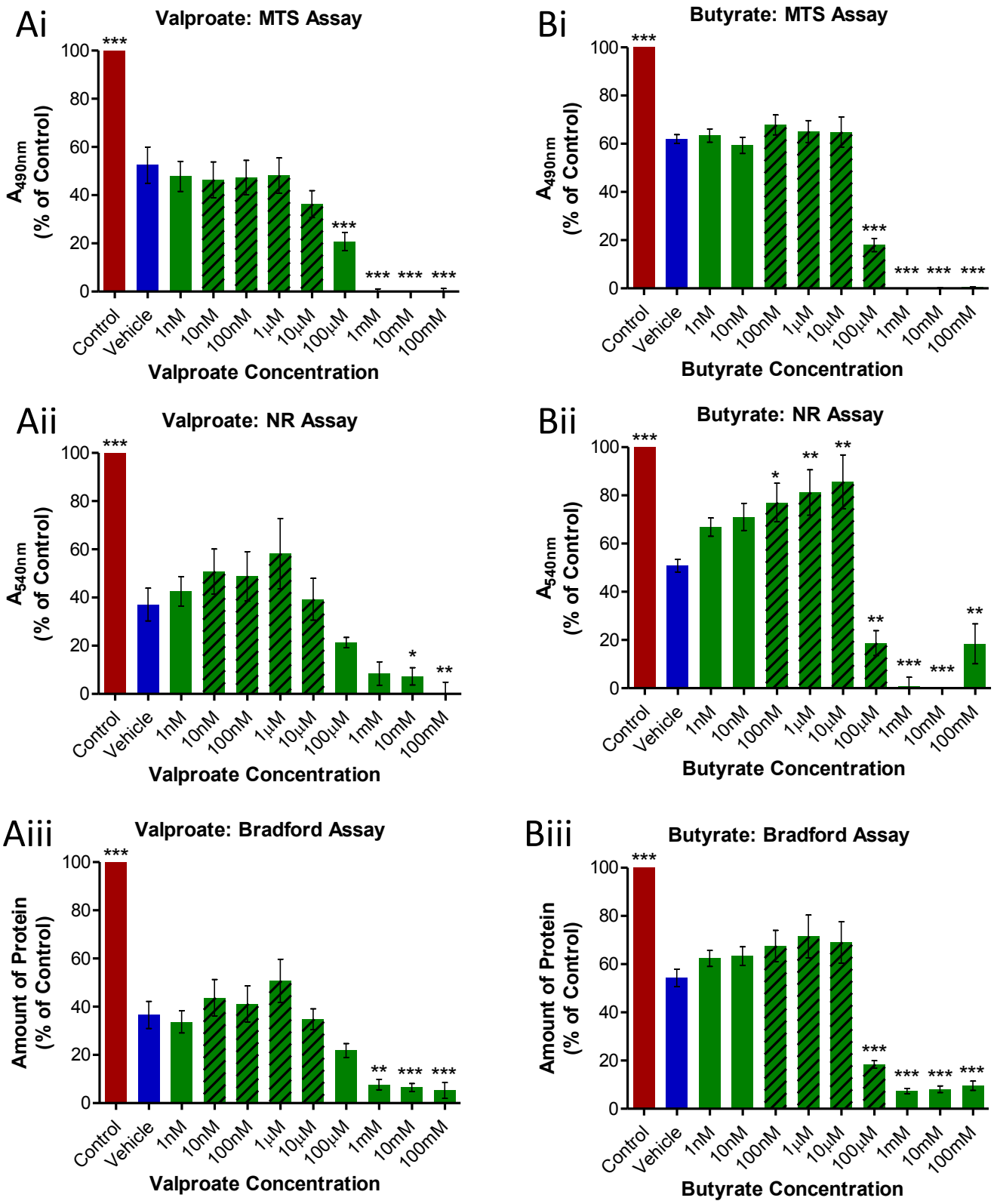

Figure 4.8 – Neuroprotective Effects of Class I and IIa HDACIs Against Lactacystin in N27 Cells
N27 cells pre-treated with HDACIs for 48hrs prior to addition of lactacystin and incubation for a further 24hrs. MTS, NR and Bradford assays were then performed for quantification of HDACI induced neuroprotection against lactacystin toxicity. Red bar indicates cells which received PBS in place of both drug and lactacystin. Blue bar indicates cells which received PBS in place of drug treatment but which received subsequent treatment with lactacystin. Green bars indicate cells treated with HDACIs and which received subsequent treatment with lactacystin. Crossed green bars indicate concentrations subsequently used for N9 experiments. (A) Valproate (class I and IIa HDACI) treated cells. (B) Butyrate (class I and IIa HDACI) treated cells. Statistical significance from vehicle treated cells indicated using asterisks: *p<0.05, **p<0.01, ***p<0.001. n=5.

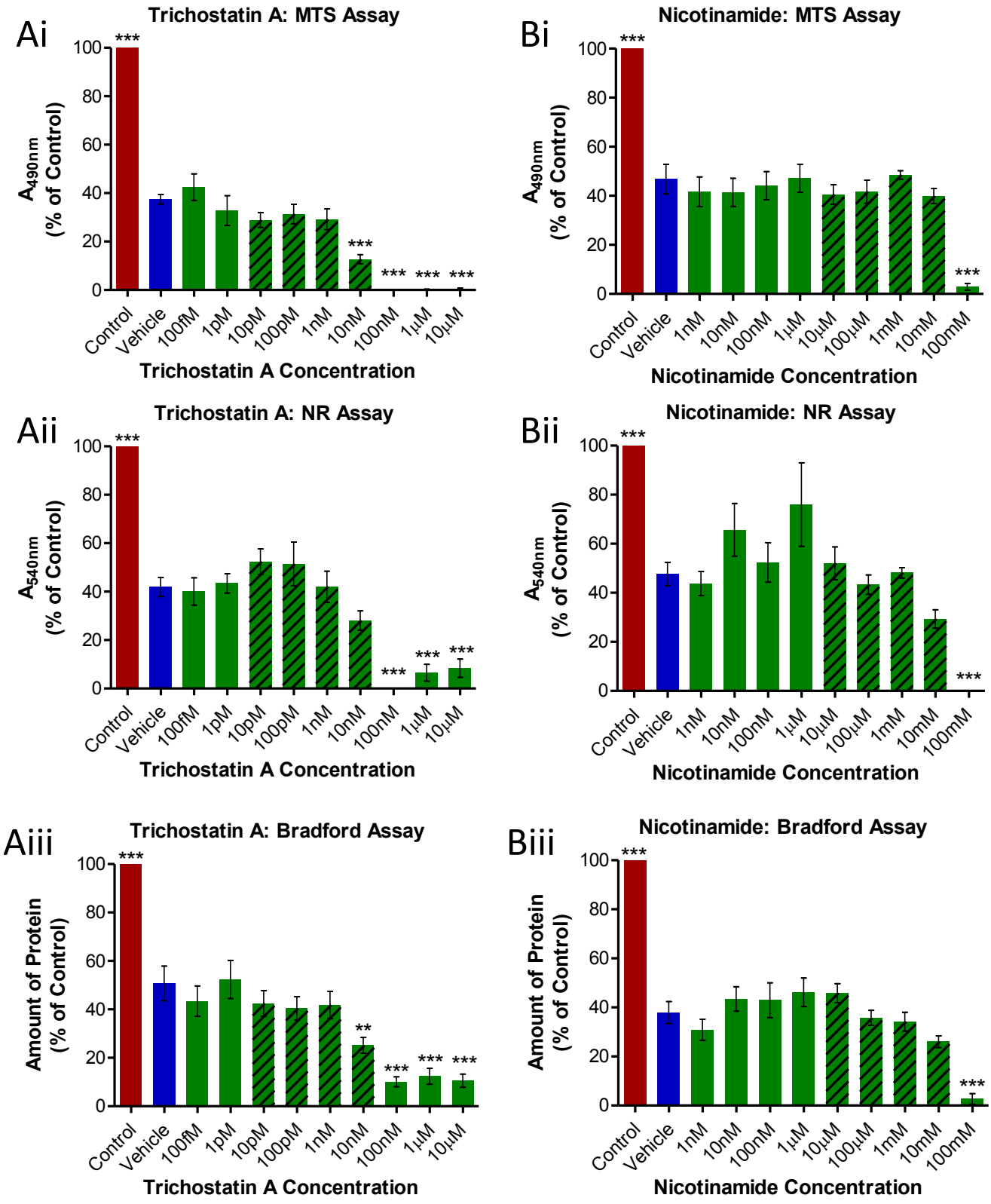

Figure 4.9 – Neuroprotective Effects of Isoform Non-Specific HADACIs Against Lactacystin in N27 Cells
N27 cells pre-treated with HDACIs for 48hrs prior to addition of lactacystin and incubation for a further 24hrs. MTS, NR and Bradford assays were then performed for quantification of HDACI induced neuroprotection against lactacystin toxicity. Red bar indicates cells which received PBS in place of both drug and lactacystin. Blue bar indicates cells which received PBS in place of drug treatment but which received subsequent treatment with lactacystin. Green bars indicate cells treated with HDACIs and which received subsequent treatment with lactacystin. Crossed green bars indicate concentrations subsequently used for N9 experiments. (A) Trichostatin A (class I, IIa and IIb HDACI) treated cells. (B) Nicotinamide (class III HDACI) treated cells. Statistical significance from vehicle treated cells indicated using asterisks: *p<0.05, **p<0.01, ***p<0.001. n=5.

4.4.4.2 – Neuroprotective Effects of Isoform Specific HDACIs

In the current study, MS275 displayed marked levels of toxicity in N27 cells, the lowest concentration of MS275 tested (100pM) inducing significant reductions in cell viability in two of the three assays (figure 4.10A, MTS assay, MS275 treated cells, 21.90 ± 7.75, vs. vehicle treated cells,48.19 ± 4.80, $p<0.001$; NR assay MS275 (100pM) treated cells, 26.99 ± 5.82, vs. vehicle treated cells, 41.70 ± 3.10, $p<0.01$). This toxicity becomes more evident at higher concentrations: MS275 given at concentrations ≥100nM inducing significantly reduced cell viability in all assays compared to vehicle treated cells, $p<0.001$ in all comparisons.

Like with all other HDACIs discussed previously higher concentrations of apicidin (≥1μM) induced cytotoxicity of N27 cells in culture evident in all three cell viability assays (figure 4.10B). No marked neuroprotective effects were observed upon incubation of N27 cells with apicidin at lower concentrations. NR assays results suggested a modest increase in cell viability most evident at 100pM however given that this effect was not observed in either of the other two assays suggest that this result appears to be artefact.

4.4.4.3 – Neuroprotective Effects of Isoform Specific Sirtuin Inhibitors

Suramin itself was observed here to be toxic towards N27 cells at concentration exceeding 10nM, reaching statistical significance form vehicle treated cells at higher concentrations tested (figure 4.11A). Due to differences between assay results it is difficult to ascertain the level of neuroprotection exhibited by the drug at lower concentrations, if any. NR and Bradford assays highlight the possibility of a very subtle level of neuroprotection at concentrations in the nM range, however these differences were not observed in MTS assay data making interpretation difficult.

Again as with many of the HDACIs mentioned thus far, EX527 was toxic at higher concentration, toxicity becoming evident at concentrations exceeding 100μM (figure 4.11B). Similarly no overt neurorprotective effect was observed with cell treatment at lower concentrations.

Of all the HDACIs tested here, Sirtuin2 inhibiting compounds exhibited the most neuroprotection against lactacystin in N27 cells. Higher concentrations (>1μM) of both of these compounds exhibited toxicity in N27 cells, however marked neuroprotection was observed upon treatment with lower concentrations of both compounds (figure 4.12A and B). With AGK2 treatment, 1μM resulted in greater cell viability than vehicle treated cells, reaching significance from vehicle treated cells in both the MTS and NR assays (figure 4.12A, AGK2 treated cells, 69.49 ± 8.80 and 65.27 ± 7.94, vs. vehicle treated cells, 32.19 ± 4.54 and 37.21 ± 5.25 in the MTS and NR assays respectively, $p<0.05$ in both comparisons). Similarly with ICL-SIRT078 treatment, protection of N27 cells was observed in all three of the cell viability assay used here, most notably but not limited to 1μM ICL-SIRT078 (figure 4.12B, ICL-SIRT078 1μM treated cells 69.25 ± 7.85, 68.80 ± 9.12 and 47.84 ±

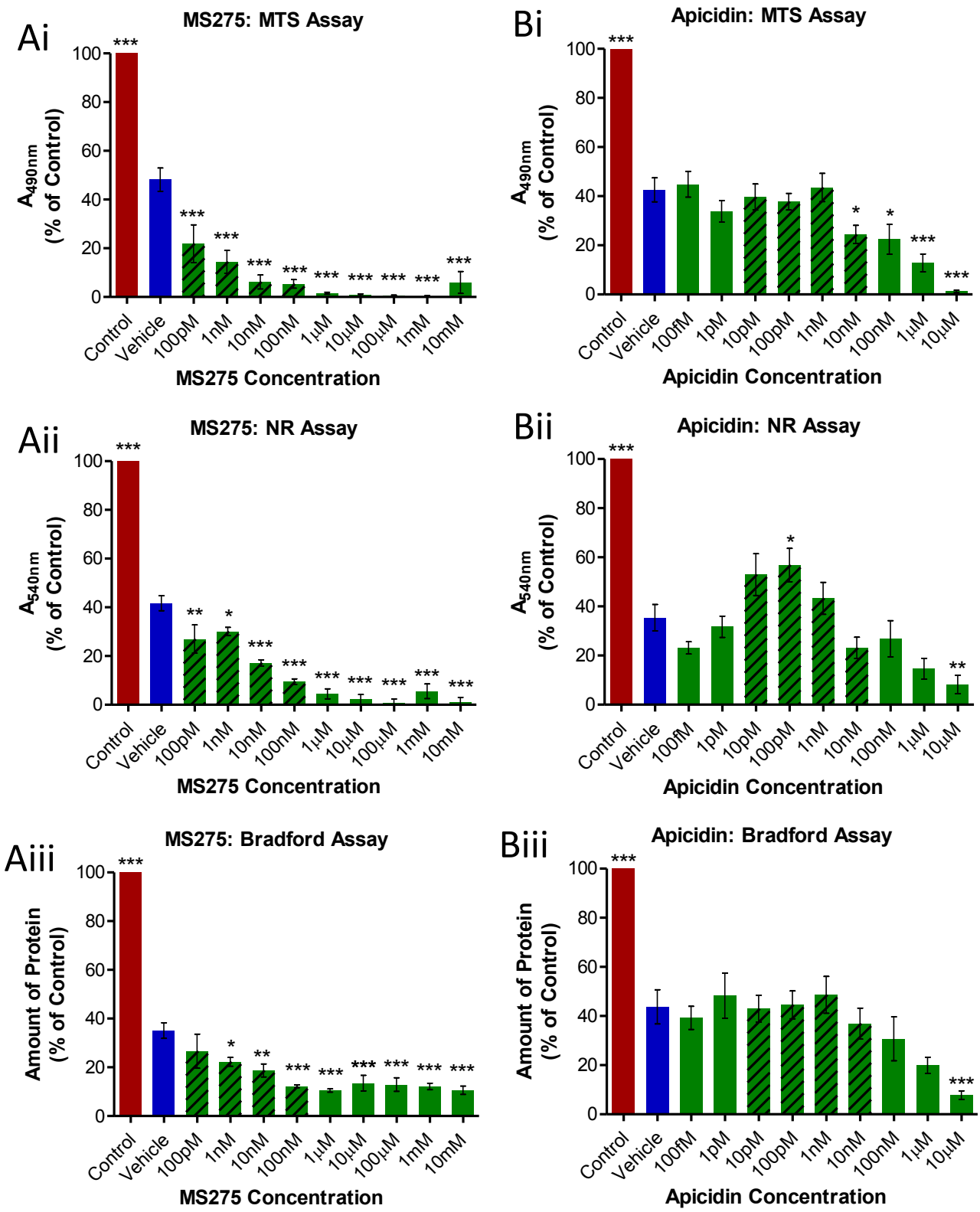

Figure 4.10 – Neuroprotective Effects of Isoform Specific HADACIs Against Lactacystin in N27 Cells
N27 cells pre-treated with HDACIs for 48hrs prior to addition of lactacystin and incubation for a further 24hrs. MTS, NR and Bradford assays were then performed for quantification of HDACI induced neuroprotection against lactacystin toxicity. Red bar indicates cells which received PBS in place of both drug and lactacystin. Blue bar indicates cells which received PBS in place of drug treatment but which received subsequent treatment with lactacystin. Green bars indicate cells treated with HDACIs and which received subsequent treatment with lactacystin. Crossed green bars indicate concentrations subsequently used for N9 experiments. (A) MS275 (HDAC1 inhibitor) treated cells. (B) Apicidin (HDAC2 and 3 inhibitor) treated cells. Statistical significance from vehicle treated cells indicated using asterisks: *p<0.05, **p<0.01, ***p<0.001. n=5.

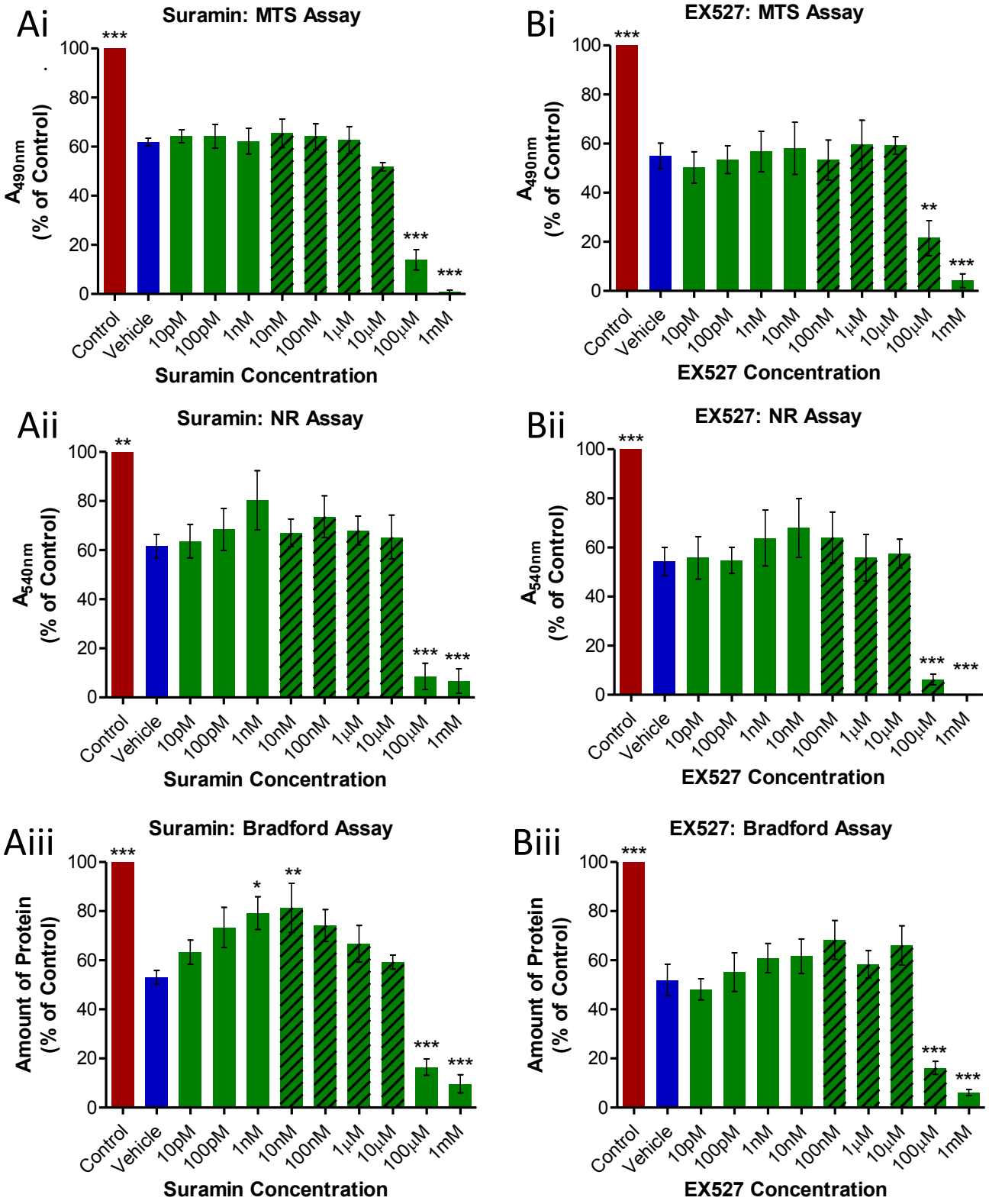

Figure 4.11 – Neuroprotective Effects of Isoform Specific Sirtuin Inhibitors Against Lactacystin in N27 Cells
N27 cells pre-treated with HDACIs for 48hrs prior to addition of lactacystin and incubation for a further 24hrs. MTS, NR and Bradford assays were then performed for quantification of HDACI induced neuroprotection against lactacystin toxicity. Red bar indicates cells which received PBS in place of both drug and lactacystin. Blue bar indicates cells which received PBS in place of drug treatment but which received subsequent treatment with lactacystin. Green bars indicate cells treated with HDACIs and which received subsequent treatment with lactacystin. Crossed green bars indicate concentrations subsequently used for N9 experiments. (A) Suramin (Sirtuin1 and 2 inhibitor) treated cells. (B) EX527 (Sirtuin1 inhibitor) treated cells. Statistical significance from vehicle treated cells indicated using asterisks: *p<0.05, **p<0.01, ***p<0.001. n=5.

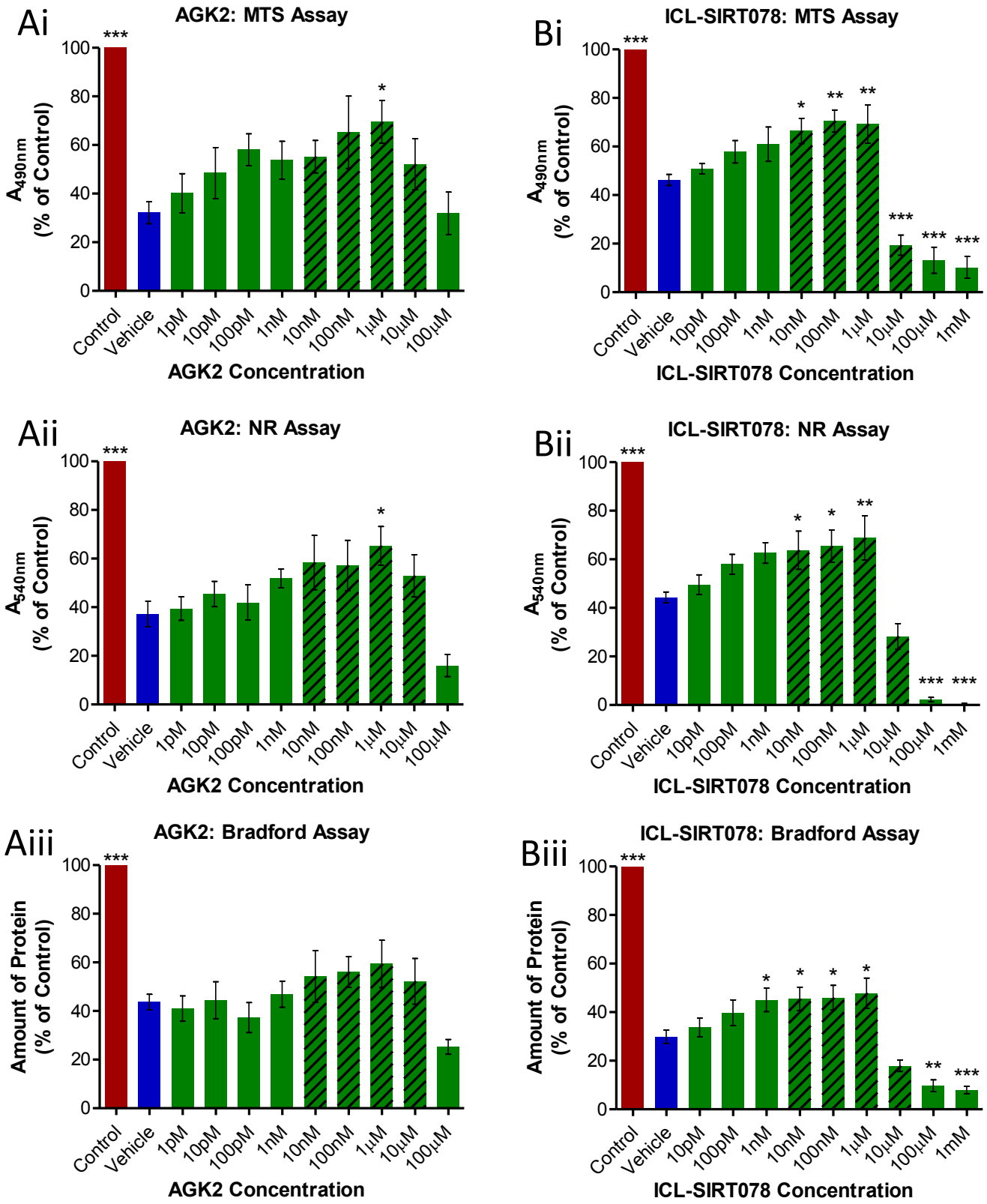

Figure 4.12 – Neuroprotective Effects of Sirtuin2 Inhibitors Against Lactacystin in N27 Cells
N27 cells pre-treated with HDACIs for 48hrs prior to addition of lactacystin and incubation for a further 24hrs. MTS, NR and Bradford assays were then performed for quantification of HDACI induced neuroprotection against lactacystin toxicity. Red bar indicates cells which received PBS in place of both drug and lactacystin. Blue bar indicates cells which received PBS in place of drug treatment but which received subsequent treatment with lactacystin. Green bars indicate cells treated with HDACIs and which received subsequent treatment with lactacystin. Crossed green bars indicate concentrations subsequently used for N9 experiments. (A) AGK2 (Sirtuin2 inhibitor) treated cells. (B) ICL-SIRT078 (Sirtuin2 inhibitor) treated cells. Statistical significance from vehicle treated cells indicated using asterisks: *p<0.05, **p<0.01, ***p<0.001. n=5.

6.21% compared to control wells vs. vehicle treated cells, 46.26 ± 2.27, 44.29 ± 2.21 and 29.86 ± 2.77% compared to control wells in vehicle treated cells in the MTS, NR and Bradford assays respectively, $p<0.01$, $p<0.01$ and $p<0.05$ respectively). Concentrations of this compound >1μM however resulted in significant toxicity towards N27 cells.

4.4.5 – Confirming the Expression of Iba-1 in N9 Cells

N9 cells were seeded at increasing densities in 6 well plates 24hrs prior to being lysed. In addition, a well void of cells and a well containing N27 cells (seeded at 20 x 10^5 cells/well) were also included as negative controls which should not contain Iba-1. The Iba-1 protein content of well lysates was then analysed using Western blot analysis. As expected the wells containing no cells and the well containing N27 cells did not show expression of Iba-1 (figure 4.13A). N9 cells seeded at increasing densities however demonstrated linearly increasing expression of Iba-1 with cell number, indicative of N9 cellular expression of this marker (figure 4.13B, linear regression analysis, $R^2>0.96$).

4.4.6 – Concentration and Incubation Period of LPS with N9 Cells to be Used in Subsequent Activation Reduction Studies

4.4.6.1 - Optimising Concentration of LPS

N9 cells were seeded in 6 well plates 24hrs prior to the addition of LPS (at a range of concentrations) or vehicle (PBS). Cells were then left to incubate for 24hrs before the medium was removed for quantification of NO using Griess assays and TNFα using ELISAs for indirect quantification of the level of microglial activation as a result of LPS incubation. Incubation of N9 cells with LPS of concentrations ≥15.625ng/ml induced significant increases of NO production as measured through the Griess assay (figure 4.14Ai). When a semi-log plot of this data was constructed, it became evident that LPS induced NO production in N9 cells through a shallow sigmoidal profile (figure 4.14Aii). With TNFα production however, all concentrations of LPS tested here induced significant increases in production in the N9 cell line (figure 4.14Bi). When a semi-log plot of this data was constructed, unlike Griess assay results, it was unclear as to the nature of the line of best fit (figure 4.14Bii). Given the large amount of NO produced by cells treated with even the lowest of concentrations, it is most likely then that the concentrations of LPS used here were too high to observe the sigmoidal curve of TNFα production in the N9 cell line. From this data 125ng/ml was chosen for subsequent studies due to its ability to produce a suitably robust sub-maximal level of microglial activation in N9 cells through quantification of NO and TNFα (7.93 ± 0.44μM nitrite and 23.92 ± 0.99μg/ml TNFα, vs. 1.96 ± 0.18μM nitrite and 1.06 ± 0.03μg/ml TNFα in LPS (125ng/ml) treated and vehicle treated cell respectively, $p<0.001$ in both comparisons).

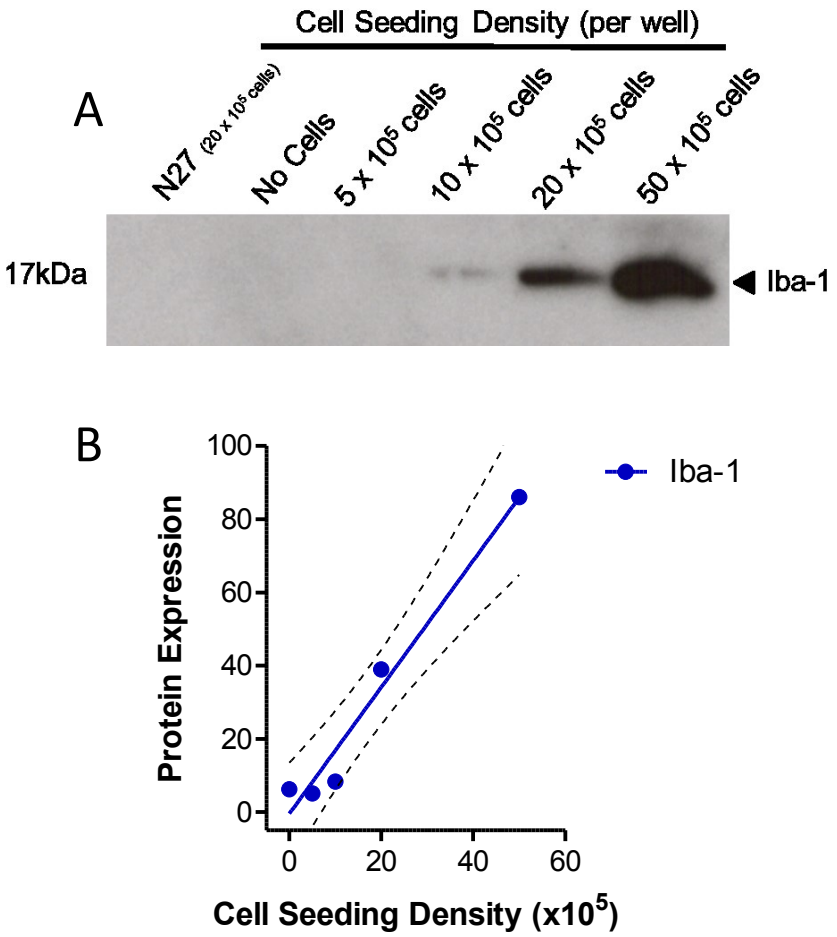

Figure 4.13 – Confirmation of N9 Expression of Microglia Marker
Iba-1 protein content of lysates from N9 cells seeded at increasing densities were quantified using Western blot analysis for confirmation of N9 expression of a marker of microglial cells. In addition a well void of cells and a well containing N27 cells (seeded at 20 x 105 cells/well) were also included as negative controls which should not contain Iba-1. Equal volumes of cell lysates for each well were run on a Western blot to confirm expression of Iba-1 marker. (B) Densitometry analysis of Iba-1 bands confirming linear expression with cell density. Lines indicate linear regression lines of best fit with respective 95% confidence intervals (dotted lines). (A) Representative blot of data presented in (B).

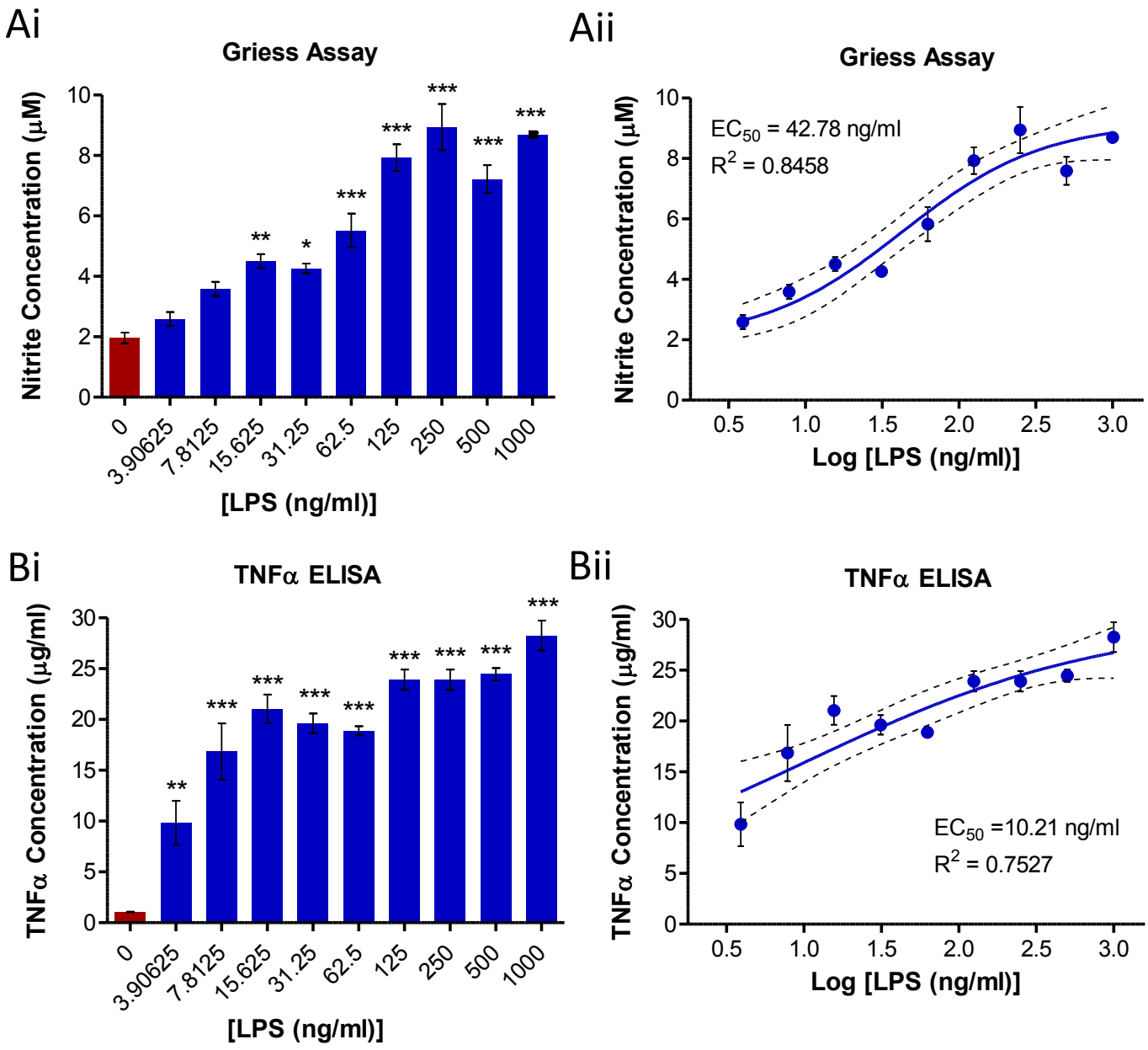

Figure 4.14 – Optimising LPS Dose for Subsequent Activation Reduction Studies in N9 Cells
N9 cells were incubated in a range of concentrations of LPS for 24hrs in order to quantify the extent microglial activation as a result of LPS. After LPS treatment, the cell medium was removed for quantification of NO using Griess assays and TNFα using ELISAs for quantification of the level of microglial activation as a result of LPS incubation. (Ai and Bi) Dose response data from the Griess assay for NO and ELISAs for TNFα respectively indicating significance from vehicle treated cells and (Aii and Bii) dose response data plotted as semi-logarithmic plot indicating IC_{50} and respective R^2 values for Griess assays and ELISAs respectively. Statistical significance from control cells indicated using asterisks: *p<0.05, **p<0.01, ***p<0.001. n=3.

4.4.6.2 - Optimising Incubation Period of LPS

N9 cells were seeded in 6 well plates 24hrs prior to the addition of LPS (125ng/ml). Cells were then left to incubate for a range of timepoints before the medium was removed for quantification of NO using Griess assays and TNFα using ELISAs for indirect quantification of the level of microglial activation as a result of LPS incubation for these timepoints. Significant increases of nitrite were not observed in the Griess assay until 15hrs post LPS treatment (time points ≥15hrs, $p<0.001$ compared to control untreated cells). After this time nitrite concentration in cell medium increased gradually with time. When a semi-log plot of this data was constructed it appeared evident that nitrite production occurs with a sigmoidal profile with time, plateauing before 48hrs of LPS incubation (figure 4.15A). TNFα production however occurred less quickly after incubation with LPS: significant increases of TNFα being observed in cell cultures incubated with LPS for ≥18hrs (figure 4.15B). When a semi log plot of this data was constructed it was evident that over the timepoints examined here TNFα is still being exponentially produced by activated microglia with time, not reaching the expected plateaux at 48hrs post LPS production. From these data, 24hrs LPS incubation was chosen for subsequent studies due to the fact that LPS induced significant yet submaximal production of both NO and TNFα, allowing for robust detection and quantification of any HDACI mediated reduction in the production of NO and TNFα in subsequent studies.

4.4.6.3 – Histone Acetylation in LPS Treated N9 Cells

For quantification of histone acetylation in N9 cells treated with the chosen concentration of LPS for the chosen incubation period, N9 cells were seeded in 6 well plates 24hrs prior to incubation with either LPS (125ng/ml) or vehicle (PBS) for 24hrs. After this time cells were lysed and the AcH3-Lys9 content of lysates quantified using Western blot analysis (figure 4.16). There was significantly more AcH3-Lys9 in cell lysates in cells treated with LPS than vehicle treated cells indicative of histone acetylation upon LPS treatment and subsequent microglial activation (LPS treated, 0.642 ± 0.056, vs. vehicle treated cells, 0.381 ± 0.066, $p<0.05$).

4.4.7 – Incubation Period of HDACIs with N9 Cells To be Used in Subsequent Activation Reduction Studies

For optimisation of the appropriate pre-treatment incubation period of HDACIs to be used in subsequent microglial activation reduction studies, cells were seeded in 6 well plates 24hrs prior to incubation with the reference HDACI, valproate (1μM) for a range of time periods. After this time cells were lysed and the AcH3-Lys9 content of lysates quantified using Western blot analysis. There was a significant time dependent increase in AcH3-Lys9 in HDACI treated cells indicative of time-dependent histone acetylation with HDACI (valproate) treatment (figure 4.17). This increase in

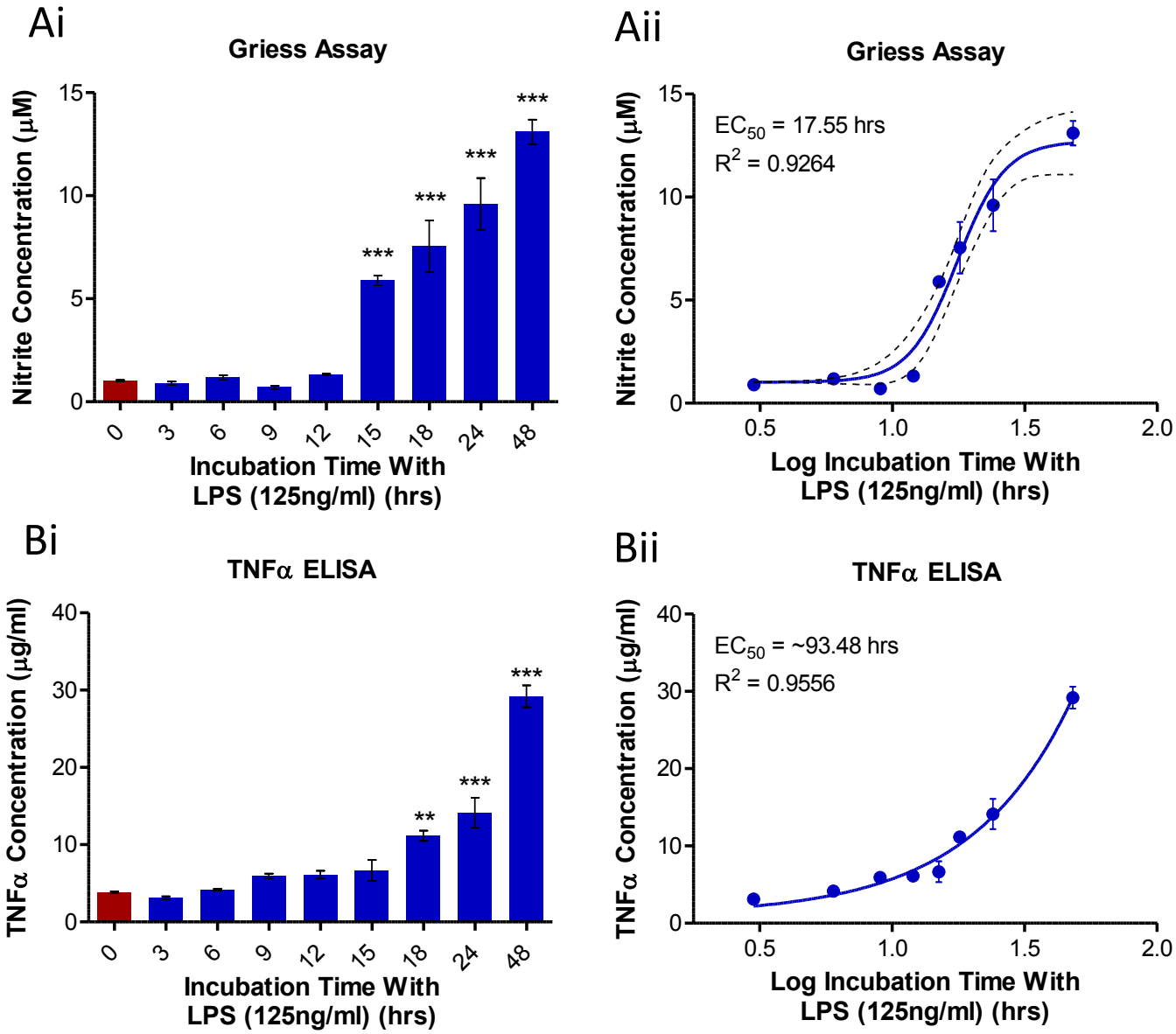

Figure 4.15 – Optimising LPS Incubation Period for Subsequent Activation Reduction Studies in N9 Cells
N9 cells were incubated with LPS (125ng/ml) for a range time periods in order to quantify the extent microglial activation as a result of LPS. After LPS treatment, the cell medium was removed for quantification of NO using Griess assays and TNFα using ELISAs for indirect quantification of the level of microglial activation as a result of LPS incubation. (Ai and Bi) Timecourse data from the Griess assay for NO and ELISAs for TNFα respectively indicating significance from vehicle treated cells and (Aii and Bii) timecourse data plotted as semi-logarithmic plot indicating IC_{50} and respective R^2 values for Griess assays and ELISAs respectively. Statistical significance from control cells indicated using asterisks: *p<0.05, **p<0.01, ***p<0.001. n=3.

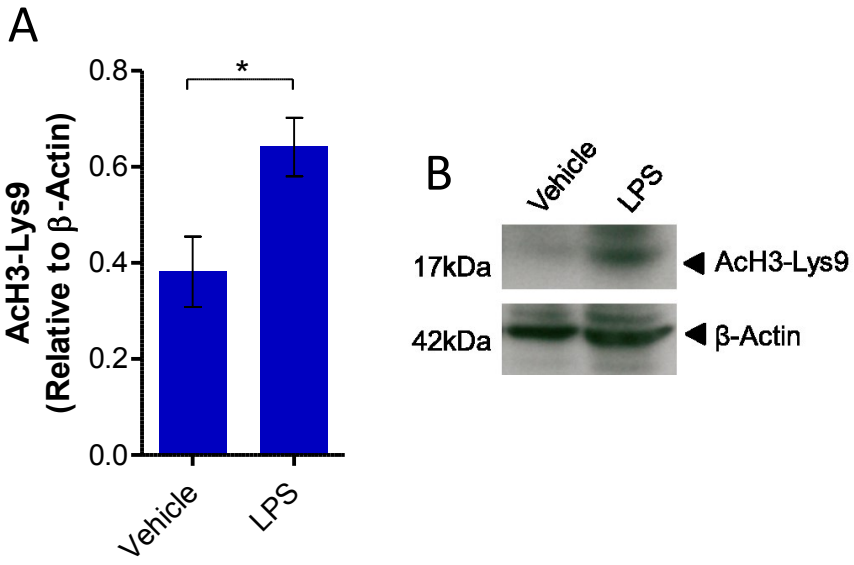

Figure 4.16 – Histone Acetylation in LPS Treated N9 Cells
AcH3-Lys9 content of lysates from cells treated with either LPS (125ng/ml) of vehicle (PBS) for 24hrs were quantified by Western blot analysis. (A) Densitometry analysis of AcH3-Lys9 bands relative to β-actin used as a loading control demonstrate that there is significantly more histone acetylation in LPSA compared to vehicle treated cells. (B) Representative blot of data presented in (A). Statistical significance indicated using asterisks: *p<0.05. n=3.

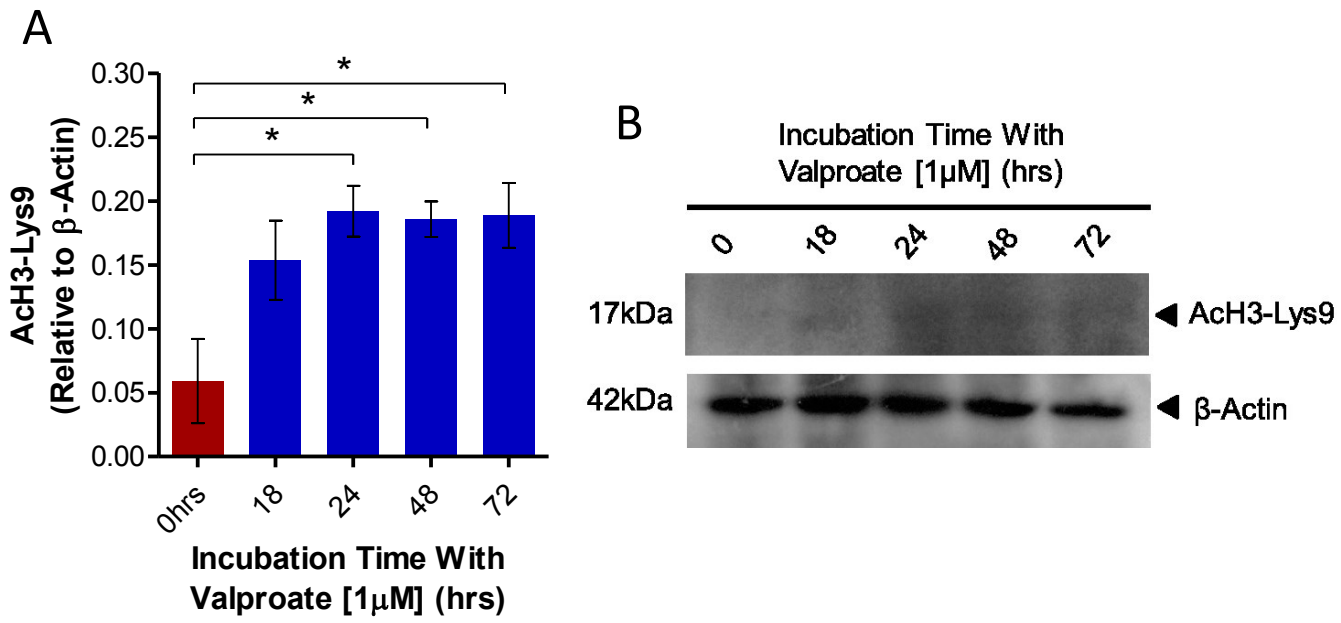

Figure 4.17 – Histone Acetylation in HDACI Treated N9 Cells
AcH3-Lys9 content of lysates from N9 cells treated with valproate (1μM) for a range of incubation periods were quantified by Western blot analysis. (A) Densitometry analysis of AcH3-Lys9 bands relative to β-actin used as a loading control demonstrate that histone acetylation increases with incubation time with valproate. (B) Representative blot of data presented in (A). Statistical significance indicated using asterisks: *p<0.05. n=3.

histone acetylation however did not become significantly different from control cell lysates until 24hrs of HDACI treatment, after which time there were no further increases in acetylation (cells treated with valproate for 24, 48 and 72hrs, 0.191 ± 0.019, 0.186 ± 0.014, 0.189 ± 0.025 respectively compared to control cells, 0.060 ± 0.033, $p<0.05$ in all comparisons).

4.4.8 - Potential of Isoform Specific and Isoform Non-Specific HDACIs at Reducing LPS Induced Activation of N9 Cells

After optimisation of the concentration and incubation period of LPS most suitable for inducing activation of N9 cells, and the appropriate pre-incubation period with HDACIs required to induce histone acetylation in the cells, the ability of the range of isoform specific and non-specific HDACI used previously at reducing LPS induced activation of N9 cells was examined. Cells were seeded in 6 well plates 24hrs prior to incubation with varying concentrations of the HDACIs for 24hr. Four concentrations of each HDACI were chosen for study in N9 cells based on the results described above, spanning the concentration range at which the HDACI was shown to be both neuroprotective and cytotoxic in N27 cells (chosen concentrations indicated by crossed green bars in figure 4.8, 4.9, 4.10, 4.11 and 4.12). After this time LPS (125ng/ml) was added to cell cultures containing HDACIs/vehicle and incubated for a further 24hrs. After this time the medium was removed for quantification of NO using Griess assays and TNFα using ELISAs for indirect quantification of the level of HDACI mediated reduction of LPS induced microglial activation. In addition to confirm that any reduction of NO or TNFα observed were a result of reduction of microglial by the HDACI and not cytotoxicity, MTS, NR and Bradford assays were then conducted on HDACI treated cell culture wells to quantify the extent of cytotoxicity, if any, exerted by the HDACI compounds.

4.4.8.1 –Effects of Isoform Non-Specific HDACIs on Microglial Activation

In both the Griess assay and TNFα ELISA, there was a strong correlation of reduction of NO and TNFα in the medium of N9 cells treated with increasing valproate concentration indicative of reduction of microglial activation with valproate treatment. At the highest concentration of valproate tested here (10μM), a marked reduction in both nitrite and TNFα were both observed (figure 4.18A, valproate treated cells, 168.64 ± 52.33 and 460.57 ± 176.71% of control vs. vehicle treated cells, 279.49 ± 45.96 and 1164.09 ± 285.20% of control, nitrite and TNFα respectively) however these differences did not reach statistical significance ($p>0.05$ in both comparisons). No reduction in cell viability was observed in valproate treated N9 cells even with the highest concentration tested, previously observed to be toxic towards N27 cells indicative that the reduction in NO and TNFα in valproate treated cells is a result of HDACI mediated reduction in LPS induced activation. Despite also inhibiting HDAC classes I and IIa with similar potency, no overt changes in the production of NO and

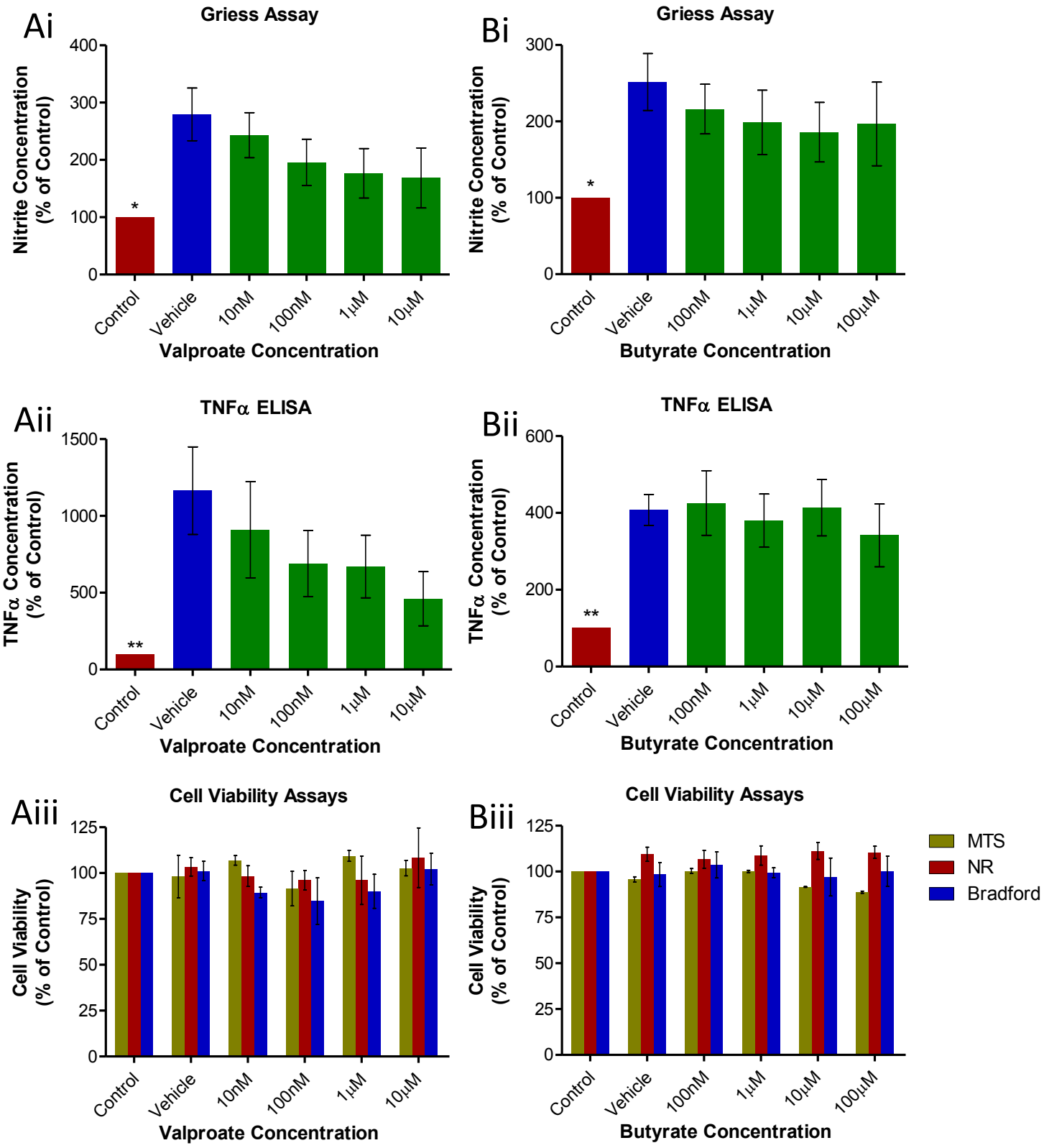

Figure 4.18 –Effects of Class I and IIa HDACIs On LPS Activated N9 Cells

N9 cells pre-treated with HDACIs for 24hrs prior to addition of LPS and incubation for a further 24hrs. Cell medium was then removed for Griess assay of NO content and ELISA of TNFα content. For cell viability assays cells were treated for 24hrs with HDACIs alone and MTS, NR and Bradford assays performed for HDACI induced cytotoxicity. Red bar indicates cells which received PBS in place of both drug and LPS. Blue bar indicates cells which received PBS in place of drug treatment but which received subsequent treatment with LPS. Green bars indicate cells treated with HDACIs and which received subsequent treatment with LPS. (A) Valproate (class I and IIa HDACI) treated cells. (B) Butyrate (class I and IIa HDACI) treated cells. Statistical significance from vehicle treated cells indicated using asterisks: *p<0.05, **p<0.01. n=5.

TNFα were observed upon treatment of cells with butyrate (figure 4.18B). A very subtle reduction of NO was observed upon increasing butyrate treatment, however this difference did not reach statistical significance. Additionally, similar to valproate, the highest concentration of butyrate used to treat the N9 cells did not result in cytotoxicity as it did with N27 cells.

Treatment of N9 cells with trichostatin A at the four concentrations examined here did not have any effect on the resulting concentration of NO or TNFα in the cell medium (figure 4.19A). Similarly no cytotoxicity was observed upon treatment of N9 cells with 10nM trichostatin A unlike in N27 cells. This was also the case with N9 cells treated with the highest dose of nicotinamide (10mM), previously shown to induce modest cytotoxicity in N27 cells. No cytotoxicity was observed in any of the three cell viability assays utilised here. However there was a concentration dependent reduction in the production of both NO and TNFα in nicotinamide treated N9 cell cultures, reaching significance from vehicle treated cells at the highest concentration tested indicative of nicotinamide induced reduction of LPS activation of N9 cells (figure 4.19B, nicotinamide (10mM) treated cells, 60.11 ± 4.59 and 282.11 ± 29.55% of control vs. vehicle treated cells, 255.88 ± 34.01 and 686.62 ± 126.95% of control, nitrite and TNFα respectively, $p<0.001$ and $p<0.01$ respectively).

4.4.8.2 –Effects of Isoform Specific HDACIs on Microglial Activation

In the above N27 cell studies, MS275 was shown to be extremely cytotoxic. This did not appear to be the case in N9 cells: there being only a slight non-significant reduction in cell viability at the highest MS275 concentration examined in N9 cells (figure 4.20A). Griess assay data does not suggest any reduction in NO production upon MS275 treatment, however there was a subtle concentration dependent decrease in TNFα production in cells treated with MS275, reaching significance from vehicle treated cells at the highest concentration tested here (MS275 (100nM) treated cells, 398.18 ± 45.40% of control vs vehicle treated cells, 552.91 ± 35.86% of control, $p<0.05$). This result however is difficult to interpret give the reduction, however subtle, in cell viability upon treatment of cells with this concentration of MS275. In N9 cells apicidin did not induce any reduction in either NO or TNFα, nor did it induce cytotoxicity of N9 at any of the concentrations examined here (figure 4.20B).

4.4.8.3 –Effects of Isoform Specific Sirtuin Inhibitors on Microglial Activation

Treatment of N9 cells with suramin at the four concentrations examined here did not have any effect on the resulting concentration of NO or TNFα in the cell medium (figure 4.21A). Similarly no cytotoxicity was observed upon treatment of N9 cells with this HDACI. EX527 however induced significant cytotoxicity at its highest concentration (100μM) in all three cell viability assays described here mirroring its effects on N27 cells shown above (figure 4.21B, $p<0.05$ compared to vehicle treated cell wells in all comparisons). In line with this change, there are subtle non-significant reductions in both nitrite and TNFα production by cell treated with this concentration of the drug,

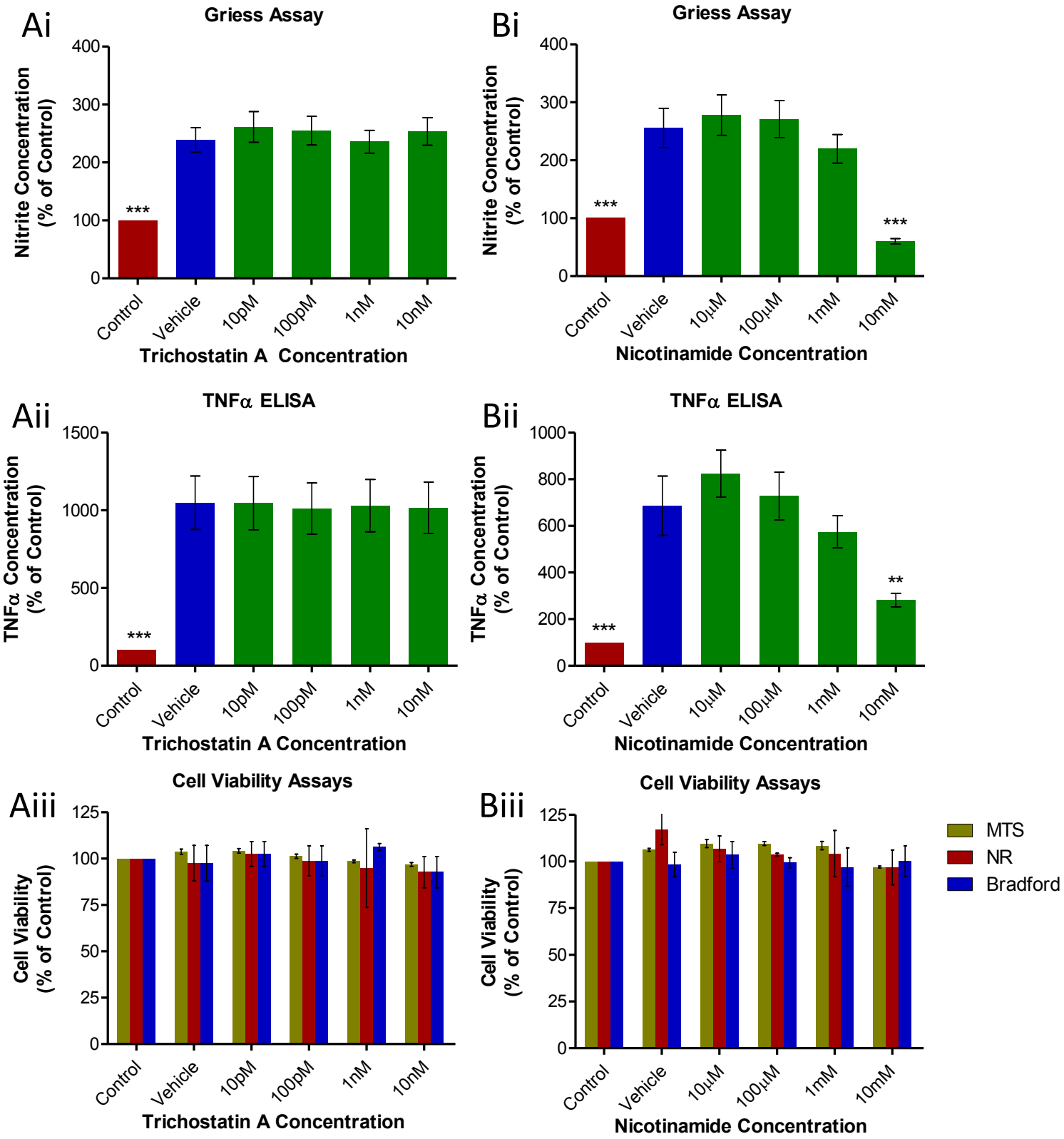

Figure 4.19 –Effects of Isoform Non-Specific HADACIs On LPS Activated N9 Cells

N9 cells pre-treated with HDACIs for 24hrs prior to addition of LPS and incubation for a further 24hrs. Cell medium was then removed for Griess assay of NO content and ELISA of TNFα content. For cell viability assays cells were treated for 24hrs with HDACIs alone and MTS, NR and Bradford assays performed for HDACI induced cytotoxicity. Red bar indicates cells which received PBS in place of both drug and LPS. Blue bar indicates cells which received PBS in place of drug treatment but which received subsequent treatment with LPS. Green bars indicate cells treated with HDACIs and which received subsequent treatment with LPS. (A) Trichostatin A (class I, IIa and IIb HDACI) treated cells. (B) Nicotinamide (class III HDACI) treated cells. Statistical significance from vehicle treated cells indicated using asterisks: **p<0.01, ***p<0.001. n=5.

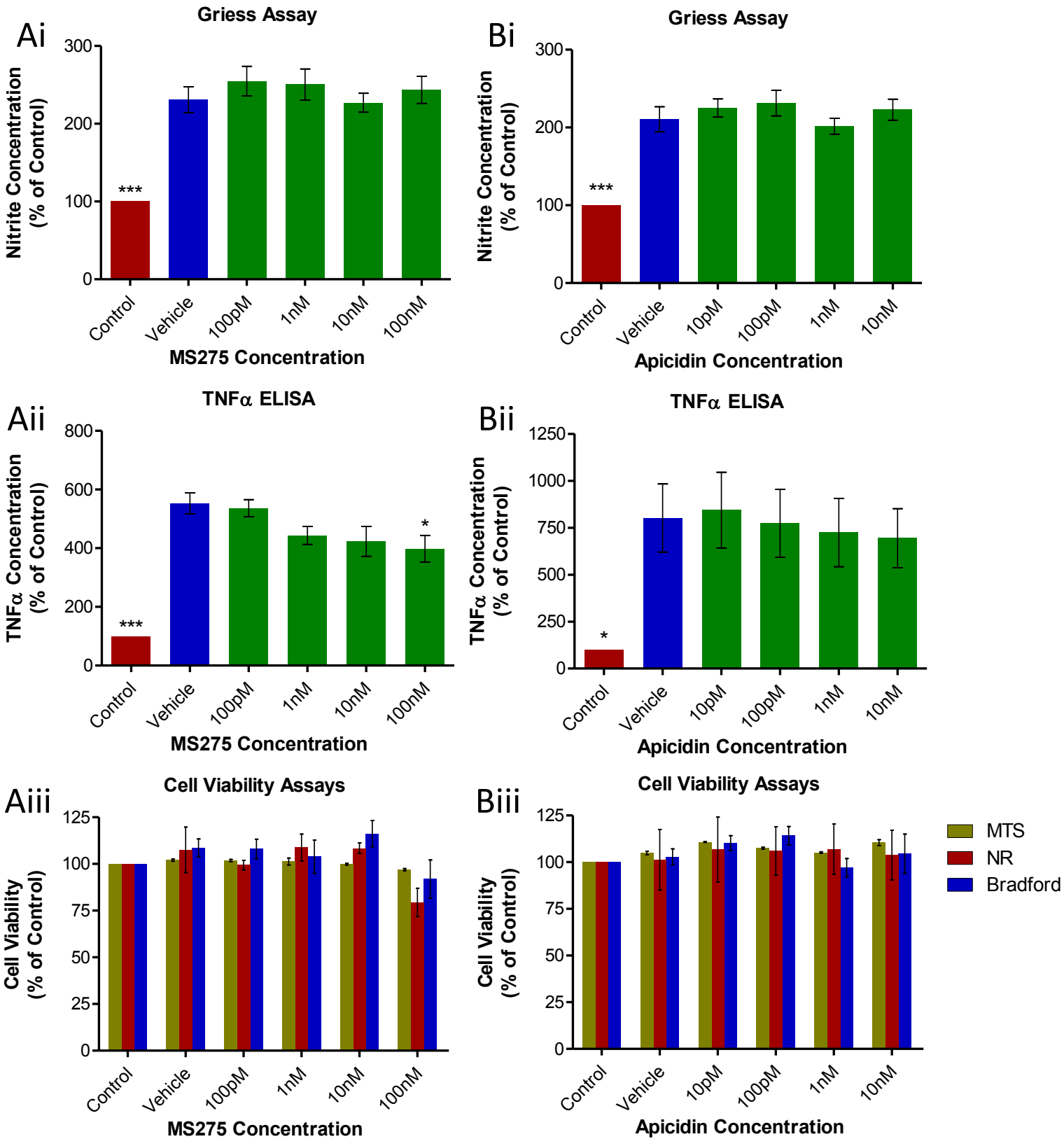

Figure 4.20 –Effects of Isoform HDACIs On LPS Activated N9 Cells

N9 cells pre-treated with HDACIs for 24hrs prior to addition of LPS and incubation for a further 24hrs. Cell medium was then removed for Griess assay of NO content and ELISA of TNFα content. For cell viability assays cells were treated for 24hrs with HDACIs alone and MTS, NR and Bradford assays performed for HDACI induced cytotoxicity. Red bar indicates cells which received PBS in place of both drug and LPS. Blue bar indicates cells which received PBS in place of drug treatment but which received subsequent treatment with LPS. Green bars indicate cells treated with HDACIs and which received subsequent treatment with LPS. (A) MS275 (HDAC1 inhibitor) treated cells. (B) Apicidin (HDAC2 and 3 inhibitor) treated cells. Statistical significance from vehicle treated cells indicated using asterisks: *p<0.05, ***p<0.001.

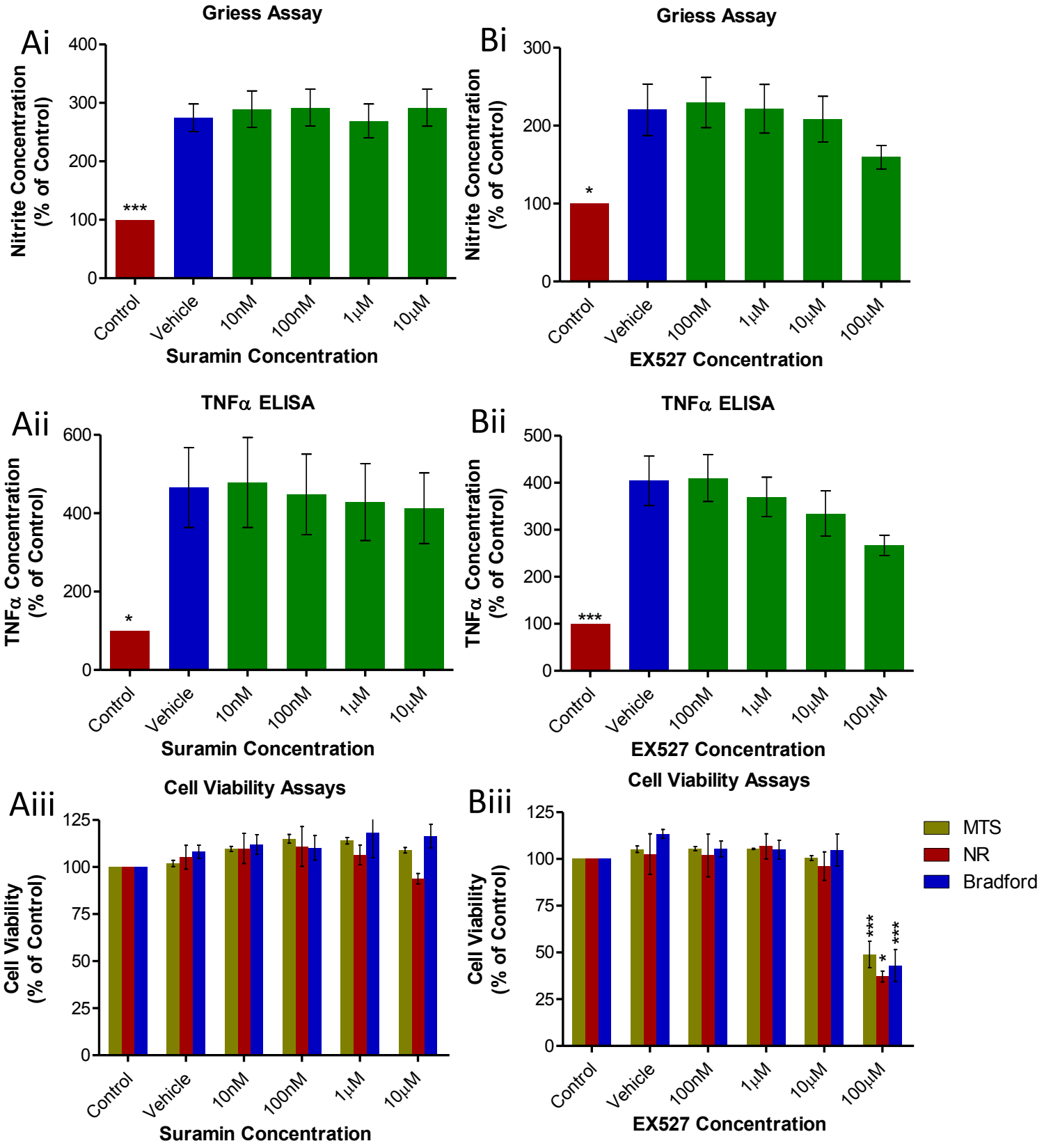

Figure 4.21 – Effects of Isoform Specific Sirtuin Inhibitors On LPS Activated N9 Cells

N9 cells pre-treated with HDACIs for 24hrs prior to addition of LPS and incubation for a further 24hrs. Cell medium was then removed for Griess assay of NO content and ELISA of TNFα content. For cell viability assays cells were treated for 24hrs with HDACIs alone and MTS, NR and Bradford assays performed for HDACI induced cytotoxicity. Red bar indicates cells which received PBS in place of both drug and LPS. Blue bar indicates cells which received PBS in place of drug treatment but which received subsequent treatment with LPS. Green bars indicate cells treated with HDACIs and which received subsequent treatment with LPS. (A) Suramin (Sirtuin1 and 2 inhibitor) treated cells. (B) EX527 (Sirtuin1 inhibitor) treated cells. Statistical significance from vehicle treated cells indicated using asterisks: *p<0.05, ***p<0.001. n=5.

likely the result of the observed cytotoxicity at this concentration.

AGK2 did not exert any cytotoxicity at any of the concentrations used here in N9 cells. However a subtle concentration dependent reduction in both NO and TNFα production were observed with AGK2 treatment in the cells (figure 4.22A). These changes however did not reach significance from vehicle treated cells. Like in N27 cells assays shown above, 10μM ICL-SIRT078 however induced significant cytotoxicity in all three cell viability assays ($p<0.01$ compared to vehicle treated cells in all comparisons). In line with this, significant reductions in NO and TNFα were observed in N9 cells treated with the concentration of the Sirtuin2 inhibitor ($p<0.001$ compared to vehicle treated cells in both comparisons). Additionally, a significant concentration dependent decrease in NO production was observed in lower, non-cytotoxic concentrations of ICL-SIRT078, reaching significance from vehicle treated cells at the highest of the non-cytotoxic concentrations of the drug (figure 4.22B, ICL-SIRT078 treated cells, 76.51 ± 17.51% of control cells vs. vehicle treated cells, 228.36 ± 40.95% of control cells, $p<0.001$). A similar concentration dependent decrease in TNFα production is also observed in with ICL-SIRT078 treatment of cells, reaching significance from vehicle treated cells in all concetrations tested (10nM, 100nM and 1μM ICL-SIRT078, $p<0.01$, $p<0.001$ and $p<0.001$ compared to vehicle treated cells respectively).

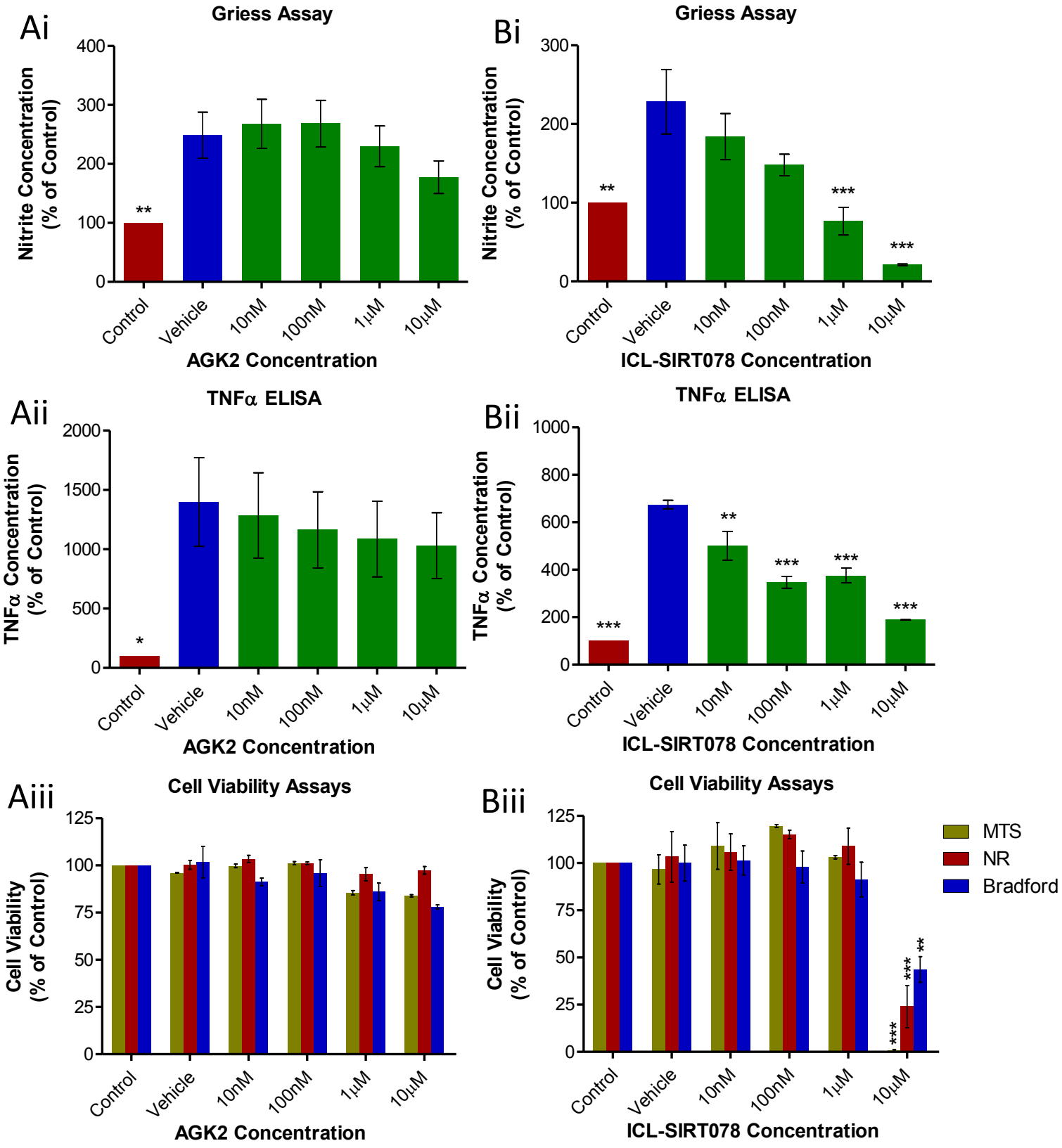

Figure 4.22 –Effects of Isoform Sirtuin2 Inhibitors On LPS Activated N9 Cells

N9 cells pre-treated with HDACIs for 24hrs prior to addition of LPS and incubation for a further 24hrs. Cell medium was then removed for Griess assay of NO content and ELISA of TNFα content. For cell viability assays cells were treated for 24hrs with HDACIs alone and MTS, NR and Bradford assays performed for HDACI induced cytotoxicity. Red bar indicates cells which received PBS in place of both drug and LPS. Blue bar indicates cells which received PBS in place of drug treatment but which received subsequent treatment with LPS. Green bars indicate cells treated with HDACIs and which received subsequent treatment with LPS. (A) AGK2 (Sirtuin2 inhibitor) treated cells. (B) ICL-SIRT078 (Sirtuin2 inhibitor) treated cells. Statistical significance from vehicle treated cells indicated using asterisks: *p<0.05, **p<0.01, ***p<0.001. n=5.

Table 4.2 – Summary of Neuroprotective/Anti-Inflammatory Effects of HDACIs *In Vitro*
Summary of the effects of HDACIs on neuronal and microglial cell culture systems in terms of their neuroprotective and anti-inflammatory respectively. Statistical significance from vehicle treated cells indicated using asterisks: ns, non-significant, *p<0.05, **p<0.01, ***p<0.001.

Drug	*Neuroprotective Concentration?*	*Significance from Vehicle Treated (MTS, NR, Bradford)*	*Anti-Inflammatory Concentration?*	*Significance from Vehicle Treated (Greiss assay, TNFα ELISA)*
Valproate	1μM	ns, ns, ns	10μM	ns, ns
Butyrate	10μM	ns, **, ns	100μM	ns, ns
Trichostatin A	-	-	-	-
Nicotinamide	10μM	ns, ns, ns	10mM	***, **
MS275	-	-	100nM	ns, *
Apicidin	100pM	ns, *, ns	10nM	ns, ns
Suramin	10nM	ns, ns, **	-	-
EX527	10μM	ns, ns, ns	10μM	ns, ns
AGK2	1μM	*, *, ns	10μM	ns, ns
ICL-SIRT078	1μM	**, **, *	1μM	***, ***

4.5 – Discussion

It has been shown here that HDACIs reduce lactacystin induced neurodegeneration in N27 cells and LPS induced activation of N9 cells (table 4.2). Dependent on the class or isoform inhibited, HDACIs vary hugely in their effects as neuroprotectants and their ability to reduce microglial activation, *in vitro*. Disparity between results from neurons and microglia also highlight the possible differing effects of HDAC isoform inhibition on Parkinsonian pathogeneses. Careful interpretation of these findings will identify suitable lead HDACIs for study in subsequent *in vivo* neuroprotection studies.

In the current study, subtle reductions in lactacystin induced neurodegeneration and LPS induced microglial activation were observed upon treatment of cells with the HDAC class I and IIa pan-inhibitor, valproate. These are consistent with previous findings in both neurons and microglia. Valproate mediated neuroprotection has been observed in cerebellar granule cell cultures treated with a glutamate excitotoxic insult (Leng and Chuang, 2006) and 6-OHDA (Monti et al., 2007), in rat cortical neurons treated with a glutamate excitotoxic insult (Marinova et al., 2009), in a neuroblastoma cell line treated with rotanone (Pan et al., 2005) and in human dopaminergic neuroblastoma derived and rat dopaminergic neuroblastoma derived cells treated with MPP+ (Kidd and Schneider, 2010). Similarly valproate has also been observed to reduce the levels of nitrite and TNFα secreted by microglial cell cultures, translating to protection of dopaminergic neurons in rat primary mescencephalic neuron-glia cultures (Peng et al., 2005). In contrast however, it has also been demonstrated that this reduction of inflammatory cytokines and markers of microglial activation induced by valproate are a result of increased microglial apoptosis (Chen et al., 2007). These results are in direct disagreement with those described here: in conjunction with nitrite and TNFα assays, cell viability assays were conducted to validate that any reduction in nitrite and TNFα observed were a direct result of reduced microglial activation rather than cell death. In contrast to Chen and colleagues observations, a reduction of nitrite and TNFα were observed here in the absence of a reduction in cell viability. This disparity is difficult to comment on given the differences in cell culture systems and concentrations of valproate used. Therefore it may be likely then at higher concentrations, valproate induces apoptosis of microglial cells, similar to those results obtained here using neuronal cultures. Regardless, at lower non-cytotoxic concentrations of valproate, marked reductions in both nitrite and TNFα are observed here, highlighting the ability of valproate to reduce microglial activation without inducing apoptosis. Extending the findings discussed thus far in neurons and microglia, astrocytes are also likely involved in valproate's neuroprotective phenotype: valproate was shown to protect against spontaneous dopaminergic neuronal cell death in microglial-depleted cell cultures (Chen et al., 2006), and protect neuron enriched cultures against the toxic effects of conditioned astrocytic medium when astrocytes were

pre-treated with valproate (Wu et al., 2008b). Taken together with the results from the experiments conducted here, valproate appears a valid candidate for further study *in vivo*.

Like valproate, butyrate is also a pan-inhibitor of HDAC classes I and IIa, however in the experiments described here it appears to exert different effects in neuronal and microglial cultures than valproate. Butyrate appears to mediate neuroprotection in N27 cell cultures, reducing lactacystin induced neurodegeneration detected through two of the three assays described. These findings are consistent with those in rat dopaminergic mescencephalic derived dopaminergic cells in which butyrate was previously observed to protect against MPP+ induced neurotoxicity (Kidd and Schneider, 2010) as well as in neuron-glia cultures treated with this same neurotoxin (Wu et al., 2008b). Unlike valproate however, butyrate was not observed here to mediate a reduction in microglial activation in N9 cultures. Previous work by others have eluded to a reduction of microglial pro-inflammatory factors as a result of butyrate treatment, however this was attributed to the significant induction of apoptosis of microglial cells caused by butyrate (Chen et al., 2007). The results presented here are encouraging however, in that butyrate was able to induce neuroprotection against a toxin such as lactacystin, be it modest and only detected through two of the three cell viability assays described. However given the difference in butyrate's effects on neuronal and microglial cultures, valproate appears a more suitable compound for further study of these two HDAC class I and IIa inhibitors.

In addition to inhibiting HDAC classes I and IIa, trichistatin A also inhibits HDAC class IIb, HDAC6 inclusive which was highlighted in human post-mortem studies. However in contrast to results produced from pan-inhibitors of HDAC classes I and IIa valproate and butyrate described above, in the current study trichostatin A does not appear to have any effect on lactacystin induced neurodegeneration or microglial activation. These findings are in conflict with previously published reports of the use of trichostatin A in culture. For example trichostatin A has been previously observed to reduce microglial activation in culture (Suh et al., 2010) and protect neurons against Parkinsonian insults such as MPTP toxicity, oxidative stress and excitotoxicity in culture (Wu et al., 2008b, Langley et al., 2008, Leng and Chuang, 2006). This difference in findings could be for a number of reasons given the different cell culture systems used and in particular the toxin used to induce neurodegeneration in the current study of N27 cells. Here, trichostatin A was unable to relieve lactacystin induced neurodegeneration and microglial activation, it does not present as a viable candidate for further investigation *in vivo*.

The other pan-inhibitor examined in the current work, nicotinamide, produces far more positive results compared to trichostatin A. Despite not being able to reduce lactacystin toxicity in N27 cells, a marked significant reduction of microglial activation was observed in N9 cell cultures. To

the authors knowledge this is the first time in which the effects of nicotinamide have been studied in microglial culture. In contrast however, despite not showing any significant neuroprotective effect in the current study, nicotinamide has previously been shown to increase neuronal cell viability in culture (Jia et al., 2008) and protect against dopaminergic neuronal cell death *in vivo* in the MPTP mouse model of PD (Anderson et al., 2006, Anderson et al., 2008) improving motor behavioural performance (Xu et al., 2012). Authors suggest that neuroprotection occurs at higher nicotinamide concentrations *in vivo,* therefore given the positive effects of nicotinamide on microglial activation at higher concentrations shown here, high concentrations of nicotinamide presents as an interesting candidate for study *in vivo* in an animal model of PD.

The benzamide MS275 is an inhibitor of HDAC1 and to a lesser degree HDAC3. In the current study, this drug had hugely contrasting effects on the cell culture systems examined: producing marked toxicity in dopaminergic neurons in culture yet reducing TNFα production in microglial cells. This latter finding however needs to be interpreted cautiously however as a slight reduction in cell viability was similarly observed with the concentration of MS275 in question and hence could have resulted in the reduction observed. However, in microglial cells, unlike neurons, this benzamide is not nearly as cytotoxic as it is in neurons. To the authors knowledge, this is the first time in which MS275 has been studied in culture in a cellular model of Parkinsonsian neurodegeneration or microglial activation. That being said, these results do not support further investigation of this HDACI in future studies as inhibition of HDAC1 (and HDAC3) does not appear sufficient to exert beneficial effects.

Likewise, the selective HDAC2, HDAC3 (and HDAC8) inhibitor apicidin fails to exert any marked affects in the assays described here in neuronal or microglial cultures. A significant level of neuroprotection from vehicle treated cells was observed upon apicidin treatment in the NR assays however given the lack of a response observed in other assays this result appears to be invalid. Apicidin did not mediate any reduction of microlgial activation either, as measured through nitrite and TNFα production from N9 cells. It would therefore also appear that HDAC2, HDAC3 (and HDAC8) inhibition is insufficient to produce a neuroprotective/anti-inflammatory phenotype similar to that observed with by other pan-inhibitors of the HDACs. This is disappointing given that HDAC2 and HDAC3 are two of the most highly expressed HDACs in the SNpc (Broide et al., 2007), effectively highlighting the attractive nature of apicidin as a PD therapeutic due to its ability to inhibit the two HDACs expressed most abundantly in the brain nuclei most associated neuronal cell death within the disease. The above mentioned results however do not support further investigation of this compound in future *in vivo* studies.

The pan-sirtuin inhibitor, nicotinamide was observed here to produce positive results in terms of its reduction of microglial activation but not protection of dopaminergic neurons in culture. It remains unknown from the experiments conducted here however whether or not this was a result of nicotinamide's effects on bioenergetics rather its inhibition of the sirtuin class of HDACs (Liu et al., 2013a). Suramin however, a selective inhibitor of only sirtuin1 and sirtuin2 did not mediate similar results. No change in TNFα or nitrite production in microglial cells was observed upon suramin treatment. In neuroprotection studies however a subtle extent of neurorprotection may have been observed, yet given that this was only shown in one of the cell viability assays, this finding may be erroneous. Recent evidence however highlights the contrasting effects of sirtuin1 and sirtuin2 in neurodegenerative disorders, it being argued that sirtuin1 inhibition is damaging towards neurons whereas sirtuin2 inhibition is neuroprotective (Donmez and Outeiro, 2013). This theory therefore may explain the lack of efficacy observed in the current study using an inhibitor of both sirtuin1 and sirtuin2: the positive effects of sirtuin2 inhibition being outweighed by sirtuin1 inhibition. If this were the case however, one would expect an inhibitor of sirtuin1 to exacerbate neurodegeneration in neuronal cultures. Upon treatment with EX527 however, little to no neuroprotection was observed here in N27 cells. Contrastingly however, both of the sirtuin2 inhibitors studied, AGK2 and ICL-SIRT078, mediated marked neuroprotection in N27 cells treated with lactacystin, and marked reduction in LPS activated microglia. ICL-SIRT078 is a sirtuin2 inhibitor developed and synthesised in-house by Dr Matthew Fuchter and colleagues (Department of Medicinal Chemistry, Imperial College London). Compared with the IC50 of AGK2 (3.5μM) (Outeiro et al., 2007), this novel compound is more than twice as potent (IC50 = 1.45μM) and far more selective than for sirtuin2 than sirtuin1 compared to AGK2 (Di Fruscia et al., 2014). This increased potency and selectively is reflected in data presented here indicative that the effects of drug treatment on cell assays are indeed an effect of sirtuin2 inhibition. Very few studies investigating the neuroprotective effects of sirtuin2 inhibition have been conducted to date: only one publication looking at the neuroprotective effects of AGK2 in PD. Outeiro and colleagues (2007) demonstrated dose dependent rescue of αSyn mediated toxicity in neuroglioma cells upon treatment with the sirtuin2 inhibitor AGK2. Furthermore it was demonstrated that AGK2 when fed to drosophila overexpressing αSyn, a dose dependent protection of TH+ dorsomedial neurons was similarly observed. Extending these observations in neurons, in the current study reductions in nitrite and TNFα were also observed in LPS activated microglia treated with sirtuin2 inhibitors. To the authors knowledge this is the first time in which the effects of sirtuin2 inhibitors have been studied in activated microglia. Taken together these results are extremely encouraging given the success of compounds in treating both lactacystin induced neurodegeneration

as well as microglial activation. Sirtuin2 inhibitors therefore warrant further investigation in subsequent *in vivo* studies.

The broad aims of this study were to test the potential of a range of HDACIs at reducing lactacystin induced neurodegeneration and LPS induced activation of neuronal and microglial cultures respectively. Based on these findings, lead compounds for subsequent testing *in vivo* would then be identified. The obvious choice would be one of the sirtuin2 inhibitors. However, there is no evidence to date on the brain penetrance of AGK2 in either animals or human, or its toxicity in experimental animals. Similarly due to the novel and experimental nature of ICL-SIRT078 neither of these issues have yet to be elucidated with this drug either. None of the isoform specific inhibitors examined here (MS275, apicidin, suramin and EX527) mediated any marked effects in the cell culture models described here ruling them out for further study. Of the four pan-inhibitors remaining (valproate, butyrate, trichostatin A and nicotinamide), trichostatin A failed to exert any neuroprotective or anti-inflammatory actions in the experiments described therefore this was ruled out also. The pan-inhibitors of HDAC class I and IIa, valproate and butyrate, mediated respectable effects in cell culture. However due to the effects of valproate on both neuronal and microglial cultures unlike butyrate, this compound was chosen for further study. Similarly unlike butyrate, this HDAC class I and IIa inhibitor has a large body of evidence suggesting its beneficial effects against Parkinsonian pathologies in neuronal, microglial and astrocytic cultures as well as its neuroprotection *in vivo*. Similarly, valproate, being already FDA-approved for the treatment of epilepsy and seizures comes with years of clinical experience for treatment of neurological disorder and if proved to be successful in pre-clinical investigations could be translated to the clinic quickly. The remaining HDACI, nicotinamide, was therefore also chosen for further study *in vivo*. Nicotinamide itself is an amide converted, *in vivo*, from its dietary precursor, niacin (or vitamin B3), found in numerous food sources, making it extremely well tolerated orally in man. This is most opportune given the wealth of previously published evidence suggesting its neuroprotection when administered at high doses *in vivo*. The neuroprotective and behavioural effects of valproate and nicotinamide on an animal model of PD will therefore be assessed in subsequent chapter.

The choice of both of these broad spectrum pan-HDACIs therefore represents an exciting prospect for their further study *in vivo* given their previous FDA-approval, making their translatability to the clinic relatively easy if found to be successful. Likewise the use of two broad spectrum pan-HDACIs which both inhibit a wide range of distinctly different sets of HDAC isoforms will hopefully add insight into the potential of inhibiting individual HDAC isoforms within classes I and IIa (valproate) and class II (nicotinamide).

4.6 – Conclusions

To conclude, this study demonstrates that pre-treatment of cell cultures with HDACIs, dependent on the class(es) or isoform(s) inhibited, results in neuroprotection against lactacystin induced neurodegeneration in dopaminergic neurons, and reduction of LPS induced activation of microglial cells in culture. From these data, valproate and nicotinamide were identified as most suitable lead compounds for further investigation *in vivo*, in the lactacystin rat model of PD.

Chapter Five

Generating and Profiling Progression of the Lactacystin Rat Model of Parkinson's Disease

5 – Generating and Profiling Progression of the Lactacystin Rat Model of Parkinson's Disease

5.1 – Introduction

In order to reliably test the efficacy of a candidate neuroprotective compound for PD *in vivo*, a reproducible animal model which recapitulates elements of Parkinsonian dopaminergic neuronal cell death, neuropathological and behavioural deficits of the disease, is essential. As has been previously introduced (section 1.2.7), numerous animal models of PD are routinely used for the study of neuroprotective agents, *in vivo*. From genetic mouse models harbouring familial PD associated mutations, to systemic and focal toxin administration induced models, animal models of PD are available which recapitulate differing aspects of the human condition dependent on the research question being asked. A relatively novel animal model of PD is one utilising the irreversible UPS inhibitor, lactacystin. Lactacystin (figure 5.1) is a naturally synthesised product of the *Streptomyces* genus of bacteria, which was first described in 1991 (Omura et al.). The discovery that lactacystin acts as a potent covalent inhibitor of the UPS by binding to 20/26S catalytic subunits came in 1995 (Fenteany et al.) making it the first non-peptidic selective proteasome inhibitor discovered. Today, lactacystin is a commonly used research tool in the biochemical study of the UPS, and more recently, in PD research in modelling UPS inhibition and dopaminergic neurodegeneration both *in vitro* and *in vivo*.

Since the discovery that activity of the UPS is reduced in PD (McNaught and Jenner, 2001, McNaught et al., 2002a), and two mutations in familial PD, namely UCH-L1 and parkin affect the functioning of the UPS (Kitada et al., 1998, Leroy et al., 1998), UPS inhibitors such as the synthetic proteasome inhibitor PSI, epoxomycin, MG-132 and lactacystin have been used in attempt to generate animal models of PD (McNaught et al., 2002c, McNaught et al., 2004). Lactacystin was first shown to induce neuronal cell death, *in vitro*, in PC12 cells, a catacholaminergic cell line, in 2001 (Rideout et al.). Subsequently, it has been shown extensively to recapitulate Parkinsonian dopaminergic neuronal cell death, *i*n vivo, in mice (Li et al., 2010, Pan et al., 2008, Xie et al., 2010, Zhu et al., 2007) and rats (McNaught et al., 2002b, Niu et al., 2009, Vernon et al., 2010, Lorenc-Koci et al., 2011, Pienaar et al., 2013). Lactacystin covalently binds to catalytic subunits of the 20/26S proteosome, this prevents accessibility of ubiquitinated proteins to the catalytic sites of UPS elements and therefore causes the cytoplasmic accumulation of unwanted proteins (McNaught et al., 2002b, McNaught et al., 2002c). Lactacystin is not brain penetrant and is therefore stereotaxically injected into the SNpc of rats to cause the formation of ubiquitin/αSyn immunopositive inclusions in nigral dopaminergic neurons (McNaught et al., 2002b, Niu et al., 2009, Vernon et al., 2010, Lorenc-Koci et al., 2011, Pienaar et al., 2013). This intracellular accumulation

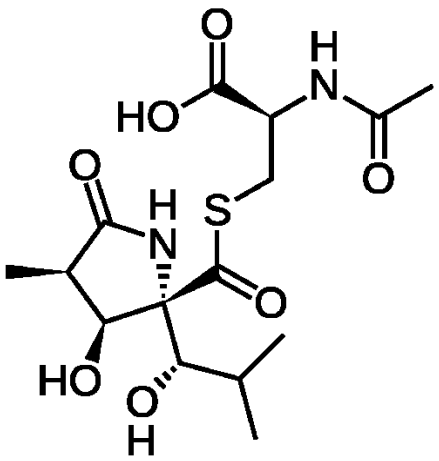

Figure 5.1 – Chemical Structure of Lactacystin
The chemical structure of lactacystin (2-(acetylamino)-3-[({3-hydroxy-2-[1-hydroxy-2-methylpropyl]-4-methyl-5-oxopyrrolidin-2-yl}carbonyl)sulfanyl]propanoic acid) is given. Unlike many other toxins used for inducing Parkinsonism in rats (e.g. 6-OHDA) lactacystin is not subject to oxidisation and hence is relatively stable when stored on ice for stereotaxic injection. It is however subject to hydrolysis and is therefore stored as a stock solution in an organic solvent and reconstituted in sterile (0.9%) saline on the day of stereotaxic surgery.

results in progressive nigral neurodegeneration and subsequent progressive development of motor behavioural deficits. For example neurological deficit scoring of lactacystin lesioned animals has previously been shown to gradually worsen post lactacystin-lesion: rats displaying progressive deficits in spontaneous motility and horizontal bar, grasping reflex and placing reaction tests (Vernon et al., 2010). Similarly lactacystin lesioned rats have also previously been shown to display deficits in forelimb grip strength, reduced performance on an accelerating rotarod and ostensible circling behaviour after apomorphine challenge (Vernon et al., 2010, Vernon et al., 2011). The behavioural symptoms have also been observed to be attenuated with chronic L-DOPA treatment (Konieczny et al., 2014). Clinically relevant changes have also been observed in lactacystin lesioned rats in PET scans (Mackey et al., 2013). Therefore unlike many other animal models of PD, the lactacystin model not only recapitulates the formation of protein inclusions in dopaminergic neurons, but also models the progressive nature of both dopaminergic neurodegeneration and development of L-DOPA attenuated motor behavioural deficits. These qualities make the lactacystin rat model of PD and ideal platform on which to study the neuroprotective potential of candidate therapeutics, allowing for simultaneous study of motor behaviour, neuropathology, and cellular and molecular changes in a single animal model.

The purpose of this chapter is to generate and profile progression of the lactacystin animal model of PD with the aim of identifying a clinically translatable therapeutic window in which pathological features and motor behavioural symptoms are evident in order to start treatment with the candidate HDACI, and model the clinical scenario in which a neuroprotective drug would be administered. Firstly the animal model of PD will be established by stereotaxic injection of lactacystin into the SNpc. MRI and behavioural testing will then be used to longitudinally monitor the neuropathological and symptomatic progression of the disease model over time. At the end of the study, animals will be culled, and the brains removed for cellular and molecular analysis. From longitudinal findings a suitable therapeutic timepoint will be identified in which neuropathological and symptomatic features of the model are evident. An additional group of animals will then be similarly lesioned with lactacystin, culled at this earlier timepoint, and cellular and molecular analyses performed on the brains in order to quantify lactacystin induced changes prior to HDACI treatment.

5.2 - Aims of Chapter

The aims of this chapter are therefore to:

1. Generate a lactacystin rat model of PD which recapitulates progressive motor behavioural symptoms and neuropathological features of the disease
    a. Profile the symptomatic progression of lactacystin induced motor behavioural symptoms in the model.
    b. Profile the progression of lactacystin induced pathological changes in brain structure in the model.
    c. Quantify the extent of lactacystin induced dopaminergic neuronal cell death in the SNpc in the model.
    d. Quantify the extent of lactacystin induced changes in histone acetylation in the model.
    e. Quantify the extent of lactacystin induced changes in expression of key neurotrophic and neuroprotective genes in the model.
2. Identify a suitable clinically translatable delayed therapeutic window in which to treat the animal model with candidate neuroprotective HDACIs.
    a. From symptomatic and neuropathological profiling of the lactacystin model, identify a suitable timepoint in which early pathological features and motor behavioural symptoms are evident.
    b. Quantify lactacystin induced dopaminergic neuronal cell death and ascertain the level of microglial activation in the SNpc of model animals at the chosen timepoint.
    c. Quantify the extent of lactacystin induced changes in histone acetylation and changes in expression of key neurotrophic and neuroprotective genes at this chosen timepoint.

5.3 – Experimental Design

5.3.1 – Generating and Profiling Disease Progression in the Lactacystin Rat Model of PD

Male Sprague-Dawley rats (n=7) were intra-nigrally lesioned with the irreversible proteasome inhibitor, lactacystin, by stereotaxic injection into the SNpc (see section 2.4.3). In order to follow the behavioural and neuropathological progression of the model of PD and to identify a suitable clinically translatable delayed therapeutic window in which to treat the animals with candidate neuroprotective HDACIs, motor behavioural testing (see section 2.4.4) and MRI of the rat brain, *in vivo* (see section 2.4.5), were conducted at baseline prior to stereotaxic lesioning and at weeks 1, 3 and 5 of the study. For comparison, a second group of male Sprague-Dawley rats (n=7) was also subjected to the same behavioural testing and MR imaging in parallel but which did not receive lactacystin lesioning surgery (table 5.1 for study groups). Both the vertical cylinder and amphetamine induced rotation tests were used to study the progression of behavioural motor asymmetry. Similarly, manual volumetric segmentation analysis, tensor based morphometry and T_2 relaxivity analysis using MR images were conducted to study the neuropathological progression of the model. Five weeks post-surgery, animals were culled and brain tissue collected (see section 2.4.6), and prepared for qRT-PCR, Western, and immunohistochemical analysis (see section 2.5) for profiling of the cellular and molecular effects of lactacystin after the five week study period (figure 5.2 for graphical illustration of study design). At the end of the study the hind brain was fixed, cryoprotected, cryosectioned and dopaminergic neurons (TH+) immunohistochemically stained and stereologically quantified in the SNpc. Frontal cortex tissue was dissected out and snap frozen for molecular analysis. Protein content was extracted from tissue samples and Western blot analyses were conducted to quantify the level of histone acetylation in the brains of lactacystin/non-lesioned animals. In addition, mRNA content was extracted for qRT-PCR analysis to quantify the expression of numerous key neurotrophic and neuroprotective factors.

5.3.2 – Identification of a Clinically Translatable Therapeutic Window in the Lactacystin Rat Model

From the experiments detailed above a clinically translatable therapeutic window in the lactacystin rat model of PD was identified based on the existence of behavioural motor asymmetry and brain morphological changes evident from behavioural testing and manual segmentation of MR images respectively. However to confirm that lactacystin induced neurodegeneration of dopaminergic neurons in the SNpc was similarly evident at this early timepoint, an additional group of animals were lesioned similar to that described above (section 5.3.1) and culled early for cellular and molecular analysis of brain changes. Male Sprague-Dawley rats (n=7) were intra-nigrally lesioned with the irreversible proteasome inhibitor, lactacystin, by stereotaxic injection into the SNpc (see

section 2.4.3). Animals were culled at the early timepoint chosen and brain tissue was collected and prepared for qRT-PCR, Western, and immunohistochemical analysis (see section 2.5) for detailing of the cellular and molecular effects of intranigral injection. As above, at the end of the study the hind brain was fixed, cryoprotected, cryosectioned and dopaminergic neurons (TH+) immunohistochemically stained and stereologically quantified in the SNpc. Frontal cortex tissue was dissected out and snap frozen for molecular analysis. Protein content was extracted from tissue samples and Western blot analyses were conducted to quantify the level of histone acetylation in the brains of lactacystin lesioned animals. In addition, mRNA content was extracted for qRT-PCR analysis to quantify the expression of numerous key neurotrophic and neuroprotective factors.

5.3.3 – Statistical Analysis

All data is presented as mean ± SEM. All Western blot datasets were analysed using a one-way ANOVA with Bonferroni post-tests. All qRT-PCR datasets were analysed using a two-way ANOVA with Bonferroni post-tests. For the five week lactacystin study, two-way (repeated measures) ANOVA with Bonferroni post-tests were used for analysis of vertical cylinder test, amphetamine induced rotations, MRI manual segmentation and T_2 relaxivity datasets analysis. An additional unpaired student t-test and one-way ANOVA with Bonferroni post-tests were used for analysis of area under curve data from vertical cylinder and amphetamine induced rotation tests, respectively. For correlation analysis of behavioural test outcomes, a non-linear one-phase decay regression line was fitted onto the data. Paired and unpaired student t-tests were used to compare stereological cell counts in the ipsilateral and contralateral hemispheres of animal brains, and percentage cell loss between hemispheres respectively. For the one week lactacystin study, two-way (repeated measures) ANOVA with Bonferroni post-tests were used for analysis of vertical cylinder test, MRI manual segmentation and T_2 relaxivity datasets analysis. A one-way ANOVA with Bonferroni post-tests was used for analysis of amphetamine induced rotation test data. An additional one-way ANOVA with Bonferroni post-tests and unpaired student t-test were used for analysis of area under curve data from vertical cylinder and amphetamine induced rotation tests, respectively. Paired student t-tests were used to compare stereological cell counts in the ipsilateral and contralateral hemispheres of animal brains and a one-way ANOVA with Bonferroni post-tests was used for analysis of percentage cell loss data between hemispheres. All statistical tests were performed using GraphPad Prism (v5.0 for Windows, GraphPad Software, San Diego, CA, USA).

Table 5.1 - Disease Model Progression Animal Treatment Groups

Group	N=	Intranigral Injection	Behavioural Tests
Lacta(-)	7	None	Vertical Cylinder Test
Lacta(+)	7	Lactacystin (10µg in 4µl saline)	Vertical Cylinder & Amphetamine Induced Rotation Tests

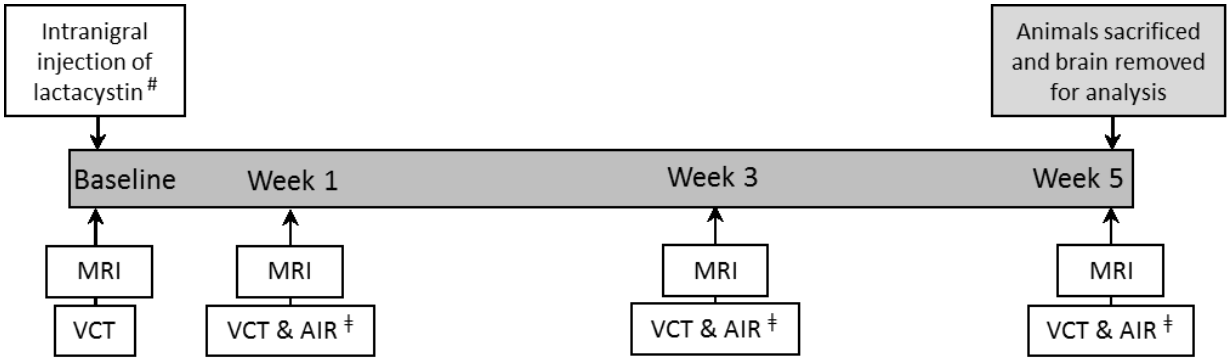

Figure 5.2 – Disease Model Progression Animal Study Design
Study design used for investigation of the behavioural and neuropathological progression of the lactacystin rat model of PD and investigation of the cellular and molecular effects of intranigral injection of lactacystin.
#Only group Lacta(+) was intranigrally injected with lactacystin.
‡Only group Lacta(+) were tested using the amphetamine induced rotation test at these time points.

5.4 – Results

5.4.1 – Confirming Lesion Accuracy in Lactacystin Injected Animals

Firstly to confirm that all of the lesioned animals received lactacystin to the left SNpc, MRI scans acquired at week 1 post-lesion were examined to confirm the location of stereotaxic injection of the toxin (see section 2.4.5.3). The SNpc containing plate of the rat brain atlas (-5.2mm from bregma) was overlaid on the acquired T_2W MR image of the rat brain most resembling the size and shape of the brain in the atlas plate. Accurate lactacystin lesioning was accepted if the needle tract was visible on the MR image (confirming anterio-posterior positioning) and the end of the needle tract was located above the left SNpc (confirming medio-lateral, and ventral-dorsal positioning). The lesion site was confirmed in all lesioned animals and therefore no animals were excluded on this basis.

5.4.2 – Progressive Development of Motor Behavioural Symptoms in the Lactacystin Rat Model

5.4.2.1 – Vertical Cylinder Test

The vertical cylinder test was conducted on both lactacystin-lesioned and non-lesioned animals at baseline and weeks 1, 3 and 5 of study. At baseline there was equal use of both the left and right forelimbs in all animals (figure 5.3A, 51.98 ± 1.67% mean contralateral forelimb use). However one week after surgery there was a significant reduction in the contralateral forelimb use of lactacystin-lesioned animals compared with non-lesioned animals (week 1, non-lesioned animals, 46.47 ± 0.95% vs. lactacystin-lesioned animals, 39.59 ± 4.11% contralateral forelimb use, $p<0.01$). From one week onwards the contralateral forelimb use of lactacystin-lesioned animals continued to decline with time (week 1, 39.59 ± 4.11%; week 3, 35.80 ± 3.37%; week 5, 35.50 ± 4.08% contralateral forelimb use, $p<0.01$ compared with non-lesioned animals at each time point). This resulted in a significantly reduced area under the curve produced from plotting percentage contralateral forelimb use vs. time compared with non-lesioned animals (figure 5.3B, lactacystin-lesioned animals, 262.04 ± 3.38 vs. non-lesioned animals, 193.31 ± 13.71 area under curve, $p<0.001$).

5.4.2.2 – Amphetamine Induced Rotation Test

In addition to vertical cylinder tests, amphetamine induced rotation tests were conducted on lactacystin-lesioned animals at week 1, 3 and 5 following lesioning surgery. At week 1 following lesioning surgery, all lactacystin-lesioned animals exhibited rotational asymmetric behaviour upon treatment with amphetamine (figure 5.3C, week 1, 24.31 ± 4.80 mean number of rotations per 5 mins). This rotational behaviour continued to develop over the further two time points examined (average number of ipsiversive rotations per 5 mins, week 1, 24.31 ± 4.80, week 3, 41.72 ± 9.84, week 5, 66.22 ± 19.43). This resulted in a significantly increased area under the curve produced from

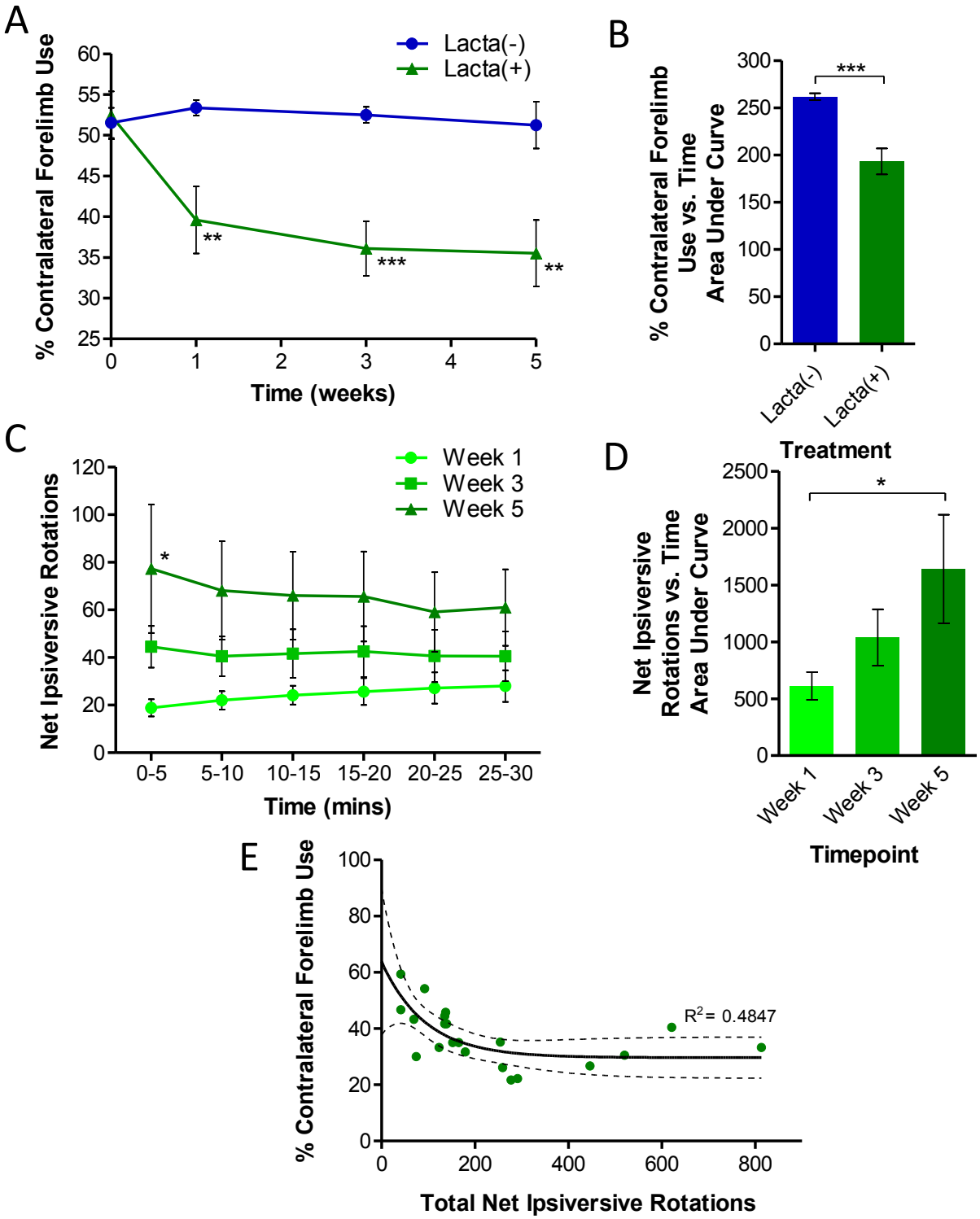

Figure 5.3 – Lactacystin Lesioning Causes Progressive Development of Motor Asymmetry
(A) Vertical cylinder test outcomes demonstrate that one week after lactacystin lesioning, animals exhibit a significant reduction in contralateral forelimb use compared with non-lesioned animals. (B) Area under the curve of data represented in (A) demonstrating more clearly the differences between percentage contralateral forelimb use in animal treatment groups. (C) Amphetamine induced rotation test outcomes demonstrate that one week after lactacystin lesioning, animals exhibit rotational asymmetric behaviour after administration of amphetamine. The extent of this behaviour continues to develop over the five weeks of study. (D) Area under the curve of data represented in (C) demonstrating more clearly the progressive nature of rotational behaviour after lactacystin lesioning. (E) Correlation analysis between contralateral forelimb use in the vertical cylinder test, and total net number of ipsilateral rotations in the amphetamine induced rotation test demonstrate the relationship between these two behavioural outcomes in lesioned animals. Black line indicates non-linear one-phase decay line of regression with 95% confidence interval (dotted lines). Statistical significance between groups/timepoints is indicated using asterisks: *p<0.05, **p<0.01, ***p<0.001. n=7.

from plotting net ipsiversive rotations vs. time, between week 1 and week 5 following lactacystin-lesioning (figure 5.3D, week 1, 612.83 ± 121.59, vs. week 5, 1641.00 ± 477.50, $p<0.05$).

5.4.2.3 – Behavioural Test Outcome Correlation Analysis

As has been seen, both vertical cylinder and amphetamine induced rotation test outcomes progress with lesion development in the lactacystin rat model of PD. Both of these behavioural paradigms demonstrate motor asymmetry, therefore to determine how they relate to one another a correlation analysis was performed between the percentage contralateral forelimb use exhibited by the animal in the vertical cylinder test and the corresponding total net number of ipsiversive rotations in the amphetamine induced rotation test performed on the same day. In the lactacystin-lesioned animals described here, the outcomes of these two motor asymmetry behavioural tests were correlated by a non-linear one-phase decay line of regression (figure 5.3E). As expected the lower the percentage contralateral forelimb use exhibited by an animal, the greater total net number of ipsiversive rotations. However due to the non-linear nature of the correlation the contralateral forelimb use of animals produces a plateaux at 29.67 ± 3.497%, meaning that animals which perform greater than ~300 ipsiversive rotations do not exhibit a deficit in contralateral forelimb use more than ~20%.

5.4.3 – Neuropathological Development of the Lactacystin Rat Model of Parkinson's Disease

5.4.3.1 – Manual Segmentation Analysis

Post-acquisition, MR images of the brains of all animal treatment groups were analysed using manual segmentation analysis to assess changes in regional brain volume over the course of the five week study (figure 5.4A). In line with rat growth there was a steady increase in whole brain volume of both treatment groups over the five weeks of examination, however this trend of volume increase with time was steeper in lactacystin-lesioned compared with non-lesioned animals (figure 5.4B, week 5, non-lesioned animals, 6.60 ± 1.18%, vs. lactacystin-lesioned animals, 9.08 ± 2.44% increase from baseline). Similar is the case with cerebellum volume: lactacystin-lesioned animals exhibit a far greater increase in cerebellum volume with time than non-lesioned animals, reaching statistical significance at week 5 of study (figure 5.4C, week 5, non-lesioned animals, 3.30 ± 2.74%, vs. lactacystin-lesioned animals, 12.91 ± 1.65% increase from baseline, $p<0.05$).

As expected in the non-lesioned animals the volume of the lateral ventricles increased comparably in both hemispheres over the 5 weeks of study (figure 5.4D). Animals which received an intranigral injection of lactacystin however exhibited a greater increase in ventricular volume than non-lesioned controls, a change which was more pronounced in the lesioned hemisphere. Neither of these changes however reached statistical significance compared with non-lesioned animals.

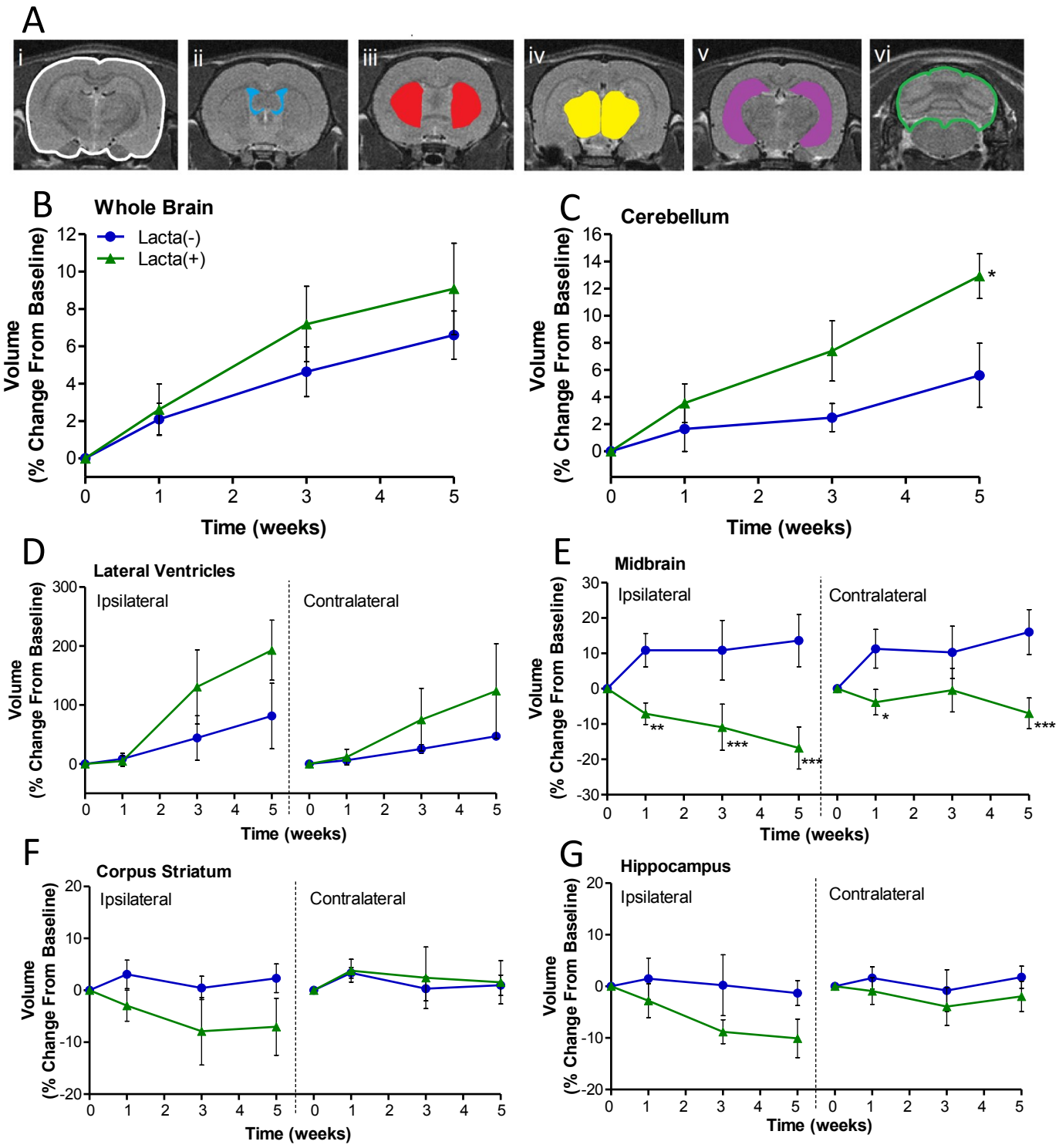

Figure 5.4 – Manual Segmentation Analysis of MR Images Reveals Dose Dependent Attenuation of Lactacystin Induced Volumetric Changes by Valproate

(A) Representative examples of the manual segmentation of (i) whole brain, (ii) lateral ventricles, (iii) corpus striatum, (iv) midbrain, (v) hippocampus and (vi) cerebellum in MR images. Administration of valproate (designated by arrow and grey shading) dose dependently attenuates volumetric changes observed in the (D) lateral ventricles and (E) the midbrain as a result of lactacystin lesioning, as ascertained through manual segmentation analysis of rat brain MR images. Similar, albeit more subtle changes are observed in the (F) corpus striatum and (G) hippocampus mirroring those seen in the midbrain. Administration of valproate and/or lactacystin also have marked effects on (B) whole brain and (C) cerebellum volume. Statistical significance between groups is indicated using asterisks: *p<0.05, **p<0.01, ***p<0.001. n=7.

The most pronounced changes in regional brain volume took place in the midbrain, the location of the SNpc and therefore the site of stereotaxic injection of lactacystin (figure 5.4E). One week after surgery, lactacystin-lesioned animals displayed a significant reduction in the volume of the ipsilateral midbrain compared with non-lesioned control animals (figure 5.4E, week 1, lactacystin-lesioned animals, -7.07 ± 3.04% change from baseline vs. non-lesioned animals 10.88 ± 4.73% change from baseline, $p<0.01$). This volume decrease in the ipsilateral midbrain continued to progress with time, resulting in the percentage change in volume from baseline being significantly different from non-lesioned animals at both weeks 3 and 5 (figure 5.4E, lactacystin-lesioned animals, -10.90 ± 6.54% and -16.76 ± 5.94%, vs. non-lesioned animals 10.89 ± 8.45 and 13.63 ± 7.41% change from baseline at weeks 3 and 5 respectively, $p<0.001$ in both comparisons). Identical, albeit more subtle changes are similarly observed upon lactacystin lesioning in the contralateral hemisphere of the midbrain.

No significant differences were observed in corpus striatum volume in either the ipsilateral or contralateral hemispheres. However a number of trends in the ipsilateral hemisphere exist mimicking those changes observed in the midbrain (figure 5.4F). There was a trend of reduced corpus striatal volume in lactacystin-lesioned animals compared with non-lesioned, however unlike the ipsilateral midbrain volume at these time points these differences were not statistically significant. No statistical differences or notable trends were observed in the contralateral corpus striatum volume. Similar non-significant differences of a reduction in ipsilateral volume were also observed in the hippocampus. However as with the case of the contralateral corpus striatum, there were no discernible trends or statistically significant differences observed in the volume of the contralateral hippocampus.

5.4.3.2 – Tensor Based Morphometry

In collaboration with Drs Anthony Vernon and William Crum at Kings College London, tensor based morphometry analysis was applied to MR images acquired at week 5 to confirm and extend observations from manual segmentation analysis (figure 5.5). After correcting for global differences in brain volume (9dof registration) to search for relative differences in structural volume, several distinct anatomical patterns were observed between treatment groups (all data shown are corrected for multiple-comparison over voxels using the False Discovery Rate with $q<0.05$).

Consistent with manual segmentation analyses, in lactacystin-lesioned animals widespread significant contraction of cortical voxels in the ipsilateral hemisphere of the brain was observed. These included the cingulate, motor, somatosensory and parietal cortical sub-fields. Sub-cortically, widespread clusters of contracted voxels were observed in the ipsilateral striatum, globus pallidus, thalamus, ventral midbrain and brainstem nuclei. Some of these clusters extended across the

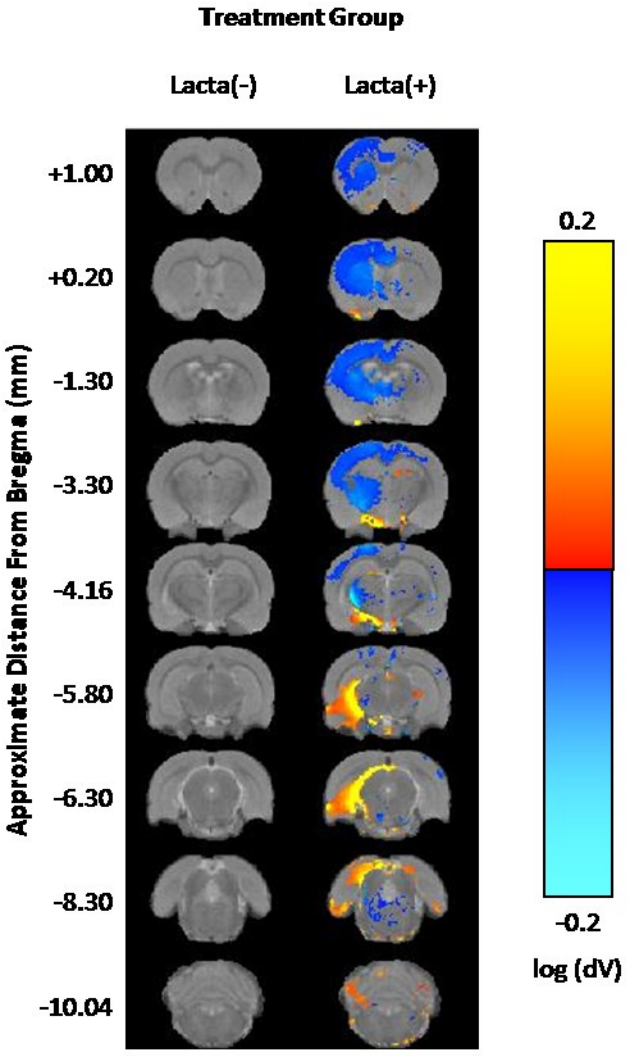

Figure 5.5 – Tensor Based Morphometry Validates Findings from Manual Segmentation Analyses of Rat Brain MR Images

Regions of significant volume difference relative to whole brain compared with non-lesioned animals at week 5 are shown. Positive differences (yellow/orange) indicate volume increases, and negative differences (blue) indicate volume decreases compared with non-lesioned animals. Results shown are significant after correction for multiple comparisons across voxels using the False Discovery Rate with $q<0.05$. n=7.

midline into the contralateral hemisphere. No significantly contracted voxels were observed in the hippocampus. Clusters of significantly expanded voxels were also observed in the ipsilateral hemisphere. Primarily this reflected an increase in cerebrospinal fluid signal accompanying deformation of the ventral midbrain. Significantly expanded voxels were however also seen in the cerebellar white matter and dorsolateral entorhinal cortex.

5.4.3.3 – T_2 Relaxivity Measurement

In conjunction with manual segmentation analysis, at each of the time points examined, inter-hemispheric differences in T_2 signal intensity were assessed in the SNpc, the midbrain and the corpus striatum. For each brain region the T_2 signal intensity ratio (ipsilateral divided by contralateral T_2 signal) was then calculated as a measure of interhemispheric difference (figure 5.6). The most marked changes in T_2 relaxivity occurred within the SNpc (figure 5.6A). In lactacystin-lesioned animals 1 week post-surgery there was a significant increase in T_2 signal intensity ratio compared with the signal ratio from non-lesioned animals (figure 5.6A, lactacystin-lesioned animals, 1.057 ± 0.010 vs. non-lesioned animals, 1.000 ± 0.016, $p<0.01$). This increase in T_2 signal intensity ratio however was reversed by week 3, and continued to decline by week 5 (lactacystin-lesion animals, 0.935 ± 0.012 vs. non-lesioned animals 0.999 ± 0.012, $p<0.001$). Subtle changes were also observed in the midbrain mimicking those seen in the SNpc (figure 5.6C). However due to the subtlety of these alterations no significant differences were observed. No noticeable alterations in T_2 signal intensity ration were observed in the corpus striatum (figure 5.6E).

5.4.4 – Neuronal Cell Death in the SNpc of Lactacystin Lesioned Animals

At week five of the study, animals were culled and the hind brain tissue collected for immunohistochemical staining and stereological counting of dopaminergic neurons TH positive) in the SNpc (figures 5.7E and F). As expected, non-lesioned animals did not shown any interhemispheric loss of TH+ dopaminergic neurons in the SNpc (figure 5.7A and C, left SNpc, 11724 ± 729 vs. right SNpc, 11652 ± 493 TH+ cells, % difference +1.30 ± 7.04%). Lactacystin-lesioned animals however exhibited a marked interhemispheric loss of TH+ neurons (left SNpc, 4257 ± 1364 vs. right SNpc, 12328 ± 580 TH+ cells, % difference -53.81 ± 14.32%, $p<0.01$). This change was similarly observed in the numbers of Nissl+ cell number in lactacystin-lesioned animals, indicative of TH+ neuronal cell death rather than loss of the TH enzyme expression in dying neurons.

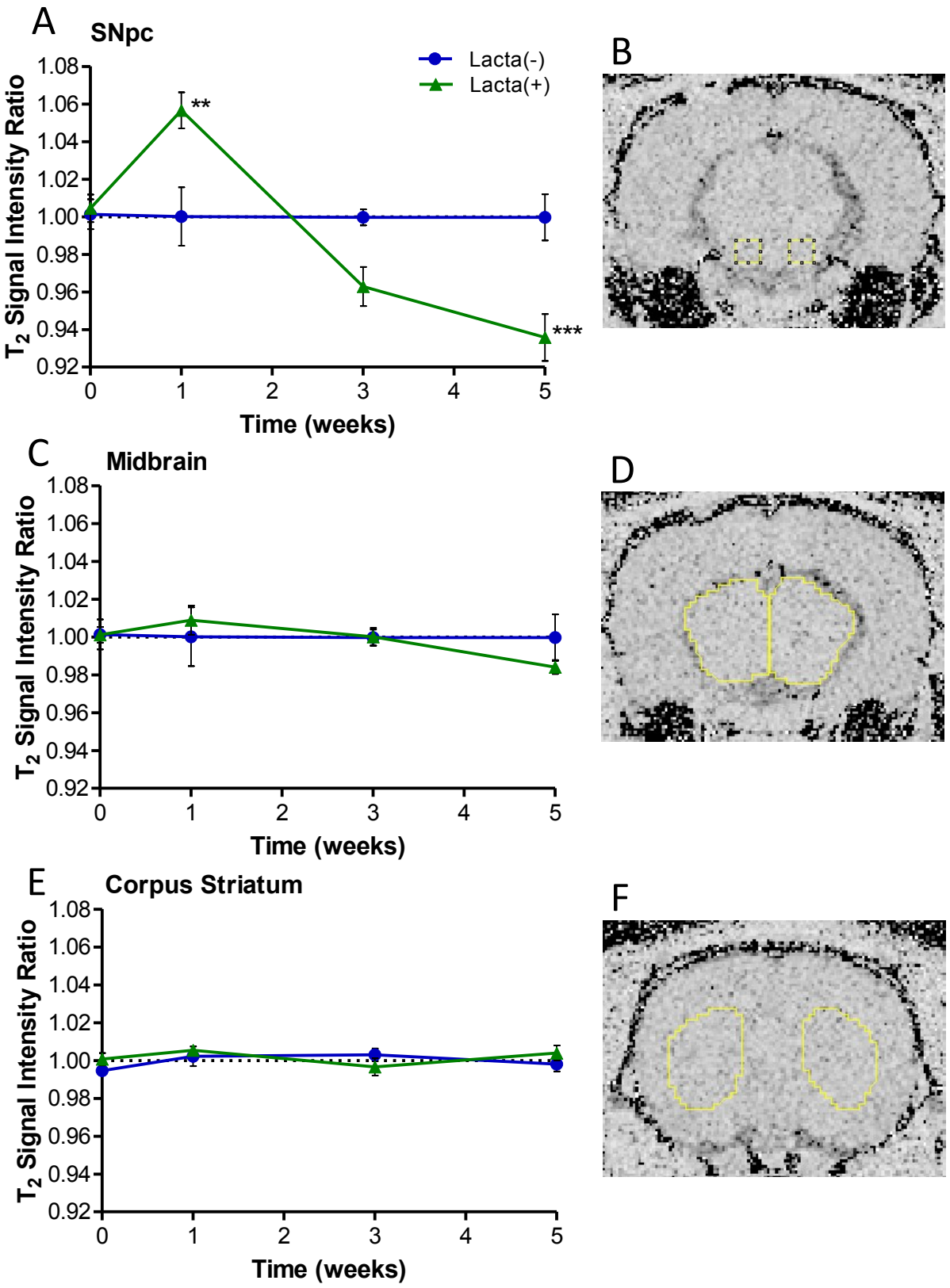

Figure 5.6 – T_2 Signal Intensity Analyses Reveal Alteration in T_2 Signal Between Hemispheres of Lactacystin-Lesioned Animals

T_2 signal intensity measurements were made from T_2 relaxivity maps in the ipsilateral and contralateral (B) SNpc, (D) midbrain, and (F) corpus striatum. Data was then expressed as the ratio between the ipsilateral and contralateral hemisphere: the T_2 signal intensity ratio. Graphs show T_2 signal intensity ratio between the ipsilateral and contralateral hemisphers over time in the (A) SNpc, (C) midbrain and (E) corpus striatum. Statistical significance between groups is indicated using asterisks: *p<0.05, **p<0.01, ***p<0.001. n=7.

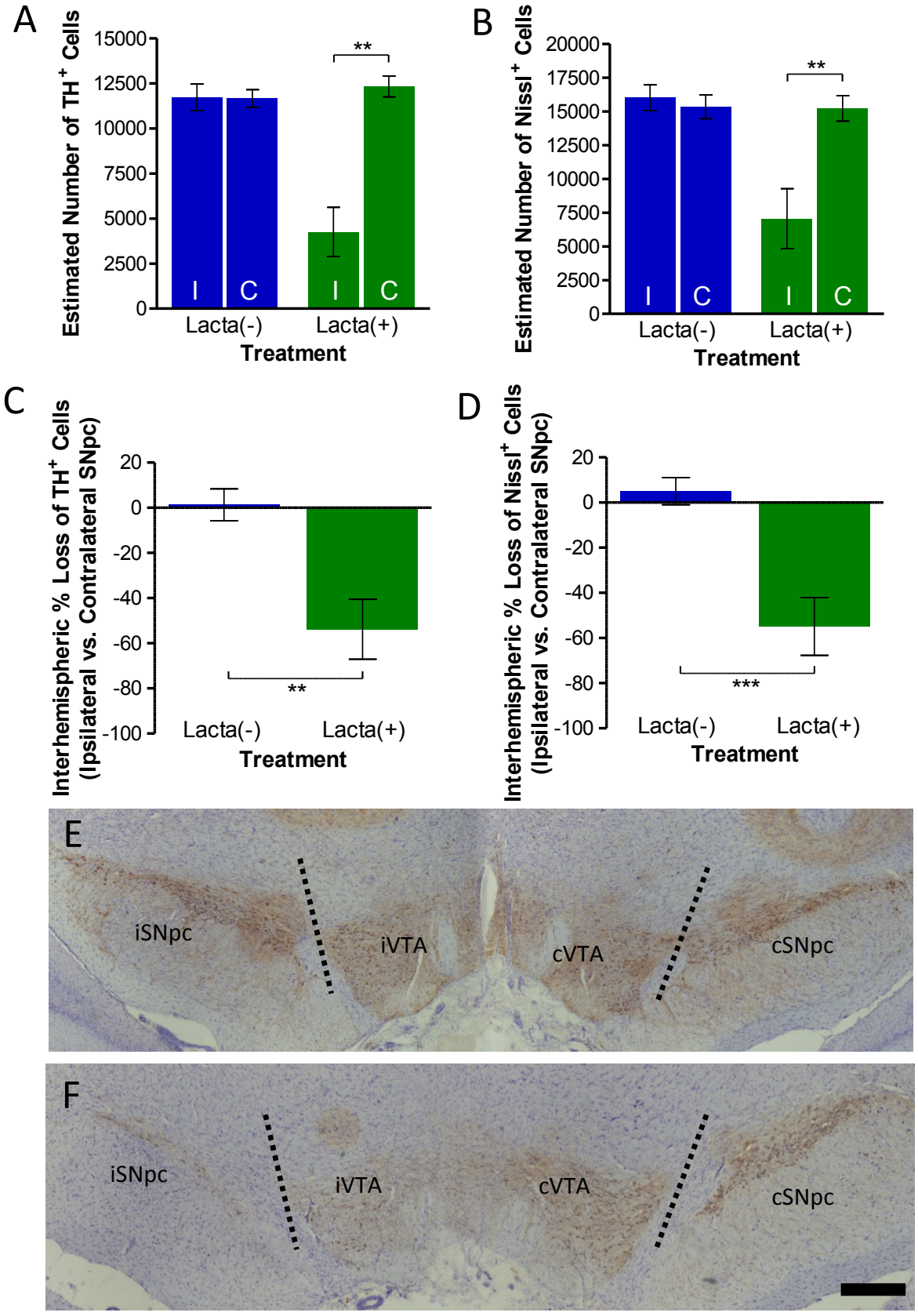

Figure 5.7 – Stereological Estimates of Cell Number Demonstrate the Toxic Effects of Lactacystin-Lesioning
Stereologically estimated (A) TH+ and (B) Nissl+ neuron numbers in the SNpc of rats demonstrate the toxic effects of lactacystin-lesioning. This is exemplified by the percentage interhemispheric loss of TH+ (C) and Nissl+ (D) neurons calculated between hemispheres of the SNpc. Statistical significance indicated with asterisks: *p<0.05, **p<0.01, ***p<0.001. n=7. Representative examples of the stained SNpc of non-lesioned (E) and lactayctsin-lesioned (F) rats demonstrating interhemispheric cell loss. Scale bar equal to 500µm. Abbreviations: I, ipsilateral; C, contralateral.

5.4.5 – Lactacystin-Lesioning Causes Histone Hypoacetylation in the Frontal Brain

At the end of the study the frontal brain tissue was removed and snap frozen for subsequent extraction of mRNA and protein for molecular analysis. Histone protein H3 acetylated on lysine 9 (AcH3-Lys9) was quantified using Western blot analysis. Significantly less AcH3-Lys9 was observed in both frontal brain hemispheres in lactacystin-lesioned animals compared to non-lesioned controls (figure 5.8, ipsilateral and contralateral frontal brain hemispheres, 2.96 ± 6.41% and 21.05 ± 11.07% of control respectively, $p<0.01$ in both comparisons).

5.4.6 – Lactacystin-Lesioning Causes Downregulation of Neurotrophic Growth Factors and Neuroprotective Protein Genes in the Frontal Brain

In conjunction with proteins for Western blot analysis, mRNA was extracted from frontal brain tissue and the expression level of a number of neuroprotective factors, apoptotic regulators and genes of interest to neurodegeneration/neuroprotection were quantified using qRT-PCR (figure 5.9). Modest reductions in the expression of αSyn, Hsp70, GSN, Bcl-2 and Bad were observed in both the ipsilateral and contralateral frontal brain hemispheres of lactacystin-lesioned compared with control animals. Additionally, marked reductions in the expression of BDNF and GDNF were observed in both brain hemispheres of lactacystin-lesioned animals compared with controls, more so in the lesioned hemisphere (BNDF and GDNF expression in the ipsilateral hemisphere, 0.14 ± 0.01 and 0.08 ± 0.02 fold change from control respectively, $p<0.05$ in both comparisons).

5.4.7 – Behavioural, Neuropathological and Molecular and Cellular Marks of Neurodegeneration are Evident Seven Days Post Lactacystin-Lesioning

From symptomatic and neuropathological profiling of the lactacystin model detailed above, week 1 was identified as a suitable timepoint in which early pathological features and motor behavioural symptoms in the model were evident, and therefore highlighted as a suitable therapeutic window in which to start HDACI treatment. Therefore to quantify the lactacystin induced cellular and molecular marks of neurodegeneration at this early timepoint, an additional group of animals was lesioned with lactacystin and culled after behavioural testing at week 1 and the brains removed for molecular and cellular analyses.

5.4.7.1 – Motor Behavioural Symptoms Comparable with Previously Lesioned Animal Group

To confirm that animals had been lesioned accurately, both the vertical cylinder test and amphetamine induced rotation tests were conducted at week 1 to compare behavioural outcomes to previously lesioned rats in which needle placement was confirmed with MRI. Lactacystin-lesioned

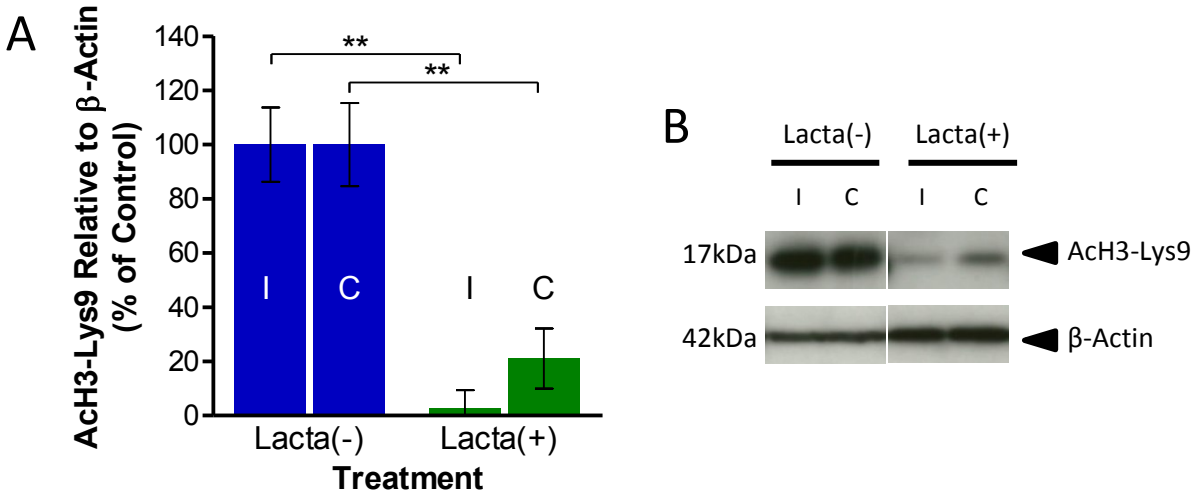

Figure 5.8 – Lactacystin-Lesioning Induces Histone Hypoacetylation in the Frontal Brain
Lactacystin-lesioning causes a reduction in histone H3-lysine 9 acetylation in the frontal brain. (A) Densitometry analysis of the AcH3-Lys9 band relative to the β-actin band used as a loading control. (B) Representative blot of data presented in (A). Statistical significance between groups is indicated using asterisks: **p<0.01. n=7. Abbreviations: I, ipsilateral; C, contralateral.

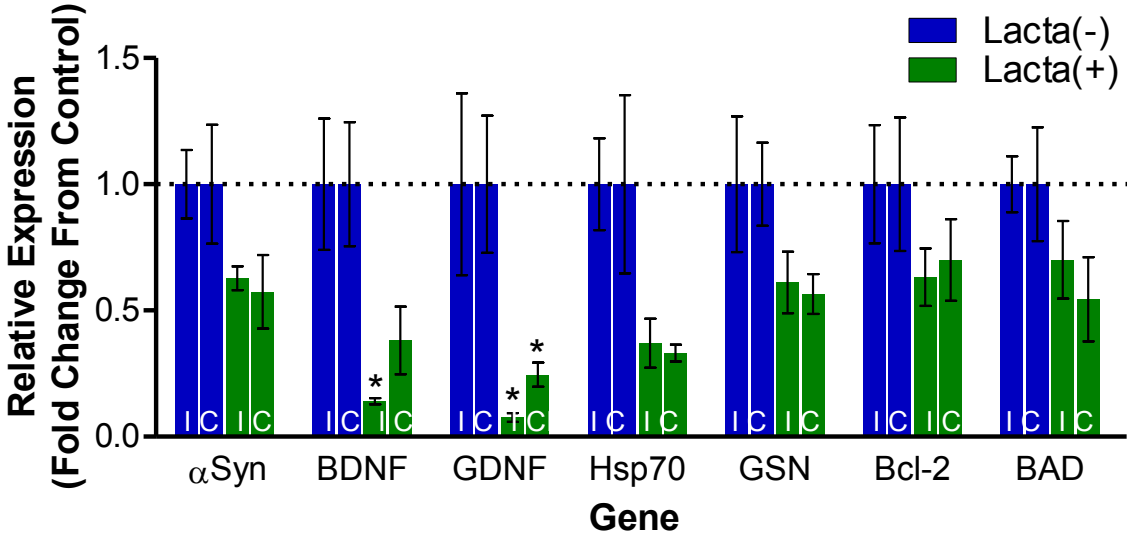

Figure 5.9 – Downregulation of Neurotrophic Growth Factors and Neuroprotective Protein Genes in Lactacystin-Lesioned Animal Brains

qRT-PCR of the frontal brain mRNA reveals downregulation of neurotrophic and neuroprotective gene proteins. Statistical significance from control is indicated using asterisks: *p<0.05. n=7. Abbreviations: I, ipsilateral; C, contralateral.

animals later culled at week 1 compared favourably with those later culled at week 5: animals developing a similar reduction in contralateral forelimb use 7 days post lesion detected through the vertical cylinder test (figure 5.10A, contralateral forelimb use of animals later culled at week 1, 39.76 ± 3.53% vs. animals later culled at week 5, 39.59 ± 4.11%, $p<0.01$ compared with non-lesioned animals in both comparisons). This resulted in a significantly reduced area under the curve produced from plotting percentage contralateral forelimb use vs. time in both lesioned groups compared to non-lesioned animals (figure 5.10B, animals later culled at week 1 and 5, 44.42 ± 2.32 and 45.12 ± 2.05 respectively compared with non-lesioned animals, 52.43 ± 0.74, $p<0.05$ in both comparisons).

In addition to vertical cylinder tests, additional animals were also subjected to amphetamine induced rotation tests at week 1 post lesion. As with vertical cylinder test outcomes from these animals at this timepoint, animal behaviour compared favourably between lactacystin-lesioned groups. Both animal groups performed similar numbers of rotations when administered amphetamine at week 1 (figure 5.10C, mean number of rotations per 5 mins, 20.51 ± 5.89 and 24.31 ± 4.80 in animals later culled at week 1 and 5 respectively). This translated to a similarly comparable area under the curve from plotting net ipsiversive rotations vs. time in both of the groups (figure 5.9D, animals later culled at week 1, 513.34 ± 149.98 vs. animals later culled at week 5, 612.08 ± 121.59).

5.4.7.2 – Progressive Neuronal Cell Death in Lactacystin-Lesioned Animals

One week post lesion, animals were culled and the hind brain tissue collected for immunohistochemical staining and stereological counting of dopaminergic neurons (TH positive) in the SNpc (figures 5.11 and 5.12A and B). Lactacystin-lesioned animals culled seven days post lesion exhibited a marked interhemispheric loss of TH+ neurons in the SNpc (left SNpc, 7817 ± 1733 vs. right SNpc, 14027 ± 538 TH+ cells, % difference -45.17 ± 10.96%, $p<0.05$). This interhemispheric difference however was lower than that observed in animals culled 5 weeks post lactacystin-lesion indicative of progressive degeneration of dopaminergic neurons after lactacystin-lesioning (animals culled at one and five weeks, -45.17 ± 10.96% and -53.81 ± 14.32% interhemispheric cell loss respectively). A similar albeit more subtle decrease in Nissl+ neurons was also observed between the left and right SNpc of animal culled at week 1 (left SNpc, 11712 ± 2890 vs. right SNpc, 18162 ± 1174 Nissl+ cells, % difference -38.23 ± 11.60%, $p<0.05$).

In addition to stereological cell quantification, comparative study of the morphology of nigral dopaminergic neurons at the two timepoints examined add insights into the pathological progression of this disease model. One week after lactacystin-lesioning, despite substantial cell loss, TH immunopositive neuropil, axonal and dendritic projections were still evident within the ipsilateral SNpc (figure 5.12Ai). By week five however this staining was reduced (figure 5.12Bi).

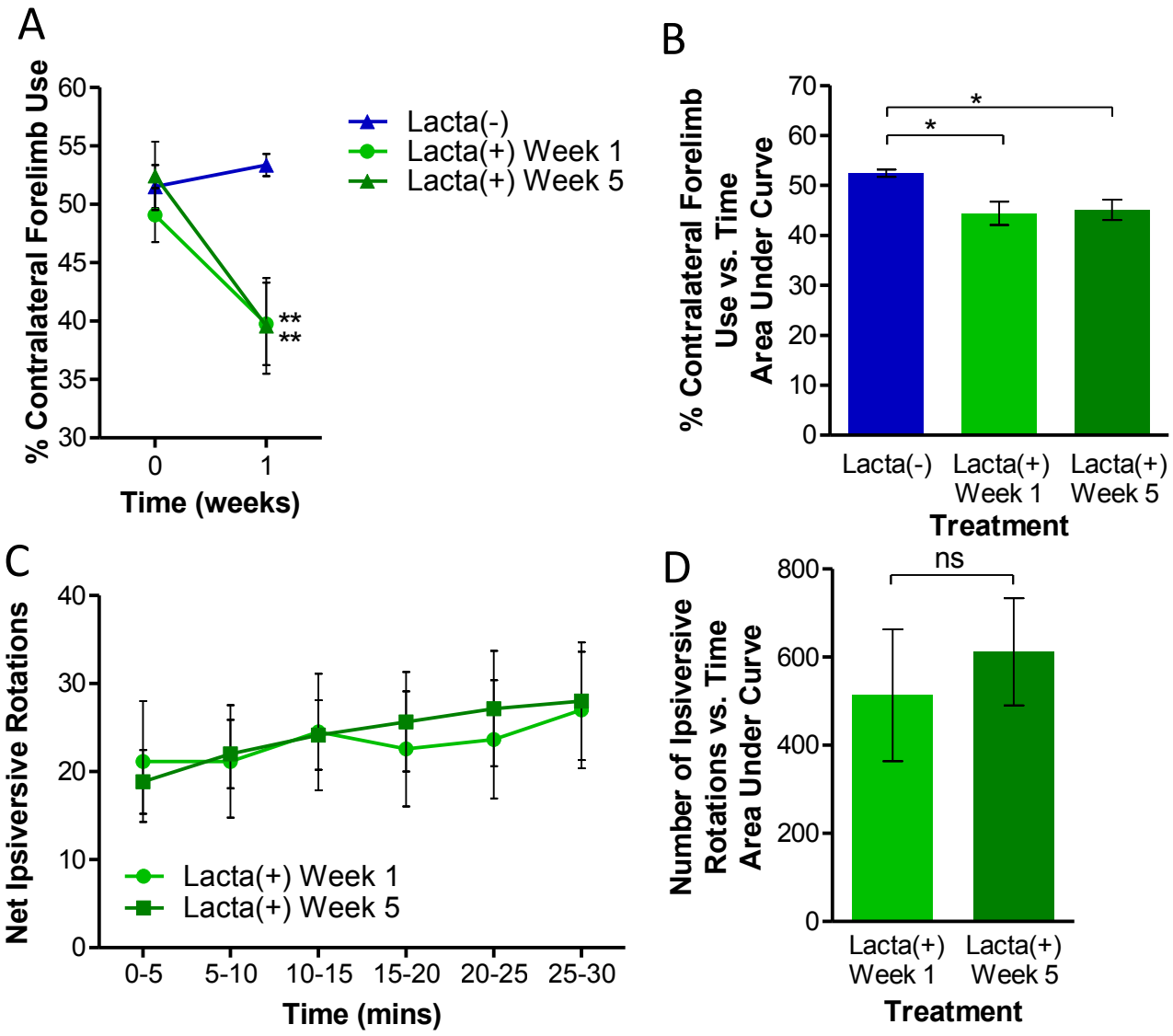

Figure 5.10 – Motor Behavioural Symptoms are Comparable with Previously Lesioned Animal Group
(A) Vertical cylinder test outcomes demonstrate that one week after lactacystin lesioning, both lesioned animal groups exhibit significant reductions in contralateral forelimb use compared with non-lesioned animals. (B) Area under the curve of data represented in (A) demonstrating more clearly the differences between percentage contralateral forelimb use in animal treatment groups. (C) Amphetamine induced rotation test outcomes demonstrate that one week after lactacystin lesioning, animals exhibit rotational asymmetric behaviour after administration of amphetamine. (D) Area under the curve of data represented in (C). Statistical significance between groups is indicated using asterisks: *p<0.05, **p<0.01. n=7.

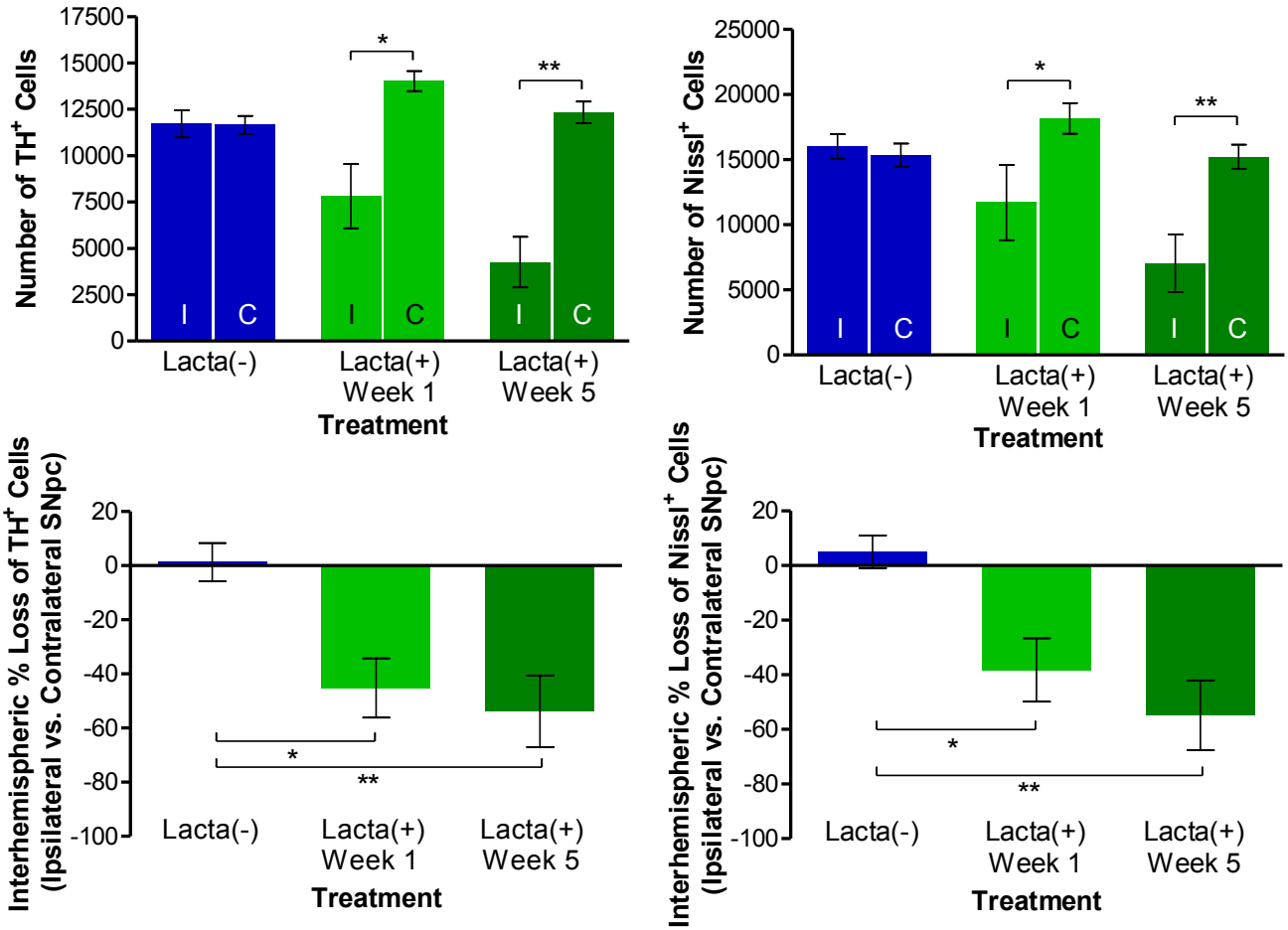

Figure 5.11 – Stereological Estimates of Cell Number One Week Post Lactacystin-Lesion
Stereologically estimated (A) TH+ and (B) Nissl+ neuron numbers in the SNpc of lactacystin-lesioned rats demonstrate progressive nature of cell death in the model, and suitability of week 1 as a therapeutic window in which to start drug treatment. This is exemplified by the percentage interhemispheric loss of TH+ (C) and Nissl+ (D) neurons calculated between hemispheres of the SNpc. Statistical significance indicated with asterisks: *p<0.05; **p<0.01. n=7. Abbreviations: I, ipsilateral; C, contralateral.

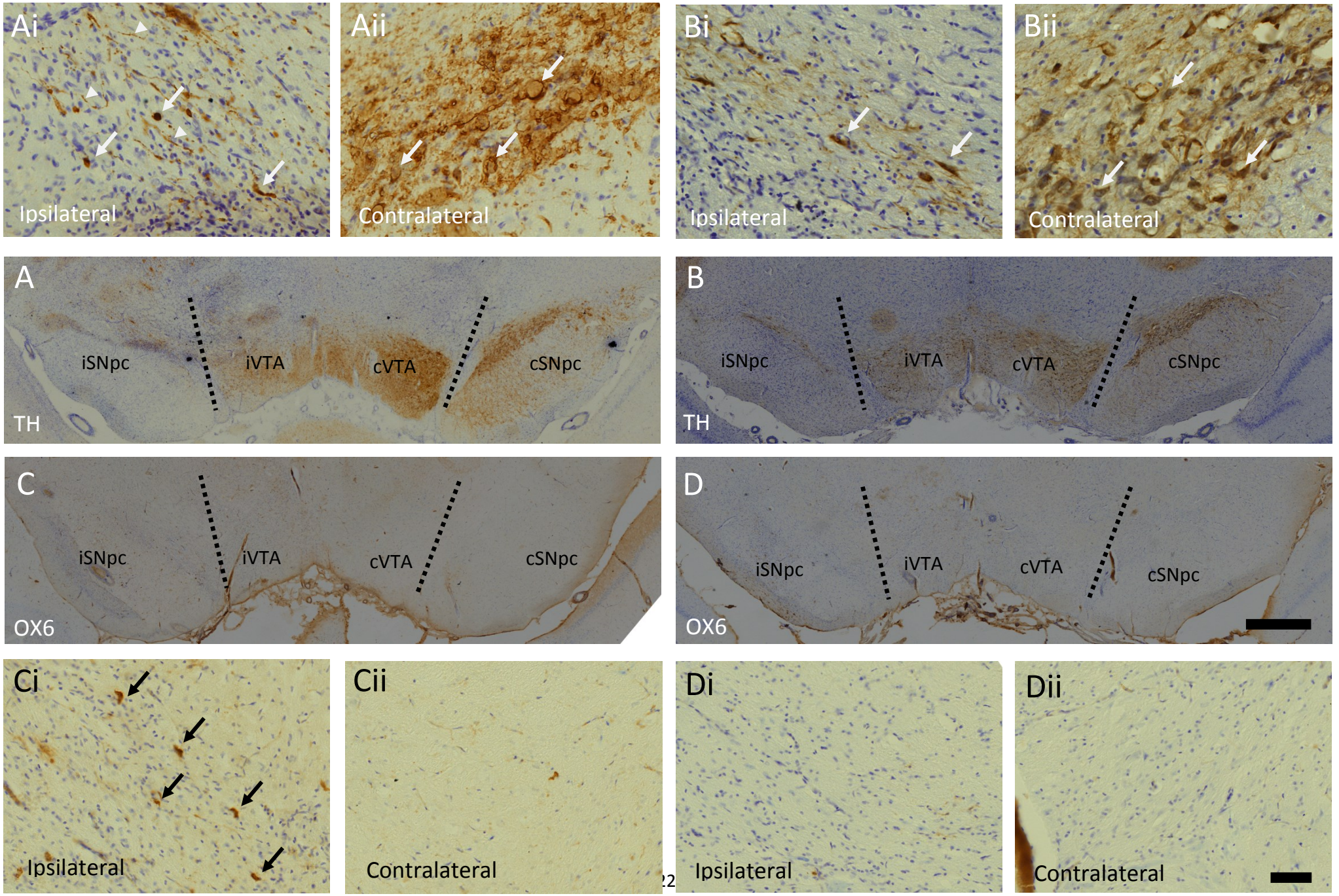
Ai
Ipsilateral
Aii
Contralateral
Bi
Ipsilateral
Bii
Contralateral
A
iSNpc
iVTA
cVTA
cSNpc
TH
B
iSNpc
iVTA
cVTA
cSNpc
TH
C
iSNpc
iVTA
cVTA
cSNpc
OX6
D
iSNpc
iVTA
cVTA
cSNpc
OX6
Ci
Ipsilateral
Cii
Contralateral
Di
Ipsilateral
Dii
Contralateral

Figure 5.12 – Immunohistochemistry in the SNpc One and Five Weeks Post Lactacystin-Lesioning
[Previous page] Immunohistochemistry for TH with Nissl counterstain in the SNpc of animals lesioned with lactacystin and culled one (A) and five (B) weeks post lesion. Higher power magnification of TH immunohistochemistry in the ipsilateral (Ai and Bi) and contralateral (Aii and Bii) hemispheres of SNpc in animals culled at week one and five respectively. Immunohistochemistry for OX6 with Nissl counterstain in the SNpc of animals lesioned with lactacystin and culled one (C) and five (D) weeks post lesion. Higher power magnification of TH immunohistochemistry in the ipsilateral (Ci and Di) and contralateral (Cii and Dii) hemispheres of SNpc in animals culled at week one and five respectively. Examples of immunopositive DAB (brown) stained cells indicated with arrows. Examples of immunopositive DAB (stained) neuropil indicated with arrowheads. Low magnification images taken at x4 magnification, scale bar equal to 50µm. High magnification images taken at x20 magnification, scale bar equal to 500µm.

5.4.7.3 – Presence of Activated Microglia One Week After Lactacystin-Lesioning

As well as TH staining of the SNpc, consecutive sections were immunohistochemically stained for OX6, a marker of activated microglia. As expected immunopositive cells were not present in contralateral hemispheres of either lactacystin-lesioned animal groups (figure 5.12Cii and Dii). However in lactacystin-lesioned animals culled seven days post-surgery, OX6+ microglia were present in the SNpc. Similar cells were not present however when animals were culled at week 5.

5.4.7.4 – Histone Hypoacetylation One Week After Lactacystin-Lesioning

Western blot analysis of extracted frontal brain proteins of animals culled one week after lactacystin-lesioning revealed marked reduction of histone acetylation in line with animals culled at five weeks post lactacystin-lesion. Compared with control non-lesioned animals, there was a significant reduction in histone protein H3 acetylated on lysine 9 (AcH3-Lys9) (figure 5.13, ipsilateral and contralateral frontal brain hemispheres, 18.24 ± 4.38% and 18.03 ± 6.58% of control respectively, $p<0.01$ in both comparisons). These reductions are in similar to those observed in animals culled five weeks post lactacystin-lesion.

5.4.7.5 - Downregulation of Neurotrophic Growth Factors and Neuroprotective Protein Genes in the Frontal Brain of Animals One Week After Lactacystin-Lesioning

As with Western blot analyses of acetylated histone protein in the frontal brain, changes observed in lactacystin-lesioned animals culled at week one mirror those observed in animals culled at five weeks post lesion (figure 5.14). Like lactacystin-lesioned animals culled at week five, modest reductions in the expression of αSyn, Hsp70, GSN, and Bad were observed in both the ipsilateral and contralateral frontal brain hemispheres of lesioned animals culled at week one compared with control animals. Additionally however, unlike animals culled at the later timepoint in which only a modest reduction of expression was observed, Bcl-2 expression was considerably reduced in animals culled at week one compared with controls. This change reached significance in the level of ipsilateral hemisphere expression (lactacystin-lesioned animals culled at week 1, ipsilateral Bcl-2 expression, 0.21 ± 0.06 fold change from control, $p<0.05$). Similar to animals culled later, marked reductions in the expression of BDNF and GDNF were also observed in both brain hemispheres of lactacystin-lesioned animals culled at week one compared with controls, more so in the lesioned hemisphere (BNDF and GDNF expression in the ipsilateral hemisphere, 0.16 ± 0.04 and 0.25 ± 0.06 fold change from control respectively, $p<0.05$ in both comparisons).

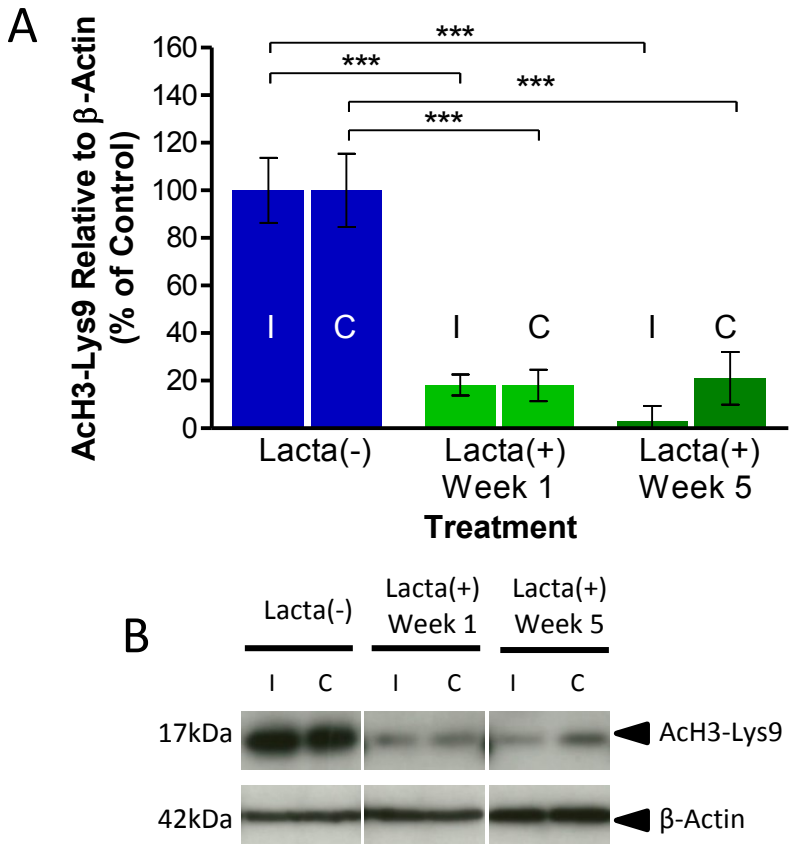

Figure 5.13 –Histone Hypoacetylation in the Frontal Brain One Week Post Lactacystin-Lesion
Lactacystin-lesioning causes a reduction in histone H3-lysine 9 acetylation in the frontal brain at week one post lesion in line with the level of histone hypoacetylation observed at week five. (A) Densitometry analysis of the AcH3-Lys9 band relative to the β-actin band used as a loading control. (B) Representative blot of data presented in (A). Statistical significance indicated with asterisks: ***p<0.001. n=7. Abbreviations: I, ipsilateral; C, contralateral.

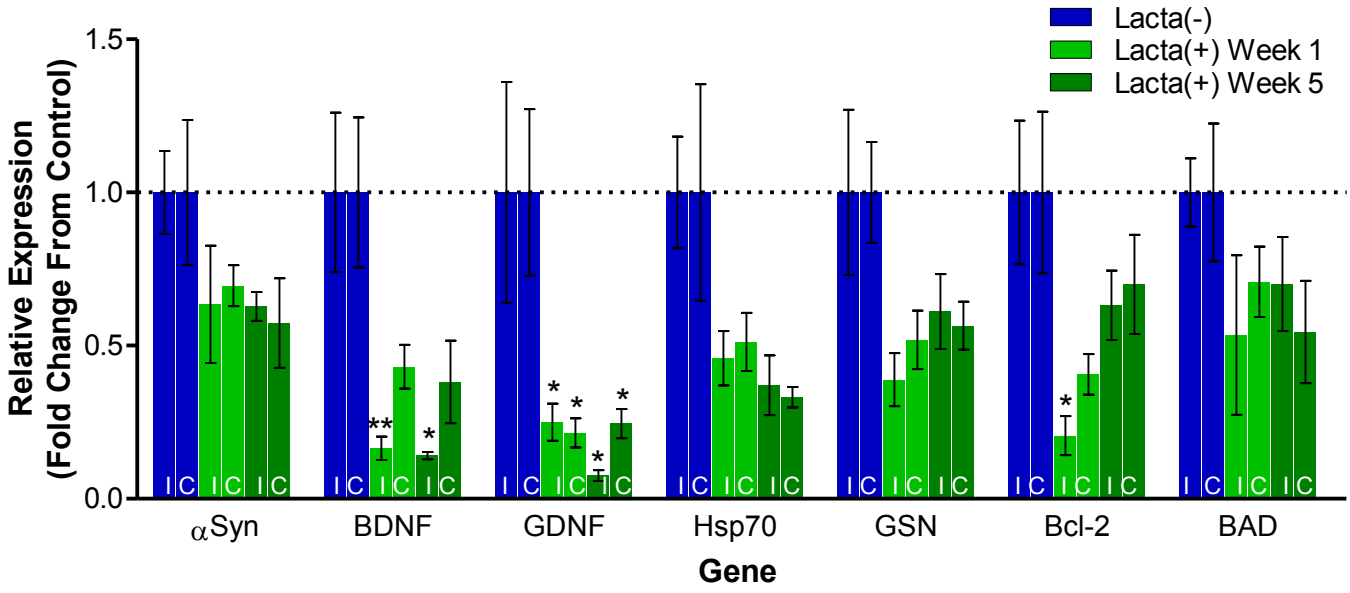

Figure 5.14 – Downregulation of Neurotrophic Growth Factors and Neuroprotective Protein Genes in Lactacystin-Lesioned Animal Brains One Week After Lesioning

qRT-PCR of the frontal brain mRNA reveals that downregulation of neurotrophic and neuroprotective gene proteins in animals one week after lesioning is comparable to those five weeks after lactacystin-lesioning. Statistical significance from control group indicated with asterisks: *p<0.05, **p<0.01. n=7. Abbreviations: I, ipsilateral; C, contralateral.

5.5 – Discussion

It has been demonstrated above that stereotaxic unilateral injection of 10µg of lactacystin into the SNpc produces a reproducible animal model of PD which recapitulates progressive motor behavioural symptoms, neuropathology and dopaminergic neurodegeneration within the SNpc. These progressive features of the model are accompanied by histone hypoacetylation in the brain and reduced mRNA expression of neurotrophic growth factors and neuroprotective proteins. Studies of the brains of animals culled one week post lactacystin-lesion suggest that cellular pathology and neurodegeneration in this model are progressive in nature and highlights this timepoint as a suitable timepoint in which to start delayed treatment with candidate HDACIs in subsequent studies to mimic the clinical scenario in which a neuroprotective/neuroregenerative drug would be administered.

Since the discovery that activity of the UPS is reduced in sporadic and familial forms of PD, UPS inhibitors such as the synthetic proteasome inhibitor PSI, epoxomycin, MG-132 and lactacystin have been used in attempt to generate animal models of PD (McNaught et al., 2002c, McNaught et al., 2004). Systemic infusions or repeated injections of lactacystin or PSI were initially proposed to produce progressive models of the disease. However despite initial findings that this caused progressive dopaminergic neurodegeneration and motor behavioural symptom development, failure to reproduce similar findings between laboratories quickly became apparent casting serious doubt on the use of UPS inhibitors as a model of PD. More recently however focal administration of UPS inhibitors such as lactacystin has become a more stable and reproducible model of the disease. Initial studies focussed largely on mice (Li et al., 2010, Pan et al., 2008, Xie et al., 2010, Zhu et al., 2007). It is only more recently in which studies using lactacystin to model PD in rats have started to appear in the literature (Konieczny et al., 2014, Mackey et al., 2013, Lorenc-Koci et al., 2011, Vernon et al., 2010, Vernon et al., 2011, Pienaar et al., 2013). Consistent with these previous observations, here we have observed that focal intranigral administration of lactacystin results in a progressive and reproducible model of dopaminergic neurodegeneration in the rat.

Behavioural test outcomes have been used extensively in the lactacystin rat model to demonstrate the effects of lactacystin-lesioning. For example neurological scoring of lactacystin lesioned animals has previously been shown to gradually worsen post lactacystin-lesion: rats displaying progressive deficits in spontaneous motility and horizontal bar, grasping reflex, placing reaction and tapered ledged beam tests (Vernon et al., 2010, Mackey et al., 2013). Similarly lactacystin lesioned rats have also previously been shown to display deficits in forelimb grip strength, reduced performance on an accelerating rotarod, and prolonged descent latency in bar tests (Vernon et al., 2010, Vernon et al., 2011, Konieczny et al., 2014). It has been shown here that lesioned animals also exhibit a similar magnitude reduction of contralateral forelimb use in the vertical cylinder test

following lactacystin lesioning compared with previously published findings (Konieczny et al., 2014), demonstrating robust reproducibility of the model between laboratories. In addition to vertical cylinder testing in the current study, amphetamine induced rotation was similarly used as an indicator of the degree of lactacystin-lesioning. Lactacystin-lesioning has previously been shown to produce ostensible circling behaviour after apomorphine challenge (Vernon et al., 2010, Vernon et al., 2011, Konieczny et al., 2014). However to our knowledge this is the first time in which amphetamine has been used as an inducer of rotational behaviour in this model. Amphetamine was chosen in the current study as it is known to be a more sensitive predictor of nigrostriatal lesion (Hudson et al., 1993). These findings therefore confirm and extent the pattern of behavioural deficits of lactacystin lesioning in the current model adding weight to its use in subsequent neuroprotection studies.

To our knowledge, a full and comprehensive study of the temporal progression of the lactacystin rat model is yet to be conducted. However according to the very limited investigation of the progression of dopaminergic neurodegeneration in the current study, the findings presented here are in agreement with behavioural and histological findings previously published by others (Vernon et al., 2010, Vernon et al., 2011, Mackey et al., 2013). From stereological cell quantification of animals culled seven days post lactacystin-lesion and longitudinal behavioural test outcomes it appears evident that the vast majority of nigral degeneration occurs in the first seven days post lesion (Vernon et al., 2010, Vernon et al., 2011, Mackey et al., 2013). Importantly however it has been observed here that a large number of TH+ neuropil, and axonal and dendritic projections remain at week 1 post lactacystin-lesion despite the significant reduction in TH+ neuronal cells bodies. Likewise Nissl+ neuronal cell degeneration is markedly less than that of TH+ cells at this early timepoint. Taken together, in addition to the observed TH+/Nissl+ neuronal degeneration at week 1 post lesion, it is likely that a number of nigral dopaminergic neuronal cells still remain present at this early timepoint, however their loss of expression of TH in conjunction with the significant amount of complete neuronal degeneration observed results in the deficits in motor behavioural tests shown here. By looking at neuronal cell counts at week 5 post lesion it is evident that neurodegeneration continues after week one resulting in the continued decline of animal performance in motor behavioural tasks. At present we cannot predict who will develop PD and by the time patients present to the clinic with the cardinal motor symptoms of the disorder, 60-70% of neurons in the SNpc have already degenerated, and ~80% of striatal dopamine has been depleted (Riederer and Wuketich, 1976). Week one post lactacystin-lesion therefore appears a suitable timepoint in which to start delayed treatment with candidate neuroprotective/neuroregenerative HDACIs in order to model the clinical scenario in which a neuroprotective drug would be administered. Likewise focal administration of lactacystin has now been successfully used in multiple neuroprotection studies (Konieczny et al., 2014, Li et al., 2010,

Pan et al., 2008, Zhu et al., 2007, Zhang et al., 2005). Moreover neuroprotection was successfully observed from initiating drug treatment at this same timepoint in the lactacystin mouse model (Pan et al., 2008) verifying the suitability of this therapeutic window in subsequent neuroprotection/neuroregeneration studies. In addition to the extent of cell death it has also been observed here that microglial activation is also present at this early model timepoint. As has been extensively discussed in previous chapters, HDACIs are thought to not only protect against neurodegenation but also reduce microglial activation. This timepoint is therefore highly appropriate for subsequent drug challenge studies using HDACIs as neuroprotectants and reducers of microglial activation.

MR imaging studies using toxin based models of PD have largely been focused on alterations in T_2 water ^1H relaxation and ^1H MR spectroscopy, whilst potential morphological changes have been overlooked. Recently however, a method of using MRI to non-invasively monitor the morphological progression and nigrostriatal neuropathology in this proteasome inhibitor rat model of PD has been established (Vernon et al., 2010, Vernon and Modo, 2011, Vernon et al., 2011). Manual segmentation analysis was performed in the current study to examine the temporal morphological progression of selected brain regions. In line with previously published data following nigrostriatal neuropathology induced as a result of stereotaxic injection of lactacystin to the SNpc (Vernon and Modo, 2011), in the current study a marked reduction in the volume of the ipsilateral midbrain in the weeks following stereotaxic surgery was observed. Similarly an increase in the volume of the lateral ventricles was observed, which was far more pronounced in the ipsilateral as opposed to the contralateral hemisphere. Subsequent TBM analysis both confirm and extend the manual data adding further weight to the findings, as well as extending prior observations. For example, unbiased, automated TBM data reinforces manual observations, and confirms lactacystin-lesioning is associated with a specific reproducible pattern of neuroanatomical changes in the brain, detectable by MRI (Vernon et al., 2011). The combination of longitudinal *in vivo* MRI and automated TBM therefore has great potential for pre-clinical assessment of drugs with disease-modifying potential in pre-clinical models of PD.

In conjunction with volumetric analysis and TBM to monitor morphological progression and nigrostriatal neuropathology in this model, T_2 signal intensity analysis was also used to follow asymmetry in T_2 signal intensity in the SNpc, midbrain and corpus striatum. Consistent with previous studies using the lactacystin rat model (Vernon et al., 2010), changes in T_2 signal intensity ratio were observed in the SNpc and to a lesser extent the midbrain, but not in the striatum. The temporal profile of T_2 relaxivity changes observed here also mirrors those previously seen in the lactacystin rat model of PD (Vernon et al., 2011). One week following lesioning, an increase in T_2 signal intensity was

observed in the ipsilateral SNpc and to a lesser extent the ipsilateral midbrain. This change is similarly observed in other animal models of PD, in the 6-OHDA rodent model (Kondoh et al., 2005) and the MPTP primate model (Miletich et al., 1994), and is suggested to be most likely due to acute inflammatory oedema in the area of interest given its appearance in nigrostriatally lesioned animals alone and its dissipation with time. By weeks three and five however the reduction in T_2 signal intensity in the ipsilateral hemisphere is likely due to cell death given the differences between treatment groups at these time points. Several studies note the accumulation of iron in the SNpc of PD patients (Dexter et al., 1989b, Brar et al., 2009, Gorell et al., 1995, Kosta et al., 2006, Martin et al., 2008) and a number of studies also note the accumulation of iron in the SNpc of the lactacystin rat model (Vernon et al., 2010, Zhu et al., 2007). Iron affects MR signal by creating inhomogeneities in magnetic field which diphase nearby water protons leading to shortening of T_2 relaxation and therefore lowering T_2 signal intensity (Chen et al., 1993). Additionally therefore this reduction in T_2 signal intensity ratio observed at weeks three and five may also be a function of iron deposition in the SNpc.

αSyn accumulation actively promotes histone hypoacetylation both *in vitro* in SH-SY5Y cells and *in vivo* in drosophila, both overexpressing αSyn (Kontopoulos et al., 2006). Lactacystin dopaminergic neurotoxicity is associated with the aggregation of α-synuclein to form inclusion bodies in the SNpc, a finding which has been extensively verified since (McNaught et al., 2002b, Vernon et al., 2011, Zhu et al., 2007, Niu et al., 2009). Therefore in line with previous observations of the effect of αSyn on histone acetylation, in the current study a reduction in histone acetylation in the brains of lactacystin-lesioned animals is observed. Removal of an acetyl group from a histone lysine residue causes the residue to become positively charged and hence causes electrostatic interaction to form between the lysine in the histone tail and the negatively charged phosphate group on DNA. This results in formation of inter- and intra-nucleosomal interactions between the histone protein and DNA hence causing condensation of the structure of chromatin and restricting transcription factor access to DNA. This would therefore cause a global reduction in gene expression. Consistently, a reduction in expression of numerous genes have been shown in the current study. Moreover, neurotrophic factors such BDNF and GDNF were shown to be significantly downregulated, likely contributing to and/or exacerbating the progressive neuropathology observed in the brain following lactacystin-lesioning.

5.6 – Conclusions

To conclude, this study demonstrates that unilateral stereotaxic injection of lactacystin produces a reproducible animal model of PD which recapitulates progressive motor behavioural symptoms, neuropathology and dopaminergic neurodegeneration within the SNpc. These changes are accompanied by a reduction in histone acetylation and downregulation of numerous neurotrophic and neuroprotective genes thought likely to contribute to and/or exacerbate neurodegeneration in the model. Seven days post lactacystin-lesion in the model has been identified as a suitable therapeutic window in which to start treatment with candidate neuroprotective/neuroregenerative HDACIs due to motor behavioural symptoms, brain pathology, dopaminergic neurodegeneration, microglial activation, histone hypoacetylation and neurotrophic gene downregulation being already evident in the model at this early timepoint. These findings therefore provide a clinically relevant drug testing platform on which to test the therapeutic potential of HDACIs at delineating the course of disease model progress in subsequent studies.

Chapter Six

Neuroprotective Effects of Valproate in the Lactacystin Rat Model of Parkinson's Disease

6 – Neuroprotective Effects of Valproate in the Lactacystin Rat Model of Parkinson's Disease

6.1 – Introduction

Valproate was first marketed as an anti-epileptic drug in France over 45 years ago (Löscher, 2002) and is now one of the most commonly prescribed mood stabilisers and anti-epileptic drugs for both generalised and partial seizures in adults and children (Perucca, 2002), appearing on the WHO's List of Essential Medicines (WHO, 2013). Valproic acid (2-propylpentanoic acid, figure 6.1) is a liquid at RT, and when reacted with a base such as sodium hydroxide forms a solid salt, sodium valproate. Numerous preparations can then be made from this salt dependent on the route and means of administration: intravenously, or orally in a capsule, tablet or syrup. Due to its relatively simple structure and low molecular weight (144.211 g/mol), valproate crosses the BBB with ease. Pharmacokinetically it is characterised by nonlinear plasma protein binding and multiple metabolic pathways of elimination (DeVane, 2003). It has an extensive record of use across its lifespan in the clinic and a good record of tolerability (DeVane, 2003).

The rational for valproate use in epilepsy and mood stabilisation, is that it has numerous effects on the brain: including effects on Glycogen Synthase Kinase 3 (GSK-3), Akt/ERK pathways, GABA/glutamate neurotransmission, Na^+ and Ca^{2+} voltage-dependent channels, phosphoinositol/TCA pathways and the oxidative phosphorylation pathway (Ximenes et al., 2012). Added to these effects in 2001 was its capacity for HDAC inhibition, noted due to its ability to relieve HDAC-dependent transcriptional repression and cause histone hyperacetylation both *in vitro* and *in vivo* (Gottlicher et al., 2001, Phiel et al., 2001). Like many short chain fatty acids, valproate acts as a pan-inhibitor of HDAC classes I and IIa (section 1.5.3), at relatively low potencies (Gurvich et al., 2004). It is thought that this weak potency is attributable to its inability to access the zinc cation in the HDAC active-site pocket, which appears to be pivotal to the deacetylation catalysis (Lu et al., 2003). It therefore appears likely that valproate uses mechanisms other than direct interface with the catalytic site of HDACs to bring about inhibition.

Valproate has been shown to produce neuroprotection in models of stroke (Kim et al., 2007, Xuan et al., 2012, Sinn et al., 2007), traumatic brain injury (Dash et al., 2010, Tai et al., 2014, Jepsen et al., 2014), and spinal cord injury (Lv et al., 2011, Yu et al., 2012). However it remains debated as to the neuroprotective potential of valproate in more chronic neurodegenerative diseases such as PD. It has been shown that *in vitro*, valproate reduces microglial activation and release of proinflammatory factors such as TNFα, nitrite and reactive oxygen species resulting in neuroprotection in neuron-glia co-cultures (Peng et al., 2005, Chen et al., 2007). Similarly, it has also been demonstrated that valproate's HDAC inhibition results in upregulation of neurotrophic factors such as BDNF and GDNF

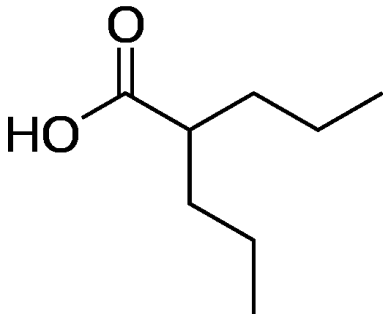

Figure 6.1 – Chemical Structure of Valproate

The chemical structure of valproic acid is given which exists as a liquid at RT. This can be reacted with a base such as sodium hydroxide to form the solid salt sodium valproate. In the majority of studies cited and in the study described in this chapter the solid salt sodium valproate was dissolved into sterile (0.9%) saline at the desired concentration for animal administration.

in astrocytic cultures translating to neuroprotection in neuron-enriched cultures (Chen et al., 2006, Wu et al., 2008a). Valproate has also been shown to directly protect neurons against cell death, through dose dependent acetylation of histone protein H3 in the αSyn promotor, increasing expression of endogenous αSyn and protecting neuronal cell cultures (Leng and Chuang, 2006). Additionally, in line with a dose dependent increase in histone acetylation, valproate treatment has been shown to increase expression of neuroprotective Hsp70 and reduce release of apoptotic regulator caspase-3 in neuronal cultures (Marinova et al., 2009, Pan et al., 2005, Kidd and Schneider, 2010).

Pre-clinical *in vivo* studies also highlight the neuroprotective potential of valproate. Neuroprotection by valproate was observed in the MPTP mouse model of PD: protecting dopaminergic neurons and preventing the reduction of striatal dopamine observed in MPTP treated mice (Kidd and Schneider, 2011). These changes were also accompanied by an increase in the histone acetylation mark AcH3-Lys9. In addition, dietary pre-treatment with valproate was shown to significantly protect against rotenone induced loss of TH+ dopaminergic neurons in rats, as well as increasing expression of endogenous αSyn in the SNpc and striatum (Monti et al., 2010). Neuroprotection of TH+ neurons and upregulation of endogenous αSyn was also observed in the 6-OHDA rat model of PD with dietary pre-treatment with valproate (Monti et al., 2012). These are extremely encouraging findings, especially studies utilising dietary administration of the drug, highlighting the translatability of valproate treatment to the clinic. However care must be taken when interpreting these data as valproate treatment was commenced prior to toxin administration: 4 week in both of these studies, highlighting the poor clinical relevance of such a study design.

Based on preclinical evidence and clinical criteria, the American Neuropsychiatric Association (ANPA) Committee on Research identify FDA-approved, first-line psychotropic drugs which affect intracellular mechanisms and merit disease modifying clinical trials in neurodegenerative disease. Given the wealth of research conducted on the use of valproate in neurodegenerative diseases such as PD, in 2011 ANPA's committee deemed valproate one of the 'most promising investigative priories' in PD (Lauterbach and Mendez, 2011). Two studies from the 1970s examined the effects of valproate on disease progression in PD patients clinically prior to its discovery as HDACI (Nutt et al., 1979, Price et al., 1978). Neither of these studies claims to notice any significant amelioration of symptoms. Hence given the age of these publications and the wealth of evidence in favour of the neuroprotective potential of valproate, the use of this drug in PD is being re-challenged. This chapter therefore aims to confirm and extend previous findings on the use of valproate in more classically used animal models of PD (the MPTP mouse model, and 6OHDA and rotenone rat models) by using the lactacystin rat model which recapitulates the formation of neurotoxic protein inclusions within the substantia nigra to cause

progressive dopaminergic cell death. Furthermore unlike many of the previous studies of valproate's neuroprotective effects *in vivo*, a delayed start study design will also be used to model the clinical scenario in which a neuroprotective drug would be administered more accurately. In addition, molecular and cellular analyses of study samples will attempt to elucidate the neuroprotective mechanism of valproate in this model.

6.2 - Aims of Chapter

The aims of this chapter are therefore to:

1. Determine the neuroprotective and behavioural effects of delayed start valproate treatment in the lactacystin rat model of PD:
    a. Determine the effects of delayed start valproate treatment on the progression of lactacystin induced motor behavioural symptoms in the model.
    b. Determine the effects of delayed start valproate treatment on lactacystin induced pathological changes in brain structure in the model.
    c. Determine the effects of delayed start valproate treatment on lactacystin induced dopaminergic neuronal cell death in the SNpc in the model.
2. Investigate the neuroprotective mechanism of delayed start valproate treatment in the lactacystin rat model of PD
    d. Quantify the level of histone acetylation in the brains of valproate treated lactacystin-lesioned animals.
    b. Quantify the expression of numerous neurotrophic and neuroprotective factors thought to be associated with HDACI mediated neuroprotection in valproate treated lactacystin-lesioned animals.

6.3 – Experimental Design

6.3.1 – Determining the Neuroprotective and Behavioural Effects of Delayed Start Valproate Treatment in the Lactacystin Rat Model of PD

Three groups of male Sprague-Dawley rats (n=6 or 7) were intra-nigrally lesioned with the irreversible proteasome inhibitor, lactacystin, by stereotaxic injection into the SNpc (see section 2.4.3). Animals were then left to recover for 7 days before receiving a daily i.p. injection of sterile saline (0.9% NaCl), or 200mg/kg or 400mg/kg valproate dissolved into saline, for 28 days. In addition to these three animal treatment group, two groups of male Sprague-Dawley rats (n=6 or 7) were also included which did not receive lactacystin lesioning surgery: which received subsequent daily treatment with saline or daily treatment with 400mg/kg valproate dissolved into saline (table 6.1 for animal treatment groups). In order to follow the neuropathological and behavioural progression of the disease model and to determine to what extent valproate was able to delineate this progression, both motor behavioural testing and MRI were conducted at baseline, and at weeks 1, 3 and 5 of the study (figure 6.1 for graphical illustration of study design). Both the vertical cylinder and amphetamine induced rotation tests were used to study the progression of behavioural motor asymmetry. Similarly, manual volumetric segmentation analysis, tensor based morphometry and T_2 relaxivity analysis using MR images were conducted to study the neuropathological progression of the model. For quantification of valproate neuroprotection, at the end of the 5 week study animals were culled and brain tissue was collected. The hind brain was fixed, cryoprotected, cryosectioned and dopaminergic neurons (TH+) immunohistochemically stained and stereologically quantified.

6.3.2 – Investigating the Neuroprotective Mechanism of Delayed Start Valproate Treatment in the Lactacystin Rat Model of PD

Upon collection of brain tissue at the end of the five week study, frontal cortex tissue was dissected and snap frozen for molecular analysis of the neuroprotective mechanism of valproate in the model. Protein content was extracted from tissue samples and Western blot analyses were conducted to quantify the level of histone acetylation in the brains of lactacystin-lesioned/valproate treated animals. In addition, mRNA content was extracted for qRT-PCR analysis to quantify the expression of numerous neurotrophic and neuroprotective factors thought to be involved in the neuroprotective effects of HDACIs such as valproate.

6.3.3 – Statistical Analysis

All data is presented as mean ± SEM. Two-way (repeated measures) ANOVA with Bonferroni post-tests were used for analysis of vertical cylinder test in the confirmation of lesioning. An additional student t-

test was used for analysis of area under curve data from vertical cylinder tests in lesion confirmation. In the valproate study a two-way (repeated measures) ANOVA with Bonferonni post-tests were used for analysis of vertical cylinder test, amphetamine induced rotation test and MRI manual segmentation analysis datasets. An additional one-way ANOVA with Bonferroni post-tests was used for comparison of percentage contralateral forelimb use vs time area under the curve data. Paired t-tests were used to compare stereological cell counts in the ipsilateral and contralateral hemispheres of animal brains. A one-way ANOVA with Bonferroni post-tests were used to compare cell loss percentages calculated from stereological cell counts. A one-way ANOVA with Bonferroni post-tests were used to compare Western blot data. A two-way ANOVA with Bonferroni post-tests were used to compare qRT-PCR data. All statistical tests were performed using GraphPad Prism (v5.0 for Windows, GraphPad Software, San Diego, CA, USA).

Table 6.1 - Valproate Neuroprotection Animal Treatment Groups

*All daily i.p. injections given as 2ml/kg: saline injections given as 2ml/kg empty saline; 400mg/kg valproate injections given as 2ml/kg of 200mg/ml solution of valproate in saline; 200mg/kg valproate injections given as 2ml/kg of 100mg/ml solution of valproate in saline.

Group	N=	Intranigral Injection	Daily i.p. Injections*	Behavioural Tests
Lacta(-)VPA(-)	7	None	Saline	Vertical Cylinder Test
Lacta(-)VPA(++)	6	None	Valproate (400mg/kg)	Vertical Cylinder Test
Lacta(+)VPA(-)	7	Lactacystin (10µg in 4µl saline)	Saline	Vertical Cylinder Test & Amphetamine Rotation
Lacta(+)VPA(+)	6	Lactacystin (10µg in 4µl saline)	Valproate (200mg/kg)	Vertical Cylinder Test & Amphetamine Rotation
Lacta(+)VPA(++)	6	Lactacystin (10µg in 4µl saline)	Valproate (400mg/kg)	Vertical Cylinder Test & Amphetamine Rotation

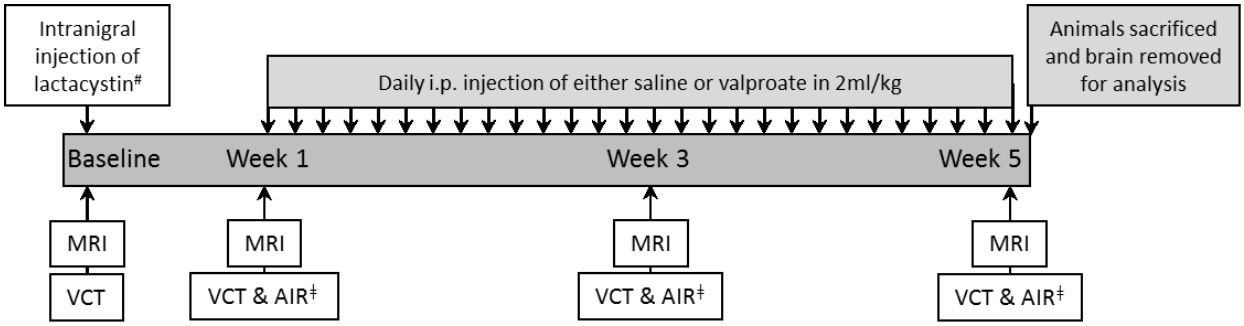

Figure 6.2 - Valproate Neuroprotection Animal Study Design
Study design used for investigation of the neuroprotective effects of delayed start valproate treatment in the lactacystin rat model of PD. Abbreviations: AIR, amphetamine induced rotations; MRI, magnetic resonance imaging; VCT, vertical cylinder test.
#Only groups Lacta(+)VPA(-), Lacta(+)VPA(+) and Lacta(+)VPA(++) intranigrally injected with lactacystin. Control groups remained surgically naïve.
‡Only groups lesioned with lactacystin were tested using the amphetamine induced rotation test at these time points.

6.4 – Results

6.4.1 – Confirming Lesion in Lactacystin Injected Animals

To confirm that all lesioned animals included in the study received lactacystin to the left SNpc, MRI scans acquired at week 1 post-lesion were examined to check the location of stereotaxic injection of the toxin (section 2.4.3, figure 6.3E). The lesion site was confirmed in all lesioned animals and therefore no animals were excluded on this basis. In addition to visual confirmation of the lesion site from MR images, behavioural tests performed at 7 days post lesioning were also used to confirm the development of early motor symptoms as a consequence of lactacystin injection into the left SNpc. For analysis of vertical cylinder test data, animals were divided into two groups dependent on whether they had received stereotaxic surgery (n=19) or not (n=13) at week 1. There was a significant reduction in the use of the contralateral forelimb of animals lesioned with lactacystin, compared to non-lesioned animals at week 1 (figure 6.3A, week 1, lactacystin-lesioned animals, 40.20 ± 2.57%, vs. non-lesioned animals, 51.59 ± 1.39% contralateral forelimb use, $p<0.001$). In addition, lactacystin-lesioned animals were injected with amphetamine to examine the degree to which they exhibited rotational behavioural, indicative of degeneration of the ipsilateral SNpc. All animals lesioned with lactacystin exhibited amphetamine induced rotations 7 days after lesioning indicative of correct needle placement and delivery of lactacystin to the left SNpc (figure 6.3C and D, 19.73 ± 1.39 mean number of rotations per 5 mins). The extent of rotational behavioural in the animals therefore compared favourably to previously lesioned animals groups (figure 5.10, 21.17 ± 3.71 mean number of rotations per 5 mins).

6.4.2 – Effects of Delayed Start Valproate Treatment on Behavioural Progression of the Lactacystin Rat Model of PD

6.4.2.1 – Vertical Cylinder Test

The vertical cylinder test was conducted in all five treatment groups at baseline and weeks 1, 3 and 5 of the study to assess motor asymmetry in rat forelimb use. At baseline there was equal use of both the left and right forelimbs in all animals (figure 6.4A, 51.69 ± 0.89% contralateral forelimb use). However one week after surgery there was a significant reduction in the contralateral forelimb use of all lactacystin-lesioned animal groups compared with non-lesioned groups (figure 6.4A, $p<0.05$ in all comparisons). From one week onwards the contralateral forelimb use of the lactacystin-lesioned saline treated animals continued to decline with time (week 1, 39.59±4.11%; week 3, 36.01±3.37%; week 5, 35.50±4.08%, $p<0.01$ compared with control animals at each time point). However once animals began daily i.p. treatment with either 200mg/kg or 400mg/kg valproate one week after lactacystin lesioning, there was a time and dose dependent reduction in contralateral forelimb use

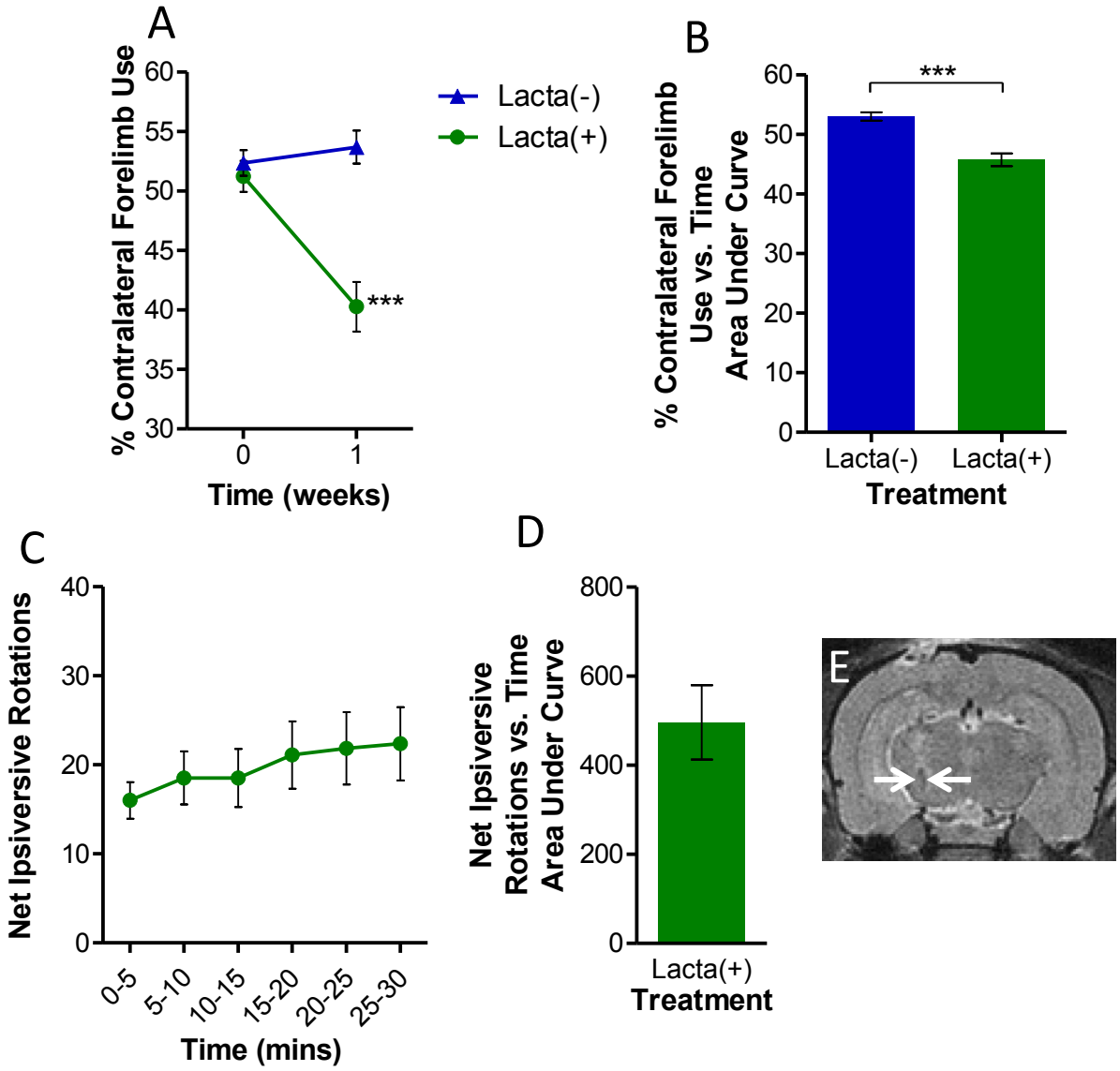

Figure 6.3 - Confirming Lesion in Lactacystin Injected Animals

(A) Percentage contralateral forelimb use in lactacystin-lesioned (Lacta(+)) and non-lesioned (Lacta(-)) rats at baseline and 7 days after surgery. (B) Area under the curve of data represented in (A) demonstrating more clearly the differences between percentage contralateral forelimb use in animal treatment groups. (C) Number of amphetamine rotations performed by lactacystin-lesioned animals in five minute intervals after administration of amphetamine. (D) Area under the curve of data represented in (C) demonstrating more clearly the progressive nature of rotational behaviour after lactacystin-lesioning. (E) Representative MR image confirming correct needle placement and therefore delivery of lactacystin to the left SNpc in a lesioned animal. Statistical significance is indicated using asterisks: ***p<0.001. n=13-19.

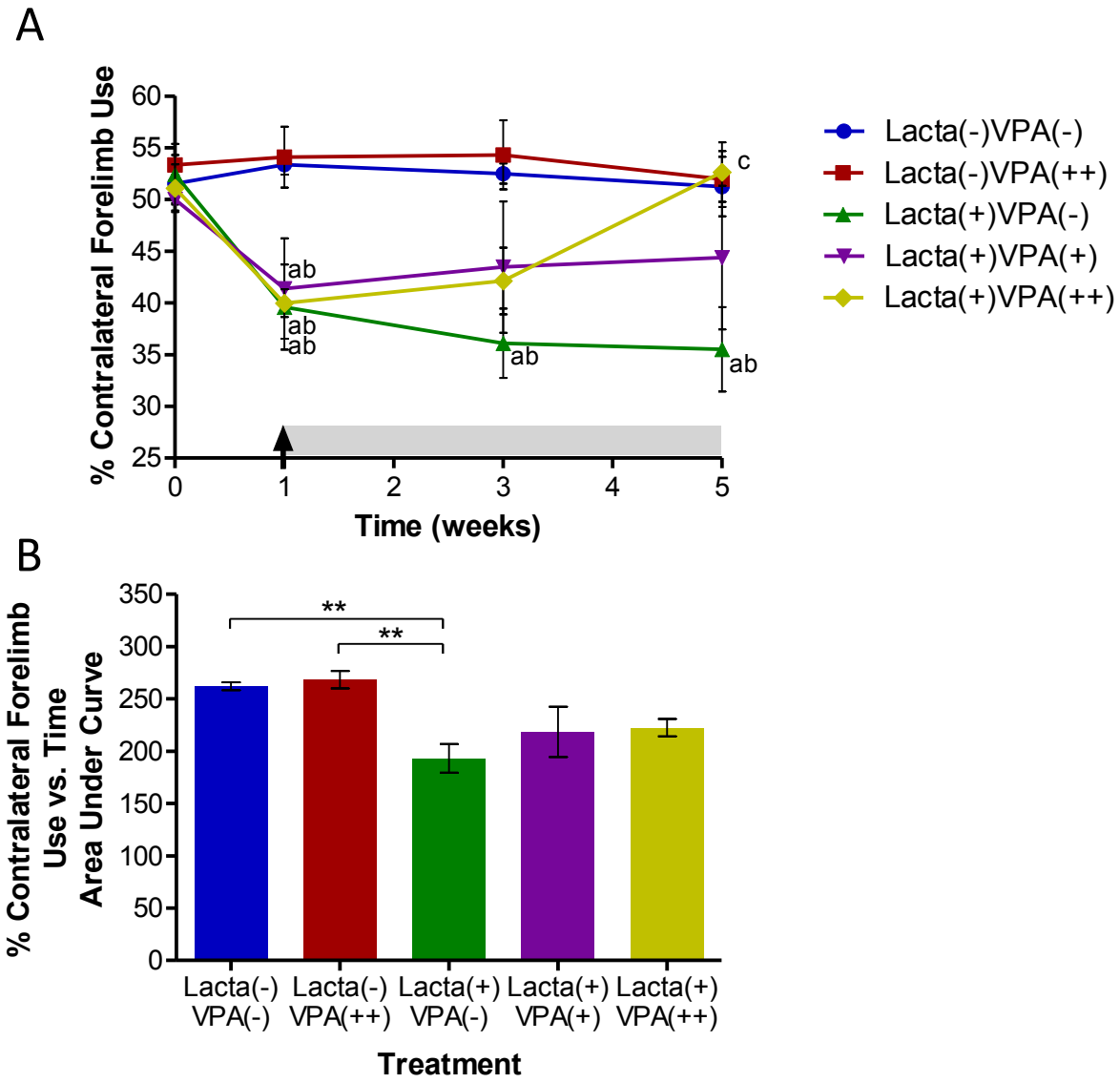

Figure 6.4 – Valproate Attenuates Motor Behavioural Deficits Caused by Lactacystin in Vertical Cylinder Test
(A) Vertical cylinder test outcomes demonstrate that once animals begin treatment with valproate at week 1 (designated by arrow and grey shading) the lactacystin induced reduction in percentage contralateral forelimb use is reversed in a dose dependent manner. Statistical significance indicated with letters: [a]significantly different from group Lacta(-)VPA(-); [b]significantly different from group Lacta(-)VPA(++); [c]significantly different from group Lacta(+)VPA(-). See text for levels of significance. (B) Area under the curve of data represented in (A) demonstrating more clearly the differences between percentage contralateral forelimb use in animals treatment groups. Statistical significance is indicated using asterisks: **p<0.01. n=6-7.

deficit. Animals treated with the lower dose of valproate (200mg/kg) displayed a reduced deficit in contralateral forelimb use with time (week 5, valproate, 44.39 ± 6.94% vs. saline treated animals, 35.50 ± 4.08%). Similarly animals treated with the highest dose of valproate (400mg/kg) displayed a reduced deficit in contralateral forelimb use with time, failing to show any deficit after 28 days of valproate treatment (week 5, valproate, 52.63 ± 2.66% vs. saline treated animals, 35.50 ± 4.08%, $p<0.01$). The area under the curve produced by plotting percentage contralateral forelimb use vs. time demonstrates the differences between treatment groups more clearly (figure 6.4B). The area under the curve produced by the saline treated group was significantly less than both non-lesioned groups (lactacystin-lesioned saline treated animals 193.31 ± 13.71 vs. non-lesioned saline treated and valproate (400mg/kg) treated animals 262.04 ± 3.68 and 268.4 ± 8.32 respectively, $p<0.01$ in both comparisons). Neither of the lactacystin-lesioned, valproate treated groups however were significantly difference from non-lesioned control groups.

6.4.2.2 – Amphetamine Induced Rotation Test

As well as the vertical cylinder test, the amphetamine induced rotation test was conducted on all lesioned animal groups at week 1, 3 and 5 following lesioning to assess the extent of drug induced rotational behaviour. Following amphetamine challenge, all lactacystin-lesioned animals produced ipsilateral rotations one week after lesioning surgery (figure 6.5A, mean number of amphetamine induced rotations per 5 minutes during recording, 24.31 ± 4.44, 18.81 ± 8.45, and 18.22 ± 1.83 for Lacta(+)VPA(-), Lacta(+)VPA(+) and Lacta(+)VPA(++) groups respectively). Over the further two time points examined, saline treated lactacystin-lesioned animals performed increasing numbers of rotations (mean number of amphetamine induced rotations per 5 minutes during recording, week 3, 41.72 ± 9.84, week 5, 66.22 ± 19.43). However valproate administration dose dependently attenuated the number of ipsiversive rotations after treatment initiation at week one. Animals treated with the lowest dose of valproate (200mg/kg) performed fewer rotations than saline treated animals after 28 days of valproate treatment (mean number of amphetamine induced rotations per 5 minutes during recording, 39.50 ± 16.39 vs. 66.22 ± 19.43 in valproate (200mg/kg) and saline treated animals respectively, $p<0.05$). Animals treated with valproate at its higher dose however performed fewer rotations than the saline treated group after both 14 and 28 days of treatment (saline treated animals, 41.72 ± 9.84 and 66.22 ± 19.43 vs. valproate (400mg/kg) treated animals 21.19 ± 4.01 and 23.28 ± 4.85 at weeks 3 and 5 respectively, $p<0.001$ in both comparisons). These differences between groups become clearer when data is expressed as the area under the curve produced by plotting net number of rotations vs. time (figure 6.5B). Animals treated with valproate at its highest dose exhibit a significantly greater area under the curve at week 5 compared with saline treated animals (valproate (400mg/kg) treated animals, 585.83 ± 123.47 vs. saline treated animals, 1641 ± 477.50, $p<0.05$).

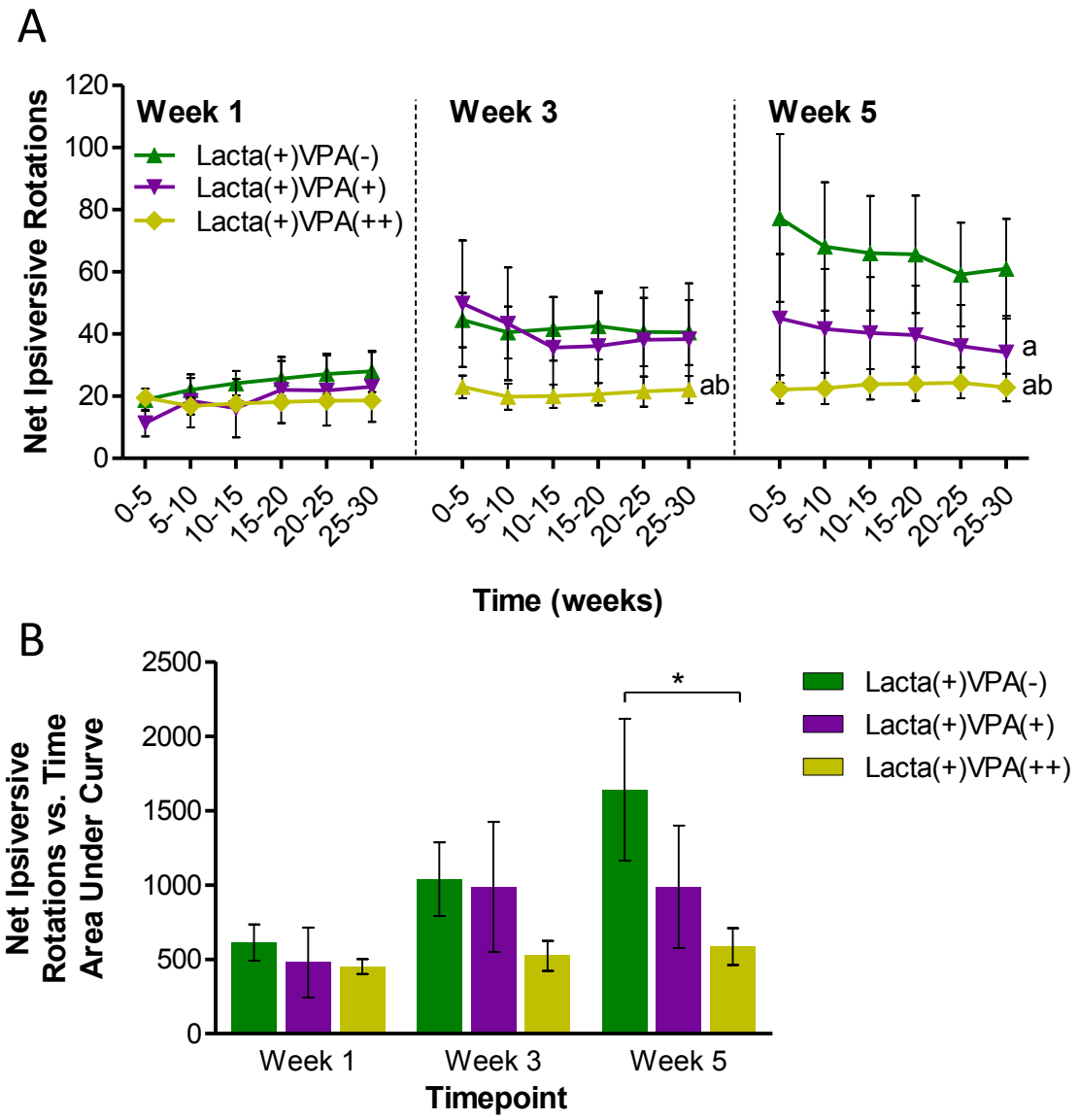

Figure 6.5 – Valproate Attenuates Amphetamine Induced Rotational Asymmetry Caused by Lactacystin
(A) Net number of ipsiversive rotations performed by animals per 5 minutes plotted against time for the 30mins in which rotational behaviour was recorded following amphetamine administration. Statistical significance indicated with letters: [a]significantly different from group Lacta(+)VPA(-); [b]significantly different from group Lacta(+)VPA(+). See text for levels of significance. (B) The area under the curve produced by plotting raw rotational values against time (A) demonstrates the attenuation of amphetamine induced rotational behaviour by valproate. Statistical significance is indicated using asterisks: *p<0.05. n=6-7.

6.4.3 - Effects of Delayed Start Valproate Treatment on Neuropathological Progression of the Lactacystin Rat Model of PD

6.4.3.1 – Manual Segmentation Analysis

Post-acquisition, MR images of the brains of all animal treatment groups were analysed using manual segmentation analysis to assess changes in regional brain volume over the course of the five week study (figure 6.6A). In line with rat growth there was a steady increase in whole brain volume in saline treated non-lesioned animals over the five weeks of examination (figure 6.6B, week 1, 2.09 ± 0.86% increase from baseline; week 3, 4.64 ± 1.33% increase from baseline; week 5, 6.60 ± 1.29% increase from baseline). The whole brain volumes of all other treatment groups also increased with time however to a greater/lesser degree than these control animals. Lactacystin-lesioned animals treated with saline and lactacystin-lesioned animals treated with valproate at its lower dose (200mg/kg) both exhibited a greater increase in brain volume compared with control animals (9.07 ± 2.44% and 9.33 ± 0.69% increase from baseline at week 5 respectively vs. 6.60 ± 1.29% increase from baseline at week 5 in non-lesioned saline treated animals). Animal groups treated with valproate at its higher dose (400mg/kg) however, both lactacystin-lesioned and non-lesioned, exhibited a discernible shallower increase in whole brain volume over the 5 weeks of treatment (3.76 ± 1.19% and 3.07 ± 1.34% increase from baseline at week 5 respectively vs. 6.60 ± 1.29% increase from baseline at week 5 in non-lesioned saline treated animals). Similar was the case with cerebellum volume: each of the treatment groups displayed an increase in volume over the five weeks of examination (figure 6.6C). However unlike with whole brain volume, all groups exhibited a comparably greater percentage cerebellum volume increase at every time points when compared to the non-lesioned saline treated group. The only statistically significant difference being between the cerebellar volume increase of lactacystin-lesioned saline treated animals and the non-lesioned saline treated animals at week five (lactacystin-lesioned animals, 12.91 ± 1.64% increase compared with non-lesioned animals, 5.60 ± 2.36% increase, $p<0.05$).

As expected in the non-lesioned saline treated animals the volume of the lateral ventricles increased comparably in both hemispheres over the 5 weeks of scan acquisition (figure 6.6D). Similarly the ventricular volumes of non-lesioned valproate treated animals also increased with time, yet unexpectedly to a greater extent than saline treated animals. This difference however was not significant. Animals which received an intranigral injection of lactacystin and were subsequently treated with saline exhibited a greater increase in ventricular volume than non-lesioned controls, a change which was more pronounced in the lesioned hemisphere. Neither of these increases however reached statistical significance compared with non-lesioned saline treated animals. In contrast the animal groups which received valproate (both 200mg/kg and 400mg/kg) one week after lactacystin

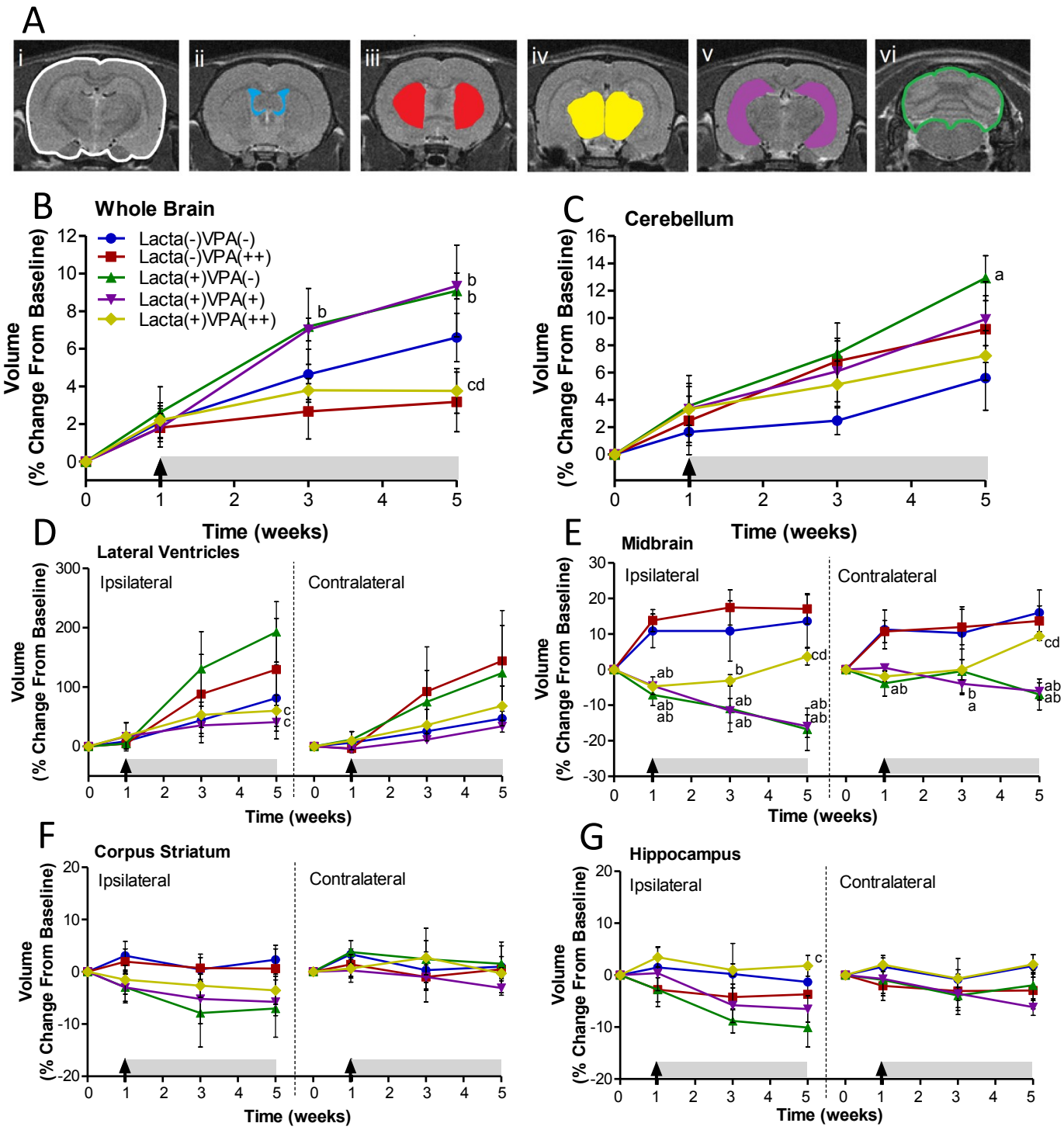

Figure 6.6 – Manual Segmentation Analysis of MR Images Reveals Dose Dependent Attenuation of Lactacystin Induced Volumetric Changes by Valproate

(A) Representative examples of the manual segmentation of (i) whole brain, (ii) lateral ventricles, (iii) corpus striatum, (iv) midbrain, (v) hippocampus and (vi) cerebellum in MR images. Administration of valproate (designated by arrow and grey shading) dose dependently attenuates volumetric changes observed in the (D) lateral ventricles and (E) the midbrain as a result of lactacystin lesioning, as ascertained through manual segmentation analysis of rat brain MR images. Similar, albeit more subtle changes are observed in the (F) corpus striatum and (G) hippocampus mirroring those seen in the midbrain. Administration of valproate and/or lactacystin also have marked effects on (B) whole brain and (C) cerebellum volume. Statistical significance indicated with letters: [a]significantly different from group Lacta(-)VPA(-); [b]significantly different from group Lacta(-)VPA(++); [c]significantly different from group Lacta(+)VPA(-); [d]significantly different from group Lacta(+)VPA(+). See text for levels of significance. n=6-7.

lesioning surgery did not exhibit these increases in ventricular volume over time: the ventricular volumes of both valproate dosed groups was comparable with non-lesioned saline treated animals in both hemispheres, reaching significance in the lactacystin-lesioned hemisphere (left ventricle at week 5, 200mg/kg and 400mg/kg valproate treated animals, 40.81 ± 28.20% and 60.05 ± 14.17% increase from baseline respectively compared with saline treated animals, 192.93 ± 61.54% increase from baseline, both $p<0.05$).

The most pronounced changes in regional brain volume took place in the midbrain, the location of the SNpc and therefore the site of stereotaxic injection of lactacystin (figure 6.6E). One week after lesioning surgery, prior to starting vehicle/drug treatment, the ipsilateral midbrain volume of all lactacystin-lesioned animal groups was significantly lower than the volume of both non-lesioned groups (lactacystin-lesioned saline, 200mg/kg and 400mg/kg valproate treated animals, 7.07 ± 3.05%, 4.51 ± 2.42% and 4.74 ± 0.83% decrease from baseline respectively vs. 10.88 ± 4.73% and 13.80 ± 3.08% increase in non-lesioned saline treated and valproate treated groups respectively, $p<0.05$ in all comparisons). The ipsilateral midbrain volume in lactacystin-lesioned saline and low dose (200mg/kg) valproate treated animals continued to decline over the further two time points examined, remaining significantly different from the volume change in non-lesioned groups at both week 3 and week 5 ($p<0.001$ in all comparisons). In contrast, animals lesioned with lactacystin and treated with the higher dose (400mg/kg) of valproate displayed a reversal of the decrease in ipsilateral midbrain volume seen at week 1 in the following two time points: reaching a significant difference from saline and low dose (200mg/kg) treated animals at week 5 (400mg/kg valproate treated animals, 3.70 ± 2.36% increase from baseline vs. saline and 200mg/kg valproate treated animals, 16.77 ± 5.94% and 15.90 ± 2.36% decrease from baseline respectively, $p<0.01$ in both comparisons). Identical albeit more subtle changes are similarly observed upon lactacystin lesioning and valproate treatment in the contralateral hemisphere of the midbrain: lactacystin-lesioned animals displayed a reduction in contralateral midbrain volume at week 1 which continued on to week 5 for saline and low dose valproate treated animals but not for high dose treated animals.

No significant differences were observed in corpus striatum volume in either the ipsilateral or contralateral hemispheres. However a number of trends in the ipsilateral hemisphere exist mimicking those changes observed in the midbrain (figure 6.6F). There was a trend of reduced corpus striatal volume in lactacystin-lesioned animals compared with non lesioned, however unlike the ipsilateral midbrain volume at this time point this trend was not statistically significant (lactacystin-lesioned saline, 200mg/kg and 400mg/kg valproate treated animals, 2.96 ± 2.99%, 2.98 ± 2.66% and 2.76 ± 2.76% decrease from baseline respectively vs. 3.07 ± 2.76% and 1.96 ± 2.43% increase in non-lesioned saline treated and valproate treated groups respectively, $p>0.05$ in all comparisons). The volume of

the ipsilateral corpus striatum continued to decrease in a dose dependent manner with valproate in lactacystin-lesioned animals. Again however these changes failed to reach statistical significance from either control non-lesioned animals or saline treated lesioned animals. No statistical differences or notable trends were observed in the contralateral corpus striatum volume.

In the hippocampus unlike the volume changes observed in the midbrain and striatum, there was no discernible reduction in volume in the ipsilateral hemisphere at week one after lactacystin lesioning (figure 6.6G). With time however, at week 3 and 5, a reduction in ipsilateral hippocampal volume became evident in lactacystin-lesioned saline treated animals, and to a lesser degree low dose valproate (200mg/kg) treated animals (lactacystin-lesioned saline treated animals, 8.81 ± 2.31% and 10.09 ± 3.74% decrease from baseline at week 3 and 5 respectively; lactacystin-lesioned valproate (200mg/kg) treated animals, 5.79 ± 3.33% and 6.51 ± 2.52% decrease from baseline respectively at week 3 and 5 respectively). Lactacystin-lesioned animals treated with the higher dose of valproate (400mg/kg) however did not display this decline in ipsilateral hippocampal volume, the volumes of which reaching statistical significance from lactacystin-lesioned saline treated ipsilateral hippocampal volume at week 5 (valproate (400mg/mg) treated animals, 1.83 ± 1.99% increase from baseline vs. saline treated animals, 10.09 ± 3.74% decrease from baseline, $p<0.05$). As with the case of the contralateral corpus striatum, there were no discernible trends or statistically significant differences observed in the volume of the contralateral hippocampus.

6.4.3.2 – Tensor Based Morphometry

In collaboration with Dr Anthony Vernon (Department of Neuroscience, Kings College London) and Dr William Crum (Department of Neuroimaging, Kings College London), tensor based morphometry analysis was applied to MR images acquired at week 5 to confirm and extend observations from manual segmentation analysis (figure 6.7). After correcting for global differences in brain volume (9dof registration) to search for relative differences in structural volume, several distinct anatomical patterns were observed across treatment groups (all data shown are corrected for multiple-comparison over voxels using the False Discovery Rate with $q<0.05$).

Non-lesioned animals treated with a high dose of valproate alone (Lacta(-)VPA(++)) showed bilateral clusters of blue contracted voxels in the globus pallidus, internal capsule, third ventricle, ventromedial thalamic nuclei, perirhinal cortex, amygdala and brainstem. Conversely, clusters of yellow/orange expanded voxels were detected in the hippocampus (dorsal and ventral regions), dorsal entorhinal cortex, external capsule and the 3rd and 4th cerebellar lobules.

In lactacystin-lesioned animals treated with saline (Lacta(+)VPA(-)) widespread significant contraction of cortical voxels in the ipsilateral hemisphere of the brain was observed. These included the cingulate, motor, somatosensory and parietal cortical sub-fields. Sub-cortically, widespread

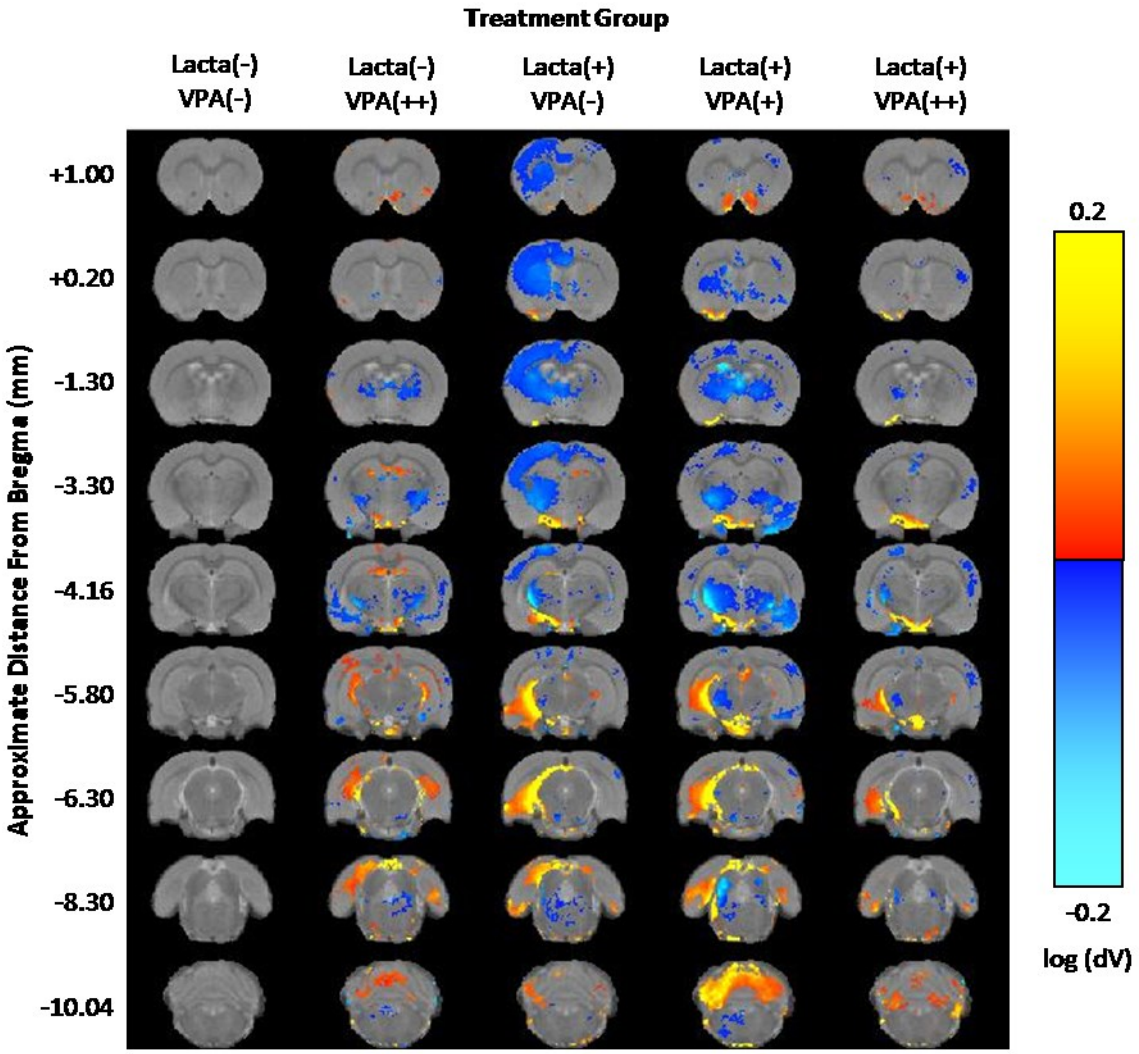

Figure 6.7 – Tensor Based Morphometry Validates Findings from Manual Segmentation Analyses of Rat Brain MR Images

Regions of significant volume difference relative to whole brain for each group compared with Lacta(-)VPA(-) at week 5 are shown. Positive differences (yellow/orange) indicate where each group has volume increases compared with Lacta(-)VPA(-) and negative differences (blue) indicate where each group has volume decreases compared with Lacta(-)VPA(-). Results shown are significant after correction for multiple comparisons across voxels using the False Discovery Rate with $q<0.05$. n=6-7.

clusters of contracted voxels were observed in the ipsilateral striatum, globus pallidus, thalamus, ventral midbrain and brainstem nuclei. Some of these clusters extended across the midline into the contralateral hemisphere. No significantly contracted voxels were observed in the hippocampus. Clusters of significantly expanded voxels were also observed in the ipsilateral hemisphere. Primarily this reflected an increase in cerebrospinal fluid signal accompanying deformation of the ventral midbrain. Significantly expanded voxels were however also seen in the cerebellar white matter and dorsolateral entorhinal cortex. In lactacystin-lesioned animals treated with low dose (200mg/kg) and high dose (400mg/kg) valproate a more complex pattern of anatomical changes were detected. Valproate treatment dose-dependently reversed cortical atrophy in the cingulate, motor, sensorimotor and parietal cortices in the ipsilateral hemisphere. Sub-cortically, valproate treatment also dose-dependently reversed atrophy of the ventromedial thalamus, ventral midbrain and expansion of CSF space. These effects were more marked at the higher dose tested.

6.4.3.3 – T_2 Relaxivity Measurement

In conjunction with manual segmentation analysis, at each of the time points examined, inter-hemispheric differences in T_2 signal intensity were assessed in the SNpc, the midbrain and the corpus striatum. For each brain region, the T_2 signal intensity ratio (ipsilateral divided by contralateral T_2 signal) was then calculated as a measure of interhemispheric difference (figure 6.8). The most marked changes in T_2 relaxivity occurred within the SNpc (figure 6.8A). As expected there were no discernable alterations in T_2 signal intensity ratio in the SNpc of non-lesioned animals treated with either saline or valproate throughout the five weeks of study. However in all groups lesioned with lactacystin, seven days post-surgery there was a significant increase in T_2 signal intensity ratio compared with the signal in both non-lesioned groups (mean T_2 signal intensity ratio in lactacystin-lesioned animals, 1.053 ± 0.012 vs. non-lesioned animals, 0.999 ± 0.011, $p<0.05$ in all comparisons). In animals subsequently treated with saline this increase in T_2 signal intensity ratio was reversed by week three and continued to decline, being significantly lower than both non-lesioned groups by week five (lactacystin lesion , saline treated animals, 0.935 ± 0.012 vs. non-lesioned , saline treated, 0.999 ± 0.012 and valproate treated animals, 1.000 ± 0.013, $p<0.001$ in both comparisons). Lactacystin-lesioned animals subsequently treated with valproate (both 200mg/kg and 400mg/kg) also exhibited this reversal in T_2 signal intensity ratio at week three and decline at week five however to a much lesser degree than saline treated animals. Notably neither of these treatment groups displayed significant differences from non-lesioned groups at either of these time points. Subtle changes were also observed in the midbrain mimicking those seen in the SNpc (figure 6.8C). However due to the subtlety of these alterations no significant differences were observed. No noticeable alterations in T_2 signal intensity ration were observed in the corpus striatum.

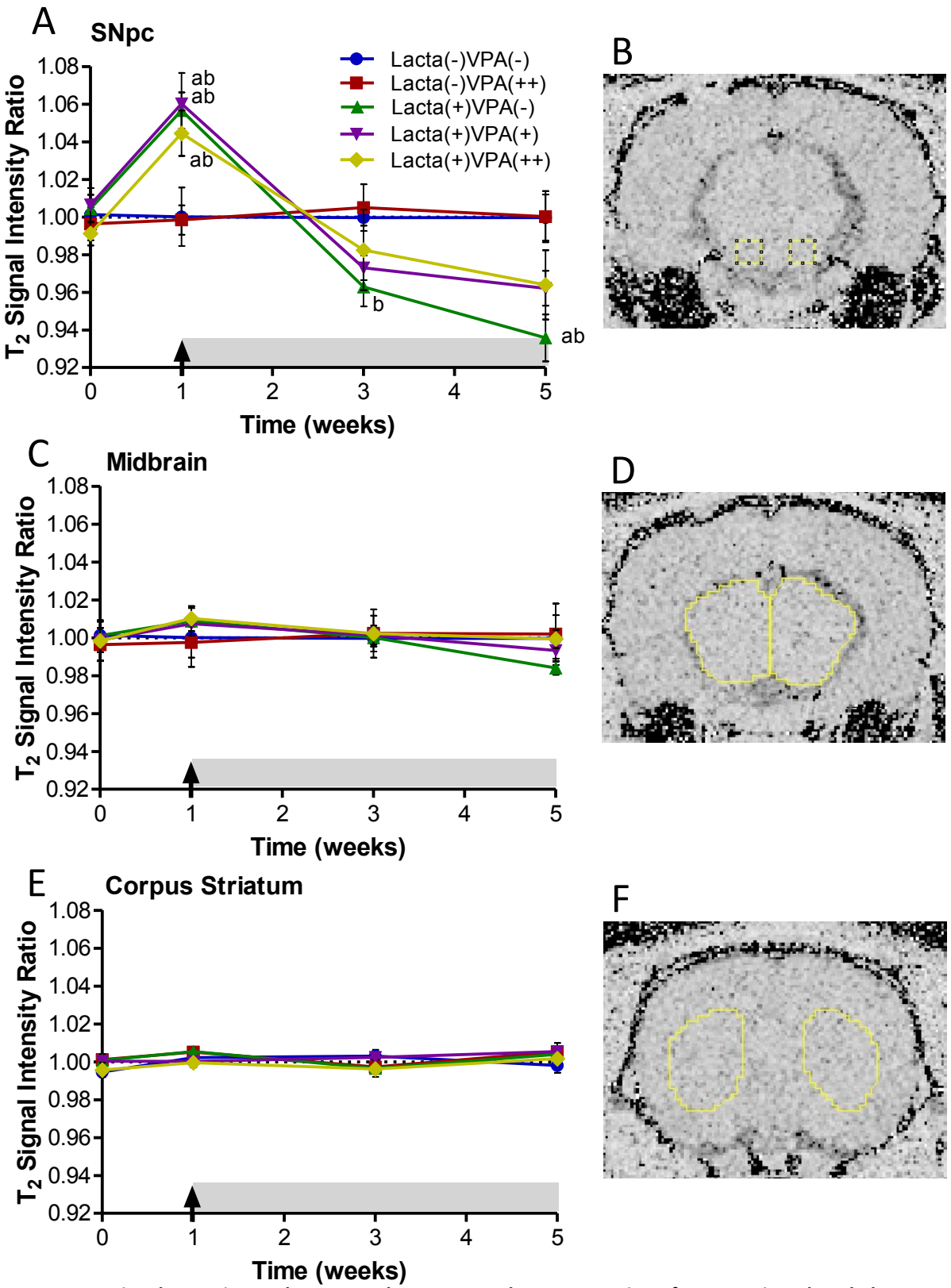

Figure 6.8 – T_2 Signal Intensity Analyses Reveal Dose Dependent Attenuation of Lactacystin Induced Changes
T_2 signal intensity measurements were made from T_2 relaxivity maps in the ipsilateral and contralateral (B) SNpc, (D) midbrain, and (F) corpus striatum. Data was then expressed as the ratio between the ipsilateral and contralateral hemisphere: the T_2 signal intensity ratio. Graphs show T_2 signal intensity ratio between the ipsilateral and contralateral hemisphers over time in the (A) SNpc, (C) midbrain and (E) corpus striatum. Statistical significance indicated with letters: [a]significantly different from group Lacta(-)VPA(-); [b]significantly different from group Lacta(-)VPA(++). n=6-7.

6.4.4 – Neuroprotective Effects of Delayed Start Valproate Treatment on Dopaminergic Neurons in the SNpc in the Lactacystin Rat Model of PD

Animals were sacrificed at week five of the study and hind brain tissue collected for immunohistochemical staining and stereological counting of dopaminergic (TH+) neurons in the SNpc (figures 6.9 and 6.10). Non-lesioned animals treated with saline did not show any interhemispheric loss of TH+ dopaminergic neurons of the SNpc (left SNpc, 11724 ± 729 vs. right SNpc, 11652 ± 493 TH+ cells). Similarly no difference was observed in the number of TH+ dopaminergic neurons in the left and right hemispheres of the SNpc in non-lesioned animals subsequently treated with valproate (400mg/kg) (left SNpc, 11706 ± 1716 vs. right SNpc, 12154 ± 1255 TH+ cells). Animals lesioned with lactacystin and treated with saline however exhibited a marked interhemispheric loss of TH+ neurons due to the intranigral injection of lactacystin (left SNpc, 4257 ± 1364 vs. right SNpc, 12328 ± 580 TH+ cells, % difference -53.81 ± 14.32%, $p<0.01$). By contrast valproate administration at its higher dose (400mg/kg) for 28 days afforded near complete protection of SNpc TH+ neurons against the toxic effects of lactacystin (left SNpc, 9729 ± 1347 vs. right SNpc, 11913 ± 578 TH+ cells, % difference -19.08 ± 10.17%, $p>0.05$). Administration of the lower dose of valproate (200mg/kg) resulted in only a partial protection of the TH+ neurons against lactacystin toxicity (left SNpc, 7659 ± 1228 vs. right SNpc, 12739 ± 862 TH+ cells, % difference -40.26 ± 9.87%, $p<0.05$). The changes observed in SNpc TH+ cell number were also similarly observed in the numbers of Nissl+ cell number, indicative of TH+ neuronal cell death rather than loss of the TH enzyme expression in dying neurons.

6.4.5 – Effects of Delayed Start Valproate Treatment on Brain Histone Acetylation Level in the Lactacystin Rat Model of PD

Upon removal of brain tissue at the end of the study the frontal brain was snap frozen for subsequent quantification of histone protein H3 acetylated on lysine 9 (AcH3-Lys9) using Western blot analysis (figure 6.11). Significantly less AcH3-Lys9 was observed in both hemispheres of animals lesioned with lactacystin and treated daily with saline (ipsilateral and contralateral hemispheres, 2.97 ± 4.05% and 21.05 ± 7.00% of control non-lesioned animals respectively, $p<0.001$ and $p<0.05$). This effect was dose dependently attenuated in both hemispheres upon treatment of valproate for 28 days, reaching significance between the amount of AcH3-Lys9 observed in the left hemisphere of lactacystin animals subsequently treated with saline compared with those treated with 400mg/kg valproate for 28 days (ipsilateral hemisphere, saline treated animals, 2.97 ± 4.05% vs. animals treated with 400mg/kg valproate, 108.67 ± 10.14% of control non-lesioned animals, $p<0.05$). No difference in the amount of AcH3-Lys9 in either hemisphere was observed in non-lesioned animals treated with valproate compared with control.

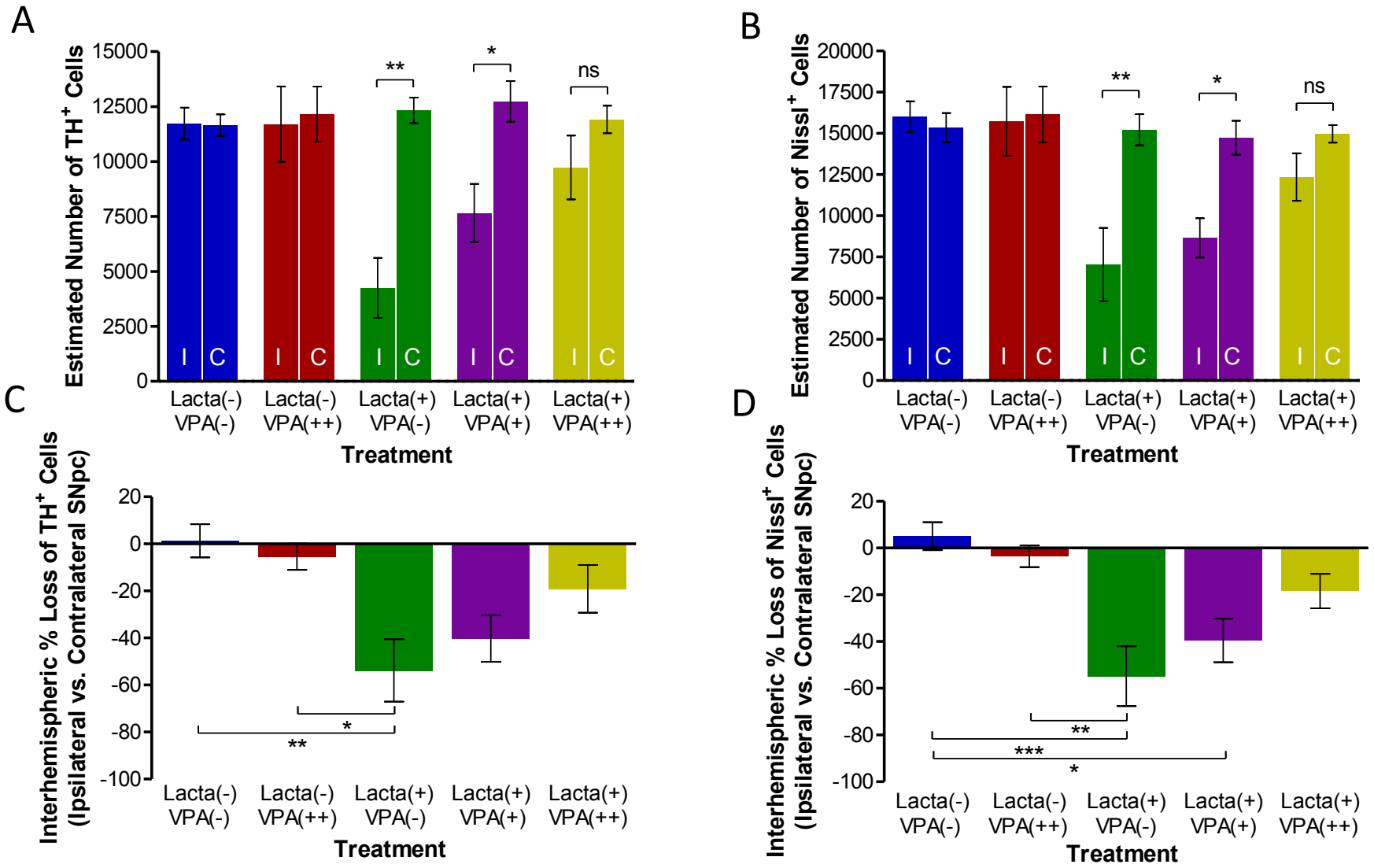

Figure 6.9 –Valproate Dose Dependently Protects Dopaminergic Neurons in the SNpc Against Lactacystin Induced Cell Death
Stereologically estimated (A) TH+ and (B) Nissl+ neuron numbers in the SNpc of rats suggest a dose dependent neuroprotective effect of valproate in this lactacystin rat model of Parkinson's disease. This is exemplified by the percentage interhemispheric loss of TH+ (C) and Nissl+ (D) neurons calculated between hemispheres of the SNpc. Statistical significance indicated with asterisks: *p<0.05; **p<0.01, ***p<0.001. n=6-7. Abbreviations: I, ipsilateral; C, contralateral.

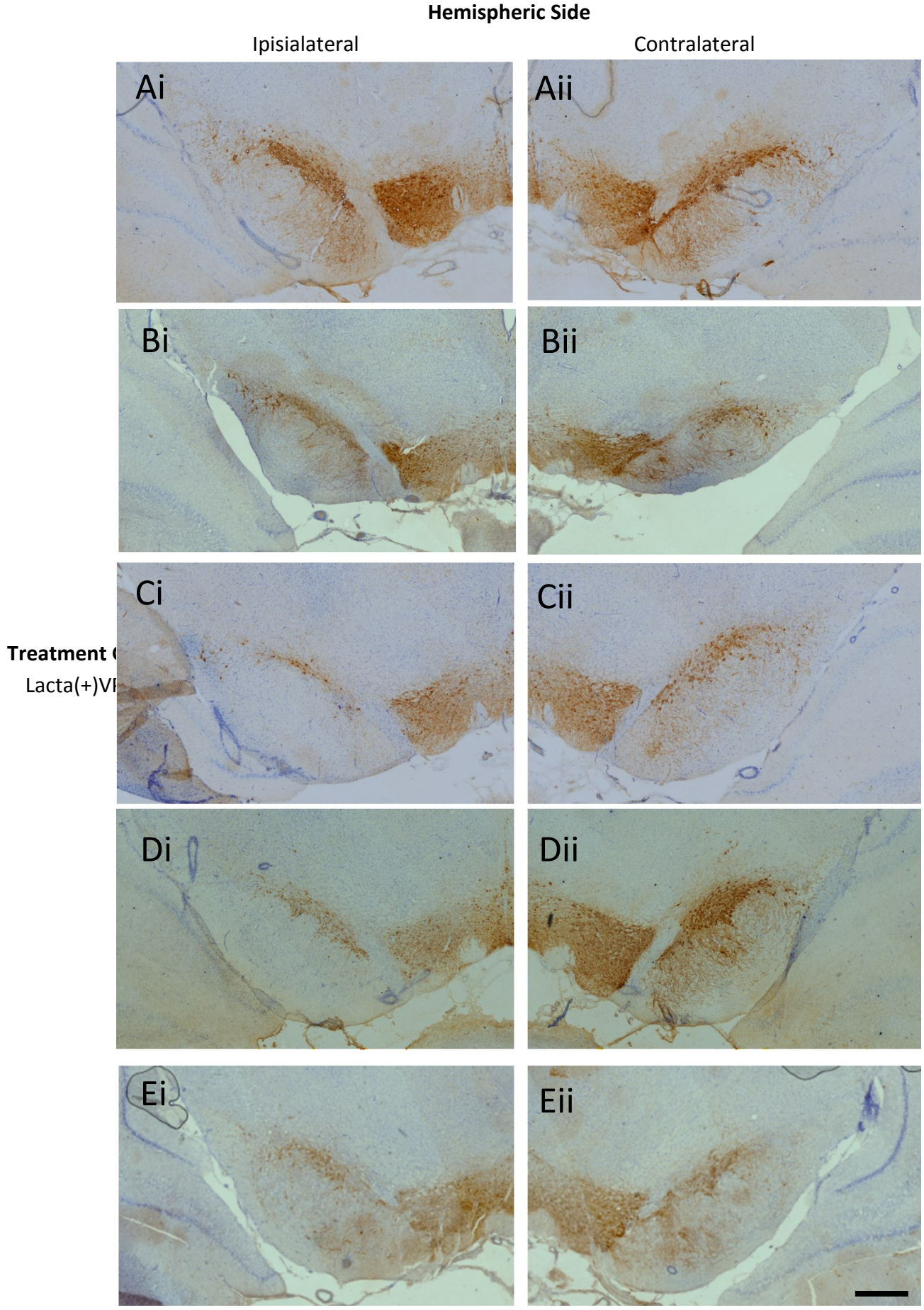

Figure 6.10 – Immunohistochemical Staining of TH+ Neurons in the SNpc of Animal Treatment Groups
Representative examples of the TH and Nissl stained ipsilateral (Ai-Ei) and contralateral (Aii-Eii) SNpc of rats in each of the five treatment groups. Scale bar equal to 500µm.

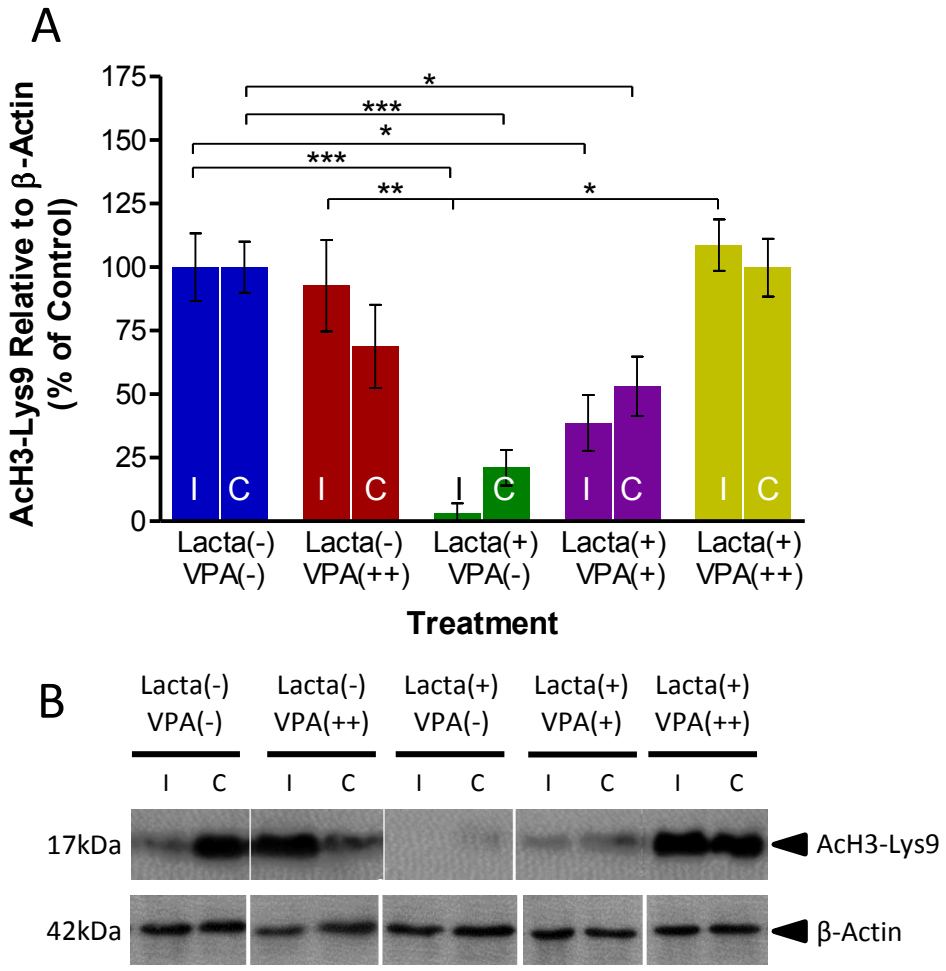

Figure 6.11 – Valproate Attenuates Lactacystin Induced Reduction in Histone Acetylation
Administration of delayed valproate treatment dose dependently reverses the reduction in histone H3-lysine 9 acetylation caused by lactacystin. (A) Densitometry analysis of the AcH3-Lys9 band relative to the β-actin band used as a loading control. (B) Representative blot of data presented in (A). Statistical significance indicated with asterisks: *p<0.05; **p<0.01, ***p<0.001. n=6-7. Abbreviations: I, ipsilateral; C, contralateral.

6.4.6 - Effects of Delayed Start Valproate Treatment on Brain Neuroprotective Gene Expression in the Lactacystin Rat Model of PD

qRT-PCR was performed on frontal brain tissue to quantify the expression of a number of different neurotrophic factors, apoptotic regulators and genes of interest previously shown to change upon treatment with HDACIs (Monti et al., 2009), to help elucidate the mechanism of valproate's neuroprotection. In non-lesioned animals, administration of valproate induced a stringent two fold upregulation of BDNF (figure 6.12, ipsilateral valproate treated, 2.14 ± 0.36 times greater than saline treated controls, $p<0.001$; contralateral valproate treated, 1.94 ± 0.36 times greater than saline treated controls, $p<0.01$). Valproate did not alter the expression of the other genes in these non-lesioned animals. However, in lactacystin-lesioned animals valproate administration significantly and dose dependently up regulated the expression of BDNF, GDNF and the anti-apoptotic factor Bcl-2, in the frontal brain hemisphere contralateral to the lesion. Most notably GDNF expression was greater in the contralateral hemisphere of valproate treated animals compared with saline treated control animals (Fig. 7b, high dose (400mg/kg) treated animals, 5.15 ± 1.48 times greater than saline treated controls; low dose (200mg/kg) treated animals 4.32 ± 1.34 times greater than saline treated control, $p<0.001$ in both comparisons). Similarly, expression of BDNF and Bcl-2 are also elevated in a dose dependent manner in the frontal brain hemisphere contralateral to the lesion, however this only reached significance at the higher dose of valproate (BDNF expression, 4.08 ± 0.88 times greater than saline treated control, $p<0.01$; Bcl-2 expression, 3.09 ± 0.32 times greater than saline treated control, $p<0.05$). Similar trends of an up regulation of gene expression of native αSyn and Hsp70 upon treatment with valproate were observed but these did not reach significance.

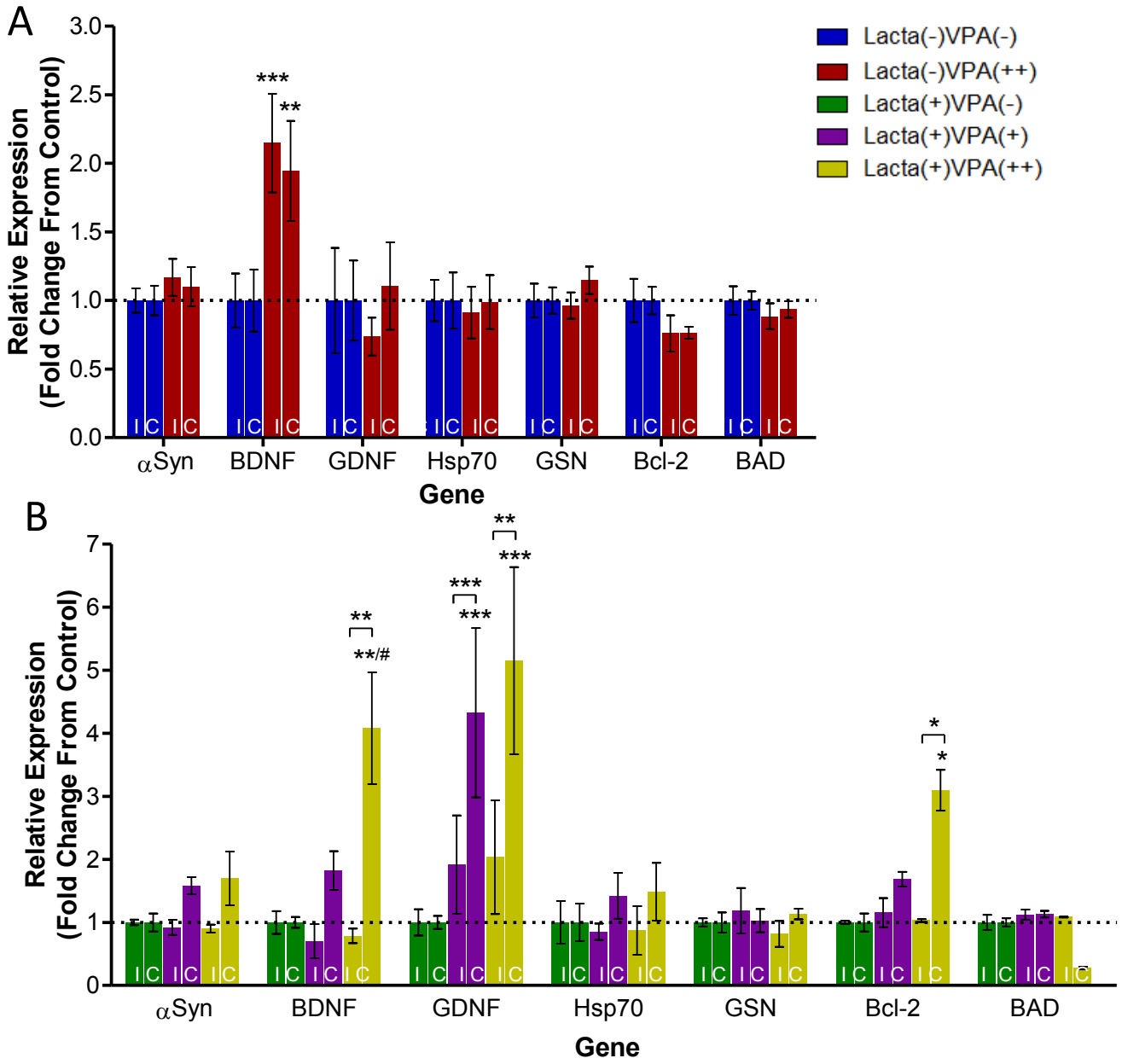

Figure 6.12 - Valproate Upregulates Expression of Neurotrophic Growth Factors and Neuroprotective Proteins

(A) Administration of systemic valproate alone, in non-lesioned rats upregulates bilateral expression of BDNF. (B) In lactacystin-lesioned animals valproate dose dependently up regulated unilateral expression of αSyn, BDNF, GDNF, Hsp70 and Bcl-2, as well as reducing the expression of BAD when given at its highest dose. Statistical significance indicated with asterisks and hashes: *p<0.05, **p<0.01, ***p<0.001 compared with the same hemisphere of saline treated group; #p<0.05, ##p<0.01, ###p<0.001 compared with the same hemisphere of Lacta(+)VPA(+). n=6-7. Abbreviations: I, ipsilateral; C, contralateral.

6.5 – Discussion

In the previous chapter it was demonstrated that the neurodegenerative process has been initiated and clinical behavioural symptoms, MRI changes, microglial activation, dopaminergic cell loss and molecular hallmarks of neurodegeneration in the animal model are already observed at seven days post-lesion. In order to model the clinical setting in which a neuroprotective agent would be administered, valproate treatment was initiated seven days post lactacystin lesion. Despite the delay in treatment, valproate dose dependently afforded neuroprotection and neuroregeneration in this animal model as evidenced by an attenuation of motor behavioural deficits, longitudinal MRI brain volume changes and quantification of the dopaminergic neurons within the SNpc. Molecular analyses of brain extracts indicate that valproate's neuroprotective/neuroregenerative effects may be at least part mediated through epigenetic changes via the inhibition of histone deacetylation to cause chromatin remodelling and upregulation of numerous neurotrophic and neuroprotective genes culminating in the observed phenotype.

The finding here that valproate acts neuroprotectively and neurorestoratively in an animal model of PD is consistent with findings from others. Notably Monti and colleagues (2010) were the first to describe the neuroprotective effects of valproate in a preclinical model of PD in 2010, in which they observed a significant preservation of SNpc TH+ dopaminergic neurons with valproate treatment in rats implanted with osmotic mini-pumps delivering a sub-chronic administration of rotenone. They also observed an attenuation of the loss of striatal dopamine and consistent with *in vitro* findings from their group (Monti et al., 2007), and in agreement with qRT-PCR analyses conducted here, they observed an increase in native αSyn expression in line with a reduction in mono-ubiquitinated αSyn and its nuclear translocation following valproate administration. As well as in the rotenone rat model of PD, Monti and colleagues also demonstrated that dietary pre-treatment with valproate resulted in protection of the dopaminergic neuronal terminals and cell bodies in the SNpc in the striatal 6-OHDA model (Monti et al., 2012). An increase in endogenous αSyn was similarly observed in both the SNpc and striatum in these animals. Lastly, Kidd and Schneider (2011) also demonstrated the neuroprotective effects of valproate in the MPTP mouse model of PD, observing dopaminergic neuroprotection when valproate was administered systemically prior to MPTP. In all of these previously mentioned studies, neuroprotection was observed following its pre-treatment prior to toxin administration. The current study extends these previous findings given that valproate mediated neuroprotection was afforded despite being administered after toxin administration in the lactacystin animal model of PD.

Valproate has previously been shown to partially protect against motor deficits in animal models of traumatic brain injury (Dash et al., 2010, Jepsen et al., 2014, Tai et al., 2014), spinal cord

injury (Lee et al., 2012), and stroke (Kim et al., 2007), yet this study is the first to examine the ability of valproate to relieve motor symptoms in an animal model of PD. Here it is observed that delayed start valproate treatment dose dependently reverses the lactacystin induced reduction in use of the forelimb contralateral to the lesioned SNpc in rats observed 7 days after lesioning, and also attenuates the number of rotations performed by these animals upon treatment with amphetamine. Additionally, using a battery of behavioural tests, Castro and colleagues (2012) have previously demonstrated that valproate pre-treatment prevented the development of early non-motor symptoms of PD e.g. cognitive and emotional deficits, in animals nasally administered MPTP (Prediger et al., 2011). Authors demonstrated that this was accompanied by a significant preservation of olfactory bulb and striatal dopamine content in MPTP treated animals (Castro et al., 2012). This suggests that valproate may also act neuroprotectively towards other neuronal systems which is particularly important since the neurodegenerative process in PD is not merely confined to the dopaminergic nigrostriatal system (Braak et al., 2003). Taken together with the cellular evidence of neuroprotection presented here and by others (Kidd and Schneider, 2011, Monti et al., 2010, Monti et al., 2012) and previous work in models of early non-motor PD (Castro et al., 2012) and other more acute neurodegenerative conditions, valproate appears an encouraging candidate for disease modification and corresponding symptomatic relief in PD.

The current study is the first to use MRI to non-invasively monitor the morphological progression and nigrostriatal neuropathology in this proteasome inhibitor rat model of PD in conjunction with a candidate neuroprotective drug to longitudinally assess its efficacy at disease modification. Manual segmentation analysis was performed here to examine the temporal morphological progression of selected brain regions in the model, and in line with previously published data following nigrostriatal neuropathology induced as a result of stereotaxic injection of lactacystin to the SNpc (Vernon and Modo, 2011), in the current study a marked reduction in the volume of the ipsilateral midbrain in the weeks following stereotaxic surgery was observed. Similarly an increase in the volume of the lateral ventricles was observed, which was far more pronounced in the ipsilateral as opposed to the contralateral hemisphere. Both of these changes were observed, in the current study, to be dose dependently attenuated by delayed valproate treatment. Subsequent TBM analysis both confirm and extend the manual data adding further weight to the findings, as well as extending prior observations. For example TBM reveals that chronic valproate treatment by itself induces a specific pattern of structural re-modelling (expansion and contraction) in the healthy brain, as observed for other psychotropic drugs (Vernon et al., 2012, Vernon et al., 2013). Similarly, unbiased, automated TBM data reinforces manual observations, and confirms lactacystin-lesioning by itself is associated with a specific reproducible pattern of neuroanatomical changes in the brain,

detectable by MRI (Vernon et al., 2011). Taken together, these data may suggest a complex drug x disease interaction driving the anatomical effects observed. That is, a dose-dependent neuroprotective effect of valproate on lactacystin-induced brain atrophy is observed. The combination of longitudinal *in vivo* MRI and automated TBM (clinically comparable technology) therefore has great potential for pre-clinical assessment of drugs with disease-modifying potential in pre-clinical models of PD.

In conjunction with volumetric analysis to monitor morphological progression and nigrostriatal neuropathology in this model, T_2 signal intensity analysis was also used to follow asymmetry in T_2 signal intensity in the SNpc, midbrain and corpus striatum. Consistent with previous studies using the lactacystin rat model (Vernon et al., 2010), changes in T_2 signal intensity ratio were observed in the SNpc and to a lesser extent the midbrain, but not in the striatum. One week following lesioning, an increase in T_2 signal intensity was observed in the SNpc of all lactacystin-lesioned animal groups consistent with findings in the 6-OHDA rodent model (Kondoh et al., 2005) and the MPTP primate model (Miletich et al., 1994), indicative of acute inflammatory oedema in the area of interest given its appearance in nigrostriatally lesioned animals alone and its dissipation with time. This increase in the SNpc is reversed at weeks three and five in lactacystin-lesioned animals likely due to the combination of cell death and iron accumulation in the area creating inhomogeneities in magnetic field, which diphase nearby water protons leading to shortening of T_2 and lowering T_2 signal intensity. Several studies note the accumulation of iron in the SNpc of PD patients (Dexter et al., 1989b, Brar et al., 2009, Gorell et al., 1995, Kosta et al., 2006, Martin et al., 2008) and a number of studies also note the accumulation of iron in the SNpc of the lactacystin rat model (Vernon et al., 2010, Zhu et al., 2007). Correspondingly a dose dependent reversal of this lowering of T_2 signal intensity ratio was observed in the current study indicative that valproate may not only be reducing cell death and inducing neuroregeneration within the SNpc but also reducing iron deposition within the area as well.

It was observed in the previous chapter from stereological cell quantification of animals culled seven days post lactacystin-lesion and longitudinal behavioural test outcomes that the vast majority of nigral degeneration occurs in the first seven days post lesion (Vernon et al., 2010, Vernon et al., 2011, Mackey et al., 2013). Importantly however it was also observed that a large number of TH+ neuropil, and axonal and dendritic projection remain at week 1 post lesion despite the significant reduction in TH+ neuronal cells bodies. Likewise, Nissl+ neuronal degeneration was markedly less than that of TH+ cells at this early timepoint. In the current study of the effects of valproate in this model of PD, valproate treatment was initiated seven days post lactacystin-lesion. Despite this delayed treatment strategy, significantly less neurodegeneration of nigral dopaminergic

neurons was observed after four weeks of valproate treatment. This appears counterintuitive given the large extent of nigral dopaminergic neurodegeneration already observed at week one previously, prior to the initiation of valproatre treatment. These findings therefore suggest that valproate is not only acting neuroprotectively towards dopaminergic nigral neurons but is also acting neuroregeneratively: rescuing unhealthy and/or dying neurons that have lost TH expression in the cell body and therefore have reduced function, yet retain TH+ projection. Additionally, valproate has been shown to be effective at reducing microglial activation (Chen et al., 2007, Peng et al., 2005). It is therefore also likely that in conjunction with its effects on nigral neurons, valproate reduces activation of microglia, reducing microglial exacerbation of further neurodegeneration and aiding the recovery/regeneration of unhealthy/dying nigral neurons. These results are extremely encouraging given the delayed initiation of valproate treatment in this study highlighting the translatability of such a treatment to the clinic to tackle Parkinsonian neurodegeneration after it is evident through motor symptom presentation and corresponding nigral dopaminergic neurodegeneration.

αSyn accumulation actively promotes histone hypoacetylation both *in vitro* in SH-SY5Y cells and *in vivo* in drosophila, both overexpressing αSyn (Kontopoulos et al., 2006). Lactacystin dopaminergic neurotoxicity is associated with the aggregation of α-synuclein to form inclusion bodies in the SNpc, a finding which has been extensively verified since (McNaught et al., 2002b, Vernon et al., 2011, Zhu et al., 2007, Niu et al., 2009, Pienaar et al., 2013). Therefore in line with previous observations of the effect of αSyn on histone acetylation, in the current study a reduction in histone acetylation in the brains of lactacystin-lesioned animals is observed. Importantly, valproate treatment was observed to dose dependently attenuate this histone hypoacetylation, in parallel with the cellular neuroprotective effect of the drug shown through stereological cell quantification of dopaminergic neurons in the SNpc. Valproate is a somewhat promiscuous drug: affecting GSK-3 and Akt/ERK pathways, GABA/glutamate neurotransmission, Na+ and Ca2+ voltage-dependent channels, phosphoinositol/TCA pathways and the oxidative phosphorylation pathway (Ximenes et al., 2012). A number of these effects too could contribute towards valproate's neuroprotective phenotype observed here. However the dose dependent attenuation of histone hypoacetylation induced by valproate in line with the extent of neuroprotection/neuroregeneration observed is suggestive that valproate's inhibition of HDACs is at least partly responsible for the phenotype observed.

Addition of an acetyl group to histone lysine residues neutralises the positive charge of the residue and hence reduces the electrostatic interaction between the lysine in the histone tail and the negatively charged phosphate group on DNA. This disrupts the inter- and intra-nucleosomal

interactions between the histone and DNA and hence relaxes the structure of the chromatin allowing transcription factor access. Inhibition of HDACs and histone acetylation in the brain have therefore been shown to be associated with transcriptional upregulation of numerous factors that are thought to contribute to the neuroprotective effects observed by valproate (Monti et al., 2009). Similarly neurotrophic factors BDNF and GDNF are significantly upregulated upon valproate treatment, confirming the studies by Wu and colleagues (2008b) who demonstrated that an astrocytic cell line treated with valproate displays a time dependent increase in expression of both BDNF and GDNF; an effect which translated to neuroprotection in midbrain neuronal cultures in medium transfer experiments. Additionally the group demonstrated, by using chromatin immunoprecipitation, that the GDNF promoter associated histone H3 is significantly hyperacetylated when astrocytes are treated with valproate. The upregulation of both of these neurotrophic factors by valproate is most advantageous given the therapeutic implications of both of them in neurodegenerative disease, more specifically PD (Allen et al., 2013). For example BDNF treatment alone has been shown to reduce amphetamine induced rotational behaviour in 6-OHDA lesioned rats (Klein et al., 1999). Additionally, direct GDNF delivery to the striatum has been shown to protect dopaminergic neurons against 6-OHDA induced death, preserving locomotor function (Kirik et al., 2001). Moreover, adding to the evidence presented here on the functional recovery and restoration of dopaminergic nigral neurons upon valproate treatment, GDNF has been previously shown to induce significant increases in nigral TH activity, associated with increased release of dopamine and its metabolites, and accompanying improvement of motor function (Lapchak et al., 1997, Martin et al., 1996). It has therefore been suggested that the functional recovery caused by GDNF is mediated by restoration of dopaminergic nigrostriatal neurons (Kirik et al., 2001). This may well be the case with valproate histone deacetylase inhibition induced upregulation of endogeneous GDNF in the current study.

In addition to BDNF and GDNF, in this animal study it was also observed that gene expression of the anti-apoptotic molecule Bcl-2 is upregulated upon valproate treatment. This is in agreement with previously experiments conducted by Kidd and Schneider (2010) in which MES23.5 dopaminergic cells treated with valproate showed a reduction in MPP+ induced activation of caspase-3 indicating the inhibition of apoptosis. The findings from the current study therefore suggest that valproate's mechanism of histone acetylation mediated neuroprotection is a multifaceted and complex affair, one which may hold therapeutic potential against a complex disorder such as PD.

The doses of valproate administered to rats in this study translate to human equivalent doses of 64 and 32mg/kg/day (400 and 200mg/kg/day rat dose respectively) (as calculated using FDA

guidelines (FDA, 2005)). Both of these doses are far greater than the usual therapeutic maintenance dose of valproate used for the treatment of epilepsy in humans (1000-2000mg/day) (Britain, 2009). This suggests that valproate itself, at the doses examined here, may not be a candidate for repositioning for PD treatment. However given the presented data, the current study acts as proof of principle that delayed start treatment with a HDACI is capable of producing a neuroprotective/neurorestorative phenotype in this animal model of PD.

6.6 – Conclusions

Utilising a clinically relevant drug testing platform this study demonstrates that valproate's inhibition of HDAC classes I and IIa is dose-dependently neuroprotective and neurorestorative in the lactacystin rodent model of PD when administered chronically starting seven days after the toxin administration when behavioural symptoms, MRI changes, microglial activation, dopaminergic cell loss and molecular hallmarks of neurodegeneration in the animal model are already observed. The neuroprotective and neurorestorative effects of valproate are associated with a reversal of histone hypoacetylation and an upregulation of neuroprotective and neurotrophic factors. These findings therefore support the potential of the use of HDACIs such as valproate as a clinically translatable treatment strategy for PD.

Chapter Seven

Neuroprotective Effects of Nicotinamide in the Lactacystin Rat Model of Parkinson's Disease

7 – Neuroprotective Effects of Nicotinamide in the Lactacystin Rat Model of Parkinson's Disease

7.1 – Introduction

Nicotinamide (niacinamide or nicotinic amide), is an amide converted, *in vivo*, from its dietary precursor niacin (nicotinic acid), otherwise known as vitamin B3. This B vitamin is found in numerous food sources, most abundantly in beef, chicken, pork, fish, peanuts, mushrooms, green beans, sunflower seeds and avocado. Both niacin and nicotinamide are precursors of the coenzymes NAD+ and NADP (Chi and Sauve, 2013). For this reason vitamin B3 and the corresponding amide nicotinamide are essential dietary vitamins, required for a wide range of biological function in the body including include energy production, synthesis of fatty acids, cholesterol and steroids, signal transduction and the maintenance of genomic integrity (Maiese and Chong, 2003, Chi and Sauve, 2013). Pharmacologically, nicotinamide does not have the same adverse effects of niacin (cutaneous flushing and itching apparent for around 60mins after administration) which occur incidental to niacin's conversion. Nicotinamide is therefore highly tolerated orally up to 3g/kg/day in man (Britain, 2009). It displays a linear pharmacokinetic profile exhibiting maximal plasma levels as little as 30mins after ingestion with higher doses maintaining high plasma levels for up to 4 hours (Dragovic et al., 1995). Nicotinamide is a solid at room temperature and is highly water soluble, making administration easy via numerous routes. It has a relatively low molecular weight (122.12 g/mol) and therefore also crossed the BBB with ease (Spector, 1987).

Being a precursor for NAD+, nicotinamide is known to inhibit class III HDACs through competition binding to the NAD+ binding site of the Sirtuin HDACs (Avalos et al., 2005). It has therefore gained increased interest as a neuroprotective agent in neurodegenerative conditions. For example nicotinamide has been shown to improve neurological outcome and reduce infarct volume in models of stroke (Mokudai et al., 2000, Liu et al., 2009, Ayoub et al., 1999), restore cognitive function in transgenic models of AD (Green et al., 2008), and improve motor deficits and upregulate neurotrophic factors in models of HD (Hathorn et al., 2011). Furthermore greater focus has been placed upon the potential use of nicotinamide in PD due to its modulatory effects of cellular energy metabolism and the implications these have upon dopaminergic cell death within the disease (Beal, 2003).

The two most notable studies came from the work of Anderson, Bradbury and Schneider (2006, 2008). The neuroprotective efficacy of nictotinamide was assessed in different mouse MPTP models taking advantage of differing dose regimes of the toxin to induce dopaminergic neuronal cell death. By analysing striatal DA levels and changes in number of TH+ and Nissl+ stained neurons in the SNpc at differing time point authors were able determine the neuroprotective profile of

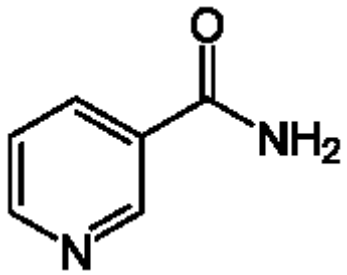

Figure 7.1 – Chemical Structure of Nicotinamide

The chemical structure of nicotinamide is given which exists as a solids a RT. It is highly water soluble making administration through numerous routes very easy.

nicotinamide. Administration of nictotinamide peripherally prior to MPTP injection, a dose dependent neuroprotective profile was observed in the 'acute' MPTP (four injections in 1 day at 2hr intervals) but not in the 'sub-acute' model (two injections per day at 4hr intervals for 5 days). The highest dose of nictotinamide was still shown to be neuroprotective in this latter 'sub-acute' model however not to the same degree as was seen in the 'acute' model. Authors suggest that this is a result of nicotinamide interacting directly with the specific mechanism of cell death operating in the two different models (Anderson et al., 2008). However, Anderson et al fail to elucidate the mechanism of neuroprotection in each of the models. Regardless, in both of these drug/MPTP dosing regimens, like many of the studies previously discussed using valproate *in vivo* in animal models of PD, drug administration was commenced prior to toxin administration highlighting the poor clinical relevance of such a study design. In addition, the focuses of their studies are not on the HDAC inhibition by nicotinamide hence they do not correlate the extent of neuroprotection with histone acetylation in any way. Therefore, it is impossible to say whether the neuroprotective effects observed are in any way a result of HDAC inhibition. Nonetheless, studies by Anderson and colleagues (2006, 2008) suggest that nicotinamide administered at higher doses, appears to be neuroprotective towards dopaminergic neurons in this model of Parkinsonian cell death.

This chapter therefore aims to confirm and extend previous findings on the use of nicotinamide in animals models of PD by using the lactacystin rat model which recapitulates the formation of neurotoxic protein inclusions within the substantia nigra to cause progressive dopaminergic cell death. Furthermore, unlike many of the previous studies, a delayed start study design will also be used to model the clinical scenario in which a neuroprotective drug would be administered more accurately. In addition, molecular and cellular analyses of study samples will attempt to elucidate the neuroprotective mechanism of nicotinamide in this model.

7.2 - Aims of Chapter

The aims of this chapter are therefore to:

1. Determine the neuroprotective and behavioural effects of delayed start nicotinamide treatment in the lactacystin rat model of PD:
    d. Determine the effects of delayed start nicotinamide treatment on the progression of lactacystin induced motor behavioural symptoms in the model.
    e. Determine the effects of delayed start nicotinamide treatment on lactacystin induced pathological changes in brain structure in the model.
    f. Determine the effects of delayed start nicotinamide treatment on lactacystin induced dopaminergic neuronal cell death in the SNpc in the model.
2. Investigate the neuroprotective mechanism of delayed start nicotinamide treatment in the lactacystin rat model of PD
    a. Quantify the level of histone acetylation in the brains of nicotinamide treated lactacystin-lesioned animals.
    b. Quantify the expression of numerous neurotrophic and neuroprotective factors thought to be associated with HDACI mediated neuroprotection in nicotinamide treated lactacystin-lesioned animals.

7.3 – Experimental Design

7.3.1 – Investigating the Neuroprotective and Behavioural Effects of Delayed Start Nicotinamide Treatment in the Lactacystin Rat Model of PD

Three groups of male Sprague-Dawley rats (n=6 or 7) were intra-nigrally lesioned with the irreversible proteasome inhibitor, lactacystin, by stereotaxic injection into the SNpc (see section 2.4.3). Animals were then left to recover for 7 days before receiving a daily i.p. injection of sterile saline (0.9% NaCl), or 250mg/kg or 500mg/kg nicotinamide dissolved into saline, for 28 days. In addition to these three animal treatment group, two groups of male Sprague-Dawley rats (n=6 or 7) were also included which did not receive lactacystin lesioning surgery: which received subsequent daily treatment with saline or daily treatment with 500mg/kg nicotinamide dissolved into saline (table 7.1 for animal treatment groups). In order to follow the neuropathological and behavioural progression of the disease model and to determine to what extent nicotinamide was able to delineate this progression, both motor behavioural testing and MRI were conducted at baseline, and at weeks 1, 3 and 5 of the study (figure 7.1 for graphical illustration of study design). Both the vertical cylinder and amphetamine induced rotation tests were used to study the progression of behavioural motor asymmetry. Similarly, manual volumetric segmentation analysis and T_2 relaxivity analysis of MR images were conducted to study the neuropathological progression of the model. For quantification of nicotinamide neuroprotection, at the end of the 5 week study animals were culled and brain tissue was collected. The hind brain was fixed, cryoprotected, cryosectioned and dopaminergic neurons (TH+) immunohistochemically stained and stereologically quantified.

7.3.2 – Investigating the Neuroprotective Mechanism of Delayed Start Nicotinamide Treatment in the Lactacystin Rat Model of PD

Upon collection of brain tissue at the end of the five week study, frontal cortex tissue was dissected and snap frozen for molecular analysis of the neuroprotective mechanism of nicotinamide in the model. Protein content was extracted from tissue samples and Western blot analyses were conducted to quantify the level of histone acetylation in the brains of lactacystin-lesioned/nicotinamide treated animals. In addition, mRNA content was extracted for qRT-PCR analysis to quantify the expression of numerous neurotrophic and neuroprotective factors thought to be involved in the neuroprotective effects of HDACIs such as nicotinamide.

7.3.3 – Statistical Analysis

All data is presented as mean ± SEM. One-way ANOVA with Bonferroni post-tests were used for analysis of vertical cylinder test in the confirmation of lesioning. In the nicotinamide study a two-way

(repeated measures) ANOVA with Bonferonni post-tests were used for analysis of vertical cylinder test, amphetamine induced rotation test and MRI manual segmentation analysis datasets. An additional one-way ANOVA with Bonferroni post-tests was used for comparison of percentage contralateral forelimb use vs time area under the curve data. Paired t-tests were used to compare stereological cell counts in the ipsilateral and contralateral hemispheres of animal brains. A one-way ANOVA with Bonferroni post-tests were used to compare cell loss percentages calculated from stereological cell counts. A one-way ANOVA with Bonferroni post-tests were used to compare Western blot data. A two-way ANOVA with Bonferroni post-tests were used to compare qRT-PCR data. All statistical tests were performed using GraphPad Prism (v5.0 for Windows, GraphPad Software, San Diego, CA, USA).

Table 7.1 - Nicotinamide Neuroprotection Animal Treatment Groups
*All daily i.p. injections given as 2ml/kg: saline injections given as 2ml/kg empty saline; 500mg/kg nicotinamide injections given as 2ml/kg of 250mg/ml solution of nicotinamide in saline; 250mg/kg nicotinamide injections given as 2ml/kg of 125mg/ml solution of nicotinamide in saline.

Group	N=	Intranigral Injection	Daily i.p. Injections*	Behavioural Tests
Lacta(-)NTA(-)	7	None	Saline	Vertical Cylinder Test
Lacta(-)NTA(++)	5	None	Nicotinamide (500mg/kg)	Vertical Cylinder Test
Lacta(+)NTA(-)	7	Lactacystin (10µg in 4µl saline)	Saline	Vertical Cylinder Test & Amphetamine Rotation
Lacta(+)NTA(+)	6	Lactacystin (10µg in 4µl saline)	Nicotinamide (200mg/kg)	Vertical Cylinder Test & Amphetamine Rotation
Lacta(+)NTA(++)	6	Lactacystin (10µg in 4µl saline)	Nicotinamide (400mg/kg)	Vertical Cylinder Test & Amphetamine Rotation

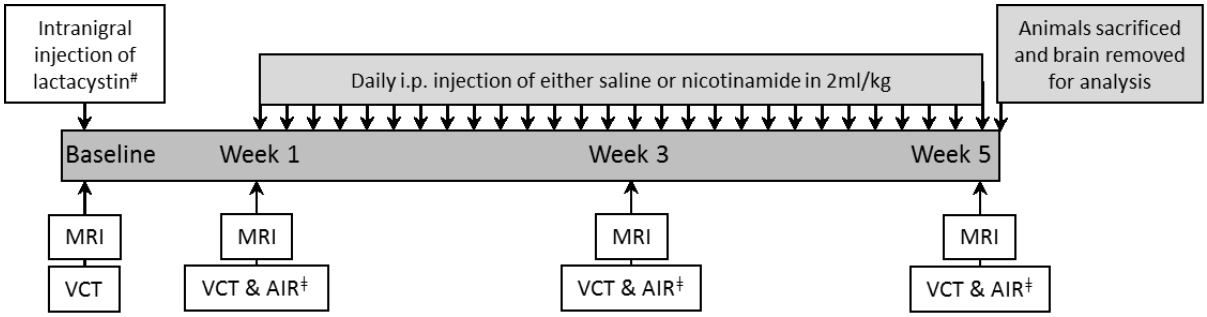

Figure 7.2 - Nicotinamide Neuroprotection Animal Study Design
Study design used for investigation of the neuroprotective effects of delayed start nicotinamide treatment in the lactacystin rat model of PD. Abbreviations: AIR, amphetamine induced rotations; MRI, magnetic resonance imaging; VCT, vertical cylinder test.
#Only groups Lacta(+)NTA(-), Lacta(+)NTA(+) and Lacta(+)NTA(++) intranigrally injected with lactacystin. Control groups remained surgically naïve.
‡Only groups lesioned with lactacystin were tested using the amphetamine induced rotation test at these time points.

7.4 – Results

7.4.1 – Confirming Lesion in Lactacystin Injected Animals

To confirm that all lesioned animals included in the study received lactacystin to the left SNpc, MRI scans acquired at week 1 post-lesion were examined to check the location of stereotaxic injection of the toxin (section 2.4.3, figure 7.3E). The lesion site was confirmed in all lesioned animals and therefore no animals were excluded on this basis. In addition to visual confirmation of the lesion site from MR images, behavioural tests performed at 7 days post lesioning were also used to confirm the development of early motor symptoms as a consequence of lactacystin injection into the left SNpc. For analysis of vertical cylinder test data, animals were divided into two groups dependent on whether they had received stereotaxic surgery (n=19) or not (n=12) at week 1. There was a significant reduction in the use of the contralateral forelimb of animals lesioned with lactacystin, compared to non-lesioned animals at week 1 (figure 7.3A, week 1, lactacystin-lesioned animals, 38.71 ± 2.06%, vs. non-lesioned animals, 50.04 ± 1.39% contralateral forelimb use, $p<0.001$). In addition, lactacystin-lesioned animals were injected with amphetamine to examine the degree to which they exhibited rotational behavioural, indicative of degeneration of the ipsilateral SNpc. All animals lesioned with lactacystin exhibited amphetamine induced rotations 7 days after lesioning indicative of correct needle placement and delivery of lactacystin to the left SNpc (figure 7.3C and D, 21.58 ± 2.25 mean number of rotations per 5 mins). The extent of rotational behavioural in the animals therefore compared favourably to previously lesioned animals groups (figure 5.10, 21.17 ± 3.71 and figure 6.3, 19.73 ± 1.39 mean number of rotations per 5 mins).

7.4.2 – Effects of Delayed Start Nicotinamide Treatment on Behavioural Progression of the Lactacystin Rat Model of PD

7.4.2.1 – Vertical Cylinder Test

The vertical cylinder test was conducted in all five treatment groups at baseline and weeks 1, 3 and 5 of the study to assess motor asymmetry in rat forelimb use. At baseline there was equal use of both the left and right forelimbs in all animals (figure 7.4A, 50.26 ± 1.10% contralateral forelimb use). However one week after surgery there was a significant reduction in the contralateral forelimb use of all lactacystin-lesioned animal groups compared with non-lesioned groups (figure 7.4A, $p<0.05$ in all comparisons). From one week onwards the contralateral forelimb use of the lactacystin-lesioned saline treated animals continued to decline with time (week 1, 39.59±4.11%; week 3, 36.01±3.37%; week 5, 35.50±4.08%, $p<0.01$ compared with control animals at each time point). However once animals began daily i.p. treatment with 250mg/kg nicotinamide one week after lactacystin-lesioning there was a time dependent reduction in contralateral forelimb use deficit (week 1, 35.76 ± 3.23%;

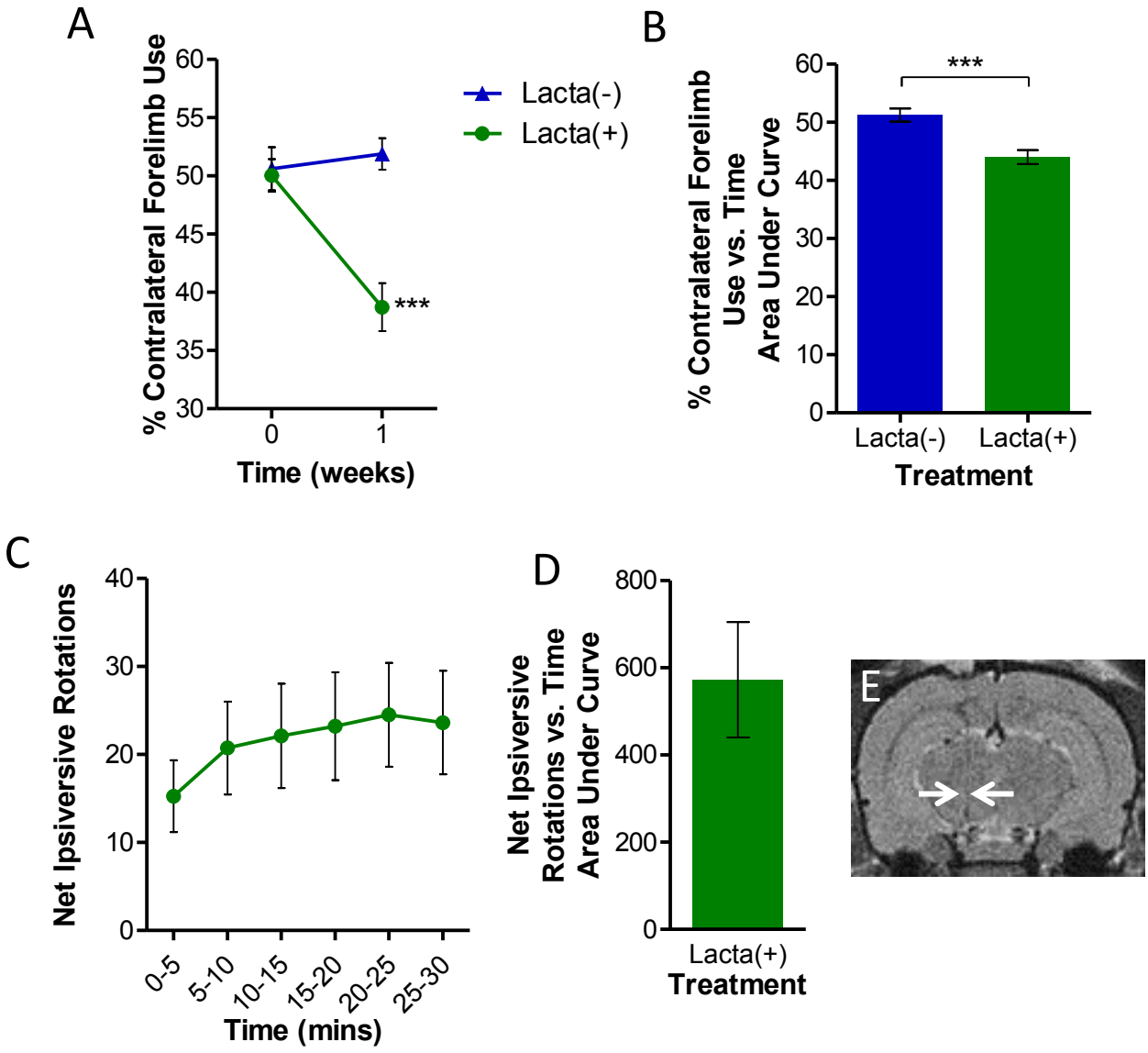

Figure 7.3 - Confirming Lesion in Lactacystin Injected Animals

(A) Percentage contralateral forelimb use in lactacystin-lesioned (Lacta(+)) and non-lesioned (Lacta(-)) rats at baseline and 7 days after surgery. (B) Area under the curve of data represented in (A) demonstrating more clearly the differences between percentage contralateral forelimb use in animal treatment groups. (C) Number of amphetamine rotations performed by lactacystin-lesioned animals in five minute intervals after administration of amphetamine. (D) Area under the curve of data represented in (C) demonstrating more clearly the progressive nature of rotational behaviour after lactacystin-lesioning. (E) Representative MR image confirming correct needle placement and therefore delivery of lactacystin to the left SNpc in a lesioned animal. Statistical significance is indicated using asterisks: ***p<0.001.

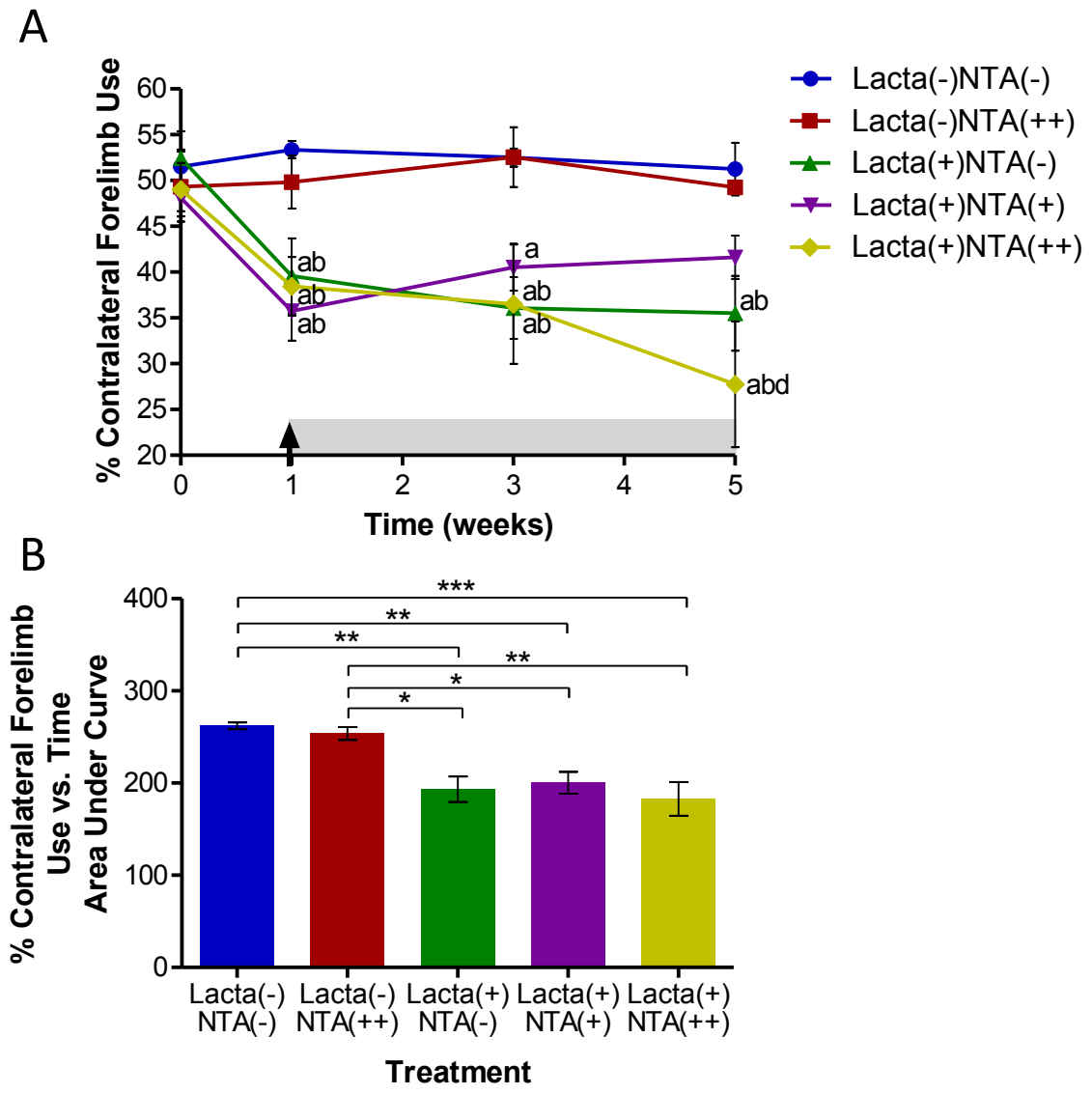

Figure 7.4 – Nicotinamide Alters Extent of Lactacystin Induced Motor Behavioural Deficits in the Vertical Cylinder Test

(A) Vertical cylinder test outcomes demonstrate that once animals begin treatment with nicotinamide at week 1 (designated by arrow and grey shading), the lactacystin induced reduction in percentage contralateral forelimb use is either reversed or exacerbated dependent on nicotinamide dose applied. Statistical significance indicated with letters: [a]significantly different from group Lacta(-)NTA(-); [b]significantly different from group Lacta(-)NTA(++); [c]significantly different from group Lacta(+)NTA(-). See text for levels of significance. (B) Area under the curve of data represented in (A) demonstrating more clearly the differences between percentage contralateral forelimb use in animals treatment groups. Statistical significance is indicated using asterisks: *, $p<0.05$, **$p<0.01$, ***$p<0.001$. n=5-7.

week 3, 40.53 ± 2.55%; week 5, 41.63 ± 2.37% contralateral forelimb use), animals failing to show a statistically significant difference from either non-lesioned groups at week 5. Lactacystin-lesioned animals subsequently treated with the higher dose of nicotinamide (500mg/kg) however exhibited a continued decline of contralateral forelimb use over the subsequent time points more so than saline treated animals (week 1, 35.76 ± 3.23%; week 3, 40.53 ± 2.55%; week 5, 41.63 ± 2.37% contralateral forelimb use), reaching statistical significance from both non-lesioned animal groups and those lactacystin-lesioned and treated with 250mg/kg nicotinamide ($p<0.05$ in all comparisons). The area under the curve produced by plotting percentage forelimb use vs. time demonstrates the differences between treatment groups more clearly (figure 7.4B).

7.4.2.2 – Amphetamine Induced Rotation Test

As well as the vertical cylinder test, the amphetamine induced rotation test was conducted on all lesioned animal groups at week 1, 3 and 5 following lesioning to assess the extent of drug induced rotational behaviour. Following amphetamine challenge, all lactacystin-lesioned animals produced ipsilateral rotations one week after lesioning surgery (figure 7.5A, mean number of amphetamine induced rotations per 5 minutes during recording, 24.30 ± 4.80, 21.00 ± 16.73, and 24.9 ± 3.71 for Lacta(+)NTA(-), Lacta(+)NTA(+) and Lacta(+)NTA(++) groups respectively). Over the further two time points examined, saline treated lactacystin-lesioned animals performed increasing numbers of rotations (mean number of amphetamine induced rotations per 5 minutes during recording, week 3, 41.72 ± 9.84, week 5, 66.22 ± 19.43). Animals treated with the lose dose of nicotinamide (250mg/kg) exhibited a similar trend of increased number of rotations with time however to a slightly lesser extent than saline treated animals (mean number of amphetamine induced rotations performed by nicotinamide (250mg/kg) treated animals per 5 minutes of recording at week 3 and 5, 29.66 ± 19.73 and 59.47 ± 18.22 respectively). Animals treated with the high dose (500mg/kg) or valproate however exhibited a far greater number of amphetamine induced rotations at the later two timepoints examined (mean number of amphetamine induced rotations performed by nicotinamide (500mg/kg) treated animals per 5 minutes of recording at week 3 and 5, 103.367 ± 7.42 and 131.37 ± 18.35 respectively, $p<0.001$ in all comparisons from both saline and low dose (250mg/kg) treated animal groups at both timepoints). These differences between groups become clearer when data is expressed as the area under the curve produced by plotting net number of rotations vs. time (figure 7.5B). At both week 3 and week 5 timepoints the area under the curve for animals treated with the high dose of nicotinamide (500mg/kg) is significantly greater than animals treated with saline ($p<0.05$ in both comparisons) and the low dose of nicotinamide ($p<0.01$ in both comparisons).

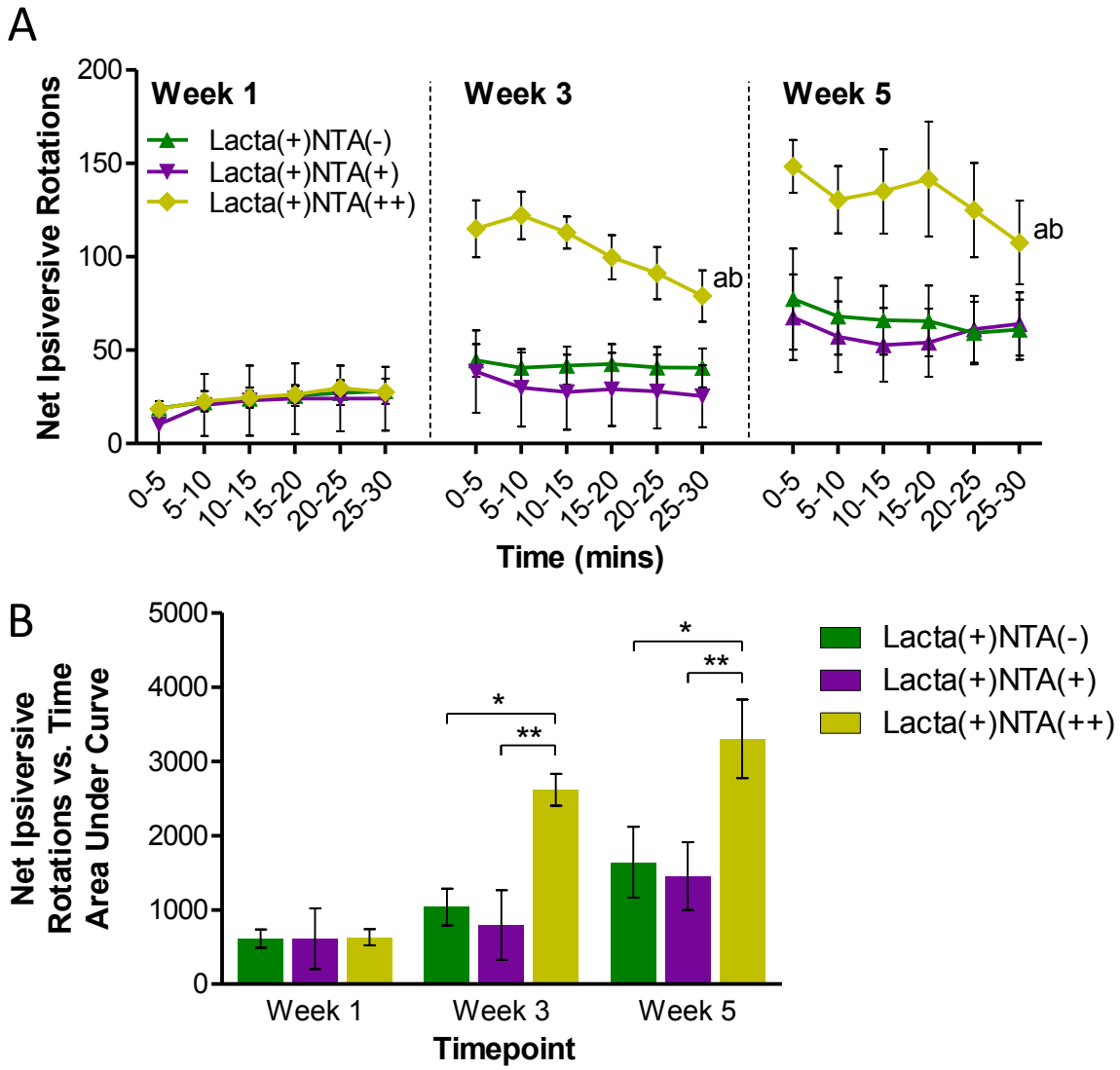

Figure 7.5 – Nicotinamide Alters Extent of Lactacystin Induced Rotational Behaviour After Amphetamine Challenge

(A) Net number of ipsiversive rotations performed by animals per 5 minutes plotted against time for the 30mins in which rotational behaviour was recorded following amphetamine administration. Statistical significance indicated with letters: [a]significantly different from group Lacta(+)NTA(-); [b]significantly different from group Lacta(+)NTA(+). See text for levels of significance. (B) The area under the curve produced by plotting raw rotational values against time (A) demonstrates differences in amphetamine induced rotational behaviour with nicotinamide treatment. Statistical significance is indicated using asterisks: *p<0.05, **p<0.01. n=5-7.

7.4.3 - Effects of Delayed Start Nicotinamide Treatment on Neuropathological Progression of the Lactacystin Rat Model of PD

7.4.3.1 – Manual Segmentation Analysis

Post-acquisition, MR images of the brains of all animal treatment groups were analysed using manual segmentation analysis to assess the changes in regional brain volume over the course of the five week study (figure 7.6A). Unfortunately due to early closure of the Biological Imaging Centre at Imperial College London, the non-lesioned animal group treated with nicotinamide (Lacta(-)NTA(++)) was not scanned. In line with rat growth there was a steady increase in whole brain volume in saline treated non-lesioned animals over the five weeks of examination (figure 7.6B, week 1, 2.09 ± 0.86% increase from baseline; week 3, 4.64 ± 1.33% increase from baseline; week 5, 6.60 ± 1.29% increase from baseline). Similar trends of increase were observed in all other treatment groups. With cerebellum volume, each of the treatment groups displayed an increase in volume over the five weeks of examination (figure 7.6C). However, unlike with whole brain volume, lactacystin-lesioned exhibited a comparatively greater percentage cerebellum volume increase at each of the time points examined compared with non-lesioned animals. These differences reach significance in lactacystin-lesioned saline and nicotinamide (250mg/kg) treated animals at week 5 (lactacystin-lesioned saline, 12.91 ± 1.65% and nicotinamide (250mg/kg) treated animals, 13.01 ± 1.88% change from baseline vs.non-lesioned animals 5.60 ± 2.36% change from baseline, $p<0.01$ and $P<0.05$ respectively). A similar trend is observed in lactacystin-lesioned animals later treated with nicotinamide at its higher dose (500mg/kg) for the first three weeks of study. However between week 3 and 5 of study, a large reduction in cerebellum volume was observed in these animals, reaching significance from the percentage volume increase from baseline of both other lactacystin-lesioned groups at this time point (week 5, lactacystin-lesioned saline, 12.91 ± 1.65% and nicotinamide (250mg/kg) treated animals, 13.01 ± 1.88% change from baseline vs. lactacystin-lesioned nicotinamide (500mg/kg) treated animals, 4.52 ± 2.14% change from baseline, $p<0.01$ and $P<0.05$ respectively).

As expected in the non-lesioned saline treated animals the volume of the lateral ventricles increase compariably in both hemispheres over the 5 weeks of scan acquisition (figure 7.6D). Animals which received an intranigral injection of lactacystin and were subsequently treated with saline exhibited a greater increase in ventricular volume than non-lesioned controls, a change which was more pronounced in the lesioned hemisphere. Neither of these increases however reached statistical significance compared with non-lesioned saline treated animals. Animals treated with nicotinamide however exhibited dose dependent exacerbation of this increase in ipsilateral ventricular volume: the ventricular volume of animals treated with nicotinamide at its highest dose (500mg/kg) reaching significance from non-lesioned animals at week 3 ($p<0.01$), and non-lesioned

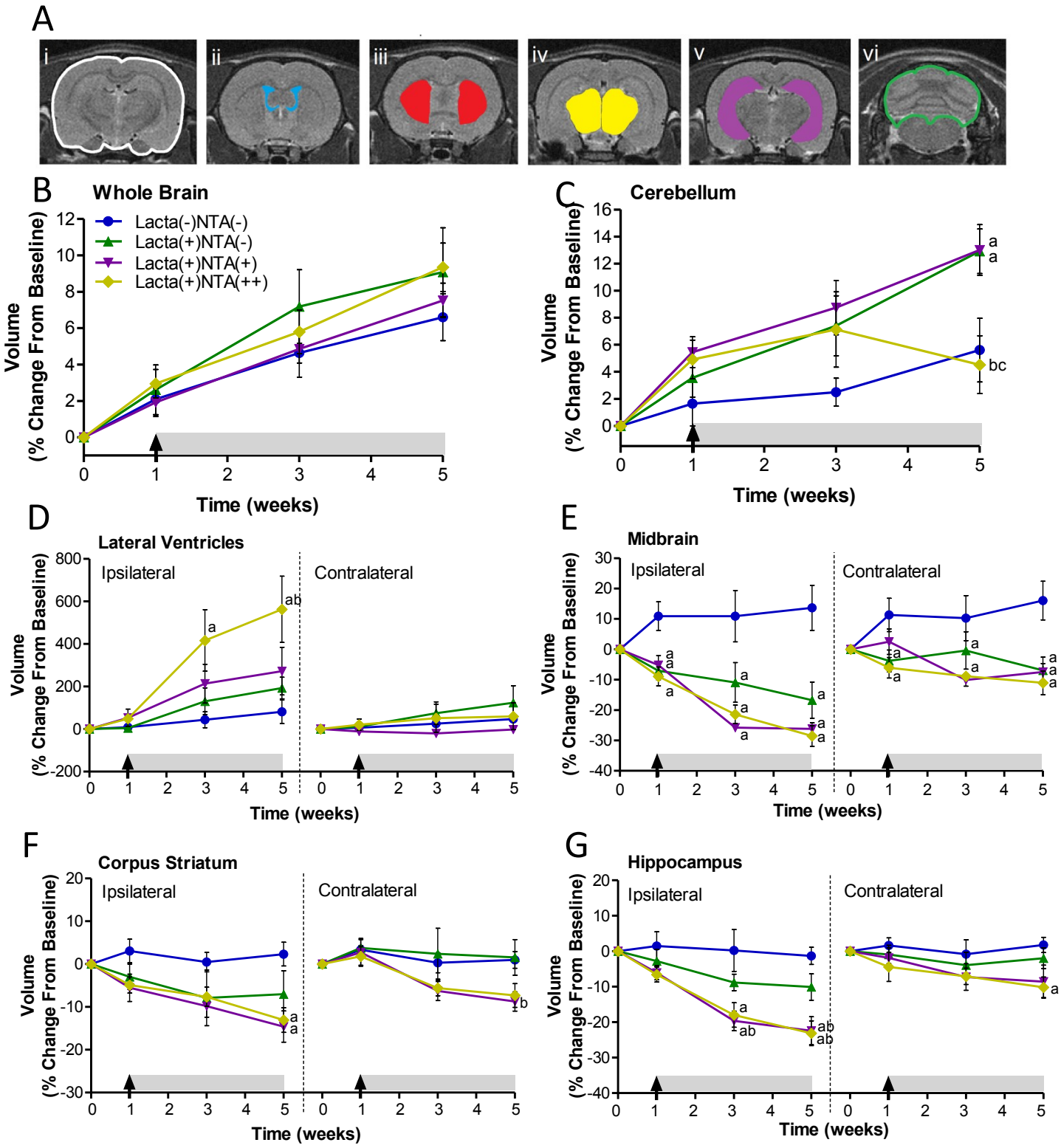

Figure 7.6 – Manual Segmentation Analysis of MR Images Reveals Exacerbation of Lactacystin Induced Volumetric Changes by Nicotinamide

(A) Representative examples of the manual segmentation of (i) whole brain, (ii) lateral ventricles, (iii) corpus striatum, (iv) midbrain, (v) hippocampus and (vi) cerebellum in MR images. Administration of nicotinamide (designated by arrow and grey shading) exacerbates volumetric changes observed in the (D) lateral ventricles, the (E) midbrain, the (F) corpus striatum and the (G) hippocampus as a result of lactacystin lesioning, as ascertained through manual segmentation analysis of rat brain MR images. Administration of nicotinamide and/or lactacystin also have marked effects on (B) whole brain and (C) cerebellum volume. Statistical significance indicated with letters: [a]significantly different from group Lacta(-)NTA(-); [b]significantly different from group Lacta(+)NTA(-); [c]significantly different from group Lacta(+)NTA(+). See text for levels of significance. n=5-7.

and lactacystin-lesioned saline treated animals at week 5 (week 5, non-lesioned and lactacystin-lesioned animals, 81.27 ± 55.50 and 192.93 ± 50.92 respectively vs. lactacystin-lesioned nicotinamide (500mg/kg) treated animals, 537.70 ± 188.71, $p<0.001$ and $p<0.05$ respectively).

The most pronounced changes in regional brain volume took place in the midbrain, the location of the SNpc and therefore the site of stereotaxic injection of lactacystin (figure 7.6E). One week after lesioning surgery, prior to starting vehicle/drug treatment, the ipsilateral midbrain volume of all lactacystin-lesioned animal groups was significantly lower than the volume of the non-lesioned group (lactacystin-lesioned saline, 250mg/kg and 500mg/kg nicotinamide treated animals, 7.07 ± 3.05%, 5.20 ± 3.14% and 8.94 ± 3.11% decrease from baseline respectively vs. 10.88 ± 4.73% increase from baseline in non-lesioned saline treated animals, $p<0.05$ in all comparisons). The ipsilateral midbrain volume of all lactacystin-lesioned saline treated animals continued to decline over the further two time points examined, remaining significantly different from the volume change in non-lesioned animals at both week 3 and 5 ($p<0.01$ and $p<0.001$ respectively). The ipsilateral midbrain volume of lactacystin-lesioned nicotinamide treated (250 and 500mg/kg) animals also decrease with time, however to a far greater extent than lactacystin-lesioned saline treated animals ($p<0.001$ in all comparisons with non-lesioned animals at weeks 3 and 5). Identical albeit more subtle changes are similarly observed upon lactacystin lesioning and nicotinamide treatment in the contralateral hemisphere of the midbrain.

A trend of reduced corpus striatal volume in lactacystin-lesioned animals compared with non-lesioned was observed at week 1, however unlike the ipsilateral midbrain volume at this time points this trend was not statistically significant (lactacystin-lesioned saline, 250mg/kg and 500mg/kg nicotinamide treated animals, 2.96 ± 2.99%, 5.54 ± 3.18% and 4.90 ± 1.89% decrease from baseline vs. 3.07 ± 2.76% increase from baseline in non-lesioned saline treated animals, $p>0.05$ in all comparisons). The volume of this region in lactacystin-lesioned animals continued to decline with time, a reduction in volume which was more pronounced in animals which later received nicotinamide (week 5, lactacystin-lesioned 250mg/kg and 500mg/kg nicotinamide treated animals, 14.59 ± 3.64% and 13.05 ± 2.87% decrease from baseline respectively vs. non-lesioned animals, 2.33 ± 2.77% increase from baseline, $p<0.05$ in both comparisons). Similar albeit more subtle trends were also observed in the contralateral corpus striatum.

Similar changes to those previously discussed in the midbrain and corpus striatum were also observed to occur within the hippocampus. A trend of reduced ipsilateral hippocampal volume in lactacystin-lesioned animals compared with non-lesioned was observed at week 1, however unlike the ipsilateral midbrain and like the ipsilateral corpus striatal volume at this time points these differences were not statistically significant (lactacystin-lesioned saline, 250mg/kg and 500mg/kg

nicotinamide treated animals, 2.78 ± 3.28%, 6.08 ± 1.98% and 6.59 ± 2.13% decrease form baseline vs. 1.47 ± 4.01% increase from baseline in non-lesioned saline treated animals, $p>0.05$ in all comparisons). The volume of this region in lactacystin-lesioned animals continued to decline with time, a reduction in volume which was more pronounced in animals which later received nicotinamide (week 5, lactacystin-lesioned 250mg/kg and 500mg/kg nicotinamide treated animals, 22.42 ± 3.93% and 23.12 ± 3.49% decrease from baseline vs. non-lesioned animals, 1.30 ± 2.41% decrease from baseline, $p<0.001$ in both comparisons). Similar albeit more subtle trends were also observed in the contralateral hippocampus.

7.4.3.2 – T_2 Relaxivity Measurement

In conjunction with manual segmentation analysis, at each of the time points examined, inter-hemispheric differences in T_2 signal intensity were assessed in the SNpc, the midbrain and the corpus striatum. For each brain region, the T_2 signal intensity ratio (ipsilateral divided by contralateral T_2 signal) was then calculated as a measure of interhemispheric difference (figure 7.7). The most marked changes in T_2 relaxivity occurred within the SNpc (figure 7.7A). As expected there were no discernable alterations in T_2 signal intensity ratio in the SNpc of non-lesioned animals treated with saline throughout the five weeks of study. However in all groups lesioned with lactacystin, seven days post-surgery there was a significant increase in T_2 signal intensity ratio compared with the signal in both non-lesioned groups (mean T_2 signal intensity ratio in lactacystin-lesioned animals, 1.048 ± 0.011 vs. non-lesioned animals, 1.00 ± 0.016, $p<0.05$ in all comparisons). In animals subsequently treated with saline this increase in T_2 signal intensity ratio was reversed by week three and continued to decline, becoming significantly different from non-lesioned animals at week five (lactacystin-lesioned , saline treated animals, 0.935 ± 0.012 vs. non-lesioned , saline treated animals, 0.999 ± 0.012, $p<0.001$ comparisons). Lactacystin-lesioned animals subsequently treated with nicotinamide (both 250mg/kg and 500mg/kg) also exhibited this reversal in T_2 signal intensity ratio at week three and decline at week five. Notably the reduction in T_2 signal intensity ratio was even greater in animals treated with nicotinamide at its highest dose (500mg/kg), resulting in a significant difference from both non-lesioned animals and lactacystin lesioned animals subsequently treated with saline at week 5 (week 5, lactacystin-lesioned nicotinamide (500mg/kg) treated animals, 0.896 ± 0.008 vs. lactacystin-lesioned saline treated animals , 0.935 ± 0.012 and non-lesioned saline treated animals, 0.999 ± 0.012, $p<0.05$ and $p<0.001$ respectively). Subtle changes were also observed in the midbrain mimicking those seen in the SNpc (figure 7.7C). However due to the subtlety of these alterations no significant differences were observed. No noticeable alterations in T_2 signal intensity ratio were observed in the corpus striatum (figure 7.7E).

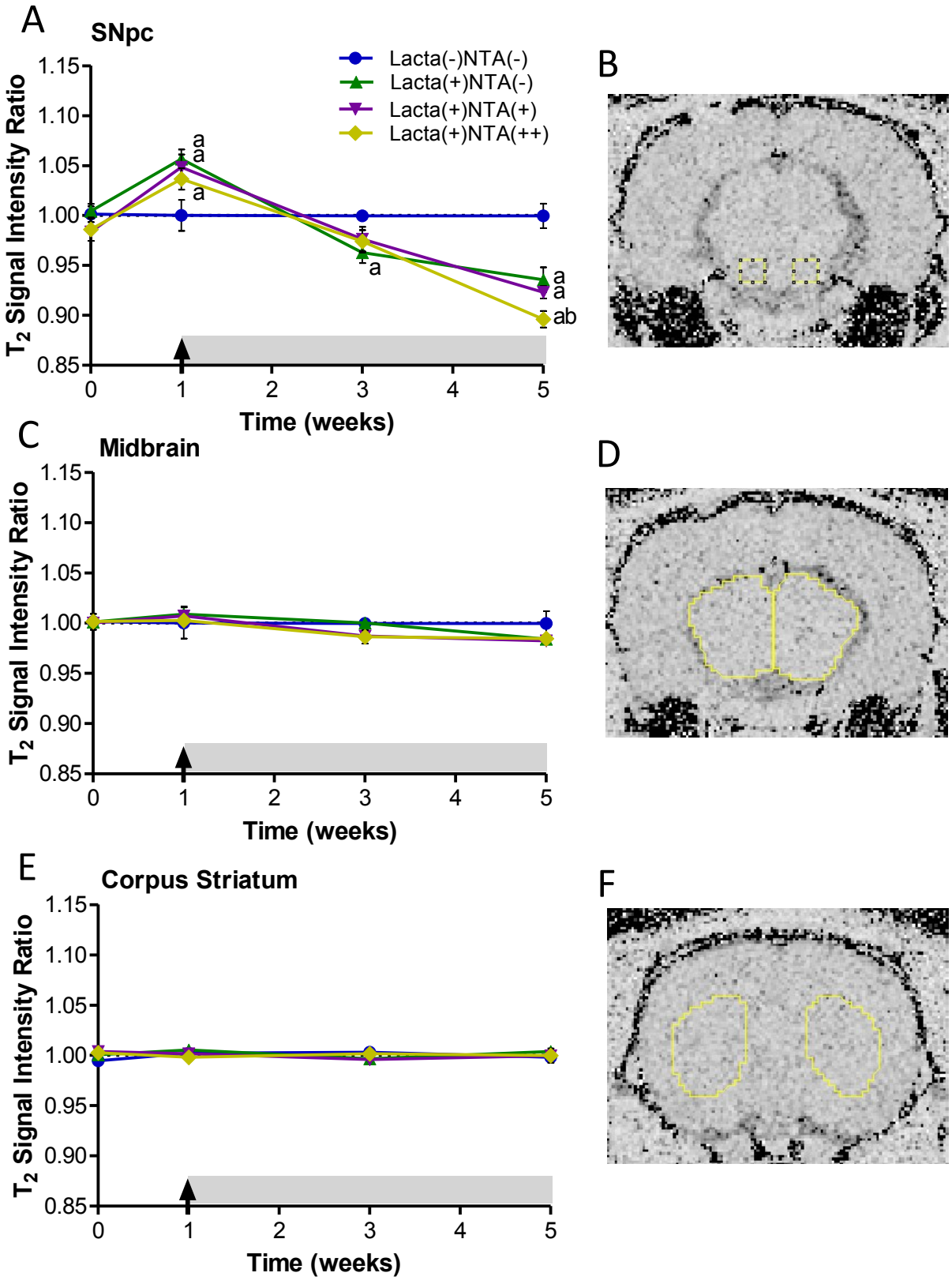

Figure 7.7 – T_2 Signal Intensity Analyses Reveal Exacerbation of Lactacystin Induced Changes by Nicotinamide

T_2 signal intensity measurements were made from T_2 relaxivity maps in the ipsilateral and contralateral (B) SNpc, (D) midbrain, and (F) corpus striatum. Data was then expressed as the ratio between the ipsilateral and contralateral hemisphere: the T_2 signal intensity ratio. Graphs show T_2 signal intensity ratio between the ipsilateral and contralateral hemispheres over time in the (A) SNpc, (C) midbrain and (E) corpus striatum. Statistical significance indicated with letters: [a]significantly different from group Lacta(-)NTA(-); [b]significantly different from group Lacta(+)NTA(-). n=5-7.

7.4.4 – Detrimental Effects of Delayed Start Nicotinamide Treatment on Dopaminergic Neurons in the SNpc in the Lactacystin Rat Model of PD

Animals were sacrificed at week five of the study and hind brain tissue collected for immunohistochemical staining and stereological counting of dopaminergic (TH+) neurons in the SNpc (figures 7.8 and 7.9). Non-lesioned animals treated with saline did not show any interhemispheric loss of TH+ dopaminergic neurons of the SNpc (left SNpc, 11724 ± 729 vs. right SNpc, 11652 ± 493 TH+ cells). Similarly no difference was observed in the number of TH+ dopaminergic neurons in the left and right hemispheres of the SNpc in non-lesioned animals subsequently treated with nicotinamide (500mg/kg) (left SNpc, 11706 ± 1716 vs. right SNpc, 12154 ± 1255 TH+ cells). Animals lesioned with lactacystin and treated with saline however exhibited a marked interhemispheric loss of TH+ neurons due to the intranigral injection of lactacystin (left SNpc, 4257 ± 1364 vs. right SNpc, 12328 ± 580 TH+ cells, % difference -53.81 ± 14.32%, $p<0.01$). Lactacystin-lesioned animals subsequently treated with the high dose of nicotinamide (500mg/kg) did not result in any neuroprotection against lactacystin toxicity of TH+ cells (left SNpc, 2551 ± 529 vs. right SNpc, 13402 ± 922 TH+ cells, % difference -81.40 ± 3.35%, $p<0.001$). Similarly, unexpectedly, lactacystin-lesioned animals treated with the low dose of nicotinamide (250mg/kg) did not result in any neuroprotection against lactacystin toxicity of TH+ cells (left SNpc, 3694 ± 1813 vs. right SNpc, 12177 ± 1246 TH+ cells, % difference -85.41 ± 4.22%, $p<0.01$). These changes observed in SNpc TH+ cell number were also similarly observed in the numbers of Nissl+ cell number, indicative of TH+ neuronal cell death rather than loss of the TH enzyme expression in dying neurons.

7.4.5 – Effects of Delayed Start Nicotinamide Treatment on Brain Histone Acetylation Level in the Lactacystin Rat Model of PD

Upon removal of brain tissue at the end of the study the frontal brain was snap frozen for subsequent quantification of histone protein H3 acetylated on lysine 9 (AcH3-Lys9) using Western blot analysis (figure 6.11). Significantly less AcH3-Lys9 was observed in both hemispheres of animals lesioned with lactacystin and treated daily with saline (ipsilateral and contralateral hemispheres, 2.97 ± 4.05% and 21.05 ± 7.00% of control non-lesioned animals respectively, $p<0.001$ and $p<0.05$). However, in animals subsequently treated with nicotinamide, both at its lower and higher dose, a more than doubling of the amount of AcH3-Lys9 was observed in both hemispheres (low dose (250mg/kg) nicotinamide treated animals, 233.62 ± 23.85% and 220.20 ± 46.34%, and high dose (500mg/kg) nicotinamide treated animals 242.01 ± 18.00% and 259.85 39.50% of control non-lesioned animals respectively, $p<0.001$ compared with lactacystin-lesioned saline treated animals in

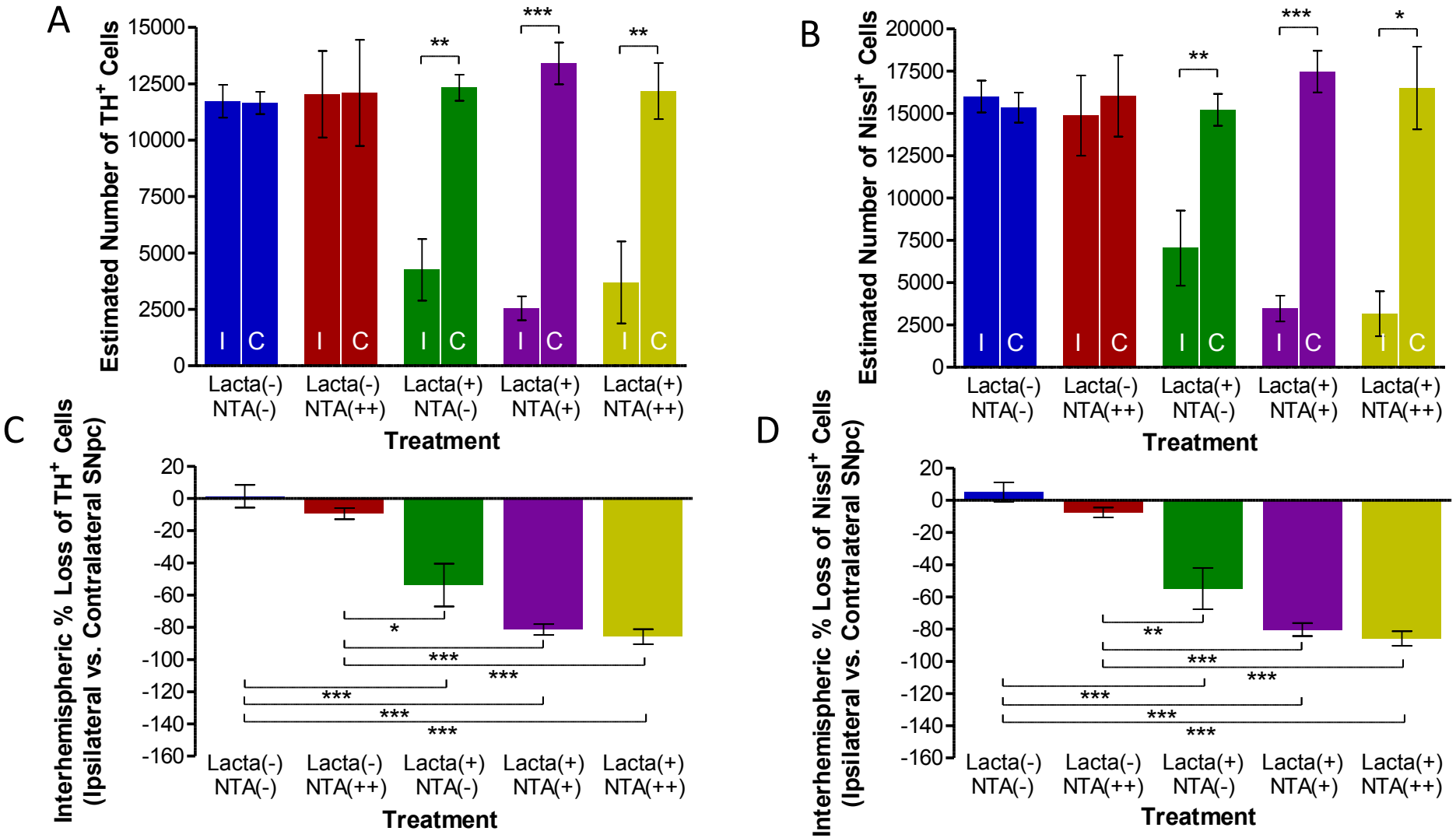

Figure 7.8 – Delayed Start Nicotinamide Treatment Exacerbates Lactacystin Induced Dopaminergic Neurodegeneration in the SNpc in the Lactacystin Rat Model of PD
Stereologically estimated (A) TH+ and (B) Nissl+ neuron numbers in the SNpc of rats suggest exacerbation of dopaminergic neurodegeneration by nicotinamide in this lactacystin rat model of Parkinson's disease. This is exemplified by the percentage interhemispheric loss of TH+ (C) and Nissl+ (D) neurons calculated between hemispheres of the SNpc. Statistical significance indicated with asterisks: *p<0.05; **p<0.01, ***p<0.001. n=5-7. Abbreviations: I, ipsilateral; C, contralateral.

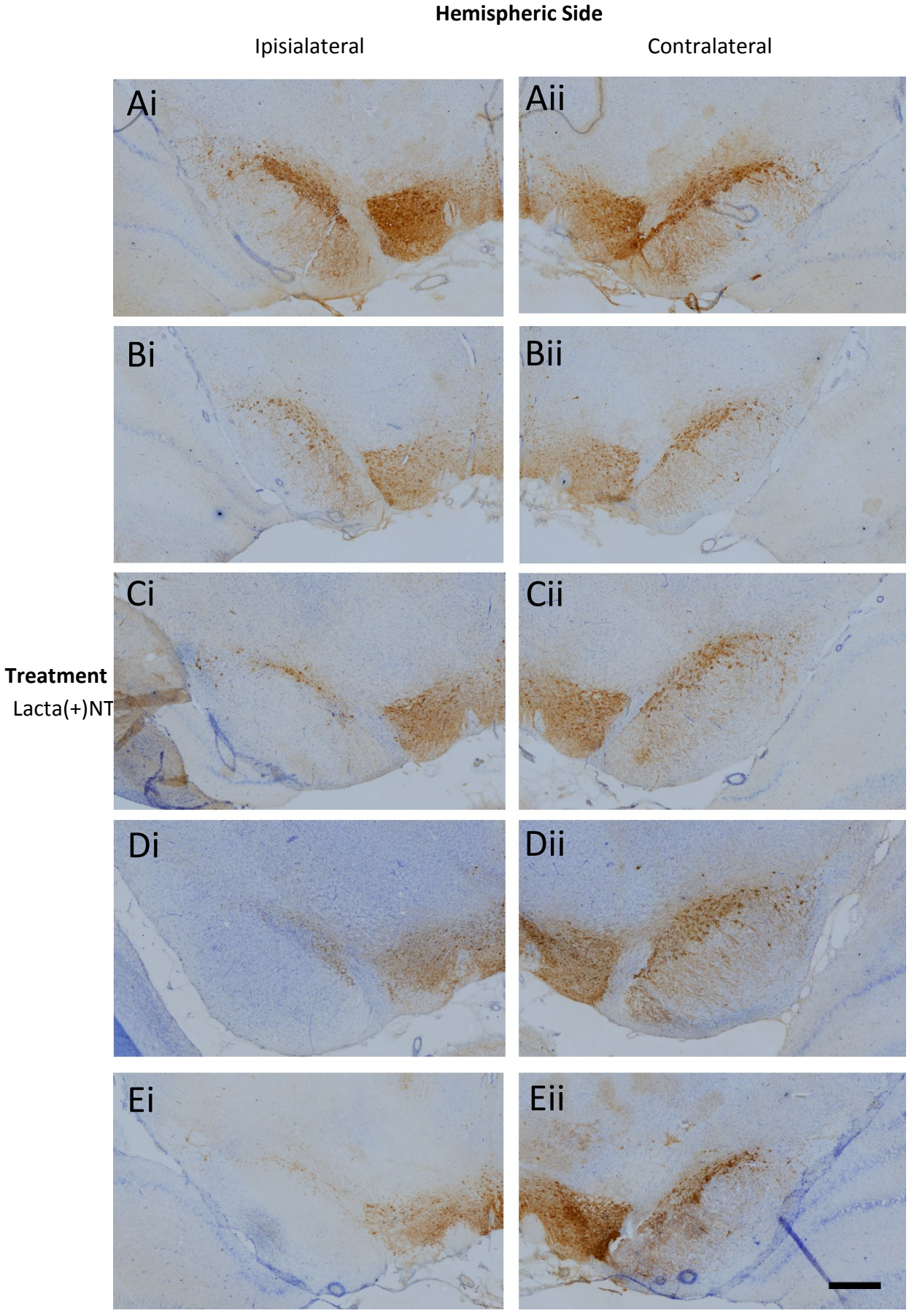

Figure 7.9 – Immunohistochemical Staining of TH+ Neurons in the SNpc of Animal Treatment Groups
Representative examples of the TH and Nissl stained ipsilateral (A-E) and contralateral (A'-E') SNpc of rats in each of the five treatment groups. Scale bar equal to 500µm.

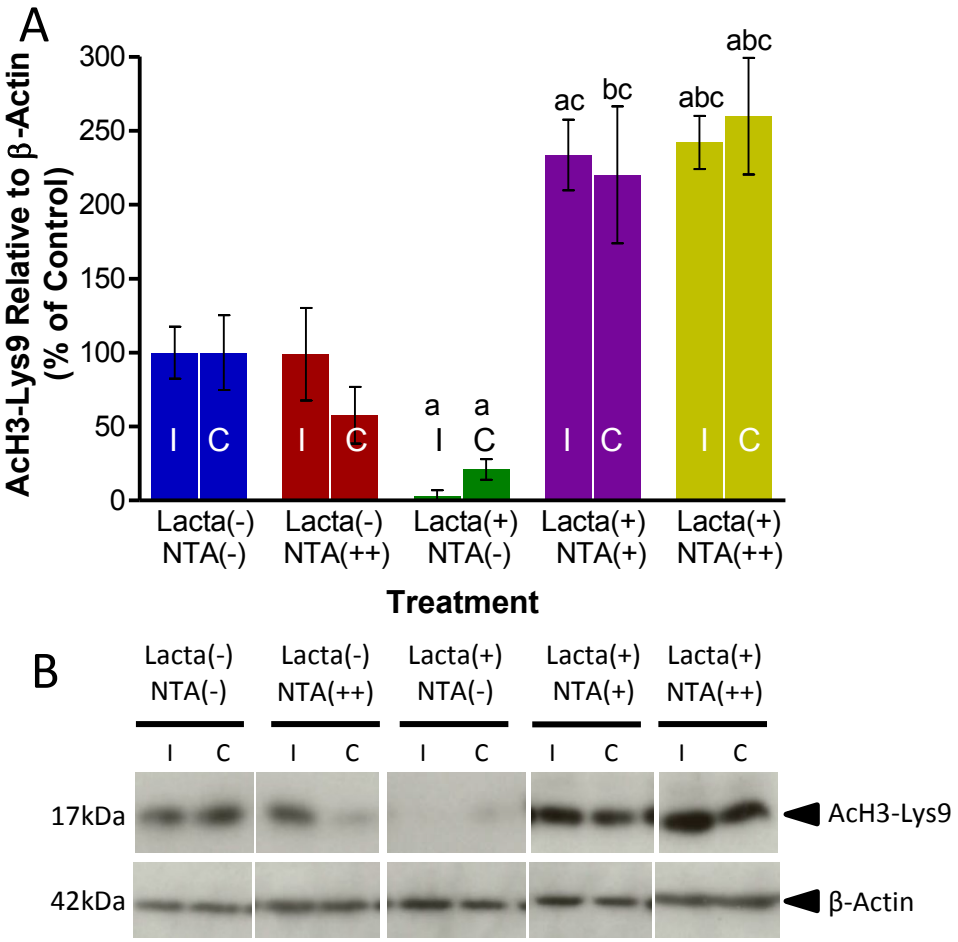

Figure 7.10 – Delayed Nicotinamide Treatment Causes Reversal of Lactacystin Induced Histone Hypoacetylation

Administration of delayed nicotinamide treatment causes reversal of the reduction in histone acetylation observed as a result of lactacystin lesioning. (A) Densitometry analysis of the AcH3-Lys9 band relative to the β-actin band used as a loading control. Statistical significance from corresponding hemisphere indicated with letters: [a]significantly different from group Lacta(-)NTA(-); [b]significantly different from group Lacta(-)NTA(++), [c]significantly different from group Lacta(+)NTA(-). See text for levels of significance. (B) Representative blot of data presented in (A). n=5-7. Abbreviations: I, ipsilateral; C, contralateral.

each comparison). Although a slight reduction was observed in the contralateral hemispheres, no significant differences in the amount of AcH3-Lys9 in either hemisphere was observed in non-lesioned animals treated with nicotinamide compared with control.

7.4.6 - Effects of Delayed Start Nicotinamide Treatment on Brain Neuroprotective Gene Expression in the Lactacystin Rat Model of PD

qRT-PCR was performed on frontal brain tissue to quantify the expression of a number of different neurotrophic factors, apoptotic regulators and genes of interest previously shown to change upon treatment with HDACIs (Monti et al., 2009), to help elucidate action of nicotinamide in the brain. In non-lesioned animals, administration of nicotinamide induced slight reductions in the expression of both GDNF and the anti-apoptotic factor, Bcl-2, however neither of these changes were significant. Nicotinamide did not overtly affect the expression of other genes in these non-lesioned animals. However, in lactacystin-lesioned animals, nicotinamide administration significantly and dose dependently upregulated expression of αSyn, GDNF, GSN, and Bcl-2 in the frontal brain hemisphere both ipsilateral and contralateral to the lactacystin-lesion. Most notably GDNF expression was expressed greater in both hemispheres in animals treated with the low (250mg/kg) dose of nicotinamide (ipsilateral and contralateral hemisphere expression, 3.46 ± 1.32 and 2.57 ± 1.41 fold change from saline treated animals respectively). Consistently, GDNF expression was even greater in the brains of animals treated with the high (500mg/kg) dose of nicotinamide (ipsilateral and contralateral hemisphere expression, 7.79 ± 2.92 and 8.18 ± 3.32 fold change from saline treated animals respectively, $p<0.05$ in both comparisons with corresponding lesioned in saline treated animals). Similar albeit more subtle dose dependent changes were also observed the expression of BDNF, Hsp70 and the pro-apoptotic factor, Bad. However these did not reach statistical significance.

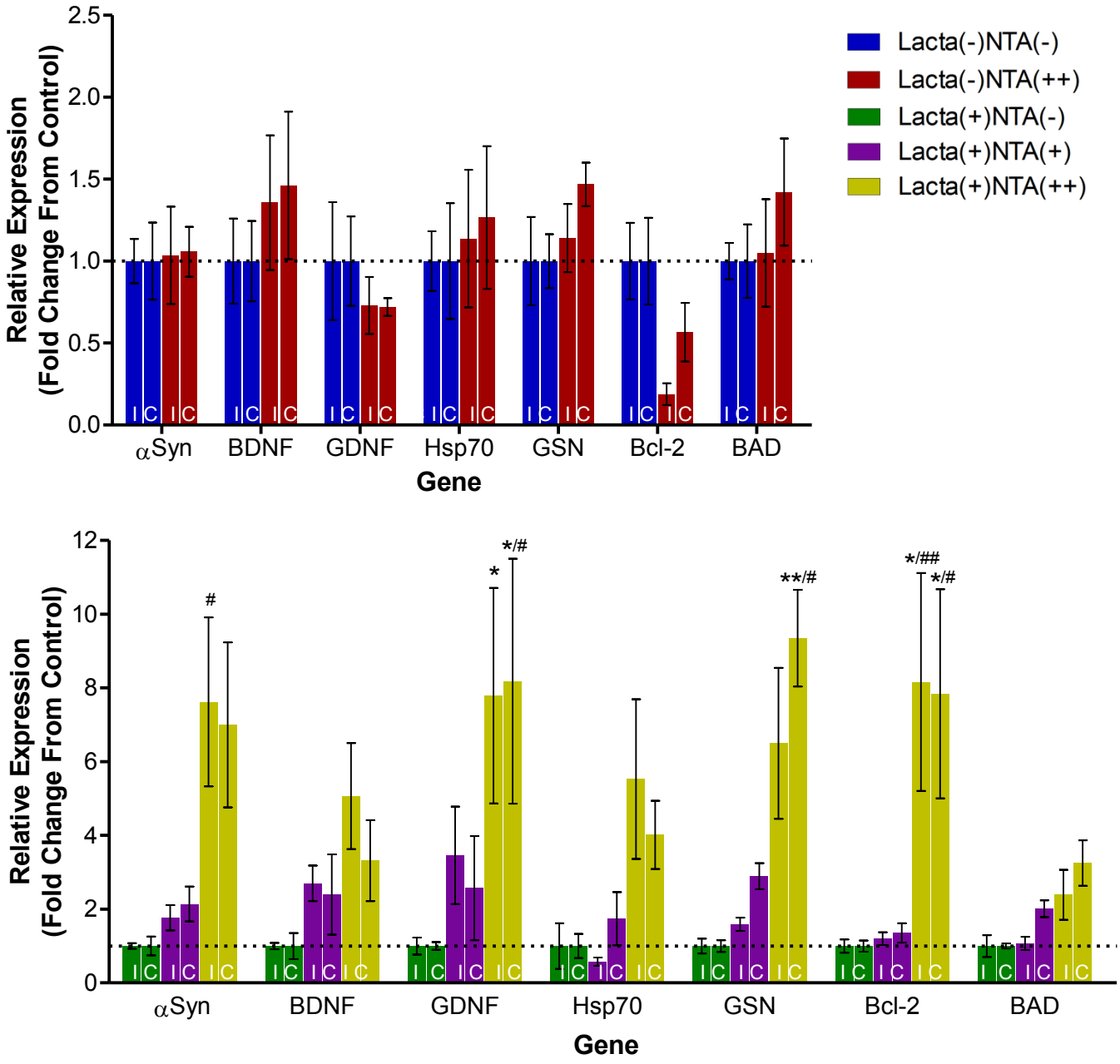

Figure 7.11 - Nicotinamide Upregulates Expression of Neurotrophic Growth Factors and Neuroprotective Proteins

(A) Administration of systemic nicotinamide alone, in non-lesioned rats causes subtle downregulation of GDNF and Bcl-2. (B) In lactacystin-lesioned animals nicotinamide dose dependently up regulated unilateral expression of αSyn, BDNF, GDNF, Hsp70, GSN, BCL-2 and Bad. Statistical significance indicated with asterisks and hashes: *p<0.05, **p<0.01, ***p<0.001 compared with the corresponding hemisphere of saline treated group; #p<0.05, ##p<0.01, ###p<0.001 compared with the same hemisphere of Lacta(+)NTA(+). n=5-7. Abbreviations: I, ipsilateral; C, contralateral.

7.5 – Discussion

In the previous chapter it was demonstrated that valproate, when administered daily for 28days starting from seven days post lactacystin-lesion, dose dependently afforded neuroprotection and neurorestoration in the lactacystin rat model of PD as evidenced by an attenuation of motor behavioural deficits, longitudinal MRI brain volume changes and quantification of the dopaminergic neurons within the SNpc. Molecular analyses of brain extracts indicated that valproate's neuroprotective/neuroregenerative effects may be at least part mediated through epigenetic changes via the inhibition of histone deacetylation to cause chromatin remodelling and upregulation of numerous neurotrophic and neuroprotective genes culminating in the observed phenotype. This was not the case with nicotinamide when administered using the same regime in the same model. At higher doses nicotinamide caused significant worsening of performance in motor behavioural tests. Nicotinamide administration also caused marked worsening of lactacystin induced nigral dopaminergic neurodegeneration as well as worsening of the morphological changes detected in the animal model through MRI. On a molecular level however, nicotinamide reversed lactacystin induced histone hypoacetylation, resulting in extensive histone hyperacetylation in nicotinamide treated animal brains translating to large upregulations of numerous neuroprotective and neurotrophic genes. Such changes however did not translate to neuroprotection. These finidings not only highlight the differential effects of HDAC class inhibition on neuroprotection *in vivo* but also highlight the possibility of valproate's other non-HDAC effects given the comparable changes in neurotrophic gene expression and differential extents of neuroprotection observed between these two drug treatments. Careful interpretation of these results and comparison to previously published similar datasets will help to understand how and why, nicotinamide, a HDACI which held such promise for neuroprotection did not translate to positive findings *in vivo* in this animal model of PD.

Nicotinamide has received increased interest in neurodegenerative disease research in recent years due to it being previously shown to improve neurological outcome and reduce infarct volume in models of stroke (Ayoub et al., 1999, Liu et al., 2009, Mokudai et al., 2000), restore cognitive function in transgenic models of AD (Green et al., 2008), and improve motor deficits and upregulate neurotrophic factors in models of HD (Hathorn et al., 2011). Additionally, in contrast to the results observed here, nicotinamide has also previously been shown to act neuroprotectively in animal models of PD (Anderson et al., 2006, 2008). Upon administration of nictotinamide peripherally prior to MPTP injection, a dose dependent neuroprotective profile was observed in the 'acute' MPTP (four injections in 1 day at 2hr intervals) but not in the 'sub-acute' model (two injections per day at 4hr intervals for 5 days). The highest dose of nicotinamide was still shown to be neuroprotective in this latter 'sub-acute' model however not to the same degree as was seen in the

'acute' model (Anderson et al., 2006, 2008). Authors suggest that this is a result of nicotinamide interacting directly with the specific mechanism of cell death operating in the two different models (Anderson et al., 2008). However, Anderson et al fail to elucidate the mechanism of cell death in each of the models. Similarly, the focus of their paper is not on the HDAC inhibition by nicotinamide hence they do not correlate the extent of neuroprotection with histone acetylation in any way. Therefore, it is impossible to say whether the neuroprotective effects observed are in any way a result of nicotinamide's HDAC inhibition. Regardless, nicotinamide at higher concentrations, appears to be neuroprotective towards dopaminergic neurons in the MPTP mouse model of PD. This finding is in direct contrast to those shown here in which the same dose of nicotinamide (500mg/kg) was shown to markedly exacerbate lactacystin induced nigral dopaminergic neurodegeneration as ascertained through stereological estimation of nigral cell number. A key difference between the designs of these two studies however is the frequency and duration of drug administration. Both studies by Anderson and colleagues (2006, 2008) administer nicotinamide subcutaneously either twice daily at 4hr intervals for five days, or four times daily at 2hr intervals for one day. In the current study however nicotinamide was administered intraperitonealy once daily for 28days. Despite it alterations in histone acetylation and neurotrophic gene expression with the dosing schecule used here, it may be likely then that neuroprotection and alleviation of behavioural deficits would only be observed in the current model if acute or lower treatment doses of nicotinamide were administered: continued chronic administration of nicotinamide exacerbating lactacystin induced dopaminergic neurodegeneration in this model. Respectively, unlike the higher dose of nicotinamide (500mg/kg) administered here, upon treatment with 250mg/kg nicotinamide, animals did not exhibit any worsening of performance in motor behavioural tests. Likewise, consistent with stereological quantification of dopaminergic nigral neurons, animals administered 500mg/kg nicotinamide perform significantly more rotations upon amphetamine challenge and have significantly reduced contralateral forelimb use compared with saline treated animals after 28days of nicotinamide treatment.

On the other hand, nicotinamide is a precursor of NAD+ and is therefore thought to be involved with brain energy metabolism and preservation of mitochondrial functionality. Bioenergetics are becoming an increasingly attractive prospect for neuroprotection in PD (Beal, 2003). Correspondingly nicotinamide has previously been observed to prevent oxidative mitochondrial dysfunction in a model of PD (Jia et al., 2008). The only other studies investigating the neuroprotective effects nicotinamide in animal models of PD all use MPTP to model dopaminergic neurodgeeration (Anderson et al., 2006, Anderson et al., 2008, Xu et al., 2012). This toxin works by inhibiting mitochondrial complex 1 to cause mitochondrial dysfunction and energy starvation in

dopaminergic neurons. It is likely then that nicotinamide, in the MPTP model, would directly counteract the effects of this mitochondrial toxin due to its effects on bioenergetics. Data presented here however demonstrate that despite the upregulation of neuroprotective factors in the lactacystin model, nicotinamide is incapable of counteracting the pathogenesis induced as a result of this toxin, i.e. accumulation of altered proteins in the SNpc.

Manual segmentation analysis of MR images was performed here to examine the temporal morphological progression of selected brain regions in the model, and in line with previously published data following nigrostriatal neuropathology induced as a result of stereotaxic injection of lactacystin to the SNpc (Vernon and Modo, 2011), in the current study a marked reduction in the volume of the ipsilateral midbrain in the weeks following stereotaxic surgery was observed. Similarly an increase in the volume of the lateral ventricles was observed, which was far more pronounced in the ipsilateral as opposed to the contralateral hemisphere. Consistent with nicotinamide's exacerbation of the effects of lactacystin lesioning in the SNpc as ascertained through stereological quantification of dopaminergic neurons, both of these MRI detected changes were observed to be dose dependently exacerbated by delayed nicotinamide treatment. In saline treated animals, lactacystin-lesioning was also observed to produce non-significant reductions in ipsilateral corpus striatal and hippocampal volume. These reductions were similarly observed to be exacerbated upon nicotinamide treatment. Moreover, nicotinamide at its higher dose (500mg/kg) was observed to induce caudal progression of lactacystin induced pathology: a significant reduction in cerebellar volume being observed after 28 days of nicotinamide treatment. From these data it is therefore evident that nicotinamide's effects on the brain are not simply restricted to the worsening of pathology at the location of toxin administration, but brain wide, exacerbating even areas of subtle lactacystin induced change.

In conjunction with volumetric analysis to monitor morphological progression and nigrostriatal neuropathology in this model, T_2 signal intensity analysis was also used to follow asymmetry in T_2 signal intensity in the SNpc, midbrain and corpus striatum. Consistent with previous studies using the lactacystin rat model (Vernon et al., 2010), changes in T_2 signal intensity ratio were observed in the SNpc and to a lesser extent the midbrain, but not in the striatum. One week following lesioning, an increase in T_2 signal intensity was observed in the SNpc of all lactacystin-lesioned animal groups consistent with findings in the 6-OHDA rodent model (Kondoh et al., 2005) and the MPTP primate model (Miletich et al., 1994), indicative of acute inflammatory oedema in the area of interest given its appearance in nigrostriatally lesioned animals alone and its dissipation with time. This increase in the SNpc is reversed at weeks three and five in lactacystin-lesioned animals likely due to the combination of cell death and iron accumulation in the area creating

inhomogeneities in magnetic field, which diphase nearby water protons leading to shortening of T_2 and lowering T_2 signal intensity. Several studies note the accumulation of iron in the SNpc of PD patients (Dexter et al., 1989b, Brar et al., 2009, Gorell et al., 1995, Kosta et al., 2006, Martin et al., 2008) and a number of studies also note the accumulation of iron in the SNpc of the lactacystin rat model (Vernon et al., 2010, Zhu et al., 2007). Consistent with previously discussed MRI findings, the reversal of this lowering of T_2 signal intensity ratio in the current study was dose dependent upon nicotinamide treatment, indicative that nicotinamide may not only be exacerbating cell death and neurodegeneration within the SNpc but also increasing iron deposition within the area as well.

Addition of an acetyl group to histone lysine residues neutralises the positive charge of the residue and hence reduces the electrostatic interaction between the lysine in the histone tail and the negatively charged phosphate group on DNA. This disrupts the inter- and intra-nucleosomal interactions between the histone and DNA and hence relaxes the structure of the chromatin allowing transcription factor access. Here, nicotinamide treatment reverses lactacystin induced histone hypoacetylation, resulting in extensive histone hyperacetylation in nicotinamide treated animals. Correspondingly, large dose dependent upregulations of neuroprotective and neurotrophic genes were observed in the brains of nicotinamide treated rats. Unlike in valproate treated animals however, as previously discussed these upregulations do not translate to neuroprotection in the current model. Interestingly however if these gene upregulation were simply a function of nicotinamide treatment via HDAC inhibition, similar levels of histone hyperacetylation along with respective gene upregulations would also be expected in non-lesioned nicotinamide treated animals. This is not the case. For that matter if the extensive progressive neuropathology observed in MR images was a result of nicotinamide treatment alone then these changes would also be expected in MR images of non-lesioned nicotinamide treated animals. Unfortunately, due to early closure of the Biological Imaging Centre at Imperial College London, this group of animals was not scanned. Taken together it is most likely that a complex drug x disease interaction is driving the anatomical and molecular and cellular effects of nicotinamide observed.

As has been previously discussed, being a precursor for NAD+, nicotinamide is known to non-selectively inhibit class III HDACs, inhibiting sirtuin1-7 through competition binding to the NAD+ binding site of the sirtuin HDACs (Avalos et al., 2005). There is currently debate within the literature however as to the effects of these sirtuins in neuronal survival and neurodegeneration. For example, sirtuin1 and 5 are known to act neuroprotectively (Pfister et al., 2008, Donmez and Outeiro, 2013, Dobbin et al., 2013), whereas sirtuin2, 3 and 6 are known to be neurotoxic (Pfister et al., 2008). Of the sirtuins, most research conducted in neurodegeneration has centred around sirtuin1 and 2: activation of sirtuin1 and inhibition of sirtuin2 emerging as novel targets for neuroprotection

(Donmez and Outeiro, 2013). Sirtuin1 is known to bind to a number of transcription factors (Donmez, 2012) e.g. NF-κB, p65, retinoic acid receptor β (RARβ), forkhead box (FOXO) family of transcription factors, and most notable to neurodegeneration, peroxisome proliferator-activated receptor gamma coactivator 1α (PGC1α) which has long held therapeutic potential in PD (Zheng et al., 2010). Sirtuin1 activation has subsequently been shown to reduce αSyn aggregation through its upregulation of molecular chaperones (Donmez et al., 2012) and activation, via its deacetylation, of PGC1α maintaining mitochondrial number and function (Austin and St-Pierre, 2012). Upon inhibition of sirtuin1 therefore the opposite occurs: αSyn accumulation due in part to lack of molecular chaperones, accompanied by mitochondrial DNA depletion and subsequent mitochondrial stress. Like sirtuin1, sirtuin2 also interacts with the FOXO family. More specifically sirtuin2 deacetylates FOXO3a which causes upregulation of Bim and subsequently induces caspase-3 activated apoptotic cell death (Liu et al., 2012, erratum in Liu et al., 2013b). Additionally, sirtuin2 is known to regulate αSyn inclusion number, size and cytotoxicity rescuing αSyn toxicity *in vivo* (Outeiro et al., 2007). Upon inhibition then, sirtuin2 is therefore thought to reduce αSyn toxicity and apoptotic cell death. Although nicotinamide is known to non-selectively inhibit the sirtuin class of HDACIs, its IC_{50} values for each of the sirtuins vary greatly. Most notably, nicotinamide's IC_{50} for sirtuin1 is 85.1μM whereas its IC_{50} for sirtuin2 is significantly less, at just 1.1μM (Peck et al., 2010). This may therefore explain the toxic effects of nicotinamide observed in the current study, for example lower doses of nicotinamide may be sufficient to inhibit sirtuin2 and yet also to a lesser degree sirtuin1. Whereas higher doses may be sufficient enough to induce extensive inhibition of sirtuin1 hence the dose dependent toxic effects of this drug in the current study. Data presented here therefore highlights the importance of target specificity within this class of HDACs, given the contrasting effects of its individual isoforms.

7.6 – Conclusions

Utilising a clinically relevant drug testing platform this study demonstrates that nicotinamide's inhibition of the sirtuin HDACs (class III) is dose-dependently neurotoxic in the lactacystin rodent model of PD when administered chronically starting seven days after the toxin administration when behavioural symptoms, MRI changes, microglial activation, dopaminergic cell loss and molecular hallmarks of neurodegeneration in the animal model are already observed. The toxic effects of nicotinamide's sirtuin inhibition are associated with exacerbation of behavioural motor based symptoms, the neuropathological progression of the model as detected through MRI, and nigral dopaminergic neurodegeneration. These changes were accompanied by reversal of lactacystin induced histone hypoacetylation resulting in excessive histone hyperacetylation and an upregulation of neuroprotective and neurotrophic factors. Such upregulations however did not translate to neuroprotection. These findings therefore highlight the importance of target specificity within this class of HDACs and demonstrate the contrasting effects of sirtuin inhibition upon cell survival in this animal model of PD.

Chapter Eight

Discussion

8 – Discussion

8.1 – Summary of Main Findings

By the time the motor based symptoms of PD first arise, 60-70% of dopaminergic nigrostriatal neurons have already degenerated, and around 80% of striatal dopamine is thought to be depleted. First line therapies for PD aim to replace this loss of dopamine signalling, yet these drugs only correct the deficit in dopamine however and such do not return patients to full normal function. Likewise, they do not protect dopaminergic neurons from death and hence are only effective if a responsive population of dopaminergic neurons remains intact in the SNpc to mediate their effects. The effectiveness of dopaminergic therapeutics against non-motor symptoms of the disease, main determinants for deteriorating quality of life and patient care costs, are also very limited and long term use is linked to the development of debilitating side effects such as L-DOPA induced dyskinesias. Hence more novel neuroprotective agents are sought which tackle the degeneration of dopaminergic nigrostriatal directly.

The overall aim of this thesis was to test the hypothesis that histone hypoacetylation and transcriptional dysfunction contribute to the pathological process of neurodegeneration in PD, hence HDAC inhibition is neuroprotective. To assess this hypothesis, the aims set out at the start were to: (1) quantify the level of histone acetylation in degenerating regions on the Parkinsonian brain in relation to healthy age matched controls, and conduct expression profiling of HDAC isoforms in these same brain regions, with the aim of identifying targetable HDAC isoforms for treatment in PD, (2) test the potential of a range of isoform specific and pan-HDACIs at reducing dopaminergic neurodegeneration and microglial activation *in vitro*, with the aim of identifying suitable lead compounds for further investigation *in vivo,* and (3) determine the neuroprotective and behavioural effects of delayed start HDACI treatment in the progressive lactacystin lesion animal model of PD, and attempt to elucidate the mechanism by which HDACI mediated neuroprotection is achieved. In the preceding chapters, these aims have sought to be fulfilled, adding to the current body of knowledge concerning both the pathogenesis of HDACs in PD as well as the potential of the use of HDACIs for the treatment of PD.

Firstly, it was shown here that a number of changes exist in the levels of both histone acetylation and HDAC expression in regions of the Parkinsonian brain. In the midbrain, disease dependent histone acetylation was accompanied by downregulation of a number of HDAC isoforms. However, this was upon a background of marked loss of dopaminergic neurons, hence the expression of HDAC isoforms in surviving neurons may be increased. In the putamen however, histone acetylation in PD remained unchanged from controls, however marked increases in HDAC isoforms unaffected in the midbrain were seen. In the frontal cortex however, reductions in the

expression levels of all the HDAC isoforms quantified here were observed, yet this was accompanied by increased histone acetylation in early stage PD cases, and reduced histone acetylation in late stage PD cases. Data presented here are the first demonstration of histone acetylation and HDAC expression quantification in PD brain.

Secondly, it was shown in cell culture that HDACIs are capable of reducing lactacystin induced neurodegeneration and LPS induced activation of microglia. However, dependent on the class(es) or isoform(s) inhibited, HDACIs vary hugely in their effects as neuroprotectants and their ability to reduce microglial activation, *in vitro*. Disparity between results from neurons and microglia also highlight the possible differing effects of HDAC isoform inhibition on Parkinsonian pathogeneses. From these data, two broad spectrum HDACIs, valproate and nicotinamide, were identified for further investigation *in vivo*, in the lactacystin rat model of PD.

Thirdly, utilising a clinically relevant drug testing platform and an animal model of PD which models the clinical setting in which a neuroprotective agent would be administered, valproate's inhibition of HDAC classes I and IIa was shown to be dose-dependently neuroprotective and neurorestorative when administered chronically starting seven days after toxin administration when behavioural symptoms, MRI changes, microglial activation, dopaminergic cell loss and molecular hallmarks of neurodegeneration in the animal model are already observed. In contrast when nicotinamide, which inhibits the sirtuin class of HDACs (class III), was administered using the same regime in the same model, at higher doses it caused significant worsening of performance in motor behavioural tests, lactacystin induced nigral dopaminergic neurodegeneration as well as worsening of the morphological changes detected in the animal model through MRI. However, on a molecular level nicotinamide reversed lactacystin induced histone hypoacetylation, resulting in extensive histone hyperacetylation in nicotinamide treated animal brains translating to large upregulations of numerous neuroprotective and neurotrophic genes. Such changes did not translate to neuroprotection.

Taken together, these data highlight the importance of HDAC isoform selection for inhibition, for potential neuroprotection in PD. For the first time it has been shown here that histone hyperacetylation is present in the midbrain in PD despite the presence of marked dopaminergic neuronal loss, rather than histone hypoacetylation which has been previously observed in animal models of neurodegeneration. Cell culture studies of histone acetylation in individual cell types, suggest that this may be a result of microglial infiltration and activation in the midbrain in PD: degenerating dopaminergic neurons display histone hypoacetylation in culture whereas activated microglia displayed histone hyperacetylation. Alteration of expression levels of HDACs in human tissue and cell culture experiments using a variety of targeted HDACIs demonstrate

that HDAC inhibition and neuroprotection/microglial activation are not as simply related as first thought. Likewise treatment of PD animal models with HDACIs targeted to different HDAC classes can produce hugely opposing effects. These findings therefore call for a reappraisal of the putative model of HDACI mediated neuroprotection.

8.2 – Putative Model of HDACI Mediated Neuroprotection

Although, there have been numerous reports of the neuroprotective effects of HDACI in neurodegenerative disease, and more specifically PD, mechanistic studies of their neuroprotection are lacking. However, based on the body of literature examining the varying aspects of HDACI mediated neuroprotection in neurons and the effects HDACIs on astrocytic and microglial culture, a putative model has arisen as to the mechanisms of HDACI mediated neuroprotection in PD. Like PD pathogenesis, it is a multifaceted mechanism of action, affecting astrocytes, microglia and neurons, which are thought to culminate in the neuroprotective phenotype of HDACIs observed in models of PD (figure 8.1).

In neurons, HDACIs are thought to induce both transcriptional and non-transcriptional effects. In the nucleus, the inhibition of HDACs causes a reduction in the deacetylation of lysine residues on histone proteins. Acetylation of histone lysine residues neutralises the positive charge of the residue and hence reduces the electrostatic interaction between the lysine in the histone tail and the negatively charged phosphate group on DNA. This disrupts the inter- and intra-nucleosomal interactions between the histone and DNA and hence relaxes the structure of the chromatin allowing transcription factor access to the DNA and transcriptional activation (Grayson et al., 2010). This has been shown to result in increased expression of numerous growth factors, neurotrophic factors and anti-apoptotic mediators in neurons thought to contribute to reduced neurodegeneration in HDACI treated neurons (Dietz and Casaccia, 2010, Marinova et al., 2009, Chuang et al., 2009, Hahnen et al., 2008, Kazantsev and Thompson, 2008, Saha and Pahan, 2006). In astrocytes, HDACIs are thought to mediate similar transcriptional effects, resulting in transctiptional upregulation of neurotrophic factors such as BDNF and GDNF thought to contribute to HDACI mediated neuroprotection (Chen et al., 2006, Suh et al., 2010, Wu et al., 2008b). Likewise, HDACI are also known to mediate an increase in glutamate uptake, thought to contribute to HDACI mediated neuroprotection by reducing glutamate excitotoxicity in dopaminergic neurons of the SNpc (Wu et al., 2008a). In the cytoplasm of neurons, HDAC inhibition also leads to a reduction in the deacetylation of tubulin, which translates to increased microtubule stabilisation, thought to also contribute to the neuroprotective effects of HDACIs (Dompierre et al., 2007, Esteves et al., 2014, Zhang et al., 2003). In microglia, on the other hand, the mechanism by which reduced activation is achieved is less well understood. However, it has been extensively demonstrated that HDACI cause reduced expression of pro-inflammatory cytokines, reduced release of ROS, as well as reduced activity of NOS resulting in reduced secretion of NO (Peng et al., 2005, Roy et al., 2012, Suh et al., 2010). Taken together, it is thought that the multicellular effects of HDACI collaborate in the production of a neuroprotective phenotype previously demonstrated in animal models of PD.

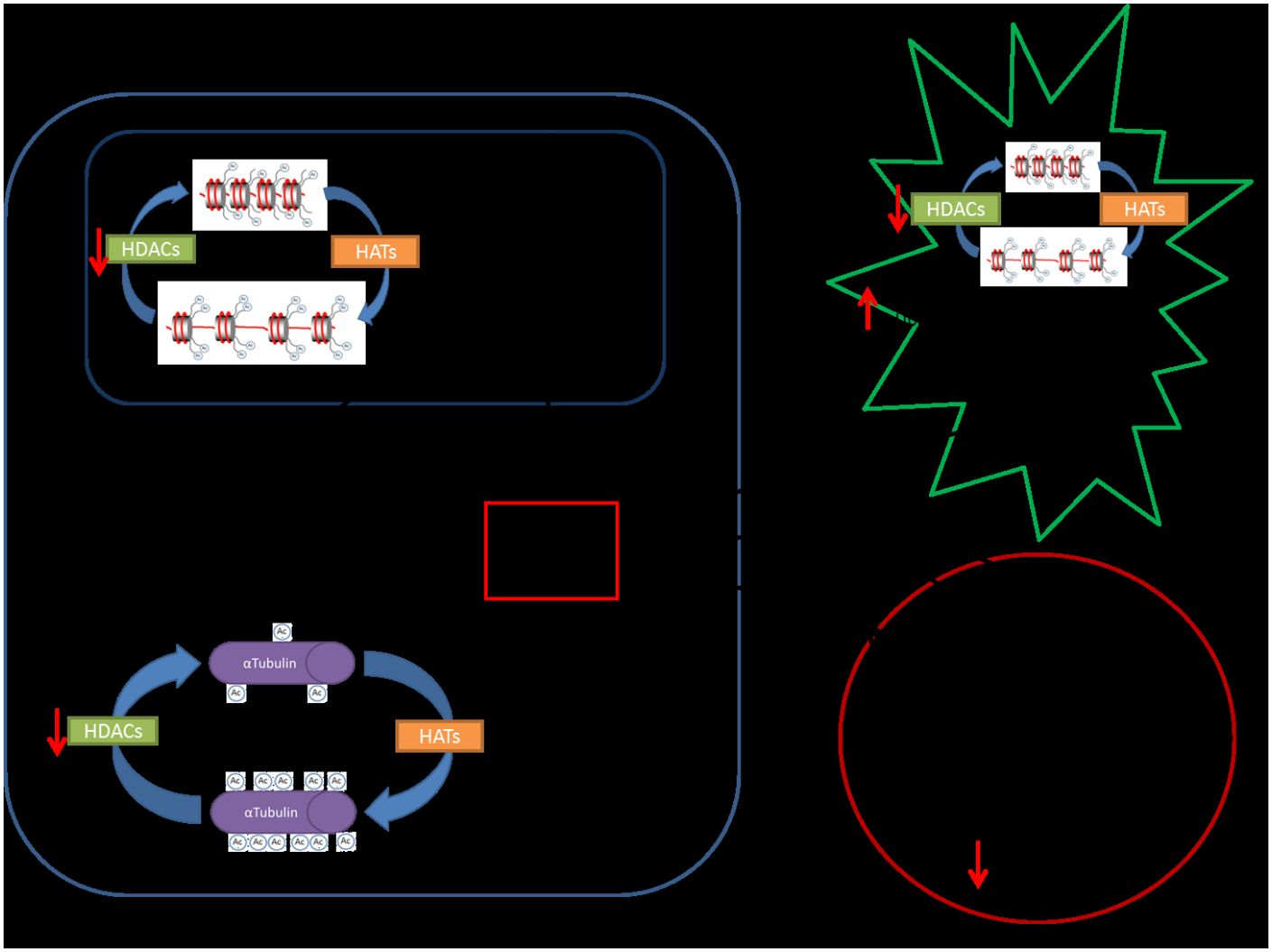

Figure 8.1 – Model of HDACI Mediated Neuroprotection in PD

Schematic of the putative model of HDACI mediated neuroprotection in PD. Effects of HDACIs shown in red. Abbreviations: HDAC, histone deacetylase; HAT, histone acetyl transferase; BDNF, brain derived neurotrophic factor; GDNF, glial derived neurotrophic factor; Hsp70, heat shock protein 70; αSyn, α-Synuclein; Bcl2, B-cell lymphoma 2; ROS, reactive oxygen species; NO, nitric oxide; iNOS, inducible nitric oxide synthase.

Consistent with this putative model of HDACI mediated neuroprotection and the involvement of HDACs and histone acetylation in PD pathogenesis, in this thesis it has been shown that histone deacetylation occurs in degenerating dopaminergic neurons in culture. Additionally, histone acetylation was observed in activated microglial culture, in line with the changes in acetylation observed in the human brain. HDACIs were shown to cause histone acetylation in neuronal cultures, which translated to protection in the absence of either astrocytes or microglia. Likewise, HDACI treatment of microglial cultures has been shown here to reduce the secretion of NO and the pro-inflammatory cytokine TNFα. The effects of HDACIs in individual cell populations observed here were not very dramatic. However, consistent with the putative multicellular mechanism of neuroprotection, the neuroprotective effects *in vivo* were far greater, illustrative of the additive effects of different cell populations, culminating in marked neuroprotection. Both valproate and nicotinamide treatment of animal models resulted in upregulation of numerous neurotrophic factors observed in the brain, including BDNF and GDNF. This resulted in a dose dependent neuroprotection upon treatment with valproate, however these increases did not translate similarly to neuroprotection in nicotinamide treated animals. When taken as a whole the findings in this thesis are in agreement with the putative model of neuroprotection exerted by HDACIs and the involvement of HDACs and histone acetylation in PD pathogenesis. However when consolidated, a number of discrepancies between data sets still exist calling for further investigation and study.

8.3 – Consolidation of Findings

In the studies utilising human post-mortem PD brains in this thesis histone acetylation was observed in the midbrain, contradictory to previously published findings in animal models of neurodegenerative disease (Kontopoulos et al., 2006, Rouaux et al., 2003). However, taken together with *in vitro* data presented here, I would hypothesise that these observations are a result of microglial infiltration in the midbrain of PD brains. In cell culture, it was demonstrated that activated microglia exhibit histone hyperacetylation, hypothesised to be because of their upregulation of and expression of numerous cytokines and inflammatory mediators. Whereas, degenerating neurons, consistent with previously published data, exhibit histone hypoacetylation. This was supported by an upregulation of HLA-DPα in the midbrain of human cases utilised, indicating accumulation of activated microglia in this area. It is therefore thought that any reduction in histone acetylation in degenerating dopaminergic neurons in the midbrain would therefore be diluted by the opposing effects of histone hyperacetylation observed in resident activated microglia. Likewise, as would be expected in the SNpc in the midbrain, post-mortem studies demonstrated that there is a disease dependent reduction of TH in this region, exacerbating this 'dilution' effect even further.

The opposing histone acetylation status of degenerating neurons and activated microglia become even more apparent in cell culture experiments given the disparity between HDACI compound effects on neuronal survival and microglial activation. Some compounds, for example ICL-SIRT078 exhibit both neuroprotection in dopaminergic neuronal cultures and reduction of LPS induced activation of microglial cultures. Whereas others, for example butyrate, exhibit marked effects on neuronal cultures but demonstrate very little effect on microglial cells. The opposite is also demonstrated with the use of other HDACIs. As discussed previously, the mechanism of HDACI mediated reduction in microglial activation is poorly understood. However, these results suggest that inhibition of different HDAC isoforms can have markedly different effects on neurons and microglia. It remains unanswered however as to why inhibition of certain classes, such as sirtuin2, affect both neurons and glia equally. The differences in cell biology between these cells types could easily account for the observed difference, however the effects of HDAC inhibition on downstream pathways in such cell systems should be elucidated, if only to better understand the mechanism by which neuroprotection and microglial activation reduction are achieved. Additionally, the putative mechanism of neuroprotection by HDACIs is thought to be achieved by the combined effects of both neurons and glia. Further study to identify the specific isoforms which when inhibited exerts effects on both neurons and glia, should provide a greater magnitude of neuroprotection through their additive effects.

From the human studies it was interestingly observed that each of the HDACs isoforms become perturbed in either the midbrain or the putamen, but rarely both simultaneous. However, it is hypothesised that due to the expected degeneration of dopaminergic terminals in the putamen, the changes observed in this region are probably due to the change in HDAC expression profile of target neurons in this nucleus. These target neurons are likely to induce a compensatory mechanism for their loss of innervation. This could therefore explain the changes observed here. Of note, only two of the HDACs examined were shown to present changes in both of these brain regions: HDAC6 and sirtuin2, prioritising them for targeting in subsequent cell culture experiments. A specific inhibitor of HDAC6 is yet to be discovered, however in cell culture the use of trichostatin A, an inhibitor of HDAC classes I, IIa and IIb, HDAC6 inclusive was not observed to produce any marked neuroprotection or reduction of microglial activation. In contrast sirtuin2 inhibition, via AGK2 or ICL-SIRT078, produced both marked neuroprotection and reduction of microglial activation in the cell culture systems examined. These findings again highlight the apparent complex nature of HDACs in neurodegeneration, it being evident that not all targets identified from human studies present viable targets for therapeutic inhibition.

In the current thesis, HDAC class I and IIa inhibition by valproate was shown to result in in significant neuroprotection and alleviation of behavioural deficits in the lactacystin rat model of PD. In cell culture however, valproate was observed to exert only subtle effects on both neuronal and microglial cultures. The difference in the magnitude of effect shown between these studies *in vitro* and *in vivo* could firstly be attributed to the additive effects of valproate on neurons and microglia *in vivo*. Likewise, consistent with the model of HDACI mediated neuroprotection put forward previously, it has also been observed that valproate exerts effects on astrocytes too, such as upregulation of neurotrophic factors and increase of glutamate uptake (Chen et al., 2006, Suh et al., 2010, Wu et al., 2008b). It is therefore suggested that the extent of neuroprotection observed upon valproate treatment in this animal model of PD is therefore a combined effects of HDAC inhibition in each of these brain cells types. Additionally however due to its current use in the clinic for the treatment of seizures, valproate is known to have multiple other effects on the brain, including effects on GSK-3, Akt/ERK pathways, GABA/Glutamate neurotransmission, Na+ and Ca2+ voltage-dependent channels, phosphoinositol/TCA pathways and the oxidative phosphorylation pathway (Ximenes et al., 2012). A number of these affects too could contribute valproate neuroprotective phenotype observed here. Likewise, outside of its effects on brain cell populations, valproate could too affect the activity of regulatory T cells given the recent discovery that inhibition of HDAC class I leads to induction of this cell population, thought to be a result of acetylation of the transcription factor FOXP3, a key regulator of the development and function of regulatory T cells (Shen and Pili,

2012, Wang et al., 2009, Tao et al., 2007, Reddy and Zou, 2007). Regulatory T cells themselves have become recently implicated in neurodegenerative disease due to their implication in suppressing autoimmunity in the brain, i.e. the pathogenic activation of microglia in PD (He and Balling, 2013, Gendelman and Appel, 2011). Likewise, adoptive transfer of regulatory T cells has been shown to be neuroprotective in animal models of PD (Reynolds et al., 2007, Reynolds et al., 2010). In the valproate study I have carried out, valproate's inhibition of class I HDACs could also induces regulatory T cells in lactacystin lesioned animals, adding to the neuroprotective effects exerted by the putative model of HDACI mediated neuroprotection discussed earlier (figure 8.1).

Nicotinamide, on the other hand despite being shown *in vitro* to exert subtle effects on both neuronal and microglial cell cultures, and its ability to reverse lactacystin induced histone hypoacetylation and upregulate the expression of numerous neurotrophic and neuroprotective factors in the brains on rats *in vivo*, did not result in neuroprotection in the lactacystin rat model of PD shown here. This finding is contradictory to the previous reports of nicotinamide induced neuroprotection in other animal models of PD (Anderson et al., 2008, Jia et al., 2008, Xu et al., 2012, Anderson et al., 2006). Outside of its effects on HDACs, nicotinamide, is a precursor of NAD+ and is therefore thought to be involved with brain energy metabolism and preservation of mitochondrial functionality. Bioenergetics are becoming an increasingly attractive prospect for neuroprotection in PD (Beal, 2003). Correspondingly, nicotinamide has previously been observed to prevent oxidative mitochondrial dysfunction in a model of PD (Jia et al., 2008). The only other studies investigating the neuroprotective effects of nicotinamide in animal models of PD all use MPTP to model dopaminergic neurodegeneration (Anderson et al., 2006, Anderson et al., 2008, Xu et al., 2012). This toxin works by inhibiting mitochondrial complex 1 to cause mitochondrial dysfunction and energy starvation in dopaminergic neurons. It is likely then that nicotinamide, in the MPTP model, would directly counteract the effects of this mitochondrial toxin due to its effects on bioenergetics. Data presented here, however demonstrate that despite the upregulation of neuroprotective factors in the lactacystin model, nicotinamide is incapable of counteracting the pathogenesis induced as a result of this toxin. Moreover, this highlights even further the implication of additional HDAC and non-HDAC effects of valproate in mediation of its neuroprotection observed here. Further investigation of nicotinamide treatment in additional animal models of PD which use different mechanisms to induce cell death (i.e. 6-OHDA and LPS) will help to unravel the effects displayed here.

8.4 – Implications and Significance of Findings

This study provides the first evidence of perturbation of histone acetylation and alteration in HDAC expression in degenerating regions of the Parkinsonian brain. This is a significant progression for field, as all previous work implicating histone acetylation and the neuroprotective effects of HDACIs in neurodegeneration have been conducted in animal models of the disease. These findings represents a vital step in the drug development process for HDACIs as without confirming the dysregulation of histone acetylation and transcriptional dysfunction in primary diseased tissue, the use of HDACIs for the treatment of PD cannot truly be rationalised. Although the current data does not elucidate whether or not dysregulation of histone acetylation and HDAC expression contribute to PD pathogenesis or whether PD pathogenesis results in dysregulation of histone acetylation and HDAC expression, the findings add insight into the state of this system in degenerating regions of the Parkinsonian brain, adding weight to the hypothesis that HDACIs represent a viable candidate for therapeutic intervention in PD.

The cell culture studies presented here are the first in which the neuroprotective effects of a range of HDACIs are tested against lactacystin induced cell death *in vitro*. Likewise, studies of HDACIs in microglial cultures represent the first parallel study of numerous HDACIs in activated microglia, allowing for direct comparison of the efficacy of numerous inhibitors with one another, and in combination with their effect in neuronal cultures as well. From these data, it was shown that of all of the HDACIs examined, inhibitors of sirtuin2 represent the most promising in terms of their concurrent effects in both degenerating neurons and in activated microglia. These therefore support further investigation of Sirtuin2 inhibitors *in vivo* animal models of PD. It is unclear as yet however, whether sirtuin2 inhibiting agents such as AGK2 and the novel inhibitor presented here, ICL-SIRT078, cross the BBB. Experiments to elucidate whether or not they cross will add significant weight as to their potential for the treatment of PD. In the interim however, neuroprotection studies using an indwelling intracerebral cannula system to deliver these drugs into the brain will add insight into their effectiveness as neuroprotective agents *in vivo*, in animal models.

The animal work conducted here and the study of the neuroprotective effects of valproate using a delayed start are hugely encouraging for the use of HDACIs for the treatment of PD. Chronic treatment of the lactacystin rat model of PD with valproate, starting seven days post lesion, dose dependently afforded neuroprotection and neuroregeneration in this animal model as evidenced by an attenuation of motor behavioural deficits, longitudinal MRI brain volume changes and quantification of the dopaminergic neurons within the SNpc. Molecular analyses of brain extracts indicate that valproate's neuroprotective/neuroregenerative effects may be at least part mediated through epigenetic changes via the inhibition of histone deacetylation to cause chromatin

remodelling and upregulation of numerous neurotrophic and neuroprotective genes culminating in the observed phenotype. Although the doses utilised here are far greater than the usual therapeutic maintenance dose of valproate used for the treatment of epilepsy in humans (1000-2000mg/day) (Britain, 2009), findings acts as proof of principle that delayed start treatment with a HDACI is capable of producing a neuroprotective/neurorestorative phenotype in this animal model of PD.

Equally, although the results of the study of nicotinamide are less positive, they represent a vital finding in the understanding of the neuroprotective effects of different HDACIs in PD. Namely, histone acetylation and upregulation of neurotrophic and neuroprotective factors alone by a HDACI do not translate to neuroprotection. The disparity between the findings presented here in the lactacystin rat model compared with previous published findings in the MPTP mouse model, encourage further investigation of the effects of nicotinamide in additional animal models of PD which rely of different mechanisms to induce cell death (i.e. 6-OHDA and LPS).

8.5 – Limitations and Technical Considerations

Although the data presented here advance the understanding of the role of HDACs in PD and the implication of the potential use of HDACIs as neuroprotective agents, a number of limitations of the current study exist. Similarly, some technical considerations need to be made when interpreting the datasets presented here. Firstly, in the initial results presented here from human post-mortem brain tissue, protein and mRNA were extracted from whole brain tissue sections from the brain block containing a region of interest. Glial cells outnumber neurons in the brain by approximately 3 to 1 and hence it is likely that in these extracted samples the majority of protein and mRNA are glial in origin. It was observed in cell culture that degenerating dopaminergic neurons exhibit histone hypoacetylation, while activated microglia exhibit histone hyperacetylation. A mixed population of both degenerating neurons and activated microglial such as that in the midbrain of a PD brain would therefore exhibit a profile of acetylation and HDAC expression unrepresentative of either cell type, but the histone acetylation and HDAC expression in the brain region alone. This therefore, makes interpretation of the data difficult when trying to ascertain acetylation and HDAC expression in an individual population of cells within it. Similarly, the histone acetylation status and HDAC expression patterns in both astrocytes and oligodendrocytes are yet to be determined, adding further complexity to the dataset.

Study of human post-mortem brain tissue comes with the added consideration as to the inhomogeneity of the study groups. Although cases were grouped based on αSyn Braak staging, groups are made up differing ratios of males and females, difference ages of disease onset, different ages and causes of death etc. Most importantly each patient received a different combination of PD medications. There is no evidence as to the effects of dopamine replacement therapies on histone acetylation, and hence the differences observed between control and PD cases may well be a result of therapeutics, i.e. greater Braak stage, greater disease duration, longer time on PD medication. These factors add an extra complexity to results observed here, and further experiments and study should aid clarification.

Cell culture is an excellent tool for high throughput screening of compounds and mechanistic study of drug action due to the various manipulations possible *in vitro* as opposed to *in vivo*. However, with this comes various downfalls. Firstly, although cells are maintained in imitated physiological conditions, i.e. nutrients, pH, temperature, CO_2 etc., even when treated with lactacystin or LPS for example as in the current study, the conditions bare very little resemblance to those in the Parkinsonian brain. Likewise, maintenance of individual cell lines such as neurons alone in culture do not represent physiology in the brain at all. Neurons are surrounding in the brain by glia: astrocytes, oligodendrocytes and microglia, which supply trophic support for functioning

neurons. The relationship between glia and neurons is vitally important in neurodegenerative disease as it is known that microglia play a specific role in PD pathogenesis. Modelling neuronal cell death or microglial activation alone in cell culture systems can therefore provide an initial indication of a drug's potential, however, as has been seen here this does not always translate to similar findings *in vivo*, i.e. nicotinamide. Likewise, both of the cell lines used in the current study are immortalised cells lines, which have been engineered to grow and divide continuously. Again such cell lines while being hugely advantageous in terms of their ease of maintenance and longevity do not accurately represent the lifespan of cells within the CNS. Further work would be to replicate the studies presented in in primary cell cultures; however these too have their limitations. The flexibility, speed of growth, cost, and reproducibility of cell lines however vastly outweigh the limitations and considerations described here. However, it is clear that great care must be taken not to over interpret *in vitro* findings.

HDACIs are thought to act neuroprotectively via a number of different mechanisms in the brain (see section 8.2). The most cited and most well understood is their inhibition of HDACs in neurons resulting in upregulation of neurotrophic and anti-apoptotic factors thought to translate to neuroprotection. Unlike many other drugs targets, such as receptor ligand interactions, this process is thought to take place less quickly: cumulative acetylation of histone proteins by HATs without the HDAC mediated deacetylation. Correspondingly, significantly increased histone acetylation was not observed in cell culture systems until 48 (N27 cells) and 24hrs (N9 cells) with a HDACI (sections 4.4.3 and 4.4.7 respectively). On the other hand, toxins used here to model dopaminergic neurodegeneration and microglial cell death exerted their action far quicker, significant cell death and microglial activation being observed after 6 and 15hrs in N27 and N9 cells respectively (sections 4.4.2.2 and 4.4.6.2 respectively). For this reason, cell culture systems were pre-treated with HDACI compounds prior to treatment with toxins. Drug pre-treatment does not accurately model the clinical scenario in which a neuroprotective agent would currently be given. That being said, cell culture models of PD represent a far cry from the clinical disease. Results presented here however act as a proof of principle that HDAC inhibition of various isoform(s) is capable of mediating neuroprotection and reduced microglial activation, encouraging future study of their effects *in vivo*.

Controversy has surrounded proteasome inhibitor models of PD in the past due to difficulty in reproducibility between laboratories (Duty and Jenner, 2011). However more recently focal administration of lactacystin to the SNpc has become a reproducible, well used model of PD used by many groups (Niu et al., 2009, Vernon et al., 2010, Lorenc-Koci et al., 2011, Pienaar et al., 2013, Konieczny et al., 2014, Mackey et al., 2013). Lactacystin, specifically and irreversibly inhibits the UPS. However, unlike many other toxins used for the modelling of PD in rats (e.g. 6-OHDA and MPTP) it is

unclear as to the dopaminergic specificity of lactacystin since UPS inhibition may also induce cell death and altered function in other cell types (Ren et al., 2009, Fine et al., 1999). Selectivity of lactacystin for dopaminergic over other neuronal types has been demonstrated at low concentrations, however higher concentrations of this UPS inhibitor are known to show reduced specificity (McNaught et al., 2002c). Focus in this thesis has been placed on the effects of lactacystin on dopaminergic neurons, however the non-specific nature of this irreversible UPS inhibitor at high concentrations highlights the possibility of its effects on other cell types e.g. microglia. Focal injection of lactacystin into the SNpc most likely leads to selective exposure of dopaminergic nigrostriatal neurons, however it must be considered that other cell types may play a part in lactacystin pathogenesis in this model.

All of the drugs investigated in this thesis are inhibitors of HDAC isoforms. However, some of the agents used here are known to also have hugely diverse actions on other cell systems in the brain in conjunction with their inhibitory action upon HDACs. Most pertinent, are the effects of the two previously approved FDA drugs chosen for study *in vivo* here: valproate and nicotinamide. In this thesis focus has been placed on valproate's inhibition of HDACs: its upregulation of neurotrophic and anti-apoptotic factors and subsequent neuroprotection *in vivo*. However, as has already been described, valproate is also known to have a number of other effects on the brain ranging from alterations in GABAergic and glutamatergic signalling, effects on Na+ and Ca2+ voltage-dependent channels and induction of regulatory T cells (Ximenes et al., 2012, Shen and Pili, 2012). These mechanisms may equally be contributing to the neuroprotective phenotype of the drug displayed here. That being said, drugs which modulate glutamatergic signalling (Williams and Dexter, 2014), and calcium channels (Hurley and Dexter, 2012), when administered at a similar stage of disease model progression do not produce such dramatic effects as neurorestoration as that seen here with valproate. Likewise, nicotinamide is a precursor of NAD+ and is therefore thought to also be involved with brain energy metabolism and preservation of mitochondrial functionality, which has become an increasingly attractive prospect for neuroprotection in PD (Beal, 2003). In the current study, it is therefore likely that both HDAC and non-HDAC mediated effects of nicotinamide are exerted yet together they were not capable of inducing neuroprotection against lactacystin in the model used here. That being said, if upregulation of neurotrophic factors by nicotinamide was not sufficient to produce neuroprotection in the model, it is unlikely that valproate's upregulation of these same factors alone would result in neuroprotection, highlighting the probably involvement of valproate's non-HDAC effects in its mechanism of neuroprotection.

8.6 – Further Work

8.6.1 – Further Study of Histone Acetylation and HDAC Expression in the Parkinsonian Brain

Firstly, in order to ascertain the specific contributions of both degenerating dopaminergic neurons and activated microglia to the changes observed in histone acetylation and HDAC expression in Parkinsonian brains, laser capture microdissection could be utilised to isolate specific cell populations from degenerating regions. More specifically, by rapidly immunohistochemically staining sections of the human midbrain under RNase free conditions, it is possible to isolate specific populations of cells for extraction of protein and mRNA (Brown et al., 2013). The level of histone acetylation and HDAC isoform expression could then be assessed specifically in these cell populations. Obvious experiments would firstly be to isolate dopaminergic neurons from the SNpc of human cases (control and early and late stage PD) to determine the level of histone acetylation and HDAC expression. Additional populations could also similarly be isolated such as activated microglia and astrocytes. Ascertaining the histone acetylation profile in each of these individual populations would build up a more focussed picture as to the state of histone acetylation within the disease. Moreover, identification of specific HDAC isoforms for therapeutic targeting in each of these cell types would better inform subsequent cell culture experiment using HDACIs.

To eliminate any confounding effects of dopaminergic replacement therapy treatment in PD cases, further work could be to conduct similar HDAC expression studies and quantification of histone acetylation in Braak stage 1/2 cases. These cases are thought to be presymptomatic and therefore would not be on any dopaminergic medication. If changes in HDAC expression and histone acetylation are indeed a function of PD development, the changes observed in these 'pre-early PD' cases would be subtle, however they would be void of any confounding effect of drug treatment.

The seminal paper by Broide et al (2007) remains the only study of HDAC distribution in the brain. In fact this study only details the 11 'classical' HDACs, the distribution of the sirtuin HDACs in the brain remaining unknown. To the best of the authors' knowledge, a full study of HDAC isoform expression using *in situ* hybridisation in the human brain is yet to be conducted. Conducting such a study would impact hugely on the field of HDACI neuroprotection as this would highlight the HDACs most abundant within areas of the brain known to be affected in PD, allowing for specific targeting with inhibitors. This would hopefully also eliminate possible side effects of HDAC inhibition in brain regions not affected within the disorder, refining the investigation of the potential use of HDACI for the treatment of PD even further.

8.6.2 – Further Study of the Neuroprotective and Anti-Inflammatory Effects of HDACIs *In Vitro*

To add to the findings presented here demonstrating the neuroprotective effects of HDACIs in cell culture, a number of additional experiments and further work could be conducted to extend results. Firstly, it was shown in animal studies that HDAC inhibition leads to upregulation of both neurotrophic and anti-apoptotic factors in the frontal cortex, an area distinctly separate from the nigrostriatal system. Therefore, it would be interesting to see whether this upregulation was similar in degenerating dopaminergic neurons in culture. Extraction of mRNA, reverse transcription, and qRT-PCR to quantify the expression of genes such as BDNF, GDNF,αSyn, Hsp70 etc., would add greatly to the findings previously presented in this thesis, and help elucidate the mechanism by which HDACIs exert their neuroprotective phenotype in dopaminergic neurons directly. In addition, the expression of a number of other genes could similarly be quantified, such as further elements associated with apoptosis (i.e. Bim, Bax, Bcl-XL, and the caspases), or conducting microarray studies to look at the expression of entire banks of related factors. Such experiments would build up a greater picture of the pathways associated with HDACI mediated neuroprotection in neurons.

It was demonstrated here that histone acetylation is increased upon LPS treatment of microglia. It therefore seems counterintuitive to expect HDACIs, agents which are expected to result in exacerbation of this histone hyperacetylation in microglia, to result in a reduction of activation. However, a number of the HDACIs examined here were observed to produce a reduction in microglial activation in culture. Understanding of the mechanism of HDACI mediated reduction of microglial activation therefore remains lacking. Further studies would therefore focus on the mechanism by which HDACIs reduce activation of microglia. For example, by determining the extent of histone acetylation before and after treatment with HDACIs, with and without LPS treatment, it may be possible to understand the mechanism by which excessive histone hyperacetylation could lead to reduction in activation, i.e. perhaps some sort of negative feedback mechanism exists in healthy active microglia which is lacking or dysfunctional in degenerating neurons. Likewise, perhaps in microglia, as in neurons, histone hyperacetylation encourages upregulation of protective, immunomodulatory factors. Further work therefore would seek to characterise this reduction of activation further. For example, additional ELISAs conducted on microglial incubated medium for other pro-inflammatory cytokines such as IL6 and IL1β and also anti-inflammatory and immune regulatory cytokines such as IL10 and TGFβ would add greatly to the picture of the effects of HDACIs on microglial activation. Additionally, ROS assays, such as the 2',7'-dichlorofluorescin diacetate (DCFDA) assay which has already shown in microglial (Seo et al., 2012), conducted on the same medium samples would also increase our knowledge on the effects of histone deacetylase inhibition

on microglial activation. Together, these assays would add greatly to our understanding of the mechanism of HDACI mediated reduction of the activation of microglia.

Another possible avenue of investigation related to the cell culture experiments conducted here is the use of medium transfer and co-cultures. The relationship between glial cells and neurons in the pathogenesis of PD is a complicated one and hence by combining use of both cell types would produce a more realistic model of PD neurodegeneration *in vitro*. Their combined use with neurons would therefore give a greater idea of the neuroprotective potential of a HDACI *in vitro*. Microglial medium transfer experiments would generally consist of treating microglial cultures with LPS (with or without HDACIs) and after a period of time, transferring their medium, rich in pro-inflammatory cytokines, NO and ROS, to neuronal cultures (with or without HDACs) and measuring cell viability. Likewise, microglia-neuron co-culture systems could also be utilised, in which varying numbers of microglia are co-cultured with neurons to determine their contribution to cell death. Additionally, one has not yet considered the role of astrocytes in the neuroprotective effects of HDACIs in the current studies. Astrocytes have been heavily implicated in HDACI mediated neuroprotection (Chen et al., 2006, Suh et al., 2010, Wu et al., 2008a, Wu et al., 2008b) and hence it would also be interesting to study both the effects of HDACIs on astrocyte cultures alone and in combination with neurons and also microglia. These experiments would help to explain why such subtle effects were observed in individual cell lines presented here, i.e. by combining cell culture systems, a greater level of drug response to HDACIs would be expected given the proposed multi-cellular mechanism of HDACI mediated neuroprotection. Similarly, these sorts of experiments would help elucidate the contribution of both of these glial cell types towards the observed neuroprotective phenotype of HDACIs in culture, which would hopefully allow for more accurate translatability into animal models.

8.6.3 – Further Study of the Effects of HDACIs in the Lactacystin Rat Model of PD

A number of questions still remain regarding the study of the effects of valproate and nicotinamide on the lactacystin rat model of PD. Firstly, it has not been addressed as to the effects of HDACIs on striatal projections from the SNpc. Possible future experiments would therefore be to quantify dopamine and its metabolites in the striatum using high-performance liquid chromatography (HPLC) of striatal homogenates in order to calculate striatal dopamine turnover. This ratio gives an indication of dopaminergic functionality and whether or not drug treatment induces any degree of compensatory action in the dopaminergic metabolism in the striatum. Alternatively, immunohistochemistry for TH of striatal sections would provide an additional measure of nigrostriatal neurodegeneration induced as a result of intra-nigral injection of lactacystin and to what extent this is avoided upon treatment of the animal model with HDACIs.

It has been observed here that valproate and nicotinamide both upregulate a number of neurotrophic and anti-apoptotic factors, however to further understand the effects of HDAC inhibition and histone acetylation, the expression of a number of other genes could similarly be quantified, such as further elements associated with apoptosis (i.e. Bim, Bax, Bcl-XL, and the caspases) or conducting microarray studies to look at the expression of entire banks of related factors. Such experiments would build up a greater picture of the pathways associated with HDACI mediated neuroprotection. Likewise, one of the non-histone targets of HDACIs is tubulin. In conjunction with Western blot analysis of AcH3-Lys9 in the current studies, quantification of acetyl-tubulin would give an indication of the extent of tubulin acetylation in the brains of the animals. Of note, fPD mutations such as those in the LRRK2 gene have been shown to lead to perturbation in microtubule dynamics, thought to contribute to the mechanisms associated with neuronal cell death on PD (Gillardon, 2009, Law et al., 2014). Similarly, rescue of microtubule stability is known to be neuroprotective in PD (Esteves et al., 2014) and tubulin acetylation is known to be associated with microtubule stabilisation and neuroprotection by HDACI (Dompierre et al., 2007). Further investigation of the extent of tubulin acetylation in the animal studies conducted here will therefore help to elucidate the extent the role tubulin acetylation plays in neuroprotective phenotype of the HDACIs described here.

As has been described above, due to the promiscuous nature of both of the HDACIs investigated *in vivo* in the current thesis, further work would also seek to understand the extent these additional effects contribute to the neuroprotective phenotype of valproate and the neurotoxic phenotype of nicotinamide. Due to valproate's inhibition of HDAC class I, the induction of regulatory T cells are of particular interest given the recent implication of their induction upon inhibition of this class (Shen and Pili, 2012, Wang et al., 2009, Tao et al., 2007, Reddy and Zou, 2007), and the neuroprotective effects of these cells in animal models of PD (Reynolds et al., 2007, Reynolds et al., 2010). These regulatory T cells are known to be CD4, CD25 and FOXP3 positive and hence a triple chromagen immunofluorescent stain for these markers would easily identify infiltrating cells into the brain parenchyma in the aim of determining if this infiltration is upregulated upon valproate treatment. Further investigation of valproate's other known mechanisms within the brain such as GABAergic and glutamatergic signalling, and its effects on Na+ and Ca2+ voltage-dependent channels would similarly add further understanding to the complexities of valproate mediated neuroprotection in the current studies. Likewise with nicotinamide, however given the lack of neuroprotection observed here, future studies should aim to determine to what extent the non-HDAC actions of nicotinamide play in its neurotoxic phenotype. Similarly, they should aim to understand why there is such disparity between previously published reports of nicotinamide's

neuroprotective effects in PD models such as the MPTP mouse model and not the lactacystin model. Further investigations of nicotinamide's effects in additional animal models of PD which use different mechanisms to induce cell death (i.e. 6-OHDA and LPS) will help to unravel the effects displayed here.

8.6.4 – Future Directions

Studies conducted on post-mortem tissue from PD brains and cell culture work using a range of available HDACIs highlight only the 'tip of the iceberg' of the complexity of HDAC involvement in PD and the potential of HDACI potential for therapeutic intervention leading to neuroprotection. Similarly, results from animal model studies indicate the degree of potential of HDACI mediated neuroprotection in PD. Future work investigating the role of HDACs in PD pathogenesis and the effects of inhibition of specific groups of individual isoforms will transform this infant field into one which has true scope for development of an effective neuroprotective agent for the treatment of PD.

In the short term studies should focus on the specific isoforms identified to have neuroprotective and anti-inflammatory potential for PD treatment. Notably, further investigation of sirtuin2 inhibitors via mechanistic cell culture studies and neuroprotection studies in animals should be a priority given the extremely encouraging results observed in cell culture work presented here. In the first instance, an animal study using an indwelling intracerebral cannula system for delivery of novel sirtuin2 inhibitors to a lesioned brain region such as the SNpc should be conducted to ascertain the neuroprotective effects of such inhibitors *in vivo*. Likewise, investigation as to the brain permeability of sirtuin2 inhibitors will help advise their use for PD. In the long term, focus should be placed on the development of novel HDAC isoform specific inhibitors and distribution studies of HDACs within the human brain. The distinct patterns of expression of HDACs in the brain crossed with design of selective target specific isoform inhibitors position HDACIs as an excellent therapeutic target in neuroscience. Equally given the small molecular nature of the vast majority of HDACI available today, they embody an exciting target for therapy of brain disorders. The multi-targeted and multi-cellular neuroprotective and neurotrophic affects induced upon HDACI treatment make HDACI the most disease relevant drug class being investigated today. Further study to facilitate understanding of the effects of the dysregulation of histone acetylation and the changes in HDAC expression in PD, and the consequences of HDAC isoform inhibition, are now required to further refine the prospective use of HDACIs in this complex disorder and translate their use to the clinic. There is concern as to the use of drugs which regulate epigenetics on the general population, especially to those of child bearing age since epigenetics is heavily implicated in fertility, conception

and foetal development. However, as neurodegenerative disorders such as PD typically affect those later in life, these concerns are not relevant to this patient group. Once better understanding of the effects of HDAC inhibition is achieved, we must learn how best to wield the power of these drugs in PD: how best to use them in the clinic, what drugs to combine them with, and how they can be translated to the treatment of other neurodegenerative diseases.

8.6 - Conclusions

In conclusion, this current thesis provides evidence for the first time of the altered levels of histone acetylation in affected regions on the Parkinsonian brain, and demonstrates that HDAC isoform expression is perturbed in human PD. Cell culture studies have revealed that the neuroprotective phenotype in neurons and the anti-inflammatory phenotype in microglia exerted by HDACIs depends greatly on the isoform specificity of the inhibitor: sirtuin2 inhibitors demonstrating most potent neuroprotection and microglial activation reduction. Furthermore, animal studies provide evidence that pan-inhibition of class I and IIa HDACs by valproate results in significant neuroprotection and neurorestoration in the lactacystin rat model of PD even when administered after toxin administration. Conversely, nicotinamide, despite inhibiting the sirtuin class of HDACs, results in a neurotoxic phenotype in this same animal model of PD. Taken together the data herein provide compelling evidence to support the concept that dependent on isoform specificity, HDAC inhibiting agents represent a novel class of neuroprotective therapeutics for the treatment of PD.

References

ADAMS, F., ROSA, F., KUMAR, S., EDWARDS-PRASAD, J., KENTROTI, S., VERNADAKIS, A., FREED, C. & PRASAD, K. (1996) Characterization and transplantation of two neuronal cell lines with dopaminergic properties. *Neurochemical Research,* 21**,** 619-627.

ALAM, Z. I., DANIEL, S. E., LEES, A. J., MARSDEN, D. C., JENNER, P. & HALLIWELL, B. (1997) A Generalised Increase in Protein Carbonyls in the Brain in Parkinson's but Not Incidental Lewy Body Disease. *Journal of Neurochemistry,* 69**,** 1326-1329.

ALLEN, S. J., WATSON, J. J., SHOEMARK, D. K., BARUA, N. U. & PATEL, N. K. (2013) GDNF, NGF and BDNF as therapeutic options for neurodegeneration. *Pharmacology & Therapeutics,* 138**,** 155-175.

ALLFREY, V. G., FAULKNER, R. & MIRSKY, A. E. (1964) Acetylation and Methylation of Histones and Their Possible Role in the Regulation of RNA Synthesis. *Proceedings of the National Academy of Sciences of the United States of America,* 51(5)**,** 786-794.

ANDERSON, D. W., BRADBURY, K. A. & SCHNEIDER, J. S. (2006) Neuroprotection in Parkinson models varies with toxin administration protocol. *European Journal of Neuroscience,* 24**,** 3174-3182.

ANDERSON, D. W., BRADBURY, K. A. & SCHNEIDER, J. S. (2008) Broad neuroprotective profile of nicotinamide in different mouse models of MPTP-induced parkinsonism. *European Journal of Neuroscience,* 28**,** 610-617.

ARMENTERO, M. T., PINNA, A., FERRÉ, S., LANCIEGO, J. L., MÜLLER, C. E. & FRANCO, R. (2011) Past, present and future of A2A adenosine receptor antagonists in the therapy of Parkinson's disease. *Pharmacology & Therapeutics,* 132**,** 280-299.

ARRANZ, M. J. & FESTING, M. F. W. (1990) Prior use of the neutral red assay and reduction of total protein determination in 96-well plate assays. *Toxicology in Vitro,* 4**,** 211-212.

ARROWSMITH, C. H., BOUNTRA, C., FISH, P. V., LEE, K. & SCHAPIRA, M. (2012) Epigenetic protein families: a new frontier for drug discovery. *Nat Rev Drug Discov,* 11**,** 384-400.

AUSTIN, S. & ST-PIERRE, J. (2012) PGC1α and mitochondrial metabolism – emerging concepts and relevance in ageing and neurodegenerative disorders. *Journal of Cell Science,* 125**,** 4963-4971.

AVALOS, J. L., BEVER, K. M. & WOLBERGER, C. (2005) Mechanism of Sirtuin Inhibition by Nicotinamide: Altering the NAD+ Cosubstrate Specificity of a Sir2 Enzyme. *Molecular cell,* 17**,** 855-868.

AYOUB, I. A., JIAN LEE, E., OGILVY, C. S., FLINT BEAL, M. & MAYNARD, K. I. (1999) Nicotinamide reduces infarction up to two hours after the onset of permanent focal cerebral ischemia in Wistar rats. *Neuroscience Letters,* 259**,** 21-24.

BEAL, M. F. (2003) Bioenergetic approaches for neuroprotection in Parkinson's disease. *Annals of Neurology,* 53**,** S39-S48.

BERARDELLI, A., ROTHWELL, J. C., THOMPSON, P. D. & HALLETT, M. (2001) Pathophysiology of bradykinesia in Parkinson's disease. *Brain,* 124**,** 2131-2146.

BERNSTEIN, B. E., MEISSNER, A. & LANDER, E. S. (2007) The Mammalian Epigenome. *Cell,* 128**,** 669-681.

BERRIDGE, M. V. & TAN, A. S. (1993) Characterization of the Cellular Reduction of 3-(4,5-dimethylthiazol-2-yl)-2,5-diphenyltetrazolium bromide (MTT): Subcellular Localization, Substrate Dependence, and Involvement of Mitochondrial Electron Transport in MTT Reduction. *Archives of Biochemistry and Biophysics,* 303**,** 474-482.

BETARBET, R., SHERER, T. B., MACKENZIE, G., GARCIA-OSUNA, M., PANOV, A. V. & GREENAMYRE, J. T. (2000) Chronic systemic pesticide exposure reproduces features of Parkinson's disease. *Nature Neuroscience,* 3**,** 1301-1306.

BLANDER, G. & GUARENTE, L. (2004) The Sir2 Family of Protein Deacetylases. *Annual Review of Biochemistry,* 73**,** 417-435.

BOLDEN, J. E., PEART, M. J. & JOHNSTONE, R. W. (2006) Anticancer activities of histone deacetylase inhibitors. *Nat Rev Drug Discov,* 5**,** 769-784.

BRAAK, H., TREDICI, K. D., RÜB, U., DE VOS, R. A. I., JANSEN STEUR, E. N. H. & BRAAK, E. (2003) Staging of brain pathology related to sporadic Parkinson's disease. *Neurobiology of Aging,* 24**,** 197-211.

BRADFORD, M. M. (1976) A rapid and sensitive method for the quantitation of microgram quantities of protein utilizing the principle of protein-dye binding. *Analytical Biochemistry,* 72**,** 248-254.

BRAR, S., HENDERSON, D., SCHENCK, J. & ZIMMERMAN, E. (2009) Iron accumulation in the substantia nigra of patients with Alzheimer disease and parkinsonism. *Arch Neurol,* 66**,** 371-4.

BREDT, D. S. & SNYDER, S. H. (1994) Nitric Oxide: A Physiologic Messenger Molecule. *Annual Review of Biochemistry,* 63**,** 175-195.

BRITAIN, B. M. A. A. T. R. P. S. O. G. (2009) *British National Formulary,* UK, BMJ Publishing Group.

BROIDE, R. S., REDWINE, J. M., AFTAHI, N., YOUNG, W., BLOOM, F. E. & WINROW, C. J. (2007) Distribution of histone deacetylases 1-11 in the rat brain. *Journal of molecular neuroscience : MN,* 31**,** 47-58.

BROWN, A. L., DAY, T. A., DAYAS, C. V. & SMITH, D. W. (2013) Purity and Enrichment of Laser-Microdissected Midbrain Dopamine Neurons. *BioMed Research International,* 2013**,** 8.

BUCK, K. & FERGER, B. (2010) L-DOPA-induced dyskinesia in Parkinson's disease: a drug discovery perspective. *Drug Discovery Today,* 15**,** 867-875.

BULLMORE, E. T., SUCKLING, J., OVERMEYER, S., RABE-HESKETH, S., TAYLOR, E. & BRAMMER, M. J. (1999) Global, Voxel, and Cluster Tests, by Theory and Permutation, for a Difference Between Two Groups of Structural MR Images of the Brain. *IEEE Trans Med Imaging,* 18.

BURRIDGE, S. (2013) Target watch: Drugging the epigenome. *Nat Rev Drug Discov,* 12**,** 92-93.

BUTLER, R. & BATES, G. P. (2006) Histone deacetylase inhibitors as therapeutics for polyglutamine disorders. *Nat Rev Neurosci,* 7**,** 784-796.

CAREY, N. & LA THANGUE, N. B. (2006) Histone deacetylase inhibitors: gathering pace. *Current Opinion in Pharmacology,* 6**,** 369-375.

CARMAN, L. S., GAGE, F. H. & SHULTS, C. W. (1991) Partial lesion of the substantia nigra: relation between extent of lesion and rotational behavior. *Brain Research,* 553**,** 275-283.

CASTRO, A. A., GHISONI, K., LATINI, A., QUEVEDO, J., TASCA, C. I. & PREDIGER, R. D. S. (2012) Lithium and valproate prevent olfactory discrimination and short-term memory impairments in the intranasal 1-methyl-4-phenyl-1,2,3,6-tetrahydropyridine (MPTP) rat model of Parkinson's disease. *Behavioural Brain Research*.

CHAUDHURI, K. R., HEALY, D. G. & SCHAPIRA, A. H. V. (2006) Non-motor symptoms of Parkinson's disease: diagnosis and management. *The Lancet Neurology,* 5**,** 235-245.

CHAUDHURI, K. R. & SCHAPIRA, A. H. V. (2009) Non-motor symptoms of Parkinson's disease: dopaminergic pathophysiology and treatment. *The Lancet Neurology,* 8**,** 464-474.

CHEN, H., JACOBS, E., SCHWARZSCHILD, M. A., MCCULLOUGH, M. L., CALLE, E. E., THUN, M. J. & ASCHERIO, A. (2005a) Nonsteroidal anti-inflammatory drug use and the risk for Parkinson's disease. *Annals of Neurology,* 58**,** 963-967.

CHEN, H., ZHANG, S. M., HERNÁN, M. A. & ET AL. (2003) Nonsteroidal anti-inflammatory drugs and the risk of parkinson disease. *Archives of Neurology,* 60**,** 1059-1064.

CHEN, J.-F., XU, K., PETZER, J. P., STAAL, R., XU, Y.-H., BEILSTEIN, M., SONSALLA, P. K., CASTAGNOLI, K., JR, N. C. & SCHWARZSCHILD, M. A. (2001) Neuroprotection by Caffeine and A2A Adenosine Receptor Inactivation in a Model of Parkinson's Disease. *The Journal of Neuroscience,* 21.

CHEN, J., HARDY, P., KUCHARCZYK, W., CLAUBERG, M., JOSHI, J., VOURLAS, A., DHAR, M. & HENKELMAN, R. (1993) MR of human postmortem brain tissue: correlative study between T2 and assays of iron and ferritin in Parkinson and Huntington disease. *AJNR Am J Neuroradiol,* 14(2)**,** 275-81.

CHEN, L., CAGNIARD, B., MATHEWS, T., JONES, S., KOH, H. C., DING, Y., CARVEY, P. M., LING, Z., KANG, U. J. & ZHUANG, X. (2005b) Age-dependent Motor Deficits and Dopaminergic Dysfunction in DJ-1 Null Mice. *Journal of Biological Chemistry,* 280**,** 21418-21426.

CHEN, P. S., PENG, G. S., LI, G., YANG, S., WU, X., WANG, C. C., WILSON, B., LU, R. B., GEAN, P. W., CHUANG, D. M. & HONG, J. S. (2006) Valproate protects dopaminergic neurons in midbrain neuron/glia cultures by stimulating the release of neurotrophic factors from astrocytes. *Mol Psychiatry,* 11**,** 1116-1125.

CHEN, P. S., WANG, C. C., BORTNER, C. D., PENG, G. S., WU, X., PANG, H., LU, R. B., GEAN, P. W., CHUANG, D. M. & HONG, J. S. (2007) Valproic acid and other histone deacetylase inhibitors induce microglial apoptosis and attenuate lipopolysaccharide-induced dopaminergic neurotoxicity. *Neuroscience,* 149**,** 203-212.

CHEN, S. H., WU, H. M., OSSOLA, B., SCHENDZIELORZ, N., WILSON, B. C., CHU, C. H., CHEN, S. L., WANG, Q., ZHANG, D., QIAN, L., LI, X., HONG, J. S. & LU, R. B. (2012) Suberoylanilide hydroxamic acid, a histone deacetylase inhibitor, protects dopaminergic neurons from neurotoxin-induced damage. *British Journal of Pharmacology,* 165**,** 494-505.

CHI, Y. & SAUVE, A. A. (2013) Nicotinamide riboside, a trace nutrient in foods, is a Vitamin B3 with effects on energy metabolism and neuroprotection. *Current Opinion in Clinical Nutrition & Metabolic Care,* 16**,** 657-661 10.1097/MCO.0b013e32836510c0.

CHUANG, D.-M., LENG, Y., MARINOVA, Z., KIM, H.-J. & CHIU, C.-T. (2009) Multiple roles of HDAC inhibition in neurodegenerative conditions. *Trends in Neurosciences,* 32**,** 591-601.

COOKSON, M. R. (2010a) DJ-1, PINK1, and their effects on mitochondrial pathways. *Movement Disorders,* 25**,** S44-S48.

COOKSON, M. R. (2010b) The role of leucine-rich repeat kinase 2 (LRRK2) in Parkinson's disease. *Nat Rev Neurosci,* 11**,** 791-797.

COSTA, J., LUNET, N., SANTOS, C., SANTOS, J. & VAZ-CARNEIRO, A. (2010) Caffeine Exposure and the Risk of Parkinson's Disease: A Systematic Review and Meta-Analysis of Observational Studiess. *Journal of Alzheimer's Disease,* 20**,** 221-238.

CRUM, W. R., GIAMPIETRO, V. P., SMITH, E. J., GORENKOVA, N., STROEMER, R. P. & MODO, M. (2013a) A comparison of automated anatomical–behavioural mapping methods in a rodent model of stroke. *Journal of Neuroscience Methods,* 218**,** 170-183.

CRUM, W. R., MODO, M., VERNON, A. C., BARKER, G. J. & WILLIAMS, S. C. R. (2013b) Registration of challenging pre-clinical brain images. *Journal of Neuroscience Methods,* 216**,** 62-77.

DASH, P. K., ORSI, S. A., ZHANG, M., GRILL, R. J., PATI, S., ZHAO, J. & MOORE, A. N. (2010) Valproate Administered after Traumatic Brain Injury Provides Neuroprotection and Improves Cognitive Function in Rats. *PLoS ONE,* 5**,** e11383.

DAUER, W. & PRZEDBORSKI, S. (2003) Parkinson's Disease: Mechanisms and Models. *Neuron,* 39**,** 889-909.

DE LA FUENTE-FERNÁNDEZ, R. (2012) Role of DaTSCAN and clinical diagnosis in Parkinson disease. *Neurology,* 78**,** 696-701.

DE LAU, L. M. L. & BRETELER, M. M. B. (2006) Epidemiology of Parkinson's disease. *The Lancet Neurology,* 5**,** 525-535.

DE RUIJTER, A. J. M., VAN GENNIP, A. H., CARON, H. N., KEMP, S. & VAN KUILENBURG, A. B. P. (2003) Histone deacetylases (HDACs): characterization of the classical HDAC family. *Biochemical Journal,* 370**,** 737-749.

DESPLATS, P., SPENCER, B., COFFEE, E., PATEL, P., MICHAEL, S., PATRICK, C., ADAME, A., ROCKENSTEIN, E. & MASLIAH, E. (2011) α-Synuclein Sequesters Dnmt1 from the Nucleus: a novel mechanism for epigenetic alterations in Lewy body diseases *Journal of Biological Chemistry,* 286**,** 9031-9037.

DEVANE, C. L. (2003) Pharmacokinetics, drug interactions, and tolerability of valproate. *Psychopharmacol Bull,* 37**,** 25-42.

DEVINE, M. J., PLUN-FAVREAU, H. & WOOD, N. W. (2011) Parkinson's disease and cancer: two wars, one front. *Nat Rev Cancer,* 11**,** 812-823.
DEXTER, D. T., CARTER, C. J., WELLS, F. R., JAVOY-AGID, F., AGID, Y., LEES, A., JENNER, P. & MARSDEN, C. D. (1989a) Basal Lipid Peroxidation in Substantia Nigra Is Increased in Parkinson's Disease. *Journal of Neurochemistry,* 52**,** 381-389.
DEXTER, D. T. & JENNER, P. (2013) Parkinson disease: from pathology to molecular disease mechanisms. *Free Radical Biology and Medicine,* 62**,** 132-144.
DEXTER, D. T., WELLS, F. R., LEE, A. J., AGID, F., AGID, Y., JENNER, P. & MARSDEN, C. D. (1989b) Increased Nigral Iron Content and Alterations in Other Metal Ions Occurring in Brain in Parkinson's Disease. *Journal of Neurochemistry,* 52**,** 1830-1836.
DI FRUSCIA, P., ZACHARIOUDAKIS, E., LIU, C., MONIOT, S., LAOHASINNARONG, S., KHONGKOW, M., HARRISON, I. F., KOLTSIDA, K., REYNOLDS, C. R., SCHMIDTKUNZ, K., JUNG, M., CHAPMAN, K. L., STEEGBORN, C., DEXTER, D. T., STERNBERG, M. J., LAM, E. W.-F. & FUCHTER, M. J. (2014) The Discovery of a Highly Isoform Selective 5,6,7,8-Tetrahydrobenzo[4,5]thieno[2,3-d]pyrimidin-4(3H)-one SIRT2 Inhibitor that is Neuroprotective in an in vitro Parkinson's Disease Model. *ChemMedChem,* 13.
DIETZ, K. C. & CASACCIA, P. (2010) HDAC inhibitors and neurodegeneration: At the edge between protection and damage. *Pharmacological Research,* 62**,** 11-17.
DOBBIN, M. M., MADABHUSHI, R., PAN, L., CHEN, Y., KIM, D., GAO, J., AHANONU, B., PAO, P.-C., QIU, Y., ZHAO, Y. & TSAI, L.-H. (2013) SIRT1 collaborates with ATM and HDAC1 to maintain genomic stability in neurons. *Nat Neurosci,* 16**,** 1008-1015.
DOMPIERRE, J. P., GODIN, J. D., CHARRIN, B. C., CORDELIÈRES, F. P., KING, S. J., HUMBERT, S. & SAUDOU, F. (2007) Histone Deacetylase 6 Inhibition Compensates for the Transport Deficit in Huntington's Disease by Increasing Tubulin Acetylation. *The Journal of Neuroscience,* 27**,** 3571-3583.
DONMEZ, G. (2012) The neurobiology of sirtuins and their role in neurodegeneration. *Trends in Pharmacological Sciences,* 33**,** 494-501.
DONMEZ, G., ARUN, A., CHUNG, C.-Y., MCLEAN, P. J., LINDQUIST, S. & GUARENTE, L. (2012) SIRT1 Protects against α-Synuclein Aggregation by Activating Molecular Chaperones. *The Journal of Neuroscience,* 32**,** 124-132.
DONMEZ, G. & OUTEIRO, T. F. (2013) SIRT1 and SIRT2: emerging targets in neurodegeneration. *EMBO Molecular Medicine,* 5**,** 344-352.
DRAGOVIC, J., KIM, S. H., BROWN, S. L. & KIM, J. H. (1995) Nicotinamide pharmacokinetics in patients. *Radiotherapy and Oncology,* 36**,** 225-228.
DURRENBERGER, P. F., FERNANDO, F. S., MAGLIOZZI, R., KASHEFI, S. N., BONNERT, T. P., FERRER, I., SEILHEAN, D., NAIT-OUMESMAR, B., SCHMITT, A., GEBICKE-HAERTER, P. J., FALKAI, P., GRÜNBLATT, E., PALKOVITS, M., PARCHI, P., CAPELLARI, S., ARZBERGER, T., KRETZSCHMAR, H., RONCAROLI, F., DEXTER, D. T. & REYNOLDS, R. (2012) Selection of novel reference genes for use in the human central nervous system: a BrainNet Europe Study. *Acta Neuropathologica,* 124**,** 893-903.
DUTY, S. & JENNER, P. (2011) Animal models of Parkinson's disease: a source of novel treatments and clues to the cause of the disease. *British Journal of Pharmacology***,** no-no.
ECHANIZ-LAGUNA, A., BOUSIGES, O., LOEFFLER, J.-P. & BOUTILLIER, A.-L. (2008) Histone Deacetylase Inhibitors: Therapeutic Agents and Research Tools for Deciphering Motor Neuron Diseases. *Current Medicinal Chemistry,* 15**,** 1263-1273.
EHRLICH, M., GAMA-SOSA, M. A., HUANG, L.-H., MIDGETT, R. M., KUO, K. C., MCCUNE, R. A. & GEHRKE, C. (1982) Amount and distribution of 5-methylcytosine in human DNA from different types of tissues or cells. *Nucleic Acids Research,* 10**,** 2709-2721.
ESTEVES, A. R., GOZES, I. & CARDOSO, S. M. (2014) The rescue of microtubule-dependent traffic recovers mitochondrial function in Parkinson's disease. *Biochimica et Biophysica Acta (BBA) - Molecular Basis of Disease,* 1842**,** 7-21.

FARACO, G., CAVONE, L. & CHIARUGI, A. (2011) The therapeutic potential of HDAC inhibitors in the treatment of multiple sclerosis. *Mol Med,* 17**,** 442-447.
FDA (2005) Guidance for Industry: Estimating the Maximum Safe Starting Dose in Initial Clinical Trials for Therapeutics in Adult Healthy Volunteers. *U.S. Department of Health and Human Services, Food and Drug Administration, Center for Drug Evaluation and Research (CDER)*
FEANY, M. B. & BENDER, W. W. (2000) A Drosophila model of Parkinson's disease. *Nature,* 404**,** 394-398.
FELLNER, L. & STEFANOVA, N. (2013) The Role of Glia in Alpha-Synucleinopathies. *Molecular Neurobiology,* 47**,** 575-586.
FENTEANY, G., STANDAERT, R., LANE, W., CHOI, S., COREY, E. & SCHREIBER, S. (1995) Inhibition of proteasome activities and subunit-specific amino-terminal threonine modification by lactacystin. *Science,* 268**,** 726-31.
FINDLEY, L. J. (2007) The economic impact of Parkinson's disease. *Parkinsonism & Related Disorders,* 13, Supplement**,** S8-S12.
FINE, S., MAGGIRWAR, S., ELLIOTT, P., EPSTEIN, L., GELBARD, H. & DEWHURST, S. (1999) Proteasome blockers inhibit TNF-alpha release by lipopolysaccharide stimulated macrophages and microglia: implications for HIV-1 dementia. *J Neuroimmunol. ,* 1**,** 55-64.
FLECKENSTEIN, A. E., VOLZ, T. J., RIDDLE, E. L., GIBB, J. W. & HANSON, G. R. (2007) New Insights into the Mechanism of Action of Amphetamines. *Annual Review of Pharmacology and Toxicology,* 47**,** 681-698.
FOLTYNIE, T. & HARIZ, M. I. (2010) Surgical management of Parkinson's disease. *Expert Review of Neurotherapeutics,* 10**,** 903-914.
FUKS, F. O. (2005) DNA methylation and histone modifications: teaming up to silence genes. *Current Opinion in Genetics & Development,* 15**,** 490-495.
FUKS, F. O., HURD, P. J., WOLF, D., NAN, X., BIRD, A. P. & KOUZARIDES, T. (2003) The Methyl-CpG-binding Protein MeCP2 Links DNA Methylation to Histone Methylation. *Journal of Biological Chemistry,* 278**,** 4035-4040.
FURUMAI, R., MATSUYAMA, A., KOBASHI, N., LEE, K.-H., NISHIYAMA, M., NAKAJIMA, H., TANAKA, A., KOMATSU, Y., NISHINO, N., YOSHIDA, M. & HORINOUCHI, S. (2002) FK228 (Depsipeptide) as a Natural Prodrug That Inhibits Class I Histone Deacetylases. *Cancer Research,* 62**,** 4916-4921.
GARCIA-RUIZ, P. J. (2004) Prehistory of Parkinson's disease. *Neurologia,* 19(10)**,** 735-737.
GARDIAN, G., YANG, L., CLEREN, C., CALINGASAN, N., KLIVENYI, P. & BEAL, M. (2004) Neuroprotective effects of phenylbutyrate against MPTP neurotoxicity. *NeuroMolecular Medicine,* 5**,** 235-241.
GENDELMAN, H. E. & APPEL, S. H. (2011) Neuroprotective activities of regulatory T cells. *Trends in Molecular Medicine,* 17**,** 687-688.
GENOVESE, C. R., LAZAR, N. A. & NICHOLS, T. (2002) Thresholding of Statistical Maps in Functional Neuroimaging Using the False Discovery Rate. *NeuroImage,* 15**,** 870-878.
GERTZ, M., FISCHER, F., NGUYEN, G. T. T., LAKSHMINARASIMHAN, M., SCHUTKOWSKI, M., WEYAND, M. & STEEGBORN, C. (2013) Ex-527 inhibits Sirtuins by exploiting their unique NAD+-dependent deacetylation mechanism. *Proceedings of the National Academy of Sciences,* 110**,** E2772-E2781.
GIASSON, B. I., DUDA, J. E., QUINN, S. M., ZHANG, B., TROJANOWSKI, J. Q. & LEE, V. M. Y. (2002) Neuronal α-Synucleinopathy with Severe Movement Disorder in Mice Expressing A53T Human α-Synuclein. *Neuron,* 34**,** 521-533.
GIBB, W. R. & LEES, A. J. (1988) The relevance of the Lewy body to the pathogenesis of idiopathic Parkinson's disease. *Journal of Neurology, Neurosurgery & Psychiatry,* 51**,** 745-752.
GILLARDON, F. (2009) Leucine-rich repeat kinase 2 phosphorylates brain tubulin-beta isoforms and modulates microtubule stability – a point of convergence in Parkinsonian neurodegeneration? *Journal of Neurochemistry,* 110**,** 1514-1522.

GILLIES, G. E., MURRAY, H. E., DEXTER, D. & MCARTHUR, S. (2004) Sex dimorphisms in the neuroprotective effects of estrogen in an animal model of Parkinson's disease. *Pharmacology Biochemistry and Behavior,* 78**,** 513-522.

GLOZAK, M. A., SENGUPTA, N., ZHANG, X. & SETO, E. (2005) Acetylation and deacetylation of non-histone proteins. *Gene,* 363**,** 15-23.

GOETZ, C. G. (2011) The History of Parkinson's Disease: Early Clinical Descriptions and Neurological Therapies. *Cold Spring Harbor Perspectives in Medicine,* 1.

GOLDBERG, M. S., FLEMING, S. M., PALACINO, J. J., CEPEDA, C., LAM, H. A., BHATNAGAR, A., MELONI, E. G., WU, N., ACKERSON, L. C., KLAPSTEIN, G. J., GAJENDIRAN, M., ROTH, B. L., CHESSELET, M.-F., MAIDMENT, N. T., LEVINE, M. S. & SHEN, J. (2003) Parkin-deficient Mice Exhibit Nigrostriatal Deficits but Not Loss of Dopaminergic Neurons. *Journal of Biological Chemistry,* 278**,** 43628-43635.

GORELL, J. M., ORDIDGE, R. J., BROWN, G. G., DENIAU, J.-C., BUDERER, N. M. & HELPERN, J. A. (1995) Increased ironâ€related MRI contrast in the substantia nigra in Parkinson's disease. *Neurology,* 45**,** 1138-1143.

GORELL, J. M., RYBICKI, B. A., COLE JOHNSON, C. & PETERSON, E. L. (1999) Occupational Metal Exposures and the Risk of Parkinson's Disease. *Neuroepidemiology,* 18**,** 303-308.

GORRELL, J., DIMONTE, D. & GRAHAM, D. (1996) The role of the environment in Parkinson's disease. *Environ Health Perspect,* 104**,** 652-654.

GOTTLICHER, M., MINUCCI, S., ZHU, P., KRAMER, O. H., SCHIMPF, A., GIAVARA, S., SLEEMAN, J. P., LO COCO, F., NERVI, C., PELICCI, P. G. & HEINZEL, T. (2001) Valproic acid defines a novel class of HDAC inhibitors inducing differentiation of transformed cells. *EMBO J,* 20**,** 6969-6978.

GRAYSON, D. R., KUNDAKOVIC, M. & SHARMA, R. P. (2010) Is There a Future for Histone Deacetylase Inhibitors in the Pharmacotherapy of Psychiatric Disorders? *Molecular Pharmacology,* 77**,** 126-135.

GREEN, K. N., STEFFAN, J. S., MARTINEZ-CORIA, H., SUN, X., SCHREIBER, S. S., THOMPSON, L. M. & LAFERLA, F. M. (2008) Nicotinamide Restores Cognition in Alzheimer's Disease Transgenic Mice via a Mechanism Involving Sirtuin Inhibition and Selective Reduction of Thr231-Phosphotau. *The Journal of Neuroscience,* 28**,** 11500-11510.

GREGORETTI, I., LEE, Y.-M. & GOODSON, H. V. (2004) Molecular Evolution of the Histone Deacetylase Family: Functional Implications of Phylogenetic Analysis. *Journal of Molecular Biology,* 338**,** 17-31.

GRIESS, P. (1879) Bemerkungen zu der Abhandlung der HH. Weselsky und Benedikt „Ueber einige Azoverbindungen". *Berichte der deutschen chemischen Gesellschaft,* 12**,** 426-428.

GURVICH, N., TSYGANKOVA, O. M., MEINKOTH, J. L. & KLEIN, P. S. (2004) Histone Deacetylase Is a Target of Valproic Acid-Mediated Cellular Differentiation. *Cancer Research,* 64**,** 1079-1086.

HABIBI, E., MASOUDI-NEJAD, A., ABDOLMALEKY, H. & HAGGARTY, S. (2011) Emerging roles of epigenetic mechanisms in Parkinson's disease. *Functional & Integrative Genomics,* 11**,** 523-537.

HAHNEN, E., HAUKE, J., TRÄNKLE, C., EYÜPOGLU, I. Y., WIRTH, B. & BLÜMCKE, I. (2008) Histone deacetylase inhibitors: possible implications for neurodegenerative disorders. *Expert Opinion on Investigational Drugs,* 17**,** 169-184.

HAIGIS, M. C. & SINCLAIR, D. A. (2010) Mammalian Sirtuins: Biological Insights and Disease Relevance. *Annual Review of Pathology: Mechanisms of Disease,* 5**,** 253-295.

HARRISON, I. F. & DEXTER, D. T. (2013) Epigenetic targeting of histone deacetylase: Therapeutic potential in Parkinson's disease? *Pharmacology & Therapeutics,* 140**,** 34-52.

HATHORN, T., SNYDER-KELLER, A. & MESSER, A. (2011) Nicotinamide improves motor deficits and upregulates PGC-1α and BDNF gene expression in a mouse model of Huntington's disease. *Neurobiology of Disease,* 41**,** 43-50.

HE, F. & BALLING, R. (2013) The role of regulatory T cells in neurodegenerative diseases. *Wiley Interdisciplinary Reviews: Systems Biology and Medicine,* 5**,** 153-180.

HERRERA, A. J., CASTAÑO, A., VENERO, J. L., CANO, J. & MACHADO, A. (2000) The Single Intranigral Injection of LPS as a New Model for Studying the Selective Effects of Inflammatory Reactions on Dopaminergic System. *Neurobiology of Disease,* 7**,** 429-447.

HIRSCH, E. C., BREIDERT, T., ROUSSELET, E., HUNOT, S., HARTMANN, A. & MICHEL, P. P. (2003) The Role of Glial Reaction and Inflammation in Parkinson's Disease. *Annals of the New York Academy of Sciences,* 991**,** 214-228.

HOBAN, D. B., CONNAUGHTON, E., CONNAUGHTON, C., HOGAN, G., THORNTON, C., MULCAHY, P., MOLONEY, T. C. & DOWD, E. (2013) Further characterisation of the LPS model of Parkinson's disease: A comparison of intra-nigral and intra-striatal lipopolysaccharide administration on motor function, microgliosis and nigrostriatal neurodegeneration in the rat. *Brain, Behavior, and Immunity,* 27**,** 91-100.

HOULDEN, H. & SINGLETON, A. (2012) The genetics and neuropathology of Parkinson's disease. *Acta Neuropathologica,* 124**,** 325-338.

HUA, X., LEOW, A. D., PARIKSHAK, N., LEE, S., CHIANG, M.-C., TOGA, A. W., JACK JR, C. R., WEINER, M. W. & THOMPSON, P. M. (2008) Tensor-based morphometry as a neuroimaging biomarker for Alzheimer's disease: An MRI study of 676 AD, MCI, and normal subjects. *NeuroImage,* 43**,** 458-469.

HUANG, C.-C. (2007) Parkinsonism Induced by Chronic Manganese Intoxication-An Experience in Taiwan. *Chang Gung Medical Journal*.

HUDSON, J. L., VAN HORNE, C. G., STRÖMBERG, I., BROCK, S., CLAYTON, J., MASSERANO, J., HOFFER, B. J. & GERHARDT, G. A. (1993) Correlation of apomorphine- and amphetamine-induced turning with nigrostriatal dopamine content in unilateral 6-hydroxydopamine lesioned rats. *Brain Research,* 626**,** 167-174.

HUGHES, A. J., DANIEL, S. E., KILFORD, L. & LEES, A. J. (1992) Accuracy of clinical diagnosis of idiopathic Parkinson's disease: a clinico-pathological study of 100 cases. *J Neurol Neurosurg Psychiatry,* 55**,** 181-4.

HURLEY, M. J. & DEXTER, D. T. (2012) Voltage-gated calcium channels and Parkinson's disease. *Pharmacology & Therapeutics,* 133**,** 324-333.

HYUN, D.-H., LEE, M., HALLIWELL, B. & JENNER, P. (2003) Proteasomal inhibition causes the formation of protein aggregates containing a wide range of proteins, including nitrated proteins. *Journal of Neurochemistry,* 86**,** 363-373.

INDEN, M., KITAMURA, Y., TAKEUCHI, H., YANAGIDA, T., TAKATA, K., KOBAYASHI, Y., TANIGUCHI, T., YOSHIMOTO, K., KANEKO, M., OKUMA, Y., TAIRA, T., ARIGA, H. & SHIMOHAMA, S. (2007) Neurodegeneration of mouse nigrostriatal dopaminergic system induced by repeated oral administration of rotenone is prevented by 4-phenylbutyrate, a chemical chaperone. *Journal of Neurochemistry,* 101**,** 1491-1504.

IPDGC & WTCCC (2011) A Two-Stage Meta-Analysis Identifies Several New Loci for Parkinson's Disease. *PLoS Genet,* 7**,** e1002142.

JANKOVIC, J. (2005) Searching for a relationship between manganese and welding and Parkinson's disease. *Neurology,* 64**,** 2021-2028.

JANKOVIC, J. (2008) Parkinson's disease: clinical features and diagnosis. *Journal of Neurology, Neurosurgery & Psychiatry,* 79**,** 368-376.

JEPSEN, C. H., DEMOYA, M. A., PERNER, A., SILLESEN, M., OSTROWSKI, S. R., ALAM, H. B. & JOHANSSON, P. I. (2014) Effect of valproic acid and injury on lesion size and endothelial glycocalyx shedding in a rodent model of isolated traumatic brain injury. *Journal of Trauma and Acute Care Surgery,* 77**,** 292-297 10.1097/TA.0000000000000333.

JIA, H., LI, X., GAO, H., FENG, Z., LI, X., ZHAO, L., JIA, X., ZHANG, H. & LIU, J. (2008) High doses of nicotinamide prevent oxidative mitochondrial dysfunction in a cellular model and improve motor deficit in a Drosophila model of Parkinson's disease. *Journal of Neuroscience Research,* 86**,** 2083-2090.

JONSSON, G. (1983) Chemical lesioning techniques: monoamine neurotoxins. IN BJÖRKLUND, A. & HÖKFELT, T. (Eds.) *Handbook of chemical neuroanatomy. Methods in chemical neuroanatomy.* 1st ed. Amsterdam, Elsevier Science Publishers.

JOWAED, A., SCHMITT, I., KAUT, O. & WULLNER, U. (2010) Methylation Regulates Alpha-Synuclein Expression and Is Decreased in Parkinson's Disease Patients' Brains. *The Journal of Neuroscience,* 30**,** 6355-6359.

KALAITZAKIS, M. E., GRAEBER, M. B., GENTLEMAN, S. M. & PEARCE, R. K. B. (2008) The dorsal motor nucleus of the vagus is not an obligatory trigger site of Parkinson's disease: a critical analysis of α-synuclein staging. *Neuropathology and Applied Neurobiology,* 34**,** 284-295.

KAZANTSEV, A. G. & THOMPSON, L. M. (2008) Therapeutic application of histone deacetylase inhibitors for central nervous system disorders. *Nat Rev Drug Discov,* 7**,** 854-868.

KEY, M. (2009) Chapter 9: Immunohistochemistry Staining Methods. IN KUMAR, G. L. & RUDBECK, L. (Eds.) *Dako Educational Guide: Immunohistochemical Staining Methods.* 5th ed. Carpinteria, California, Dako.

KHAN, N., JEFFERS, M., KUMAR, S., HACKETT, C., BOLDOG, F., KHRAMTSOV, N., QIAN, X., MILLS, E., BERGHS, S. C., CAREY, N., FINN, P. W., COLLINS, L. S., TUMBER, A., RITCHIE, J. W., JENSEN, P. B., LICHENSTEIN, H. S. & SEHESTED, M. (2008) Determination of the class and isoform selectivity of small-molecule histone deacetylase inhibitors. *Biochem J,* 409**,** 581-589.

KIDD, S. K. & SCHNEIDER, J. S. (2010) Protection of dopaminergic cells from MPP+-mediated toxicity by histone deacetylase inhibition. *Brain Research,* 1354**,** 172-178.

KIDD, S. K. & SCHNEIDER, J. S. (2011) Protective effects of valproic acid on the nigrostriatal dopamine system in a 1-methyl-4-phenyl-1,2,3,6-tetrahydropyridine mouse model of Parkinson's disease. *Neuroscience,* 194**,** 189-194.

KIELAR, C., SAWIAK, S. J., NAVARRO NEGREDO, P., TSE, D. H. Y. & MORTON, A. J. (2012) Tensor-Based Morphometry and Stereology Reveal Brain Pathology in the Complexin1 Knockout Mouse. *PLoS ONE,* 7**,** e32636.

KIM, H. J., ROWE, M., REN, M., HONG, J.-S., CHEN, P.-S. & CHUANG, D.-M. (2007) Histone Deacetylase Inhibitors Exhibit Anti-Inflammatory and Neuroprotective Effects in a Rat Permanent Ischemic Model of Stroke: Multiple Mechanisms of Action. *Journal of Pharmacology and Experimental Therapeutics,* 321**,** 892-901.

KIRIK, D., GEORGIEVSKA, B., ROSENBLAD, C. & BJÖRKLUND, A. (2001) Delayed infusion of GDNF promotes recovery of motor function in the partial lesion model of Parkinson's disease. *European Journal of Neuroscience,* 13**,** 1589-1599.

KIRIK, D., ROSENBLAD, C., BURGER, C., LUNDBERG, C., JOHANSEN, T. E., MUZYCZKA, N., MANDEL, R. J. & BJÖRKLUND, A. (2002) Parkinson-Like Neurodegeneration Induced by Targeted Overexpression of α-Synuclein in the Nigrostriatal System. *The Journal of Neuroscience,* 22**,** 2780-2791.

KITADA, T., ASAKAWA, S., HATTORI, N., MATSUMINE, H., YAMAMURA, Y., MINOSHIMA, S., YOKOCHI, M., MIZUNO, Y. & SHIMIZU, N. (1998) Mutations in the parkin gene cause autosomal recessive juvenile parkinsonism. *Nature,* 392**,** 605-608.

KITADA, T., PISANI, A., PORTER, D. R., YAMAGUCHI, H., TSCHERTER, A., MARTELLA, G., BONSI, P., ZHANG, C., POTHOS, E. N. & SHEN, J. (2007) Impaired dopamine release and synaptic plasticity in the striatum of PINK1-deficient mice. *Proceedings of the National Academy of Sciences,* 104**,** 11441-11446.

KIYOHARA, C. & KUSUHARA, S. (2011) Cigarette smoking and Parkinson's disease: a meta-analysis. *Fukuoka Igaku Zasshi.,* 102**,** 254-65.

KLEIN, R. L., LEWIS, M. H., MUZYCZKA, N. & MEYER, E. M. (1999) Prevention of 6-hydroxydopamine-induced rotational behavior by BDNF somatic gene transfer. *Brain Research,* 847**,** 314-320.

KONDOH, T., BANNAI, M., NISHINO, H. & TORII, K. (2005) 6-Hydroxydopamine-induced lesions in a rat model of hemi-Parkinson's disease monitored by magnetic resonance imaging. *Experimental Neurology,* 192**,** 194-202.

KONIECZNY, J., CZARNECKA, A., LENDA, T., KAMIŃSKA, K. & LORENC-KOCI, E. (2014) Chronic l-DOPA treatment attenuates behavioral and biochemical deficits induced by unilateral lactacystin administration into the rat substantia nigra. *Behavioural Brain Research,* 261**,** 79-88.

KONSOULA, Z. & BARILE, F. A. (2012) Epigenetic histone acetylation and deacetylation mechanisms in experimental models of neurodegenerative disorders. *Journal of Pharmacological and Toxicological Methods*.

KONTOPOULOS, E., PARVIN, J. D. & FEANY, M. B. (2006) α-synuclein acts in the nucleus to inhibit histone acetylation and promote neurotoxicity. *Human Molecular Genetics,* 15**,** 3012-3023.

KOSTA, P., ARGYROPOULOU, M., MARKOULA, S. & KONITSIOTIS, S. (2006) MRI evaluation of the basal ganglia size and iron content in patients with Parkinson's disease. *Journal of Neurology,* 253**,** 26-32.

KOUZARIDES, T. (2007) Chromatin Modifications and Their Function. *Cell,* 128**,** 693-705.

KRACK, P., LIMOUSIN, P., BENABID, A. L. & POLLAK, P. (1997) Chronic stimulation of subthalamic nucleus improves levodopa-induced dyskinesias in Parkinson's disease. *The Lancet,* 350**,** 1676.

LANGLEY, B., D'ANNIBALE, M. A., SUH, K., AYOUB, I., TOLHURST, A., BASTAN, B. L., YANG, L., KO, B., FISHER, M., CHO, S., BEAL, M. F. & RATAN, R. R. (2008) Pulse Inhibition of Histone Deacetylases Induces Complete Resistance to Oxidative Death in Cortical Neurons without Toxicity and Reveals a Role for Cytoplasmic p21waf1/cip1 in Cell Cycle-Independent Neuroprotection. *The Journal of Neuroscience,* 28**,** 163-176.

LANGSTON, J., BALLARD, P., TETRUD, J. & IRWIN, I. (1983) Chronic Parkinsonism in humans due to a product of meperidine-analog synthesis. *Science,* 219**,** 979-980.

LAPCHAK, P. A., MILLER, P. J., COLLINS, F. & JIAO, S. (1997) Glial cell line-derived neurotrophic factor attenuates behavioural deficits and regulates nigrostriatal dopaminergic and peptidergic markers in 6-hydroxydopamine-lesioned adult rats: comparison of intraventricular and intranigral delivery. *Neuroscience,* 78**,** 61-72.

LAUTERBACH, E. C. & MENDEZ, M. F. (2011) Psychopharmacological Neuroprotection in Neurodegenerative Diseases, Part III: Criteria-Based Assessment: A Report of the ANPA Committee on Research. *The Journal of Neuropsychiatry & Clinical Neurosciences,* 23**,** 242-260.

LAW, B. M. H., SPAIN, V. A., LEINSTER, V. H. L., CHIA, R., BEILINA, A., CHO, H. J., TAYMANS, J.-M., URBAN, M. K., SANCHO, R. M., RAMÍREZ, M. B., BISKUP, S., BAEKELANDT, V., CAI, H., COOKSON, M. R., BERWICK, D. C. & HARVEY, K. (2014) A Direct Interaction between Leucine-rich Repeat Kinase 2 and Specific β-Tubulin Isoforms Regulates Tubulin Acetylation. *Journal of Biological Chemistry,* 289**,** 895-908.

LAWLESS, M. W., NORRIS, S., O'BYRNE, K. J. & GRAY, S. G. (2009) Targeting histone deacetylases for the treatment of disease. *Journal of Cellular and Molecular Medicine,* 13**,** 826-852.

LEE, J. Y., KIM, H. S., CHOI, H. Y., OH, T. H., JU, B. G. & YUNE, T. Y. (2012) Valproic acid attenuates blood–spinal cord barrier disruption by inhibiting matrix metalloprotease-9 activity and improves functional recovery after spinal cord injury. *Journal of Neurochemistry,* 121**,** 818-829.

LEE, M. G., WYNDER, C., SCHMIDT, D. M., MCCAFFERTY, D. G. & SHIEKHATTAR, R. (2006) Histone H3 Lysine 4 Demethylation Is a Target of Nonselective Antidepressive Medications. *Chemistry & Biology,* 13**,** 563-567.

LEE, M. K., STIRLING, W., XU, Y., XU, X., QUI, D., MANDIR, A. S., DAWSON, T. M., COPELAND, N. G., JENKINS, N. A. & PRICE, D. L. (2002) Human α-synuclein-harboring familial Parkinson's disease-linked Ala-53 → Thr mutation causes neurodegenerative disease with α-synuclein aggregation in transgenic mice. *Proceedings of the National Academy of Sciences,* 99**,** 8968-8973.

LEE, V. M. Y. & TROJANOWSKI, J. Q. (2006a) Mechanisms of Parkinson's Disease Linked to Pathological α-Synuclein: New Targets for Drug Discovery. *Neuron,* 52**,** 33-38.

LEE, V. M. Y. & TROJANOWSKI, J. Q. (2006b) Mechanisms of Parkinson's Disease Linked to Pathological α-Synuclein: New Targets for Drug Discovery. *Neuron,* 52**,** 33-38.
LEES, A. J. (2007) Unresolved issues relating to the Shaking Palsy on the celebration of James Parkinson's 250th birthday. *Movement Disorders,* 22**,** S327-S334.
LENG, Y. & CHUANG, D.-M. (2006) Endogenous α-Synuclein Is Induced by Valproic Acid through Histone Deacetylase Inhibition and Participates in Neuroprotection against Glutamate-Induced Excitotoxicity. *The Journal of Neuroscience,* 26**,** 7502-7512.
LEROY, E., BOYER, R., AUBURGER, G., LEUBE, B., ULM, G., MEZEY, E., HARTA, G., BROWNSTEIN, M. J., JONNALAGADA, S., CHERNOVA, T., DEHEJIA, A., LAVEDAN, C., GASSER, T., STEINBACH, P. J., WILKINSON, K. D. & POLYMEROPOULOS, M. H. (1998) The ubiquitin pathway in Parkinson's disease. *Nature,* 395**,** 451-452.
LEVIN, J., HÖGEN, T., HILLMER, A. S., BADER, B., SCHMIDT, F., KAMP, F., KRETZSCHMAR, H. A., BÖTZEL, K. & GIESE, A. (2011) Generation of Ferric Iron Links Oxidative Stress to α-Synuclein Oligomer Formation. *Journal of Parkinson's Disease,* 1**,** 205-216.
LI, C., GUO, Y., XIE, W., LI, X., JANOKOVIC, J. & LE, W. (2010) Neuroprotection of Pramipexole in UPS Impairment Induced Animal Model of Parkinson's Disease. *Neurochemical Research,* 35**,** 1546-1556.
LI, F., MACFARLAN, T., PITTMAN, R. N. & CHAKRAVARTI, D. (2002) Ataxin-3 Is a Histone-binding Protein with Two Independent Transcriptional Corepressor Activities. *Journal of Biological Chemistry,* 277**,** 45004-45012.
LI, Y., LIU, W., OO, T. F., WANG, L., TANG, Y., JACKSON-LEWIS, V., ZHOU, C., GEGHMAN, K., BOGDANOV, M., PRZEDBORSKI, S., BEAL, M. F., BURKE, R. E. & LI, C. (2009) Mutant LRRK2R1441G BAC transgenic mice recapitulate cardinal features of Parkinson's disease. *Nat Neurosci,* 12**,** 826-828.
LIM, S., FOX, S. H. & LANG, A. E. (2009) Overview of the extranigral aspects of parkinson disease. *Archives of Neurology,* 66**,** 167-172.
LIN, X., PARISIADOU, L., GU, X.-L., WANG, L., SHIM, H., SUN, L., XIE, C., LONG, C.-X., YANG, W.-J., DING, J., CHEN, Z. Z., GALLANT, P. E., TAO-CHENG, J.-H., RUDOW, G., TRONCOSO, J. C., LIU, Z., LI, Z. & CAI, H. (2009) Leucine-Rich Repeat Kinase 2 Regulates the Progression of Neuropathology Induced by Parkinson's-Disease-Related Mutant α-synuclein. *Neuron,* 64**,** 807-827.
LIU, D., GHARAVI, R., PITTA, M., GLEICHMANN, M. & MATTSON, M. (2009) Nicotinamide Prevents NAD+ Depletion and Protects Neurons Against Excitotoxicity and Cerebral Ischemia: NAD+ Consumption by SIRT1 may Endanger Energetically Compromised Neurons. *NeuroMolecular Medicine,* 11**,** 28-42.
LIU, D., PITTA, M., JIANG, H., LEE, J.-H., ZHANG, G., CHEN, X., KAWAMOTO, E. M. & MATTSON, M. P. (2013a) Nicotinamide forestalls pathology and cognitive decline in Alzheimer mice: evidence for improved neuronal bioenergetics and autophagy procession. *Neurobiology of Aging,* 34**,** 1564-1580.
LIU, L., ARUN, A., ELLIS, L., PERITORE, C. & DONMEZ, G. (2012) Sirtuin 2 (SIRT2) Enhances 1-Methyl-4-phenyl-1,2,3,6-tetrahydropyridine (MPTP)-induced Nigrostriatal Damage via Deacetylating Forkhead Box O3a (Foxo3a) and Activating Bim Protein. *Journal of Biological Chemistry,* 287**,** 32307-32311.
LIU, L., ARUN, A., ELLIS, L., PERITORE, C. & DONMEZ, G. (2013b) Sirtuin 2 (SIRT2) enhances 1-methyl-4-phenyl-1,2,3,6-tetrahydropyridine (MPTP)-induced nigrostriatal damage via deacetylating forkhead box O3a (Foxo3a) and activating Bim protein. *Journal of Biological Chemistry,* 288**,** 14672.
LIU, M. & BING, G. (2011) Lipopolysaccharide Animal Models for Parkinson's Disease. *Parkinson's Disease,* 2011.
LIVAK, K. J. & SCHMITTGEN, T. D. (2001) Analysis of Relative Gene Expression Data Using Real-Time Quantitative PCR and the 2−ΔΔCT Method. *Methods,* 25**,** 402-408.

LO BIANCO, C., RIDET, J.-L., SCHNEIDER, B. L., DÉGLON, N. & AEBISCHER, P. (2002) α-Synucleinopathy and selective dopaminergic neuron loss in a rat lentiviral-based model of Parkinson's disease. *Proceedings of the National Academy of Sciences,* 99**,** 10813-10818.

LORENC-KOCI, E., LENDA, T., ANTKIEWICZ-MICHALUK, L., WARDAS, J., DOMIN, H., ŚMIAŁOWSKA, M. & KONIECZNY, J. (2011) Different effects of intranigral and intrastriatal administration of the proteasome inhibitor lactacystin on typical neurochemical and histological markers of Parkinson's disease in rats. *Neurochemistry International,* 58**,** 839-849.

LU, Q., YANG, Y.-T., CHEN, C.-S., DAVIS, M., BYRD, J. C., ETHERTON, M. R., UMAR, A. & CHEN, C.-S. (2003) Zn2+-Chelating Motif-Tethered Short-Chain Fatty Acids as a Novel Class of Histone Deacetylase Inhibitors. *Journal of Medicinal Chemistry,* 47**,** 467-474.

LUCIO-ETEROVIC, A., CORTEZ, M., VALERA, E., MOTTA, F., QUEIROZ, R., MACHADO, H., CARLOTTI, C., NEDER, L., SCRIDELI, C. & TONE, L. (2008) Differential expression of 12 histone deacetylase (HDAC) genes in astrocytomas and normal brain tissue: class II and IV are hypoexpressed in glioblastomas. *BMC Cancer,* 8**,** 243.

LUK, K. C., KEHM, V., CARROLL, J., ZHANG, B., O'BRIEN, P., TROJANOWSKI, J. Q. & LEE, V. M.-Y. (2012) Pathological α-Synuclein Transmission Initiates Parkinson-like Neurodegeneration in Nontransgenic Mice. *Science,* 338**,** 949-953.

LV, L., SUN, Y., HAN, X., XU, C.-C., TANG, Y.-P. & DONG, Q. (2011) Valproic acid improves outcome after rodent spinal cord injury: Potential roles of histone deacetylase inhibition. *Brain Research,* 1396**,** 60-68.

MACKEY, S., JING, Y., FLORES, J., DINELLE, K. & DOUDET, D. J. (2013) Direct intranigral administration of an ubiquitin proteasome system inhibitor in rat: Behavior, positron emission tomography, immunohistochemistry. *Experimental Neurology,* 247**,** 19-24.

MAGGIO, R., RIVA, M., VAGLINI, F., FORNAI, F., MOLTENI, R., ARMOGIDA, M., RACAGNI, G. & CORSINI, G. U. (1998) Nicotine Prevents Experimental Parkinsonism in Rodents and Induces Striatal Increase of Neurotrophic Factors. *Journal of Neurochemistry,* 71**,** 2439-2446.

MAIESE, K. & CHONG, Z. Z. (2003) Nicotinamide: necessary nutrient emerges as a novel cytoprotectant for the brain. *Trends in Pharmacological Sciences,* 24**,** 228-232.

MARAGANORE, D. M., LESNICK, T. G., ELBAZ, A., CHARTIER-HARLIN, M.-C., GASSER, T., KRÜGER, R., HATTORI, N., MELLICK, G. D., QUATTRONE, A., SATOH, J.-I., TODA, T., WANG, J., IOANNIDIS, J. P. A., DE ANDRADE, M. & ROCCA, W. A. (2004) UCHL1 is a Parkinson's disease susceptibility gene. *Annals of Neurology,* 55**,** 512-521.

MARAMBAUD, P., DRESES-WERRINGLOER, U. & VINGTDEUX, V. (2009) Calcium signaling in neurodegeneration. *Molecular Neurodegeneration,* 4**,** 20.

MARINOVA, Z., REN, M., WENDLAND, J. R., LENG, Y., LIANG, M.-H., YASUDA, S., LEEDS, P. & CHUANG, D.-M. (2009) Valproic acid induces functional heat-shock protein 70 via Class I histone deacetylase inhibition in cortical neurons: a potential role of Sp1 acetylation. *Journal of Neurochemistry,* 111**,** 976-987.

MARKS, P. A., RICHON, V. M., BRESLOW, R. & RIFKIND, R. A. (2001a) Histone deacetylase inhibitors as new cancer drugs. *Current Opinion in Oncology,* 13**,** 477-483.

MARKS, P. A., RICHON, V. M., MILLER, T. & KELLY, W. K. (2004) Histone Deacetylase Inhibitors. *Advances in Cancer Research.* Academic Press.

MARKS, P. A., RIFKIND, R. A., RICHON, V. M., BRESLOW, R., MILLER, T. & KELLY, W. K. (2001b) Histone deacetylases and cancer: causes and therapies. *Nat Rev Cancer,* 1**,** 194-202.

MARTIN, D., MILLER, G., CULLEN, T., FISCHER, N., DIX, D. & RUSSELL, D. (1996) Intranigral or intrastriatal injections of GDNF: effects on monoamine levels and behavior in rats. *European Journal of Pharmacology,* 317**,** 247-256.

MARTIN, W. R. W., WIELER, M. & GEE, M. (2008) Midbrain iron content in early Parkinson disease: A potential biomarker of disease status. *Neurology,* 70**,** 1411-1417.

MATSUMOTO, L., TAKUMA, H., TAMAOKA, A., KURISAKI, H., DATE, H., TSUJI, S. & IWATA, A. (2010) CpG Demethylation Enhances Alpha-Synuclein Expression and Affects the Pathogenesis of Parkinson's Disease. *PLoS ONE,* 5**,** e15522.

MATSUOKA, Y., VILA, M., LINCOLN, S., MCCORMACK, A., PICCIANO, M., LAFRANCOIS, J., YU, X., DICKSON, D., LANGSTON, W. J., MCGOWAN, E., FARRER, M., HARDY, J., DUFF, K., PRZEDBORSKI, S. & DI MONTE, D. A. (2001) Lack of Nigral Pathology in Transgenic Mice Expressing Human α-Synuclein Driven by the Tyrosine Hydroxylase Promoter. *Neurobiology of Disease,* 8**,** 535-539.

MAYEUX, R., MARDER, K., COTE, L. J., DENARO, J., HEMENEGILDO, N., MEJIA, H., TANG, M.-X., LANTIGUA, R., WILDER, D., GURLAND, B. & HAUSER, A. (1995) The Frequency of Idiopathic Parkinson's Disease by Age, Ethnic Group, and Sex in Northern Manhattan, 1988–1993. *American Journal of Epidemiology,* 142**,** 820-827.

MAZE, I., NOH, K.-M. & ALLIS, C. D. (2012) Histone Regulation in the CNS: Basic Principles of Epigenetic Plasticity. *Neuropsychopharmacology,* 38(1)**,** 3-22.

MCGEER, P. L., ITAGAKI, S., BOYES, B. E. & MCGEER, E. G. (1988) Reactive microglia are positive for HLA-DR in the substantia nigra of Parkinson's and Alzheimer's disease brains. *Neurology,* 38**,** 1285.

MCNAUGHT, K. S. P., BELIZAIRE, R., JENNER, P., OLANOW, C. W. & ISACSON, O. (2002a) Selective loss of 20S proteasome α-subunits in the substantia nigra pars compacta in Parkinson's disease. *Neuroscience Letters,* 326**,** 155-158.

MCNAUGHT, K. S. P., BJORKLUND, L. M., BELIZAIRE, R., ISACSON, O., JENNER, P. & OLANOW, C. W. (2002b) Proteasome inhibition causes nigral degeneration with inclusion bodies in rats. *NeuroReport,* 13**,** 1437-1441.

MCNAUGHT, K. S. P. & JENNER, P. (2001) Proteasomal function is impaired in substantia nigra in Parkinson's disease. *Neuroscience Letters,* 297**,** 191-194.

MCNAUGHT, K. S. P., MYTILINEOU, C., JNOBAPTISTE, R., YABUT, J., SHASHIDHARAN, P., JENNER, P. & OLANOW, C. W. (2002c) Impairment of the ubiquitin-proteasome system causes dopaminergic cell death and inclusion body formation in ventral mesencephalic cultures. *Journal of Neurochemistry,* 81**,** 301-306.

MCNAUGHT, K. S. P., PERL, D. P., BROWNELL, A.-L. & OLANOW, C. W. (2004) Systemic exposure to proteasome inhibitors causes a progressive model of Parkinson's disease. *Annals of Neurology,* 56**,** 149-162.

MEANEY, M. J. (2010) Epigenetics and the Biological Definition of Gene × Environment Interactions. *Child Development,* 81**,** 41-79.

MILETICH, R. S., BANKIEWICZ, K. S., QUARANTELLI, M., PLUNKETT, R. J., FRANK, J., KOPIN, I. J. & DI CHIRO, G. (1994) MRI detects acute degeneration of the nigrostriatal dopamine system after MPTP exposure in hemiparkinsonian monkeys. *Annals of Neurology,* 35**,** 689-697.

MIMASU, S., SENGOKU, T., FUKUZAWA, S., UMEHARA, T. & YOKOYAMA, S. (2008) Crystal structure of histone demethylase LSD1 and tranylcypromine at 2.25 A. *Biochemical and Biophysical Research Communications,* 366**,** 15-22.

MINUCCI, S. & PELICCI, P. G. (2006) Histone deacetylase inhibitors and the promise of epigenetic (and more) treatments for cancer. *Nat Rev Cancer,* 6**,** 38-51.

MIRANDA, T. B. & JONES, P. A. (2007) DNA methylation: The nuts and bolts of repression. *Journal of Cellular Physiology,* 213**,** 384-390.

MOCHIZUKI, A., KOMATSUZAKI, Y. & SHOJI, S. I. (2002) Association of Lewy bodies and glial cytoplasmic inclusions in the brain of Parkinson's disease. *Acta Neuropathologica,* 104**,** 534-537.

MOKUDAI, T., AYOUB, I. A., SAKAKIBARA, Y., LEE, E.-J., OGILVY, C. S. & MAYNARD, K. I. (2000) Delayed Treatment With Nicotinamide (Vitamin B3) Improves Neurological Outcome and Reduces Infarct Volume After Transient Focal Cerebral Ischemia in Wistar Rats. *Stroke,* 31**,** 1679-1685.

MONTI, B., GATTA, V., PIRETTI, F., RAFFAELLI, S., VIRGILI, M. & CONTESTABILE, A. (2010) Valproic Acid is Neuroprotective in the Rotenone Rat Model of Parkinson's Disease: Involvement of α-Synuclein. *Neurotoxicity Research,* 17**,** 130-141.

MONTI, B., MERCATELLI, D. & CONTESTABILE, A. (2012) Valproic acid neuroprotection in 6-OHDA lesioned rat, a model for parkinson's disease. *HOAJ Biology,* 1**,** 4-4.

MONTI, B., POLAZZI, E., BATTI, L., CROCHEMORE, C., VIRGILI, M. & CONTESTABILE, A. (2007) Alpha-synuclein protects cerebellar granule neurons against 6-hydroxydopamine-induced death. *Journal of Neurochemistry,* 103**,** 518-530.

MONTI, B., POLAZZI, E. & CONTESTABILE, A. (2009) Biochemical, Molecular and Epigenetic Mechanisms of Valproic Acid Neuroprotection. *Current Molecular Pharmacology,* 2**,** 95-109.

MOORE, L. D., LE, T. & FAN, G. (2012) DNA Methylation and Its Basic Function. *Neuropsychopharmacology,* 38(1)**,** 23-38.

MORRISON, B., MAJDZADEH, N. & D'MELLO, S. (2007) Histone deacetylases: Focus on the nervous system. *Cellular and Molecular Life Sciences,* 64**,** 2258-2269.

NAKAMURA, Y., SI, Q. S. & KATAOKA, K. (1999) Lipopolysaccharide-induced microglial activation in culture: temporal profiles of morphological change and release of cytokines and nitric oxide. *Neuroscience Research,* 35**,** 95-100.

NICHOLAS, A. P., LUBIN, F. D., HALLETT, P. J., VATTEM, P., RAVENSCROFT, P., BEZARD, E., ZHOU, S., FOX, S. H., BROTCHIE, J. M., SWEATT, J. D. & STANDAERT, D. G. (2008) Striatal histone modifications in models of levodopa-induced dyskinesia. *Journal of Neurochemistry,* 106**,** 486-494.

NIU, C., MEI, J., PAN, Q. & FU, X. (2009) Nigral Degeneration with Inclusion Body Formation and Behavioral Changes in Rats after Proteasomal Inhibition. *Stereotactic and Functional Neurosurgery,* 87**,** 69-81.

NUSSBAUM, R. L. & ELLIS, C. E. (2003) Alzheimer's Disease and Parkinson's Disease. *New England Journal of Medicine,* 348**,** 1356-1364.

NUTT, J., WILLIAMS, A., PLOTKIN, C., ENG, N., ZIEGLER, M. & CALNE, D. B. (1979) Treatment of Parkinson's disease with sodium valproate: clinical, pharmacological, and biochemical observations. *Can J Neurol Sci,* 6**,** 337-43.

OGURA, K.-I., OGAWA, M. & YOSHIDA, M. (1994) Effects of ageing on microglia in the normal rat brain: immunohistochemical observations. *NeuroReport,* 5**,** 1224-1226.

OLIVERAS-SALVA, M., VAN DER PERREN, A., CASADEI, N., STROOBANTS, S., NUBER, S., D'HOOGE, R., VAN DEN HAUTE, C. & BAEKELANDT, V. (2013) rAAV2/7 vector-mediated overexpression of alpha-synuclein in mouse substantia nigra induces protein aggregation and progressive dose-dependent neurodegeneration. *Molecular Neurodegeneration,* 8**,** 44.

OMURA, S., FUJIMOTO, T. O., K., MATSUZAKI, K., MORIGUCHI, R., TANAKA, H. & SASAKI, Y. (1991) Lactacystin, a novel microbial metabolite, induces neuritogenesis of neuroblastoma cells. *J Antibiot,* 44**,** 113-6.

ONO, K., IKEMOTO, M., KAWARABAYASHI, T., IKEDA, M., NISHINAKAGAWA, T., HOSOKAWA, M., SHOJI, M., TAKAHASHI, M. & NAKASHIMA, M. (2009) A chemical chaperone, sodium 4-phenylbutyric acid, attenuates the pathogenic potency in human alpha-synuclein A30P + A53T transgenic mice. *Parkinsonism & Related Disorders,* 15**,** 649-654.

OUTEIRO, T. F., KONTOPOULOS, E., ALTMANN, S. M., KUFAREVA, I., STRATHEARN, K. E., AMORE, A. M., VOLK, C. B., MAXWELL, M. M., ROCHET, J.-C., MCLEAN, P. J., YOUNG, A. B., ABAGYAN, R., FEANY, M. B., HYMAN, B. T. & KAZANTSEV, A. G. (2007) Sirtuin 2 Inhibitors Rescue α-Synuclein-Mediated Toxicity in Models of Parkinson's Disease. *Science,* 317**,** 516-519.

OUTEIRO, T. F., MARQUES, O. & KAZANTSEV, A. (2008) Therapeutic role of sirtuins in neurodegenerative disease. *Biochimica et Biophysica Acta (BBA) - Molecular Basis of Disease,* 1782**,** 363-369.

PACHECO, M. & NIELSEN, T. O. (2012) Histone deacetylase 1 and 2 in mesenchymal tumors. *Mod Pathol,* 25**,** 222-230.

PADMAJA, M. V., JAYARAMAN, M., SRINIVASAN, A. V., SRISAILAPATHY, C. R. S. & RAMESH, A. (2012) PARK2 gene mutations in early onset Parkinson's disease patients of South India. *Neuroscience Letters,* 523**,** 145-147.

PAN, T., KONDO, S., ZHU, W., XIE, W., JANKOVIC, J. & LE, W. (2008) Neuroprotection of rapamycin in lactacystin-induced neurodegeneration via autophagy enhancement. *Neurobiology of Disease,* 32**,** 16-25.

PAN, T., LI, X., XIE, W., JANKOVIC, J. & LE, W. (2005) Valproic acid-mediated Hsp70 induction and anti-apoptotic neuroprotection in SH-SY5Y cells. *FEBS Letters,* 579**,** 6716-6720.

PARIHAR, M. S., PARIHAR, A., FUJITA, M., HASHIMOTO, M. & GHAFOURIFAR, P. (2008) Mitochondrial association of alpha-synuclein causes oxidative stress. *Cellular and Molecular Life Sciences,* 65**,** 1272-1284.

PARISH, C. & MULLBACHER, A. (1983) Automated colorimetric assay for T cell cytotoxicity. *J Immunol Methods,* 11**,** 225-37.

PARKINSON, J. (2002) An Essay on the Shaking Palsy. *J Neuropsychiatry Clin Neurosci,* 14**,** 223-236.

PAULY, J. R., CHARRIEZ, C. M., GUSEVA, M. V. & SCHEFF, S. W. (2004) Nicotinic Receptor Modulation for Neuroprotection and Enhancement of Functional Recovery Following Brain Injury or Disease. *Annals of the New York Academy of Sciences,* 1035**,** 316-334.

PAXINOS, G. & WATSON, C. (2009) *The Rat Brain in Stereotaxic Coordinates, 6th Ed.,* New York, Accademic Press.

PECK, B., CHEN, C.-Y., HO, K.-K., DI FRUSCIA, P., MYATT, S. S., COOMBES, R. C., FUCHTER, M. J., HSIAO, C.-D. & LAM, E. W.-F. (2010) SIRT Inhibitors Induce Cell Death and p53 Acetylation through Targeting Both SIRT1 and SIRT2. *Molecular Cancer Therapeutics,* 9**,** 844-855.

PENDLETON, R. G., PARVEZ, F., SAYED, M. & HILLMAN, R. (2002) Effects of Pharmacological Agents upon a Transgenic Model of Parkinson's Disease in Drosophila melanogaster. *Journal of Pharmacology and Experimental Therapeutics,* 300**,** 91-96.

PENG, G.-S., LI, G., TZENG, N.-S., CHEN, P.-S., CHUANG, D.-M., HSU, Y.-D., YANG, S. & HONG, J.-S. (2005) Valproate pretreatment protects dopaminergic neurons from LPS-induced neurotoxicity in rat primary midbrain cultures: role of microglia. *Molecular Brain Research,* 134**,** 162-169.

PFISTER, J., MA, C., MORRISON, B. & D'MELLO, S. (2008) Opposing Effects of Sirtuins on Neuronal Survival: SIRT1-Mediated Neuroprotection Is Independent of Its Deacetylase Activity. *PLoS ONE,* 3.

PHIEL, C. J., ZHANG, F., HUANG, E. Y., GUENTHER, M. G., LAZAR, M. A. & KLEIN, P. S. (2001) Histone Deacetylase Is a Direct Target of Valproic Acid, a Potent Anticonvulsant, Mood Stabilizer, and Teratogen. *Journal of Biological Chemistry,* 276**,** 36734-36741.

PIENAAR, I. S., HARRISON, I. F., ELSON, J. L., BURY, A., WOLL, P., SIMON, A. K. & DEXTER, D. T. (2013) An animal model mimicking pedunculopontine nucleus cholinergic degeneration in Parkinson's disease. *Brain Structure and Function***,** 1-22.

PLUMB, J. A., FINN, P. W., WILLIAMS, R. J., BANDARA, M. J., ROMERO, M. R., WATKINS, C. J., LA THANGUE, N. B. & BROWN, R. (2003) Pharmacodynamic Response and Inhibition of Growth of Human Tumor Xenografts by the Novel Histone Deacetylase Inhibitor PXD101. *Molecular Cancer Therapeutics,* 2**,** 721-728.

POEWE, W., ANTONINI, A., ZIJLMANS, J. C. M., BURKHARD, P. R. & VIGERHOETS, F. (2010) Levodopa in the treatment of Parkinson's disease: an old drug still going strong. *Clin Interv Aging,* 5**,** 229-238.

PORTELA, A. & ESTELLER, M. (2010) Epigenetic modifications and human disease. *Nat Biotechnol,* 28**,** 1057-68.

POSSEL, H., NOACK, H., PUTZKE, J., WOLF, G. & SIES, H. (2000) Selective upregulation of inducible nitric oxide synthase (iNOS) by lipopolysaccharide (LPS) and cytokines in microglia: In vitro and in vivo studies. *Glia,* 32**,** 51-59.

POYET, C., JENTSCH, B., HERMANNS, T., SCHWECKENDIEK, D., SEIFERT, H.-H., SCHMIDTPETER, M., SULSER, T., MOCH, H., WILD, P. & KRISTIANSEN, G. (2014) Expression of histone deacetylases 1, 2 and 3 in urothelial bladder cancer. *BMC Clinical Pathology,* 14**,** 10.

PRASAD, K., CARVALHO, E., KENTROTI, S., EDWARDS-PRASAD, J., FREED, C. & VERNADAKIS, A. (1994) Establishment and characterization of immortalized clonal cell lines from fetal rat mesencephalic tissue. *In Vitro Cellular & Developmental Biology - Animal,* 30**,** 596-603.

PREDIGER, R., AGUIAR, A. J., MOREIRA, E., MATHEUS, F., CASTRO, A., WALZ, R., DE BEM, A., LATIN, I. A., TASCA, C., FARINA, M. & RAISMAN-VOZARI, R. (2011) The intranasal administration of 1-methyl-4-phenyl-1,2,3,6-tetrahydropyridine (MPTP): a new rodent model to test palliative and neuroprotective agents for Parkinson's disease. *Curr Pharm Des,* 17**,** 489-507.

PRICE, P. A., PARKES, J. D. & MARSDEN, C. D. (1978) Sodium valproate in the treatment of levodopa-induced dyskinesia. *J Neurol Neurosurg Psychiatry,* 41**,** 702-706.

PRZEDBORSKI, S., JACKSON-LEWIS, V., DJALDETTI, R., LIBERATORE, G., VILA, M., VUKOSAVIC, S. & ALMER, G. (2000) The parkinsonian toxin MPTP: action and mechanism. *Restorative Neurology and Neuroscience,* 16**,** 135-142.

QUIK, M., PEREZ, X. A. & BORDIA, T. (2012) Nicotine as a potential neuroprotective agent for Parkinson's disease. *Movement Disorders,* 27**,** 947-957.

RANE, P., SHIELDS, J., HEFFERNAN, M., GUO, Y., AKBARIAN, S. & KING, J. A. (2012) The histone deacetylase inhibitor, sodium butyrate, alleviates cognitive deficits in pre-motor stage PD. *Neuropharmacology,* 62**,** 2409-2412.

RANG, H. P., DALE, M. M., RITTER, J. M. & FLOWER, R. J. (2007) Neurodegenerative Disease. IN RANG, H. P., DALE, M. M., RITTER, J. M. & FLOWER, R. J. (Eds.) *Rang and Dale's Pharmacology.* 6th ed., Churchill Livingstone Elsevier.

REDDY, P. & ZOU, W. (2007) Blocking HDACs boosts regulatory T cells. *Nat Med,* 13**,** 1282-1284.

REN, Q.-G., YU, Y., PAN, D.-J., LUO, X., WANG, X.-Z. & WANG, W. (2009) Lactacystin Stimulates Stellation of Cultured Rat Cortical Astrocytes. *Neurochemical Research,* 34**,** 859-866.

REPETTO, G., PESO, A. D. & ZURITA, J. L. (2008) Neutral red uptake assay for the estimation of cell viability/cytotoxicity. *Nature Protocols,* 3**,** 1125-1131.

REYNOLDS, A. D., BANERJEE, R., LIU, J., GENDELMAN, H. E. & MOSLEY, R. L. (2007) Neuroprotective activities of CD4+CD25+ regulatory T cells in an animal model of Parkinson's disease. *Journal of Leukocyte Biology,* 82**,** 1083-1094.

REYNOLDS, A. D., STONE, D. K., HUTTER, J. A. L., BENNER, E. J., MOSLEY, R. L. & GENDELMAN, H. E. (2010) Regulatory T Cells Attenuate Th17 Cell-Mediated Nigrostriatal Dopaminergic Neurodegeneration in a Model of Parkinson's Disease. *The Journal of Immunology,* 184**,** 2261-2271.

RIDEOUT, H. J., LARSEN, K. E., SULZER, D. & STEFANIS, L. (2001) Proteasomal inhibition leads to formation of ubiquitin/α-synuclein-immunoreactive inclusions in PC12 cells. *Journal of Neurochemistry,* 78**,** 899-908.

RIEDERER, P. & WUKETICH, S. (1976) Time course of nigrostriatal degeneration in parkinson's disease. A detailed study of influential factors in human brain amine analysis. *Journal of Neural Transmission,* 38**,** 277-301.

RIGHI, M., MORI, L., LIBERO, G. D., SIRONI, M., BIONDI, A., MANTOVANI, A., DONINI, S. D. & RICCIARDI-CASTAGNOLI, P. (1989) Monokine production by microglial cell clones. *European Journal of Immunology,* 19**,** 1443-1448.

RODRIGUEZ, M. C., OBESO, J. A. & OLANOW, C. W. (1998) Subthalamic nucleus-mediated excitotoxicity in parkinson's disease: A target for neuroprotection. *Annals of Neurology,* 44**,** S175-S188.

ROTH, S. Y., DENU, J. M. & ALLIS, C. D. (2001) Histone Acetyltransferases. *Annual Review of Biochemistry,* 70**,** 81-120.

ROTTACH, A., LEONHARDT, H. & SPADA, F. (2009) DNA methylation-mediated epigenetic control. *Journal of Cellular Biochemistry,* 108**,** 43-51.

ROUAUX, C., JOKIC, N., MBEBI, C., BOUTILLIER, S., LOEFFLER, J.-P. & BOUTILLIER, A.-L. (2003) Critical loss of CBP/p300 histone acetylase activity by caspase-6 during neurodegeneration. *EMBO J,* 22**,** 6537-6549.

ROY, A., GHOSH, A., JANA, A., LIU, X., BRAHMACHARI, S., GENDELMAN, H. E. & PAHAN, K. (2012) Sodium Phenylbutyrate Controls Neuroinflammatory and Antioxidant Activities and Protects Dopaminergic Neurons in Mouse Models of Parkinson's Disease. *PLoS ONE,* 7**,** e38113.

SADRI-VAKILI, G. & CHA, J.-H. J. (2006) Histone Deacetylase Inhibitors: A Novel Therapeutic Approach to Huntington's Disease (Complex Mechanism of Neuronal Death). *Current Alzheimer Research,* 3**,** 403-408.

SAHA, R. N. & PAHAN, K. (2006) HATs and HDACs in neurodegeneration: a tale of disconcerted acetylation homeostasis. *Cell Death Differ,* 13**,** 539-550.

SALMINEN, A., TAPIOLA, T., KORHONEN, P. & SUURONEN, T. (1998) Neuronal apoptosis induced by histone deacetylase inhibitors. *Molecular Brain Research,* 61**,** 203-206.

SAUNDERS-PULLMAN, R. (2003) Estrogens and parkinson disease: neuroprotective, symptomatic, neither, or both? *Endocrine,* 21**,** 81-87.

SAUNDERS, L. R. & VERDIN, E. (2007) Sirtuins: critical regulators at the crossroads between cancer and aging. *Oncogene,* 26**,** 5489-5504.

SCHALLERT, T., FLEMING, S. M., LEASURE, J. L., TILLERSON, J. L. & BLAND, S. T. (2000) CNS plasticity and assessment of forelimb sensorimotor outcome in unilateral rat models of stroke, cortical ablation, parkinsonism and spinal cord injury. *Neuropharmacology,* 39**,** 777-787.

SCHMALBACH, S. & PETRI, S. (2010) Histone Deacetylation and Motor Neuron Degeneration. *CNS & Neurological Disorders - Drug Targets (Formally Current Drug Targets - CNS & Neurological Disorders),* 9**,** 279-284.

SCHMIDT, D. M. Z. & MCCAFFERTY, D. G. (2007) trans-2-Phenylcyclopropylamine Is a Mechanism-Based Inactivator of the Histone Demethylase LSD1â€ *Biochemistry,* 46**,** 4408-4416.

SEO, J.-W., KIM, J.-H., KIM, J.-H., SEO, M., HAN, H., PARK, J. & SUK, K. (2012) Time-dependent effects of hypothermia on microglial activation and migration. *Journal of Neuroinflammation,* 9**,** 164.

SHAHBAZIAN, M. D. & GRUNSTEIN, M. (2007) Functions of Site-Specific Histone Acetylation and Deacetylation. *Annual Review of Biochemistry,* 76**,** 75-100.

SHEN, L. & PILI, R. (2012) Class I histone deacetylase inhibition is a novel mechanism to target regulatory T cells in immunotherapy. *OncoImmunology,* 1**,** 948-950.

SHI, Y., LAN, F., MATSON, C., MULLIGAN, P., WHETSTINE, J. R., COLE, P. A., CASERO, R. A. & SHI, Y. (2004) Histone Demethylation Mediated by the Nuclear Amine Oxidase Homolog LSD1. *Cell,* 119**,** 941-953.

SINN, D.-I., KIM, S.-J., CHU, K., JUNG, K.-H., LEE, S.-T., SONG, E.-C., KIM, J.-M., PARK, D.-K., KUN LEE, S., KIM, M. & ROH, J.-K. (2007) Valproic acid-mediated neuroprotection in intracerebral hemorrhage via histone deacetylase inhibition and transcriptional activation. *Neurobiology of Disease,* 26**,** 464-472.

SONG, D. D., SHULTS, C. W., SISK, A., ROCKENSTEIN, E. & MASLIAH, E. (2004) Enhanced substantia nigra mitochondrial pathology in human α-synuclein transgenic mice after treatment with MPTP. *Experimental Neurology,* 186**,** 158-172.

SOTO, C. (2003) Unfolding the role of protein misfolding in neurodegenerative diseases. *Nat Rev Neurosci,* 4**,** 49-60.

SPANGE, S., WAGNER, T., HEINZEL, T. & KRÄMER, O. H. (2009) Acetylation of non-histone proteins modulates cellular signalling at multiple levels. *The International Journal of Biochemistry & Cell Biology,* 41**,** 185-198.

SPATOLA, M. & WIDER, C. (2014) Genetics of Parkinson's disease: the yield. *Parkinsonism & Related Disorders,* 20**,** S35-38.

SPECTOR, R. (1987) Niacinamide transport through the blood-brain barrier. *Neurochemical Research,* 12**,** 27-31.

SPILLANTINI, M. G., SCHMIDT, M. L., LEE, V. M.-Y., TROJANOWSKI, J. Q., JAKES, R. & GOEDERT, M. (1997) α−Synuclein in Lewy bodies. *Nature,* 388**,** 839-840.

STOLL, G., JANDER, S. & SCHROETER, M. (2000) Cytokines in CNS disorders: neurotoxicity versus neuroprotection. IN JELLINGER, K., SCHMIDT, R. & WINDISCH, M. (Eds.) *Advances in Dementia Research.* Springer Vienna.

SUH, H. S., CHOI, S., KHATTAR, P., CHOI, N. & LEE, S. C. (2010) Histone deacetylase inhibitors suppress the expression of inflammatory and innate immune response genes in human microglia and astrocytes. *Journal of Neuroimmune Pharmacology,* 5**,** 521-532.

TAI, Y.-T., LEE, W.-Y., LEE, F.-P., LIN, T.-J., SHIH, C.-L., WANG, J.-Y., CHIU, W.-T. & HUNG, K.-S. (2014) Low Dose of Valproate Improves Motor Function after Traumatic Brain Injury. *BioMed Research International,* 2014**,** 8.

TAO, R., DE ZOETEN, E. F., OZKAYNAK, E., CHEN, C., WANG, L., PORRETT, P. M., LI, B., TURKA, L. A., OLSON, E. N., GREENE, M. I., WELLS, A. D. & HANCOCK, W. W. (2007) Deacetylase inhibition promotes the generation and function of regulatory T cells. *Nat Med,* 13**,** 1299-1307.

TOFARIS, G. K., LAYFIELD, R. & SPILLANTINI, M. G. (2001) α-Synuclein metabolism and aggregation is linked to ubiquitin-independent degradation by the proteasome. *FEBS Letters,* 509**,** 22-26.

TOLOSA, E., WENNING, G. & POEWE, W. (2006) The diagnosis of Parkinson's disease. *The Lancet Neurology,* 5**,** 75-86.

TONG, Y. & SHEN, J. (2009) α-Synuclein and LRRK2: Partners in Crime. *Neuron,* 64**,** 771-773.

TRAPP, J., MEIER, R., HONGWISET, D., KASSACK, M. U., SIPPL, W. & JUNG, M. (2007) Structure–Activity Studies on Suramin Analogues as Inhibitors of NAD+-Dependent Histone Deacetylases (Sirtuins). *ChemMedChem,* 2**,** 1419-1431.

TRINH, K., ANDREWS, L., KRAUSE, J., HANAK, T., LEE, D., GELB, M. & PALLANCK, L. (2010) Decaffeinated Coffee and Nicotine-Free Tobacco Provide Neuroprotection in Drosophila Models of Parkinson's Disease through an NRF2-Dependent Mechanism. *The Journal of Neuroscience,* 30**,** 5525-5532.

TSUKADA, Y.-I., FANG, J., ERDJUMENT-BROMAGE, H., WARREN, M. E., BORCHERS, C. H., TEMPST, P. & ZHANG, Y. (2006) Histone demethylation by a family of JmjC domain-containing proteins. *Nature,* 439**,** 811-816.

UNGERSTEDT, U. & ARBUTHNOTT, G. W. (1970) Quantitative recording of rotational behavior in rats after 6-hydroxy-dopamine lesions of the nigrostriatal dopamine system. *Brain Research,* 24**,** 485-493.

VERNON, A., JOHANSSON, S. & MODO, M. (2010) Non-invasive evaluation of nigrostriatal neuropathology in a proteasome inhibitor rodent model of Parkinson's disease. *BMC Neuroscience,* 11**,** 1.

VERNON, A. & MODO, M. (2011) Non-invasive MR Imaging of Neurodegeneration in a Rodent Model of Parkinson's Disease. IN MODO, M. & BULTE, J. W. M. (Eds.) *Magnetic Resonance Neuroimaging.* Humana Press.

VERNON, A. C., CRUM, W. R., JOHANSSON, S. M. & MODO, M. (2011) Evolution of Extra-Nigral Damage Predicts Behavioural Deficits in a Rat Proteasome Inhibitor Model of Parkinson's Disease. *PLoS ONE,* 6**,** e17269.

VERNON, A. C., CRUM, W. R., LERCH, J. P., CHEGE, W., NATESAN, S., MODO, M., COOPER, J. D., WILLIAMS, S. C. R. & KAPUR, S. (2013) Reduced Cortical Volume and Elevated Astrocyte Density in Rats Chronically Treated with Antipsychotic Drugs—Linking Magnetic Resonance Imaging Findings to Cellular Pathology. *Biological Psychiatry*.

VERNON, A. C., NATESAN, S., CRUM, W. R., COOPER, J. D., MODO, M., WILLIAMS, S. C. R. & KAPUR, S. (2012) Contrasting Effects of Haloperidol and Lithium on Rodent Brain Structure: A Magnetic Resonance Imaging Study with Postmortem Confirmation. *Biological Psychiatry,* 71**,** 855-863.

VILLAR-GAREA, A. & ESTELLER, M. (2004) Histone deacetylase inhibitors: Understanding a new wave of anticancer agents. *International Journal of Cancer,* 112**,** 171-178.

VONSATTEL, J. P. G., ALZAWA, H., DIFIGLIA, M., MCKEE, A. C., MACDONALD, M., GUSELLA, J. E., LANDWEHRMEYER, G. B., BIRD, E. P., RICHARDSON, E. P. J. & HEDLEY-WHYTE, E. T. (1995) An Improved Approach to Prepare Human Brains for Research. *Journal of Neuropathology & Experimental Neurology,* 54**,** 42-56.

WAGNER, J. M., HACKANSON, B., LÜBBERT, M. & JUNG, M. (2010) Histone deacetylase (HDAC) inhibitors in recent clinical trials for cancer therapy. *Clin Epigenetics,* 1(3-4)**,** 117-136.

WANG, L., DE ZOETEN, E. F., GREENE, M. I. & HANCOCK, W. W. (2009) Immunomodulatory effects of deacetylase inhibitors: therapeutic targeting of FOXP3+ regulatory T cells. *Nat Rev Drug Discov,* 8**,** 969-981.

WEST, M. J., SLOMIANKA, L. & GUNDERSEN, H. J. G. (1991) Unbiased stereological estimation of the total number of neurons in the subdivisions of the rat hippocampus using the optical fractionator. *The Anatomical Record,* 231**,** 482-497.

WHITFIELD, A. C., MOORE, B. T. & DANIELS, R. N. (2014) Classics in Chemical Neuroscience: Levodopa. *ACS Chemical Neuroscience*.

WHO (2013) *18th WHO Model List of Essential Medicines*, WHO.

WILLIAMS, C. J. & DEXTER, D. T. (2014) Neuroprotective and symptomatic effects of targeting group III mGlu receptors in neurodegenerative disease. *Journal of Neurochemistry,* 129**,** 4-20.

WILLIAMS, D. R., WATT, H. C. & LEES, A. J. (2006) Predictors of falls and fractures in bradykinetic rigid syndromes: a retrospective study. *Journal of Neurology, Neurosurgery & Psychiatry,* 77**,** 468-473.

WILSON, A. J., BYUN, D.-S., POPOVA, N., MURRAY, L. B., L'ITALIEN, K., SOWA, Y., ARANGO, D., VELCICH, A., AUGENLICHT, L. H. & MARIADASON, J. M. (2006) Histone Deacetylase 3 (HDAC3) and Other Class I HDACs Regulate Colon Cell Maturation and p21 Expression and Are Deregulated in Human Colon Cancer. *Journal of Biological Chemistry,* 281**,** 13548-13558.

WU, J. Y., NIU, F. N., HUANG, R. & XU, Y. (2008a) Enhancement of glutamate uptake in 1-methyl-4-phenylpyridinium-treated astrocytes by trichostatin A. *NeuroReport,* 19**,** 1209-1212.

WU, X., CHEN, P. S., DALLAS, S., WILSON, B., BLOCK, M. L., WANG, C.-C., KINYAMU, H., LU, N., GAO, X., LENG, Y., CHUANG, D.-M., ZHANG, W., LU, R. B. & HONG, J.-S. (2008b) Histone deacetylase inhibitors up-regulate astrocyte GDNF and BDNF gene transcription and protect dopaminergic neurons. *The International Journal of Neuropsychopharmacology,* 11**,** 1123-1134.

XIE, W., LI, X., LI, C., ZHU, W., JANKOVIC, J. & LE, W. (2010) Proteasome inhibition modeling nigral neuron degeneration in Parkinson's disease. *Journal of Neurochemistry,* 115**,** 188-199.

XIMENES, J. C. M., VERDE, E. C. L., NAFFAH-MAZZACORATTI, M. D. G. & VIANA, G. S. D. B. (2012) Valproic Acid, a Drug with Multiple Molecular Targets Related to Its Potential Neuroprotective Action. *Neuroscience and Medicine,* 3**,** 107-123.

XU, J., XU, S.-Q., LIANG, J., LU, Y., LUO, J.-H. & JIN, J.-H. (2012) [Protective effect of nicotinamide in a mouse Parkinson's disease model]. *Zhejiang da xue xue bao. Yi xue ban = Journal of Zhejiang University. Medical sciences,* 41**,** 146-152.

XU, K., DAI, X. L., HUANG, H. C. & JIANG, Z. F. (2011) Targeting HDACs: A Promising Therapy for Alzheimer's Disease. *Oxidative Medicine and Cellular Longevity,* 2011.

XU, K., XU, Y., BROWN-JERMYN, D., CHEN, J.-F., ASCHERIO, A., DLUZEN, D. E. & SCHWARZSCHILD, M. A. (2006) Estrogen Prevents Neuroprotection by Caffeine in the Mouse 1-Methyl-4-Phenyl-1,2,3,6-Tetrahydropyridine Model of Parkinson's Disease. *The Journal of Neuroscience,* 26**,** 535-541.

XU, W. S., PARMIGIANI, R. B. & MARKS, P. A. (2007) Histone deacetylase inhibitors: molecular mechanisms of action. *Oncogene,* 26**,** 5541-5552.

XUAN, A., LONG, D., LI, J., JI, W., HONG, L., ZHANG, M. & ZHANG, W. (2012) Neuroprotective effects of valproic acid following transient global ischemia in rats. *Life Sciences,* 90**,** 463-468.

YEUNG, F., HOBERG, J. E., RAMSEY, C. S., KELLER, M. D., JONES, D. R., FRYE, R. A. & MAYO, M. W. (2004) *Modulation of NF-κB-dependent transcription and cell survival by the SIRT1 deacetylase*.

YORITAKA, A., HATTORI, N., UCHIDA, K., TANAKA, M., STADTMAN, E. R. & MIZUNO, Y. (1996) Immunohistochemical detection of 4-hydroxynonenal protein adducts in Parkinson disease. *Proceedings of the National Academy of Sciences,* 93**,** 2696-2701.

YU, S.-H., CHO, D.-C., KIM, K.-T., NAM, K.-H., CHO, H.-J. & SUNG, J.-K. (2012) The Neuroprotective Effect of Treatment of Valproic Acid in Acute Spinal Cord Injury. *J Korean Neurosurg Soc,* 51**,** 191-198.

ZHANG, J., PERRY, G., SMITH, M. A., ROBERTSON, D., OLSON, S. J., GRAHAM, D. G. & MONTINE, T. J. (1999) Parkinson's Disease Is Associated with Oxidative Damage to Cytoplasmic DNA and RNA in Substantia Nigra Neurons. *The American Journal of Pathology,* 154**,** 1423-1429.

ZHANG, X., XIE, W., QU, S., PAN, T., WANG, X. & LE, W. (2005) Neuroprotection by iron chelator against proteasome inhibitor-induced nigral degeneration. *Biochemical and Biophysical Research Communications,* 333**,** 544-549.

ZHANG, Y., LI, N., CARON, C., MATTHIAS, G., HESS, D., KHOCHBIN, S. & MATTHIAS, P. (2003) HDAC-6 interacts with and deacetylates tubulin and microtubules in vivo. *EMBO J,* 22**,** 1168-79.

ZHANG, Z., YAMASHITA, H., TOYAMA, T., SUGIURA, H., OMOTO, Y., ANDO, Y., MITA, K., HAMAGUCHI, M., HAYASHI, S.-I. & IWASE, H. (2004) HDAC6 Expression Is Correlated with Better Survival in Breast Cancer. *Clinical Cancer Research,* 10**,** 6962-6968.

ZHENG, B., LIAO, Z., LOCASCIO, J. J., LESNIAK, K. A., RODERICK, S. S., WATT, M. L., EKLUND, A. C., ZHANG-JAMES, Y., KIM, P. D., HAUSER, M. A., GRÜNBLATT, E., MORAN, L. B., MANDEL, S. A., RIEDERER, P., MILLER, R. M., FEDEROFF, H. J., WÜLLNER, U., PAPAPETROPOULOS, S., YOUDIM, M. B., CANTUTI-CASTELVETRI, I., YOUNG, A. B., VANCE, J. M., DAVIS, R. L., HEDREEN, J. C., ADLER, C. H., BEACH, T. G., GRAEBER, M. B., MIDDLETON, F. A., ROCHET, J.-C., SCHERZER, C. R. & CONSORTIUM, T. G. P. G. E. (2010) PGC-1α, A Potential Therapeutic Target for Early Intervention in Parkinson's Disease. *Science Translational Medicine,* 2**,** 52ra73.

ZHOU, W., BERCURY, K., CUMMISKEY, J., LUONG, N., LEBIN, J. & FREED, C. R. (2011) Phenylbutyrate Up-regulates the DJ-1 Protein and Protects Neurons in Cell Culture and in Animal Models of Parkinson Disease. *Journal of Biological Chemistry,* 286**,** 14941-14951.

ZHU, W., XIE, W., PAN, T., XU, P., FRIDKIN, M., ZHENG, H., JANKOVIC, J., YOUDIM, M. B. H. & LE, W. (2007) Prevention and restoration of lactacystin-induced nigrostriatal dopamine neuron degeneration by novel brain-permeable iron chelators. *The FASEB Journal,* 21**,** 3835-3844.

Appendices

Appendix 1 – Copyright Agreement

Copyright agreement from Elsevier allowing reprint of parts of Pharmacology & Therapeutics, 140, HARRISON, I.F. & DEXTER, D.T., "Epigenetic targeting of histone deacetylase: Therapeutic potential in Parkinson's disease?" Pages 32-52, Copyright 2013.

ELSEVIER LICENSE
TERMS AND CONDITIONS

Oct 17, 2014

This is a License Agreement between Ian F Harrison ("You") and Elsevier ("Elsevier") provided by Copyright Clearance Center ("CCC"). The license consists of your order details, the terms and conditions provided by Elsevier, and the payment terms and conditions.

All payments must be made in full to CCC. For payment instructions, please see information listed at the bottom of this form.

Supplier	Elsevier Limited The Boulevard,Langford Lane Kidlington,Oxford,OX5 1GB,UK
Registered Company Number	1982084
Customer name	Ian F Harrison
Customer address	Department of Medicine
	London, W12 0NN
License number	3480721424500
License date	Oct 02, 2014
Licensed content publisher	Elsevier
Licensed content publication	Pharmacology & Therapeutics
Licensed content title	Epigenetic targeting of histone deacetylase: Therapeutic potential in Parkinson's disease?
Licensed content author	Ian F. Harrison,David T. Dexter
Licensed content date	October 2013
Licensed content volume number	140
Licensed content issue number	1
Number of pages	19
Start Page	34
End Page	52
Type of Use	reuse in a thesis/dissertation
Intended publisher of new work	other
Portion	full article
Format	electronic
Are you the author of this Elsevier article?	Yes
Will you be translating?	No
Order reference number	3480720879369
Title of your thesis/dissertation	Investigating the Neuroprotective Effects of Histone Deacetylase Inhibitors in Parkinson's Disease
Expected completion date	Oct 2014
Estimated size (number of pages)	350
Elsevier VAT number	GB 494 6272 12
Permissions price	0.00 GBP
VAT/Local Sales Tax	0.00 GBP / 0.00 GBP
Total	0.00 GBP
Terms and Conditions	